ADVANCES IN POLLEN RESEARCH: BIOLOGY, BIOTECHNOLOGY AND PLANT BREEDING APPLICATIONS

EDITED BY: Concepción Gómez-Mena, Pilar S. Testillano, David Honys and Raju Datla

PUBLISHED IN: Frontiers in Plant Science

frontiers Research Topics

frontiers

ISSN 1664-8714
ISBN 978-2-88974-962-1
DOI 10.3389/978-2-88974-962-1

About Frontiers

Frontiers is more than just an open-access publisher of scholarly articles: it is a pioneering approach to the world of academia, radically improving the way scholarly research is managed. The grand vision of Frontiers is a world where all people have an equal opportunity to seek, share and generate knowledge. Frontiers provides immediate and permanent online open access to all its publications, but this alone is not enough to realize our grand goals.

Frontiers Journal Series

The Frontiers Journal Series is a multi-tier and interdisciplinary set of open-access, online journals, promising a paradigm shift from the current review, selection and dissemination processes in academic publishing. All Frontiers journals are driven by researchers for researchers; therefore, they constitute a service to the scholarly community. At the same time, the Frontiers Journal Series operates on a revolutionary invention, the tiered publishing system, initially addressing specific communities of scholars, and gradually climbing up to broader public understanding, thus serving the interests of the lay society, too.

Dedication to Quality

Each Frontiers article is a landmark of the highest quality, thanks to genuinely collaborative interactions between authors and review editors, who include some of the world's best academicians. Research must be certified by peers before entering a stream of knowledge that may eventually reach the public - and shape society; therefore, Frontiers only applies the most rigorous and unbiased reviews.
Frontiers revolutionizes research publishing by freely delivering the most outstanding research, evaluated with no bias from both the academic and social point of view. By applying the most advanced information technologies, Frontiers is catapulting scholarly publishing into a new generation.

What are Frontiers Research Topics?

Frontiers Research Topics are very popular trademarks of the Frontiers Journals Series: they are collections of at least ten articles, all centered on a particular subject. With their unique mix of varied contributions from Original Research to Review Articles, Frontiers Research Topics unify the most influential researchers, the latest key findings and historical advances in a hot research area! Find out more on how to host your own Frontiers Research Topic or contribute to one as an author by contacting the Frontiers Editorial Office: frontiersin.org/about/contact

ADVANCES IN POLLEN RESEARCH: BIOLOGY, BIOTECHNOLOGY AND PLANT BREEDING APPLICATIONS

Topic Editors:
Concepción Gómez-Mena, Polytechnic University of Valencia, Spain
Pilar S. Testillano, Margarita Salas Center for Biological Research, Spanish National Research Council (CSIC), Spain
David Honys, Institute of Experimental Botany, Academy of Sciences of the Czech Republic, Czechia
Raju Datla, Global Institute for Food Security (GIFS), Canada

Citation: Gómez-Mena, C., Testillano, P. S., Honys, D., Datla, R., eds. (2022). Advances in Pollen Research: Biology, Biotechnology and Plant Breeding Applications. Lausanne: Frontiers Media SA. doi: 10.3389/978-2-88974-962-1

Table of Contents

05 ***Editorial: Advances in Pollen Research: Biology, Biotechnology, and Plant Breeding Applications***
Concepción Gómez-Mena, David Honys, Raju Datla and Pilar S. Testillano

08 ***Development of the Middle Layer in the Anther of* Arabidopsis**
Jing-Shi Xue, Chi Yao, Qin-Lin Xu, Chang-Xu Sui, Xin-Lei Jia, Wen-Jing Hu, Yong-Lin Lv, Yi-Feng Feng, Yu-Jia Peng, Shi-Yi Shen, Nai-Ying Yang, Yu-Xia Lou and Zhong-Nan Yang

17 ***A Maize Male Gametophyte-Specific Gene Encodes ZmLARP6c1, a Potential RNA-Binding Protein Required for Competitive Pollen Tube Growth***
Lian Zhou, Zuzana Vejlupkova, Cedar Warman and John E. Fowler

29 ***The Role of INAPERTURATE POLLEN1 as a Pollen Aperture Factor Is Conserved in the Basal Eudicot* Eschscholzia californica *(Papaveraceae)***
Ismael Mazuecos-Aguilera, Ana Teresa Romero-García, Božena Klodová, David Honys, María C. Fernández-Fernández, Samira Ben-Menni Schuler, Anna A. Dobritsa and Víctor N. Suárez-Santiago

43 ***Occurrence and Prevention of Delayed Autonomous Selfing in* Salvia umbratica *(Lamiaceae)***
Han-Wen Xiao, Yan-Bo Huang, Yu-Hang Chang, Yun Chen, Richard J. Abbott, Yu-Kun Wei and Yong-Peng Ma

53 ***Sequential Deposition and Remodeling of Cell Wall Polymers During Tomato Pollen Development***
Syeda Roop Fatima Jaffri and Cora A. MacAlister

69 ***Impact of Storage Temperature on Pollen Viability and Germinability of Four Serbian Autochthon Apple Cultivars***
Dušica Ćalić, Jelena Milojević, Maja Belić, Rade Miletić and Snežana Zdravković-Korać

75 ***Mapping and Analysis of a Novel Genic Male Sterility Gene in Watermelon (*Citrullus lanatus*)***
Wei Dong, Dewei Wu, Chen Yan and Defeng Wu

87 ***The Toughest Material in the Plant Kingdom: An Update on Sporopollenin***
Etienne Grienenberger and Teagen D. Quilichini

96 ***Hormonome Dynamics During Microgametogenesis in Different* Nicotiana *Species***
Lenka Záveská Drábková, Eva Pokorná, Petre I. Dobrev, Jana Kůrková, Lenka Steinbachová, David Honys and Václav Motyka

112 **PsEND1 *Is a Key Player in Pea Pollen Development Through the Modulation of Redox Homeostasis***
Rim Hamza, Edelín Roque, Concepción Gómez-Mena, Francisco Madueño, José Pío Beltrán and Luis A. Cañas

127 ***Androgenesis-Based Doubled Haploidy: Past, Present, and Future Perspectives***
Brett Hale, Alison M. R. Ferrie, Sreekala Chellamma, J. Pon Samuel and Gregory C. Phillips

142 ***Pollen Number and Ribosome Gene Expression Altered in a Genome-Editing Mutant of* REDUCED POLLEN NUMBER1 *Gene***
Hiroyuki Kakui, Takashi Tsuchimatsu, Misako Yamazaki, Masaomi Hatakeyama and Kentaro K. Shimizu

155 ***Molecular Control of Sporophyte-Gametophyte Ontogeny and Transition in Plants***
Saurabh Pandey, Amir Bahram Moradi, Oleksandr Dovzhenko, Alisher Touraev, Klaus Palme and Ralf Welsch

164 ***Transcript Profiling Analysis and ncRNAs' Identification of Male-Sterile Systems of* Brassica campestris *Reveal New Insights Into the Mechanism Underlying Anther and Pollen Development***
Dong Zhou, Caizhi Chen, Zongmin Jin, Jingwen Chen, Sue Lin, Tao Lyu, Dandan Liu, Xinpeng Xiong, Jiashu Cao and Li Huang

182 ***A Plastid-Bound Ankyrin Repeat Protein Controls Gametophyte and Early Embryo Development in* Arabidopsis thaliana**
Katarína Kulichová, Janto Pieters, Vinod Kumar, David Honys and Said Hafidh

frontiers in Plant Science

EDITORIAL
published: 29 March 2022
doi: 10.3389/fpls.2022.876502

Editorial: Advances in Pollen Research: Biology, Biotechnology, and Plant Breeding Applications

Concepción Gómez-Mena[1], David Honys[2], Raju Datla[3] and Pilar S. Testillano[4]**

[1] Department of Plant Development and Hormone Action, Instituto de Biología Molecular y Celular de Plantas (CSIC-Universitat Politècnica de València), Ciudad Politécnica de la Innovación, Valencia, Spain, [2] Laboratory of Pollen Biology, Institute of Experimental Botany of the Czech Academy of Sciences, Prague, Czechia, [3] Global Institute for Food Security, University of Saskatchewan, Saskatoon, SK, Canada, [4] Pollen Biotechnology of Crop Plants Group, Margarita Salas Center of Biological Research, CIB -CSIC, Madrid, Spain

Keywords: pollen, anther, biotechnology, breeding, crops

Editorial on the Research Topic

Advances in Pollen Research: Biology, Biotechnology, and Plant Breeding Applications

OPEN ACCESS

Edited and reviewed by:
Michael Gerard Muszynski, University of Hawaii at Manoa, United States

****Correspondence:***
Concepción Gómez-Mena
cgomezm@ibmcp.upv.es
Pilar S. Testillano
testillano@cib.csic.es

Specialty section:
This article was submitted to Plant Development and EvoDevo, a section of the journal Frontiers in Plant Science

Received: *15 February 2022*
Accepted: *10 March 2022*
Published: *29 March 2022*

Citation:
Gómez-Mena C, Honys D, Datla R and Testillano PS (2022) Editorial: Advances in Pollen Research: Biology, Biotechnology, and Plant Breeding Applications. Front. Plant Sci. 13:876502. doi: 10.3389/fpls.2022.876502

In flowering plants, mature pollen grains are produced within the developing anthers of the flowers in two successive phases, microsporogeneseis and microgametogenesesis. Anther and pollen development involves the coordinated growth and differentiation of tissues and cell types required for the formation of viable male gametes, but also, to permit pollen release and ensure successful fertilization. The identification of the genetic networks and regulatory molecules involved in the formation of the anther remains a highly unexplored topic in many crops. Evolutionary and functional studies in crops are helping to unravel new functions for genes originally identified in model plants (Rojas-Gracia et al., 2017) and the changes in transcriptional profiles associated with plant domestication (Xiang et al., 2019). Under the global changes in environmental conditions, pollen development is probably one of the most vulnerable and challenged stages of plant reproduction (Chaturvedi et al., 2021). In this context, increasing basic research will provide valuable information to assist the design of biotechnological tools to mitigate this effect especially in crop systems in the future.

New advances in the functional characterization of genes involved in different aspects of pollen development and function are described in the following articles of this Research Topic. In the original research article by Hamza et al., the authors functionally characterized *Pisum sativum ENDOTHECIUM* 1 (*PsEND1*), a pea anther-specific gene that encodes a protein containing four hemopexin domains. Gain and loss-of-function experiments showed that PsEND1 is a central player in the maintenance of balanced redox levels during pollen and anther development. Zhou L. et al. demonstrated pollen-specific regulatory function of ZmLarp6c1, maize ortholog of Arabidopsis AtLARP6C, particularly during the progamic phase. The respective Ds-GFP transposable element insertion line showed reduced transmission through the male wich was associated with altered germination dynamics and slower growth of mutant pollen tubes. Considering that LARP6C also orchestrates posttranscriptional reprogramming of gene expression during hydration in Arabidopsis (Billey et al., 2021),

these findings highlight the general regulatory role of LARP6C in angiosperms. The original research article by Mazuecos-Aguilera et al. describes the functional study of the *INAPERTURATE POLLEN1* (*INP1*) ortholog from the basal eudicot *Eschscholzia californica* (California poppy), a gene involved in pollen aperture formation. This study substantiates the importance of *INP1* homologs for aperture formation across angiosperms and opens up new avenues for functional studies of other aperture candidate genes. The role of the Arabidopsis Ankyrin-repeat protein (AT5G66055, AKRP), during male and female gametogenesis is analyzed by Kulichová et al. using the new mutant allele *akrp-3*. AKRP is a plastid-localized protein with a putative function in plastid differentiation and morphogenesis. The findings provide insight into the role of this protein in both the differentiation of gametophytes and the coupling of embryo development with chlorophyll synthesis. In the research article by Dong et al., the authors reported a new major gene *Cla006625* controlling "Genic Male Sterility" (GMS) in watermelon. Molecular and genomics studies revealed that this gene renamed as *ClaPEX1* encodes a leucine-rich repeat protein, and the recessive mutant of this locus causes pollen abortion conferring GMS. The targeted RNAi based evidence further confirmed the functionality for this gene in GMS, and the authors propose potential applications in hybrid seed production technology to capture heterosis in watermelon. Kakui et al. studied pollen number variation in Arabidopsis and discovered the first gene responsible for pollen number, *REDUCED POLLEN NUMBER1* (*RDP1*), encoding the large ribosomal subunit assembly factor. CRISPR/Cas9-generated *rdp1-3* mutants revealed the pleiotropic effect of RDP1 in flowering and pollen development. Subsequent transcriptome analysis supported the hypothesis that ribosome biogenesis, critical for pollen development, is disturbed in the *rdp1-3* mutant pollen and highlighted three key bHLH transcription factors (ABORTED MICROSPORES, bHLH010, and bHLH089).

The identification and characterization of regulatory molecules during anther or pollen development is the subject of the remaining articles in this Research Topic. The role of hormone dynamics during microgametogenesis has been explored by Záveská Drábková et al. in several *Nicotiana* species. The article describes the dynamic changes in endogenous phytohormones during pollen ontogeny, highlighting that unequal levels of endogenous hormones and the presence of specific derivatives which may be characteristic for pollen development in different phylogenetic plant groups. In the original research article by Zhou D. et al., the author used male-sterile systems of *Brassica campestris* (Chinese cabbage) to study anther and pollen development in this species. Differentially expressed lncRNAs (DELs), miRNAs (DEMs), and genes (DEGs) were identified providing new insights into molecular regulation especially the ncRNA interaction during pollen development in Brassica crops.

Several of the articles submitted to this Research Topic investigated global developmental aspects of pollen development and its impact on plant performance. Xue et al., developed several live imaging methods for the study of anther development. They created the marker line *ProUBQ10:H2B:VENUS* and used it to study the development of the middle layer in the anther of *Arabidopsis thaliana*. The results showed that the middle layer was derived from both inner and outer secondary parietal cells, indicating that the cell fate determination of the middle layer was non-cell-autonomous in Arabidopsis. In the new research report by Xiao et al., the authors investigated the adaptive and evolutionary features of "Delayed Autonomous Selfing" (DAS) in *Salvia umbractica*. The observations and findings from the field and controlled experiments showed outcrossing using insect pollinators first, wich failed to fertilize, lead to execution of DAS to ensure fertilization for successful fruit and seed production. The authors presented strong supporting evidence by detailed documentation of changes in the reproductive organs' specific behaviors linked with morphological and developmental activities of these two built-in alternative pollination options in *Salvia* species. In the research article by Calić et al., the authors investigated the influence of long-term storage temperature on pollen viability of four Serbian autochthon apple cultivars. Interestingly, the pollen could be efficiently maintained at −20°C and later used for breeding purposes. The results will surely contribute to the preservation of these old autochthon cultivars as unique genetic resources with important ecological and economic value. Jaffri and MacAlister utilized histology and immunostaining to show the structure of the tomato pollen wall, characterized dynamic changes in pectin composition, and established a developmental timeline of its formation. Following meiosis, the microspores losing their cellulose primary wall remain connected by a temporary callose wall in tetrads. Release of early microspores initiates sporopollenin secretion to form exine, wich is completed in late microspores. The tomato pollen wall formation is finished by the formation of intine from pollen mitosis I to pollen maturation. Grienenberger and Quilichini highlighted significant progress in the field of sporopollenin research; they examined the cross-disciplinary efforts to solve the sporopollenin composition puzzle and presented a working model of sporopollenin's molecular structure and biosynthesis. They further discussed the controversies and remaining knowledge gaps, including the degree of aromaticity, cross-linkage profiles, and extent of chemical conservation of sporopollenin among land plants. Finally, the authors highlighted opportunities for practical utilization of this extraordinary biomaterial.

Pollen biotechnology offers a wide range of possibilities for plant breeding. Doubled-haploid technology, based on the reprogramming of immature pollen grains or microspores toward embryogenesis, promises to accelerate crop breeding programs and shorten the time to obtain new varieties. Investigations in recent years have shown the complex regulatory mechanisms underlying microspore embryogenesis (Testillano, 2019), opening promising avenues for improving its efficiency in crop species of economic and environmental interest. In addition, genetically engineered male-sterile plants offer a valuable trait for plant breeding programs for many crops. Recently, CRISPR/Cas9 editing technology has become an efficient and versatile option to obtain new plant varieties and accelerate breeding practices. In the review by et al., the authors recapitulated past and present research on obtaining male-derived haploid progeny by microspore embryogenesis.

The authors evaluated basic breeding applications of this process, explored the utility of genomics and gene editing technologies for protocol development, and provided considerations to overcome genotype specificity and morphogenic recalcitrance in non-model plant systems. In the article by Pandey et al., the authors reviewed the molecular mechanisms controlling the alternation of generations between the sporophytic and gametophytic stages from an evolutionary perspective. The article compares the genetic factors and mechanisms regulating the separation of the two developmental programs and discusses its biotechnological applications for accelerating the breeding of crop plants.

The goal of this Research Topic was to highlight the latest advances in pollen research and the potential of pollen in the development of biotechnological applications for plant breeding. Fifteen articles have been published on this Research Topic including two reviews, one mini-review, and 12 original research articles covering different aspects of pollen biology, biotechnology, and breeding applications. Remarkably, many of the research articles were carried out on important crops including studies in apple, pea, maize, watermelon, or tomato. Globally this Research Topic of articles successfully represents some major advances in pollen research across different plant species contributing to increasing knowledge in the field and to the generation of new opportunities to implement crop improvement programs in the coming years.

AUTHOR CONTRIBUTIONS

All authors listed have made a substantial, direct, and intellectual contribution to the work and approved it for publication.

ACKNOWLEDGMENTS

We thank the Frontiers Editorial Staff for their support throughout the elaboration of this Research Topic and the authors that submitted the articles for their invaluable contribution.

REFERENCES

Billey, E., Hafidh, S., Cruz-Gallardo, I., Litholdo, C. G. Jr., Jean, V., Carpentier, M. C., et al. (2021). LARP6C orchestrates posttranscriptional reprogramming of gene expression during hydration to promote pollen tube guidance. *Plant Cell* 33, 2637–2661. doi: 10.1093/plcell/koab131

Chaturvedi, P., Wiese, A. J., Ghatak, A., Záveská Drábková, L., Weckwerth, W., and Honys, D. (2021). Heat stress response mechanisms in pollen development. *New Phytol.* 231, 571–585. doi: 10.1111/nph.17380

Rojas-Gracia, P., Roque, E., Medina, M., Rochina, M., Hamza, R., Angarita-Díaz, M. P., et al. (2017) The parthenocarpic hydra mutant reveals a new function for a SPOROCYTELESS-like gene in the control of fruit set in tomato. *New Phytol.* 214, 1198–1212. doi: 10.1111/nph.14433

Testillano, P. S. (2019). Microspore embryogenesis: targeting the determinant factors of stress-induced cell reprogramming for crop improvement. *J. Exp. Bot.* 70, 2965–2978. doi: 10.1093/jxb/ery464

Xiang, D., Quilichini, T. D., Liu, Z., Gao, P., Pan, Y., Li, Q., et al. (2019). The transcriptional landscape of polyploid wheats and their diploid ancestors during embryogenesis and grain development. *Plant Cell* 31, 2888–2911. doi: 10.1105/tpc.19.00397

Conflict of Interest: The authors declare that the research was conducted in the absence of any commercial or financial relationships that could be construed as a potential conflict of interest.

frontiers in Plant Science

ORIGINAL RESEARCH
published: 10 February 2021
doi: 10.3389/fpls.2021.634114

Development of the Middle Layer in the Anther of *Arabidopsis*

*Jing-Shi Xue†, Chi Yao†, Qin-Lin Xu, Chang-Xu Sui, Xin-Lei Jia, Wen-Jing Hu, Yong-Lin Lv, Yi-Feng Feng, Yu-Jia Peng, Shi-Yi Shen, Nai-Ying Yang, Yu-Xia Lou and Zhong-Nan Yang**

Shanghai Key Laboratory of Plant Molecular Sciences, College of Life Sciences, Shanghai Normal University, Shanghai, China

The middle layer is an essential cell layer of the anther wall located between the endothecium and tapetum in *Arabidopsis*. Based on sectioning, the middle layer was found to be degraded at stage 7, which led to the separation of the tapetum from the anther wall. Here, we established techniques for live imaging of the anther. We created a marker line with fluorescent proteins expressed in all anther layers to study anther development. Several staining methods were used in the intact anthers to study anther cell morphology. We clarified the initiation, development, and degradation of the middle layer in *Arabidopsis*. This layer is initiated from both the inner and outer secondary parietal cells at stage 4, stopped cell division at stage 6, and finally degraded at stage 11. The neighboring cell layers, the epidermis, and endothecium continued cell division until stage 10, which led to a thin middle layer. The degradation of the tapetum cell wall at stage 7 lead to its isolation from the anther wall. This work presents fundamental information on the development of the middle layer, which facilitates the further investigation of anther development and plant fertility. These live imaging methods could be useful in future studies.

Keywords: anther development, pollen, *Arabidopsis*, middle layer, living images

OPEN ACCESS

Edited by:
Pilar S. Testillano, Spanish National Research Council, Spain

Reviewed by:
Gwyneth Ingram, Université de Lyon, France
Jorge Lora, Consejo Superior de Investigaciones Científicas (CSIC), Spain

***Correspondence:**
Zhong-Nan Yang
znyang@shnu.edu.cn

† These authors have contributed equally to this work

Specialty section:
This article was submitted to Plant Development and EvoDevo, a section of the journal Frontiers in Plant Science

Received: *27 November 2020*
Accepted: *08 January 2021*
Published: *10 February 2021*

Citation:
Xue J-S, Yao C, Xu Q-L, Sui C-X, Jia X-L, Hu W-J, Lv Y-L, Feng Y-F, Peng Y-J, Shen S-Y, Yang N-Y, Lou Y-X and Yang Z-N (2021) Development of the Middle Layer in the Anther of Arabidopsis. Front. Plant Sci. 12:634114. doi: 10.3389/fpls.2021.634114

INTRODUCTION

The anther is the male reproductive organ in seed plants. Its main function is to produce and disperse pollen. Defects in anther development leading to male sterility are widely used in agriculture to increase crop yields (Tester and Langridge, 2010). In angiosperms, anther structure is generally conserved. The anther wall contains four layers called the epidermis, endothecium, middle layer, and tapetum. Inside anther locules, pollen mother cells undergo meiosis to form microspores enclosed in the tetrad. After release, microspores further develop into mature pollen (Goldberg et al., 1993; van der Linde and Walbot, 2019). Anther wall layers carry out different functions for pollen formation and release. The epidermis plays a protective role in anther development. The tapetum provides nutrients for microspore development and materials for pollen wall formation. The endothecium is responsible for anther dehiscence to disperse pollen when they are mature (van der Linde and Walbot, 2019). The middle layer is located between the

tapetum and endothecium. Currently, knowledge of its development and function during anther development is limited.

Arabidopsis is the most celebrated model plant. Its anther development has been extensively investigated. The development of anthers in *Arabidopsis* is divided into 14 stages. The section technique is generally used to assess anther development. Based on this technique, the middle layer was shown to be a short-lived, transient cell type in *Arabidopsis* (Goldberg et al., 1993; Sanders et al., 1999; van der Linde and Walbot, 2019). This layer is established at stage 4 together with the four-lobed anther. The middle layer becomes thinner at stage 5 and is mechanically crushed or undergoes programmed cell death at stage 6 prior to the completion of meiosis. Only remnants of this layer are present at stage 7 when meiosis is finished and tetrads are formed. Finally, the middle layer completely disappears at stage 8 when the callose wall surrounding tetrads degenerates (Goldberg et al., 1993; Sanders et al., 1999; van der Linde and Walbot, 2019). However, by using transmission electron microscopy (TEM), the middle layer is observed at the late uninucleate microspore stage (Owen and Makaroff, 1995; Quilichini et al., 2014). Although current knowledge about the middle layer is quite limited, several mutants with defective middle layers have been reported. Loss-of-function mutants of several receptor-like kinases display defects in the middle layer and pollen formation (Mizuno et al., 2007; Cui et al., 2018). These mutant phenotypes indicate that the middle layer is essential for anther development and pollen formation.

The anther primordium cell layers are designated L1, L2, and L3. The endothelium, middle layer, and tapetum are derived from L2. L2 cells develop into archesporial cells, which divide into parietal cells and sporogenous cells. Parietal cells generate inner secondary parietal (ISP) cells and outer secondary parietal (OSP) cells (Goldberg et al., 1993; van der Linde and Walbot, 2019). OSP and ISP cells further develop into the endothecium and tapetum. The middle layer is located between the endothecium and tapetum. In a study of the *EXCESS MICROSPOROCYTES1* gene, the middle layer was observed to originate from OSP cells (Zhao et al., 2002; Zhao, 2009; Chang et al., 2011). In the study of tapetum development, ISP cells were shown to perform periclinal division to form the tapetum and the middle layer (Feng and Dickinson, 2010). Therefore, middle layer initiation still needs to be clarified.

Semithin sections observed by bright-field microscopy are the major method for cellular analysis of anther development. However, sections may damage the tissue morphology, and the resolution of bright-field microscopes is not sufficient to detect detailed information on anther development. Optical observation of intact plant tissue could be achieved by laser scanning confocal microscopy (LSCM). It provides high-resolution and dynamic images *in vivo* without fixing, sectioning, and dehydrating (Sappl and Heisler, 2013). However, plant tissues contain various components with different refractive indexes, leading to light scattering and low-quality LSCM images in the deep tissue (Kurihara et al., 2015). To enhance the signals in deep tissue, researchers have used transgenic marker lines expressing fluorescent proteins with LSCM. Several chemical reagents are used to "clear" (improve transparency and decrease light scattering) plant tissue. Through these treatments, cell patterning in the intact organ can be visualized (Kurihara et al., 2015). Many histological staining techniques are combined with one clearing method, ClearSee (Kurihara et al., 2015) and LSCM in intact tissues (Ursache et al., 2018). These methods improve the resolution of images and decrease the cost of fixing and sectioning. Together, these new methods have been used to visualize cell patterning in complex organs such as roots, leaves, or shoot apical meristems (SAMs) *in vivo* (Truernit et al., 2008; Andriankaja et al., 2012; Kurihara et al., 2015; Xue et al., 2015; Ursache et al., 2018).

The major method for anther cellular analysis is semithin sections of fixed samples (Cui et al., 2018; Jacobowitz et al., 2019; Xu et al., 2019; Yamamoto et al., 2020). In this study, we used an appropriate promoter for the ubiquitous expression of fluorescent proteins in anthers. A marker line for cell morphology was created for live imaging of the anther. Histological staining and clearing methods were also used with anthers to analyze the cell morphology. Through these methods, we clarified the initial process, development, and degradation of the middle layer in *Arabidopsis*. Further cell proliferation analyses showed the division patterns of different anther layers. Together, these studies provide fundamental knowledge of anther development. The application of new imaging techniques in anther development may provide further information for future studies.

RESULTS

The Promoter of *POLYUBIQUITIN 10* Drives the Expression of Fluorescent Proteins in Cells of All Anther Layers

The 35S promoter of the cauliflower mosaic virus is the most commonly used promoter in plants (Benfey and Chua, 1990). We introduced the *Pro35S:GFP* transgenic construct into *Arabidopsis*. GFP signals could be detected in the leaf epidermis, mesophyll, anther epidermis, and endothecium (**Supplementary Figure 1** and **Figure 1A**). However, no GFP signal was detected in the middle layer, tapetum, or microspores of these transgenic lines (**Figure 1A**). To screen appropriate promoters for the *in vivo* analysis of anthers, we analyzed the expression of several housekeeping genes in anthers (**Supplementary Figure 2**). Among these genes, *TUBULINA6* (*TUA6*), *TUBULIN6* (*TUB6*), *GLYCERALDEHYDE 3 PHOSPHATE DEHYDROGENASE A SUBUNIT* (*GAPA*), and *POLYUBIQUITIN 10* (*UBQ10*) were highly expressed in anthers. We cloned the promoters of these genes to generate the constructs *ProTUA6: VENUS*, *Pro TUB6: VENUS*, *ProGAPA: VENUS*, and *ProUBQ10: VENUS*. After introduction into wild-type *Arabidopsis*, at least three independent transgenic lines for each construct were analyzed. Through LSCM, VENUS signals were detected in the leaf epidermis and mesophyll of all these transgenic lines (**Supplementary Figures 1,3**). However, no VENUS signals of TUA6-VENUS, TUB6-VENUS, or GAPA-VENUS were detected in the tapetum, microspore mother cells, or microspores of these plants (**Figure 1A** and **Supplementary Figures 1,3**). Thus, the *TUA6*, *TUB6*, and *GAPA* promoters

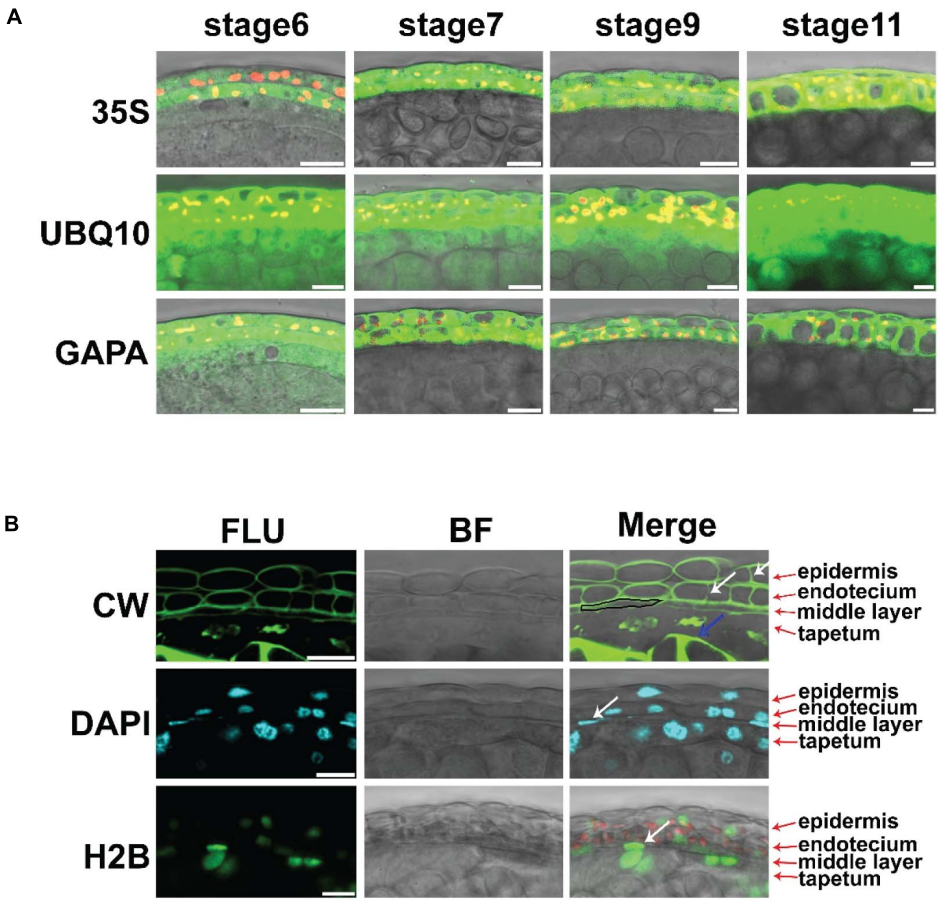

FIGURE 1 | The live imaging methods for intact anther. **(A)** Expression of VENUS driven by the promoters of *35S, GAPA,* and *UBQ10* in anther stages 6, 7, 9, and 11. The VENUS signals are colored green, and the chloroplasts are colored red. Scale bar = 10 μm. **(B)** Fluorescence images of anthers stained with CW in anther stage 7 are shown in the first row. Arrows show the newly formed cell wall. The images of anthers stained with DAPI in anther stage 7 are shown in the second row. The images in the third row show the expression of *ProUBQ10-H2B-VENUS* in anther stage 7. The VENUS signals are colored green. The CW signals are colored green. The DAPI signals are colored cyan, and the chloroplasts are colored red; 35S: Pro35S: GFP. UBQ10: ProUBQ10: VENUS. GAPA: ProGAPA: VENUS. CW, Calcofluor white staining; DAPI, DAPI staining; H2B, ProUBQ10; H2B, VENUS; FLU, fluorescence signals; BF, bright field signals; Merge, merge signals. White arrows show the dividing cells and middle layer nucleus. The blue arrow shows the callose. The black box shows the middle layer cell. Scale bar = 10 μm.

could not drive VENUS expression in every anther layer. In the *ProUBQ10:VENUS* transgenic plants, VENUS signals were detected ubiquitously at stages 4–5 in anthers (**Supplementary Figure 1**). At stages 6–10, strong VENUS signals were detected in the epidermis, endothecium, and middle layer (**Figure 1A**). Thus, the *UBQ10* promoter conferred ubiquitous expression in anthers. This promoter could be used to construct marker lines for anther developmental analysis.

The Establishment of Live Imaging Methods in Intact Anthers

Plant tissues with different compositions can cause light scattering. This phenomenon leads to difficulty in observing deep plant tissue using LSCM. In this study, the clearing method of ClearSee combined with the cell wall polysaccharide dye Calcofluor white (CW) (Ursache et al., 2018), as described in another study. The CW signals clearly showed the cell wall of the anther layers at stage 7 (**Figure 1B**). Newly formed cell walls showed weak signals in the epidermis and endothecium layer (**Figure 1B**). The middle layer was thinner than its neighboring layers (**Figure 1B**). The tapetum cell wall was degraded (**Figure 1B**). Strong CW signals of the callose surrounding tetrads were identified in the anther locules (**Figure 1B**). Together, the different cell types of anthers were clearly identified. The classic dye 4′6-diamidino-2-phenylindole (DAPI) is used to stain DNA in nuclei. Here, a simplified clearing method (see "Materials and Methods" section) was combined with DAPI staining to show the nuclei in intact anthers. Through this staining, the epidermis, endothecium, tapetum, and tetrads showed typical rounded nuclei, while oblong nuclei were observed in the middle layer (**Figure 1B**). Only the tapetum contains two nuclei at this stage (**Figure 1B**). Histone 2B (H2B) is a marker protein of nucleosomes. To confirm the DAPI staining, we constructed *ProUBQ10:H2B:VENUS* and transferred it into wild-type *Arabidopsis* to visualize the nucleosomes. The VENUS

signals were detected by LSCM and showed a similar shape to DAPI in the transgenic plants *in vivo* (**Figure 1B**). Together, these methods clearly showed the characteristics of the cell layers in the intact anther of *Arabidopsis*.

The Middle Layer Is Derived From Both Inner Secondary Parietal (ISP) and Outer Secondary Parietal (OSP) Cells in the Anther

ISP and OSP cells are derived from parietal cells at stage 3 (Sanders et al., 1999). Generally, anticlinal division increases the cell number of each layer, while periclinal division leads to the formation of new cell layers. Direct observation of the axial cell division could be based on nuclear division directions and the axial direction of the newly formed cell wall. The middle layer is established at stage 4 (Sanders et al., 1999). After the establishment of this layer, the original axial cell division could not be detected. To identify anthers that were at stage 4 and were undergoing periclinal division, we analyzed the relationship between flower size and anther stages (**Supplementary Figure 4**). Anthers of approximately 339 μm^2 that were at stage 4 were collected. LSCM was used to identify the maximum longitudinal section of each anther (**Supplementary Figure 5**). In this section, the axial division of the ISP and OSP layers was analyzed in *Arabidopsis* ecotype Col-0 (**Figure 2A**). CW staining was used to show the axis of the newly formed cell wall. We identified 71 anthers that had established their middle layer (**Figure 2D**). The signals of newly formed cell walls that separated two daughter cells were detected in all the cell layers (**Figure 2B**). In the epidermis, newly formed cell walls were perpendicular to the long side (**Figure 2B**), indicating anticlinal division in these layers. However, in ISP and OSP cells, newly formed cell walls were perpendicular to both the short side and long side in different cells (**Figure 2B**). These results showed that periclinal division appeared in both ISP and OSP cells, indicating that the middle layer was derived from both layers. To further confirm this result, we performed DAPI staining. Consistent with the CW staining,

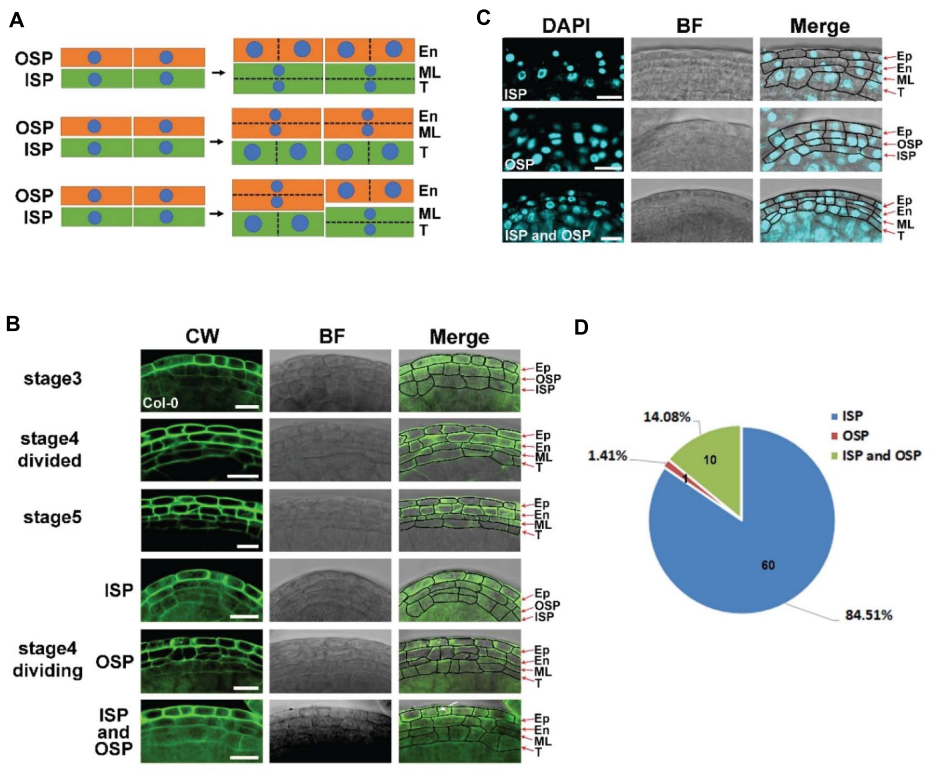

FIGURE 2 | The middle layer is derived from both inner secondary parietal (ISP) and outer secondary parietal (OSP) cells in the anther. **(A)** Model of the origin of the middle layer. The first model shows periclinal division in ISP cells to form the endothecium and middle layer. The second model shows periclinal division in OSP cells to form the tapetum and middle layer. The last model shows periclinal division in both OSP and ISP cells. **(B)** Images of Col-0 anthers stained with CW at stages 3, 4, and 5. The images in the left column show the CW signals. The images in the middle showed bright field signals. The right images are the merged signals of Calcoflour white (CW) and the bright field. Arrow shows the newly formed cell wall. Stage 4 divided: the anther finished periclinal division at stage 4 with the middle layer fully formed. Stage 4 division: the anther was undergoing periclinal division. The middle layers were derived from inner secondary parietal cells (ISPs), outer secondary parietal cells (OSPs), and both inner secondary parietal cells and outer secondary parietal cells (ISPs and OSPs) in the same anther. Scale bar = 10 μm. **(C)** Fluorescence images of Col-0 anthers stained with 4′,6-diamidine-2-phenylindole (DAPI) at stage 4. The images in the left column show the DAPI signals. The images in the middle showed bright field signals. The right images merge the DAPI signals and the bright field signals. Scale bar = 10 μm. **(D)** The statistics of CW staining anthers undergoing periclinal division in stage 4. ISP: middle layer derived from inner secondary parietal cells. OSP: middle layer derived from outer secondary parietal cells. ISP and OSP: middle layer derived from both inner secondary parietal cells and outer secondary parietal cells in the same anther.

DAPI signals increased by periclinal division were also detected in both the ISP and OSP layers (**Figure 2C**). Thus, evidence of nuclear division and newly formed cell walls consistently showed that the middle layer originates from both ISP and OSP cells. Statistics showed that the middle layer was generated from ISP cells in 84.51% of the anthers, from both ISP and OSP cells in 14.08% of the anthers, and from OSP cells in 1.41% of the anthers in Col-0 (**Figure 2D**). This result indicates that the initial middle layer varies in Col-0.

The Cell Division and Expansion of the Middle Layer

Sections reveal that the morphology of the middle layer is similar to that of the tapetum at stage 4, while this layer becomes thinner at stages 5–6 and finally cannot be detected at stage 8 (Sanders et al., 1999). Cell division and expansion are critical for cell morphology and organ development (Anastasiou and Lenhard, 2007). To study cell division in anthers, we introduced a cell cycle marker into *Arabidopsis*. B-type CYCLIN (CYCB) is a key factor in the G_2/M transitions (De Veylder et al., 2007). *ProCYCB1;1*: *CYCB1;1*: *VENUS* was constructed and transferred to wild-type Col-0 to generate a proper marker line. VENUS signals were detected at all the cell layers before stage 6 in these transgenic plants (**Figure 3A**). At stage 6, the VENUS signals of CYCB disappeared in the middle layer and tapetum. However, in the epidermis and endothecium, the signals of the marker protein were detected until stage 10 (**Figure 3A**). These results indicated that the cell division of the middle layer and tapetum stops at stage 6, while the epidermis and endothecium undergo cell division from stage 5 to 10. To confirm these results, we determined the cell number in the anther layer. CW staining was performed in intact anthers at stages 6–10. At the maximum longitudinal sections (**Supplementary Figure 5**), the cell numbers of each layer were counted (**Figure 3B**). In the middle layer, no significant cell number increase was detected from stage 6 to 10 (**Figure 3C**). However, the endothecium and epidermis cell numbers showed a significant increase in these stages (**Figure 3C**). Taken together, these results showed a distinct cell division regulation of anther layers.

Anther size dramatically increased in stages 4–11 (**Supplementary Figure 4**). To study the correlated cell expansion, we analyzed cell areas of the epidermis, endothecium, and middle layer. The cell area of the middle layer showed no increase at stages 6–7 (**Figure 3C**). In stages 7–10, the cell area of middle layer cells was increased significantly (**Figure 3C**), suggesting that cell expansion occurred in these stages. The cell areas of the endothecium and epidermis showed a significant increase from stage 5 to 10 (**Figure 3C**), together with the results of the cell cycle marker, indicating that both cell division and cell expansion occurred in the endothecium and epidermis at these stages. Taken together, after the establishment of anther layers at stage 4, the middle layer underwent cell division at stages 4–6 and cell expansion at stages 7–10. The cells of the endothecium and epidermis layer underwent both cell division and cell expansion at stages 5–10 (**Figure 3**). The side length of the anther cells was measured to analyze the cell shape of each layer. The aspect ratio of the middle layer was dramatically

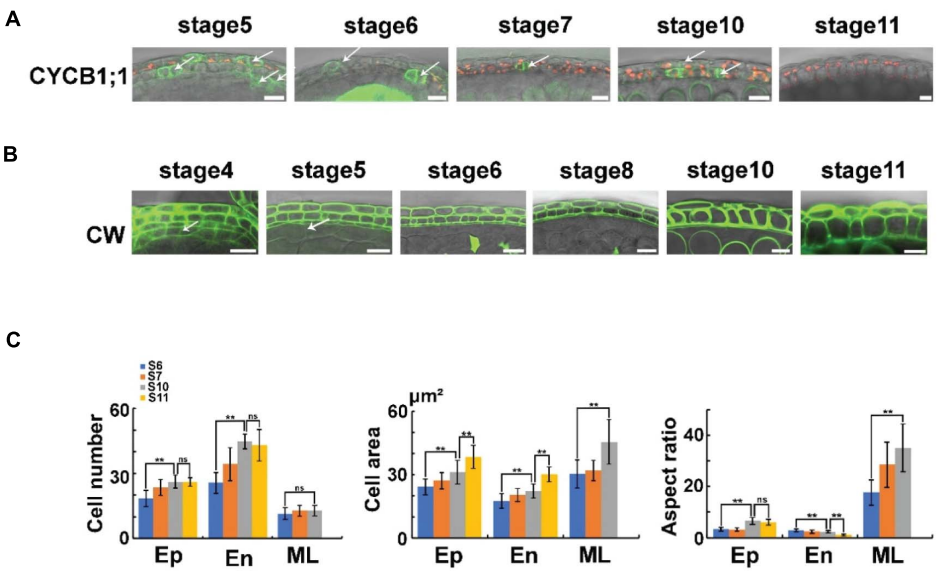

FIGURE 3 | The cell division and expansion of anther layers. **(A)** The expression of *ProCYCB1;1*: *CYCB1;1*: *VENUS* in anther stages 5–11. The VENUS signals are colored green, and the chloroplasts are colored red. Arrows show the dividing cells. Scale bar = 10 μm. **(B)** The CW staining in anther stages 4–11. The CW signals are colored green. Arrows show the tapetum cell wall. Scale bar = 10 μm. **(C)** Statistical analysis of anthers in anther stages 6, 7, 10, and 11. The first image on the left shows the cell number. The second image shows the cell area. The third shows the aspect ratio. For each layer, the cell number was quantified from at least 10 anthers per stage with three biological repeats. The cell area and aspect ratio were quantified from five cells in each layer. At least 10 anthers per stage were used for the analysis with three biological repeats. Further statistical analysis was performed by R. Asterisks indicate statistically significant differences ($P < 0.01$, ANOVA by R). Ep, epidermis; En, endothecium; ML, middle layer; S6, stage 6; S7, stage 7; S10, stage 10; S11, stage 11; Ns, not significant.

increased (**Figure 3C**). This increase leads to an increasingly thin middle layer that is hard to detect in sections after stage 8 (Sanders et al., 1999). The epidermal and endothelial cells showed a similar aspect ratio at stage 6 (**Figures 3B,C**). However, in stages 7–11, the aspect ratio was increased in the epidermis but decreased in the endothecium (**Figure 3C**), resulting in a thin epidermis and a thick endothecium layer. These results showed a distinct regulation of cell expansion in different anther layers.

The Degradation of the Middle Layer Started at Stage 10

The middle layer is considered to be degraded at stage 7 (Goldberg et al., 1993; Sanders et al., 1999; Walbot and Egger, 2016). However, in the intact anther, our results showed that the middle layer was not degraded in this stage (**Figure 3B**), which was consistent with previous reports (Owen and Makaroff, 1995; Quilichini et al., 2014). The cell size of the middle layer was still increasing during stages 7–10 (**Figures 3B,C**). To study the degradation of the middle layer, we performed CW and DAPI staining in *Arabidopsis* to individually show the degradation of the cell wall and nucleus. DAPI staining showed that the DNA signals in the nucleus were still detectable at stage 10 (**Figure 4A**). In stage 11, no DAPI signals could be detected in the middle layer (**Figure 4A**). Consistently, CW staining showed that signals in the cell wall of the middle layer could be detected at stage 10 but completely disappeared at stage 11 (**Figure 3B**). To further confirm the staining results, we used the marker line *ProUBQ10*: *H2B*: *VENUS*. The H2B-VENUS signals showed similar results with DAPI staining (**Figure 4A**). Together, evidence from both cell wall and nuclear degradation studies demonstrated that the middle layer survived until stage 10 and completely disappeared at stage 11. This finding is similar to the degradation of the tapetum. Thus, we showed that the middle layer and tapetum were degraded at the same stage.

DISCUSSION

Anther development is critical for pollen formation. The traditional evidence of anther development is mainly from semithin sections (Zhao et al., 2002; Feng and Dickinson, 2010). In this work, we developed several live imaging methods for the study of anther development. After screening the ubiquitously expressed promoter UBQ10, we created the marker line *ProUBQ10*: *H2B*: *VENUS*, which is a useful tool in the study of cell morphology and proliferation. The marker line is not only used for live imaging analysis of the middle layer in this work but could also be used in the study of other layers in anthers. In this study, we used CW and DAPI staining in intact anthers to avoid damage to sections. These easy-to-use and low-cost methods provide better images than current methods for developmental studies *in vivo*. Through these methods, we clearly showed the developmental process of the middle layer. Other anther layers could also be analyzed through these methods.

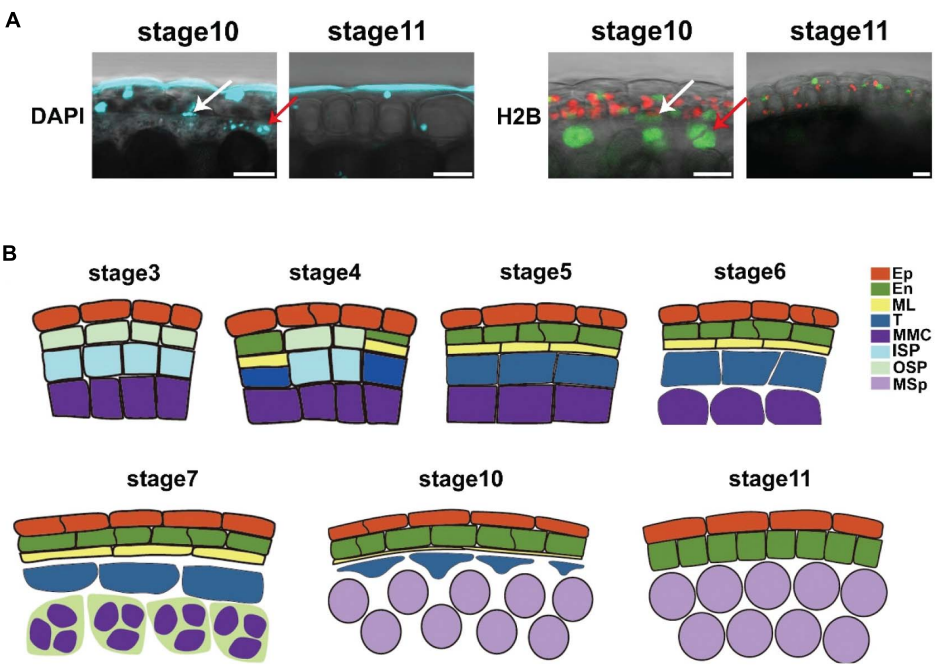

FIGURE 4 | The degradation of the middle layer started at stage 10. **(A)** DAPI staining and ProUBQ10-H2B-VENUS signals in anther stages 10 and 11. Arrows show the middle layer and tapetum cells. The VENUS signals are colored green, the chloroplasts are colored red, and the DAPI signals are colored cyan. DAPI, DAPI staining; H2B, ProUBQ10-H2B-VENUS. Scale bar = 10 μm. **(B)** Model of anther development. Images showed anther cell morphology during anther development. Ep, epidermis; En, endothecium; ML, middle layer; T, tapetum; MMC, microspore mother cell; ISP, inner secondary parietal cell; OSP; outer secondary parietal cell; MSp, microspores.

L2 anther primordium cells develop into parietal cells, which further generate ISP and OSP cells (Goldberg et al., 1993; Sanders et al., 1999). Middle layer formation is studied in both monocotyledon plant maize and rice, and dicotyledon plant *Arabidopsis*. In maize, OSP cells are considered to only undergo anticlinal divisions to form the endothecium layer, and ISP cells undergo periclinal divisions to produce both the middle layer and tapetum (Sheridan et al., 1999). In rice, the middle layer is also considered to be divided only from ISP cells (Raghavan, 1988). Thus, the identity of individual cell layers is proposed to be determined by genetically controlled periclinal cell divisions (Kelliher and Walbot, 2011). However, in *Arabidopsis*, OSP cells are also reported to generate middle layer cells (Zhao et al., 2002; Feng and Dickinson, 2010). In this study, we used staining methods to analyze the initiation of the middle layer in *Arabidopsis*. Evidence of both nuclear division and new cell wall formation showed that the middle layer was derived from both the ISP and OSP cells in Col-0 (**Figure 2**), indicating that the cell fate determination of the middle layer was non-cell-autonomous in *Arabidopsis*.

Cell division and expansion are the basis of anther size enlargement. In this study, we showed that different anther layers exhibited distinct cell proliferation and expansion strategies to support anther development. For the epidermis and endothecium, cell division is maintained for a long time, providing enough cells to build anther locules with enough space for microspore development and pollen formation. The endothecium is required for the anther dehiscence. This layer is lignified at stage 11 to provide resistance to bending and stretching, and is essential for final anther dehiscence (Steiner-Lange et al., 2003; Yang et al., 2007, 2017; Xu et al., 2019). For this layer, more cell divisions occur than in the epidermis. The aspect ratio of this layer decreases from stage 5 to 11, forming a quadratic cell layer. These quadratic types of cells provide a thick layer, which may provide more strength for anther dehiscence after lignification of their cell walls.

The middle layer is very thin at stages 6–7 and is considered to be degraded before the completion of meiosis, as shown by semithin sections (Goldberg et al., 1993; Sanders et al., 1999; van der Linde and Walbot, 2019). Transverse sections showed that the tapetum is usually isolated from the anther wall at stage 8 (Sanders et al., 1999). The degradation of the middle layer is believed to separate the endothecium from the tapetum (van der Linde and Walbot, 2019). We showed that the middle layer was undergoing cell division with an increasing aspect ratio at stages 4–6, which led to a very thin middle layer that was hard to detect in the semithin sections (**Figure 3**). However, this layer survived after meiosis, and the cell size was still increasing with an even higher aspect ratio at stages 7–10. These results showed that this layer existed much longer than previously believed. The tapetum provides material and nutrition for microspore development and pollen formation (Zhu et al., 2011). Through the sections, the tapetum was found to be isolated from the anther wall and detected in the anther locules at stages 7–10 (Sanders et al., 1999). The degradation of the middle layer is assumed to be responsible for the dissociation of the tapetum from the anther wall and avoids the direct influence of the endothecium on the tapetum (van der Linde and Walbot, 2019). However, we showed that the middle layer was not degraded until stage 11. By staining semithin sections, the cellulosic wall of the tapetum is degraded before the onset of meiosis (Matsuo et al., 2013). We observed the cell wall of the tapetum through CW staining in intact anthers. The signals of the tapetum cell wall were normally detected at stage 4 (**Figure 3B**). However, CW signals of the tapetum cell wall dramatically decreased at stage 5 (**Figure 3B**) and disappeared at stages 67 (**Figures 1B**,**3B**). This result was consistent with a previous investigation (Matsuo et al., 2013) that showed that the tapetum cell wall was degraded at stage 7. The degradation of the tapetum cell wall may lead to the isolation of this layer from the anther wall. Taken together, these studies provide fundamental information on anther development (**Figure 4B**), which is important for pollen formation and plant reproduction.

MATERIALS AND METHODS

Plant Materials and Growth Conditions

Plants were grown under long-day conditions (16 h light/8 h dark) in an ∼22°C growth room. Ecotype Col-0 was obtained from ABRC.

Plasmid Construction and Plant Transformation

For generation of *Pro35S-GFP*, *ProTUA6-VENUS*, *ProTUB6-VENUS*, *ProGAPA-VENUS*, and *ProUBQ10-VENUS*, the promoters of *35S*, *TUA6*, *TUB6*, *GAPA*, and *UBQ10* were fused with the P1300-VENUS plasmid by using the pEASY Uni-Seamless Cloning and Assembly Kit (Yao et al., 2018). For generation of *ProUBQ10-H2B-VENUS*, the genomic DNA of *H2B* was fused with the P1300-UBQ10-VENUS plasmid by using the same method as above. For generation of *ProCYCB1;1-CYCB1;1-VENUS*, the genome of CYCB1;1 was fused with the P1300-VENUS plasmid. For plant transformation, the plasmid was introduced into *Agrobacterium* strain GV3101 and transformed into plants by the floral dip method (Clough and Bent, 2010).

DAPI Staining

DAPI (4′,6-diamidino-2-phenylindole) solution was prepared as previously described (Scali and Tinti, 1992). Briefly, flowers without petals and calyxes were dissected and immersed in DAPI solution, vacuumed for 20 min and stained at 4°C in the dark for 48 h. After this treatment, the transparency was increased, and DAPI signals in intact anthers were visualizable.

CW Staining

ClearSee, a clearing agent, was prepared as previously described (Ursache et al., 2018). Briefly, flowers without petals and calyxes were dissected and treated with ClearSee solution for 7 days. The treated anthers were then stained with 2 mg/ml Calcofluor white (Fluorescent brightener 28) (Sigma, cat# 4404-43-7) in ClearSee

for 6 h (Ursache et al., 2018). The anther was washed five times using ClearSee solution before analysis.

Confocal Microscopy

All fluorescence images were obtained with an Olympus FV3000 laser scanning microscope. For monitoring of VENUS signals, a 514 nm laser line was used for excitation, and a 525–570 nm bandpass filter was used for detection (Xue et al., 2020). For GFP fluorescence, a 488 nm laser was used for excitation, and a 498–532 nm bandpass filter was used for detection. For DAPI signals, we used 405 nm for excitation, and emission spectra were recorded in the range of 425–475 nm. For the CW signals, we used 405 nm for excitation, and emission spectra were recorded at 430–470 nm. For the cell division, cell number, and cell area analyses, we used z-stacks to identify the maximum light cross-sections of every intact anther. Then, ImageJ was used to analyze the cell area, aspect ratio, and cell number.

DATA AVAILABILITY STATEMENT

The original contributions presented in the study are included in the article/**Supplementary Material**, further inquiries can be directed to the corresponding author/s.

AUTHOR CONTRIBUTIONS

Z-NY and J-SX conceived and designed the experiments. CY, J-SX, X-LJ, S-YS, C-XS, Y-JP, Q-LX, Y-FF, N-YY, Y-LL, and W-JH performed the experiments. J-SX, CY, and Z-NY analyzed the data. J-SX, CY, Y-XL, and Z-NY wrote the manuscript. All authors have read the manuscript and approved it for submission.

FUNDING

This work was supported by grants from the National Natural Science Foundation of China (31670314 and 31900165), the Science and Technology Commission of Shanghai Municipality (17DZ2252700 and 18DZ2260500), and the Shanghai Municipal Education Commission (2019-01-07-00-02-E00006).

SUPPLEMENTARY MATERIAL

The Supplementary Material for this article can be found online at: https://www.frontiersin.org/articles/10.3389/fpls.2021.634114/full#supplementary-material

Supplementary Figure 1 | Expression of the promoters of *35S, GAPA,* and *UBQ10* in leaf epidermis, mesophyll, and anther stage 4. The VENUS signals are colored green, and the chloroplasts are colored red. Ep: epidermis. Me: mesophyll. 35S: Pro35S: GFP. UBQ10: ProUBQ10: VENUS. GAPA: ProGAPA: VENUS. Scale bar = 10 μm.

Supplementary Figure 2 | Expression levels of several housekeeping genes in the anthers of young flowers. The expression data is obtained from TraVA (travadb.org).

Supplementary Figure 3 | Expression of Pro*TUA6* and Pro*TUB6* in leaf and anther. Expression of the promoters of *TUA6* and *TUB6* in leaf epidermis, mesophyll, and anther stages 4, 6, 7, 9, and 11. The VENUS signals are colored green, and the chloroplasts are colored red. Ep: epidermis. Me: mesophyll. TUA6: ProTUA6: VENUS. TUB6: ProTUB6: VENUS. Scale bar = 10 μm.

Supplementary Figure 4 | The relationship between flower size and anther stages during anther development. **(A)** The top row shows the images of buds from stage 4 to stage 11, and the bottom row shows the images of anthers from stage 4 to stage 11. Scale bars = 1 mm in the first row and 20 μm in the bottom row. **(B)** Statistical analysis of the anther area.

Supplementary Figure 5 | The identification of the maximum light cross-section of intact anthers in stage 7. **(A)** The LSCM anther analysis model for cell division, cell area, and cell morphology. A Z-stack was performed to identify the maximum light sections of the intact anther. **(B)** The z-stack of a stage 7 anther. The epidermis layer was artificially set as 0 μm. The step size for the z-stack was 8 μm. Arrows show the region with four anther wall layers in the maximum light sections of the intact anther. Cell number counting was performed in this region. Five cells in the middle of the anther wall were used for the cell area and aspect ratio analysis. The CW signals were colored green. Scale bar = 10 μm. **(C)** Statistical analysis of the anther locule area in light sections for the identification of the maximum light section. The maximum light section was further used for other analyses.

REFERENCES

Anastasiou, E., and Lenhard, M. (2007). Growing up to one's standard. *Curr. Opin. Plant Biol.* 10, 63–69.

Andriankaja, M., Dhondt, S., De Bodt, S., Vanhaeren, H., Coppens, F., De Milde, L., et al. (2012). Exit from proliferation during leaf development in *Arabidopsis thaliana*: a not-so-gradual process. *Dev. Cell* 22, 64–78. doi: 10.1016/j.devcel.2011.11.011

Benfey, P. N., and Chua, N. H. (1990). The cauliflower mosaic virus 35S promoter: combinatorial regulation of transcription in plants. *Science* 250, 959–966. doi: 10.1126/science.250.4983.959

Chang, F., Wang, Y., Wang, S., and Ma, H. (2011). Molecular control of microsporogenesis in *Arabidopsis*. *Curr. Opin. Plant Biol.* 14, 66–73. doi: 10.1016/j.pbi.2010.11.001

Clough, S. J., and Bent, A. F. (2010). Floral dip: a simplified method for Agrobacterium-mediated transformation of *Arabidopsis thaliana*. *Plant J.* 16, 735–743. doi: 10.1046/j.1365-313x.1998.00343.x

Cui, Y., Hu, C., Zhu, Y., Cheng, K., Li, X., Wei, Z., et al. (2018). CIK receptor kinases determine cell fate specification during early anther development in *Arabidopsis*. *Plant Cell* 30, 2383–2401. doi: 10.1105/tpc.17.00586

De Veylder, L., Beeckman, T., and Inzé, D. (2007). The ins and outs of the plant cell cycle. *Nat. Rev. Mol. Cell Biol.* 8, 655–665. doi: 10.1038/nrm2227

Feng, X., and Dickinson, H. G. (2010). Tapetal cell fate, lineage and proliferation in the *Arabidopsis* anther. *Development* 137, 2409–2416. doi: 10.1242/dev.049320

Goldberg, R. B., Beals, T. P., and Sanders, P. M. (1993). Anther development: basic principles and practical applications. *Plant Cell* 5, 1217–1229. doi: 10.2307/3869775

Jacobowitz, J. R., Doyle, W. C., and Weng, J.-K. (2019). PRX9 and PRX40 are extensin peroxidases essential for maintaining tapetum and microspore cell wall integrity during *Arabidopsis* anther development. *Plant Cell* 31, 848–861. doi: 10.1105/tpc.18.00907

Kelliher, T., and Walbot, V. (2011). Emergence and patterning of the five cell types of the zea mays anther locule. *Dev. Biol.* 350, 32–49. doi: 10.1016/j.ydbio.2010.11.005

Kurihara, D., Mizuta, Y., Sato, Y., and Higashiyama, T. (2015). ClearSee: a rapid optical clearing reagent for whole-plant fluorescence imaging. *Development* 142, 4168–4179. doi: 10.1242/dev.127613

Matsuo, Y., Arimura, S., and Tsutsumi, N. (2013). Distribution of cellulosic wall in the anthers of *Arabidopsis* during microsporogenesis. *Plant Cell Rep.* 32, 1743–1750. doi: 10.1007/s00299-013-1487-1

Mizuno, S., Osakabe, Y., Maruyama, K., Ito, T., Osakabe, K., Sato, T., et al. (2007). Receptor-like protein kinase 2 (RPK 2) is a novel factor controlling anther development in *Arabidopsis thaliana*. *Plant J. Cell Mol. Biol.* 50, 751–766. doi: 10.1111/j.1365-313x.2007.03083.x

Owen, H. A., and Makaroff, C. A. (1995). Ultrastructure of microsporogenesis and microgametogenesis in *Arabidopsis thaliana* (L.) heynh. ecotype wassilewskija (*Brassicaceae*). *Protoplasma* 185, 7–21. doi: 10.1007/bf01272749

Quilichini, T. D., Douglas, C. J., and Samuels, A. L. (2014). New views of tapetum ultrastructure and pollen exine development in *Arabidopsis thaliana*. *Ann. Bot.* 114, 1189–1201. doi: 10.1093/aob/mcu042

Raghavan, V. (1988). Anther and pollen development in rice (*Oryza sativa*). *Am. J. Bot.* 75, 183–196. doi: 10.1002/j.1537-2197.1988.tb13430.x

Sanders, P. M., Bui, A. Q., Weterings, K., Mcintire, K. N., Hsu, Y. C., Pei, Y. L., et al. (1999). Anther developmental defects in *Arabidopsis thaliana* male-sterile mutants. *Sex Plant Reprod.* 11, 297–322. doi: 10.1007/s004970050158

Sappl, P. G., and Heisler, M. G. (2013). Live-imaging of plant development: latest approaches. *Curr. Opin. Plant Biol.* 16, 33–40. doi: 10.1016/j.pbi.2012.10.006

Scali, V., and Tinti, F. (1992). Rapid assessment of maturation stage and reproductive mode in centrolecytic eggs of stick insects (*Phasmatodea*) using DAPI stain. *Biotechnic Histochem.* 67, 356–359. doi: 10.3109/10520299209110049

Sheridan, W. F., Golubeva, E. A., Abrhamova, L. I., and Golubovskaya, I. N. (1999). The mac1 mutation alters the developmental fate of the hypodermal cells and their cellular progeny in the maize anther. *Genetics* 153, 933–941.

Steiner-Lange, S., Unte, U. S., Eckstein, L., Yang, C., Wilson, Z. A., Schmelzer, E., et al. (2003). Disruption of *Arabidopsis thaliana* MYB26 results in male sterility due to non-dehiscent anthers. *Plant J.* 34, 519–528. doi: 10.1046/j.1365-313x.2003.01745.x

Tester, M., and Langridge, P. (2010). Breeding technologies to increase crop production in a changing world. *Science* 327, 818–822. doi: 10.1126/science.1183700

Truernit, E., Bauby, H., Dubreucq, B., Grandjean, O., Runions, J., Barthelemy, J., et al. (2008). High-resolution whole-mount imaging of three-dimensional tissue organization and gene expression enables the study of Phloem development and structure in *Arabidopsis*. *Plant Cell* 20, 1494–1503. doi: 10.1105/tpc.107.056069

Ursache, R., Andersen, T. G., Marhavy, P., and Geldner, N. (2018). A protocol for combining fluorescent proteins with histological stains for diverse cell wall components. *Plant J.* 93, 399–412. doi: 10.1111/tpj.13784

van der Linde, K., and Walbot, V. (2019). Pre-meiotic anther development. *Curr. Top. Dev. Biol.* 131, 239–256. doi: 10.1016/bs.ctdb.2018.11.001

Walbot, V., and Egger, R. L. (2016). Pre-meiotic anther development: cell fate specification and differentiation. *Annu. Rev. Plant Biol.* 67, 365–395. doi: 10.1146/annurev-arplant-043015-111804

Xu, X. F., Wang, B., Feng, Y. F., Xue, J. S., Qian, X. X., Liu, S. Q., et al. (2019). Auxin response factor17 directly regulates MYB108 for anther dehiscence. *Plant Physiol.* 181, 645–655. doi: 10.1104/pp.19.00576

Xue, J.-S., Zhang, B., Zhan, H., Lv, Y.-L., Jia, X.-L., Wang, T., et al. (2020). Phenylpropanoid derivatives are essential components of sporopollenin in vascular plants. *Mol. Plant* 13, 1644–1653. doi: 10.1016/j.molp.2020.08.005

Xue, J., Luo, D., Xu, D., Zeng, M., Cui, X., Li, L., et al. (2015). CCR1, an enzyme required for lignin biosynthesis in *Arabidopsis*, mediates cell proliferation exit for leaf development. *Plant J.* 83, 375–387. doi: 10.1111/tpj.12902

Yamamoto, M., Uji, S., Sugiyama, T., Sakamoto, T., Kimura, S., Endo, T., et al. (2020). ERdj3B-mediated quality control maintains anther development at high temperatures. *Plant Physiol.* 182, 1979–1990. doi: 10.1104/pp.19.01356

Yang, C., Song, J., Ferguson, A. C., Klisch, D., Simpson, K., Mo, R., et al. (2017). Transcription factor MYB26 is key to spatial specificity in anther secondary thickening formation. *Plant Physiol.* 175, 333–350. doi: 10.1104/pp.17.00719

Yang, C., Xu, Z., Song, J., Conner, K., Vizcay Barrena, G., and Wilson, Z. A. (2007). Arabidopsis MYB26/MALE STERILE35 regulates secondary thickening in the endothecium and is essential for anther dehiscence. *Plant Cell* 19, 534–548. doi: 10.1105/tpc.106.046391

Yao, X., Yang, H., Zhu, Y., Xue, J., Wang, T., Song, T., et al. (2018). The canonical E2Fs are required for germline development in *Arabidopsis*. *Front. Plant Sci.* 9:638.

Zhao, D. (2009). Control of anther cell differentiation: a teamwork of receptor-like kinases. *Sex Plant Reprod.* 22, 221–228. doi: 10.1007/s00497-009-0106-3

Zhao, D. Z., Wang, G. F., Speal, B., and Ma, H. (2002). The EXCESS MICROSPOROCYTES1 gene encodes a putative leucine-rich repeat receptor protein kinase that controls somatic and reproductive cell fates in the *Arabidopsis* anther. *Genes Dev.* 16, 2021–2031. doi: 10.1101/gad.997902

Zhu, J., Lou, Y., Xu, X., and Yang, Z. N. (2011). A genetic pathway for tapetum development and function in *Arabidopsis*. *J. Integr. Plant Biol.* 53, 892–900. doi: 10.1111/j.1744-7909.2011.01078.x

Conflict of Interest: The authors declare that the research was conducted in the absence of any commercial or financial relationships that could be construed as a potential conflict of interest.

frontiers in Plant Science

ORIGINAL RESEARCH
published: 25 February 2021
doi: 10.3389/fpls.2021.635244

A Maize Male Gametophyte-Specific Gene Encodes ZmLARP6c1, a Potential RNA-Binding Protein Required for Competitive Pollen Tube Growth

Lian Zhou[1], Zuzana Vejlupkova[2], Cedar Warman[2] and John E. Fowler[2]**

[1] Maize Research Institute, College of Agronomy and Biotechnology, Southwest University, Chongqing, China, [2] Department of Botany and Plant Pathology, Oregon State University, Corvallis, OR, United States

OPEN ACCESS

Edited by:
David Honys,
Institute of Experimental Botany, Czech Academy of Sciences, Czechia

Reviewed by:
Jorge Muschietti,
CONICET Instituto de Investigaciones en Ingeniería Genética y Biología Molecular "Dr. Héctor N. Torres" (INGEBI), Argentina
Hua Jiang,
Leibniz Institute of Plant Genetics and Crop Plant Research (IPK), Germany

***Correspondence:**
Lian Zhou
zhoulianjojo@swu.edu.cn
John E. Fowler
john.fowler@oregonstate.edu

Specialty section:
This article was submitted to Plant Development and EvoDevo, a section of the journal Frontiers in Plant Science

Received: 30 November 2020
Accepted: 08 February 2021
Published: 25 February 2021

Citation:
Zhou L, Vejlupkova Z, Warman C and Fowler JE (2021) A Maize Male Gametophyte-Specific Gene Encodes ZmLARP6c1, a Potential RNA-Binding Protein Required for Competitive Pollen Tube Growth. Front. Plant Sci. 12:635244. doi: 10.3389/fpls.2021.635244

Members of the La-related protein family (LARPs) contain a conserved La module, which has been associated with RNA-binding activity. Expression of the maize gene GRMZM2G323499/Zm00001d018613, a member of the LARP family, is highly specific to pollen, based on both transcriptomic and proteomic assays. This suggests a pollen-specific RNA regulatory function for the protein, designated ZmLARP6c1 based on sequence similarity to the LARP6 subfamily in *Arabidopsis*. To test this hypothesis, a *Ds-GFP* transposable element insertion in the *ZmLarp6c1* gene (*tdsgR82C05*) was obtained from the Dooner/Du mutant collection. Sequencing confirmed that the *Ds-GFP* insertion is in an exon, and thus likely interferes with ZmLARP6c1 function. Tracking inheritance of the insertion via its endosperm-expressed GFP indicated that the mutation was associated with reduced transmission from a heterozygous plant when crossed as a male (ranging from 0.5 to 26.5% transmission), but not as a female. Furthermore, this transmission defect was significantly alleviated when less pollen was applied to the silk, reducing competition between mutant and wild-type pollen. Pollen grain diameter measurements and nuclei counts showed no significant differences between wild-type and mutant pollen. However, *in vitro*, mutant pollen tubes were significantly shorter than those from sibling wild-type plants, and also displayed altered germination dynamics. These results are consistent with the idea that ZmLARP6c1 provides an important regulatory function during the highly competitive progamic phase of male gametophyte development following arrival of the pollen grain on the silk. The conditional, competitive nature of the *Zmlarp6c1::Ds* male sterility phenotype (i.e., reduced ability to produce progeny seed) points toward new possibilities for genetic control of parentage in crop production.

Keywords: maize, ZmLARP6c1, pollen competition, pollen germination, pollen tube growth, RNA-binding protein

INTRODUCTION

The life cycle of plants alternates between haploid and diploid phases, called the gametophyte and sporophyte, respectively (Walbot and Evans, 2003). Flowering plants have male and female gametophytes, both of which consist of multiple cells and require regulation of gene expression for their function. For the male gametophyte, pollen grain development initiates inside the anther post-meiosis, with the unicellular microspore. In maize, the mature pollen grain consists of a vegetative cell and two sperm cells after two mitoses during its development. When the pollen grain arrives at the maize silk, progamic development commences, as the pollen tube germinates and its growth is directed to the embryo sac for fertilization (Cheung et al., 1995; Hulskamp et al., 1995; Johnson et al., 2019). Proper elongation of the pollen tube is essential for fertilization (Dresselhaus et al., 2016; Hafidh et al., 2016).

Analysis of the male gametophyte transcriptome in multiple plant species, including maize, indicates that there are numerous genes specifically expressed in the male gametophyte, apparently distinct from any expression or function in the sporophyte (Honys and Twell, 2004; Pina et al., 2005; Chettoor et al., 2014; Rutley and Twell, 2015; Warman et al., 2020). Relatively few of these genes have been characterized *in vivo* with respect to their effect on reproductive success, i.e., their contribution to successful pollen tube growth, sperm cell delivery, fertilization and seed set, particularly in monocots (Procissi et al., 2001; Lalanne and Twell, 2002; Kim et al., 2019; Lopes et al., 2019). Notably, mutations in genes active in the male haploid gametophyte are associated with reduced transmission through the male, as loss of important genetic functions can impair the ability to compete with wild-type pollen tubes, therefore reduce reproductive success, i.e., fitness (Arthur et al., 2003; Warman et al., 2020). This reduced transmission can make the generation of mutant homozygotes difficult, and it can also conceivably reduce the recovery or maintenance of such mutations in a population. Notably, although a number of cell biological regulators active during progamic development have been characterized by mutation (Chang et al., 2013; Kaya et al., 2014; Huang et al., 2017), few direct regulators of gene expression enabling pollen tube growth have been genetically defined (Lago et al., 2005; Adamczyk and Fernandez, 2009; Reňák et al., 2012).

In higher plants, post-transcriptional regulation is essential for proper gene expression during floral development and hormone signaling (Fedoroff, 2002; Kramer et al., 2018; Cho et al., 2019; Prall et al., 2019). RNA-binding proteins are associated with post-transcriptional regulation, including pre-mRNA processing, transport, localization, translation and stability of mRNAs (Dreyfuss et al., 2002; Dedow and Bailey-Serres, 2019). In particular, RNA-binding proteins harboring an RNA recognition motif (RRM) at the N-terminus and a glycine-rich region at the C-terminus are thought to play crucial roles in plant growth and stress responses (Ciuzan et al., 2015; Koster et al., 2017).

The La-related proteins (LARP) are a large and diverse superfamily, each member harboring the La module, comprised of two conserved and closely juxtaposed domains that are thought to promote RNA binding: the La motif followed by an RRM motif (Koster et al., 2017; Maraia et al., 2017). The superfamily is further divided into five families: LARP1, LARP3 (encompassing the original La protein), LARP4, LARP6, and LARP7, based on structural features and evolutionary history (Bousquet-Antonelli and Deragon, 2009; Bayfield et al., 2010; Deragon, 2020). Several members of these families have been proven to be RNA-binding proteins. The La protein binds to RNA polymerase III (RNAP III) transcripts at the single-stranded UUU-3′OH (Wolin and Cedervall, 2002). LARP7 family members most closely resemble LARP3 but function with a single RNAP III nuclear transcript, 7SK, or telomerase RNA (Krueger et al., 2008; Eichhorn et al., 2016, 2018; Mennie et al., 2018). In animal cells, LARP1 and LARP4 bind to the 5′ and 3′ untranslated regions of mRNAs to regulate translation and degradation (Aoki et al., 2013; Merret et al., 2013b; Lahr et al., 2015). In plants, the roles of the LARP superfamily are only beginning to be characterized. For example, in *Arabidopsis*, the *AtLa1* gene, a true La ortholog in the LARP3 family, is required for completion of embryogenesis, perhaps in part due to its role in promoting translation of the WUSCHEL (WUS) transcription factor, which is required for stem cell homeostasis. At the molecular level, AtLa1 appears to promote translation via interaction with the 5′UTR of the *WUS* mRNA (Fleurdepine et al., 2007; Cui et al., 2015). Members of the *Arabidopsis* LARP1 family have been linked to both leaf senescence and heat-induced mRNA decay (Zhang et al., 2012; Merret et al., 2013a). Most recently, LARP1 has been shown to regulate the translation of the subset of *Arabidopsis* transcripts bearing the 5′-terminal oligopyrimidine stretch (TOP) motif, as a key component of the target of rapamycin (TOR) pathway regulating cellular metabolism (Scarpin et al., 2020).

In contrast, there is no analogous cellular or organismal function yet identified for the LARP6 family. Only one endogenous RNA ligand has been identified: in mammals, LARP6 binds to a secondary structure element in the 5′UTR of type I collagen mRNAs (Cai et al., 2010). The LARP6 interdomain linker between the La motif and the RRM plays a critical role in this RNA binding activity (Martino et al., 2015). Intriguingly, certain members of the plant LARP6 family interact with the major plant poly(A)-binding protein (PAB2), and also show differential RNA-binding activity *in vitro* (Merret et al., 2013b).

Bioinformatics analyses (Merret et al., 2013b) showed that, in the maize genome, there are six genes encoding LARP6 family proteins (ZmLARP6a, ZmLARP6b1-b3, and ZmLARP6c1-c2). Here, we report that one of these genes (GRMZM2G323499/Zm00001d018613), which encodes ZmLARP6c1, is specifically and highly expressed in mature pollen. To begin defining the function of this gene, a *Ds-GFP* transposable element insertion (Li et al., 2013) in its coding sequence was obtained and confirmed. Characterization of this mutation and its phenotypes points toward an important male-specific function for ZmLARP6c1 in the haploid gametophyte during the highly competitive phase of pollen tube germination and growth following pollination.

MATERIALS AND METHODS

Plant Materials, Growth Conditions

The *Ds-GFP* allele used in this study (*tdsgR82C05*) was requested from the Maize Genetics Cooperation Stock Center based on its insertion location in the coding sequence of the *larp6c1* gene[1]. The mutation was backcrossed to a *c1* homozygous, predominantly W22 inbred line at least twice to insure heterozygosity and the presence of a single *Ds-GFP* locus before use in the experiments described. Primers used to PCR-genotype mutant and wild-type alleles in plants from segregating families are listed in **Supplementary Table 1**. Genetic studies were carried out using standard procedures at the OSU Botany & Plant Pathology Farm in Corvallis, OR, United States.

Sequence Alignment and Phylogenetic Analysis

The full-length sequences of ZmLARP6 and AtLARP6 family proteins were obtained from MaizeGDB[2] and TAIR[3]. Multiple amino acid sequence alignment was conducted using MegAlign Software. Phylogenetic analysis was conducted using MEGA6 by neighbor-joining method (Tamura et al., 2013).

RNA Extraction

Plants for RNA were grown in summer field conditions in Corvallis, OR, United States. Fresh mature pollen was collected upon shedding between 11:00 am and 12:00 pm. Fifty milligrams pollen of each plant was quickly harvested, frozen in liquid nitrogen and stored at −80°C. Total RNA was isolated from mature pollen using Trizol Reagent (Thermo Fisher scientific, Cat no. 15569026) with added PEG (20,000 MW) to 2% (Tattersall et al., 2005) and quantified via Nanodrop (ND-1000).

Real-Time qRT-PCR

First-strand cDNAs were synthesized from total RNA using SuperScript III First-strand synthesis system for RT-PCR kit (Invitrogen). Real-time qRT-PCR was performed using SYBR Premix EX TaqTM II (TAKARA) on a CFX96 Real-Time system (Bio-Rad), according to the manufacturer's instructions. The amplification program was performed at 95°C for 5 s, 60°C for 30 s, and 72°C for 30 s. Triplicate quantitative assays were performed on each cDNA sample. The relative expression was calculated using the formula $2^{-\Delta(\Delta cp)}$. The housekeeping gene *ZmUbiquitin1* was used as an internal control. All primers used for real-time qRT-PCR are listed in **Supplementary Table 1**.

In vitro Pollen Germination

Plants for pollen germination experiments were grown in summer field conditions in Corvallis, OR, United States. Pollen was germinated in pollen germination medium (PGM – 10% sucrose, 0.0005% H_3BO_3, 10 mM $CaCl_2$, 0.05 mM KH_2PO_4, 6% PEG 4000) (Schreiber and Dresselhaus, 2003) and imaged at 15 or 30 min after exposure to media. Germinated, ungerminated, and ruptured pollen were quantified from digital images using the FIJI distribution of ImageJ (Schindelin et al., 2012), with a minimum of 125 grains categorized for each datapoint. Pollen tube lengths were measured from homozygous *larp6c1::Ds-GFP* mutants and closely related wild-type comparator plants. Four replicates were measured with FIJI, with three homozygous mutants and three wild type plants used per replicate, and a minimum of 50 pollen tubes measured for each pollen collection.

Statistical Analysis

Statistical significance was determined using *t*-test or lm functions either in SAS (SAS Institute Inc.[4]) or with R. Analysis of the categorical response in pollen germination (i.e., the proportion of germinated, ruptured, and ungerminated pollen grains) via logistic regression used the mblogit function (Baseline-Category Logit Models for Categorical and Multinomial Responses) of the mclogit package in R. The categorical dataset was modeled using Genotype + Timepoint + Replicate as factors, with dispersion estimated using the "Afroz" default. R code and the original dataset are available upon request.

Counting of Fluorescent Kernels

Maize ears were scanned using a custom-built scanner and image projection pipeline (Warman et al., 2020, 2021). Green fluorescent (GFP) kernels and non-GFP kernels were counted using the digital image projections and the 'Cell Counter' plugin of the FIJI distribution of ImageJ.

DyeCycle Green Pollen Staining

Fresh pollen was collected from each plant, immediately fixed in ethanol: acetic acid (3:1 ratio) solution, and later rehydrated through an ethanol series for size measurements and staining. To visualize nuclei, fixed pollen grains were stained with DyeCycle Green (Thermo Fisher Scientific, Cat no. V35004) at a final concentration of 1 μM in water, incubated in dark for 30 min and washed with sterile water. Stained pollen was then imaged on a Zeiss Axiovert S100 microscope equipped with HBO 50 Illuminator and Chroma #41017 filter set (470/40 excitation, 495 long-pass dichroic, 525/50 emission) using Qimaging (Retiga ExI) camera.

RESULTS

ZmLarp6c1 Encodes a Pollen-Specific Member of the LARP6 Family

Members of the La-related protein family (LARPs) contain a conserved La motif (LAM) and an RNA recognition motif (RRM), which has been associated with RNA-binding activity. GRMZM2G323499/Zm00001d018613 is a member of the LARP family, and is predicted to encode a 505 amino

[1] acdsinsertions.org

[2] https://maizegdb.org

[3] http://www.arabidopsis.org/

[4] http://www.sas.com

acid protein that harbors conserved La and RRM-like motifs (RRM-L) (**Figure 1A**). The presence of a conserved glycine-rich C-terminal domain (the LSA: LAM and S1 associated motif) in six members of the maize LARP family is diagnostic for placing them in the LARP6 subgroup (**Figure 1B**). Consistent with earlier analyses, all but one of these also harbors the PABP-interacting motif 2 (PAM2) (**Figure 1B**), which may mediate binding to Poly(A)-Binding Protein (PABP) (Merret et al., 2013b). A phylogenetic tree was constructed based on the amino acid sequence alignment of LARP6 subgroups of maize and *Arabidopsis*. Phylogenetic analysis confirms that ZmLARP6c1 has a high degree of sequence similarity with other ZmLARP6s and that the evolutionarily closest *Arabidopsis* protein is AtLARP6c (**Figure 1C**). The closest LARP in maize, designated ZmLARP6c2, is encoded by GRMZM2G411041/Zm00001d032397 on chromosome 1, which is non-syntenic with *ZmLarp6c1* near telomere of the chromosome 7S.

Expression of *ZmLarp6c1* is highly specific to pollen, based on both transcriptomic and proteomic datasets (**Supplementary Figure 1**; Walley et al., 2016; Warman et al., 2020). To assess directly expression of all genes encoding members of the LARP6 family in maize pollen, total RNA was isolated from mature pollen collected from inbred line B73. Real-time qRT-PCR results showed that *ZmLarp6c1* had the highest transcriptional abundance of all six *ZmLarp6* family members in mature pollen (**Figure 1D**). Together, these data suggest a pollen-specific RNA regulatory function for Zm LARP6c1.

A ZmLarp6c1 Mutation Is Associated With Reduced Transmission When Crossed as a Male

To investigate the function of *ZmLARP6c1* during pollen development, a line carrying a *Ds-GFP* transposable element insertion in *ZmLARP6c1* (*Zmlarp6c1::Ds-GFP*) was obtained from the Dooner/Du population (Li et al., 2013). Sequencing confirmed that the *tdsgR82C05* insertion is in the fifth exon (**Figure 2A**) in the RRM-L domain coding region, and thus likely interferes with *ZmLARP6c1* function. PCR genotyping primers were designed to confirm the co-segregation with the GFP marker, and identify the genotype (**Figure 2B**).

Neither heterozygous nor homozygous *Zmlarp6c1::Ds-GFP* plants showed any obvious differences in vegetative and floral development. As an initial assessment of effects on gametophytic development and function, *Zmlarp6c1::Ds-GFP* heterozygous mutant plants were reciprocally crossed with wild-type plants in the field. Inheritance of the insertion was tracked via its endosperm-expressed GFP, with the mutant and wild-type kernels quantified via annotation of 360° ear projections (**Figure 3**). When crossed through the male, GFP transmission ranged from 0.5 to 26.5%, showing significantly reduced

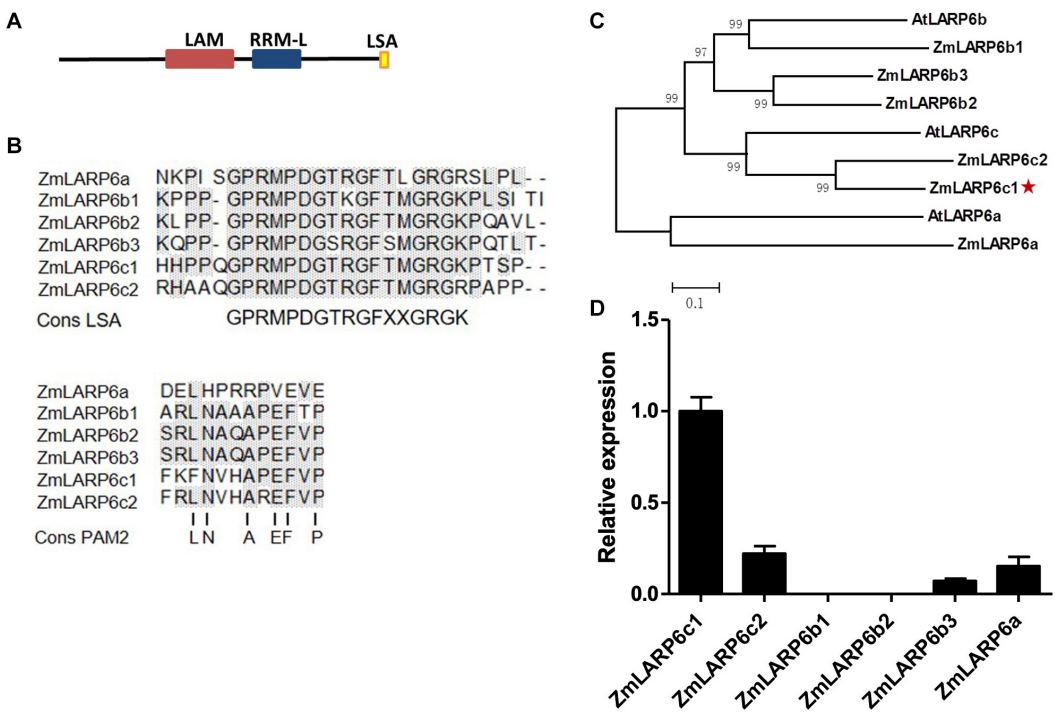

FIGURE 1 | Bioinformatic analysis and expression profiling of the maize LARP6 family members points toward a role for *ZmLarp6c1* in maize pollen. **(A)** Predicted conserved domain architecture of ZmLARP6c1. **(B)** Alignments of maize LARP6 amino acid sequences alongside consensus sequences for the LSA motif and the PAM2 motif. Gray shade, matched residues. **(C)** Phylogenetic tree, using the entire amino acid alignment and the distance method. The bar indicates a mean distance of 0.1 changes per amino acid residue. **(D)** Relative transcript levels of *ZmLARP6* genes in mature pollen of maize. Total RNA was extracted from mature pollen for qRT-PCR. All data are means of three biological replicates with error bars indicating SD.

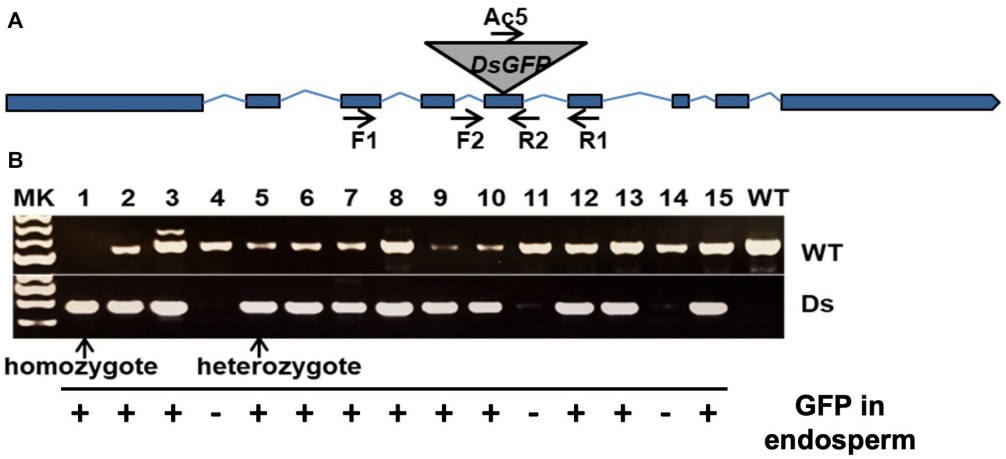

FIGURE 2 | A *Ds-GFP* transposable element insertion line provides a tool to investigate *Zmlarp6c1* function. **(A)** Sequencing confirmed that the insertion was in the 5th exon; thus, the mutation, likely a knockout, could be easily tracked genetically by observing GFP fluorescence in the endosperm. **(B)** PCR genotyping of progeny (using primers F1, R1, and Ac5) from a self-pollinated heterozygote confirms co-segregation of the insertion with the GFP marker, and helps clarify genotype (homozygote vs. heterozygote).

transmission in every outcross in two field seasons (χ^2 test, p-values $< 10^{-6}$), averaging 12.4% transmission across nine ears (**Table 1**). In contrast, female GFP transmission ranged from 47.2 to 56.7%, averaging 51.4%, with only a single cross significantly different from expected Mendelian inheritance (56.7%, $p = 0.008$) (**Table 1**). Self-crosses of heterozygous plants average a GFP transmission rate of 53.7%, consistent with the expectation based on the male and female rates observed above (**Supplementary Table 2**). Notably, pollen from plants homozygous for *Zmlarp6c1::Ds-GFP* generated full ears when used in hand pollinations onto wild-type females, with seed set similar to that generated by comparable pollinations with wild-type homozygotes (**Figures 3C,D**). No significant difference was observed between the total number of seeds from mutant homozygotes vs. from wild-type homozygotes ($p = 0.43$, t-test).

To create derivative excision alleles to confirm that the insertion is causal for the male-specific transmission defect, *Zmlarp6c1::Ds-GFP* was crossed into an *Ac-im* active line (Conrad and Brutnell, 2005). Progeny were screened by PCR for excision, and 6 putative revertant alleles were identified. Two of these alleles were heritable and confirmed by sequencing (**Figures 4A,B**). As expected, there was a 8 bp duplication in the original *Zmlarp6c1::Ds-GFP* insertion allele compared to wild-type. *Ds* excision generated distinct nucleotide footprints in the two derivatives, with one footprint (*dX549B2*) adding six base pairs relative to the wild-type sequence and the other (*dX550A8*) adding eight base pairs (**Figure 4B**). Given an insertion in the coding region, the eight-bp insertion would be predicted to generate a frameshift, and thus a likely non-functional LARP6c1 protein, whereas the six-bp footprint would insert two amino acids but retain the frame (**Supplementary Figure 2**), and thus potentially restore protein function. To test for altered functionality associated with these variant sequences, plants heterozygous for each of the two alleles were outcrossed as males with a heavy pollen load, and transmission was assessed via PCR genotyping. As expected, the 8-bp footprint *dX550A8* allele retained a strongly reduced transmission rate (12.5%, **Figure 4C**). However, the 6-bp footprint *dX549B2* allele recovered a wild-type transmission rate (54.2%, **Figure 4D**), indicating reversion of gene function. These data confirm that the interruption of the *Zmlarp6c1* coding sequence by the original *tdsgR82C05* insertion was causal for the transmission defect, rather than an unknown, linked mutation.

ZmLARP6c1 Contributes to Pollen Competitive Ability *in vivo* and to Robust Pollen Tube Growth *in vitro*

Notable in the transmission tests was the observation that the male transmission rate was associated with high variance (standard deviation = 9.6%), relative to female transmission (standard deviation = 3.1%). This raised the possibility that *Zmlarp6c1::Ds* pollen is particularly sensitive to an environmental factor that was variable across these ears. One such factor that can be easily tested is the level of competition – i.e., the number of wild-type pollen grains competing with mutant pollen grains on each silk. A defect that is only expressed in competition with wild-type pollen would also explain how pollen from homozygous mutant plants can generate good seed set in hand pollinations (**Figure 3C**). In four independent experiments, a single pollen collection from a mutant heterozygote was used to heavily pollinate silks of one ear (HVY), and to sparsely pollinate three other ears with limiting pollen (SPS) to reduce competition. In three of the four experiments, sparse pollination significantly relieved the GFP transmission defect, relative to the comparator heavy pollination, with transmission rates from 37.7 to 53.3% (**Table 2**). Because these experiments are inherently imprecise, we sought to find a measure to assess pollen load for each pollination. The total number of seeds per ear provides such an assessment,

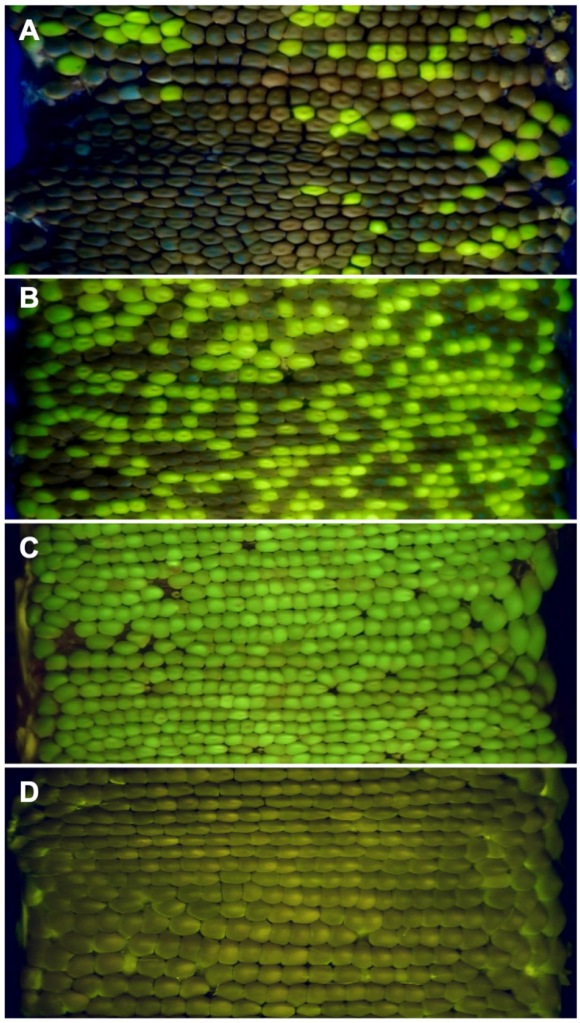

FIGURE 3 | Maize ear projections demonstrate a strong male-specific transmission defect associated with the GFP-expressing *Zmlarp6c1::DsgR82C05* allele. **(A)** *Zmlarp6c1::Ds*/+ crossed as a male (52 GFP kernels/420 total kernels = 12.4% transmission). **(B)** The same *Zmlarp6c1::Ds*/+ plant crossed as a female (246 GFP kernels/479 total kernels = 51.4% transmission). **(C)** Representative ear resulting from a cross of a homozygous *Zmlarp6c1::Ds* plant as a male to a wild-type female (average seed set = 319, standard deviation 101, *n* = 5 ears). **(D)** Representative ear resulting from a cross of a homozygous wild-type plant (a sibling from a closely related *Zmlarp6c1::Ds* family) as a male to a wild-type female (average seed set = 277, standard deviation 50, *n* = 5 ears).

indirectly, given that seed production is limited to ovules successfully pollinated and fertilized. Analysis of all ears in the dataset individually showed a significant correlation between GFP transmission rate and the total number of seeds on an ear (**Figure 5**) (p = 0.0003). This is consistent with a strong effect of the level of competition with wild-type pollen on the ability of *Zmlarp6c1::Ds* pollen to successfully fertilize and generate a seed. These data argue that *Zmlarp6c1* is a crucial contributor to pollen competitive ability *in vivo*, and suggest that its function is manifested post-pollination.

One possibility to explain the competitive defect would be slowed pollen tube germination, and/or a reduced growth rate for pollen tubes. To assess these possibilities, we characterized pollen tube germination and growth *in vitro* (**Figure 6A**). Pollen populations from homozygous mutant and wild-type field-grown plants was scored at 15 and 30 min after exposure to pollen growth medium (PGM), with germinated, ungerminated and ruptured pollen grains counted. (Ruptured pollen grains have ceased growing after releasing cytoplasm into the media, apparently due to loss of cell wall integrity at the growing pollen tube tip.) Altered germination dynamics were associated with loss of *Zmlarp6c1* function (**Figure 6B**). Analysis of four replicates comparing wild-type and *Zmlarp6c1::Ds* pollen grown *in vitro* shows the expected significant effect of time on germination, with significant decrease in the percentage of ungerminated pollen from 15 to 30 min in both genotypes (p = 1.02E-05), along with a concomitant increase in germinated and ruptured pollen. Genotype was also a significant predictor of germination response (p = 0.0047), confirming that *Zmlarp6c1::Ds* pollen is associated with a higher proportion of ungerminated pollen grains. Notably, although the proportion of ungerminated *Zmlarp6c1::Ds* pollen was higher than wild-type at both time points, by 30 min the proportional response in the mutant was similar to that of wild-type pollen at 15 min (**Figure 6B**, and individual replicates in **Supplementary Figure 3**). These data are consistent with the *Zmlarp6c1::Ds* defect causing a delay in pollen tube germination, rather than an absolute inhibition of germination. Finally, pollen tube lengths were measured at the 30 min timepoint for both *Zmlarp6c1::Ds-GFP* mutant and wild-type populations. Consistent with the competitive defect detected *in vivo*, mutant pollen was associated with significantly shorter pollen tubes than wild-type, with an average 31.5% tube length reduction associated with loss of *Zmlarp6c1* function (**Figure 6C** and **Supplementary Figure 4**).

As an initial assessment as to whether the *Zmlarp6c1::Ds-GFP* mutant pollen was associated with defects prior to the progamic phase (i.e., aberrant pollen grain development, potentially leading to reduced competitiveness following pollination), we measured pollen grain diameter and determined nuclei number in pollen fixed upon anthesis. No significant differences were found in pollen grain diameters comparing sibling wild-type and *Zmlarp6c1::Ds-GFP* heterozygotes, nor did Dyecyle Green staining of DNA identify significant differences in the number of nuclei between these pollen populations (**Supplementary Figure 5**). Collectively, these findings suggest that the important role played by *ZmLARP6c1* in male gametophyte function is primarily manifested in the post-pollination, progamic phase of gametophytic development, rather than in the development of the pollen grain itself.

DISCUSSION

Flowering plants have a complex sexual reproduction system, which includes the short but critical gametophytic generation, involving pollination followed by double fertilization, and triggering development of the progeny seed. Notably,

TABLE 1 | Transmission of *larp6c1::DsGFP* in reciprocal outcrosses.

larp6c1::DsGFP/+ plant/season	Direction of outcross to wild-type	# GFP kernels	# wt kernels	% GFP	*p*-value (χ^2)
1/2018	Male	30	83	26.5	$<10^{-6}$
	Female	124	98	55.9	0.081
2/2018	Male	32	160	16.7	$<10^{-6}$
	Female	187	209	47.2	0.269
3/2018	Male	19	257	6.9	$<10^{-6}$
	Female	238	228	51.1	0.643
4/2018	Male	63	285	18.1	$<10^{-6}$
	Female	184	193	48.8	0.643
1/2019	Male	38	119	24.2	$<10^{-6}$
	Female	221	211	51.2	0.630
2/2019	Male	12	439	2.7	$<10^{-6}$
	Female	224	171	56.7	0.008
3/2019	Male	52	368	12.4	$<10^{-6}$
	Female	246	233	51.4	0.553
4/2019	Male	9	256	3.4	$<10^{-6}$
	Female	221	210	51.3	0.596
5/2019	Male	1	187	0.5	$<10^{-6}$
	Female	148	154	49.0	0.730

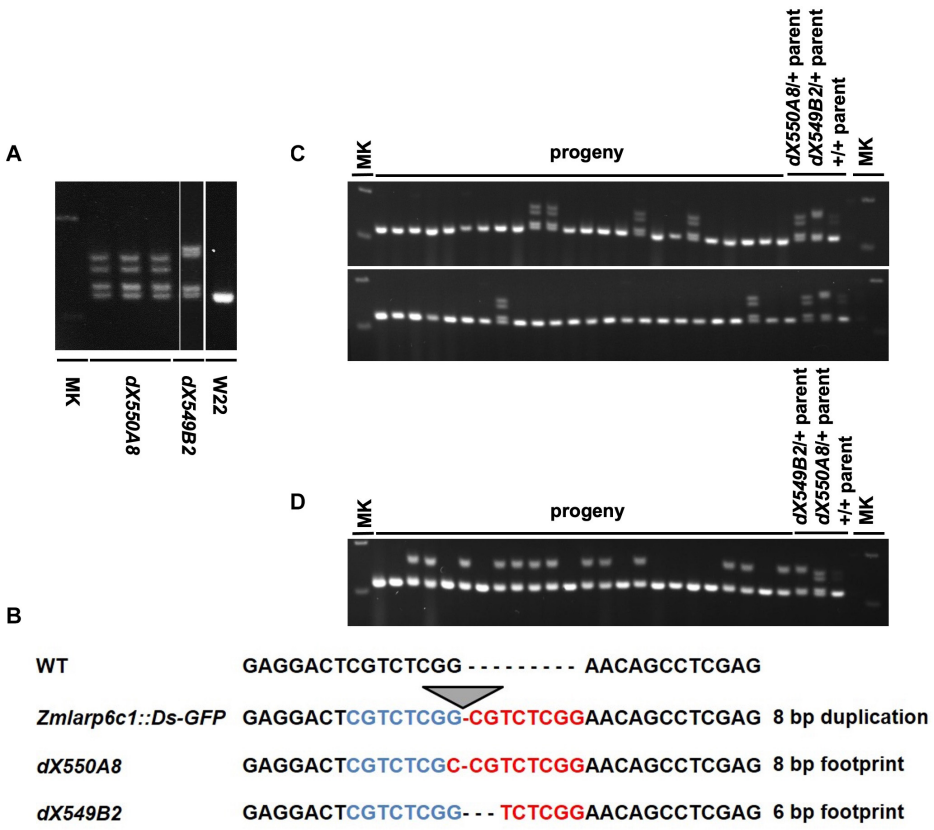

FIGURE 4 | *Ds* excision alleles derived from *Zmlarp6c1::DsgR82C05* validate that the male specific transmission defect is due to loss of ZmLARP6c1 function. **(A)** PCR genotyping using primers F2 and R2 (**Figure 2**) documents isolation of two derivative alleles (*dX550A8* and *dX549B2*) due to excision of the *Ds-GFP* element from *Zmlarp6c1::DsgR82C05*. W22: comparator wild-type inbred; MK: DNA size marker. **(B)** Sequencing of the derivative alleles shows that *dX550A8* and *dX549B2* are associated with an 8-bp and 6-bp footprints, respectively, in the *Zmlarp6c1* coding sequence. **(C)** *Zmlarp6c1-dX550A8* is associated with a male-specific transmission defect, with 6 out of 48 progeny from a heterozygous male outcross inheriting the footprint (12.5%). **(D)** *Zmlarp6c1-dX549B2* segregates at a Mendelian ratio when transmitted through the male (13:11 from a heterozygous outcross).

TABLE 2 | Transmission of *larp6c1::DsGFP* through the male when pollen load is varied.

Experiment/ Pollen load		# GFP kernels	# wt kernels	% GFP	*p*-value (χ^2)
1	HVY	30	83	26.5	0.010 (6.6151)
	SPS	16	14	53.3	
2	HVY	32	160	16.7	∼0 (30.9695)
	SPS	127	184	40.8	
3	HVY	19	257	6.9	∼0 (88.6719)
	SPS	247	409	37.7	
4	HVY	63	285	18.1	0.976 (0.0009)
	SPS	135	599	18.4	

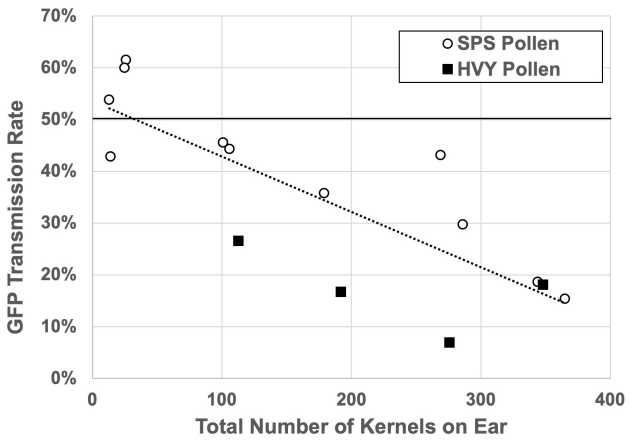

FIGURE 5 | Transmission of *Zmlarp6c1::DsgR82C05* mutation is sensitive to pollen load. Outcomes of each separate ear with more than 10 kernels in the experiments from **Table 2** are plotted. Pollination with heavy, near-saturating (HVY) pollen is associated with reduced transmission of *Zmlarp6c1::Ds*, relative to sparse (SPS) pollen (*t*-test, $p = 0.002601$). Moreover, linear regression (dotted line) indicates a significant correlation between total kernels per ear and transmission rate ($p = 0.0003$, $R^2 = 0.647$). Note that the two ears with ∼60% transmission are not significantly higher than 1:1, given the smaller populations they represent.

gametophytes express a significant subset of genes in plant genomes, which although reduced relative to the sporophyte (Honys and Twell, 2003; Chettoor et al., 2014; Rutley and Twell, 2015), enable developmental programs and environmental responses. Given that male gametophytic gene expression occurs after the genetic recombination of meiosis, and in organisms that are independent and have a free-living stage, there is considerable potential for expression of phenotypes, upon which evolutionary forces can act (Reese and Williams, 2019). In maize, with its prodigious production of large populations of pollen, lack of a biotic vector, and the extended stigma surface and transmitting tract of the female silk, there appears to be ample opportunity for gametophytic competition in the progamic phase of development (i.e., during pollen tube germination and growth). Assessing transmission rates can give an initial measure of the magnitude of a mutation's effect on gametophytic fitness (and presumably, biological function), and the same measure can also be used to determine whether competition itself influences fitness upon manipulation of pollen load (Arthur et al., 2003; Cole et al., 2005). The seed-expressed GFP phenotype linked to the *Ds* mutagenic element in the publicly available *Ds-GFP* population (Li et al., 2013), not only facilitates the initial determination of mutant transmission rate (Warman et al., 2020), but also broadens the feasibility and precision of analytical approaches for assessing the influence of pollen competition on defects like that associated with *Zmlarp6c1::Ds-GFP* (**Figure 5**).

The biological processes that enable gametophytic function (and the genes that underlie them) are regulated developmentally, but the associated regulatory mechanisms remain unclear. Interestingly, evidence in multiple species indicates that a significant component enabling the transition from quiescent pollen grain to actively growing pollen tube is post-transcriptional control (Hafidh et al., 2016). In pollen of tobacco and *Arabidopsis*, cytoplasmic complexes are likely mechanistically important for storage of transcripts generated earlier in development, and eventual translation during pollen tube growth (Honys et al., 2009; Scarpin et al., 2017). Although such complexes have not been observed in maize pollen, the rapid germination response *in vitro* (pollen tube growth apparent in less than 15 min) (**Figure 6**) is consistent with a transition that does not require *de novo* transcription. The detection of significant proteomic differences in germinated maize pollen at 30 min after exposed to media is also suggestive that control of translation plays a role in the regulation of pollen tube growth in maize (Walley et al., 2016). The protein homology, expression pattern and mutant phenotypes documented in this study raise the possibility that *ZmLarp6c1* is a component of a translational control and/or RNA storage regulatory mechanism.

Few putative RNA-binding proteins have been characterized in detail in mature pollen in any species (Park et al., 2006), and until recently, none have been phenotypically associated with aberrant progamic development. However, a number of conserved sequence elements in transcript UTRs with potential or proven roles in influencing mRNA translation or stability have been identified (Hulzink et al., 2003), most notably in the tobacco *ntp303* transcript (Hulzink et al., 2002). These are potential interaction sites for RNA-binding proteins, possibly including those of the LARP family (e.g., as observed for AtLARP1 and the TOP motif; Scarpin et al., 2020). As this report was in submission, a study of the *Arabidopsis* ortholog, AtLARP6C, provided data indicating that this protein is a *bona fide* RNA-binding protein, also specific to pollen grain and pollen tube, which targets transcripts with specific sequence motifs (the B-box) in the 5′ UTR (Billey et al., 2020). LARP6C binding, in a complex with the Poly-A Binding Protein (PABP), is proposed to regulate translation, decay and storage of its target transcripts. The data from Arabidopsis should facilitate the investigation of analogous putative RNA targets of ZmLARP6c1 in mature pollen and growing pollen tubes in maize.

The severe transmission defect for the *Zmlarp6c1::Ds* mutation indicates that the encoded protein is critical for wild-type pollen function *in vivo*. Moreover, the cellular phenotypes detected via assessment of *Zmlarp6c1::Ds* pollen germination and growth *in vitro* indicate that the encoded protein plays a role in maize pollen post-germination, causing delayed germination

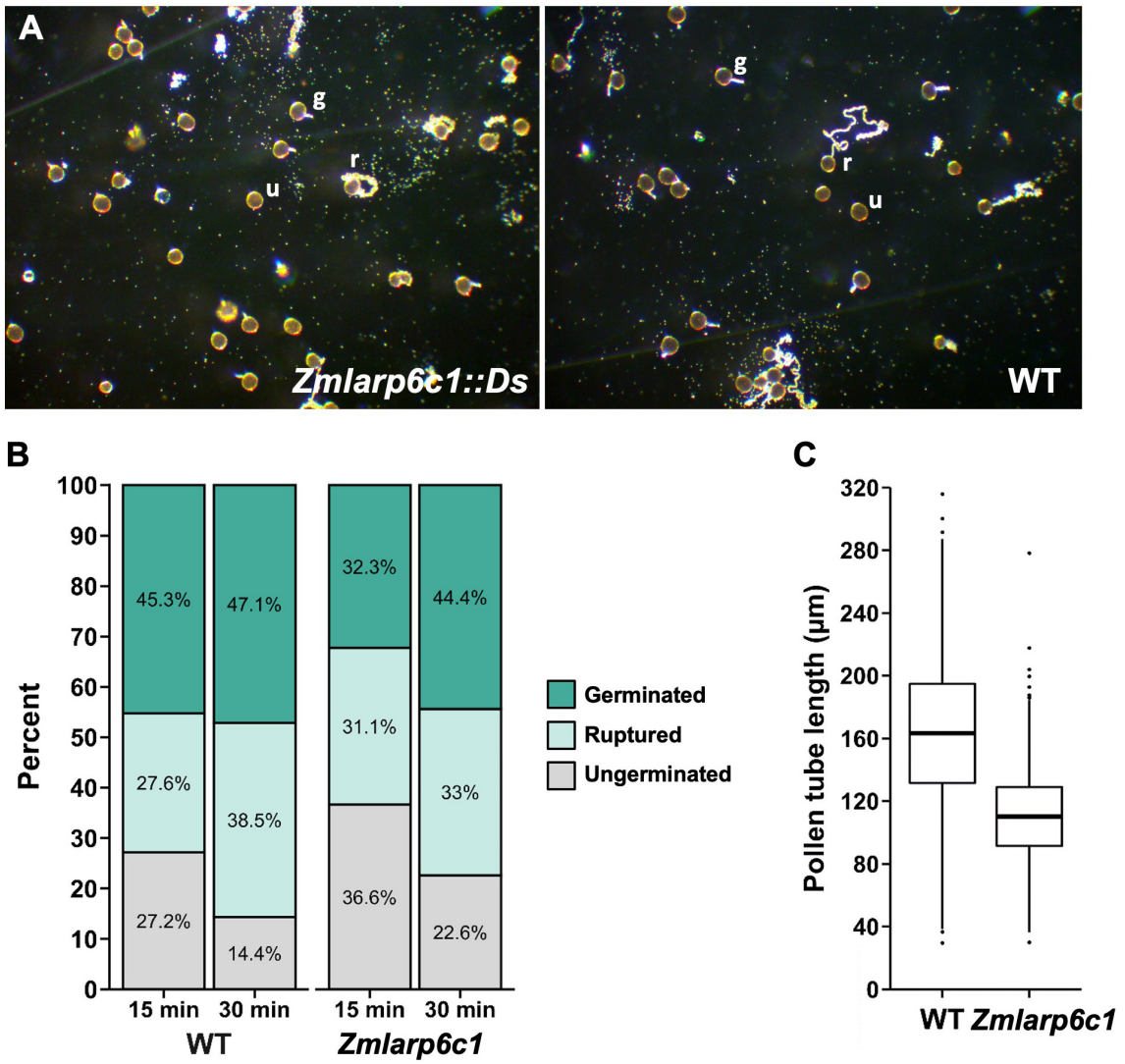

FIGURE 6 | *In vitro*, pollen from *Zmlarp6c1::Ds* plants is associated with shorter pollen tubes and altered germination dynamics. **(A)** Representative fields of pollen germinated *in vitro*, at 15 min post-exposure to liquid media. Pollen was collected from either a homozygous *Zmlarp6c1::Ds* plant, or a comparator wild-type (WT) plant. Fields were scored blindly (four biological replicates of three plants of each genotype, at least 125 pollen grains from each plant), categorizing pollen grains as germinated (g), ruptured (r), or ungerminated (u). **(B)** Combined data from four biological replicates, at 15 and 30 min after plating in PGM. Modeling the categorical response using a multinomial baseline-category logit model indicates genotype is a significant predictor ($p = 0.0047$), as is timepoint ($p = 1.02e\text{-}05$). **(C)** Mutant pollen tube lengths at 30 min were significantly shorter than wild-type in all replications (Welch's *t*-test, all *p*-values $< 10^{-15}$). Averaged across all four replicates, mutant pollen tubes were 31.5% shorter than wild-type sibling tubes.

dynamics and shorter pollen tubes when mutant. This is in contrast to the lack of a significant effect on two cellular parameters that indicative of effects earlier in development, pollen grain diameter and number of nuclei. Comparing across individual replicates, *Zmlarp6c1::Ds* pollen also appeared to show a higher variance in germination response, relative to the wild-type, raising the possibility that loss of *Zmlarp6c1* function is associated with a more general loss of cellular robustness during pollen tube growth *in vitro* (**Supplementary Figure 3**). Notably, these phenotypes are distinct from those identified for mutants of the *Arabidopsis AtLARP6C* ortholog, which is primarily defective during a later stage of pollen tube growth, during guidance of the pollen tube to the embryo sac at the ovule (Billey et al., 2020). This raises the possibility of an evolutionary shift in the timing of LARP6C function in pollen in different plant lineages, with the protein acting earlier in maize relative to *Arabidopsis*. It will be important to investigate whether *Zmlarp6c1::Ds* pollen tubes also display guidance defects, which we have not assessed.

Genetically encoded male sterility is of interest for plant breeding, crop production, and protection of patented varieties, for example, in the production of hybrid seeds. Currently, female lines with cytoplasmic male sterility (cms) or genic male-sterility based on expression in the sporophyte (gms) are the preferred biological approaches for insuring only a single male

parent during hybrid seed production, and obviate the need for mechanical detasseling (Wan et al., 2019). The observation that a single mutation such as *Zmlarp6c1::Ds* can cause a severe male-specific competitive, rather than absolute, defect raises the possibility of an alternative approach for controlling seed production via genic male sterility based on gametophytic expression (which we are designating "gms-g"). The conditional nature of the gametophytic *Zmlarp6c1::Ds* defect – i.e., its ability to generate progeny is hindered only in the presence of wild-type pollen (**Figure 3**) – could be exploited to facilitate not only the generation of hybrid seed, but also seed for the parent female inbred line. This contrasts with sporophytic-based male-sterility of typical gms lines, in which production of any viable pollen is inhibited, complicating the large-scale production of these lines via self-pollination (Wan et al., 2019). In this scenario, a gms-g line that is homozygous for a competition-defective male gametophyte can easily generate seed at scale via open self-pollination in plots isolated from wild-type pollen, eliminating competition. However, for hybrid seed production, the competitive male defect in the female gms-g parent would inhibit productive self-pollination in the presence of wild-type pollen from the hybrid partner male inbred. Similarly, such a genetically encoded competitive male gametophytic defect could be utilized for discouraging accidental transgene flow or loss of other patented alleles into non-target seed stock. It remains to be seen whether, in an open pollinated field that also provides a robust wild-type pollen source, a defective *Zmlarp6c1* alone is a strong enough barrier to insure effective male sterility. The expression of the closely related *Zmlarp6c2* at a low level in pollen (**Figure 1**) raises the possibility that this gene provides some remnant redundant function in the *Zmlarp6c1::Ds-GFP* line. Obtaining knockout mutations in this second gene would not only allow testing for genetic redundancy, but potentially also enhance gms-g effectiveness through a combination of both mutations.

DATA AVAILABILITY STATEMENT

The original contributions presented in the study are included in the article/**Supplementary Materials**, further inquiries can be directed to the corresponding author/s.

AUTHOR CONTRIBUTIONS

JF, CW, and LZ conceived and designed the experiments. LZ, ZV, and CW conducted the experiments and analyzed the data. LZ, CW, and JF discussed and wrote the manuscript. All the authors edited, read and approved the manuscript.

FUNDING

This work was supported by the US Natural Science Foundation (IOS-1340050) and the National Natural Science Foundation of China (31601312).

ACKNOWLEDGMENTS

The authors thank the Dooner/Du collection for the *Ds-GFP* transposable element insertion mutant *tdsgR82C05*. The authors would like to acknowledge statistical guidance from D. Jiang, OSU Statistics. Finally, thanks to S. Leiboff and other members of the OSU Botany & Plant Pathology PF1 group for their helpful questions and comments.

SUPPLEMENTARY MATERIAL

The Supplementary Material for this article can be found online at: https://www.frontiersin.org/articles/10.3389/fpls.2021.635244/full#supplementary-material

Supplementary Table 1 | Primers used in this study.

Supplementary Table 2 | Transmission of *larp6c1::DsGFP* in self crosses.

Supplementary Figure 1 | *Zmlarp6c1* expression is enriched specifically in mature pollen. **(A)** Expression profiling data from the Walley et al. (2016) maize developmental atlas, for GRMZM2G323499/Zm00001d018613. RNA-seq data for all 23 different tissue types assessed (blue), with corresponding proteomic (orange), and phosphoproteomic (gray) profiling data for the same tissues. Two additional, relevant samples were assessed for proteomic data: B73 (inbred line) Germinated Pollen and W23 (inbred line) Mature Pollen. Although *Zmlarp6c1* transcript is detected in mature leaf, the translated protein is only detected in pollen samples. FPKM, fragments per kilobase of exon model per million reads mapped; dNSAF, distributed normalized spectral abundance factor. **(B)** Focused transcriptome profiling of maize male gametophyte development (Warman et al., 2020) indicates that the *Zmlarp6c1* transcript (Zm00001d018613_T004) is highest in mature pollen, but largely excluded from the sperm cells isolated from mature pollen. This suggests the transcript is specifically enriched in the pollen vegetative cell, which drives pollen tube germination and growth.

Supplementary Figure 2 | Alignments of WT, *dX550A8* and *dX549B2* amino acid sequences. Red shade, La motif; blue shade, RRM-L; black dot shade, altered residues in derivative alleles; orange oval, two amino acids added by the *dX549B2* 6 bp footprint at the insertion site.

Supplementary Figure 3 | *Zmlarp6c1::Ds-GFP* and wild-type pollen germination, separated by replicate. Variance across each replicate is apparent. However, all show a trend toward a smaller percentage of ungerminated pollen grains at 30 min than at 15 min, in both genotypes; and *Zmlarp6c1* pollen associated with a higher fraction of ungerminated pollen than wild-type. Modeling the categorical response using a multinomial baseline-category logit model indicates Replicate 2 is a significant factor predictive of a high proportion of Ruptured grains ($p = 0.02059$), whereas Replicate 4 is a significant factor predictive of a low proportion of Ungerminated grains ($p = 0.0134$).

Supplementary Figure 4 | Pollen from homozygous *Zmlarp6c1::Ds-GFP* plants is associated with shorter pollen tubes. Pollen from homozygous *Zmlarp6c1::Ds-GFP* and comparator wild-type plants was germinated in pollen growth medium for 30 min, imaged, and pollen tube lengths from four replicates were measured. Mutant pollen tubes were significantly shorter than wild-type in all replicates (Welch's *t*-test, all *p*-values $< 10^{-15}$).

Supplementary Figure 5 | Pollen grain diameter and nuclei count showed no differences between wild-type and mutant pollen. **(A)** At least 150 pollen grains were measured per replicate. **(B)** DyeCycle green fluorescent dye was used to stain DNA in fixed pollen, and distinct nuclei visible in each grain were counted blindly. Although maize pollen grains are expected to have three nuclei at maturity (vegetative cell plus two sperm cells), not every nucleus is discernible in every grain, due to the large size of the pollen grain and presumed variation in staining efficiency. All data are means of four biological replicates with error bars indicating SD.

REFERENCES

Adamczyk, B. J., and Fernandez, D. E. (2009). MIKC* MADS domain heterodimers are required for pollen maturation and tube growth in *Arabidopsis*. *Plant Physiol.* 149, 1713–1723. doi: 10.1104/pp.109.135806

Aoki, K., Adachi, S., Homoto, M., Kusano, H., Koike, K., and Natsume, T. (2013). LARP1 specifically recognizes the 3′ terminus of poly(A) mRNA. *FEBS Lett.* 587, 2173–2178. doi: 10.1016/j.febslet.2013.05.035

Arthur, K. M., Vejlupkova, Z., Meeley, R. B., and Fowler, J. E. (2003). Maize ROP2 GTPase provides a competitive advantage to the male gametophyte. *Genetics* 165, 2137–2151.

Bayfield, M. A., Yang, R., and Maraia, R. J. (2010). Conserved and divergent features of the structure and function of La and La-related proteins (LARPs). *Biochim. Biophys. Acta* 1799, 365–378. doi: 10.1016/j.bbagrm.2010.01.011

Billey, E., Hafidh, S., Cruz-Gallardo, I., Litholdo, C. G., Jean, V., Marie-Christine Carpentier, M. C., et al. (2020). LARP6C regulates selective mRNA translation to promote pollen tube guidance in *Arabidopsis thaliana*. *bioRxiv* [Preprint]. doi: 10.1101/2020.11.27.401307

Bousquet-Antonelli, C., and Deragon, J. M. (2009). A comprehensive analysis of the La-motif protein superfamily. *RNA* 15, 750–764. doi: 10.1261/rna.1478709

Cai, L., Fritz, D., Stefanovic, L., and Stefanovic, B. (2010). Binding of LARP6 to the conserved 5′ stem-loop regulates translation of mRNAs encoding type I collagen. *J. Mol. Biol.* 395, 309–326. doi: 10.1016/j.jmb.2009.11.020

Chang, F., Gu, Y., Ma, H., and Yang, Z. (2013). AtPRK2 promotes ROP1 activation via RopGEFs in the control of polarized pollen tube growth. *Mol. Plant* 6, 1187–1201. doi: 10.1093/mp/sss103

Chettoor, A. M., Givan, S. A., Cole, R. A., Coker, C. T., Unger-Wallace, E., Vejlupkova, Z., et al. (2014). Discovery of novel transcripts and gametophytic functions via RNA-seq analysis of maize gametophytic transcriptomes. *Genome Biol.* 15:414. doi: 10.1186/s13059-014-0414-2

Cheung, A. Y., Wang, H., and Wu, H. M. (1995). A floral transmitting tissue-specific glycoprotein attracts pollen tubes and stimulates their growth. *Cell* 82, 383–393. doi: 10.1016/0092-8674(95)90427-1

Cho, H., Cho, H. S., and Hwang, I. (2019). Emerging roles of RNA-binding proteins in plant development. *Curr. Opin. Plant Biol.* 51, 51–57. doi: 10.1016/j.pbi.2019.03.016

Ciuzan, O., Hancock, J., Pamfil, D., Wilson, I., and Ladomery, M. (2015). The evolutionarily conserved multifunctional glycine-rich RNA-binding proteins play key roles in development and stress adaptation. *Physiol. Plant* 153, 1–11. doi: 10.1111/ppl.12286

Cole, R. A., Synek, L., Zarsky, V., and Fowler, J. E. (2005). SEC8, a subunit of the putative *Arabidopsis* exocyst complex, facilitates pollen germination and competitive pollen tube growth. *Plant Physiol.* 138, 2005–2018. doi: 10.1104/pp.105.062273

Conrad, L. J., and Brutnell, T. P. (2005). Ac-immobilized, a stable source of Activator transposase that mediates sporophytic and gametophytic excision of Dissociation elements in maize. *Genetics* 171, 1999–2012. doi: 10.1534/genetics.105.046623

Cui, Y., Rao, S., Chang, B., Wang, X., Zhang, K., Hou, X., et al. (2015). AtLa1 protein initiates IRES-dependent translation of WUSCHEL mRNA and regulates the stem cell homeostasis of *Arabidopsis* in response to environmental hazards. *Plant Cell Environ.* 38, 2098–2114. doi: 10.1111/pce.12535

Dedow, L. K., and Bailey-Serres, J. (2019). Searching for a match: structure, function and application of sequence-specific RNA-binding proteins. *Plant Cell Physiol.* 60, 1927–1938. doi: 10.1093/pcp/pcz072

Deragon, J. M. (2020). Distribution, organization an evolutionary history of La and LARPs in eukaryotes. *RNA Biol.* 19, 1–9. doi: 10.1080/15476286.2020.1739930

Dresselhaus, T., Sprunck, S., and Wessel, G. M. (2016). Fertilization mechanisms in flowering plants. *Curr. Biol.* 26, R125–R139. doi: 10.1016/j.cub.2015.12.032

Dreyfuss, G., Kim, V. N., and Kataoka, N. (2002). Messenger-RNA-binding proteins and the messages they carry. *Nat. Rev. Mol. Cell Biol.* 3, 195–205. doi: 10.1038/nrm760

Eichhorn, C. D., Chug, R., and Feigon, J. (2016). hLARP7 C-terminal domain contains an xRRM that binds the 3′ hairpin of 7SK RNA. *Nucleic Acids Res.* 44, 9977–9989. doi: 10.1093/nar/gkw833

Eichhorn, C. D., Yang, Y., Repeta, L., and Feigon, J. (2018). Structural basis for recognition of human 7SK long noncoding RNA by the La-related protein Larp7. *Proc. Natl. Acad. Sci. U.S.A.* 115, E6457–E6466. doi: 10.1073/pnas.1806276115

Fedoroff, N. V. (2002). RNA-binding proteins in plants: the tip of an iceberg? *Curr. Opin. Plant Biol.* 5, 452–459. doi: 10.1016/s1369-5266(02)00280-7

Fleurdepine, S., Deragon, J. M., Devic, M., Guilleminot, J., and Bousquet-Antonelli, C. (2007). A bona fide La protein is required for embryogenesis in *Arabidopsis thaliana*. *Nucleic Acids Res.* 35, 3306–3321. doi: 10.1093/nar/gkm200

Hafidh, S., Fila, J., and Honys, D. (2016). Male gametophyte development and function in angiosperms: a general concept. *Plant Reprod.* 29, 31–51. doi: 10.1007/s00497-015-0272-4

Honys, D., Rěnák, D., Feciková, J., Jedelský, P. L., Nebesárová, J., Dobrev, P., et al. (2009). Cytoskeleton-associated large RNP complexes in tobacco male gametophyte (EPPs) are associated with ribosomes and are involved in protein synthesis, processing, and localization. *J Proteome Res.* 8, 2015–2031. doi: 10.1021/pr8009897

Honys, D., and Twell, D. (2003). Comparative analysis of the *Arabidopsis* pollen transcriptome. *Plant Physiol.* 132, 640–652. doi: 10.1104/pp.103.020925

Honys, D., and Twell, D. (2004). Transcriptome analysis of haploid male gametophyte development in *Arabidopsis*. *Genome Biol.* 5:R85. doi: 10.1186/gb-2004-5-11-r85

Huang, J. T., Wang, Q., Park, W., Feng, Y., Kumar, D., Meeley, R., et al. (2017). Competitive ability of maize pollen grains requires paralogous serine threonine protein kinases STK1 and STK2. *Genetics* 207, 1361–1370. doi: 10.1534/genetics.117.300358

Hulskamp, M., Schneitz, K., and Pruitt, R. E. (1995). Genetic evidence for a long-range activity that directs pollen tube guidance in *Arabidopsis*. *Plant Cell* 7, 57–64. doi: 10.1105/tpc.7.1.57

Hulzink, R. J., de Groot, P. F., Croes, A. F., Quaedvlieg, W., Twell, D., Wullems, G. J., et al. (2002). The 5′-untranslated region of the ntp303 gene strongly enhances translation during pollen tube growth, but not during pollen maturation. *Plant Physiol.* 129, 342–353. doi: 10.1104/pp.001701

Hulzink, R. J., Weerdesteyn, H., Croes, A. F., Gerats, T., van Herpen, M. M., and van Helden, J. (2003). In silico identification of putative regulatory sequence elements in the 5′-untranslated region of genes that are expressed during male gametogenesis. *Plant Physiol.* 132, 75–83. doi: 10.1104/pp.102.014894

Johnson, M. A., Harper, J. F., and Palanivelu, R. (2019). A fruitful journey: pollen tube navigation from germination to fertilization. *Annu. Rev. Plant Biol.* 70, 809–837. doi: 10.1146/annurev-arplant-050718-100133

Kaya, H., Nakajima, R., Iwano, M., Kanaoka, M. M., Kimura, S., Takeda, S., et al. (2014). Ca2+-activated reactive oxygen species production by *Arabidopsis* RbohH and RbohJ is essential for proper pollen tube tip growth. *Plant Cell* 26, 1069–1080. doi: 10.1105/tpc.113.120642

Kim, Y. J., Zhang, D., and Jung, K. H. (2019). Molecular basis of pollen germination in cereals. *Trends Plant Sci.* 24, 1126–1136. doi: 10.1016/j.tplants.2019.08.005

Koster, T., Marondedze, C., Meyer, K., and Staiger, D. (2017). RNA-binding proteins revisited - the emerging *Arabidopsis* mRNA interactome. *Trends Plant Sci.* 22, 512–526. doi: 10.1016/j.tplants.2017.03.009

Kramer, M. C., Anderson, S. J., and Gregory, B. D. (2018). The nucleotides they are a-changin': function of RNA binding proteins in post-transcriptional messenger RNA editing and modification in *Arabidopsis*. *Curr. Opin. Plant Biol.* 45(Pt A), 88–95. doi: 10.1016/j.pbi.2018.05.010

Krueger, B. J., Jeronimo, C., Roy, B. B., Bouchard, A., Barrandon, C., Byers, S. A., et al. (2008). LARP7 is a stable component of the 7SK snRNP while P-TEFb, HEXIM1 and hnRNP A1 are reversibly associated. *Nucleic Acids Res.* 36, 2219–2229. doi: 10.1093/nar/gkn061

Lago, C., Clerici, E., Dreni, L., Horlow, C., Caporali, E., Colombo, L., et al. (2005). The *Arabidopsis* TFIID factor AtTAF6 controls pollen tube growth. *Dev. Biol.* 285, 91–100. doi: 10.1016/j.ydbio.2005.06.006

Lahr, R. M., Mack, S. M., Héroux, A., Blagden, S. P., Bousquet-Antonelli, C., Deragon, J. M., et al. (2015). The La-related protein 1-specific domain repurposes HEAT-like repeats to directly bind a 5′TOP sequence. *Nucleic Acids Res.* 43, 8077–8088. doi: 10.1093/nar/gkv748

Lalanne, E., and Twell, D. (2002). Genetic control of male germ unit organization in *Arabidopsis*. *Plant Physiol.* 129, 865–875. doi: 10.1104/pp.003301

Li, Y., Segal, G., Wang, Q., and Dooner, H. K. (2013). Gene tagging with engineered Ds elements in maize. *Methods Mol. Biol.* 1057, 83–99. doi: 10.1007/978-1-62703-568-2_6

Lopes, A. L., Moreira, D., Ferreira, M. J., Pereira, A. M., and Coimbra, S. (2019). Insights into secrets along the pollen tube pathway in need to be discovered. *J. Exp. Bot.* 70, 2979–2992. doi: 10.1093/jxb/erz087

Maraia, R. J., Mattijssen, S., Cruz-Gallardo, I., and Conte, M. R. (2017). The La and related RNA-binding proteins (LARPs): structures, functions, and evolving perspectives. *Wiley Interdiscip. Rev. RNA* 8:e1430. doi: 10.1002/wrna.1430

Martino, L., Pennell, S., Kelly, G., Busi, B., Brown, P., Atkinson, R. A., et al. (2015). Synergic interplay of the La motif, RRM1 and the interdomain linker of LARP6 in the recognition of collagen mRNA expands the RNA binding repertoire of the La module. *Nucleic Acids Res.* 43, 645–660. doi: 10.1093/nar/gku1287

Mennie, A. K., Moser, B. A., and Nakamura, T. M. (2018). LARP7-like protein Pof8 regulates telomerase assembly and poly(A)+TERRA expression in fission yeast. *Nat. Commun.* 9:586. doi: 10.1038/s41467-018-02874-0

Merret, R., Descombin, J., Juan, Y. T., Favory, J. J., Carpentier, M. C., Chaparro, C., et al. (2013a). XRN4 and LARP1 are required for a heat-triggered mRNA decay pathway involved in plant acclimation and survival during thermal stress. *Cell Rep.* 5, 1279–1293. doi: 10.1016/j.celrep.2013.11.019

Merret, R., Martino, L., Bousquet-Antonelli, C., Fneich, S., Descombin, J., Billey, E., et al. (2013b). The association of a La module with the PABP-interacting motif PAM2 is a recurrent evolutionary process that led to the neofunctionalization of La-related proteins. *RNA* 19, 36–50. doi: 10.1261/rna.035469.112

Park, J. I., Endo, M., Kazama, T., Saito, H., Hakozaki, H., Takada, Y., et al. (2006). Molecular characterization of two anther-specific genes encoding putative RNA-binding proteins. AtRBP45s, in *Arabidopsis thaliana*. *Genes Genet. Syst.* 81, 355–359. doi: 10.1266/ggs.81.355

Pina, C., Pinto, F., Feijo, J. A., and Becker, J. D. (2005). Gene family analysis of the *Arabidopsis* pollen transcriptome reveals biological implications for cell growth, division control, and gene expression regulation. *Plant Physiol.* 138, 744–756. doi: 10.1104/pp.104.057935

Prall, W., Sharma, B., and Gregory, B. D. (2019). Transcription is just the beginning of gene expression regulation: the functional significance of RNA-binding proteins to post-transcriptional processes in plants. *Plant Cell Physiol.* 60, 1939–1952. doi: 10.1093/pcp/pcz067

Procissi, A., de Laissardière, S., Férault, M., Vezon, D., Pelletier, G., and Bonhomme, S. (2001). Five gametophytic mutations affecting pollen development and pollen tube growth in *Arabidopsis thaliana*. *Genetics* 158, 1773–1783.

Reese, J. B., and Williams, J. H. (2019). How does genome size affect the evolution of pollen tube growth rate, a haploid performance trait? *Am. J. Bot.* 106, 1011–1020. doi: 10.1002/ajb2.1326

Reňák, D., Dupl'áková, N., and Honys, D. (2012). Wide-scale screening of T-DNA lines for transcription factor genes affecting male gametophyte development in *Arabidopsis*. *Sex Plant Reprod.* 25, 39–60. doi: 10.1007/s00497-011-0178-8

Rutley, N., and Twell, D. (2015). A decade of pollen transcriptomics. *Plant Reprod.* 28, 73–89. doi: 10.1007/s00497-015-0261-7

Scarpin, M. R., Leiboff, S., and Brunkard, J. O. (2020). Parallel global profiling of plant TOR dynamics reveals a conserved role for LARP1 in translation. *eLife* 9:e58795. doi: 10.7554/eLife.58795

Scarpin, M. R., Sigaut, L., Temprana, S. G., Boccaccio, G. L., Pietrasanta, L. I., and Muschietti, J. P. (2017). Two *Arabidopsis* late pollen transcripts are detected in cytoplasmic granules. *Plant Direct.* 1:e00012. doi: 10.1002/pld3.12

Schindelin, J., Arganda-Carreras, I., Frise, E., Kaynig, V., Longair, M., Pietzsch, T., et al. (2012). Fiji: an open-source platform for biological-image analysis. *Nat. Methods* 9, 676–682. doi: 10.1038/nmeth.2019

Schreiber, D. N., and Dresselhaus, T. (2003). In vitro pollen germination and transient transformation ofZea mays and other plant species. *Plant Mol. Biol.Rep.* 21, 31–41. doi: 10.1007/BF02773394

Tamura, K., Stecher, G., Peterson, D., Filipski, A., and Kumar, S. (2013). MEGA6: molecular evolutionary genetics analysis version 6.0. *Mol. Biol. Evol.* 30, 2725–2729. doi: 10.1093/molbev/mst197

Tattersall, E. A. R., Ergul, A., AlKayal, F., DeLuc, L., Cushman, J. C., and Cramer, G. R. (2005). Comparison of methods for isolating high-quality RNA from leaves of grapevine. *Am. J. Enol. Vit.* 56, 400–406.

Walbot, V., and Evans, M. M. (2003). Unique features of the plant life cycle and their consequences. *Nat. Rev. Genet.* 4, 369–379. doi: 10.1038/nrg1064

Walley, J. W., Sartor, R. C., Shen, Z., Schmitz, R. J., Wu, K. J., Urich, M. A., et al. (2016). Integration of omic networks in a developmental atlas of maize. *Science* 353, 814–818. doi: 10.1126/science.aag1125

Wan, X., Wu, S., Li, Z., Dong, Z., An, X., Ma, B., et al. (2019). Maize genic male-sterility genes and their applications in hybrid breeding: progress and perspectives. *Mol. Plant* 12, 321–342. doi: 10.1016/j.molp.2019.01.014

Warman, C., Panda, K., Vejlupkova, Z., Hokin, S., Unger-Wallace, E., Cole, R. A., et al. (2020). High expression in maize pollen correlates with genetic contributions to pollen fitness as well as with coordinated transcription from neighboring transposable elements. *PLoS Genet.* 16:e1008462. doi: 10.1371/journal.pgen.1008462

Warman, C., Sullivan, C. M., Preece, J., Buchanan, M. E., Vejlupkova, Z., Jaiswal, P., et al. (2021). A cost-effective maize ear phenotyping platform enables rapid categorization and quantification of kernels. *Plant J.* doi: 10.1111/tpj.15166

Wolin, S. L., and Cedervall, T. (2002). The La protein. *Annu. Rev. Biochem.* 71, 375–403.

Zhang, B., Jia, J., Yang, M., Yan, C., and Han, Y. (2012). Overexpression of a LAM domain containing RNA-binding protein LARP1c induces precocious leaf senescence in *Arabidopsis*. *Mol. Cells* 34, 367–374. doi: 10.1007/s10059-012-0111-5

Conflict of Interest: The authors declare that the research was conducted in the absence of any commercial or financial relationships that could be construed as a potential conflict of interest.

frontiers in Plant Science

ORIGINAL RESEARCH
published: 07 July 2021
doi: 10.3389/fpls.2021.701286

The Role of INAPERTURATE POLLEN1 as a Pollen Aperture Factor Is Conserved in the Basal Eudicot *Eschscholzia californica* (Papaveraceae)

*Ismael Mazuecos-Aguilera[1], Ana Teresa Romero-García[1], Božena Klodová[2,3], David Honys[2], María C. Fernández-Fernández[4], Samira Ben-Menni Schuler[1], Anna A. Dobritsa[5] and Víctor N. Suárez-Santiago[1]**

[1] Department of Botany, Faculty of Sciences, University of Granada, Granada, Spain, [2] Laboratory of Pollen Biology, Institute of Experimental Botany of the Czech Academy of Sciences, Prague, Czechia, [3] Department of Experimental Plant Biology, Faculty of Science, Charles University, Prague, Czechia, [4] Department of Cell Biology, Faculty of Sciences, University of Granada, Granada, Spain, [5] Department of Molecular Genetics and Center for Applied Plant Sciences, Ohio State University, Columbus, OH, United States

OPEN ACCESS

Edited by:
Stefan de Folter,
UGA-Langebio, Center for Research and Advanced Studies (CINVESTAV), Mexico

Reviewed by:
Silvia Vieira Coimbra,
University of Porto, Portugal
Lei Guo,
University of Maryland, College Park, United States

***Correspondence:**
Víctor N. Suárez-Santiago
vsuarez@ugr.es

Specialty section:
This article was submitted to Plant Development and EvoDevo, a section of the journal Frontiers in Plant Science

Received: 27 April 2021
Accepted: 17 June 2021
Published: 07 July 2021

Citation:
Mazuecos-Aguilera I, Romero-García AT, Klodová B, Honys D, Fernández-Fernández MC, Ben-Menni Schuler S, Dobritsa AA and Suárez-Santiago VN (2021) The Role of INAPERTURATE POLLEN1 as a Pollen Aperture Factor Is Conserved in the Basal Eudicot Eschscholzia californica (Papaveraceae). Front. Plant Sci. 12:701286. doi: 10.3389/fpls.2021.701286

Pollen grains show an enormous variety of aperture systems. What genes are involved in the aperture formation pathway and how conserved this pathway is in angiosperms remains largely unknown. *INAPERTURATE POLLEN1* (*INP1*) encodes a protein of unknown function, essential for aperture formation in Arabidopsis, rice and maize. Yet, because INP1 sequences are quite divergent, it is unclear if their function is conserved across angiosperms. Here, we conducted a functional study of the *INP1* ortholog from the basal eudicot *Eschscholzia californica* (*EcINP1*) using expression analyses, virus-induced gene silencing, pollen germination assay, and transcriptomics. We found that *EcINP1* expression peaks at the tetrad stage of pollen development, consistent with its role in aperture formation, which occurs at that stage, and showed, via gene silencing, that the role of *INP1* as an important aperture factor extends to basal eudicots. Using germination assays, we demonstrated that, in *Eschscholzia*, apertures are dispensable for pollen germination. Our comparative transcriptome analysis of wild-type and silenced plants identified over 900 differentially expressed genes, many of them potential candidates for the aperture pathway. Our study substantiates the importance of *INP1* homologs for aperture formation across angiosperms and opens up new avenues for functional studies of other aperture candidate genes.

Keywords: *Eschscholzia californica*, INAPERTURATE POLLEN1, Papaveraceae, pollen, pollen aperture, RNA-seq, transcriptome analysis, VIGS

INTRODUCTION

Pollen, the male gametophyte of spermatophytes, is surrounded by a robust, sporopollenin-based pollen wall, called exine, which isolates and protects it from the external environment (Ariizumi and Toriyama, 2011). Although most of the pollen surface is covered by exine, in many plants certain regions of the pollen surface receive little to no exine deposition. These regions, known as

pollen apertures, represent some of the most characteristic and well-defined elements of the pollen surface (Furness and Rudall, 2004; Zhou and Dobritsa, 2019). Apertures often serve as the sites for pollen tube exit (Heslop-Harrison and Heslop-Harrison, 1985; Edlund et al., 2004; Edlund et al., 2016). They are also involved in the exchange of water and solutes with the medium and allow the rigid exine to adjust to changes in pollen volume due to dehydration/rehydration during pollination (Heslop-Harrison, 1979).

Numerous studies have been carried out to characterize the large diversity of aperture patterns in angiosperms (e.g., Wodehouse, 1935; Blackmore et al., 1995; Furness and Rudall, 2004; Pérez-Gutiérrez et al., 2015; Wortley et al., 2015; Matamoro-Vidal et al., 2016). Although the number, morphology and position of apertures often vary among species, these attributes usually remain stable at the intraspecific level, suggesting a genetic control of aperture patterning which changed multiple times during the evolution of flowering plants. However, few studies so far have probed the molecular mechanisms of aperture formation.

Genetic screening in *Arabidopsis thaliana* has made it possible to identify mutants defective in aperture formation (Dobritsa et al., 2011; Lee et al., 2018; Plourde et al., 2019). One of the genes discovered in these screens, *INAPERTURATE POLLEN1* (*INP1*), encodes a protein of unknown function that is essential for aperture formation (Dobritsa and Coerper, 2012). In the Arabidopsis *inp1* mutant, pollen completely lacks apertures, producing inaperturate phenotype.

During pollen development, Arabidopsis *INP1* (*AtINP1*) first becomes expressed in pollen mother cells, where its protein is evenly distributed in the cytoplasm. Later, at the post-meiotic tetrad stage, INP1 accumulates at the specific plasma-membrane (PM) regions in each microspore (the predecessor of the pollen grain) and assembles into punctate lines at the sites where apertures will be formed (Dobritsa and Coerper, 2012; Dobritsa et al., 2018). Arabidopsis *INP1* reaches peak expression at the tetrad stage, and after the release of microspores from tetrads its expression quickly disappears. At the aperture PM domains, AtINP1 appears to localize at the interface between the PM and the callose wall surrounding the tetrad of microspores, where it may act as a bridge, keeping the aperture domains of each microspore attached to the callose wall to prevent sporopollenin deposition at these regions (Dobritsa et al., 2018). It is not known whether AtINP1 interacts with other proteins to form these bridges (Zhou and Dobritsa, 2019).

Although both aperture patterns and the INP1 protein sequences are quite divergent across angiosperms, the involvement of INP1 proteins in the process of aperture formation seems to be conserved, as indicated by the loss of apertures in the *inp1* mutants of maize and rice (Li et al., 2018; Zhang et al., 2020). Normally, these two monocot species have the ulcerate aperture pattern characteristic of the Poaceae family, with a single pore-like polar aperture, very different from the typical eudicot tricolpate pattern of Arabidopsis pollen, with its three meridional furrows. Also, while the INP1 protein sequences are very similar between maize and rice, they share only ∼35% sequence identity with AtINP1 (Dobritsa and Coerper, 2012; Li et al., 2018). It was, therefore, surprising that these quite divergent proteins are all involved in the same process. Like AtINP1, the rice INP1 (OsINP1) localizes to the aperture PM domains in microspores, assembling into a single ring-like structure that pre-marks the position of a single pore-like aperture (Zhang et al., 2020). Interestingly, although *inp1* pollen in Arabidopsis is fertile, *inp1* pollen in rice and maize loses its ability to germinate pollen tubes and becomes completely sterile, demonstrating that apertures in these species, but not in Arabidopsis, are essential for pollen fertility.

Although the INP1 homologs from several species are all involved in the same process, they cannot readily substitute for each other. The sequence divergence among INP1 homologs was suggested to be responsible for the fact that only proteins from closely related species from Brassicaceae were able to restore apertures in the Arabidopsis *inp1* mutants during the interspecific complementation experiments, while the orthologs from Solanaceae, Papaveraceae, and Poaceae were unable to do it (Dobritsa and Coerper, 2012; Li et al., 2018). Based on these results, the need for species-specific partners to cooperate with INP1 in the control of aperture formation was postulated (Li et al., 2018). However, a functional analysis of the INP1 homologs from more plant lineages is necessary to ascertain that the role of INP1 as an aperture factor is conserved across angiosperms.

In this study, we investigated the functional conservation of the INP1 ortholog EcINP1 from *Eschscholzia californica* (California poppy), a species of Papaveraceae family. This is an early divergent family within the order Ranunculales, the lineage that first diverged from the large group of eudicots (Wang et al., 2009; Hoot et al., 2015). At the base of the eudicot clade there was a transition in the pollen grain aperture system, from pollen with one polar aperture –typical of basal angiosperms and monocots– to pollen with three apertures in equatorial positions, which may have been a key innovation involved in the success and diversification of eudicots (Furness and Rudall, 2004). Because of the phylogenetic position of Ranunculales, between monocots and the core eudicots, and its high pollen aperture system diversity (Blackmore et al., 1995; Pérez-Gutiérrez et al., 2016; Zhang et al., 2017), the Ranunculales species provide the opportunity to study the conservation of genetic mechanisms involved in the aperture system and its evolution. Unlike pollen from the species in which INP1 was previously studied, pollen of *E. californica* develops between five and seven colpate apertures. AtINP1 and EcINP1 share only ∼44% sequence identity, and it was previously shown that EcINP1 cannot substitute for AtINP1 in Arabidopsis (Li et al., 2018). However, it remained unclear if this was due to the EcINP1's dependence on additional factors from *E. californica* or because EcINP1 is no longer involved in aperture formation. Here, we (1) analyzed patterns of *EcINP1* expression to demonstrate that it is also expressed in anthers during the tetrad stage of pollen development, (2) inactivated *EcINP1* with virus-induced gene silencing (VIGS) to reveal that the *INP1* involvement in aperture formation is conserved in *E. californica*, (3) tested whether pollen germination in this species requires the presence of apertures, and (4) identified genes whose expression was affected by the silencing of *EcINP1*,

which might represent candidates involved in the aperture formation mechanisms.

MATERIALS AND METHODS

Plant Material

The seeds of *Eschscholzia californica* Cham. were purchased from the company Seedaholic (Cloghbrack, Clonbur, Galway, Ireland). They were sown in pots ($9 \times 9 \times 9$ cm^3) with universal substrate and vermiculite mixed in a 3:1 ratio and kept in a greenhouse at a temperature range between 26 and 14°C under a light/dark cycle of 16/8 h. Each pot was fertilized once at the beginning of the experiment and watered every day.

DNA/RNA Extraction, PCR Amplification of *EcINP1* Analysis of Intraspecific Variability, and Phylogenetic Analysis

Genomic DNA (gDNA) was isolated from fresh leaves using the NucleoSpin® Plant II Kit (Macherey-Nagel GmbH and Co., Germany), and total RNA was extracted using the NucleoSpin® RNA Plant kit (Macherey-Nagel GmbH and Co., Germany), following the manufacturer's instructions. 1 μg of RNA was reverse-transcribed to cDNA using SuperScript III Reverse Transcriptase (Invitrogen, Karlsruhe, Germany) and oligo(dT)18 (ThermoFisher Scientific, United States).

The full-length coding sequence of *EcINP1* was published in Li et al. (2018; ENA accession number LT840341). To study intraspecific variation of *EcINP1*, PCR amplification was carried out on both gDNA and cDNA from bulked individuals (5 individuals for gDNA and 5 for cDNA) using the primers EcaINP1-F and EcaINP1-R (Li et al., 2018; **Supplementary Table 1**). PCR products were cloned using the Strataclon blunt PCR cloning kit (Agilent Technologies, United States), and 17 cDNA and 10 gDNA clones were sequenced. In addition, we included four sequences from the RNA-seq data generated in our laboratory, the sequence published in Li et al. (2018), one complete sequence from the 1000 Plants Project (1KP; Wickett et al., 2014), and the genomic sequence retrieved from the *Eschscholzia* Genome Database (Hori et al., 2018). The nucleotide sequences were aligned in Bioedit (Hall, 1999) and, after intron removal from the gDNA sequences, the observed genetic distances (*p*-distance) were estimated with MEGA X (Kumar et al., 2018).

For phylogenetic analyses, nucleotide sequences from other Papaveraceae and different angiosperm species were obtained by BLAST searches from NCBI, 1KP, Phytozome[1], and Phytometasyn (Xiao et al., 2013[2]) databases (**Supplementary Table 2**). Sequences from the same species with DNA identity of >95% were regarded as possible alleles, so only one sequence was considered. After translating the nucleotide sequences, all the protein sequences were aligned using the Clustal algorithm in Bioedit and adjusted manually. The aligned sequences were used to generate a Maximum Likelihood (ML) tree. The ML analysis was performed with the program PhyML v3.0 (Guindon and Gascuel, 2003) through the web platform "ATCG: Montpellier Bioinformatics Platform," applying the substitution model JTT automatically selected by Smart Model Selection in PhyML (Lefort et al., 2017) and the Akaike Information Criterion (AIC; Akaike, 1974). The search for the optimal tree was carried out using the subtree-pruning and regrafting algorithm from five random starting trees generated by the parsimony algorithm (Guindon et al., 2010). Branch support was assessed using the approximated likelihood ratio test (aLRT) with the Shimodaira-Hasegawa-like test interpretation (Anisimova and Gascuel, 2006; Guindon et al., 2010).

A ML phylogenetic analysis was also performed to establish the homology relationships of two genes of interest, identified by transcriptome analyses (see below), related to the AGC1 group kinases from Arabidopsis. This analysis was based on the protein sequences of the kinase domain of all AGC1 kinases from Arabidopsis and those sequences obtained by BLAST from the genomes of *E. californica* and *Papaver somniferum*. The sequences of the AGC3-group kinases from Arabidopsis were used as an outgroup. Sequence alignment and ML analysis were conducted as described above.

Semi-Quantitative Reverse Transcription-Polymerase Chain Reaction (Semi-qRT-PCR) and Quantitative RT-PCR (qRT-PCR)

The spatial pattern of expression of the *EcINP1* gene was tested by semi-qRT-PCR on vegetative organs, floral organs of flowers at anthesis, and immature and mature fruits. The temporal expression pattern in anthers at different stages of pollen development was tested by qRT-PCR. Stages of pollen development were determined by optical microscopy (Olympus-CX31, Japan) using glycerin gelatine with basic fuchsin (50 ml of glycerin, 7 g of gelatine, 1 g of phenol, a few crystals of basic fuchsin, and 42 ml of distilled water) pre-warmed to 30–35°C before staining pollen grains. RNA extraction and cDNA synthesis were performed as described above and cDNA pools were diluted to 50 ng/μl for subsequent semi-qRT-PCR and qRT-PCR analyses. Quantitative RT-PCR was also used to test for reduction in the *EcINP1* expression in the VIGS experiments, to validate the expression levels of eight genes of interest selected with the help of transcriptome analyses, and to analyse the temporal expression pattern of three of these eight genes throughout pollen ontogeny. *ACTIN* served as the reference gene for calculating the relative expression intensities in both semi-qRT-PCR and qRT-PCR analyses, using the $2^{\Delta\ \Delta\ Ct}$ method (Livak and Schmittgen, 2001). Quantitative RT-PCR was performed using the FastGene IC Green 2x qPCR mix (NIPPON Genetics, Tokyo, Japan) according to the manufacturer's instructions, and the qTower 2.2 real-time PCR thermocycler (Analytik Jena, Germany). Gene-specific primers used for semi-qRT-PCR and qRT-PCR reactions were designed using the software Primer3 (Untergasser et al., 2012; **Supplementary Table 1**). All experiments were repeated with three biological and three technical replicates.

[1]https://phytozome.jgi.doe.gov/pz/portal.html

[2]https://bioinformatics.tugraz.at/phytometasyn/

Western Blot

Anthers of wild-type plants were collected when pollen grains were at the pre-meiosis, tetrad, microspore and mature stages. For protein extraction, the anthers were crushed in the extraction buffer (50 mM Tris-HCl, 9 M Urea, 1% (v/v) Triton X-100, pH 7.4), and the insoluble material was removed by centrifugation at 10,000 g for 10 min at 4°C. The protein extracts were subjected to sodium dodecyl sulfate–polyacrylamide gel electrophoresis (SDS-PAGE). Protein profiles were determined by means of Stain-free technology using a Gel DocTM EZ System (Bio-Rad; **Supplementary Figure 1**), and were used as a loading control as described by Welinder and Ekblad (2011) and using AlphaView software (Cell Biosciences, Santa Clara, CA) for protein quantification. Proteins were electroblotted from the gel onto a PVDF membrane in a Semi-Dry Transfer Cell (Bio-Rad), and the membrane was blocked for 1 h at room temperature in Tris-buffered saline (TBS) buffer, pH 7.4 containing 5% (w/v) defatted milk and 0.1% (v/v) Tween-20. Immunodetection of EcINP1 was carried out by incubation with a polyclonal antibody SAN-ESK generated against the epitope ESKQEILKTVEKDLMVEIEE (synthesized by Davids Biotechnologie GmbH, Regensburg, Germany) diluted 1:500 in TBS buffer (pH 7.4) containing 0.3% (v/v) Tween-20, overnight at 4°C. An HRP-conjugated anti-chicken IgY (Abcam, ref. ab97135, Cambridge, United Kingdom), diluted 1:2000, served as the secondary antibody. Protein bands were visualized in a C-Digit scanner (LI-COR Biotechnology, United States).

Virus Induced Gene-Silencing

The tobacco rattle virus (TRV)-based system (Liu et al., 2002) was used for VIGS experiments. A pTRV2:*EcINP1* construct was made by cloning a 480-bp fragment of the *EcINP1* coding region, amplified with the Phusion High-Fidelity DNA polymerase (ThermoFisher Scientific, United States) and primers EcaINP1-F2-*Eco*RI and EcaINP1-R2-*Bam*HI (**Supplementary Table 1**), between the *Eco*RI and *Bam*HI restriction sites. pTRV2:*EcINP1* as well as negative- and positive-control constructs (respectively, pTRV2:empty, without any insert, and pTRV2:*PDS*, with a fragment of the phytoene desaturase gene) were transformed into *Agrobacterium tumefaciens* strain pGV3101. Three-week-old plants were inoculated with *Agrobacterium* in the hypocotyl following Tekleyohans et al. (2013) and left at 4°C overnight, after which they were transferred to the greenhouse at a temperature range between 15 and 24°C. 78 plants were infected with pTRV2:*EcINP1*, 15 with pTRV2:*PDS*, and 30 with pTRV2:empty. In addition, 50 non-treated plants were grown to observe the wild-type phenotype.

Pollen phenotypes were observed by optical microscopy in the fully open flowers. For 55 plants, pollen was collected from three flowers and three anthers per flower and stained with glycerin gelatine with basic fuchsin. Phenotypes were classified as follows: wild-type, with normal 5-7-colpate apertures; inaperturate, without apertures; and affected, with abnormal apertures that were shorter or shallower than normal. In addition, anthers from three *EcINP1*-silenced plants and three wild-type plants were fixed according to Fernández et al. (1992) and pollen was observed with a scanning electron microscope (model SMT; Zeiss) at the Centro de Instrumentación Científica (University of Granada). Pollen was also stained with auramine O as previously described (Reeder et al., 2016) and observed with confocal microscopy (Nikon A1+, Japan).

In order to test the effectiveness of VIGS, the expression levels of *EcINP1* were measured by qRT-PCR on the first bud (2–3 mm; pollen at the tetrad/free-microspore stage) of four silenced (one with the affected phenotype and three with the inaperturate phenotype) and three non-silenced (pTRV2:empty; wild-type phenotype) plants, as described above.

In vitro Pollen Germination

Pollen grains were cultured for 2 h on plates with 5 ml of liquid germination medium (15 g sucrose, 30 mg $Ca(NO_3)_2$, 20 mg $MgSO_4$, 10 mg KNO_3, and 10 mg H_3BO_3 in 100 ml of distilled water) at 25°C under moist conditions and in the dark. For both wild-type and inaperturate pollen from three wild-type plants and two VIGS plants, we counted 100 pollen grains from three anthers per flower and three flowers per plant. The pollen count was carried out using an inverted optical microscope (ZEISS Axio Scope A1, Germany) and, after checking the normality of the data, an analysis of variance (ANOVA) was carried out using IBM SPSS statistics (SPSS Inc., IBM Company, 2020).

Transcriptome Sequencing, RNA-seq Data Analysis and Annotation

RNA from anthers with pollen at the free-microspore stage was extracted from three inaperturate and three wild-type plants as described above. The extracts were sent to Macrogen Inc. (Korea), where libraries were prepared using the Illumina TruSeq Stranded Total RNA Sample Preparation Kit with Ribo-Zero Plant and sequenced on an Illumina Hiseq 2500 platform as 150 nucleotides paired-ends. Raw data was generated using the Illumina package bcl2fastq.

Raw single reads (in FASTQ format) were subjected to sequence quality control using FastQC v0.11.8[3]. Adaptors and low-quality sequences were removed from the data set using TrimGalore v0.6.4[4] and a minimum quality score of 20. The library's characteristics and trimming efficiency were checked and reads aligned to the genome of *Eschscholzia californica*[5] using the software HISAT2 v2.1.0[6] (Pertea et al., 2016). Transcripts were assembled and quantified using the software StringTie v2.0[7], with the merge option (Pertea et al., 2016). Analysis of differentially expressed genes (DEGs) was performed with the DESeq2 R package (v1.24.0) using the coverage produced by StringTie. DEGs were annotated by BLASTX search against the genome of *Papaver somniferum*[8] and the SwissProt Database[9], using default

[3]http://www.bioinformatics.babraham.ac.uk/projects/fastqc/

[4]https://github.com/FelixKrueger/TrimGalore

[5]ftp://ftp.kazusa.or.jp/pub/eschscholzia/ECA_r1.0.cds.fa.gz

[6]https://ccb.jhu.edu/software/hisat2/

[7]https://ccb.jhu.edu/software/stringtie/

[8]https://www.ncbi.nlm.nih.gov/assembly/GCF_003573695.1

[9]https://data.broadinstitute.org/Trinity/Trinotate_v3_RESOURCES/uniprot_sprot.pep.gz

parameters and extracting only the top hit for each sequence. To assign a function to each DEG, annotated DEGs were further annotated with Gene Ontology (GO, Ashburner et al., 2000) and Kyoto Encyclopedia of Genes and Genomes (KEGG, Kanehisa and Goto, 2000) databases using the Blast2GO v5.2.5 application (Götz et al., 2008) and the GhostKoala mapping tool (Kanehisa et al., 2016), respectively. To predict putative plant transcription factors (TF), coding sequences were aligned to TF domains from the Plant Transcription Factor Database (PlantTFDB, Zhang et al., 2011).

To validate the gene expression results, qRT-PCR experiments were performed for eight DEGs. These genes were selected because their predicted functions make them interesting candidates for a role in pollen aperture formation. The primer sequences used are listed in **Supplementary Table 1**.

Data Availability

All raw sequences for transcriptome are available in the European Nucleotide Archive (ENA) under the accession numbers ERS6376182-ERS6376184 for wild-type samples and ERS6376185-ERS6376187 for VIGS-treated samples.

RESULTS

Intraspecific Variability and Phylogeny of *EcINP1*

INP1 is a novel protein whose structure and domain organization are not well understood. Previously, AtINP1 was divided into five regions, based on their evolutionary conservation and position relative to the single predicted domain in this protein, the domain of unknown function DOG1 (Li et al., 2018). To better understand the relative importance of different INP1 regions, we explored the extent of the intraspecific variation of the EcINP1 sequences. To this end, we amplified and analyzed the gDNA and cDNA sequences from multiple plants of *E. californica*, as well as retrieved information from sequence databases. In total, we obtained 34 different *EcINP1* sequences: 31 by us (17 from cDNA, 10 from gDNA, and four from our RNA-seq data) and three from databases (two transcriptomic and one genomic sequences). After *in silico* translating these sequences, we found that five cDNA sequences had substitutions resulting in stop codons, and those were removed from the alignment and not analyzed further. The combination of sequences obtained from cDNA and gDNA made it possible to determine the location of an intron near the beginning of the coding sequence (as in *INP1* orthologs from several other species), as well as to discover a possible second intron, which was found in four cases near the very end of the coding sequence, suggesting the existence of a second possible transcript isoform (**Supplementary Figure 2**).

The intraspecific variation of *EcINP1* was low. The mean observed genetic distance between sequences was 0.92%, with a total of 34 variable nucleotide positions. In 11 sequences, an insertion of one triplet (AAT) was present at the beginning of the acidic domain (one of the protein regions proposed for AtINP1 by Li et al., 2018). All pairwise comparisons were always at more than 97.5% sequence identity. At the protein level, the number of variable positions was 17, distributed within the protein regions as follows: 3 N-terminal; 5 DOG1; 3 acidic; 2 middle; 4 C-terminal. The sequences with the extra triplet in the acidic region contained an extra asparagine, and one of the transcripts included three additional amino acidic residues at the end of the C-terminal domain (**Supplementary Figure 2**, sequence 5).

Curiously, in our intraspecific library of *EcINP1* we uncovered a sequence with significant homology to multiple dispersed *EcINP1* fragments that also included 255 bp of the ubiquitin-like domain-containing CTD phosphatase (**Supplementary Figure 3**, *EcUBCL1*). Portions of this sequence correspond to fragments from the *5'UTR*, the N-terminal region, the DOG1 domain, the acidic region, as well as portions of the C-terminal region and the 3'UTR of *EcINP1* (**Supplementary Figure 3**). This sequence was also found by BLAST searches in the GenBank (JG611242), the 1KP (TUHA-2032598, NJKC-2028667, RKGT-2014503, EVOD-2107709), and the *Eschscholzia* Genome (Eca_sc001433.1_4218210.424882) databases. We performed a VIGS experiment to silence this sequence, using a 493 bp region that included the ubiquitin-like domain-containing CTD phosphatase region (**Supplementary Figure 3**; see **Supplementary Table 1** for primer sequences), but did not observe any abnormal phenotypes in the treated plants (data not shown), so the functional significance of this chimeric sequence remains unknown.

To verify the relationships of the *EcINP1* gene with *INP1* homologs from other plants, we conducted a phylogenetic analysis using sequences from other members of Papaveraceae and from other angiosperm species. The ML tree shows that EcINP1 is grouped with the rest of INP1 sequences from Papaveraceae, which all fall into the Ranunculales clade, together with sequences from Ranunculaceae and Berberidaceae (**Figure 1**). In general, the INP1 tree follows a pattern according to the angiosperm phylogeny.

EcINP1 Is Expressed in Anthers During Pollen Aperture Development

To test where EcINP1 is expressed, we performed a semi-qRT-PCR on multiple plant organs. *EcINP1* transcripts were found in all tested vegetative, floral, and fruit organs. The highest signal intensity was observed in stamens, followed by the gynoecium (**Figure 2A**).

We then used qRT-PCR to assess the pattern of temporal expression of *EcINP1* in anthers during different stages of pollen ontogeny (**Figure 2B**). The *EcINP1* expression starts at the end of the microsporogenesis process, during the pre-mother cell stage. It reaches maximal levels during the tetrad stage, and essentially disappears during the microspore stage. We have also developed an antibody against an epitope in the middle region of EcINP1. Western blot analysis on protein extracts from anthers at different stages revealed a main band with a molecular weight corresponding to the ∼35 kDa expected for EcINP1, and a secondary band that might represent protein dimers. This analysis showed that EcINP1 protein was highly expressed at the tetrad stage and was still present at high concentration at the free-microspore stage (**Figure 2C**), suggesting that the protein may

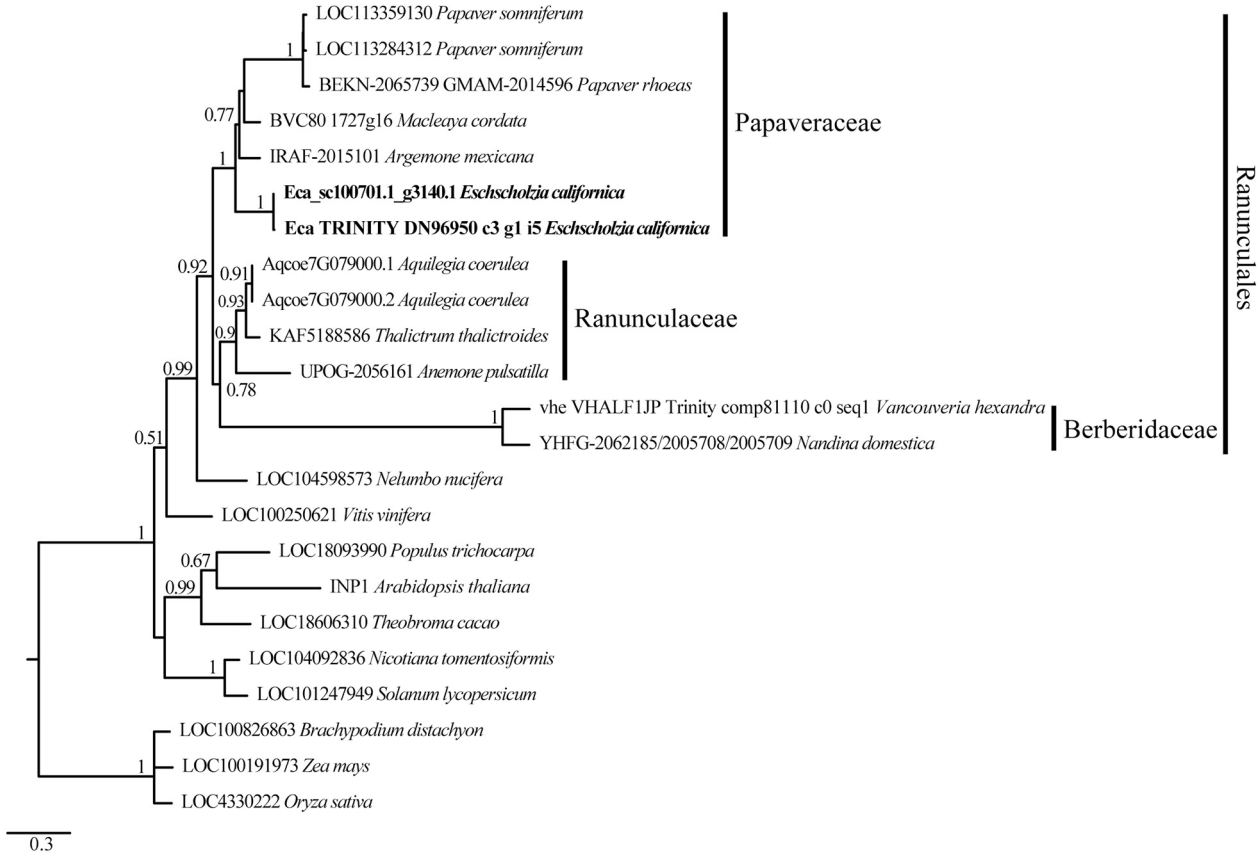

FIGURE 1 | Maximum likelihood phylogenetic tree of INP1-like protein sequences showing EcINP1 homology relationships of *Eschscholzia californica*. The name of each sequence is composed of the locus identifier followed by the species name. Sequence accession numbers can be found in **Supplementary Table 2**. The EcINP1 sequences representing two protein isoforms are in bold type. The families to which the selected sequences from the order Ranunculales belong are indicated on the right.

persist longer than the transcript. Taken together, these results indicate that EcINP1 is produced in developing pollen at the stages concurrent to aperture development.

EcINP1 Is Required for the Formation of Pollen Apertures

To test whether the INP1 involvement in aperture formation is conserved in *E. californica*, we attempted to silence *EcINP1* using the tobacco rattle virus (TRV)-based VIGS system (Liu et al., 2002). To this end, we infected plants with the pTRV2:*EcINP1* construct containing a 480-bp fragment of the *EcINP1* coding region.

The silencing of *EcINP1* did not affect vegetative growth, branching, or leaf morphology in any of the 78 plants treated with pTRV2:*EcINP1*, compared to controls (untreated plants and plants treated with the empty vector). 55 of the 78 pTRV2:*EcINP1* plants flowered and did not show any variation in the floral-organ phenotypes.

Yet, when we examined their pollen, we found that their aperture phenotypes showed significant abnormalities. We observed pollen from 139 flowers (34 plants produced three flowers, 16 plants – two flowers, and 5 plants – one flower), collecting three anthers per flower, so, in total, pollen from 417 anthers was analyzed. Within each anther, all pollen presented the same phenotype, but, occasionally, the phenotypes differed between pollen grains from different anthers of the same flower. 33.3% of the observed anthers in pTRV2:*EcINP1* plants presented pollen with some aperture defect (**Table 1**), compared to 0% in wild-type plants or in those infected with the empty vector. In pTRV2:*EcINP1* plants, 15.3% of anthers had pollen that completely lacked apertures (inaperturate phenotype), while 18% of anthers showed pollen with apertures that were shorter or shallower than normal (affected phenotype) (**Table 1**; **Figure 3A**). This result provides strong evidence that, like its homologs from Arabidopsis, rice and maize, EcINP1 is involved in the formation of pollen apertures.

Since we tracked the developmental order of the flowers collected from each plant, we noticed that the occurrence of anthers with inaperturate pollen often correlated with the order of flower development, decreasing from the oldest flower (the second in development, where the first bud was used to extract RNA) to the youngest flower (the fourth) in the same silenced plant (**Figure 3B**). This was likely due to the decrease of the silencing effect as flowering progressed (Wege et al., 2007).

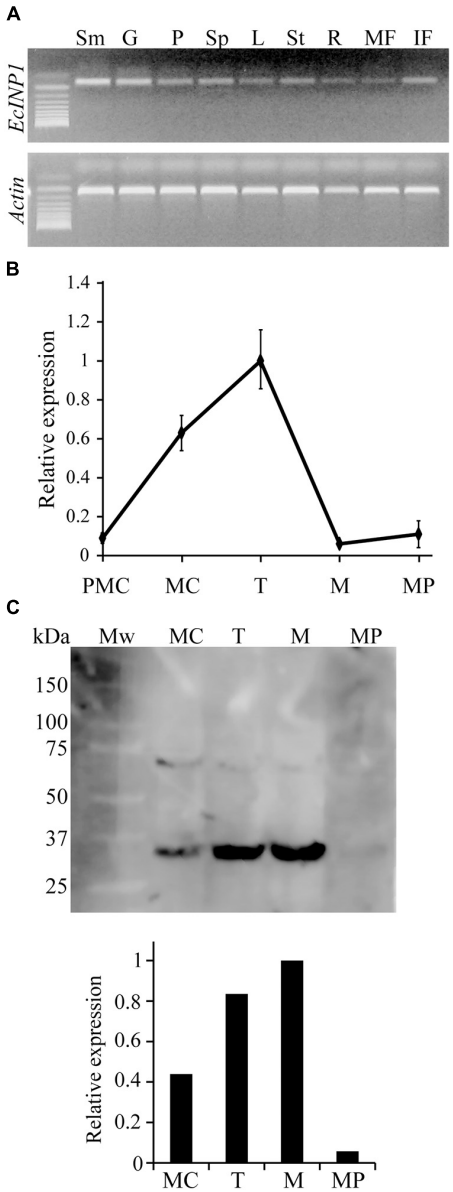

FIGURE 2 | Expression patterns of *EcINP1*. **(A)** Expression analysis of *EcINP1*, based on semi-quantitative RT-PCR, in different plant organs. Sm, stamen; G, gynoecium; P, petal; Sp, sepal; L, leaf; St, stem; R, root; MF, mature fruit; IF, immature fruit. **(B)** qRT-PCR-based expression analysis of *EcINP1* in anthers at different pollen development stages. Actin was used as a normalization control. **(C)** Detection of EcINP1 protein levels by Western blot immunoassay in anthers at different pollen development stages. The bar plot shows the relative expression of EcINP1 (normalized to total proteins detected with a Stain-free technology gel as a loading control and quantified with the AlphaView software). PMC, pre-mother cell; MC, mother cell; T, tetrad; M, microspore; MP, mature pollen.

qRT-PCR performed on young buds confirmed the downregulation of *EcINP1* in the pTRV2:*EcINP1* plants, with an approximately two-fold reduction in the *EcINP1* levels in these plants compared to the plants infected with the empty vector (**Figure 3C**).

TABLE 1 | Summary of VIGS experiments to silence the *EcINP1* gene of *Eschscholzia californica*.

	pTRV2:*EcINP1*	pTRV2:empty	Wild-type
No. of plants observed	78	30	50
No. of flowering plants	55	24	36
No. of anthers observed	417	180	246
No. of anthers with wild-type pollen	278 (66.6%)	180 (100%)	246 (100%)
No. of anthers with inaperturate pollen	64 (15.3%)	0	0
No. of anthers with affected pollen	75 (18%)	0	0

Apertures in *E. californica* Are Dispensable for Pollen Germination

As mentioned earlier, pollen apertures are usually thought to serve as the sites for pollen tube exit during germination. Consistent with this notion, inaperturate pollen grains in rice and maize lose their ability to germinate (Li et al., 2018; Zhang et al., 2020). However, in Arabidopsis, *inp1* pollen still shows normal fertility in the absence of apertures (Dobritsa et al., 2011; Albert et al., 2018). Therefore, using an *in vitro* germination test, we tested whether apertures were essential or dispensable for pollen tube germination in *E. californica*. No significant difference was found between the germination of wild-type pollen and the inaperturate pollen from the silenced plants (**Figures 4A,B**). Thus, the presence of apertures is not essential for pollen germination, and pollen tubes in *E. californica*, like those in Arabidopsis, are capable of emerging directly through the pollen wall (**Figure 4C**).

Transcriptome in the *EcINP1*-Silenced Plants Changes Significantly

To determine if silencing of *EcINP1* could affect expression of any genes, we performed RNA-seq analysis of the anthers from the pTRV2:*EcINP1* VIGS plants and compared them with the results for the wild-type plants. Sequencing, using the Illumina platform with Phred quality score, yielded an average of 50,566,911 high-quality (HQ) reads per sample (**Supplementary Table 3**), after initial quality filtering. On average, 53.53% of reads were aligned to the *E. californica* reference genome and assembled into 34,729 contigs with an average length of 1,006 bp (**Supplementary Table 3**).

The hierarchical clustering, heatmap and principal component analyses showed that there were significant differences between the wild-type and VIGS samples (**Figures 5A–C**). The filtering of the genes with the $\log_2$-fold change of > 2 and with the *p*-value and *p*-adj of <0.05 identified 971 differentially expressed genes (DEGs), of which 488 were upregulated and 483 were downregulated. As expected, *EcINP1* itself was one of the DEGs, showing downregulation in the VIGS samples with a $\log_2$-fold change of 2.49, consistent with the result of the qRT-PCR. Out of the 971 DEGs, 211 were annotated through BLASTX with the genome of *Papaver somniferum*, 677 with SwissProt Database, and the remaining 83 did not give hits

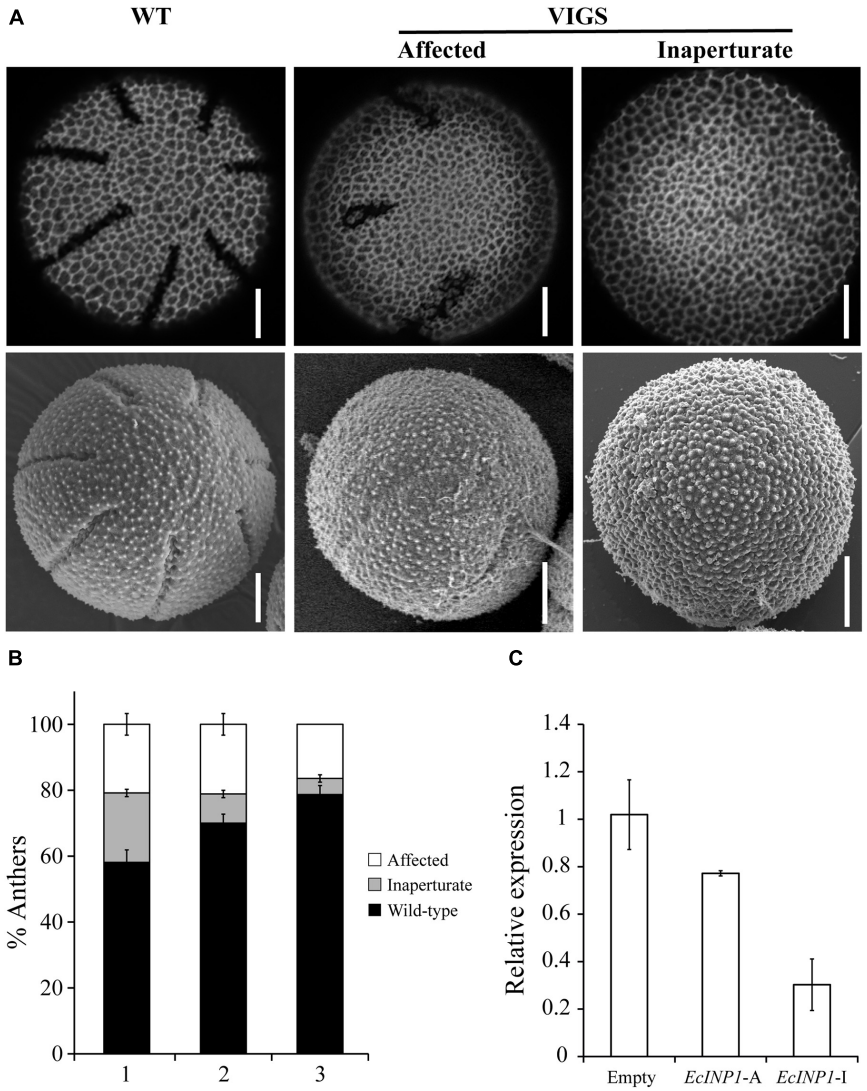

FIGURE 3 | Results of *EclNP1* silencing by VIGS. **(A)** Images showing the observed pollen phenotypes: normal aperturate wild-type (WT), on the left; affected, with shorter and/or shallower apertures, in the middle; inaperturate, on the right. Top images were taken with a confocal microscope and bottom images with a scanning electron microscope. Scale bars = 0.5 μm **(B)** Stacked bar plot showing the distribution of observed phenotypes (black: wild-type, gray: inaperturate, white: affected) according to the developmental order of the three flowers (second = (1), third = (2), and fourth = (3)) sampled for each plant treated with pTRV2:*EclNP1*. Quantification of phenotypes is shown as the percentage of anthers with pollen of each phenotype, since within each anther all pollen grains showed the same phenotype. **(C)** Comparison of *EclNP1* expression, by qRT-PCR analysis of the first flower bud, in plants treated with pTRV2:empty (*n* = 3) and pTRV2:*EclNP1*, differentiating between the affected (*EclNP1*-A*; n* = 1) and inaperturate (*EclNP1*-I*; n* = 3) phenotypes. ANOVA test *P*-value = 0.015.

in any database (**Supplementary Table 4**). As transcription factors (TFs) play important roles in plant development, we used the Plant Transcription Factor Database (PlantTFDB) to align DEGs with TF domains. 30 DEGs showed high homology to 16 known TF families, among which the NAC family, with 8 genes, was the most represented (**Supplementary Table 4** and **Supplementary Figure 4A**). With respect to functional characterization, 277 (28.5%) of 971 DEGs were classified using GhostKoala into different functional categories, with proteins involved in processing of genetic information being the most common category, followed by proteins involved in carbohydrate metabolism and in signaling and cellular processes, all processes that could be relevant to aperture formation (**Supplementary Figure 4B** and **Supplementary Table 4**). We further describe the identity of some of the most interesting DEGs in the Discussion. For eight of those genes, their differential expression was confirmed with qRT-PCR (**Figure 6**).

Phylogenetic and Expression Analyses of Three Interesting DEGs

Among the DEGs, we found two upregulated transcripts of the AGCVIII protein serine-threonine kinases from the AGC1 group (in the nomenclature of Galván-Ampudia and Offringa, 2007),

A

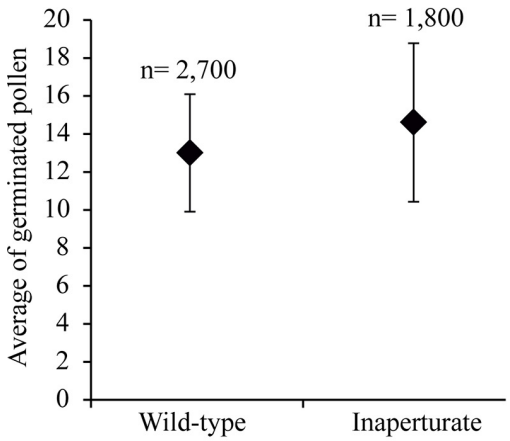

B

Source of variation	df	Sum of Squares	Mean Sum of Squares	F	*P-value*
Between groups	1	28.03	28.03	2.21	0.144
Within groups	43	544.28	12.66		
Total	44	572.31			

C

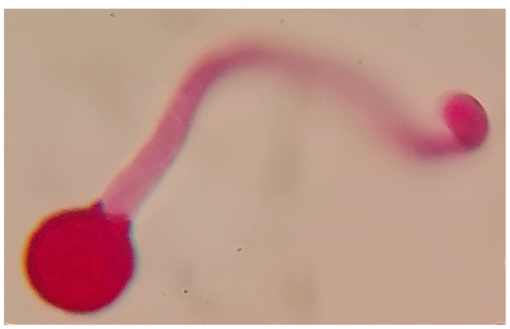

FIGURE 4 | Results of the *Eschscholzia californica* pollen germination test. **(A)** Scatter plot of the mean number of germinated pollen grains per each 100 pollen grains counted, for wild-type and inaperturate pollen. n, total number of pollen grains counted. **(B)** Summary table of the ANOVA analysis. **(C)** Optic microscope image of a germinated inaperturate pollen, stained with basic fuchsin, with the pollen tube emerging through the pollen wall.

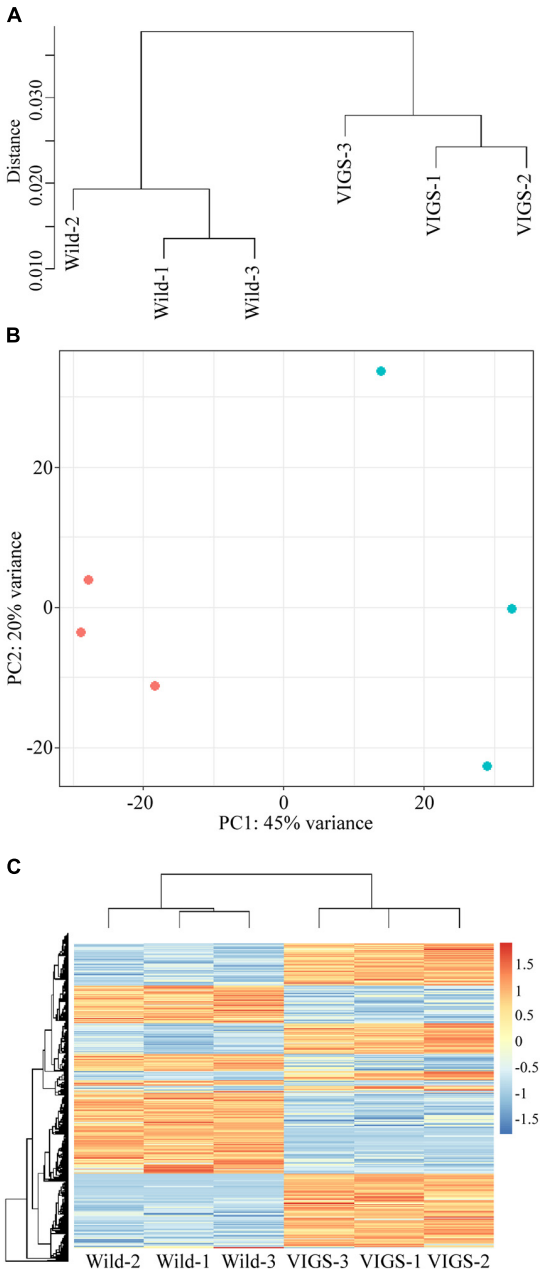

FIGURE 5 | Analysis of differentially expressed genes (DEGs) between transcriptomes of wild-type and VIGS-treated plants. **(A)** Hierarchical clustering shows dissimilarity among the transcriptome samples; distance is calculated by Pearson correlation coefficient. **(B)** Principal component analysis of the transcriptome samples. Red points represent wild-type plants; blue points represent pTRV2:*EclNP1*-treated plants. **(C)** Heatmap of transcriptomes of wild-type and pTRV2:*EclNP1*-treated plants. Heatmap scale bars indicate $\log_2$fold changes.

putatively annotated as D6 PROTEIN KINASE-LIKE1 (D6PKL1; scaffold Eca_sc004639.1_g0030.1) and D6 PROTEIN KINASE-LIKE2 (D6PKL2; Eca_sc095603.1_g0010.1). In Arabidopsis, the protein D6 PROTEIN KINASE-LIKE3 (D6PKL3) belonging to the same group of kinases is involved in aperture formation (Lee et al., 2018). To clarify the homology relationships of the two D6PKL genes found in our DEG set, we carried out phylogenetic analysis on sequences of the AGC1 group kinases from Arabidopsis, *E. californica* and *Papaver somniferum*. The DEG sequence Eca_sc095603.1_g0010.1 was not included in the analysis due to its incompleteness in the database. However, it appears to be identical to Eca_sc000153.1_g1520.1, which was used instead.

This analysis showed two distinct clades within the D6PK family (**Supplementary Figure 5**), suggesting a duplication event and a posterior divergence before the eudicot diversification from their common ancestor, with one strongly supported clade, including the Arabidopsis D6PK, D6PKL1, D6PKL2 and their

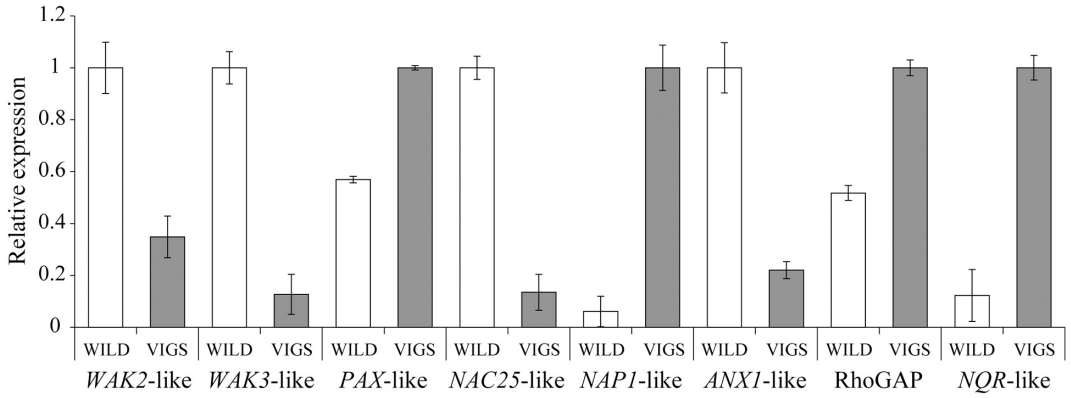

FIGURE 6 | Results of the qRT-PCR analysis to confirm the differential expression of eight DEGs detected through the transcriptome analysis in *Eschscholzia californica*. *WAK2*-like, Eca_sc194563.1_g0010.1; *WAK3*-like, Eca_sc000051.1_g1410.1; *PAX*-like, Eca_sc095603.1_g0010.1; *NAC25*-like, Eca_sc194734.1_g0710.1; *NAP1*-like, Eca_sc004324.1_g2710.1; *ANX1*-like, Eca_sc194691.1_g0370.1; Rho GTPase-activating protein (RhoGAP), Eca_sc009796.1_g0090.1; *NADPH:quinone oxidoreductase* (*NQR*)-like, Eca_sc194522.1_g0180.1.

orthologs, and a more weakly supported clade, which included D6PKL3 and the rest of the *E. californica* and *P. somniferum* sequences. Eca_sc004639.1_g0030.1, affected by the *EcINP1* silencing, belongs to this second clade, falling into a subclade unique to the Papaveraceae. The Papaveraceae sequences in the first clade are clearly related to D6PKL2, suggesting that an ancestral D6PKL2 sequence diverged from the lineage leading to D6PK-D6PKL1 in the ancestor of the eudicots. In Arabidopsis, D6PKL3 is the most diverged sequence in the D6PK family. In *E. californica*, the DEG sequence Eca_sc004639.1_g0030.1 is also clearly differentiated from the other members of the family (**Supplementary Figure 5**). The second D6PK family related DEG, Eca_sc000153.1_g1520.1, is clearly linked to a close relative of the D6PK family, the Arabidopsis gene At2g44830, encoding PROTEIN KINASE ASSOCIATED WITH BRX (PAX) (**Supplementary Figure 5**).

Another DEG we considered interesting was the homolog of *NUCLEOSOME ASSEMBLY PROTEIN 1* (*NAP1*). In dioecious wild grapevine *Vitis vinifera* subsp. *sylvestris*, this gene, together with the *INP1* homolog, is part of the sexual locus whose members are functional/present in the male but not the female genome (Badouin et al., 2020). To find out if NAP1 and the two AGC1 kinases (D6PK-like and PAX-like) could be acting simultaneously with INP1, we analyzed their transcript expression at different stages of pollen development. The results showed that all three genes reach maximal expression levels during the tetrad stage (**Supplementary Figure 6**), mimicking the expression pattern of *EcINP1* (**Figure 2B**).

DISCUSSION

The molecular mechanisms involved in the formation of pollen apertures remain largely unknown. Studies in this area have so far been mostly carried out in two model species, the core eudicot *A. thaliana* (Brassicaceae, with tricolpate pollen) and the monocot *O. sativa* (Poaceae, with ulcerate pollen). This study is the first functional characterization of an *INP1*-like gene in a basal eudicot, *E. californica* (Papaveraceae, Ranunculales, with penta- to heptacolpate pollen), and therefore, in the evolutionary context, it complements our understanding of the role of this gene in the diversification of the angiosperm apertural system. Moreover, this is the first study in which a comparative transcriptome analysis was performed for identifying potential candidate genes involved in aperture formation, calling for further functional studies.

Our functional study showed that *EcINP1* is required for the formation of apertures in *E. californica*, similar to its homologs in Arabidopsis, maize and rice. This result extends the conserved role of the gene to basal eudicots and supports the hypothesis that INP1 was involved in the aperture formation in the monocot-eudicot common ancestor (Li et al., 2018). In the interspecies complementation experiments conducted by Li et al. (2018), EcINP1 failed to restore apertures in the Arabidopsis *inp1* mutants. Our results now demonstrate the functionality of EcINP1 and support sequence divergence as the cause of this failure.

At the intraspecific level, we have detected a single copy of *EcINP1* in *E. californica*, as deduced from BLAST searches in the *Eschscholzia* genome database and from the high identity among the observed variants of the gene (>97.5%). One of the most variable regions of the gene and protein is the very end of the C-terminus, where we even detected a second intron and a shift in the reading frame resulting in extra amino acids (**Supplementary Figure 2**). Li et al. (2018) showed that this region was dispensable for the formation of the punctate INP1 lines and apertures in Arabidopsis, and that it was poorly conserved among the INP1 homologs from other species. This evidence suggests that the low functional significance of the C-terminal region leads to relaxation of the selective pressure acting on it, allowing its divergence at the sequence level even within a species. At the interspecific level, this region is highly variable and had to be excluded from the phylogenetic analysis due to alignment ambiguity. In addition, a 30-bp region located

in the acidic region was also excluded because of its high variability. This region, together with the DOG1 domain and the middle region, is part of the INP1 central region, essential for the function and stability of the protein and containing amino acids critical for species-specific interactions (Li et al., 2018). However, whether the acidic region itself is involved in species-specific interactions is not known. At the intraspecific level, we have detected moderate variation in the acidic region, with three amino acid substitutions and an indel of an asparagine. We have also detected intraspecific changes in other important areas of the central portion of EcINP1 (five in the DOG1 domain and two in the middle region). Further studies will be required to understand whether these changes in the regions critical for species-specific interactions could be related to the observed variability of the pollen aperture system in *E. californica* (e.g., in the number of apertures or their length).

The gene expression pattern of *INP1* homologs during microsporogenesis also seems to be conserved across angiosperms. Similar to its counterparts in Arabidopsis and rice (Dobritsa and Coerper, 2012; Zhang et al., 2020), *EcINP1* begins expression in pollen mother cells, reaches the maximum level at the early tetrad stage, and, after the release of microspores, its transcript practically disappears. In Arabidopsis, the AtINP1 protein signal disappears soon after the release of microspores from the tetrad, suggesting rapid degradation of the protein (Dobritsa and Coerper, 2012; Dobritsa et al., 2018). The EcINP1 protein, unlike AtINP1, reaches its maximum concentration during the free microspore period (**Figure 2C**), so degradation of the protein does not occur until after that stage. A delay in the degradation of OsINP1 has also been documented in rice and could be associated with the functional diversification of that protein, which, together with the lectin receptor-like kinase (RLK) DEFECTIVE IN APERTURE FORMATION1 (OsDAF1) with which it interacts, is involved in the formation of the pore annulus (Zhang et al., 2020). Thus, a delay in the EcINP1 degradation beyond aperture formation may suggest a possibility of its functional diversification.

Our pollen germination assay showed that apertures in *E. californica*, like those in Arabidopsis, are not essential for the exit of pollen tubes, and that pollen tubes can break through exine in inaperturate pollen grains. This is different from grasses, in which inaperturate mutants fail to germinate pollen tubes and show complete male sterility (Li et al., 2018; Zhang et al., 2020). Differences in exine morphology (thickness and tectum sculpture; Li et al., 2018) as well as in physiology of pollen and stigma (Edlund et al., 2016) have been proposed as possible causes for differences in dependence of pollen tubes on the presence of apertures. Inaperturate sterile pollen in dioecious species, produced by female flowers and acting as a reward or attractant for pollinators, is a character that has independently evolved at least six times among eudicots (Furness, 2007). Recently, Badouin et al. (2020) found that in female flowers of *Vitis vinifera* subsp. *sylvestris* the *INP1* homolog has an 8-bp deletion in the DOG1 domain, which results in a premature stop codon and is probably responsible for the absence of apertures. However, they did not study whether the lack of apertures in this pollen is sufficient to cause sterility. In this taxon, *INP1* is located within the sex locus, where four other genes, present in male plants, are missing in the female plants and could also be the candidates for pollen sterility. Interestingly, we discovered one of these four genes, *NUCLEOSOME ASSEMBLY PROTEIN 1* (*NAP1*), as part of the DEG set in the *EcINP1*-silenced plants, suggesting that a possibility of its interaction with *INP1* should be examined. Consistent with this notion, we found that *EcNAP1*-like is most strongly expressed during the tetrad stage of pollen ontogeny (**Supplementary Figure 6A**), when *EcINP1* expression is also maximal and when the process of aperture development begins.

INAPERTURATE POLLEN1 (INP1) is an essential factor for the development of apertures, but it is not the main factor defining aperture number, positions, and morphology (Reeder et al., 2016; Dobritsa et al., 2018; Zhou and Dobritsa, 2019). Still, in Arabidopsis, it has been observed that there is a relationship between the INP1 levels and aperture length, with the lower transcript levels correlating with shorter apertures (Dobritsa and Coerper, 2012). In *E. californica*, this relationship also appears to exist, since older VIGS-silenced plants, in which *EcINP1* was likely inactivated only partially, often produced pollen with apertures that were shorter or shallower than normal (**Figure 3B**). However, in no case were the changes in number, position or shape of apertures observed.

Although accumulating evidence indicates the need for species-specific partners to cooperate with INP1 in different species to control the formation of apertures (Li et al., 2018; Zhou and Dobritsa, 2019; Zhang et al., 2020), these other molecular players remain largely unknown. Our transcriptome analysis presents a basis for identifying DEGs that may represent some candidates with which EcINP1 interacts. Among the 971 DEGs, we found two belonging to the AGC1 kinases: one related to D6PKL3 of Arabidopsis and the other to PAX. In Arabidopsis, the four membrane-associated kinases of the D6PK family directly regulate the PIN-FORMED (PIN)-mediated auxin transport required for phototropic responses (Zourelidou et al., 2009). However, D6PKL3 is also involved in pollen aperture formation (Lee et al., 2018). D6PKL3 appears to act upstream of INP1, possibly specifying domains in the PM to indicate the sites where INP1 must attach. At the same time, INP1 also seems to control D6PKL3 localization at the aperture domains (Lee et al., 2018). Similar to the D6PK-family proteins, PAX regulates the activity of PIN1 in developing protophloem sieve elements (Marhava et al., 2018). Marhava et al. (2020) have shown that PAX and its partner BREVIS RADIX (BRX) influence the local abundance of PIN1 by recruiting phosphatidylinositol-4-phosphate 5-kinases (PIP5Ks) to partition the PM into distinct domains. In the Arabidopsis aperture formation process a possible link between AGC1 kinases and phosphatidylinositol lipids in the aperture PM domains was also proposed (Lee et al., 2018). The upregulation of the transcripts of these AGC1 kinases in the *E. californica* VIGS-silenced plants suggests their direct or indirect interaction with EcINP1. The temporal expression pattern of these kinases, coincident with that of *EcINP1* (**Supplementary Figures 6B,C**; **Figure 2B**), provides further evidence pointing toward the connection between these genes in determining the formation of apertures. Thus, further studies will be necessary to test possible roles of D6PK-like and

PAX-like in the establishment of the PM domains of future apertures and EcINP1 polarization.

Among the annotated DEGs, we also found several RLKs. In rice, the above-mentioned lectin RLK OsDAF1 was recently shown to be involved in the formation of pollen apertures (Zhang et al., 2020). Interestingly, one of the upregulated DEGs was annotated as a G-type lectin S-receptor-like serine/threonine-protein kinase (homologous to the Arabidopsis At2g19130). Also, among the downregulated genes we found homologs of two *WALL-ASSOCIATED RECEPTOR KINASES* (*WAK*), *WAK2,* and *WAK3* (**Figure 6**), encoding cell wall-associated RLKs (He et al., 1999). In *Oryza sativa,* a WAK-RLK gene *DEFECT IN EARLY EMBRYO SAC1* (*OsDEES1*) was shown to have some effect on pollen viability and pollen tube growth (Kohorn, 2001; Wang et al., 2012).

In addition, ten other RLKs were found in our DEG set. Among them was a downregulated homolog of the pollen-specific RLK *ANXUR1* (*ANX1*) (**Figure 6**). In Arabidopsis, ANX1, together with its homolog ANX2, controls cell wall integrity and pollen tube rupture by regulating pollen-expressed NADPH oxidases, as well as exocytosis and secretion of cell wall materials (Miyazaki et al., 2009; Boisson-Dernier et al., 2009; Fehér and Lajkó, 2015). Related to the possible role of ANX1 in aperture formation, we also found an upregulated homolog of *NADPH:quinone oxidoreductase* (*NQR*) (**Figure 6**), proposed to be a part of the ANX pathway (Fehér and Lajkó, 2015). Also, we found an upregulated DEG coding for the homolog of the leucine-rich repeat RLK PXY-LIKE1 (PXL1), very closely related to PXY which helps to maintain cell polarity required for the orientation of cell division during vascular development (Fisher and Turner, 2007). Since cell polarity in developing microspores likely plays a role in the establishment of aperture domains (Lee et al., 2018; Zhou and Dobritsa, 2019), polarity-related proteins could be good candidates for functional testing in the future. Additionally, among the upregulated DEGs, we found an uncharacterized Rho GTPase-activating protein (RhoGAP) (**Figure 6**). Rho GTPases, acting as molecular switches that cycle between the inactive cytosolic GDP-bound state and the active membrane-bound GTP-state, have been implicated in the control of cell polarity, cellular domain formation, and cytoskeletal organization (Craddock et al., 2012), all of which could be important for the formation of aperture domains.

So far, nothing is known about the factors regulating expression of genes involved in pollen aperture formation. Among the annotated DEGs, we found 30 that correspond to transcription factors. Eight belong to the NAC family, whose members regulate many developmental processes in plants. One of them, downregulated in the VIGS plants (**Figure 6**), is annotated as a homolog of *NAC TRANSCRIPTION FACTOR 25* or *TAPNAC*, known to be expressed in the tapetum of the Arabidopsis anthers (Alvarado et al., 2011).

In summary, our study extends INP1 involvement in aperture formation to basal eudicots. This functional conservation is quite remarkable, given the low protein conservation of INP1 and the large variations in aperture patterns across angiosperms. There are many questions to be answered about the aperture pathway. Characterizing the function of known genes in species from relevant angiosperm groups will allow a better assessment of the functional conservation of these genes in the phylogenetic scale of flowering plants. Of particular importance would be the identification of new factors involved in aperture formation. Characterization of proteins interacting with INP1 and/or D6PKL3, as well as genes responsible for abnormal aperture systems, such as the recently discovered *macaron* and *doughnut* mutants (Plourde et al., 2019), or the regulatory genetic network, would help to better understand the process of aperture formation and its evolution in angiosperms.

DATA AVAILABILITY STATEMENT

The original contributions presented in the study are publicly available. These data can be found here: EBI repository, accession numbers: ERS6376182, ERS6376183, ERS6376184, ERS6376185, ERS6376186, and ERS6376187.

AUTHOR CONTRIBUTIONS

IM-A performed the experiments and analyzed the transcriptomic data with the help of BK and DH. IM-A and VS-S analyzed the functional study data. AD provided critical information and confocal images of pollen. VS-S and AR-G conceived and designed the studies. VS-S, IM-A, and AD drafted the manuscript and all the authors participated in the editing of the manuscript.

FUNDING

This study was supported by the Spanish Ministry of Economy and Competitiveness (project CGL2015-70290-P to VS-S) and by the US National Science Foundation (MCB-1817835 to AD). IM-A was supported by a predoctoral grant (F.P.I. program) from the Spanish Government. BK was supported by the Ministry of Education, Youth and Sports of the Czech Republic (project LTC20050) and DH was supported by Czech Science Foundation (project 21-15856S).

ACKNOWLEDGMENTS

We thank Juan de Dios Arché for his help with the EcINP1 immunodetection.

SUPPLEMENTARY MATERIAL

The Supplementary Material for this article can be found online at: https://www.frontiersin.org/articles/10.3389/fpls.2021.701286/full#supplementary-material

REFERENCES

Akaike, H. (1974). A new look at the statistical model identification. *IEEE Trans. Automat. Contr.* 19, 716–723. doi: 10.1109/TAC.1974.1100705

Albert, B., Ressayre, A., Dillmann, C., Carlson, A. L., Swanson, R. J., Gouyon, P. H., et al. (2018). Effect of aperture number on pollen germination, survival and reproductive success in *Arabidopsis thaliana*. *Ann. Bot.* 121, 733–740. doi: 10.1093/aob/mcx206

Alvarado, V. Y., Tag, A., and Thomas, T. L. (2011). A cis regulatory element in the TAPNAC promoter directs tapetal gene expression. *Plant Mol. Biol.* 75, 129–139. doi: 10.1007/s11103-010-9713-5

Anisimova, M., and Gascuel, O. (2006). Approximate likelihood-ratio test for branches: a fast, accurate, and powerful alternative. *Syst. Biol.* 55, 539–552. doi: 10.1080/10635150600755453

Ariizumi, T., and Toriyama, K. (2011). Genetic regulation of sporopollenin synthesis and pollen exine development. *Ann. Rev. Plant Biol.* 62, 437–460. doi: 10.1146/annurev-arplant-042809-112312

Ashburner, M., Ball, C. A., Blake, J. A., Botstein, D., Butler, H., Cherry, J. M., et al. (2000). Gene ontology: tool for the unification of biology. *Nat. Genet.* 25, 25–29.

Badouin, H., Velt, A., Gindraud, F., Flutre, T., Dumas, V., Vautrin, S., et al. (2020). The wild grape genome sequence provides insights into the transition from dioecy to hermaphroditism during grape domestication. *Genome Biol.* 21, 1–24. doi: 10.1186/s13059-020-02131-y

Blackmore, S., Stafford, P., and Persson, V. (1995). "Systematics and evolution of the Ranunculiflorae," in *Plant Systematics and Evolution*, eds U. Jensen and J. W. Kadereit (Viena: Springer), 71–82.

Boisson-Dernier, A., Roy, S., Kritsas, K., Grobei, M. A., Jaciubek, M., Schroeder, J. I., et al. (2009). Disruption of the pollen-expressed FERONIA homologs ANXUR1 and ANXUR2 triggers pollen tube discharge. *Development* 136, 3279–3288. doi: 10.1242/dev.040071

Craddock, C., Lavagi, I., and Yang, Z. (2012). New insights into Rho signaling from plant ROP/Rac GTPases. *Trends Cell Biol.* 22, 492–501. doi: 10.1016/j.tcb.2012.05.002

Dobritsa, A. A., and Coerper, D. (2012). The novel plant protein INAPERTURATE POLLEN1 marks distinct cellular domains and controls formation of apertures in the Arabidopsis pollen exine. *Plant Cell.* 24, 4452–4464. doi: 10.1105/tpc.112.101220

Dobritsa, A. A., Geanconteri, A., Shrestha, J., Carlson, A., Kooyers, N., Coerper, D., et al. (2011). A large-scale genetic screen in Arabidopsis to identify genes involved in pollen exine production. *Plant Physiol.* 157, 947–970. doi: 10.1104/pp.111.179523

Dobritsa, A. A., Kirkpatrick, A. B., Reeder, S. H., Li, P., and Owen, H. A. (2018). Pollen aperture factor INP1 acts late in aperture formation by excluding specific membrane domains from exine deposition. *Plant Physiol.* 176, 326–339. doi: 10.1104/pp.17.00720

Edlund, A. F., Swanson, R., and Preuss, D. (2004). Pollen and stigma structure and function: the role of diversity in pollination. *Plant Cell* 16(Suppl. 1), S84–S97. doi: 10.1105/tpc.015800

Edlund, A. F., Zheng, Q., Lowe, N., Kuseryk, S., Ainsworth, K. L., Lyles, R. H., et al. (2016). Pollen from Arabidopsis thaliana and other Brassicaceae are functionally omniaperturate. *Am. J. Bot.* 103, 1006–1019. doi: 10.3732/ajb.1600031

Fehér, A., and Lajkó, D. B. (2015). Signals fly when kinases meet Rho-of-plants (ROP) small G-proteins. *Plant Sci.* 237, 93–107. doi: 10.1016/j.plantsci.2015.05.007

Fernández, M. C., Romero García, A. T., and Rodríguez García, M. I. (1992). Aperture structure, development and function in Lycopersicum esculentum Miller (Solanaceae) pollen grain. *Rev. Palaeobot. Palynol.* 72, 41–48. doi: 10.1016/0034-6667(92)90173-E

Fisher, K., and Turner, S. (2007). PXY, a receptor-like kinase essential for maintaining polarity during plant vascular-tissue development. *Curr. Biol.* 17, 1061–1066. doi: 10.1016/j.cub.2007.05.049

Furness, C. A., and Rudall, P. J. (2004). Pollen aperture evolution – a crucial factor for eudicot success? *Trends Plant Sci.* 9, 154–158. doi: 10.1016/j.tplants.2004.01.001

Furness, C. A. (2007). Why does some pollen lack apertures? A review of inaperturate pollen in eudicots. *Bot. J. Linn. Soc.* 155, 29–48. doi: 10.1111/j.1095-8339.2007.00694.x

Galván-Ampudia, C. S., and Offringa, R. (2007). Plant evolution: AGC kinases tell the auxin tale. *Trends Plant Sci.* 12, 541–547. doi: 10.1016/j.tplants.2007.10.004

Guindon, S., Dufayard, J. F., Lefort, V., Anisimova, M., Hordijk, W., and Gascuel, O. (2010). New algorithms and methods to estimate maximum-likelihood phylogenies: assessing the performance of PhyML 3.0. *Syst. Biol.* 59, 307–321. doi: 10.1093/sysbio/syq010

Guindon, S., and Gascuel, O. (2003). A simple, fast, and accurate algorithm to estimate large phylogenies by maximum likelihood. *Syst. Biol.* 52, 696–704. doi: 10.1080/10635150390235520

Götz, S., García-Gómez, J. M., Terol, J., Williams, T. D., Nagaraj, S. H., Nueda, M. J., et al. (2008). High-throughput functional annotation and data mining with the Blast2GO suite. *Nucleic Acids Res.* 36, 3420–3435. doi: 10.1093/nar/gkn176

Hall, T. A. (1999). BioEdit: a user-friendly biological sequence alignment editor and analysis program for Windows 95/98/NT. *Nucl. Acids. Symp. Ser.* 41, 95–98.

He, Z. H., Cheeseman, I., He, D., and Kohorn, B. D. (1999). A cluster of five cell wall-associated receptor kinase genes, Wak1–5, are expressed in specific organs of Arabidopsis. *Plant Mol. Biol.* 39, 1189–1196.

Heslop-Harrison, J., and Heslop-Harrison, Y. (1985). Surfaces and secretions in the pollen–stigma interaction: a brief review. *J. Cell Sci.* 2, 287–300.

Heslop-Harrison, J. (1979). Pollen walls as adaptive systems. *Ann. Missouri Bot. Gard.* 66, 813–829. doi: 10.2307/2398920

Hoot, S. B., Wefferling, K. M., and Wulff, J. A. (2015). Phylogeny and character evolution of Papaveraceae sl (Ranunculales). *Syst. Bot.* 40, 474–488. doi: 10.1600/036364415X688718

Hori, K., Yamada, Y., Purwanto, R., Minakuchi, Y., Toyoda, A., Hirakawa, H., et al. (2018). Mining of the uncharacterized cytochrome P450 genes involved in alkaloid biosynthesis in California poppy using a draft genome sequence. *Plant Cell Physiol.* 59, 222–233. doi: 10.1093/pcp/pcx210

Kanehisa, M., and Goto, S. (2000). KEGG: kyoto encyclopedia of genes and genomes. *Nucleic Acids Res.* 28, 27–30. doi: 10.1093/nar/28.1.27

Kanehisa, M., Sato, Y., and Morishima, K. (2016). BlastKOALA and GhostKOALA: KEGG tools for functional characterization of genome and metagenome sequences. *J. Mol. Biol.* 428, 726–731. doi: 10.1016/j.jmb.2015.11.006

Kohorn, B. D. (2001). WAKs; cell wall associated kinases. *Curr. Opin. Cell Biol.* 13, 529–533. doi: 10.1016/S0955-0674(00)00247-7

Kumar, S., Stecher, G., Li, M., Knyaz, C., and Tamura, K. (2018). MEGA X: molecular evolutionary genetics analysis across computing platforms. *Mol. Biol. Evol.* 35, 1547–1549. doi: 10.1093/molbev/msy096

Lee, B. H., Weber, Z. T., Zourelidou, M., Hofmeister, B. T., Schmitz, R. J., Schwechheimer, C., et al. (2018). Arabidopsis protein kinase D6PKL3 is involved in the formation of distinct plasma membrane aperture domains on the pollen surface. *Plant Cell.* 30, 2038–2056. doi: 10.1105/tpc.18.00442

Lefort, V., Longueville, J. E., and Gascuel, O. (2017). SMS: smart model selection in PhyML. *Mol. Biol. Evol.* 34, 2422–2424. doi: 10.1093/molbev/msx149

Li, P., Ben-Menni Schuler, S., Reeder, S. H., Wang, R., Suárez Santiago, V. N., and Dobritsa, A. A. (2018). INP1 involvement in pollen aperture formation is evolutionarily conserved and may require species-specific partners. *J. Exp. Bot.* 69, 983–996. doi: 10.1093/jxb/erx407

Livak, K. J., and Schmittgen, T. D. (2001). Analysis of relative gene expression data using real-time quantitative PCR and the $2^{-\Delta\Delta CT}$ method. *Methods.* 25, 402–408. doi: 10.1006/meth.2001.1262

Liu, Y., Schiff, M., and Dinesh-Kumar, S. P. (2002). Virus-induced gene silencing in tomato. *Plant J.* 31, 777–786. doi: 10.1046/j.1365-313X.2002.01394.x

Marhava, P., Bassukas, A. E. L., Zourelidou, M., Kolb, M., Moret, B., Fastner, A., et al. (2018). A molecular rheostat adjusts auxin flux to promote root protophloem differentiation. *Nature.* 558, 297–300. doi: 10.1038/s41586-018-0186-z

Marhava, P., Fandino, A. C. A., Koh, S. W., Jelínková, A., Kolb, M., Janacek, D. P., et al. (2020). Plasma membrane domain patterning and self-reinforcing polarity in Arabidopsis. *Dev. Cell.* 52, 223–235. doi: 10.1016/j.devcel.2019.11.015

Matamoro-Vidal, A., Prieu, C., Furness, C. A., Albert, B., and Gouyon, P. H. (2016). Evolutionary stasis in pollen morphogenesis due to natural selection. *New Phytol.* 209, 376–394. doi: 10.1111/nph.13578

Miyazaki, S., Murata, T., Sakurai-Ozato, N., Kubo, M., Demura, T., Fukuda, H., et al. (2009). ANXUR1 and 2, sister genes to FERONIA/SIRENE, are male factors for coordinated fertilization. *Curr. Biol.* 19, 1327–1331. doi: 10.1016/j.cub.2009.06.064

Pérez-Gutiérrez, M. A., Suárez-Santiago, V. N., Fernández, M. C., Salinas-Bonillo, M. J., and Romero-García, A. T. (2015). Pollen morphology and post-tetrad wall development in the subfamily Fumarioideae (Papaveraceae). *Rev. Palaeobot. Palynol.* 222, 33–47. doi: 10.1016/j.revpalbo.2015.07.009

Pérez-Gutiérrez, M. A., Fernández, M. C., Salinas-Bonillo, M. J., Suárez-Santiago, V. N., Ben-Menni Schuler, S., and Romero-García, A. T. (2016). Comparative exine development from the post-tetrad stage in the early-divergent lineages of Ranunculales: the genera Euptelea and Pteridophyllum. *J. Plant Res.* 129, 1085–1096. doi: 10.1007/s10265-016-0862-8

Pertea, M., Kim, D., Pertea, G. M., Leek, J. T., and Salzberg, S. L. (2016). Transcript-level expression analysis of RNA-seq experiments with HISAT, StringTie and ballgown. *Nat. Prot.* 11:1650. doi: 10.1038/nprot.2016.095

Plourde, S. M., Amom, P., Tan, M., Dawes, A. T., and Dobritsa, A. A. (2019). Changes in morphogen kinetics and pollen grain size are potential mechanisms of aberrant pollen aperture patterning in previously observed and novel mutants of Arabidopsis thaliana. *PLoS Comput. Biol.* 15:e1006800. doi: 10.1371/journal.pcbi.1006800

Reeder, S. H., Lee, B. H., Fox, R., and Dobritsa, A. A. (2016). A ploidy-sensitive mechanism regulates aperture formation on the Arabidopsis pollen surface and guides localization of the aperture factor INP1. *PLoS Genet.* 12:e1006060. doi: 10.1371/journal.pgen.1006060

Tekleyohans, D. G., Lange, S., and Becker, A. (2013). "Virus-induced gene silencing of the alkaloid-producing basal eudicot model plant Eschscholzia californica (California Poppy)"," in *Virus-Induced Gene Silencing*, ed. A. Becker (Totowa, NJ: Humana Press), 83–98.

Untergasser, A., Cutcutache, I., Koressaar, T., Ye, J., Faircloth, B. C., Remm, M., et al. (2012). Primer3 – new capabilities and interfaces. *Nucleic Acids Res.* 40, e115–e115. doi: 10.1093/nar/gks596

Wang, H., Moore, M. J., Soltis, P. S., Bell, C. D., Brockington, S. F., Alexandre, R., et al. (2009). Rosid radiation and the rapid rise of angiosperm-dominated forests. *Proc. Nat. Acad. Sci. U.S.A.* 106, 3853–3858. doi: 10.1073/pnas.0813376106

Wang, N., Huang, H. J., Ren, S. T., Li, J. J., Sun, Y., Sun, D. Y., et al. (2012). The rice wall-associated receptor-like kinase gene OsDEES1 plays a role in female gametophyte development. *Plant Physiol.* 160, 696–707. doi: 10.1104/pp.112.203943

Wege, S., Scholz, A., Gleissberg, S., and Becker, A. (2007). Highly efficient virus-induced gene silencing (VIGS) in California poppy (Eschscholzia californica): an evaluation of VIGS as a strategy to obtain functional data from non-model plants. *Ann. Bot.* 100, 641–649. doi: 10.1093/aob/mcm118

Welinder, C., and Ekblad, L. (2011). Coomassie staining as loading control in Western blot analysis. *J. Proteome Res.* 10, 1416–1419. doi: 10.1021/pr1011476

Wickett, N. J., Mirarab, S., Nguyen, N., Warnow, T., Carpenter, E., Matasci, N., et al. (2014). Phylotranscriptomic analysis of the origin and early diversification of land plants. *Proc. Nat. Acad. Sci. U.S.A.* 111, E4859–E4868. doi: 10.1073/pnas.1323926111

Wodehouse, R. P. (1935). *Pollen Grains. Their Structure, Identification And Significance in Science And Medicine*. London: Mcgraw-Hill Book Company, Inc.

Wortley, A. H., Wang, H., Lu, L., Li, D. Z., and Blackmore, S. (2015). Evolution of angiosperm pollen. 1. Introduction. *Ann. Missouri Bot. Gard.* 100, 177–226.

Xiao, M., Zhang, Y., Chen, X., Lee, E. J., Barber, C. J., Chakrabarty, R., et al. (2013). Transcriptome analysis based on next-generation sequencing of non-model plants producing specialized metabolites of biotechnological interest. *J. Biotechnol.* 166, 122–134. doi: 10.1016/j.jbiotec.2013.04.004

Zhang, H., Jin, J., Tang, L., Zhao, Y., Gu, X., Gao, G., et al. (2011). PlantTFDB 2.0: update and improvement of the comprehensive plant transcription factor database. *Nucleic Acids Res.* 39, D1114–D1117. doi: 10.1093/nar/gkq1141

Zhang, M. Y., Lu, L., Wortley, A. H., Wang, H., Li, D. Z., and Blackmore, S. (2017). Evolution of angiosperm pollen: 4. basal eudicots. *Ann. Missouri Bot. Gard.* 102, 141–182. doi: 10.3417/2015035

Zhang, X., Zhao, G., Tan, Q., Yuan, H., Betts, N., Zhu, L., et al. (2020). Rice pollen aperture formation is regulated by the interplay between OsINP1 and OsDAF1. *Nat. Plants.* 6, 394–403.

Zhou, Y., and Dobritsa, A. A. (2019). Formation of aperture sites on the pollen surface as a model for development of distinct cellular domains. *Plant Sci.* 288, 110222.

Zourelidou, M., Müller, I., Willige, B. C., Nill, C., Jikumaru, Y., Li, H., et al. (2009). The polarly localized D6 PROTEIN KINASE is required for efficient auxin transport in *Arabidopsis thaliana*. *Development* 136, 627–636.

Conflict of Interest: The authors declare that the research was conducted in the absence of any commercial or financial relationships that could be construed as a potential conflict of interest.

frontiers in Plant Science

ORIGINAL RESEARCH
published: 26 July 2021
doi: 10.3389/fpls.2021.635310

Occurrence and Prevention of Delayed Autonomous Selfing in *Salvia umbratica* (Lamiaceae)

Han-Wen Xiao[1,2†], *Yan-Bo Huang*[1,2†], *Yu-Hang Chang*[3], *Yun Chen*[1,2], *Richard J. Abbott*[4], *Yu-Kun Wei*[1,2*] *and Yong-Peng Ma*[3*]

[1] *Shanghai Chenshan Botanical Garden, Shanghai, China,* [2] *Eastern China Conservation Center for Wild Endangered Plant Resources, Shanghai, China,* [3] *Yunnan Key Laboratory for Integrative Conservation of Plant Species With Extremely Small Populations, Kunming Institute of Botany, Chinese Academy of Sciences, Kunming, China,* [4] *School of Biology, University of St Andrews, St Andrews, United Kingdom*

Delayed autonomous selfing (DAS) provides reproductive assurance under conditions of pollinator and/or pollen-limitation. Few plant species have been investigated to determine if DAS is terminated when a flower is sufficiently pollinated by a pollen vector, thereby saving plant resources for other purposes. We examined this possibility in bumblebee-pollinated *Salvia umbratica*. We first showed that DAS resulting in high fruit set (100%) and seed set (>80%) per flower occurred in the absence of insect pollinators by means of style recurvature and was completed in 94% of flowers 72 h after they opened. In contrast, in flowers pollinated immediately after opening, DAS was prevented by corollas dropping away before styles recurve toward the upper thecae. We next showed that hand-pollination of flowers immediately after they opened resulted in high fruit set (100%) and seed set (>80%) when 5–10 pollen grains or more were deposited on their stigmas, whereas fruit set and seed set were reduced to 45.00 and 22.50%, respectively, when pollen loads were reduced to 1–3 pollen grains. Finally, we showed that on average single pollinator visits deposited 26 pollen grains on stigmas of flowers that had just opened, which is more than enough to ensure high fruit and seed set. Our results indicate that flower longevity is highly correlated with the pollinator environment and female fitness of *S. umbratica*, with extended flower longevity allowing DAS to occur being advantageous when pollinators are absent, while reduced floral longevity and prevention of DAS being favored when flowers are pollinated by pollinators. Thus, flower longevity in *S. umbratica* varies so as to optimize reproductive output and resource efforts, and is dependent on the availability and effectiveness of pollinators to pollinate flowers.

Keywords: delayed self-pollination, pollen-limitation, recurving styles, seed set, *Salvia*, Lamiaceae, floral longevity, resource use

OPEN ACCESS

Edited by:
Raju Datla,
Global Institute for Food Security (GIFS), Canada

Reviewed by:
Chengjiang Ruan,
Dalian Nationalities University, China
Scott Zona,
University of North Carolina System, United States
Sunojkumar P,
University of Calicut, India

***Correspondence:**
Yu-Kun Wei
ykwei@aliyun.com
Yong-Peng Ma
mayongpeng@mail.kib.ac.cn

[†] These authors have contributed equally to this work and share first authorship

Specialty section:
This article was submitted to Plant Development and EvoDevo, a section of the journal Frontiers in Plant Science

Received: *20 January 2021*
Accepted: *29 June 2021*
Published: *26 July 2021*

Citation:
Xiao H-W, Huang Y-B, Chang Y-H, Chen Y, Abbott RJ, Wei Y-K and Ma Y-P (2021) Occurrence and Prevention of Delayed Autonomous Selfing in Salvia umbratica (Lamiaceae). Front. Plant Sci. 12:635310. doi: 10.3389/fpls.2021.635310

INTRODUCTION

Delayed autonomous selfing (DAS), which occurs after opportunities for pollination by a pollen-vector have passed, can provide reproductive assurance and for this reason has been termed a "best-of-both-worlds" mating strategy (Goodwillie and Weber, 2018). DAS is expected to be favored by selection when inbreeding depression caused by selfing is >0 and <1 (Lloyd, 1992; Goodwillie and Weber, 2018; Hildesheim et al., 2019). DAS has been reported in 23 orders, 40 families, 56 genera, and 68 species of plants (Chaudhary et al., 2018; Goodwillie and Weber, 2018; Lemos et al., 2020), but for ca. 94% of these species, analyses have not described how floral changes involved in delayed selfing might be terminated if prior, successful and sufficient pollination by a pollen-vector occurs. In fact, DAS has generally been regarded as a process that continues, irrespective of prior pollination by a pollen-vector (Sun et al., 2005; Fan and Li, 2012; Brys et al., 2013; Chaudhary et al., 2018). Furthermore, most previous studies have examined species possessing a large number of ovules per flower and have not assessed the extent to which ovules are fertilized through pollination by insects or as a result of DAS.

Flowering plants exhibit high diversity in floral longevity, often reflecting adaptive responses to prevailing ecological conditions, efficient pollinators, and pollen dissemination/receipt (Ashman and Schoen, 1994; Castro et al., 2008; Roddy et al., 2021). The effects of pollination on floral longevity variation have been evaluated in several plant species, showing, for example, that it may be curtailed after pollination to prevent further expenditure on floral resources (Roddy et al., 2021) and/or to direct pollinators to non-pollinated flowers (Milet-Pinheiro et al., 2015). In contrast, floral longevity may be extended when rain reduces pollen viability, thus increasing the probability of pollinators depositing viable pollen on stigmas and securing high seed set (Domingos-Melo et al., 2020). In some species, flower wilting or abscission have been shown to trigger DAS to increase seed set in the absence of pollinators or when pollen is limited (Costa and Machado, 2017; Domingos-Melo et al., 2018). However, if pollinators are present and cross-pollination is completely successful, flower abscission causing termination of DAS might be expected, so as to reduce floral maintenance costs (Ashman and Schoen, 1994; Hildesheim et al., 2019). This may be especially true in annual herbs where resources allocated to flowers are generally limited, and also in species producing few ovules per flower.

To our knowledge, few studies have evaluated experimentally the possibility of termination of processes leading to DAS following prior successful pollination of flowers by insects. We tested this hypothesis in *Salvia umbratica* Hance (Lamiaceae), an annual herb native to northern China, which produces four ovules per flower. Previous reports suggest that *Salvia* species are self-compatible (Jorge et al., 2014; Barrionuevo et al., 2021), and personal observations show that insect pollinators (bumblebees) frequently visit several flowers consecutively on a plant, and therefore often carry on their bodies a mixture of pollen grains from the same and other plants. A preliminary investigation of flower longevity in a natural population of *S. umbratica* showed that single flowers can remain opening for about 85 h in the absence of pollinators with high levels of fruit and seed set, indicating that delayed selfing occurs in the species. DAS has not been previously reported in Lamiaceae (Goodwillie and Weber, 2018), although there have been suggestions of different levels of autonomous selfing occurring in *Salvia* (Haque and Ghoshal, 1981; Navarro, 1997; Jorge et al., 2014; Rosas-Guerrero et al., 2017; Cuevas et al., 2018; Barrionuevo et al., 2021). Here we report an examination of the flowering process of *S. umbratica* in the presence and absence of pollinators, as well as investigations of fruit and seed set following different pollination treatments. We show that DAS occurs in this species and results in high fruit and seed set, but that floral changes leading to it are terminated by prior successful and sufficient pollination of flowers by a pollinator.

MATERIALS AND METHODS

Species Distribution and Floral Structure

Salvia umbratica Hance. (Lamiaceae) is an annual herb with erect stems of 1–1.2 m in height. It grows between 600 and 2,000 m a.s.l. on hillsides, and in valleys or roadsides in northern China where it is native to Anhui, Gansu, Hebei, Hubei, Shaanxi, and Shanxi provinces. The type specimen of the species was collected from Beijing (Wu and Li, 1977; Li and Hedge, 1994). The flower of *S. umbratica* is typical of *Salvia* being composed of a bilateral symmetrical corolla (**Figure 1**), the upper lip (hood) of which is formed from two petals, while the lower lip (palate) develops from the remaining three petals. The two stamens are each composed of two anther thecae and two connective arms attached to a filament by a joint (Huang et al., 2014). The upper anther theca (upper theca) of each stamen is positioned in the hood of the corolla just below the style of the pistil and is connected to the lower anther theca (lower theca) via the connective arm. A much larger quantity of pollen is produced in the upper than the lower thecae. In fully developed flowers, the stigma is bifid and protrudes slightly from the upper lip with its receptive surface facing outwards. At the base of the corolla tube is a disc containing a nectary, above this is an ovary containing four ovules (Strelin et al., 2017).

Study Sites

Field studies were conducted in 2018 and 2020 at the Beijing Forest Ecosystem Research Station (BFERS) located on Dongling Mountain (115°25′33″ E, 39°57′29″ N, elevation 1,200 m) where a semi-humid and monsoon climate prevails, with an average annual temperature of 5–10°C and annual precipitation of 500–650 mm (Xu et al., 2018). The studies included observations on insect pollinators and amount of pollen deposited during a single pollinator visit, the process of DAS in the absence and presence of pollinators, and seed set following various pollination treatments.

To confirm further the occurrence and prevention of DAS and the reproductive fitness of *S. umbratica*, greenhouse studies were conducted at the Shanghai Chenshan Botanical Garden (SCBG) on plants transplanted in May 2020 from the wild at the BFERS. These studies investigated the amount of pollen required for sufficient pollination and high seed set, the prevention of DAS by

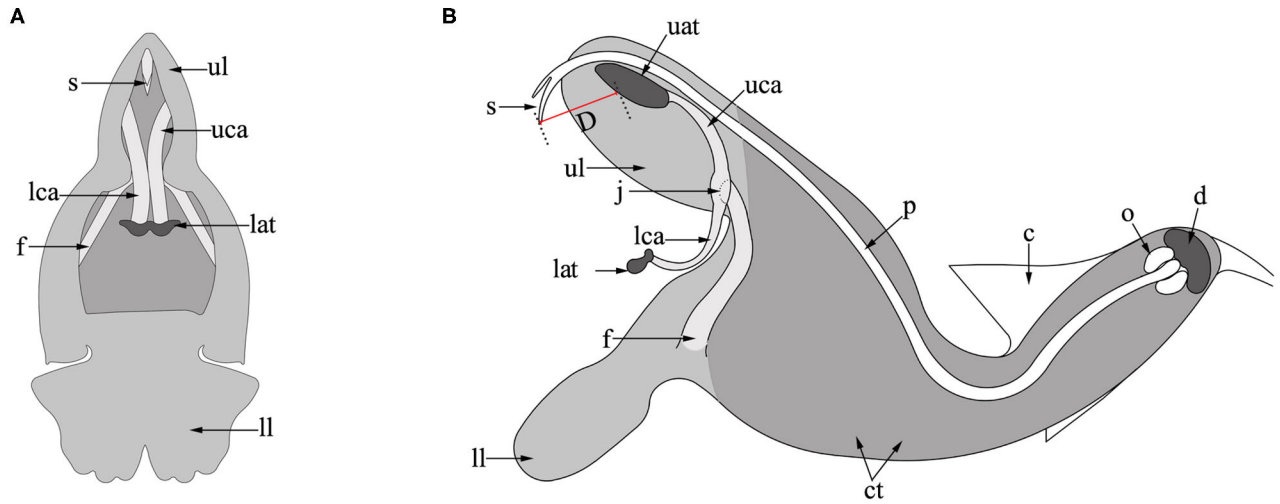

FIGURE 1 | Flower structure of *S. umbratica*. **(A)** Front view; **(B)** lateral view. ct, corolla tube; ul, upper lip; ll, lower lip; uat, upper anther theca; lat, lower anther theca; uca, upper connective arm; lca, lower connective arm; j, joint; f, filament; p, pistil; s, stigma; c, calyx; o, ovary; d, disc; D, distance (between the stigma and upper anther thecae).

prior sufficient pollination, and levels of seed set resulting from DAS in the absence of pollinators. Both field and greenhouse studies were conducted in August and September during the natural blooming period of *S. umbratica*.

Observations on Insect Pollinators and Amount of Pollen Grains Deposited on Stigmas During a Single Pollinator Visit

Pollinator visits to *S. umbratica* flowers were recorded in the field during the natural flowering period on sunny days on the 27, 28, and 31 of August, 2018. For this purpose, we established two 1 × 1 m quadrats at the field site, each of which contained four or five individual plants of *S. umbratica* and an average of 26 and 28 blooming flowers. Two SONY HDR-CX510E cameras were used to record the types, numbers, number of visits, and visit duration of flower-visiting insects in each quadrat between 08:00 and 17:00 each day. We noted the behavior of insect visitors within the quadrats, recording legitimate visits to flowers, i.e., where a pollinator contacted the stigma and stamens while searching for nectar (see Li and Huang, 2009; Ma et al., 2014), and illegitimate visits, i.e., where a pollinator robs nectar and pollen without pollinating the flower. Specimens of pollinators were captured with an insect-net and stored in ethanol (70%) for accurate identification. Vouchers were deposited at the entomological collection at the Horticulture Department of SCBG.

To detect the amount of pollen deposited on a stigma during a single pollinator visit, 45 flower buds were randomly selected from 15 *S. umbratica* plants (3 flowers per plant) that grew naturally at the field site outside the quadrats. Each bud was enclosed in a nylon mesh bag which was removed immediately after the bud opened allowing pollinators to visit the flower produced. After a single visit by a pollinator, the pistil was immediately removed from the flower and pollen deposited on the stigma was counted using a STV-120m portable microscope (Japan, Kenko).

Process of DAS in Absence and Presence of Pollinators

The process and timing of DAS in flowers of *S. umbratica* were investigated first in the absence of pollinators. Two flower buds from each of 10 plants of *S. umbratica* growing naturally at the field site were placed in nylon mesh bags. Photographs of the development of the stigma and upper thecae of each flower were taken using a Nikon D300s digital camera, and records of the distance, D (see **Figure 1B**), between the stigma and upper thecae (measured using Photoshop CS3, Adobe, USA), were made when each flower first opened (0 h) and thereafter at 24 h intervals until DAS was completed, i.e., when $D = 0$. Flowers were deemed to have first opened when the upper and lower lips of the corolla mouth had just separated. This experiment was then repeated with minor modifications in the presence of pollinators. Thus, another two flower buds from each of 10 different plants of *S. umbratica* were placed in nylon mesh bags with a record taken of distance between the upper thecae and the stigma when each flower opened (0 h). Bags were then removed from flowers to allow pollinators to visit them. After a pollinator had entered the corolla tube and successfully pollinated a selected flower, stigma-upper thecae distance was measured again and at intervals of 24 h thereafter.

Fruit and Seed Set Following Different Pollination Treatments at Field Site

To confirm the breeding and mating system characteristics of *S. umbratica*, flowers on a number of different plants in the field were subjected to five different pollination treatments after which fruit and seed set was recorded per flower. These treatments were:

(1) autogamy, involving bagging flowers to allow autonomous selfing to occur; (2) simulated geitonogamy, involving hand-pollination of emasculated and bagged flowers using pollen from another flower of the same plant; (3) simulated xenogamy, as in (2) above but using pollen from a different plant; (4) detection of apomixis, involving emasculation and bagging of flowers to determine if seed were produced; and (5) open-pollination, to determine seed set in flowers left to be naturally pollinated. Each of the five treatments was repeated on three flowers on each of 30 plants (90 flowers per treatment), with fruit production and seed set (number of seeds/4 ovules) per flower recorded 3–4 weeks after pollination had occurred.

Amount of Pollen Required for Sufficient Pollination and High Seed Set

To determine the amount of pollen required for sufficient pollination and fertilization of ovules in a flower, flowers on a number of greenhouse cultivated plants were subjected to five different pollination treatments using a mixture of pollen grains. Pollen was obtained from an equal number of newly dehiscent anthers from a flower on the same plant and a different plant, mixed on parchment and deposited on stigmas using a dissecting needle. The number of pollen grains deposited was determined using a STV-120m portable microscope (Japan, Kenko). The five treatments involved depositing on the stigma of a flower 1–3, 4, 5–10, 11–20, or >20 pollen grains from the mixture. Each treatment was applied to two flowers on each of 10 plants, i.e., 20 flowers per treatment, with fruit production and seed set per flower recorded 3–4 weeks after pollination had occurred.

Prevention of DAS by Sufficient Prior Pollination

To test the hypothesis that sufficient prior pollination by a pollinator likely prevents DAS from occurring, 40 flowers across 10 greenhouse cultivated plants were hand-pollinated immediately after they opened in either of two ways using a mixture of pollen grains. In 20 flowers, 1–3 pollen grains were deposited on their stigmas, whereas in the other 20 flowers >20 grains were deposited. Stigma-upper thecae distance in flowers (D) was recorded at the stage they were pollinated and at 24 h intervals thereafter. Because *Salvia* produces four ovules per flower, for 20 flowers the number of pollen grains deposited on a stigma was less than the number required to fertilize all ovules (i.e., there was pollen-limitation), whereas for the other 20 flowers the number of pollen grains deposited on the stigma was more than required to fertilize all ovules (i.e., no pollen-limitation; Knight et al., 2005; Jorge et al., 2014).

Fruit and Seed Set Resulting From DAS in Absence of Pollinators

In a follow-up study, the effect of DAS on seed set was determined on five plants cultivated in a greenhouse in the absence of pollinators. Flower number per plant averaged 174 and ranged between 48 and 244 across the five plants. During the period from the first flower opening to the last flower dropping, we recorded at 24 h intervals the proportion of flowers on a plant that had completed the process of DAS (when stigma-upper thecae distance was zero), and subsequently the fruit and seed set of these flowers.

Statistical Analyses

All statistical analyses were performed using SPSS 22.0 (Chicago, IL, USA). The analysis of differences in mean stigma-upper thecae distances at different times in flowers pollinated with 1–3 pollen grains was conducted using a generalized linear mixed model (GLMM), with distances as dependent variable, time as fixed effect, and plant as a random factor. A *t*-test was performed to analyze differences of stigma-upper thecae distances at the time of pollination and 24 h later in pollination treatment with >20 pollen grains. Differences in mean fruit set and seed set among different pollination treatments were analyzed by one-way ANOVA followed by a *post-hoc* Tukey's test after excluding treatment 4 (emasculation and bagging of flowers produced no seed indicating an absence of apomixis).

RESULTS

Observations on Insect Pollinators and Amount of Pollen Deposited on a Stigma During a Single Pollinator Visit

Over the 3 days that observations were made, a total of 174 legitimate pollinator visits to flowers in quadrats were recorded. These were by the bumblebees *Bombus opulentus*, *B. longipes*, *B. consobrinus,* and *B. hedini*. On entering the corolla tube, bumblebees searched for and fed on nectar. In doing so, pollen on their backs was deposited on the stigma. Furthermore, they pushed against the lower connective arms of the thecae (**Figure 1**), causing the upper connective arms to bend downwards, resulting in pollen from the upper thecae being deposited on their backs (**Figure 2E**). On average, the number of visits per flower was 1.23 ± 0.31 per day with visits per flower lasting 2.19 ± 0.09 s.

Counts of pollen grains deposited on the stigma of a flower during a single pollinator visit after the flower opened showed that, on average, 26.31 ± 2.07 (11–65 pollen grains per stigma, $n = 45$) pollen grains were deposited, which is more than enough to result in a high level of fruit and seed set (see below).

Process of DAS in Absence and Presence of Pollinators

Based on observations made on bagged flowers (**Figures 2A–D**) and measurements of distance between the stigma and upper anther thecae from the time a flower first opens until DAS is completed ($D = 0$) (**Figure 3A**), it was evident that DAS occurs in *S. umbratica* when flowers are not pollinated by insects. ANOVA showed that stigma-upper thecae distance decreased significantly with time [$F_{(5,74)} = 8.808$, $p < 0.001$]. At 24 h after a flower first opened the style had begun to recurve causing the receptive stigma surface to become angled toward the upper thecae (**Figure 2C**). At this stage, mean stigma-anther thecae distance was reduced from the initial mean of 3.17 mm at the time of flower opening (**Figure 3A**). Recurvature of the stigma

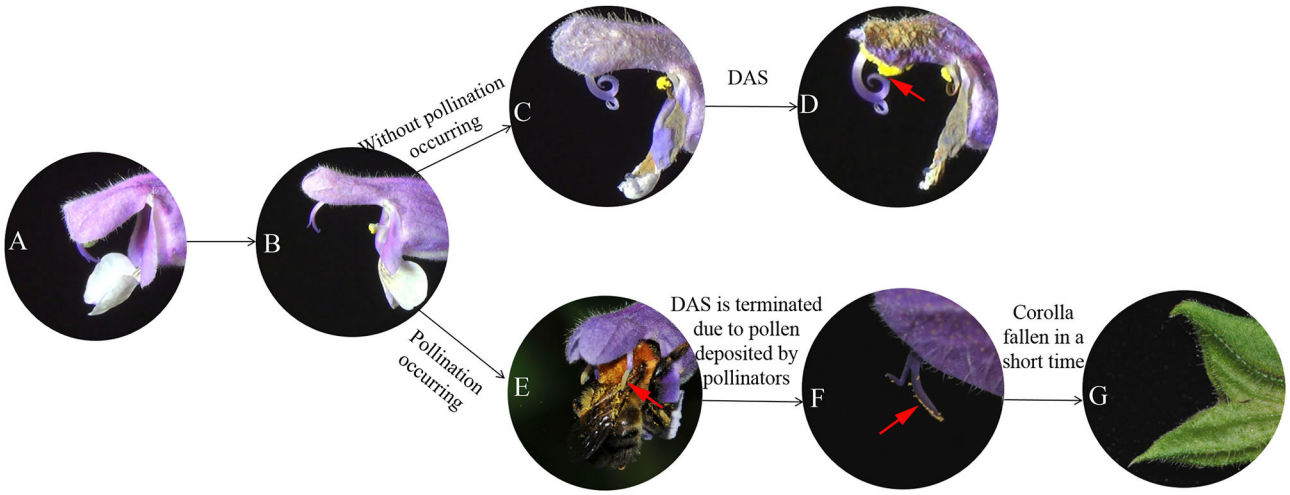

FIGURE 2 | (A–D) Different stages of flower development during the process of DAS, and **(E,F)** when DAS is terminated after bumblebee pollination. **(A)** Flower opens when upper and lower lips of corolla separate (0 h); **(B)** fully opened flower shows stigma with receptive surface oriented outward and unfurled; **(C)** style begins to recurve, orienting receptive surface of stigma toward upper thecae; **(D)** receptive surface of stigma makes contact with upper thecae resulting in selfing (arrow shows stigma receptive surface touching upper thecae); **(E)** flower pollinated by a bumblebee; **(F)** style does not recurve toward upper thecae, arrow indicates stigmatic receptive surface has pollen deposited on it by pollinator; **(G)** corolla has fallen away (dropped) from flower a short time after pollination.

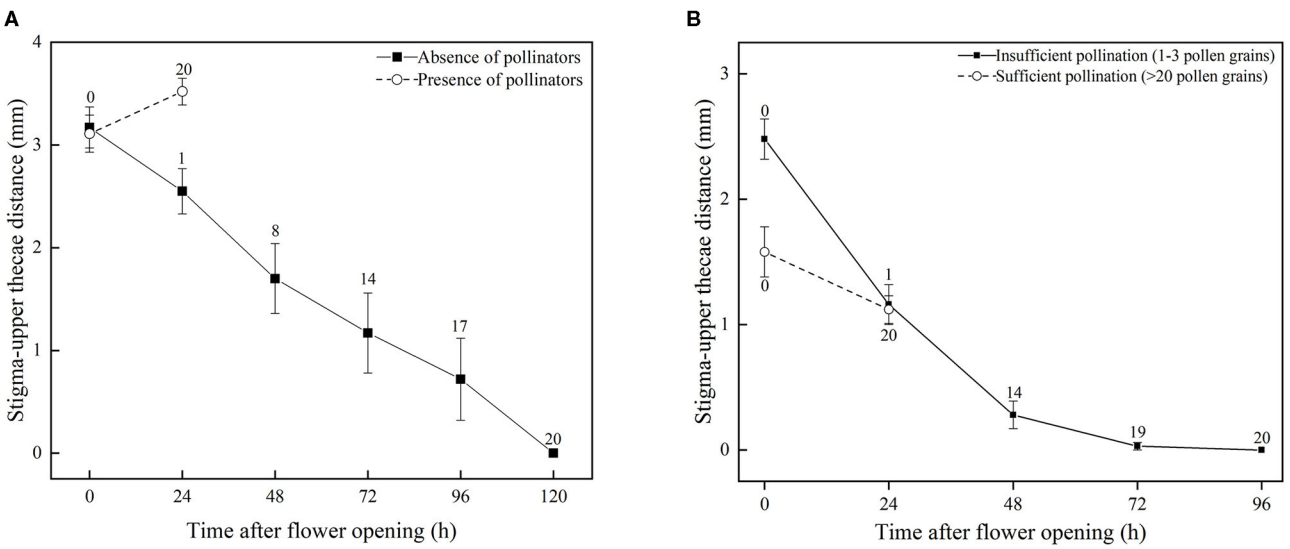

FIGURE 3 | Occurrence and prevention of DAS in *S. umbratica* (bars indicate standard errors). **(A)** Mean stigma-upper thecae distance of flowers in absence of pollinators and also after pollination by a pollinator (presence of pollinators). Records were taken when a flower first opened (0 h) and thereafter at 24 h intervals until pollination was completed in all flowers. Numbers above standard error bars indicate total number of flowers pollinated at given time. **(B)** Mean stigma-upper thecae distance of flowers subjected to insufficient pollination (stigmas hand-pollinated with 1–3 pollen grains) and sufficient pollination (hand-pollinated with >20 pollen grains) treatments. Records were taken of stigma-upper thecae distance when a flower was pollinated with a mix of pollen grains causing either insufficient fertilization or sufficient fertilization (0 h) and thereafter at 24 h intervals. Numbers above standard error bars indicate total number of flowers self-pollinated (stigma-thecae distance, $D = 0$) at given time.

toward the thecae continued at different rates in different flowers. In 70% of flowers (14 out of 20), DAS ($D = 0$) was completed by 72 h after the flower first opened. However, in three flowers it took 120 h to complete. On average, DAS took 66.7 h to complete across the 20 flowers examined. Corollas began to fade in color and dry out after styles started to recurve (**Figures 2C,D**). The entire sequence of events leading to DAS are shown in **Supplementary Video 1**.

For flowers that were accessible to pollinators, mean stigma-upper thecae distance was 3.11 ± 0.80 mm at time of flower opening (0 h) (**Figure 3A**). All marked flowers were visited and pollinated by insects (**Figure 2E**) during the following 24 h (mean

time to successful pollination equaled 19.7 h) and by 24 h mean stigma-upper thecae distance was 3.52 ± 0.59 mm (**Figure 3A**). The two means were not significantly different from each other ($t = -1.796$; $p = 0.081$). The receptive surface of the stigma remained facing outwards from the corolla with large amounts of pollen deposited on it (**Figure 2F**). The corolla quickly dropped from a flower after a pollinator visited it (**Figure 2G**) and the floral processes leading to DAS were terminated.

Effect of Pollination Treatment on Fruit and Seed Set

No fruits and seeds were produced by emasculated and bagged flowers, and it was concluded, therefore, that apomixis did not occur in the species. Fruit set for all other treatments was 100% (**Figure 4A**). High levels of seed set were recorded across these other treatments (**Figure 4A**); however, a one-way ANOVA showed that differences were significant [$F_{(3,324)} = 7.163$, $p < 0.001$]. *Post-hoc* pairwise comparisons of means using Tukey's test indicated that mean seed set of bagged flowers (90.38%, resulting from DAS) was significantly lower than mean seed sets of flowers subjected to either cross-pollination by flowers of the same plant (98.03%, geitonogamy, $p = 0.002$) or different plants (98.29%, xenogamy, $p = 0.001$). However, mean seed set of bagged flowers was not significantly different from that of open-pollinated flowers (94.88%, $p = 0.098$), which, in turn, was not significantly different from the means of the two other treatments. Flowers subjected to the geitonogamy and xenogamy pollination treatments had equivalent high seed set ($p = 0.999$).

Amount of Pollen Required for Sufficient Pollination and High Seed Set

High levels of fruit set (100%) and seed set (>80%) resulted when the number of pollen grains deposited by hand on a stigma of a bagged flower was 5–10 or greater, but were reduced to 45.00 ± 11.12% and 22.50 ± 6.59%, respectively, when 1–3 grains were deposited [**Figure 4B**; One-way ANOVA, Fruit set, $F_{(4,95)} = 12.579$, $p < 0.001$; Seed set, $F_{(4,95)} = 20.432$, $p < 0.001$]. There was no significant difference for fruit set when 4 or more pollen grains were deposited on a stigma (80 vs. 100%, $p = 0.235$), however seed set increased when >4 grains were deposited (**Figure 4B**).

Prevention of DAS by Sufficient Prior Pollination

In flowers in which 1–3 pollen grains were deposited on the stigma, mean stigma-upper thecae distance decreased gradually over time (**Figure 3B**) in a similar, though more rapid, way to when pollinators were excluded from flowers (and presumably zero pollen grains were deposited on stigmas) (**Figure 3A**). Thus, DAS was completed in 14 of the 20 flowers by 48 h after they opened, and in all flowers by 96 h, and on average took 55.2 h to complete. This average time to completion was not significantly different to that (66.7 h) estimated for bagged flowers where access by pollinators was prevented ($t = 1.807$, $df = 38$, $p = 0.079$). In marked contrast, DAS did not occur in flowers in which >20 pollen grains were deposited on stigmas. Mean stigma-upper thecae distance in these flowers remained >1 mm at 24 h after they were pollinated, and was not significantly different from D at the time stigmas were pollinated (**Figure 3B**; $t = 2.00$; $p = 0.053$). After 24 h, the corollas of these flowers quickly dropped, indicating that sufficient prior pollination and fertilization had occurred preventing DAS from occurring.

Fruit and Seed Set Due to DAS in Absence of Pollinators

Records made on bagged flowers of five plants showed that DAS was completed after flower opening in ∼17% of flowers by 24 h, a further 52% of flowers by 48 h, and another 24% by 72 h (**Figure 4C**). Thus, DAS was completed in ∼94% of flowers by 72 h after opening, with only a small proportion of flowers taking longer to complete this process. There was no significant difference in fruit set (all 100%) and seed set (always >80%) of flowers in which DAS was completed at different times over the 24–120 h period that records were taken [**Figure 4C**; One-way ANOVA, seed set, $F_{(4,765)} = 0.813$, $p = 0.517$].

DISCUSSION

Salvia species have an effective floral mechanism for promoting cross-pollination (Claßen-Bockhoff et al., 2003, 2004) and previous studies have shown that bumblebees which pollinate most of these species carry large pollen loads (up to 400 pollen grains) on their body parts (Celep et al., 2014). Our results show that a minimum of 5–10 pollen grains per stigma (i.e., 1–2 pollen grains per ovule) is required to achieve high seed set in *S. umbratica* and that on average, 26 pollen grains per stigma (range 11–65) are deposited by a single pollinator (bumblebee) visit in the field (representing the average of four bumblebee species operating as pollinators). This is more than enough pollen to ensure sufficient pollination and high seed set. However, in the absence of pollinators, we showed that delayed autonomous selfing (DAS) occurs in *S. umbratica* as a result of style recurvature, causing the receptive surface of the bifid stigma to come into contact with the upper anther thecae so that self-pollen is deposited upon it. This is the first demonstration of DAS occurring in the Lamiaceae, despite considerable previous and current interest in the pollination biology of *Salvia* (Celep et al., 2014; Cairampoma et al., 2020; Drew, 2020; Barrionuevo et al., 2021). Our results also showed that a single bumblebee visit to a flower prevents DAS from occurring, because it results in sufficient cross-pollination and fertilization, causing the flower to drop before the style recurves.

For ca. 82% of species (56/68) reported to exhibit DAS, the number of ovules per flower is greater than the four present in *S. umbratica* (Chaudhary et al., 2018; Goodwillie and Weber, 2018; Lemos et al., 2020). Theoretical models predict that stochastic variation in floral mating success creates an advantage to producing many ovules per flower because a plant will often gain greater fitness from occasional abundant seed production in randomly successful flowers than it loses in resource commitment to less successful flowers (Burd et al., 2009). However, species with high numbers of ovules per flower may frequently experience pollen-limitation, i.e., insufficient

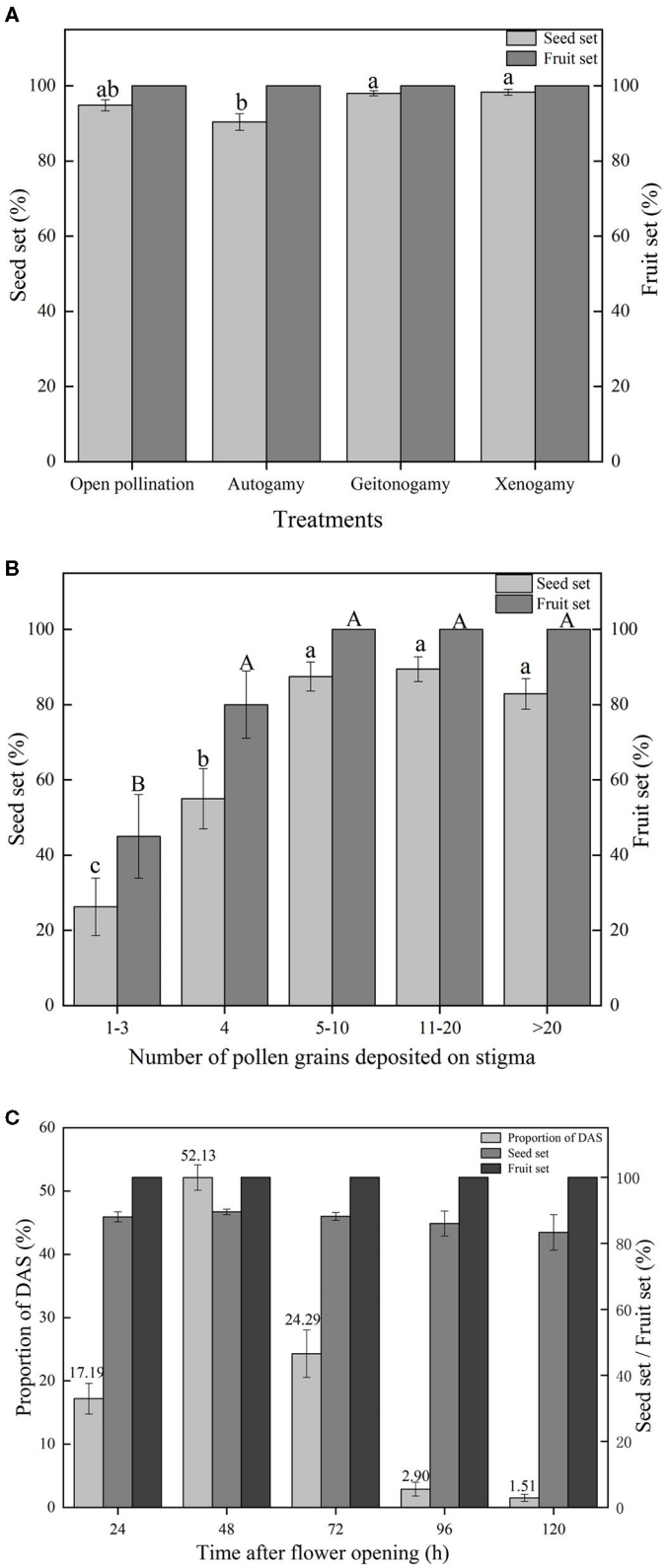

FIGURE 4 | (A) Mean fruit set and seed set of flowers subjected to different pollination treatments (bars indicate standard errors). Treatments sharing the same letters placed above bars are not significantly different according to Tukey's test. N.B. Autogamy, Geitonogamy, and Xenogamy refer to treatments where seed was produced after autonomous selfing, hand-pollination with pollen from same plant, and hand-pollination with pollen from a different plant, respectively. **(B)** Mean fruit set and seed

(Continued)

FIGURE 4 | set of flowers hand-pollinated with different amounts of pollen. Bars indicate standard errors, with treatments sharing the same letters above bars not significantly different according to Tukey's test. **(C)** Proportion of flowers in which DAS was completed at different times after flower opening. Numbers above standard error bars indicate total proportion of DAS flowers (stigma-upper thecae distance, $D = 0$) at given time. Fruit set and seed set in these flowers is also shown.

pollen is deposited on the stigmas of their flowers during one or several visits by a pollinator to fertilize all ovules. In these species, DAS might be advantageous and be expected to continue after flowers have been pollinated by a vector, so as to increase the amount of pollen deposited on stigmas and the probability of all ovules being fertilized. Supporting evidence for this comes from the genus *Centaurium,* in which species commonly produce flowers containing >200 ovules. Brys and Jacquemyn (2011) showed that though stigmas of these flowers are receptive to foreign pollen on the first day a flower opens, during the second and third days after opening, the anthers curl toward the stigma to bring about delayed selfing. In addition, in *Hedychium yunnanense* which produces ∼60 ovules per flower, it has been shown that floral processes continue after hand cross-pollination to bring about contact between stigmas and anthers so as to effect selfing (Ma et al., 2012). Of course, if during a single pollinator visit sufficient pollen is deposited to fertilize all ovules of a species that produces large numbers of ovules per flower, there would seem no advantages to having a DAS mechanism except in environments where pollinators were rare or absent. In the Orchidaceae and subfamily Asclepiadaceae, for example, deposition of a single pollinium containing millions of pollen grains is more than sufficient to fertilize all ovules of a flower (Johnson and Edwards, 2000). However, even in these plant groups some species have mechanisms enabling selfing to occur should cross-pollination fail (Yamashiro and Maki, 2005; Tałałaj et al., 2019).

Species such as *S. umbratica*, which produce one or a few ovules per flower, are unlikely to experience pollen-limitation following a single visit by a pollinator. However, the occurrence of DAS in these species should be favored if they occur in environments where pollinators are often rare or absent. This may be the case for *S. umbratica*, which has spread to northern and eastern parts of China far away from where most other members of subg. *Sclarea* Benth. occur in the Hengduan Mountains and Himalayas. Our studies show that floral longevity in *S. umbratica* is highly variable and dependent on whether or not flowers are cross-pollinated. If flowers are cross-pollinated soon after opening, floral longevity is cut short, with corollas dropping within 24 h of a single bumblebee visit. In contrast, when flowers remain unpollinated, floral longevity is extended allowing DAS to take place. The ability to reduce quickly the longevity of a flower and terminate DAS following cross-pollination will allow resources used in maintenance of floral structures to be diverted for other purposes and should be favored if this leads to an increase in fitness of an individual. This might be particularly important in an annual herb like *S. umbratica* with limited resources available for reproduction.

Some interesting comparisons can be drawn between our findings for *S. umbratica* and those for *Kosteletzkya virginica* (Malvaceae), a herbaceous species native to North America that was introduced to China <20 years ago. Although we are unaware of any reported data regarding floral characteristics and reproductive biology of *K. virginica* in areas where it is native, the species has been shown to exhibit DAS in its introduced range (Ruan et al., 2008). Like *S. umbratica*, it possesses a low number of ovules (five) per flower but in contrast has a five-lobed stigma. Pollination of these stigma lobes prevents their recurvature and therefore terminates floral processes leading to DAS (Ruan et al., 2008). However, recurvature of each stigma lobe is independent of that of other stigma lobes; thus, if only one lobe is pollinated it remains erect, whereas each of the four adjacent unpollinated lobes recurve. Ruan et al. (2008) showed that pollination of a stigma lobe by only one pollen grain prevents recurvature of the lobe provided that a pollen tube is produced which grows beyond the stigma lobe. In contrast, we found that in *S. umbratica* pollination by >4 pollen grains is required to prevent style recurvature. Ruan et al. (2008) further demonstrated that pollen tube growth rather than pollen quantity is the signal that halts stigma lobe curvature in *K. virginica*. It will be interesting to establish in future work if the same is true for style recurvature in *S. umbratica*.

A further difference between *K. virginica* and *S. umbratica* concerns the speed at which recurvature of stigma lobes or styles occurs. Whereas, unpollinated stigma lobes of *K. virginica* begin recurving within 1 h of a flower opening and contact with anthers is made after a further 8–10 h (Ruan et al., 2008), style recurvature is much slower in *S. umbratica,* such that in flowers not accessed by pollinators or hand-pollinated with only 1–3 pollen grains per stigma, contact between the stigma and upper anther thecae occurred on average ca. 55–67 h after they opened. Why the process of delayed selfing is completed much more quickly in *K. virginica* than in *S. umbratica* is an interesting question. Flowers remain open for only a day in *K. virginica* but for several days in *S. umbratica*. It is possible that pollinators are more plentiful in habitats where *K. virginica* occurs compared with those occupied by *S. umbratica*, and that cross-pollination is normally completed very soon after a flower of *K. virginica* opens. If this is the case, it might be expected that selection has favored reduced flower longevity in *K. virginica*. In support, Castro et al. (2008) showed that in *Polygala vayredae* flower longevity varied in response to the abundance of efficient pollinators indicating that increased longevity might maintain the opportunity for cross-pollination and fertilization in this species when pollinators are scarce. However, there are many factors that can influence flower longevity (Ashman and Schoen, 1994; Costa and Machado, 2017; Domingos-Melo et al., 2018; Roddy et al., 2021) and further research is required to establish why non-cross-pollinated flowers of *S. umbratica* remain open for a much longer time than those of *K. virginica.*

Termination of floral processes resulting in delayed selfing, following prior pollination by a pollen-vector, might not be uncommon, although as far as we are aware it has only been demonstrated previously in Malvaceae (Buttrose et al., 1977;

Klips and Snow, 1997; Ruan et al., 2004, 2008; Seed et al., 2006). There are indications, however, that it also occurs in self-compatible Asteraceae. For one such species, *Senecio vulgaris*, it has been shown that florets (each containing a single ovule) often produce elongated styles with no or little self-pollen on their bifid stigmas (Irwin et al., 2016; Love et al., 2016). If stigmatic lobes of these styles are not pollinated by a pollen-vector, they are thought to recurve and pick up pollen from within the floret below. This process is terminated by prior pollination with either self- or cross-pollen, after which styles quickly shrivel before stigmatic lobes recurve.

In view of the findings of the present study, those in Malvaceae, and the possibility that DAS is terminated in self-compatible Asteraceae when prior, vector-mediated pollination occurs, future studies should determine how widespread termination of DAS is in plants, particularly in species that produce few ovules per flower.

DATA AVAILABILITY STATEMENT

The raw data supporting the conclusions of this article will be made available by the authors, without undue reservation.

AUTHOR CONTRIBUTIONS

Y-KW and Y-PM designed the research. H-WX, Y-BH, Y-HC, and YC performed the experiments. H-WX analyzed the date and wrote a preliminary version of the manuscript. RA, Y-KW, and Y-PM revised the manuscript. All authors read and approved the manuscript.

FUNDING

This work was supported by Specific Project for Strategic Biological Resources and Technology Supporting System from the Chinese Academy of Sciences (No. ZSZY-001), Chenshan Special Foundations from Shanghai Municipal Administration of Forestation and City Appearances (Nos. G162408, G172410, and G182409), the Science and Technology Program of Shanghai Science and Technology Committee (No. 20392000600), the Reserve Talents for Academic and Technical Leaders of Middle-aged and Young People in Yunnan Province (Grant No. 2018HB066), and Ten Thousand Talent Program of Yunnan Province (Grant No. YNWR-QNBJ-2018-174).

ACKNOWLEDGMENTS

We thank BFERS of the Chinese Academy of Sciences (CAS) for allowing use of the study site. We thank Jian Yao (Institute of Zoology, CAS) for identifying insect specimens, Dr. Zongxin Ren (Kunming Institute of Botany, CAS) for his comments and suggestions for writing, and Juan Luo for assisting with experiments. We further thank four referees for their helpful comments on earlier versions of the manuscript.

SUPPLEMENTARY MATERIAL

The Supplementary Material for this article can be found online at: https://www.frontiersin.org/articles/10.3389/fpls.2021.635310/full#supplementary-material

REFERENCES

Ashman, T. L., and Schoen, D. J. (1994). How long should flowers live? *Nature* 371, 788–791. doi: 10.1038/371788a0

Barrionuevo, C. N., Santiago, B. V., and Federico, S. (2021). Floral biology of *Salvia stachydifolia*, a species visited by bees and birds: connecting sexual phases, nectar dynamics and breeding system to visitors' behaviour. *J. Plant Ecol.* 14, 580–590. doi: 10.1093/jpe/rtab012

Brys, R., Geens, B., Beeckman, T., and Jacquemyn, H. (2013). Differences in dichogamy and herkogamy contribute to higher selfing in contrasting environments in the annual *Blackstonia perfoliata* (Gentianaceae). *Ann. Bot.* 111, 651–661. doi: 10.1093/aob/mct031

Brys, R., and Jacquemyn, H. (2011). Variation in the functioning of autonomous self-pollination, pollinator services and floral traits in three *Centaurium* species. *Ann. Bot.* 107, 917–925. doi: 10.1093/aob/mcr032

Burd, M., Ashman, T., Campbell, D. R., Dudash, M. R., Johnston, M. O., Knight, T. M., et al. (2009). Ovule number per flower in a world of unpredictable pollination. *Am. J. Bot.* 96, 1159–1167. doi: 10.3732/ajb.0800183

Buttrose, M. S., Grant, W. J. R., and Lott, J. N. A. (1977). Reversible curvature of style branches of *Hibiscus trionum* L., a pollination mechanism. *Aust. J. Bot.* 25, 567–570. doi: 10.1071/BT9770567

Cairampoma, L., Tello, J. A., and Claßen-Bockhoff, R. (2020). Pollination in the desert: adaptation to bees and birds in *Salvia rhombifolia*. *Int. J. Plant Sci.* 181, 857–870. doi: 10.1086/710219

Castro, S., Silveira, P., and Navarro, L. (2008). Effect of pollination on floral longevity and costs of delaying fertilization in the out-crossing *Polygala vayredae* Costa (Polygalaceae). *Ann. Bot.* 102, 1043–1048. doi: 10.1093/aob/mcn184

Celep, F., Atalay, Z., Dikmen, F., Dogan, M., and Claßen-Bockhoff, R. (2014). Flies as pollinators of melittophilous *Salvia* species (Lamiaceae). *Am. J. Bot.* 101, 2148–2159. doi: 10.3732/ajb.1400422

Chaudhary, A., Yadav, S. R., and Tandon, R. (2018). Delayed selfing ensures reproductive assurance in *Utricularia praeterita* and *Utricularia babui* in Western Ghats. *J. Plant Res.* 131,599–610. doi: 10.1007/s10265-018-1016-y

Claßen-Bockhoff, R., Speck, T., Tweraser, E., Wester, P., Thimm, S., and Reith, M. (2004). The staminal lever mechanism in *Salvia* L. (Lamiaceae): a key innovation for adaptive radiation? *Organ. Divers. Evol.* 4, 189–205. doi: 10.1016/j.ode.2004.01.004

Claßen-Bockhoff, R., Wester, P., and Tweraser, E. (2003). The staminal lever mechanism in *Salvia* L. (Lamiaceae)-a review. *Plant Biol.* 5, 33–41. doi: 10.1055/s-2003-37973

Costa, A. C. G., and Machado, I. C. (2017). Pin-monomorphism in *Palicourea crocea* (SW.) Roem. & Schult. (Rubiaceae): reproductive traits and role of floral visitors. *Brazil. J. Bot.* 40, 1063–1070. doi: 10.1007/s40415-017-0406-z

Cuevas, E., Espino, J., and Marques, I. (2018). Reproductive isolation between *Salvia elegans* and *S. fulgens*, two hummingbird-pollinated sympatric sages. *Plant Biol.* 20, 1075–1082. doi: 10.1111/plb.12874

Domingos-Melo, A., Bezerra, S. M. D. S., Nadia, T. D. L., and Machado, I. C. (2020). The dark side of the rain: self-pollination setbacks due to water exposure in *Pavonia varians* Moric (Malvaceae), a species with rain-dependent flowering. *Acta Bot. Brasilica* 34, 437–441. doi: 10.1590/0102-33062020abb0023

Domingos-Melo, A., Nadia, T. L., and Machado, I. C. (2018). At the beginning and at the end: combined mechanisms of prior and delayed self-pollination interact to make a "winner" species. *Flora* 249, 24–30. doi: 10.1016/j.flora.2018.09.007

Drew, B. T. (2020). Evolution, pollination biology, and species richness in *Salvia*. *Int. J. Plant Sci.* 181, 767–769. doi: 10.1086/710711

Fan, Y. L., and Li, Q. J. (2012). Stigmatic fluid aids self-pollination in *Roscoea debilis* (Zingiberaceae): a new delayed selfing mechanism. *Ann. Bot.* 110, 969–975. doi: 10.1093/aob/mcs169

Goodwillie, C., and Weber, J. J. (2018). The best of both worlds? A review of delayed selfing in flowering plants. *Am. J. Bot.* 105, 641–655. doi: 10.1002/ajb2.1045

Haque, M., and Ghoshal, K. (1981). Floral biology and breeding system in the genus *Salvia* L. *Proc. Indian Natl. Sci. Acad.* 47, 716–724.

Hildesheim, L. S., Opedal, Ø. H., Armbruster, W. S., and Pélabon, C. (2019). Fitness costs of delayed pollination in a mixed-mating plant. *Ann. Bot.* 124, 869–881. doi: 10.1093/aob/mcz141

Huang, Y. B., Wei, Y. K., Ge, B. J., and Wang, Q. (2014). Pollination mechanisms of genus *Salvia* (Lamiaceae) in East Asia (China). *Acta Ecol. Sin.* 34, 2282–2289. doi: 10.5846/stxb201308152084

Irwin, J. A., Ashton, P. A., Bretagnolle, F., and Abbott, R. J. (2016). The long and the short of it: long-styled florets are associated with higher outcrossing rate in *Senecio vulgaris* and result from delayed self-pollen germination. *Plant Ecol. Divers.* 9, 159–165. doi: 10.1080/17550874.2016.1181116

Johnson, S. D., and Edwards, T. J. (2000). The structure and function of orchid pollinaria. *Plant Syst. Evol.* 222, 243–269. doi: 10.1007/BF00984105

Jorge, A., Loureiro, J., and Castro, S. (2014). Flower biology and breeding system of *Salvia sclareoides* Brot (Lamiaceae). *Plant Syst. Evol.* 301, 1485–1497. doi: 10.1007/s00606-014-1169-7

Klips, R. A., and Snow, A. A. (1997). Delayed autonomous self-pollination in *Hibiscus laevis* (Malvaceae). *Am. J. Bot.* 84, 48–53. doi: 10.2307/2445882

Knight, T. M., Steets, J. A., Vamosi, J. C., Mazer, S. J., Burd, M., Campbell, D. R., et al. (2005). Pollen limitation of plant reproduction: pattern and process. *Ann. Rev. Ecol. Evol. Syst.* 36, 467–497. doi: 10.1146/annurev.ecolsys.36.102403.115320

Lemos, A. L., Moreira, M. M., Benevides, C. R., Miranda, A. S., and Lima, H. A. D. (2020). Reproductive biology of *Prepusa hookeriana* (Gentianaceae): an endangered species of high-altitude grasslands in Brazil. *Brazil. J. Bot.* 43, 379–387. doi: 10.1007/s40415-020-00611-w

Li, H. W., and Hedge, I. C. (1994). "*Salvia*," in *Flora of China, Vol. 17 (Verbenaceae through Solanaceae),* eds Z. Y. Wu, P. H. Raven, and D. Y. Hong (Beijing; St Louis, MO: Science Press, Missouri Botanical Garden Press), 196–224. Available online at: http://www.iplant.cn/info/Salvia%20umbratica?t=foc (accessed November 29, 2020).

Li, J. K., and Huang, S. Q. (2009). Effective pollinators of Asian sacred lotus (*Nelumbo nucifera*): contemporary pollinators may not reflect the historical pollination syndrome. *Ann. Bot.* 104, 845–851. doi: 10.1093/aob/mcp173

Lloyd, D. G. (1992). Self- and cross-fertilization in plants. II. The selection of self-fertilization. *Int. J. Plant Sci.* 153, 370–380. Available online at: https://www.journals.uchicago.edu/doi/10.1086/297041

Love, J., Graham, S. W., Irwin, J. A., Ashton, P. A., Bretagnolle, F., and Abbott, R. J. (2016). Self-pollination, style length development and seed set in self-compatible Asteraceae: evidence from *Senecio vulgaris* L. *Plant Ecol. Divers.* 9, 371–379. doi: 10.1080/17550874.2016.1244576

Ma, Y. P., Wu, Z. K., Dong, K., Sun, W. B., and Marczewski, T. (2014). Pollination biology of *Rhododendron cyanocarpum* (Ericaceae): an alpine species endemic to NW Yunnan, China. *J. Syst. Evol.* 53, 63–71. doi: 10.1111/jse.12114

Ma, Y. P., Wu, Z. K., Tian, X. L., Zhang, C. Q., and Sun, W. B. (2012). Growth discrepancy between filament and style facilitates autonomous self-fertilization in *Hedychium yunnanense*. *Plant Ecol. Evol.* 145, 185–189. doi: 10.5091/plecevo.2012.652

Milet-Pinheiro, P., Navarro, D. M. D. A.F., Dötterl, S., Carvalho, A. T., Pinto, C. E., Ayasse, M., et al. (2015). Pollination biology in the dioecious orchid *Catasetum uncatum*: how does floral scent influence the behaviour of pollinators? *Phytochemistry* 116, 149–161. doi: 10.1016/j.phytochem.2015.02.027

Navarro, L. (1997). Is the dichogamy of *Salvia verbenaca* (Lamiaceae) an effective barrier to self-fertilization? *Plant Syst. Evol.* 207, 111–117. doi: 10.1007/bf00985212

Roddy, A. B., Martínez-Perez, C., Teixido, A. L., Cornelissen, T. G., Olson, M. E., Oliveira, R. S., et al. (2021). Towards the flower economics spectrum. *New Phytol.* 229, 665–672. doi: 10.1111/nph.16823

Rosas-Guerrero, V., Hernández, D., and Cuevas, E. (2017). Influence of pollen limitation and inbreeding depression in the maintenance of incomplete dichogamy in *Salvia elegans*. *Ecol. Evol.* 7, 4129–4134. doi: 10.1002/ece3.2827

Ruan, C. J., Li, H., and Mopper, S. (2008). The impact of pollen tube growth on stigma lobe curvature in *Kosteletzkya virginica*: the best of both worlds. *South Afr. J. Bot.* 74, 65–70. doi: 10.1016/j.sajb.2007.08.012

Ruan, C. J., Qin, P., He, Z. X., and Staden, J. V. (2004). Delayed autonomous selfing in *Kosteletzkya virginica* (Malvaceae). *South Afr. J. Bot.* 70, 640–645. doi: 10.1016/S0254-6299(15)30204-0

Seed, L., Vaughton, G., and Ramsey, M. (2006). Delayed autonomous selfing and inbreeding depression in the Australian annual *Hibiscus trionum* var. *vesicarius* (Malvaceae). *Austral. J. Bot.* 54, 27–34. doi: 10.1071/BT05017

Strelin, M. M., Sazatornil, F., Benitez-Vieyra, S., and Mariano, O. (2017). Bee, hummingbird, or mixed-pollinated *Salvia*, species mirror pathways to pollination optimization: a morphometric analysis based on the Pareto front concept. *Botany* 95, 139–146. doi: 10.1139/cjb-2016-0145

Sun, S. G., Guo, Y. H., Gituru, R. W., and Huang, S. Q. (2005). Corolla wilting facilitates delayed autonomous self-pollination in *Pedicularis dunniana* (Orobanchaceae). *Plant Syst. Evol.* 251, 229–237. doi: 10.1007/s00606-004-0260-x

Tałałaj, I., Kotowicz, J., Brzosko, E., Ostrowiecka, B., Aleksandrowicz, O., and Wróblewska, A. (2019). Spontaneous caudicle reconfiguration in *Dactylorhiza fuchsii*: a new self-pollination mechanism for Orchideae. *Plant Syst. Evol.* 305, 269–280. doi: 10.1007/s00606-019-01570-w

Wu, C. Y., and Li, H. W. (1977). "Lamiaceae," in *Florae Republicae Popularis Sinicae, Vol. 66* (Beijing: Science Press), 1–647. [In Chinese, with scientific nomenclature]. Available online at: http://www.iplant.cn/info/Salvia%20umbratica?t=z (accessed November 29, 2020).

Xu, G., Zhang, S., Zhang, Y., and Ma, K. (2018). Environmental correlates underlying elevational richness, abundance, and biomass patterns of multi-feeding guilds in litter invertebrates across the treeline. *Sci. Total Environ.* 633, 529–538. doi: 10.1016/j.scitotenv.2018.03.212

Yamashiro, T., and Maki, M. (2005). A comparative study of the reproductive character and genetic diversity of an autogamous *Tylophora matsumurae* and its progenitor *Tylophora tanakae* (Apocynaceae-Asclepiadoideae). *Plant Syst. Evol.* 256, 55–67. doi: 10.1007/s00606-005-0360-2

Conflict of Interest: The authors declare that the research was conducted in the absence of any commercial or financial relationships that could be construed as a potential conflict of interest.

Publisher's Note: All claims expressed in this article are solely those of the authors and do not necessarily represent those of their affiliated organizations, or those of the publisher, the editors and the reviewers. Any product that may be evaluated in this article, or claim that may be made by its manufacturer, is not guaranteed or endorsed by the publisher.

frontiers in Plant Science

ORIGINAL RESEARCH
published: 27 July 2021
doi: 10.3389/fpls.2021.703713

Sequential Deposition and Remodeling of Cell Wall Polymers During Tomato Pollen Development

*Syeda Roop Fatima Jaffri and Cora A. MacAlister**

Department of Molecular, Cellular and Developmental Biology, University of Michigan, Ann Arbor, MI, United States

The cell wall of a mature pollen grain is a highly specialized, multilayered structure. The outer, sporopollenin-based exine provides protection and support to the pollen grain, while the inner intine, composed primarily of cellulose, is important for pollen germination. The formation of the mature pollen grain wall takes place within the anther with contributions of cell wall material from both the developing pollen grain as well as the surrounding cells of the tapetum. The process of wall development is complex; multiple cell wall polymers are deposited, some transiently, in a controlled sequence of events. Tomato (*Solanum lycopersicum*) is an important agricultural crop, which requires successful fertilization for fruit production as do many other members of the Solanaceae family. Despite the importance of pollen development for tomato, little is known about the detailed pollen gain wall developmental process. Here, we describe the structure of the tomato pollen wall and establish a developmental timeline of its formation. Mature tomato pollen is released from the anther in a dehydrated state and is tricolpate, with three long apertures without overlaying exine from which the pollen tube may emerge. Using histology and immunostaining, we determined the order in which key cell wall polymers were deposited with respect to overall pollen and anther development. Pollen development began in young flower buds when the premeiotic microspore mother cells (MMCs) began losing their cellulose primary cell wall. Following meiosis, the still conjoined microspores progressed to the tetrad stage characterized by a temporary, thick callose wall. Breakdown of the callose wall released the individual early microspores. Exine deposition began with the secretion of the sporopollenin foot layer. At the late microspore stage, exine deposition was completed and the tapetum degenerated. The pollen underwent mitosis to produce bicellular pollen; at which point, intine formation began, continuing through to pollen maturation. The entire cell wall development process was also punctuated by dynamic changes in pectin composition, particularly changes in methyl-esterified and de-methyl-esterified homogalacturonan.

Keywords: pollen, exine development, intine, cell wall, tomato, pectin, cellulose, callose (β-1,3-glucan)

OPEN ACCESS

Edited by:
David Honys, Institute of Experimental Botany, Czechia

Reviewed by:
Jingbo Zhang, St. John's University, United States
Humberto Herrera-Ubaldo, Instituto Politécnico Nacional de México (CINVESTAV), Mexico

****Correspondence:***
Cora A. MacAlister
macalist@umich.edu

Specialty section:
This article was submitted to Plant Development and EvoDevo, a section of the journal Frontiers in Plant Science

Received: *30 April 2021*
Accepted: *21 June 2021*
Published: *27 July 2021*

Citation:
Jaffri SRF and MacAlister CA (2021) Sequential Deposition and Remodeling of Cell Wall Polymers During Tomato Pollen Development. Front. Plant Sci. 12:703713. doi: 10.3389/fpls.2021.703713

INTRODUCTION

The production of pollen was a major innovation during the evolution of land plants. The pollen grain is a highly specialized structure, which includes a complex and unique cell wall supporting its functions. The mature pollen wall can be broadly divided into two layers, an outer sporopollenin-rich exine and an inner intine, which has a composition similar to other plant cell walls. In addition to the differences in their composition, these two layers have markedly different developmental origins and functions (Heslop-Harrison, 1968). The exine protects the pollen cytoplasm from excess dehydration and other environmental insults and mediates adhesion to pollinators and the stigmatic surface (Zinkl et al., 1999). Once the relevant interactions between pollen and stigma take place, the pollen grain hydrates and the intine serves as the organizing site for the formation of a pollen tube. Once initiated, the pollen tube expands at its tip to complete pollen germination. The pollen tube will then carry the sperm nuclei from the pollen grain through the female floral tissue to a receptive ovule (Taylor and Hepler, 1997).

Pollen development takes place in the anthers, beginning in early immature buds, with the specification of microspore mother cells (MMCs) and proceeding through meiosis, microspore mitosis, and pollen development to mature pollen release at anther dehiscence (Canales et al., 2002; Scott et al., 2004; Gómez et al., 2015). During this process, the cell wall is radically altered with many cell wall polymers deposited, removed, or remodeled. The mature pollen cell wall contains material produced by both the developing pollen itself and by the sporophytic tapetum, a layer of cells lining the locule cavity in which the microspores develop (Owen and Makaroff, 1995).

Before the initiation of meiosis, the MMCs are surrounded by a simple primary cell wall; during early prophase, the middle lamella expands, followed by a reduction in the flanking fibrillous wall layers and the initiation of callose (β-1,3-glucan) deposition between the plasma membrane and the primary wall (Polowick and Sawhney, 1992). The deposition of callose continues during and after meiosis, eventually producing a thick callose wall, which holds the four products of meiosis in a tetrad (Polowick and Sawhney, 1993a; Owen and Makaroff, 1995). The callose wall serves as a scaffold for exine development, first by the deposition of primexine, a poorly defined microfibrillar polysaccharide matrix formed by the microspore (Hess and Frosch, 1994). Secretion of callase by the tapetal tissue causes the breakdown of the callose wall separating the individual microspores (Chasan, 1992; Polowick and Sawhney, 1993b; Rhee et al., 2003; Quilichini et al., 2014). The primexine serves as a scaffold for the deposition of sporopollenin produced by the tapetum. The sporopollenin polymerizes onto the primexine, producing the foot layer (Quilichini et al., 2014). The exine may be further elaborated with additional sporopollenin deposition, e.g., production of inner-column-shaped baculae and the surface decoration tectum. Together, the sporopollenin foot layer (nexine), tectum, and baculae (sexine) form the mature pollen exine (Polowick and Sawhney, 1992; Chebli et al., 2012; Jiang et al., 2013; Renzaglia et al., 2020). After exine deposition, the tapetal cell layer breaks down, releasing material for the outermost layer of the pollen, the pollen coat also called "pollenkitt" or "tryphine" (El-Ghazaly and Jensen, 1986). The pollen coat is required for the pollen-stigma interface and promotes pollen hydration (Ishiguro et al., 2010), and is largely composed of proteins and lipids (Piffanelli and Murphy, 1998; Bashir et al., 2013; Rejón et al., 2016).

Concurrent with the later stages of exine formation, the intine develops. Unlike the exine, which is composed primarily of specialized sporopollenin, the composition of intine is similar to that of other plant cell types with major components, including cellulose, pectin, and cell wall-associated proteins (Hess, 1993; Suárez-Cervera et al., 2002; Persson et al., 2007; Fang et al., 2008). The apertures, which will serve as possible sites for pollen tube initiation and pollen germination, develop a unique pollen wall, completely or partially lacking exine and, in some species, highly elaborating the intine into a specialized structure called the "Zwischenkörper" (Picken, 1984; El-Ghazaly and Jensen, 1986; Dobritsa and Reeder, 2017).

Mutants with defects in pollen wall formation have been identified in several species, providing insight into the molecular basis of pollen wall development and the roles of cell wall components. The process of exine deposition is relatively well studied, and there are many well-characterized exine mutants with male sterility phenotypes (Blackmore et al., 2007; Dobritsa et al., 2011; Jiang et al., 2013; Shi et al., 2015a). Broadly speaking, these mutants can be classified into overlapping functional categories, including biosynthesis and transport of sporopollenin precursors, primexine formation, and tryphine synthesis. Proteins falling in the sporopollenin biosynthesis class include ACYL-CoA SYNTHETASE5 (ACOS5), the fatty acyl reductase MALE STERILE2 (MS2), along with its rice ortholog DEFECTIVE POLLEN WALL (DPW), and acyl-CoA-binding proteins (AtACBP4, 5, and 6), among others (Aarts et al., 1997; Souza et al., 2009; Shi et al., 2011; Zhang et al., 2011; Hsiao et al., 2015). Since the synthesis of sporopollenin precursors takes place in the tapetum, they must be transported into the anther locule, which requires the ATP-binding cassette transporter superfamily member ABCG26/WBC27 (Quilichini et al., 2010; Choi et al., 2011). Notable primexine genes include Arabidopsis *DEFECTIVE IN EXINE FORMATION 1* (*DEX1*) and its rice ortholog *OsDEX1*(Yu et al., 2016). DEX1 is a membrane calcium-binding protein, and *dex1* pollen has reduced primexine and abnormal exine (Paxson-sowders et al., 2001). Examples of tryphine synthesis mutants include mutants of phosphoserine phosphatase, an enzyme required to catalyze the last step of the phosphorylated pathway of serine biosynthesis (PPSB). These mutants show a normal exine without any tryphine (Flores-Tornero et al., 2015).

Cellulose synthesis and callose synthesis and degradation are also required for pollen wall development. Arabidopsis triple mutants in the cellulose synthase complex members *cesa6*, *cesa9*, and *cesa2* produced deformed pollen with abnormally thickened intines, possibly due to a compensation by other cell wall polymers in the absence of cellulose (Persson et al., 2007). In Arabidopsis, the callose synthase CalS5 is required for callose wall formation and pollen fertility. In *cals5* mutants, the exine wall organization is also disrupted with malformed

baculae and tectum as well as randomly deposited globular tryphine, showing that the callose wall is required for exine sculpting (Dong et al., 2005). Similarly, a knockdown or a knockout of rice Glucan Synthase-Like 5 (GSL5) reduces callose production during pollen development, compromising exine deposition and pollen fertility (Shi et al., 2015b). The timely degradation of callose is also required for pollen fertility. Rice plants silenced for the β-1,3-glucanase gene *Osg1* have delayed release of the microspores from the tetrad, leading to their degeneration and male sterility (Wan et al., 2011).

Several mutants also suggest an important role for pectin throughout pollen development (Suárez-Cervera et al., 2002; Phan et al., 2011; Chebli et al., 2012; Jiang et al., 2013; Cankar et al., 2014). The major form of pectin, homogalacturonan (HG, β-1, 4-galacturonic acid), is initially synthesized in the Golgi in a methyl-esterified form (meHG). After secretion, the methyl groups may be enzymatically removed by pectin methyl-esterases (PMEs) to form de-methyl-esterified HG (dmeHG), exposing negative charges, which can form Ca^{2+} salt bridges between neighboring polymers, rigidifying the wall (Bosch and Hepler, 2005). De-methyl-esterification can also promote pectin degradation by polygalacturonases (PGs) (Verlag et al., 2003). The separation of the microspores at the tetrad stage requires pectin remodeling as evidenced by the Arabidopsis *quartet* mutants (*qrt1*, *qrt2*, and *qrt3*) in which the pollen completes development as a tetrad (Preuss et al., 1993; Rhee et al., 2003). *QRT1* encodes a PME and *QRT2* and *QRT3* encode PGs (Aouali et al., 2001; Rhee et al., 2003; Francis et al., 2006; Ogawa et al., 2009). Pectin remodeling is also important for the formation of the intine as demonstrated by Arabidopsis *pme48* mutants in which the intine accumulates high levels of meHG, resulting in defective pollen imbibition and germination defects (Leroux et al., 2015). In Chinese cabbage, co-inhibition of two closely related PGs, Brassica campestris Male Fertility 26a (BcMF26a) and BcMF26b, has defective pollen intine and severely inhibited male fertility (Lyu et al., 2015).

While broad landmarks of anther and pollen development are well-known and generally conserved, the molecular events of PG wall formation have received much more limited attention, particularly with respect to the development of the intine (Gómez et al., 2015; Ma et al., 2021). Here, we focus on elucidating this process during tomato pollen development. Tomato is an important agricultural crop, which requires successful pollination for a fruit set (Picken, 1984). It is also highly sensitive to environmental disruptions of fertility, particularly high-temperature stress (Pressman et al., 2002; Giorno et al., 2010, 2013; Müller et al., 2016). Therefore, understanding the development of pollen is an important preliminary step in safeguarding production against environmental insults. Tomato also serves as a model system for the large Solanaceae family, which includes many other agriculturally important plants. Given the importance of the pollen grain wall to pollen fertility, we have established a timeline of polymer deposition and remodeling during tomato pollen grain wall formation.

MATERIALS AND METHODS

Plant Material and Growth Conditions

Solanum lycopersicum cv. Micro-Tom (Carvalho et al., 2011) was grown under 16-h light:8-h-dark cycles in temperature-controlled growth chambers maintained at 23°C. Buds were staged by measuring the length from the bud tip to the pedicle with a vernier caliper. For scanning electron microscopy (SEM) of pollinated pistils, anthers were removed from 6-mm flower buds, and pistils were covered with open 0.2-ml PCR tubes and allowed to mature for 48 h. Pollen was collected by vortexing freshly collected mature anthers in 1.5-ml epitubes and applied to pistils with a paint brush. Pollinated plants were returned to the growth chamber, watered, and covered with a clear plastic dome to increase humidity. Five hours after pollination, pistils were fixed and treated for SEM as described below.

Scanning Electron Microscopy

For scanning electron microscopy (SEM), manually pollinated pistils were collected and submerged in fresh fixative (acetic acid/ethanol, 1:3), and fixed under a vacuum for 2 h. Pistils were then transferred to fresh 100% ethanol and kept at 4°C overnight in a tightly closed glass vial. The tissue was then dehydrated, using chemical drying with graded hexamethyldisilazane (HDMS) (Sigma-Aldrich catalog number 440191) series (Lee and Chow, 2012). Ethanol was slowly replaced with HDMS for 20 min each in ethanol: HDMS series of 1:0, 3:1, 3:2. 1:1, and 1:3, and three times 100% HDMS. Afterwards, tissue was left overnight in the HDMS in an open tube under the fume hood. In the morning, the HDMS evaporated, and the tissue was dry and ready for gold coating. Tissue was attached to SEM stubs with double-sided tape, and sputter coated with gold particles in a vacuum at 200-m Amps for 120 s (∼15–20 nm of gold), using a Denton Desk II sputter coater. For imaging of pollen grains, dry mature pollen grains were collected in epitubes from healthy, mature dehiscent flowers. Pollen was sprinkled on adhesive SEM stubs with paint brush bristles and sputter coated with gold particles in a vacuum for 90 s. Gold-coated pollen and pistils were imaged, using the EMAL JEOL JSM-7800FLV field-emission scanning electron microscope. For pore diameter measurements, three random pictures, each of four individual pollen grain, were taken, and diameters of all the pores in each micrograph were measured. The shown values are average across all measurements.

Transmission Electron Microscopy

Pollen grains were suspended in ice-cold fixative, containing 2% formaldehyde, 2.5% glutaraldehyde, .025-M PIPES buffer pH 7.2, and 0.001% Tween 20 *via* vortexing. After 2-h incubation under a vacuum, the solution was replaced with fresh fixative, and vials were sealed and kept at 4°C overnight. Pollen was then pelleted by centrifugation at room temperature and washed with 0.025-M phosphate buffer pH 7 for 10 min, followed by a PIPES buffer pH 7.2 wash for 20 min. Pollen was then post fixed in 1% osmium tetroxide (Sigma-Aldrich catalog number 75633) in phosphate buffer pH 7 for 1 h. This was followed by another 10-min phosphate buffer wash, followed by 20-min PIPES buffer wash. Pollen was then dehydrated for 20 min each in an ethanol

series (25, 35, 50, 70, 80, 90, and three times 100%). Ethanol was then replaced slowly with an LR white plastic polymer (Agar Scientific catalog number AGR 1281) by an LR white: ethanol series of 1:3, 2:3, 1:1, 3:2, 3:1,1:0, 1:0, and 1:0, with each step of the series having a 4°C incubation of 24 h. At this stage, pollen was put in a gelatin capsule with fresh LR white and polymerized at 58°C for 24 h. Solid polymer blocks were sectioned into 80-nm ultrathin sections and stained with 7% uranyl acetate and lead citrate. Sections were imaged with the JOEL JEM-1400 plus electron microscope with an XR401 SCMOS camera. For cell wall measurements, three pollen grains were measured at 10 random positions per grain, excluding the apertures; the average across all measurements was taken.

Paraffin Embedding, Sectioning, and Toluidine Blue Staining

To identify appropriate bud length for each pollen development stage, flower buds of 2, 4, 5, 6, 8-mm, and fully mature dehiscent flowers were fixed by submerging in ice cold fixative (4% PFA and 0.3% Tween20 in PBS) and vacuum infiltrated for 20 min. Fresh fixative and a vacuum were applied until the tissue sunk to the bottom. The tissue was then dehydrated in a PBS-ethanol series of 10, 30, 50, 70, 85, and 100% ethanol for 1 h each at 4°C. The tissue was then infiltrated with histoclear (Avantor, Electron Microscopy sciences, catalog number 101412-878) in ethanol: histoclear series (3:1, 1:1, 0:1, 0:1, and 0:1) at room temperature. Histoclear was then slowly replaced with molten paraffin at 60°C by replacing the histoclear with a histoclear: paraffin series (3:1, 1:1, 1:3, 0:1, 0:1, and 0:1) for 24 h each at 60°C. Final paraffin-embedded tissue was sectioned with a microtome to 8-μm thick sections and placed on polylysine-coated slides. Sections were dewaxed by submerging in histoclear and dehydrated by dipping in an ethanol series (10, 30, 50, 70, 85, and 100%) ethanol in PBS. Dewaxed and dehydrated sections were stained with 0.1% toluidine blue (Cankar et al., 2014) by applying the stain and heating the slide to 60°C for 30 s. After stain application, slides were washed with distilled water and permanently mounted by applying Permount (Fischer Scientific catalog number SP15-500) and cover slip.

LR White Embedding, Semi-thin Sectioning, and Immunostaining

Immunohistochemistry analysis was done as previously described (Luis da Costa et al., 2017). Briefly, flower buds of the appropriate length were removed from the plant, and, for buds bigger than 2 mm, the anthers were dissected out. The tissue was fixed and LR white embedded as described for TEM above, without the osmium tetroxide post-fixation step. Hardened samples were sectioned with glass knife ultramicrotome in 200-nm semi-thin sections. Sections were observed and imaged with light microscopy by staining with 0.1% toluidine blue in the water. For calcofluor white staining, one drop of calcofluor white solution (containing Calcofluor White 1 g/l, Evans blue 0.5 g/l; Sigma-Aldrich, 18909) was added to the well of the slide and imaged after applying the coverslip. For aniline blue staining of callose, one drop of aniline blue fluorochrome (0.1-mg/ml in distilled water; Biosupplies, 18,909) was applied to the well of the slide and imaged after applying the coverslip. For immunostaining, sections were placed in welled 0.001% poly-L-Lysine-coated slides. After drying at 50°C overnight, sections were incubated in blocking solution (5% non-fat dried milk in 1x PBS) for 10 min in a humid chamber. Then the sections were washed for 10 min with PBS. Sections were incubated at room temperature for 2 h, followed by 4°C incubation overnight in primary antibody solution (Rat monoclonal LM19 or LM20; a 1:5 antibody in blocking solution; Verhertbruggen et al., 2009). Sections were then washed two times with PBS for 10 min and then incubated with secondary antibody solution (Anti-Rat conjugated with FITC, Sigma-Aldrich, F6258; 1:100 in blocking solution) for 3–4 h at room temperature in the dark. Sections were then washed two times with PBS for 10 min each. Sections were imaged after adding one drop of calcofluor white and applying a drop of Vectashield® antifade (Vector laboratories catalog number H-1000-10) and applying the coverslip. Sections were imaged, using the Leica SP5 laser scanning confocal microscope.

RESULTS

The Structure of Mature Tomato Pollen

To observe the general shape and structure of the tomato pollen, we imaged mature-released pollen grains, using scanning electron microscopy (SEM). SEM micrographs showed that the tomato pollen exhibits features of a typical dicot pollen grain, with a prolate spheroid shape, containing three radially equidistant elongated apertures (**Figure 1A**). The outer surface of the pollen was textured with spines of exine interspersed with small pores with an average diameter of 38 ± 9 nm (**Supplementary Figures 1B–D**).

To observe the internal morphology of the pollen grain, we used transmission electron microscopy (TEM) to image transverse sections of the mature pollen grain (**Figure 1B**). Inside, the pollen was populated with an extensive ER network, vegetative and generative nuclei, numerous mitochondria, vacuoles as well as starch granules. In some sections, Golgi stacks were also visible. Upon close-up examination of the pollen wall structure (**Figure 1C**), intine was apparent as the inner, lighter, less electron dense layer around the pollen compared with the outer exine, which stained much darker. The layered organization of the exine was also apparent with the nexine layer directly adjacent to the intine, followed by the columnal baculae and, finally, the outermost tectum layer (**Figure 1C**). We measured the thickness of the overall pollen wall (658.54 ± 58 nm) and the cell wall layers (intine 151 ± 28 nm, sexine 398 ± 38 nm, nexine 112 ± 30 nm). The intine wall was continuous around the perimeter of the pollen grain, but exine was absent at the apertures. At the apertures, while the exine was absent, the inner layer of intine formed a curved outward projection at the aperture site, called the "Zwischenkörper." The intine at this site was thickened and with a layered and spongy appearance (**Figure 1D**).

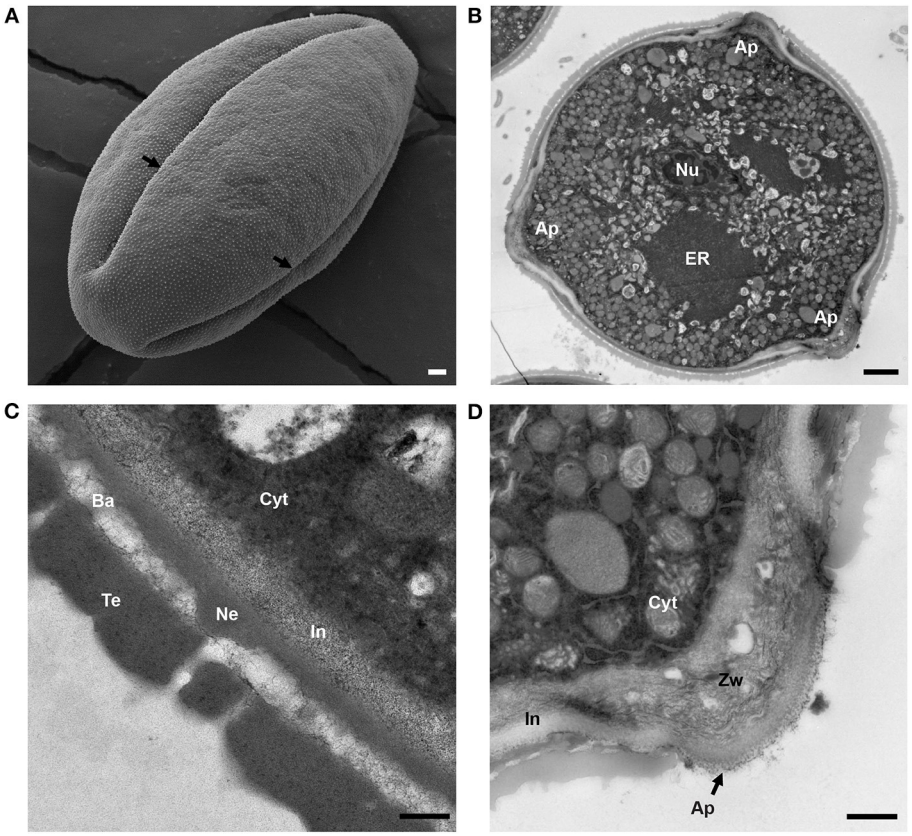

FIGURE 1 | Structure of mature tomato pollen grain. **(A)** Scanning electron micrograph of a mature, released tomato pollen grain. Arrows mark the apertures (Ap). **(B)** Transmission electron micrograph of a mature pollen grain cross section. Nu, nucleus; ER, endoplasmic reticulum; Ap, aperture. **(C)** TEM of mature pollen, showing the layers of the pollen wall. Cyt, cytoplasm; In, intine; Ne, nexine; Ba, bacula; Te, tectum. **(D)** TEM close-up of pollen aperture. Arrow marks the aperture. Cyt, cytoplasm; In, intine; Zw, zwischenkorper. Scale bars 1 μm in **(A)**, 2 μm in **(B)**, 200 nm in **(C)**, and 600 nm in **(D)**.

The Pollen Development Stage Correlates With Flower Bud Length

To establish a reproducible staging method for pollen development, we compared the morphology of anthers and developing pollen in toluidine blue-stained sections of floral buds at various bud sizes. We found that flower bud length correlated well with developmental stages of the pollen grain and could be effectively used to non-destructively estimate the developmental stage of the pollen (**Figure 2A**).

In the anthers of 2-mm-long buds, the microspore mother cells (MMCs) were visible with enlarged nuclei (**Figures 2B–D**). Cells in the center of the anther were continuous at this stage without locular pockets (**Figure 2B**, **Supplementary Figure 2A**). At the 4-mm bud stage, meiosis was complete, and the meiotic products were still joined in a tetrad. The tetrad cells had distinct centrally located nuclei, with no obvious vacuoles or visible nucleolus. The thick pollen wall did not stain with toluidine blue at this stage, but its outer edge was visible in sections (**Figures 2B–D**). In the anther, there was a distinct tapetal cell layer surrounding four locular pockets, larger and smaller pockets in each anther lobe (**Supplementary Figure 2B**).

Pollen in the 5-mm flower buds was at the early microspore stage. The microspores had an ameboid shape, and their nuclei had a distinct outline and visible nucleolus (**Figures 2B–D**). In the anthers, the locules on each side of the anther considerably enlarged but were still separated by interlocular septa and were still lined with a distinct visible tapetum cell layer (**Supplementary Figure 2C**). By this stage, the non-staining tetrad wall had disappeared. In the 6-mm flower bud, the first pollen mitosis occurred, producing bicellular pollen with a more rounded shape and a large central vacuole. The anthers were yellow, and the two locule pockets on each side had joined to make one continuous locule cavity after the deterioration of interlocular septa (**Supplementary Figure 2D**). The tapetum had also broken down, with the leftover vestiges visible in the locular cavity and around the pollen.

Pollen in the 8-mm flower was fully mature, with a well-rounded shape and one or two nuclei visible in sections. In tomato, the second pollen mitosis, producing the two sperm nuclei, occurs during pollen tube elongation (Brukhin et al., 2003). The pollen at this stage also had a distinct, two layered wall differentially stained with toluidine blue. The purple inner layer was especially prominent at the aperture sites. The pollen also

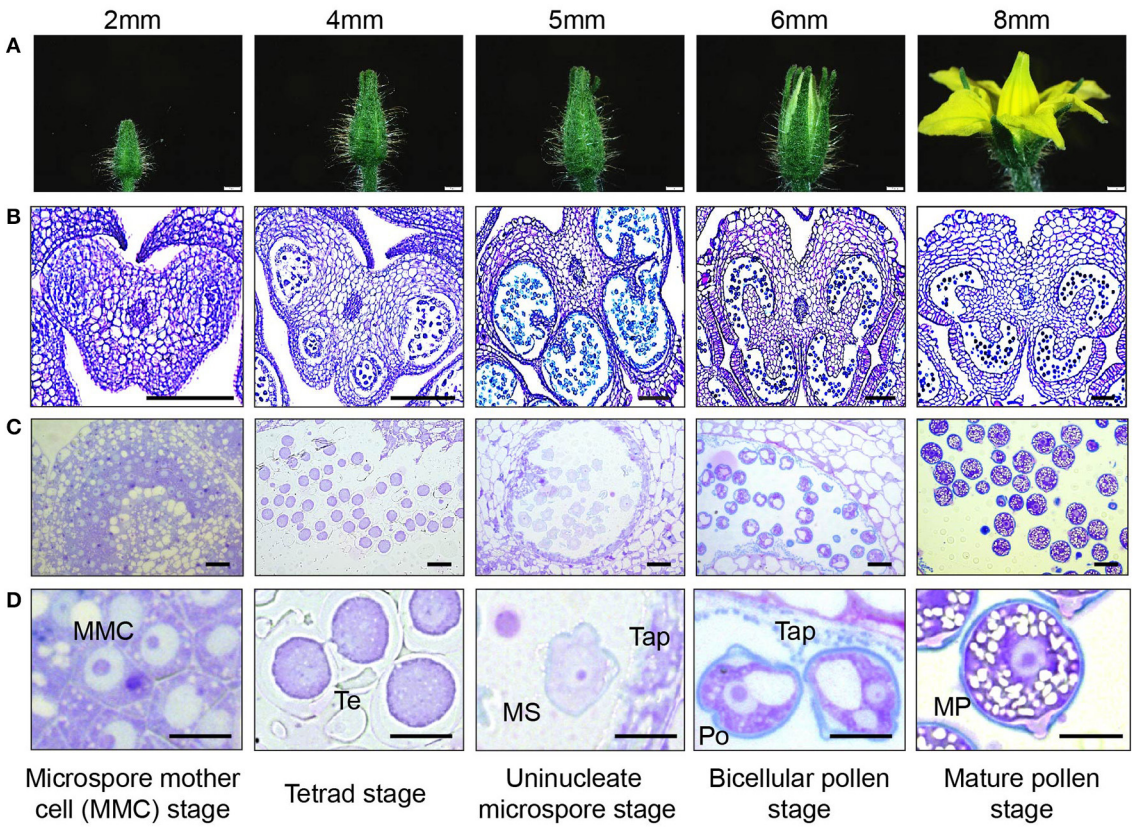

FIGURE 2 | Tomato pollen development staging. **(A)** photographic series of floral development in tomato, with bud length as a marker for each stage in pollen development inside the anther. Bud lengths, 2 mm (microspore mother cell stage), 4 mm (tetrad stage), 5 mm (uninucleate microspore stage), 6 mm (bicellular pollen stage), and 8 mm (mature pollen stage). **(B)** Micrographs of paraffin-embedded 8-μm-thick anther cross sections, stained with toluidine blue. **(C)** Micrographs of LR White embedded 500-nm-thick anther cross sections, also stained with toluidine blue. **(D)** Developing pollen grain at higher magnification, close-up of individual cells. MMC, microspore mother cell; Te, tetrad; MS, microspore; Tap, tapetum; Po, pollen; MP, mature pollen. Scale bars 1 mm in **(A)**, 100 μm in **(B)**, 20 μm in **(C)**, and 10 μm in **(D)**.

contained abundant, unstained starch granules (**Figures 2B–D**). The tapetum fully disappeared. The flower was open, and the anther was close to dehiscence upon breakage of the weak anther stomium (**Figure 2A**).

Exine Deposition Occurs Post Tetrad

Sporopollenin is a distinct biological polymer, composed of fatty acid derivatives and phenolic compounds (Piffanelli et al., 1998; Blackmore et al., 2007). It is only found in the exine layer of the pollen grains and plant spores and is one of the most resilient biological molecules. Toluidine blue (TD) is a basic thiazine metachromatic dye and differentially stains acidic residues with high affinity (Sridharan and Shankar, 2012). Since sporopollenin is acidic, it stains differently with toluidine blue stain (bluer as compared with intine, which stains purple) (Dobritsa et al., 2011). We used toluidine blue-stained sections to observe exine deposition in developing pollen. After no cell wall staining with TD in the tetrad stage (4-mm buds), a thin layer of exine was visible in the early microspores (a 5-mm bud) (**Figure 3A**). This foot layer had visible breaks at the slightly invaginated future aperture sites (**Figure 3A**, right). In the bicellular pollen stage (a 6-mm bud), the exine was much thicker, indicated by a thicker, bluer pollen outline, and the aperture sites were visible as indentations in the exine (**Figure 3B**). By this stage, tapetum had degenerated, leaving behind pollenkitt and pollen coat particles. In the 8-mm buds, the mature pollen had a solid blue outline, showing a fully developed exine wall, as well as a differentially stained intine also clearly visible (**Figure 3C**).

Cellulose and Callose Dynamics

While certain cell wall changes were apparent in sections stained with toluidine blue, the status of other cell wall polymers required further investigation. Therefore, to follow pollen wall development, we stained anther sections of the defined developmental stages with various carbohydrate-binding dyes and cell wall antibodies. The fluorescent dye Calcofluor white is a fluorochrome with a high affinity for cellulose (β-1,4-glucan), and chitin and is regularly used to observe pollen intine, although it also possesses some affinity for callose (Fang et al., 2008; Herburger and Holzinger, 2016; Li et al., 2017; Renzaglia et al., 2020; Takebe et al., 2020). Aniline blue fluorochrome (ABF) is a callose-specific dye often used to stain pollen tube cell walls

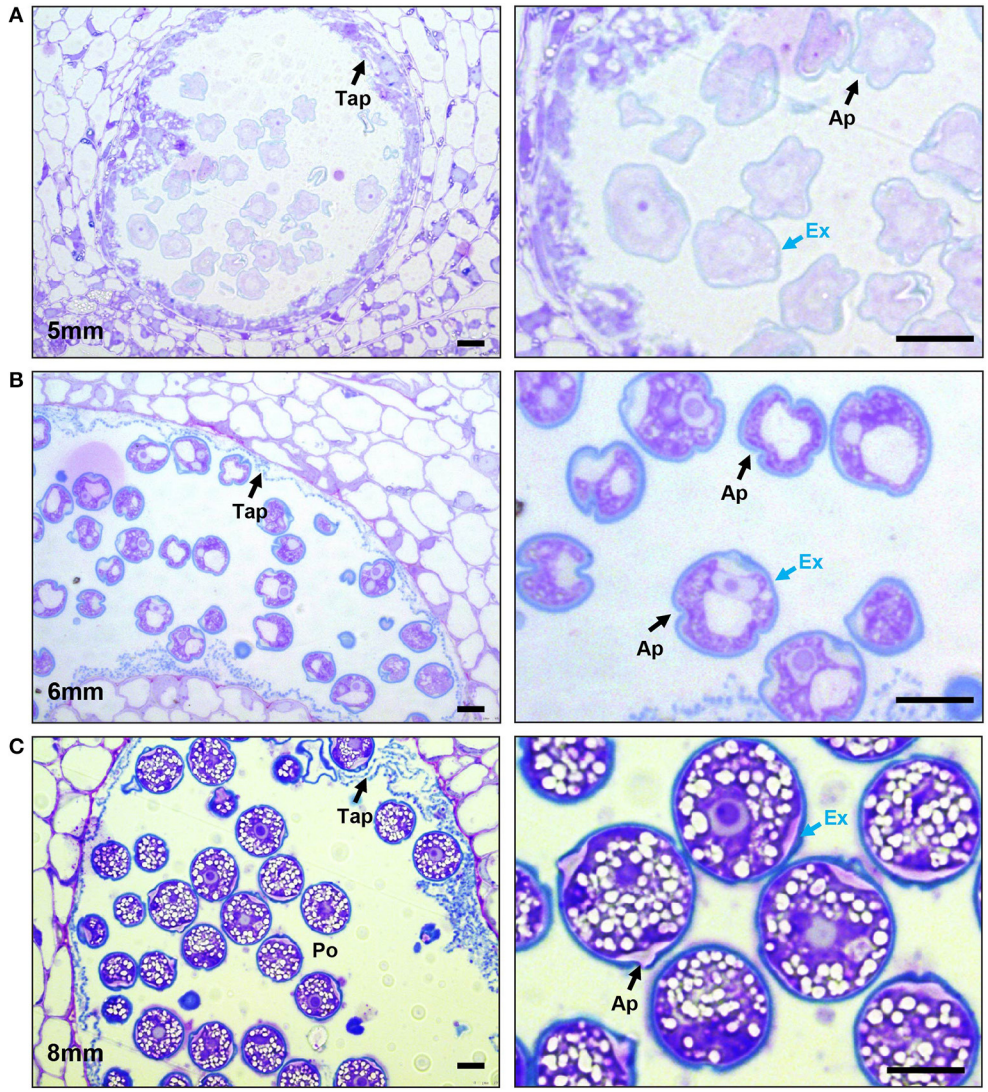

FIGURE 3 | Progression of exine deposition. Micrographs of LR White embedded 500-nm thick anther cross sections, stained with toluidine blue. **(A)** The uninucleate microspore stage at 5-mm bud length. Cross section of anther locule (Left), The arrow marks the tapetum. Close-up of microspores (right), black arrow marks aperture; the blue arrow marks the exine. **(B)** The bicellular pollen stage at 6-mm bud length. Cross section of anther locule (left); the arrow marks the tapetum. Close-up of microspores (right), black arrow marks aperture; the blue arrow marks the exine. **(C)** The mature pollen stage at 8-mm bud length. Cross section of anther locule (left); the arrow marks the tapetum. Close-up of microspores (right); the black arrow marks aperture; the blue arrow marks the exine. Ex, exine; Tap, tapetum; Po, pollen; Ap, aperture. All scale bars are 10 μm.

(Fang et al., 2008; Herburger and Holzinger, 2016; Renzaglia et al., 2020).

In 2-mm buds, calcofluor white weakly stained the MMC cell walls but strongly stained the cell walls of the surrounding anther tissue, suggesting reduced cellulose content in the MMC walls (**Figure 4A**). In 4-mm buds, the tetrad-stage pollen wall stained strongly with both calcofluor white (**Figure 4B**) and ABF (**Figure 5**). ABF did not stain the pollen or the surrounding anther tissue during any other stage of development (not shown). After dissolution of the transient callose wall, in 5-mm buds, no calcofluor white signal was observed around the uninucleate microspore (**Figure 4C**), although light microscopy at this stage showed there is a thin wall around the pollen (**Figure 2D**). In the 6-mm bud, the bicellular pollen had a thin rim of calcofluor white signal but a robust signal at the aperture sites, consistent with the development of the thick intine of the Zwischenkörper (**Figure 4D**). In the mature pollen in the 8-mm flower bud, the pollen had a continuous calcofluor white-positive layer around the perimeter of the pollen, with particularly prominent signal at the apertures (**Figure 4E**).

Pectin Dynamics

To examine the pattern of meHG and dmeHG during pollen development, we immuno-stained anther sections with rat

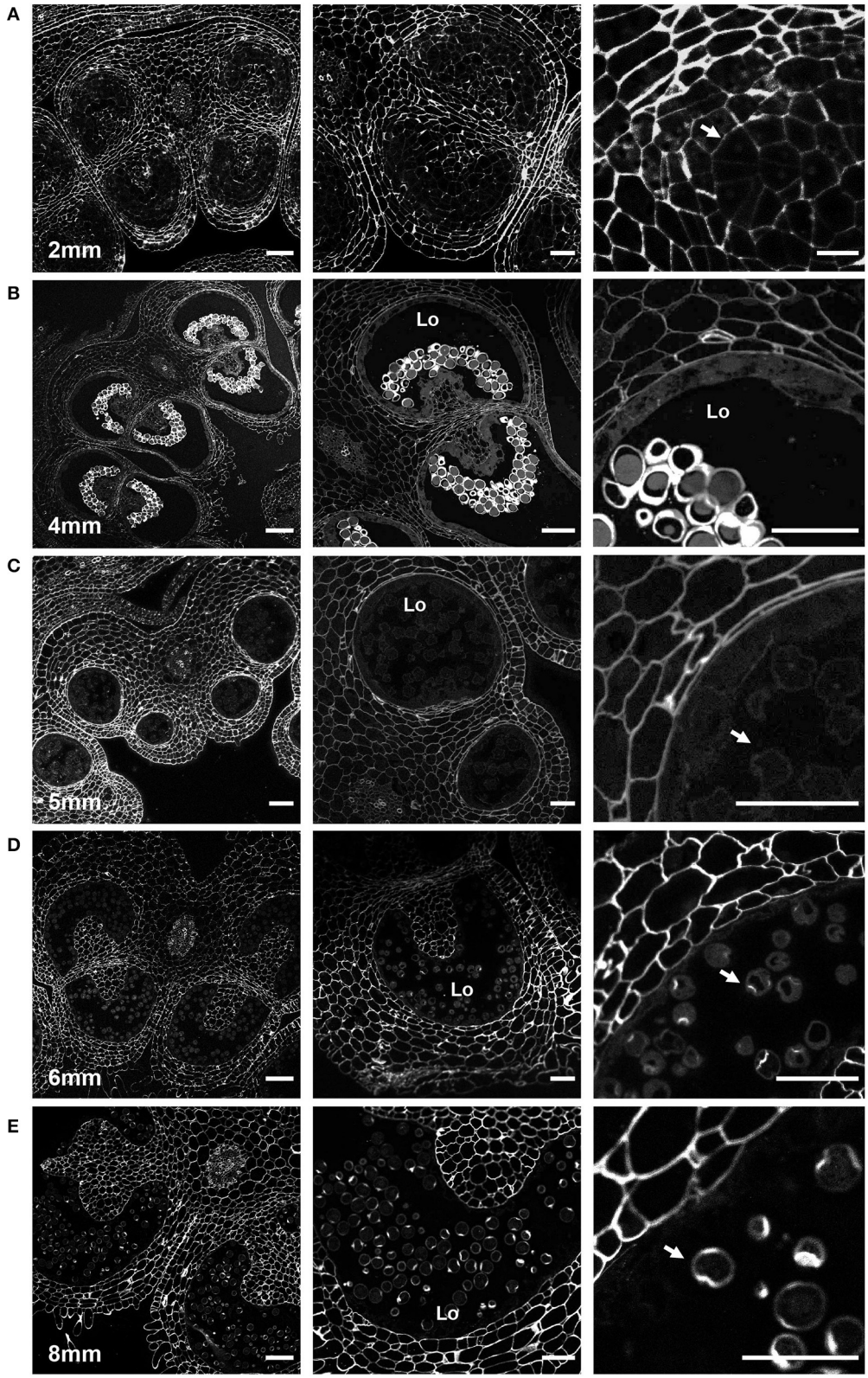

FIGURE 4 | Calcofluor white staining of pollen development. Fluorescent micrographs of anther cross sections (500 nm) in LR white, stained with calcofluor white. **(A)** The microspore mother cell stage in the 2-mm bud anther. **(B)** The tetrad stage in the 4-mm bud anther. **(C)** The uninucleate microspore stage in the 5-mm bud anther. The arrow marks the microspore wall. **(D)** Bicellular pollen in 6-mm bud anther. The arrow marks the pollen wall. **(E)** Mature pollen in 8-mm bud anther. The

(Continued)

FIGURE 4 | arrow marks pollen wall. Te, tetrad. Scale bars. **(A)** 50 μm (left), 25 μm (center and right). **(B)** 75 μm (left), 50 μm (center and right). **(C)** 50 μm (left), 25 μm (center and right). **(D)** 75 μm (left), 50 μm (center and right). **(E)** 75 μm (left), 50 μm (center and right).

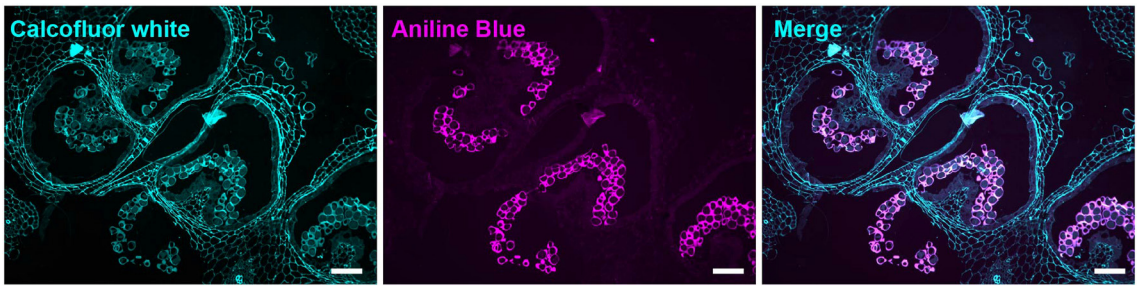

FIGURE 5 | Aniline blue staining of the tetrad callose wall. Fluorescent micrographs of anther cross sections (500 nm) in LR white, of the 4-mm bud anther, stained with calcofluor white and aniline blue fluorochrome. Calcofluor white staining (cyan) (left). Aniline blue staining (magenta) (center). Merged staining (right). Scale bars 50 μm.

monoclonal antibodies LM20 and LM19 (Verhertbruggen et al., 2009). LM19 preferentially binds HG with a lower degree of esterification (i.e., deHG), while LM20 shows a complementary affinity, binding to more heavily methylated HG, although a degree of overlap does exist in their binding abilities (Christiaens et al., 2011). As a preliminary to the use of these antibodies, we first demonstrated that the fluorophore-conjugated secondary antibody did not bind to our anther sections (**Supplementary Figure 3**).

In the 2-mm bud, while the MMCs had a weak calcofluor signal, indicating low levels of cellulose, the LM20 signal was robust and generally stronger than that of the surrounding anther tissue (**Figure 6A**). Close-up observation of the MMC walls showed boundaries of each cell thickly marked with LM20. To observe the pattern of dmeHG at this stage, we also stained with LM19. While the boundaries of MMCs did stain with LM19, the signal was considerably less robust than that of LM20, and, generally, the MMC signal was consistent with the signal observed for the cell wall of the surrounding anther cells (**Figure 6B**).

At the tetrad stage in the 4-mm bud, the callose wall also stained positive for the LM20 and LM19 epitopes (**Figures 6C,D**). At this stage, the LM19 signal was more robust, and the tetrad walls were strongly stained relative to other anther cells (**Figure 6D**). Therefore, the pollen wall at the tetrad stage contained abundant meHG and dmeHG in addition to callose (**Figure 5**). However, at the early microspore stage in 5-mm buds, pectin distribution was largely altered. meHG, as detected by LM20 binding, was considerably reduced with only a faint signal detectable around the microspores, although the surrounding anther tissue stained robustly (**Figure 7A**). The LM19 signal at this stage was similarly reduced compared with the tetrad stage, but a clear outline of the microspore was visible and was more robust than the corresponding LM20 signal (**Figure 7B**). Therefore, the loss of the callose wall coincided with a major loss of pectin during the transition between the tetrad and microspore stages.

In the bicellular stage, pollen in the 6-mm bud, we observed a diffuse LM20 signal throughout the pollen. In addition, we also found a robust signal at the inner surface of the aperture sites (**Figure 8A**). The LM19 signal was similarly diffuse in the pollen grain but was not enriched at the aperture sites at this stage (**Figure 8B**). In the mature pollen, in the 8-mm buds, there was a distinct boundary around the pollen with LM20 signal (**Figure 8C**) and a similar, though the more robust boundary of the LM19 signal (**Figure 8D**). The mature apertures sites were robustly stained with calcofluor white at this stage but were generally deficient in the LM19 and LM20 signals relative to the non-aperture regions of the pollen wall.

DISCUSSION

The transition from the general cell wall of a non-specialized anther cell to the structurally distinct wall of the mature pollen grain requires considerable remodeling. Here, we have combined imaging techniques to observe the structure of the tomato pollen wall and to establish the sequence of cell wall polymer remodeling events taking place during pollen development, beginning with the MMCs and continuing to pollen maturation (**Figure 9**). In the premeiotic anthers of 2-mm buds, we observed significant differences in cell wall composition between the MMCs and the surrounding anther cells. Weak calcofluor white staining (**Figure 4A**) and the robust LM20 signal (**Figure 6A**) in the cell walls of the MMCs are consistent with a reduction in cellulose and higher levels of meHG in these cells compared with other anther cells. These observations support the interpretation of previous tomato anther TEM data, which described an approximately 10-fold expansion of the width of the middle lamella between premeiotic MMC and those in early prophase and the loss of microfibrils adjacent to the plasma membrane by late prophase (Polowick and Sawhney, 1992). Reduced cellulose, combined with increased meHG, would be consistent with a more extensible cell wall, possibly facilitating the expansion and remodeling required for further pollen development. Therefore, even in this early stage of pollen development, the cell wall composition of the pollen lineage cells was already distinct.

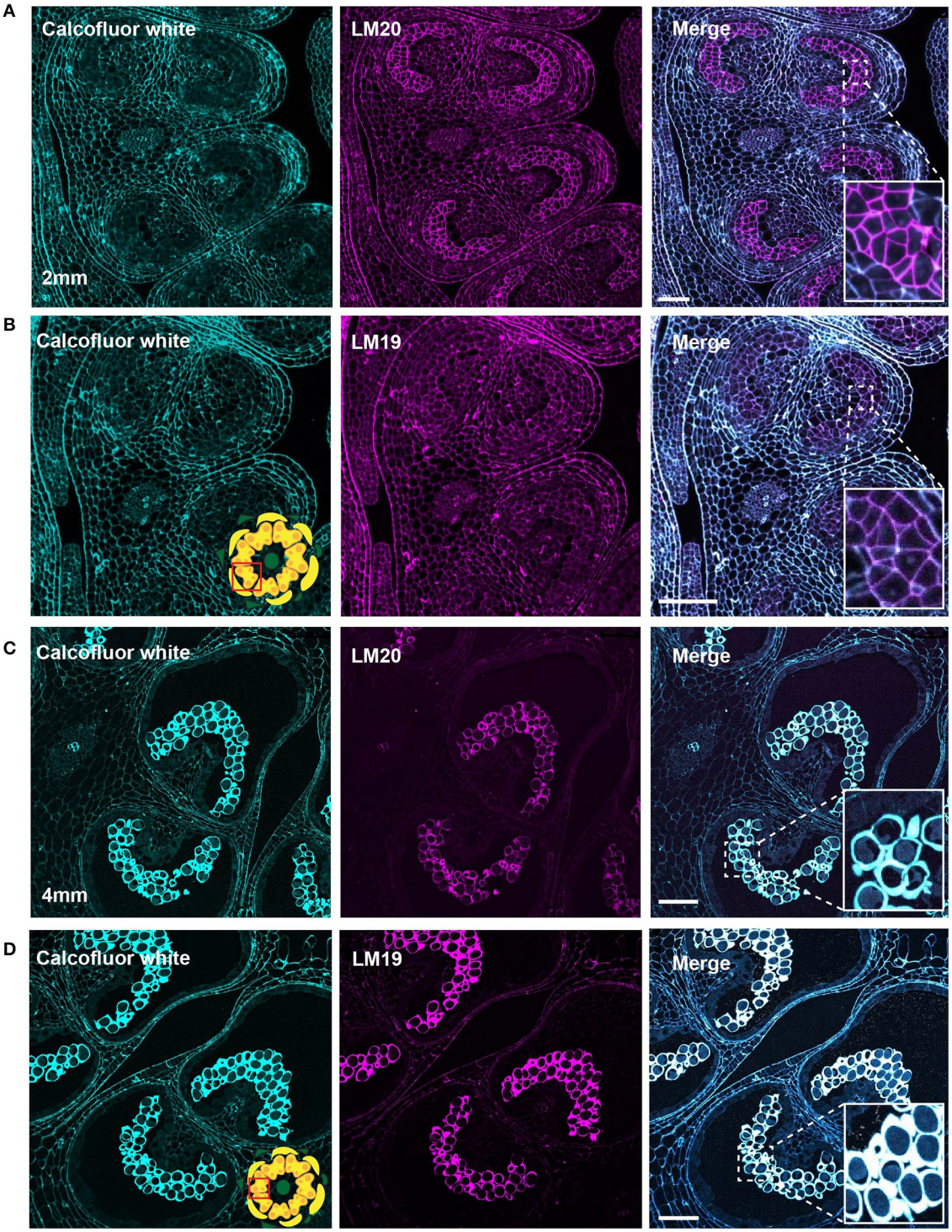

FIGURE 6 | LM20 and LM19 immunostaining of the 2-mm and 4-mm bud anthers. Fluorescent micrographs of anther cross sections (500 nm) in LR white, of the 2-mm and 4-mm bud anther, stained with Calcofluor white and FITC conjugated anti-rat secondary for LM20 or LM19. Calcofluor white staining (Cyan) (left). Aniline blue staining (magenta) (center). Merged staining (right). **(A)** LM20 staining of the 2-mm anther. The right panel inset, showing zoomed-in view of the MMCs wall with the merged staining. **(B)** LM19 staining of the 2-mm anther. The right panel inset, showing zoomed-in view of the MMCs with the merged staining. **(C)** LM20 staining of the 4-mm anther. The right panel inset, showing zoomed-in view of the tetrad cells with the merged staining. **(D)** LM19 staining of the 4-mm anther. The right panel inset, showing zoomed-in view of the tetrad cells with the merged staining. Scale bars 50 μm.

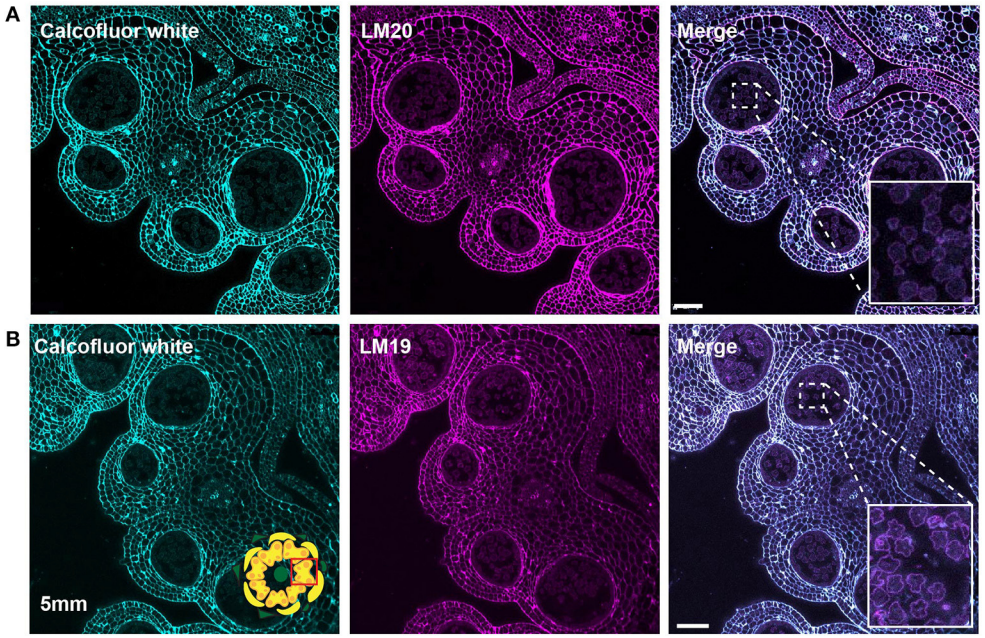

FIGURE 7 | LM20 and LM19 immunostaining of the 5-mm bud anthers. Fluorescent micrographs of anther cross sections (500 nm) in LR white, of the 5-mm bud anther, stained with Calcofluor white and FITC conjugated secondary for LM20 or LM19. Calcofluor white staining (Cyan) (left). Aniline blue staining (magenta) (center). Merged staining (right). **(A)** LM20 staining of the 5-mm anther. The right panel inset, showing zoomed-in view of the microspore wall with the merged staining. **(B)** LM19 staining of the 5-mm anther. The right panel inset, showing zoomed-in view of the microspore with the merged staining. Scale bars 50 μm.

At the tetrad stage in 4-mm buds, a thick callose wall surrounding the postmeiotic tetrads was apparent in ABF-stained sections (**Figure 5**). Unlike cellulose, which is a common plant cell wall component, callose occurs transiently during cell division and in some specialized cell types or under specific conditions (Chasan, 1992; Mollet et al., 2013; Renzaglia et al., 2020). The tetrad stage was the only stage at which we observed callose, and it was limited to the tetrad wall. While the ABF signal, indicating the presence of callose was clear, the observation of calcofluor white binding at this stage (**Figure 4B**) must be interpreted with caution as it may indicate the presence of cellulose or might result from non-specific binding to callose. In terms of pectin content, we observed both LM20 and LM19 signals, indicating that the tetrad wall also contained HG of low and high degrees of methylesterification (**Figure 6B**). Furthermore, enhancement of the LM19 signal in the tetrad wall suggests that dmeHG might serve a significant functional role here, possibly providing stiffness to the callose wall. Lack of aniline blue staining in the 5-mm bud anther demonstrated that the callose wall is temporary and after meiosis degrades to separate the tetrads into individual microspores (Polowick and Sawhney, 1993a; Owen and Makaroff, 1995; Paxson-Sowders et al., 1997; Kravchik et al., 2019; Zhang et al., 2020). At this stage, most of the LM19 and LM20 signals were also lost (**Figure 7**). These observations are also consistent with the effect of the Arabidopsis *qrt* mutants and their disruption of pectin remodeling enzymes, blocking tetrad separation (Preuss et al., 1993; Aouali et al., 2001; Rhee et al., 2003; Francis et al., 2006; Ogawa et al., 2009). The calcofluor white signal was also weak in the early microspore stage (**Figure 4C**), indicating little cellulose. We also detected a thin layer of exine at this stage, which may further support the wall structure (**Figure 3**). The primexine has an important function during this stage; unfortunately, the composition of the primexine is poorly understood, making it difficult to study (Li et al., 2017; Wang and Dobritsa, 2018). Other possible microspore cell wall components include cell wall-associated proteins, for example, the extensins or arabinogalactan glycoproteins (AGPs). The extensins are moderately glycosylated, highly repetitive proteins, which can be covalently cross-linked in the wall by secreted peroxidases, possibly forming a scaffold for pectin assembly (Schnabelrauch et al., 1996; Cannon et al., 2008; Petersen et al., 2021). In Arabidopsis *peroxidase9* (*prx9*) and *prx40* double mutants, microspores and tapetal cells have a swollen phenotype, suggesting compromised cell wall integrity due to a reduction in extensin cross-linking during pollen development (Jacobowitz et al., 2019). Evidence for possible AGP involvement at this stage of pollen development comes from *UNEQUAL PATTERN OF EXINE1/KAONASHI4* (*UPEX1/KNS4*), a β-(1,3)-galactosyltransferase responsible for the synthesis of the AG glycans found on AGPs and rhamnogalacturonan I, a pectic polysaccharide. *upex1/kns4* mutants have lower levels, and an altered pattern of AGPs at the microspore stage and disrupted primexine formation and exine patterning (Dobritsa et al., 2011; Li et al., 2017; Suzuki et al., 2017).

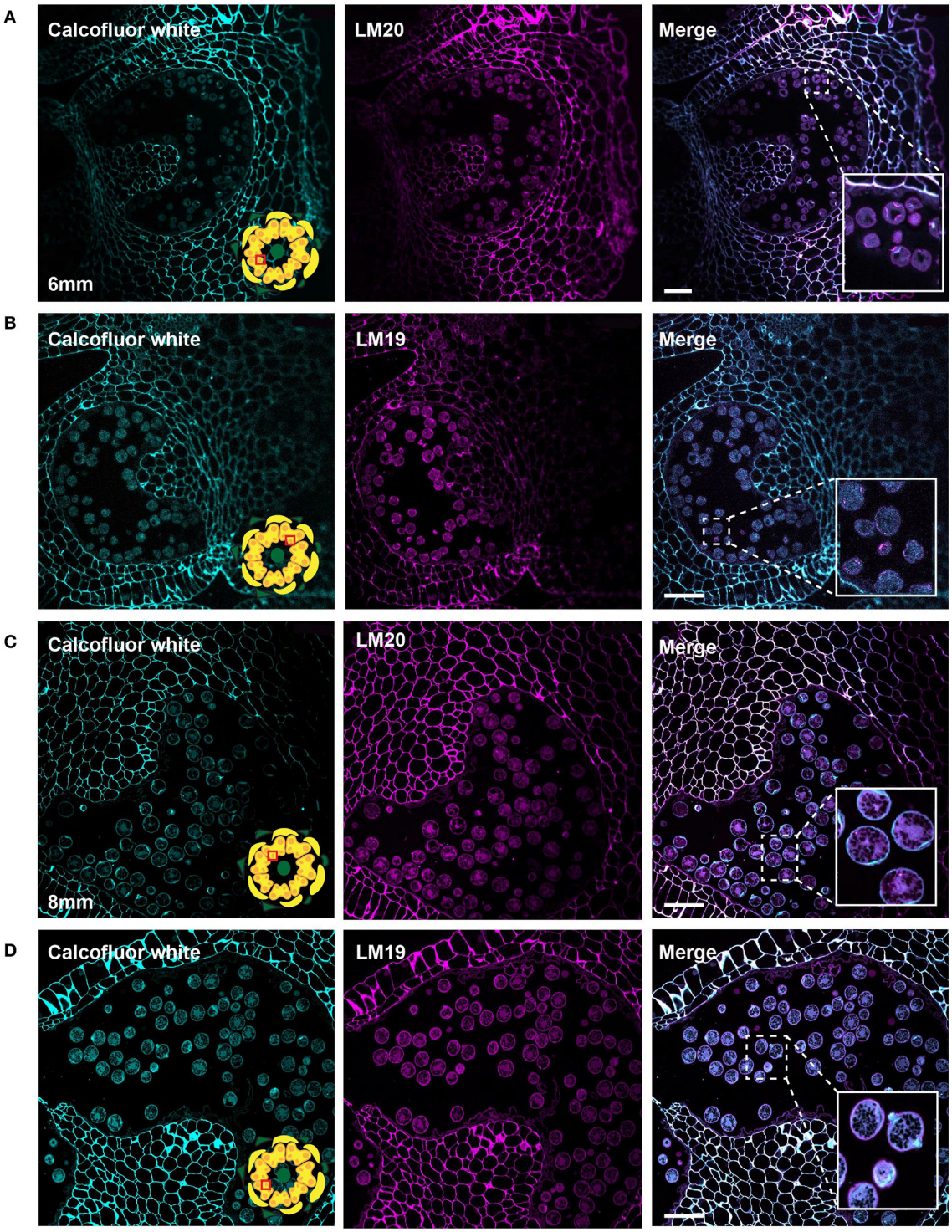

FIGURE 8 | LM20 and LM19 immunostaining of the 6-mm and 8-mm bud anthers. Fluorescent micrographs of anther cross sections (500 nm) in LR white, of the 6-mm and 8-mm bud anther, stained with Calcofluor white and FITC conjugated anti-rat secondary for LM20 or LM19. Calcofluor white staining (cyan) (left). Aniline blue staining (magenta) (center). Merged staining (right). **(A)** LM20 staining of the 6-mm anther.The right panel inset, showing zoomed-in view of the pollen wall with the merged staining. **(B)** LM19 staining of the 6-mm anther. The right panel inset, showing zoomed-in view of the pollen with the merged staining. **(C)** LM20 staining of the 8-mm anther. The right panel inset, showing zoomed-in view of the pollen wall with the merged staining. **(D)** LM19 staining of the 8-mm anther. The right panel inset, showing zoomed-in view of the pollen wall with the merged staining. Scale bars 50 μm.

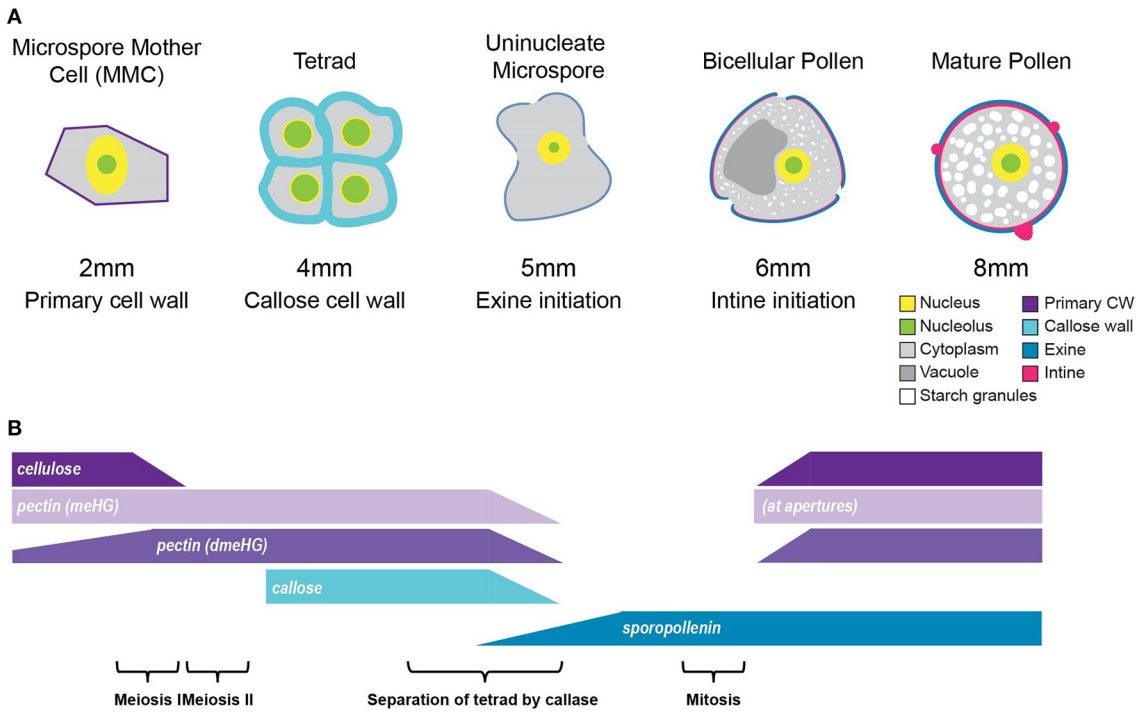

FIGURE 9 | Summary of tomato pollen wall development process. **(A)** A graphic summary of the major hallmarks of the tomato pollen development timeline. The pollen development stage is given above, and the bud length corresponding to each stage is given below, along with the major cell wall identities. **(B)** Cell wall polymer changes during development. The cellulose of the primary cell wall of the MMC breaks down at the 2-mm bud stage. Following meiosis, the tetrad cells are surrounded by a thick callose and pectin wall, which is broken down to separate the tetrad cells into free uninucleate microspores. Exine deposition by the tapetal cells begins at the 5-mm bud stage and continues through pollen maturation. The deposition of the cellulose and pectin, which make up the intine, initiates at the 6-mm bud stage and also continues through maturation. meHG deposition at the bicellular pollen stage is initially limited to the aperture regions, later spreading to the whole intine.

The aperture sites began to take on a distinct cell wall identity by the bicellular stage (6-mm buds) when the cytoplasmic face of the future aperture sites accumulates cellulose and meHG as indicated by the LM20 signal (**Figure 8A**). The accumulation of LM20 at this location suggests delivery of newly synthesized meHG through targeted exocytosis to these sites. By the mature stage, the apertures had a complex organization with a calcofluor-positive inner core and a ring rich in LM19 and LM20 epitopes visible in some pollen sections (**Figures 8C,D**). The completion of wall development in the inter-aperture regions was marked by the return of reinforcing polymers. The return of cellulose to these regions was a relatively late event, evident in the return of clacofluor white signal at the 8 mm stage when exine deposition was already complete. The later stages of pollen development were also associated with changes in pectin content. In particular, the LM19 pollen wall signal was weak in the bicellular pollen stage but much more robust in the mature pollen, forming a continuous layer around the pollen grain. This result suggests considerable enzymatic conversion of meHG to dmeHG between these stages. The defective intine produced by Arabidopsis *pme48* mutants, which are compromised in the reduction of meHG, suggests this conversion is important for ultimate intine formation and function during pollen hydration (Leroux et al., 2015).

Despite similarities in the overall process of pollen wall development, different species produce pollen with markedly different forms. This is particularly apparent for the structure of the exine, which is easily observable and, due to the resistance of sporopollenin to degradation, highly stable in the environment. Pollen also varies in the number, shape, and positioning of its apertures, with some groups lacking them entirely (Furness, 2007). Apertures serve not only as the sites for pollen tube initiation but also facilitate hydration, communication with the stigma, and help accommodate volume changes required during dehydration and rehydration (Matamoro-Vidal et al., 2016). Like many dicots, including Arabidopsis, tomato pollen is tri-aperturate, with exine deposition excluded from the aperture regions (**Figure 1B**). Our observation of pollinated pistils, using SEM, showed all pollen tubes originating at the aperture site, suggesting that tomato pollen germination is constrained to the aperture sites. However, this is not the case for Arabidopsis and several other species in the Brassicaceae where pollen has been observed to germinate at inter-aperture regions, taking the shortest path to the stigma (Edlund et al., 2016). One possible explanation for this difference between obligate-aperturate (tomato) and omni-aperturate (Arabidopsis) pollen may be differences in inter-aperture region pollen wall stiffness (Furness and Rudall, 2004; Edlund et al., 2016). However, this

possible difference in mechanical properties cannot be simply due to differences in exine thickness as Arabidopsis pollen exine is thicker (∼1 μm) compared with that of tomato (∼0.5 μm) (Dobritsa et al., 2011; Li et al., 2017). In careful examination of the pollen surface, we also noted the presence of small pores (38 ± 9 nm), which were also visible in TEM sections as exine channels (**Figure 1C**). While the mechanism of their development and the exact chemical nature of the lining of these channels are unknown, they are ubiquitous among land plants, and it is hypothesized that they facilitate hydration in advance of pollen germination (Edlund et al., 2004).

Because pollen wall development is a highly dynamic and complex process, understanding how the pollen wall is constructed requires a temporal understanding of the events of pollen wall remodeling. The work presented here describes the changes of the major cell wall polymers during pollen development in tomato (**Figure 9**) and will serve as a useful reference point for studies of the perturbation of the pollen wall in this important agricultural species.

DATA AVAILABILITY STATEMENT

The original contributions presented in the study are included in the article/**Supplementary Material**, further inquiries can be directed to the corresponding author.

AUTHOR CONTRIBUTIONS

CM and SJ designed the study and wrote and edited the manuscript. SJ carried out the experiments. Both authors contributed to the article and approved the submitted version.

FUNDING

This work was supported by the National Science Foundation under grant no. IOS-1755482.

ACKNOWLEDGMENTS

We would like to thank Gregg Sobocinski (University of Michigan, Ann Arbor) in the Molecular, Cellular and Developmental Biology (MCDB) department, Imaging Core for training and help with ultramicrotome sectioning, and confocal microscopy. We would also like to thank Sasha Meshinchi (University of Michigan, Ann Arbor) in the biomedical research core facilities, Microscopy Core for training and help with transmission electron microscopy. We would also like to thank Dr. Owen K. Neill at the Robert B. Mitchell Electron Microbeam Analysis Lab, part of the University of Michigan's Department of Earth and Environmental Sciences for training and help with scanning electron microscopy.

SUPPLEMENTARY MATERIAL

The Supplementary Material for this article can be found online at: https://www.frontiersin.org/articles/10.3389/fpls.2021.703713/full#supplementary-material

Supplemental Figure 1 | Structure of the tomato pollen grain surface. **(A)** Scanning electron micrograph (SEM) of tomato pollen, growing a pollen tube. Arrows mark the apertures (Ap) and pollen tube (Pt). **(B)** SEM of a mature pollen grain. **(C)** Close-up of the box insert from **(B)** showing exine patterning. **(D)** SEM of pollen wall. The arrow marks the Sp, exine spines; and Aq, aquapores. Scale bars 10 μm (**A**, top left), 1 μm (**B**, top right), 1 μm (**C**, bottom left), 100 nm (**D**, bottom right).

Supplemental Figure 2 | Structure of tomato anther during pollen development. Micrographs of paraffin-embedded anther sections stained with toluidine blue. **(A)** Sections of 2-mm bud. **(B)** Sections of 4-mm bud. **(C)** Sections of 5-mm bud. **(D)** Sections of 6-mm bud. **(E)** Sections of 8-mm bud. The arrow marks the Pe, petal; An, anther; Se, sepal; Pi, pistil; MMC, microspore mother cell; Loc, locule; Te, tetrad; Tap, tapetum; MS, microspore; BCP, bicellular pollen; scale bars **(A)** 75 μm (left) 50 μm (right) **(B–E)** 200 75 μm (left) 50 μm.

Supplemental Figure 3 | No primary antibody control for LM antibody staining. Fluorescent micrographs of anther cross sections (500 nm) in LR white, of 8-mm bud anther, stained with Calcofluor white and an FITC-conjugated secondary antibody only. **(A)** Calcofluor white staining (Left). **(B)** FITC-conjugated secondary only. Scale bars 25 μm.

REFERENCES

Aarts, M. G., Hodge, R., Kalantidis, K., Florack, D., Wilson, Z. A., Mulligan, B. J., et al. (1997). The Arabidopsis MALE STERILITY 2 protein shares similarity with reductases in elongation/condensation complexes. *Plant J.* 12, 615–623. doi: 10.1046/j.1365-313X.1997.00615.x

Aouali, N., Laporte, P., and Clément, C. (2001). Pectin secretion and distribution in the anther during pollen development in Lilium. *Planta* 213, 71–79. doi: 10.1007/s004250000469

Bashir, M. E. H., Lui, J. H., Palnivelu, R., Naclerio, R. M., and Preuss, D. (2013). Pollen lipidomics: lipid profiling exposes a notable diversity in 22 allergenic pollen and potential biomarkers of the allergic immune response. *PLoS ONE* 8:e57566. doi: 10.1371/journal.pone.0057566

Blackmore, S., Wortley, A. H., Skvarla, J. J., and Rowley, J. R. (2007). Pollen wall development in flowering plants. *New Phytol.* 174, 483–498. doi: 10.1111/j.1469-8137.2007.02060.x

Bosch, M., and Hepler, P. K. (2005). Pectin methylesterases and pectin dynamics in pollen tubes. *Plant Cell* 17, 3219–3226. doi: 10.1105/tpc.105.037473

Brukhin, V., Hernould, M., Gonzalez, N., and Chevalier, C. (2003). Flower development schedule in tomato Lycopersicon esculentum cv. sweet cherry. *Sex. Plant Reprod.* 15, 311–320. doi: 10.1007/s00497-003-0167-7

Canales, C., Bhatt, A. M., Scott, R., and Dickinson, H. (2002). EXS, a putative LRR receptor kinase, regulates male germline cell number and tapetal identity and promotes seed development in Arabidopsis. *Curr. Biol.* 12, 1718–1727. doi: 10.1016/S0960-9822(02)01151-X

Cankar, K., Kortstee, A., Toonen, M. A. J., Wolters-Arts, M., Houbein, R., Mariani, C., et al. (2014). Pectic arabinan side chains are essential for pollen cell wall integrity during pollen development. *Plant Biotechnol. J.* 12, 492–502. doi: 10.1111/pbi.12156

Cannon, M. C., Terneus, K., Hall, Q., Tan, L., Wang, Y., Wegenhart, B. L., et al. (2008). Self-assembly of the plant cell wall requires an extensin scaffold. *Proc. Natl. Acad. Sci. USA*. 105, 2226–2231. doi: 10.1073/pnas.0711980105

Carvalho, R. F., Campos, M. L., Pino, L. E., Crestana, S. L., Zsögön, A., Lima, J. E., et al. (2011). Convergence of developmental mutants into a single tomato model system: "Micro-Tom" as an effective toolkit for plant development research. *Plant Methods* 7, 1–14. doi: 10.1186/1746-4811-7-18

Chasan, R. (1992). Breaching the callose walI. *Plant Cell* 4, 745–749. doi: 10.1105/tpc.4.7.745

Chebli, Y., Kaneda, M., Zerzour, R., and Geitmann, A. (2012). The cell wall of the Arabidopsis pollen tube-spatial distribution, recycling, and network formation of polysaccharides. *Plant Physiol.* 160, 1940–1955. doi: 10.1104/pp.112.199729

Choi, H., Jin, J., Choi, S., Hwang, J., Kim, Y., Suh, M. C., et al. (2011). An ABCG/WBC-type ABC transporter is essential for transport of sporopollenin precursors for exine formation in developing pollen. *Plant J.* 65, 181–193. doi: 10.1111/j.1365-313X.2010.04412.x

Christiaens, S., Van Buggenhout, S., Ngouémazong, E. D., Vandevenne, E., Fraeye, I., Duvetter, T., et al. (2011). Anti-homogalacturonan antibodies: a way to explore the effect of processing on pectin in fruits and vegetables? *Food Res. Int.* 44, 225–234. doi: 10.1016/j.foodres.2010.10.031

Dobritsa, A. A., Geanconteri, A., Shrestha, J., Carlson, A., Kooyers, N., Coerper, D., et al. (2011). A large-scale genetic screen in Arabidopsis to identify genes involved in pollen exine production. *Plant Physiol.* 157, 947–970. doi: 10.1104/pp.111.179523

Dobritsa, A. A., and Reeder, S. H. (2017). Formation of pollen apertures in Arabidopsis requires an interplay between male meiosis, development of INP1-decorated plasma membrane domains, and the callose wall. *Plant Signal. Behav.* 12, 1–4. doi: 10.1080/15592324.2017.1393136

Dong, X., Hong, Z., Sivaramakrishnan, M., Mahfouz, M., and Verma, D. P. S. (2005). Callose synthase (CalS5) is required for exine formation during microgametogenesis and for pollen viability in Arabidopsis. *Plant J.* 42, 315–328. doi: 10.1111/j.1365-313X.2005.02379.x

Edlund, A. F., Swanson, R., and Preuss, D. (2004). Pollen and stigma structure and function: The role of diversity in pollination. *Plant Cell* 16, S84–S97. doi: 10.1105/tpc.015800

Edlund, A. F., Zheng, Q., Lowe, N., Kuseryk, S., Ainsworth, K. L., Lyles, R. H., et al. (2016). Pollen from Arabidopsis thaliana and other Brassicaceae are functionally omniaperturate. *Am. J. Bot.* 103, 1006–1019. doi: 10.3732/ajb.1600031

El-Ghazaly, G., and Jensen, W. A. (1986). Studies of the development of wheat (*Triticum aestivum*) pollen:I. formation of the pollen wall and ubisch bodies. *Grana* 25, 1–29. doi: 10.1080/00173138609429929

Fang, K., Wang, Y., Yu, T., Zhang, L., Baluška, F., Šamaj, J., et al. (2008). Isolation of de-exined pollen and cytological studies of the pollen intines of *Pinus bungeana* Zucc. *Ex Endl. and Picea wilsonii Mast. Flora: Morphol. Distrib. Funct. Ecol. Plants* 203, 332–340. doi: 10.1016/j.flora.2007.04.007

Flores-Tornero, M., Anoman, A. D., and Ros, R. (2015). Lack of phosphoserine phosphatase activity alters pollen and tapetum development in *Arabidopsis thaliana*. *Plant Sci.* 235, 81–88. doi: 10.1016/j.plantsci.2015.03.001

Francis, K. E., Lam, S. Y., and Copenhaver, G. P. (2006). Separation of arabidopsis pollen tetrads is regulated by *QUARTET1*, a pectin methylesterase gene. *Plant Phisiol.* 142, 1004–1013. doi: 10.1104/pp.106.085274

Furness, C. A. (2007). Why does some pollen lack apertures? A review of inaperturate pollen in eudicots. *Bot. J. Linnean Soc.* 155, 29–48. doi: 10.1111/j.1095-8339.2007.00694.x

Furness, C. A., and Rudall, P. J. (2004). Pollen aperture evolution - A crucial factor for eudicot success? *Trends Plant Sci.* 9, 154–158. doi: 10.1016/j.tplants.2004.01.001

Giorno, F., Wolters-Arts, M., Grillo, S., Scharf, K. D., Vriezen, W. H., and Mariani, C. (2010). Developmental and heat stress-regulated expression of HsfA2 and small heat shock proteins in tomato anthers. *J. Exp. Bot.* 61, 453–462. doi: 10.1093/jxb/erp316

Giorno, F., Wolters-Arts, M., Mariani, C., and Rieu, I. (2013). Ensuring reproduction at high temperatures: the heat stress response during anther and pollen development. *Plants* 2, 489–506. doi: 10.3390/plants2030489

Gómez, J. F., Talle, B., and Wilson, Z. A. (2015). Anther and pollen development: A conserved developmental pathway. *J. Integr. Plant Biol.* 57, 876–891. doi: 10.1111/jipb.12425

Herburger, K., and Holzinger, A. (2016). Aniline blue and calcofluor white staining of callose and cellulose in the streptophyte green algae Zygnema and Klebsormidium. *Bio-Protocol* 6, 6–10. doi: 10.21769/BioProtoc.1969

Heslop-Harrison, J. (1968). Pollen wall development. *Science* 161, 230–237. doi: 10.1126/science.161.3838.230

Hess, M. W. (1993). Cell-wall development in freeze-fixed pollen: Intine formation of *Ledebouria socialis* (Hyacinthaceae). *Planta* 189, 139–149. doi: 10.1007/BF00201354

Hess, M. W., and Frosch, A. (1994). Subunits of forming pollen exine and Ubisch bodies as seen in freeze substituted *Ledebouria socialis* Roth (Hyacinthaceae). *Protoplasma* 182, 10–14. doi: 10.1007/BF01403683

Hsiao, A., Yeung, E. C., Ye, Z., and Chye, M. (2015). The Arabidopsis Cytosolic Acyl-CoA-Binding proteins play combinatory roles in pollen development. *Plant Cell Physiol.* 56, 322–333. doi: 10.1093/pcp/pcu163

Ishiguro, S., Nishimori, Y., Yamada, M., Saito, H., Suzuki, T., Nakagawa, T., et al. (2010). The Arabidopsis *FLAKY POLLEN1* gene encodes a 3-hydroxy-3-methylglutaryl- coenzyme a synthase required for development of tapetum-specific organelles and fertility of pollen grains. *Plant Cell Physiol.* 51, 896–911. doi: 10.1093/pcp/pcq068

Jacobowitz, J. R., Doyle, W. C., and Weng, J. (2019). PRX9 and PRX40 Are extensin peroxidases essential for maintaining tapetum and microspore cell wall integrity during arabidopsis anther development. *Plant Cell* 31, 848–861. doi: 10.1105/tpc.18.00907

Jiang, J., Zhang, Z., and Cao, J. (2013). Pollen wall development: the associated enzymes and metabolic pathways. *Plant Biol.* 15, 249–263. doi: 10.1111/j.1438-8677.2012.00706.x

Kravchik, M., Stav, R., Belausov, E., and Arazi, T. (2019). Functional characterization of microRNA171 family in Tomato. *Plants* 8:10. doi: 10.3390/plants8010010

Lee, J. T. Y., and Chow, K. L. (2012). SEM sample preparation for cells on 3D scaffolds by freeze-drying and HMDS. *Scanning* 34, 12–25. doi: 10.1002/sca.20271

Leroux, C., Bouton, S., Fabrice, T. N., Mareck, A., Guénin, S., Fournet, F., et al. (2015). PECTIN METHYLESTERASE48 is involved in Arabidopsis pollen grain germination. *Plant Physiol.* 167, 367–380. doi: 10.1104/pp.114.250928

Li, W. L., Liu, Y., and Douglas, C. J. (2017). Role of glycosyltransferases in pollen wall primexine formation and exine patterning. *Plant Physiol.* 173, 167–182. doi: 10.1104/pp.16.00471

Luis da Costa, M., Lopes, A. L., Amorim, M. I., and Coimbra, S. (2017). Immunolocalization of AGPs and pectins in *Quercus suber*gamethophytic structures. *Plant Germline Develop. Methods Protoc. Methods Mol. Bio.* 1669, 117–137. doi: 10.1007/978-1-4939-7286-9_11

Lyu, M., Yu, Y., Jiang, J., Song, L., Liang, Y., Ma, Z., et al. (2015). *BcMF26a* and *BcMF26b*are duplicated polygalacturonase genes with divergent expression patterns and functions in pollen development and pollen tube formation in *Brassica campestris*. *PLoS ONE* 10:e0131173. doi: 10.1371/journal.pone.0131173

Ma, X., Wu, Y., and Zhang, G. (2021). Formation pattern and regulatory mechanisms of pollen wall in Arabidopsis. *J. Plant Physiol.* 260, 153388. doi: 10.1016/j.jplph.2021.153388

Matamoro-Vidal, A., Raquin, C., Brisset, F., Colas, H., Izac, B., Albert, B., et al. (2016). Links between morphology and function of the pollen wall: an experimental approach. *Bot. J. Linnean Soc.* 180, 478–490. doi: 10.1111/boj.12378

Mollet, J. C., Leroux, C., Dardelle, F., and Lehner, A. (2013). Cell wall composition, biosynthesis and remodeling during pollen tube growth. *Plants Basel* 2, 107–147. doi: 10.3390/plants2010107

Müller, F., Xu, J., Kristensen, L., Wolters-Arts, M., De Groot, P. F. M., Jansma, S. Y., et al. (2016). High-temperature-induced defects in tomato (*Solanum lycopersicum*) anther and pollen development are associated with reduced expression of B-class floral patterning genes. *PLoS ONE* 11:e0167614. doi: 10.1371/journal.pone.0167614

Ogawa, M., Kay, P., Wilson, S., and Swain, S. M. (2009). ARABIDOPSIS DEHISCENCE ZONE POLYGALACTURONASE1 required for cell separation during reproductive development in Arabidopsis. *Plant Cell* 21, 216–233. doi: 10.1105/tpc.108.063768

Owen, H. A., and Makaroff, C. A. (1995). Ultrastructure of microsporogenesis and microgametogenesis in *Arabidopsis thaliana* (L.) Heynh. ecotype Wassilewskija (Brassicaceae). *Protoplasma* 185, 7–21. doi: 10.1007/BF01272749

Paxson-sowders, D. M., Dodrill, C. H., Owen, H. A., and Makaroff, C. A. (2001). DEX1, a novel plant protein, is required for exine pattern formation during pollen development in Arabidopsis. *Plant Physiol.* 127, 1739–1749. doi: 10.1104/pp.010517

Paxson-Sowders, D. M., Owen, H. A., and Makarow, C. A. (1997). A comparative ultrastructural analysis of exine pattern development in wild-type Arabidopsis and a mutant defective in pattern formation. *Protoplasma* 198, 53–65. doi: 10.1007/BF01282131

Persson, S., Paredez, A., Carroll, A., Palsdottir, H., Doblin, M., Poindexter, P., et al. (2007). Genetic evidence for three unique components in primary cell-wall cellulose synthase complexes in Arabidopsis. *Proc. Natl. Acad. Sci. U.S.A.* 104, 15566–15571. doi: 10.1073/pnas.0706592104

Petersen, B. L., Macalister, C. A., Petersen, B. L., and Ulvskov, P. (2021). Plant protein O-arabinosylation. *Front. Plant Sci.* 12: 645219. doi: 10.3389/fpls.2021.645219

Phan, H. A., Iacuone, S., Li, S. F., and Parish, R. W. (2011). The MYB80 transcription factor is required for pollen development and the regulation of tapetal programmed cell death in *Arabidopsis thaliana*. *Plant Cell* 23, 2209–2224. doi: 10.1105/tpc.110.082651

Picken, A. J. F. (1984). A review of pollination and fruit set in the tomato (*Lycopersicon esculentum Mill.*). *J. Hortic. Sci.* 59, 1–13. doi: 10.1080/00221589.1984.11515163

Piffanelli, P., and Murphy, D. J. (1998). Novel organelles and targeting mechanisms in the anther tapetum. *Trends Plant Sci.* 3, 250–252. doi: 10.1016/S1360-1385(98)01260-6

Piffanelli, P., Ross, J. H. E., and Murphy, D. J. (1998). Biogenesis and function of the lipidic structures of pollen grains. *Sex. Plant Reprod.* 11, 65–80. doi: 10.1007/s004970050122

Polowick, P. L., and Sawhney, V. K. (1992). Ultrastructural changes in the cell wall, nucleus and cytoplasm of pollen mother cells during meiotic prophase I in *Lycopersicon esculentum* (Mill.). *Protoplasma* 169, 139–147. doi: 10.1007/BF01323613

Polowick, P. L., and Sawhney, V. K. (1993a). An ultrastructural study of pollen development in tomato (*Lycopersicon esculentum*). *I.* Tetrad to early binucleate microspore stage. *Can. J. Bot.* 71, 1039–1047. doi: 10.1139/b93-120

Polowick, P. L., and Sawhney, V. K. (1993b). Differentiation of the tapetum during microsporogenesis in tomato (*Lycopersicon esculentum Mill.*), with special reference to the tapetal cell wall. *Ann. Bot.* 72, 595–605. doi: 10.1006/anbo.1993.1150

Pressman, E., Peet, M. M., and Pharr, D. M. (2002). The effect of heat stress on tomato pollen characteristics is associated with changes in carbohydrate concentration in the developing anthers. *Ann. Bot.* 90, 631–636. doi: 10.1093/aob/mcf240

Preuss, D., Lemieux, B., Yen, G., and Davis, R. W. (1993). A conditional sterile mutation eliminates surface components from Arabidopsis pollen and disrupts cell signaling during fertilization. *Genes Develop.* 7, 974–985. doi: 10.1101/gad.7.6.974

Quilichini, T. D., Douglas, C. J., and Samuels, A. L. (2014). New views of tapetum ultrastructure and pollen exine development in *Arabidopsis thaliana*. *Ann. Bot.* 114, 1189–1201. doi: 10.1093/aob/mcu042

Quilichini, T. D., Friedmann, M. C., Samuels, A. L., and Douglas, C. J. (2010). ATP-Binding Cassette Transporter G26 is required for male fertility and pollen exine formation in Arabidopsis. *Plant Physiol.* 154, 678–690. doi: 10.1104/pp.110.161968

Rejón, J. D., Delalande, F., Schaeffer-Reiss, C., Alch,é, J., de, D., Rodríguez-García, M. I., et al. (2016). The pollen coat proteome: at the cutting edge of plant reproduction. *Proteomes* 4, 1–23. doi: 10.3390/proteomes4010005

Renzaglia, K. S., Lopez, R. A., Welsh, R. D., Owen, H. A., and Merced, A. (2020). Callose in sporogenesis: novel composition of the inner spore wall in hornworts. *Plant System. Evol.* 306, 1–9. doi: 10.1007/s00606-020-01631-5

Rhee, S. Y., Osborne, E., Poindexter, P. D., and Somerville, C. R. (2003). Microspore separation in the *quartet3* mutants of Arabidopsis is impaired by a defect in a developmentally regulated polygalacturonase required for pollen mother cell wall degradation. *Plant Physiol.* 133, 1170–1180. doi: 10.1104/pp.103.028266

Schnabelrauch, L. S., Kieliszewski, M. J., Upham, B. L., Alizedeh, H., and Lamport, D. T. A. (1996). Isolation of pl4.6 extensin peroxidase from tomato cell suspension cultures and identification of Val-Tyr-Lys as putative intramolecular cross-link site. *Plant J.* 9, 477–489. doi: 10.1046/j.1365-313X.1996.09040477.x

Scott, R. J., Spielman, M., and Dickinson, H. G. (2004). Stamen structure and function. *Plant Cell* 16, 46–61. doi: 10.1105/tpc.017012

Shi, J., Cui, M., Yang, L., Kim, Y. J., and Zhang, D. (2015a). Genetic and biochemical mechanisms of pollen wall development. *Trends Plant Sci.* 20, 741–753. doi: 10.1016/j.tplants.2015.07.010

Shi, J., Tan, H., Yu, X., Liu, Y., Liang, W., Ranathunge, K., Franke, R. B., et al. (2011). Defective pollen wall is required for anther and microspore development in rice and encodes a fatty acyl carrier protein reductase. *Plant Cell* 23, 2225–2246. doi: 10.1105/tpc.111.087528

Shi, X., Sun, X., Zhang, Z., Feng, D., Zhang, Q., Han, L., et al. (2015b). GLUCAN SYNTHASE-LIKE 5 (GSL5) plays an essential role in male fertility by regulating callose metabolism during microsporogenesis in rice. *Plant Cell Physiol.* 5, 497–509. doi: 10.1093/pcp/pcu193

Souza, C. D. A., Kim, S. S., Koch, S., Kienow, L., Schneider, K., Mckim, S. M., et al. (2009). A novel Fatty Acyl-CoA synthetase is required for pollen development and sporopollenin biosynthesis in Arabidopsis. *Plant Cell* 21, 507–525. doi: 10.1105/tpc.108.062513

Sridharan, G., and Shankar, A. A. (2012). Toluidine blue : A review of its chemistry and clinical utility. *J. Oral Maxillofacial Pathol.* 16, 251–255. doi: 10.4103/0973-029X.99081

Suárez-Cervera, M., Arcalís, E., Le Thomas, A., and Seoane-Camba, J. A. (2002). Pectin distribution pattern in the apertural intine of *Euphorbia peplus L. (Euphorbiaceae)* pollen. *Sex. Plant Reprod.* 14, 291–298. doi: 10.1007/s00497-001-0121-5

Suzuki, T., Narciso, J. O., Zeng, W., van de Meene, A., Yasutomi, M., Takemura, S., et al. (2017). Kns4/upex1: a type II arabinogalactan β-(1,3)-galactosyltransferase required for pollen exine development. *Plant Physiol.* 173, 183–205. doi: 10.1104/pp.16.01385

Takebe, N., Nakamura, A., Watanabe, T., Miyashita, A., Satoh, S., and Iwai, H. (2020). Cell wall Glycine-rich Protein2 is involved in tapetal differentiation and pollen maturation. *J. Plant Res.* 133, 883–895. doi: 10.1007/s10265-020-01223-x

Taylor, L. P., and Hepler, P. K. (1997). Pollen germination and tube growth. *Ann. Rev. Plant Physiol. Plant Molec. Bio.* 48, 461–491. doi: 10.1146/annurev.arplant.48.1.461

Verhertbruggen, Y., Marcus, S. E., Haeger, A., Ordaz-ortiz, J. J., and Knox, J. P. (2009). An extended set of monoclonal antibodies to pectic homogalacturonan. *Carbohydr. Res.* 344, 1858–1862. doi: 10.1016/j.carres.2008.11.010

Verlag, F., Wakabayashi, K., Hoson, T., and Huber, D. J. (2003). Methyl de-esterification as a major factor regulating the extent of pectin depolymerization during fruit ripening: a comparison of the action of avocado (*Persea americana*) and tomato (*Lycopersicon esculentum*) polygalacturonases. *J. Plant Physiol.* 673, 667–673. doi: 10.1078/0176-1617-00951

Wan, L., Zha, W., Cheng, X., Liu, C., Lv, L., Liu, C., et al. (2011). A rice beta-1,3-glucanase gene Osg1 is required for callose degradation in pollen development. *Planta* 309–323. doi: 10.1007/s00425-010-1301-z

Wang, R., and Dobritsa, A. A. (2018). Exine and Aperture patterns on the pollen surface: their formation and roles in plant reproduction. *Ann. Plant Rev.* 1, 1–40. doi: 10.1002/9781119312994.apr0625

Yu, J., Meng, Z., Liang, W., Behera, S., Kudla, J., Tucker, M. R., et al. (2016). A Rice Ca 2+ Binding protein is required for tapetum function and pollen formation. *Plant Physiol.* 172, 1772–1786. doi: 10.1104/pp.16.01261

Zhang, D., Chen, W., Yu, X., Zhang, K., Shi, J., Oliveira, S., et al. (2011). *Male Sterile2* encodes a plastid-localized fatty acyl carrier protein reductase required for pollen exine development in Arabidopsis. *Plant Phisiol.* 157, 842–853. doi: 10.1104/pp.111.181693

Zhang, X., Zhao, G., Tan, Q., Yuan, H., Betts, N., Zhu, L., et al. (2020). Rice pollen aperture formation is regulated by the interplay between OsINP1 and OsDAF1. *Nat. Plants* 6, 394–403. doi: 10.1038/s41477-020-0630-6

Zinkl, G. M., Zwiebel, B. I., Grier, D. G., and Preuss, D. (1999). Pollen-stigma adhesion in Arabidopsis : a species-specific interaction mediated by lipophilic molecules in the pollen exine. *Development* 5440, 5431–5440. doi: 10.1242/dev.126.23.5431

Conflict of Interest: The authors declare that the research was conducted in the absence of any commercial or financial relationships that could be construed as a potential conflict of interest.

Publisher's Note: All claims expressed in this article are solely those of the authors and do not necessarily represent those of their affiliated organizations, or those of the publisher, the editors and the reviewers. Any product that may be evaluated in this article, or claim that may be made by its manufacturer, is not guaranteed or endorsed by the publisher.

frontiers in Plant Science

ORIGINAL RESEARCH
published: 29 July 2021
doi: 10.3389/fpls.2021.709231

Impact of Storage Temperature on Pollen Viability and Germinability of Four Serbian Autochthon Apple Cultivars

Dušica Ćalić[1], Jelena Milojević[1], Maja Belić[1], Rade Miletić[2] and Snežana Zdravković-Korać[1]*

[1] *Department of Plant Physiology, Institute for Biological Research "Siniša Stanković," National Institute of Republic of Serbia, University of Belgrade, Belgrade, Serbia,* [2] *Fruit Research Institute-Čačak, Čačak, Serbia*

Globalization has drastically reduced the number of autochthon apple cultivars in the Serbian market and most of them have nearly disappeared; however, some of these cultivars, such as Petrovača, Budimka, Kolačara Pozna, and Kožara, have extraordinary quality, good pomological characteristics, and pest and disease resistance. The present study was conducted to develop a protocol for the storage of pollen for further use in the conservation and breeding of these cultivars. Viability and germination of the mature pollen were tested *in vitro*, at four storage temperatures (20, 4, −20, and −80°C), right after harvest or 1, 2, 3, 4, 5, and 6 months after storage. Differences in fresh pollen viability and germination between cultivars were statistically significant and ranged from 60 to 88% and 59 to 98%, respectively. Fresh pollen of cv. Budimka showed the highest viability and germination in comparison with other cultivars, especially cv. Kožara. Pollen viability and germination decreased over the storage period, and it was the lowest after 6 months of storage at room temperature in all tested cultivars. Storage at 4°C prolonged the pollen viability and germinability of 1–5 fold, depending on the cultivar and treatment duration; however, the pollen longevity of all cultivars was significantly extended when stored at −20 or −80°C. After 6 months, pollen of cv. Budimka stored at −20 and −80°C showed 14–15 fold higher germination rates in relation to pollen storage at room temperature for the same period. The results of the present study suggest that the pollen of these apple cultivars could be efficiently maintained at −20°C and could be further used for breeding purposes, e.g., for crossings between cultivars that flower at different times of the year.

Keywords: apple, cultivars, pollen germination, pollen storage, viability

OPEN ACCESS

Edited by:
Pilar S. Testillano, Spanish National Research Council, Spain

Reviewed by:
Juan M. Losada, Institute of Subtropical and Mediterranean Horticulture La Mayora, Spain
Muriel Quinet, Catholic University of Louvain, Belgium

****Correspondence:***
Dušica Ćalić
calic@ibiss.bg.ac.rs
orcid.org/0000-0002-8987-2563

Specialty section:
This article was submitted to Plant Development and EvoDevo, a section of the journal Frontiers in Plant Science

Received: *17 May 2021*
Accepted: *24 June 2021*
Published: *29 July 2021*

Citation:
Ćalić D, Milojević J, Belić M, Miletić R and Zdravković-Korać S (2021) Impact of Storage Temperature on Pollen Viability and Germinability of Four Serbian Autochthon Apple Cultivars. Front. Plant Sci. 12:709231. doi: 10.3389/fpls.2021.709231

INTRODUCTION

Apple (*Malus* × *domestica* Borkh.) is one of the most important and widely cultivated fruit species around the world with over 7,500 cultivars (Elzebroek and Wind, 2008). China is the largest apple producer, while the USA is the second (FAO, 2016). It is the most produced fruit in temperate climate zones, but currently, its production is expanding into subtropical and tropical zones (Brown, 2012).

Globalization and standardization in the Serbian apple market have drastically reduced the numbers of autochthon cultivars and most of them have nearly disappeared; however, some of these cultivars, such as Petrovača, Budimka, Kolačara Pozna, and Kožara, have extraordinary quality, good pomological characteristics, and pest and disease resistance (Mratinić, 2005; Mratinić and Fotirić Akšić, 2011, 2012).

These autochthon apple cultivars were chosen because of the following features: cv. Budimka is resistant to spring frosts, cv. Petrovača gives fruits at the beginning of summer, cv. Kolačara has the tastiest fruits for cakes, and cv. Kozara has fruits suitable for long-term storage (Mratinić, 2005).

Apple is a self-incompatible and insect-pollinated species. Pollination is the key event for apple fruits production, and fertilization normally occurs among the cultivars. The production of pollen grains with high viability, suitable for storage and transport, is of great importance in selective breeding programs (Chagas et al., 2010). It advances the fertilization process and permits crossings between genotypes that flower at different times (Machado et al., 2014). Efficient pollen storage and high viability are also important for biodiversity, biotechnology, conservation, and other studies.

Several reports have shown that pollen stored at low temperatures was effective for long-term preservation, such as pollen of almond (Martínez-Gómez et al., 2002), mango (Dutta et al., 2013), hazel (Novara et al., 2017), and date palm (Maryam et al., 2017). Pollen stored at −20 or −196°C has extended longevity for at least a year (Bhat et al., 2012). The storage conditions, including temperature, have an immense effect on pollen viability (Deng and Harbaugh, 2004). Pollen age, physiological state of a flower as well as pollen moisture content affect pollen viability during storage. There is little data available in the literature on the storage of apple pollen at low temperatures, except for a few other apple cultivars (Imani et al., 2011).

The *in vitro* germination of pollen grains is the most commonly used viability assay in genetic improvement programs (Imani et al., 2011; Soares et al., 2013; Machado et al., 2014); however, each species requires a specific protocol and culture medium to obtain effective germination *in vitro* (Zambon et al., 2014). The viability of pollen grains could be also determined by indirect methods based on cytological observations following the staining of pollen grains with vital fluorescent dyes (Ćalić et al., 2013; Impe et al., 2020).

Currently, no report is available on the cold pollen storage of any Serbian autochthon apple cultivar. Therefore, the objective of this study was to investigate appropriate temperature conditions for long-term pollen storage of four selected Serbian apple cultivars for possible use in the breeding of these cultivars.

MATERIALS AND METHODS

Plant Materials

Mature pollen of four Serbian autochthon apple cultivars (Petrovača, genotypes VI 49–51; Budimka, genotypes IV 1–3; Kolačara Pozna, genotypes VIII 10–12; and Kožara, genotypes IX 16–18) was harvested in spring 2016. The selected apple belongs to the fruit collection of Fruit Research Institute, Čačak, Serbia. The pollen was collected in the sterile Falcon tubes in the noon of the sunny days to collect samples with low humidity.

Storage

To evaluate the best conditions for pollen storage and extended longevity, different storage periods (0, 1, 2, 3, 4, 5, and 6 months) and temperatures (20, 4, −20, and −80°C) were tested. Pollen was transferred from Falcon tubes to Petri dishes and dehydrated over silica gel at room temperature. Samples from Petri dishes were divided into several Eppendorf tubes to reduce the freeze-thaw stress. Eppendorf tubes were sealed and stored at the above-mentioned temperature treatments. After thawing, stored pollen samples were incubated at room temperature for 24 h.

Fluorescein Diacetate Viability Test

Fluorescein diacetate (FDA) test, as a rapid test, was used to determine pollen viability (Heslop-Harrison and Heslop-Harrison, 1970). FDA (2 mg L^{-1}), dissolved in acetone, was diluted by 0.5 M sucrose solution (1:1). Pollen grains were stained with 1–2 drops of FDA for 1 h, and then preparations were observed under the fluorescent Axiovert microscope (Zeiss, Jena, Germany) with fluorescence filters. Pollen grains showing bright fluorescence were taken as viable and scored.

In vitro Pollen Germination

In vitro pollen germination was performed by using the hanging drop technique (Deng and Harbaugh, 2004; Ćalić et al., 2013) with some modifications as described below. A liquid medium containing 1.2 M sucrose, 0.3 g L^{-1} calcium nitrate [$Ca(NO_3)_2$], 0.10 g L^{-1} boric acid (H_3BO_3), 0.1 g L^{-1} potassium nitrate (KNO_3), 0.2 g L^{-1} magnesium sulfate ($MgSO_4 \cdot 7H_2O$), and 15 %, w/v polyethylene glycol (PEG) was used. A germination test was recorded after a 24 h-incubation period. Pollen was adjudged as having germinated when the length of the pollen tube was equal to or exceeded the pollen diameter. Pollen grains were counted under a light microscope (Leica DMRB, Wetzlar, Germany) at × 20 magnification. Germination of pollen was tested after harvest (0 times), and at 1, 2, 3, 4, 5, and 6 months after storage.

Pollen Nucleus Status

Pollen nuclei number was determined by 4′, 6-diamidino-2-phenylindole (DAPI) (Coleman and Goffm, 1985). The content of anthers was removed by squeezing and was stained with 1–2 drops of DAPI (1 μg mL^{-1}) solution prepared using distilled water. DAPI-treated microspores were examined under the Zeiss Axiovert fluorescent microscope equipped with a camera.

Statistical Analysis

The measurements of the pollen germination and viability were taken on 300 randomly chosen pollen grains (in three repetitions, each with 100 pollen grains) per treatment. To analyze the main effects and interaction effects, the data were subjected to analysis of variance (three-way ANOVA), and the means were separated using an LSD test at $p \leq 0.05$.

TABLE 1 | Effect of different storage temperatures and duration on *in vitro* pollen germination of four autochthon apple cultivars.

Cultivars	Temperature	0 month of storage	1 month of storage	2 month of storage	3 month of storage	4 month of storage	5 month of storage	6 month of storage	Anova *P*-Value
Petrovača	+20°C	68 ± 3.8b/A	24 ± 2.2h/B	14 ± 1.2g/C	7 ± 0.7h/D	5 ± 0.6i/E	3 ± 0.3g/F	2 ± 0.2i/G	≤0.0001
	+4°C	68 ± 3.8b/A	55 ± 4.9c/B	40 ± 3.5c/C	26 ± 2.3d/D	21 ± 1.8f/E	2 ± 0.2h/F	6 ± 0.5f/G	≤0.0001
	−20°C	68 ± 3.8b/A	63 ± 4.0b/B	57 ± 4.6b/B	53 ± 5.1bc/C	49 ± 4.3c/C	46 ± 5.3b/C	44 ± 6.2b/C	≤0.0001
	−80°C	68 ± 3.8b/A	64 ± 3.2b/B	61 ± 4.8b/B	59 ± 3.3b/B	55 ± 3.2b/BC	51 ± 4.9c/BC	47 ± 3.3b/C	≤0.0001
Budimka	+20°C	88 ± 7.9a/A	40 ± 3.7e/B	26 ± 2.1e/C	15 ± 1.3g/D	11 ± 1.0h/E	7 ± 0.6e/F	4 ± 0.5g/G	≤0.0001
	+4°C	88 ± 7.9a/A	66 ± 6.5b/B	55 ± 5.2b/C	39 ± 3.4c/D	29 ± 2.5e/E	20 ± 1.9d/F	13 ± 1.2e/G	≤0.0001
	−20°C	88 ± 7.9a/A	69 ± 6.8b/B	67 ± 5.1a/B	66 ± 5.9a/B	64 ± 4.1a/B	59 ± 3.7a/C	56 ± 5.4a/C	≤0.0001
	−80°C	88 ± 7.9a/A	81 ± 6.7a/B	72 ± 5.7a/C	70 ± 6.4a/C	68 ± 6.5a/C	61 ± 6.0a/D	59 ± 5.5a/D	≤0.0001
Kolačara Pozna	+20°C	64 ± 3.4c/A	33 ± 3.1f/B	9 ± 0.8h/C	5 ± 0.6i/D	3 ± 0.3j/E	2 ± 0.2h/F	1 ± 0.1j/G	≤0.0001
	+4°C	64 ± 3.4c/A	46 ± 4.4d/B	30 ± 3.2d/C	21 ± 1.8e/D	14 ± 1.3g/E	5 ± 0.5f/F	3 ± 0.3h/G	≤0.0001
	−20°C	64 ± 3.4c/A	55 ± 5.2c/B	52 ± 5.0b/B	50 ± 4.5bc/BC	47 ± 4.2c/BC	45 ± 4.2b/C	36 ± 3.8c/D	≤0.0001
	−80°C	64 ± 3.4c/A	56 ± 5.4c/B	55 ± 5.1b/B	52 ± 4.8bc/B	49 ± 4.6c/BC	47 ± 4.3b/C	39 ± 4.0c/D	≤0.0001
Kožara	+20°C	60 ± 3.1d/A	28 ± 2.6g/B	6 ± 0.7i/C	3 ± 0.3j/D	2 ± 0.2k/E	1 ± 0.1i/F	1 ± 0.1j/G	≤0.0001
	+4°C	60 ± 3.1d/A	34 ± 3.2f/B	20 ± 1.8f/C	17 ± 1.5f/D	11 ± 1.0g/E	3 ± 0.3g/F	2 ± 0.2i/G	≤0.0001
	−20°C	60 ± 3.1d/A	50 ± 3.8cd/B	45 ± 4.1bc/C	42 ± 4.1c/CD	38 ± 3.7d/CD	35 ± 4.2c/D	31 ± 4.7d/D	≤0.0001
	−80°C	60 ± 314d/A	51 ± 3.6cd/B	48 ± 4.4bc/B	43 ± 4.2c/C	41 ± 4.2d/C	38 ± 3.4c/CD	34 ± 3.3d/D	≤0.0001
	Anova *P*-value	≤0.001	≤0.0001	≤0.0001	≤0.0001	≤0.0001	≤0.0001	≤0.0001	

Means followed by the same lower case letters in a column and capital letters in a row are not significantly different by an LSD test ($p \leq 0.05$).

TABLE 2 | Effect of different storage temperatures and duration on *in vitro* pollen viability of four autochthon apple cultivars.

Cultivars	Temperature	0 month of storage	1 month of storage	2 month of storage	3 month of storage	4 month of storage	5 month of storage	6 month of storage	Anova *P*-Value
Petrovača	+20°C	79 ± 6.1b/A	34 ± 3.0f/B	22 ± 1.9f/C	18 ± 1.6g/D	15 ± 2.4h/E	11 ± 1.4k/F	9 ± 1.0i/G	≤0.0001
	+4°C	79 ± 6.1b/A	65 ± 5.4c/B	30 ± 2.7e/C	28 ± 2.4e/C	26 ± 2.3f/D	22 ± 2.5h/E	19 ± 2.1f/E	≤0.0001
	−20°C	79 ± 6.1b/A	74 ± 7.8b/A	70 ± 3.8b/B	68 ± 3.6b/B	66 ± 3.1b/B	62 ± 3.1c/C	60 ± 4.3b/C	≤0.0001
	−80°C	79 ± 6.1b/A	75 ± 6.4b/A	72 ± 5.1b/A	70 ± 4.2b/AB	69 ± 4.0b/AB	67 ± 3.0b/AB	63 ± 3.3b/B	≤0.0001
Budimka	+20°C	98 ±8.7a/A	55 ± 5.3d/B	30 ± 2.4e/C	24 ± 2.6f/D	20 ± 2.1g/E	16 ± 1.9i/F	12 ± 1.4g/G	≤0.0001
	+4°C	98 ± 8.7a/A	72 ± 7.3b/B	56 ± 3.2cd/C	48 ± 4.5d/D	35 ± 3.1e/E	30 ± 3.4g/F	28 ± 2.9e/F	≤0.0001
	−20°C	98 ± 8.7a/A	95 ± 9.7a/A	90 ± 8.9a/A	86 ± 6.8a/AB	80 ± 5.2ab/B	79 ± 6.2a/B	73 ± 7.6a/B	≤0.0001
	−80°C	98 ± 8.7a/A	96 ± 8.9a/A	93 ± 7.7a/A	90 ± 5.3a/A	86 ± 3.7a/AB	81 ± 3.5a/B	79 ± 4.1a/B	≤0.0001
Kolačara pozna	+20°C	68 ± 6.3c/A	41 ± 4.3e/B	17 ± 1.5g/C	13 ± 1.4h/D	10 ± 1.4i/E	9 ± 0.9k/F	7 ± 0.8j/G	≤0.0001
	+4°C	68 ± 6.3c/A	46 ± 4.5e/B	30 ± 2.5e/C	21 ± 2.3f/D	15 ± 1.6h/E	14 ± 1.5j/EF	13 ± 1.5g/F	≤0.0001
	−20°C	68 ± 6.3c/A	65 ± 5.6c/A	60 ± 5.0c/AB	58 ± 3.2c/AB	57 ± 5.6c/AB	56 ± 3.8d/AB	51 ± 3.4c/B	≤0.0001
	−80°C	68 ± 6.3c/A	66 ± 6.7c/A	62 ± 5.8c/A	59 ± 3.1c/AB	58 ± 3.9c/AB	57 ± 3.9d/B	56 ± 3.7c/B	≤0.0001
Kožara	+20°C	59 ± 5.6d/A	37 ± 3.9f/B	12 ± 1.3h/C	9 ± 0.8i/D	7 ± 0.9j/E	6 ± 0.7l/F	5 ± 5.1k/G	≤0.0001
	+4°C	59 ± 5.6d/A	40 ± 4.1e/B	33 ± 3.1e/C	28 ± 2.5e/D	17 ± 1.8h/E	14 ± 1.6j/F	11 ± 1.2g/G	≤0.0001
	−20°C	59 ± 5.6d/A	56 ± 5.7d/A	52 ± 4.7d/AB	49 ± 3.2d/AB	48 ± 2.7d/AB	44 ± 3.7f/B	40 ± 4.2 d/B	≤0.0001
	−80°C	59 ± 5.6d/A	58 ± 6.0d/A	57 ± 3.2cd/A	54 ± 3.1cd/A	50 ± 3.8d/B	49 ± 3.1e/B	44 ± 4.6d/C	≤0.0001
	Anova *P*-value	≤0.0001	≤0.0001	≤0.0001	≤0.0001	≤0.0001	≤0.0001	≤0.0001	

Means followed by the same lower case letters in a column and capital letters in a row are not significantly different by the LSD test ($p \leq 0.05$).

RESULTS

Fresh Pollen Characteristics

Fresh pollen showed a high percentage of germination and viability for all cultivars. Pollen germination rate ranged from 60% in cv. Kožara to 88% in cv. Budimka (**Table 1**), while pollen viability rate ranged from 59% in cv. Kožara to 98% in cv. Budimka at 0 months of storage (**Table 2**). Fresh pollen of cv. Budimka showed significantly higher viability and germination rates than the pollen of other cultivars (**Figure 1D**). Interestingly, a greater variation was observed among the cultivars in the pollen viability than in pollen germination rates (**Tables 1**, **2**).

Pollen Characteristics at Room Temperature

Germination and viability of pollen stored at room temperature decreased over time. So, pollen of all apple cultivars lost more

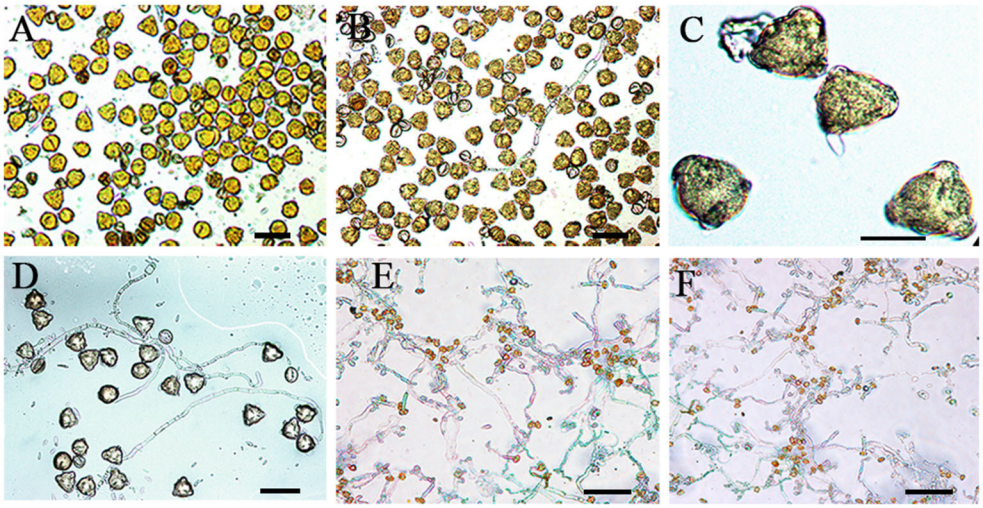

FIGURE 1 | Pollen germination after storage treatment. **(A)** Pollen germination of cv. Kožara at + 20°C (bar = 50 μm), at +4°C **(B)** (bar = 50 μm), at −80°C (**C**) (bar = 20 μm) after 6 months. **(D)** Fresh pollen germination of cv. Budimka at +20°C (bar = 50 μm). **(E)** Pollen germination of cv. Budimka on −20°C and on −80°C (**F**) after 6 months (bars = 100 μm).

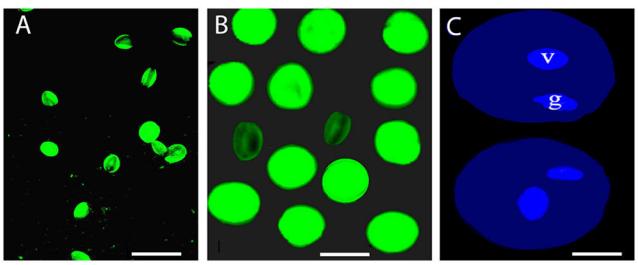

FIGURE 2 | Pollen viability after storage treatment. **(A)** Pollen viability of cv. Kožara (bar = 50 μm) and cv. Budimka **(B)** after 6 months of storage at −80°C (bar = 20 μm). **(C)** Vegetative (v) and generative (g) nucleus of fresh cv. Budimka pollen after staining with DAPI (bar =10 μm).

TABLE 3 | Mixed factorial design showing the effect of storage temperature and storage duration on pollen germination and viability of four Serbian autochthon apple cultivars.

Source of variation	*df*	Pollen germination		Pollen viability	
		***F*-Value**	***P***	***F*-Value**	***P***
Cultivar (A)	3	7,085	≤0.0001	7,710	≤0.0001
Storage duration (B)	6	558	≤0.0001	616	≤0.0001
Temperature (C)	3	148	≤0.001	250	≤0.001
A × B	18	104	≤0.0001	211	≤0.0001
A × C	9	244	≤0.001	519	≤0.001
B × C	18	348	≤0.001	452	≤0.001
A × B × C	54	66	≤0.001	78	≤0.001

than 70 and 90% of germination ability and viability after 2 and 6 months of storage at room temperature, respectively (**Tables 1**, **2**, **Figure 1A**). The decrease in pollen germination and viability rates was significantly faster at room temperature than at lower temperatures. Storage at 4°C prolonged the pollen viability and germinability 1–5 fold compared with room temperature, depending on cultivars and treatment duration (**Figure 1B**).

Pollen Characteristics at Low Temperature

Pollen longevity was further significantly extended when stored at −20 and −80°C ($P \leq 0.0001$; **Tables 1**, **2**, **Figures 1C,E,F**); however, pollen of all cultivars stored at −20°C showed similar germination and viability rates as pollen stored at −80°C (**Figures 1E,F**).

After 6 months of storage, pollen of cv. Budimka kept about 56 and 59% of germination and 73 and 79% of viability when stored at −20 and −80°C, respectively (**Tables 1**, **2**, **Figure 2B**), The germination rates were 14–15 fold higher compared with germination rates in pollen stored at room temperature for the same period ($P \leq 0.0001$).

A significant difference between pollen stored at −20 and 4°C for all cultivars was noticed ($P \leq 0.0001$, of each); however, no statistical differences in pollen germination rates were observed between pollen stored at −20 and −80°C for all cultivars, after 6 months of storage. In addition, pollen of all cultivars showed a 0.3–7 fold higher viability than germination at the same temperature conditions, after 6 months of storage (**Tables 1**, **2**); however, both pollen germination and viability significantly declined throughout the treatment in all cultivars under all storage temperatures (**Tables 1**, **2**, **Figure 1**, **Figures 2A,B**).

Data analysis showed that the effects of apple cultivar and the interactions between cultivar, storage temperature, and storage duration on pollen germination and pollen viability rates were significant ($P < 0.001$; **Table 3**).

Storage of viable pollen of Serbian autochthon apple cultivars for 6 months at −20 to −80°C is adequate for allowing breeders to efficiently carry out hybridization of germplasm flowering at different times and locations.

Pollen Nuclear Status

An analysis of the nuclei number stained with DAPI showed that mature pollen grains of all cultivars were binucleate (**Figure 2C**).

DISCUSSION

Viability and Germinability in Storage Pollen

Since there are no reports of temperature influence on long-term storage of pollen of Serbian apple cultivars on its viability, the present report aimed at providing information on the best storage conditions of pollen to be further used for raising the fertilization potentials of selected autochthon apple cultivars. These results showed that viability and pollen germination varied significantly depending on cultivar, storage conditions, and tests used for germination assessment. The results obtained in the present study are in agreement with results obtained by other authors (Osborne et al., 1992; Lora et al., 2006; Masum-Akond et al., 2012; Dutta et al., 2013; Novara et al., 2017; Yuan et al., 2018).

Variations in pollen longevity among plant species have been attributed to the difference in desiccation tolerance of the pollen (Song and Tachibana, 2007). Pollen of most Serbian autochthon apple cultivars lost viability (up to 12–30%) and germination potential (up to 6–26%) after 2 months at room temperature. These cultivars keep their pollen germination at 31–66% and 35–69% if stored at −20 and −80°C, respectively, for 6 months.

Pollen longevity has been reported to be extended by storing at lower temperatures (4, −20, and −80°C) in other plant species, e.g., in almond (Martínez-Gómez et al., 2002), cherimoya (Lora et al., 2006), mango (Dutta et al., 2013), hazel (Novara et al., 2017), date palm (Maryam et al., 2017), and many others.

Also, Dutta et al. (2013) and Novara et al. (2017) reported that the longevity of pollen of mango and hazel may retain viability for years with low-temperature storage, but pollen viability was generally not extended at the lowest temperature tested in their study (−20°C). This indicates that harmful physical and chemical changes proceed gradually in refrigerator-stored dry pollen (Hanna and Towill, 1995). Studies have indicated that pollen spoilage during aging involves disarranged intracellular integrity, decreased activity of enzymes, accumulation of free radicals, and de-esterification and lipid peroxidation leading to increased leakage of cellular components upon rehydration (Taylor and Hepler, 1997). It has been shown that the aging-mediated membrane damage of pollen is not associated with protein denaturation (Wolkers and Hoekstra, 1995). Reduction in the viability of tomato pollen during long-term dry storage in a freezer involves a decline in the capacity to enhance gene expression for polyamine biosynthetic enzymes upon rehydration (Song and Tachibana, 2007).

The inclusion of 15% PEG in the liquid medium had a positive effect on pollen germination of the autochthon apple cultivars in the present study (data are not shown) and in a previous study on pollen germination of plum (Ćalić et al., 2013). PEG functions as an osmoticum, and it improves *in vitro* pollen germination frequency by preventing tube bursting (Ćalić et al., 2013).

Nuclear Status of Pollen

These results showed that all apple cultivars had binucleate pollen grains. Binucleate pollen has weaker germination but longer survival time than trinucleate pollen. Plants that have binucleate pollen grains are pollinated *via* insects (Gottsberger, 1989). Trinucleate pollen is associated with higher metabolic activity and moisture content in comparison to binucleate pollen. Therefore, a common feature of trinucleate pollen is more sensitive to trauma by desiccation (Lora et al., 2006). Storage techniques with low temperature are more easily improved for desiccation-tolerant binucleate pollen than trinucleate pollen.

Since there is no difference in the pollen viability and germination of the Serbian autochthon apple cultivars after storage at −20 and −80°C for up to 6 months, there is no need to keep pollen at −80°C, as was also recommended for pollen of some other plant species, such as crape myrtle (Masum-Akond et al., 2012).

The significance of this study points to the necessity of preserving these old autochthon cultivars as unique genetic resources with enormous ecological, and potential economic value.

CONCLUSION

From the results of this study, it can be concluded that the pollen of the four apple cultivars tested has different viability and germination capacity. Furthermore, germination of all apple cultivars tested is best maintained over 6 months when pollen is stored at −20 to −80°C.

The long period of this pollen viability makes it suitable for most breeding program applications.

DATA AVAILABILITY STATEMENT

The original contributions presented in the study are included in the article/supplementary material, further inquiries can be directed to the corresponding author/s.

AUTHOR CONTRIBUTIONS

DĆ and SZ-K conceived and designed the experiments. DĆ, JM, MB, RM, and SZ-K performed the experiments. JM, MB, DĆ, and SZ-K analyzed the data. DĆ and SZ-K wrote the manuscript. All authors have read the manuscript and approved it for submission.

FUNDING

This work was supported by the Ministry of Education, Science and Technological Development of the Republic of Serbia, Grant no. 451-03-9/2021-14/200007.

ACKNOWLEDGMENTS

The authors like to express their deepest gratitude to the late colleague Dr. Rade Milić, Fruit Research Institute, Čačak, Serbia, for providing plant material used in this study.

REFERENCES

Bhat, Z. A., Dhillon, W. S., Shafi, R. H. S., Rather, J. A., Mir, A. H., Shafi, W., et al. (2012). Influence of storage temperature on viability and *in vitro* germination capacity of pear *(Pyrus* spp.) pollen. *J. Agric. Sci.* 4, 128–135. doi: 10.5539/jas.v4n11p128

Brown, S. (2012). "Apple," in *Fruit Breeding*, eds M. L. Badenes, and D. H. Byrne (New York, NY: Springer), 329–367.

Ćalić, D., Devrnja, N., Kostić, I., and Kostić, M. (2013). Pollen morphology, viability, and germination of *Prunus domestica* cv. *PoŽegača. Sci. Hortic.* 155, 118–122. doi: 10.1016/j.scienta.2013.03.017

Chagas, E. A., Pio, R., Chagas, P. C., Pasqual, M., and Bettiol Neto, J. E. (2010). Composição de meio de cultura e condições ambientais para germinação de grãos de pólen de porta-enxertos de pereira. *Ciênc. Rural* 40, 231–236. doi: 10.1590/S0103-84782010000200002

Coleman, A. W., and Goffm, L. J. (1985). Applications of fluorochromes to pollen biology. Mithramycin and 4',6-diamidino-2-phenylindole (DAPI) as vital stains and for quantitation of nuclear DNA. *Stain Technol.* 60, 145–154. doi: 10.3109/10520298509113905

Deng, Z., and Harbaugh, B. (2004). Technique for in vitro pollen germination and short term pollen storage in caladium. *Hortscience* 39, 365–367. doi: 10.21273/HORTSCI.39.2.365

Dutta, S. K., Srivastav, M., Chaudhary, R., Lal, K., Patil, P., Singh, S. K., et al. (2013). Low temperature storage of mango (*Mangifera inidica* L.) pollen. *Sci. Hortic.* 161, 193–197. doi: 10.1016/j.scienta.2013.06.022

Elzebroek, A. T. G., and Wind, K. (2008). "Edible fruits and nuts," in *Guide to Cultivated Plants*, eds A. T. G. Elzebroek, and K. Wind (Wallingford: CAB International), 25–131.

FAO (2016). *Food and Agriculture Data*. FAO. Available online at: http://faostat3.fao.org/faostat-gateway/go/to/download/~Q/QC/E

Gottsberger, G. (1989). Comments on flower evolution and beetle pollination in the genera annona and rollina (*Annonaceae*). *Plant Syst. Evol.* 167, 89–94. doi: 10.1007/BF00936405

Hanna, W. W., and Towill, L. W. (1995). "Long-term pollen storage," in *Plant Breeding Reviews*, ed J. Janic (Chichester: John Wiley and Sons), 197–207.

Heslop-Harrison, J., and Heslop-Harrison, Y. (1970). Evaluation of pollen viability by enzymatically induced fluorescence; intracellular hydrolysis of fluorescein diacetate. *Biotech. Histochem.* 45, 115–120. doi: 10.3109/10520297009085351

Imani, A., Barzegar, K., Piripireivatlou, S., and Masomi, S. H. (2011). Storage of apple pollen and *in vitro* germination. *Afr. J. Agr. Res.* 6, 624–629. doi: 10.5897/AJAR10.905

Impe, D., Reitz, J., Köpnick, C., Rolletschek, H., Börner, A., Senula, A., et al. (2020). Assessment of pollen viability for wheat. *Front. Plant Sci.* 10:1588. doi: 10.3389/fpls.2019.01588

Lora, J., Pérez de Oteyza, M. A., Fuentetaja, P., and Hormaza, J. I. (2006). Low temperature storage and *in vitro* germination of cherimoya (*Annona cherimola* Mill.) pollen. *Sci. Hortic.* 108, 91–94. doi: 10.1016/j.scienta2005.12.003

Machado, C. A., Moura, C. R. F., Lemos, E. E. P., Ramos, S. R. R., Ribeiro, F. E., and Lédo, A. S. (2014). Pollen grain viability of coconut accessions at low temperatures. *Acta Sci. Agron.* 36, 227–232. doi: 10.4025/actasciagron.v36i2.17346

Martínez-Gómez, P., Gradziel, T. M., Ortega, E., and Dicenta, F. (2002). Low temperature storage of almond pollen. *Hortscience* 37, 691–692 doi: 10.21273/HORTSCI.37.4.691

Maryam, A., Jaskani, M. J., and Naqvi, S. A. (2017). Storage and viability assessment of date palm pollen. *Methods Mol. Biol.* 1638, 3–13. doi: 10.1007/978-1-4939-7159-6_1

Masum-Akond, A. S. M. G., Pounders, C. T., Blythe, E. K., and Wang, X. W. (2012). Longevity of crape myrtle pollen stored at different temperatures. *Sci. Hortic.* 139, 53–57. doi: 10.1016/j.scienta.2012.02.021

Mratinić, E. (2005). *Autochton Apple Cultivars in Serbia and Montenegro*. Draganić.

Mratinić, E., and Fotirić Akšić, M. (2011). Evaluation of phenotypic diversity of apple *(Malus sp.)* germplasm through the principle component analysis. *Genetika Belgrade* 43, 331–340. doi: 10.2298/GENSR1102331M

Mratinić, E., and Fotirić Akšić, M. (2012). Phenotypic diversity of apple *(Malus sp.)* germplasm in South Serbia. *Braz. Arch. Biol. Technol.* 55, 349–358. doi: 10.1590/S1516-89132012000300004

Novara, C., Ascari, L., La Morgia, V., Reale, L., Genre, A., and Siniscalco, C. (2017). Viability and germinability in long term storage of *Corylus avellana* pollen. *Sci. Hortic.* 214, 295–303. doi: 10.1016/j.scienta.2016.11.042

Osborne, R., Robbertse, P. J., and Claassen, M. L. (1992). The longevity of cycad pollen in storage. *S. Afri. J. Bot.* 58, 250–254. doi: 10.1016/S0254-6299(16)3 0842-03

Soares, T. L., Jesus, O. N., Souza, E. H., Santos-Serejo, J. A., and Oliveira, E. J. (2013). Morphology and viability of pollen grains from passion fruit species (*Passiflora* spp.). *Acta Bot. Bras.* 27, 779–787. doi: 10.1590/S0102-33062013000400018

Song, J., and Tachibana, S. (2007). Loss of viability of tomato pollen during long-term dry storage is associated with reduced capacity for translating polyamine biosynthetic enzyme genes after rehydration. *J. Exp. Bot.* 58, 4235–4244. doi: 10.1093/jxb/erm280

Taylor, L. P., and Hepler, P. K. (1997). Pollen germination and tube growth. *Ann. Rev. Plant Physiol. Plant Mol. Biol.* 48, 461–491. doi: 10.1146/annurev.arplant.48.1.461

Wolkers, W. F., and Hoekstra, F. A. (1995). Aging of dry desiccation-tolerant pollen does not affect protein secondary structure. *Plant Physiol.* 109, 907–915. doi: 10.1104/pp.109.3.907

Yuan, S. C., Chin, S. W., Lee, C. Y., and Chen, F. C. (2018). *Phalaenopsis pollinia* storage at sub-zero temperature and its pollen viability assessment. *Bot. Stud.* 59, 1–8. doi: 10.1186/s40529-017-0218-2

Zambon, C. R., Silva, L. F. O., Pio, R., Figueiredo, M. A., and Silva, K. N. (2014). Estabelecimento de meio de cultura e quantificação da germinação de grãos de pólen de cultivares de marmeleiros. *Rev. Bras. Frutic.* 36, 400–407. doi: 10.1590/0100-2945-095/13

Conflict of Interest: The authors declare that the research was conducted in the absence of any commercial or financial relationships that could be construed as a potential conflict of interest.

frontiers in Plant Science

ORIGINAL RESEARCH
published: 01 September 2021
doi: 10.3389/fpls.2021.639431

Mapping and Analysis of a Novel Genic Male Sterility Gene in Watermelon (*Citrullus lanatus*)

Wei Dong[1], *Dewei Wu*[2], *Chen Yan*[1] *and Defeng Wu*[1]*

[1] School of Life Science, Henan University, Kaifeng, China, [2] Jiangsu Provincial Key Laboratory of Crop Genetics and Physiology, Yangzhou University, Yangzhou, China

Seed production is critical for watermelon production, which mostly involves first-generation hybrid varieties. However, watermelon hybrid seed production currently requires complex procedures, including artificial isolation and pollination. Therefore, the development and use of a male-sterile system to generate watermelon hybrids can simplify the process. The scarcity of male-sterile watermelon germplasm resources necessitates the use of molecular breeding methods. Unfortunately, the genes responsible for male sterility in watermelon have not been cloned. Thus, the genetic basis of the male sterility remains unknown. In this study, two DNA pools derived from male-sterile and normal plants in the F_2 population were used for whole-genome resequencing. The Illumina high-throughput sequencing resulted in 62.99 Gbp clean reads, with a Q30 of 80% after filtering. On the basis of the SNP index association algorithm, eight candidate regions (0.32 Mb) related to specific traits were detected on chromosome 6. Expression pattern analyses and watermelon transformation studies generated preliminary evidence that *Cla006625* encodes a pollen-specific leucine-rich repeat protein (ClaPEX1) influencing the male sterility of watermelon. The identification and use of genic male sterility genes will promote watermelon male sterility research and lay the foundation for the efficient application of seed production technology.

Keywords: watermelon (*Citrullus lanatus* L.), genic male sterility, fine mapping, pollen-specific leucine-rich repeat protein, seed production technology

OPEN ACCESS

Edited by:
Raju Datla, Global Institute for Food Security (GIFS), Canada

Reviewed by:
Cecilia McGregor, University of Georgia, United States
Wenge Liu, Zhengzhou Fruit Research Institute (CAAS), China

***Correspondence:**
Defeng Wu
wudefeng@163.com

Specialty section:
This article was submitted to Plant Development and EvoDevo, a section of the journal Frontiers in Plant Science

Received: *06 January 2021*
Accepted: *19 March 2021*
Published: *01 September 2021*

Citation:
Dong W, Wu D, Yan C and Wu D (2021) Mapping and Analysis of a Novel Genic Male Sterility Gene in Watermelon (Citrullus lanatus). Front. Plant Sci. 12:639431. doi: 10.3389/fpls.2021.639431

INTRODUCTION

Watermelon (*Citrullus lanatus*) is a monoecious and diclinous species, which makes it very useful for research applying heterosis for crop improvement. Heterosis generally refers to the phenomenon in which a few or many traits of hybrid varieties (heterozygotes) are superior to those of the parent varieties (homozygotes) (Gusmini and Wehner, 2005). A previous study revealed that the total fruit weight and total number of fruits were 22 and 32% greater in F_1 hybrids than in the best parents (Gusmini and Wehner, 2005). Moreover, triploid watermelon breeding, which is based on the heterotic effects associated with different combinations of diploid and tetraploid genomes, requires the production of F_1 hybrids (Saminathan et al., 2015).

Detasseling is a necessary step during the production of high-quality watermelon hybrid seeds. However, it is a time-consuming and labor-intensive process that is not conducive to plant growth, and it may lead to a decreased hybrid seed yield (Wan et al., 2019). This problem may be addressed by using male-sterile watermelon lines to generate hybrids. There are two main types of male sterility, namely, cytoplasmic male sterility (CMS)

and genic male sterility (GMS). More specifically, CMS is maternally inherited and may be related to the genes in the mitochondria and chloroplasts of plants, whereas GMS is controlled by nuclear genes and leads to pollen abortion and stable sterility. Many male-sterile mutants have been identified among members of the family Cucurbitaceae, including watermelon, cucumber (*Cucumis sativus* L.), and melon (*Cucurbita pepo* L.). In cucumber, the genetic material of the natural male-sterile mutant plants in the "YL-5" inbred line population was sequenced, after which the *MS-3* gene was fine-mapped based on a Kompetitive Allele Specific PCR analysis (Han et al., 2018). The following five single recessive genes control male sterility in melon: *ms-1*, *ms-2*, *ms-3*, *ms-4*, and *ms-5* (Bohn and Whitaker, 1949; Bohn and Principe, 1964; McCreight and Elmstrom, 1984; Lecouviour et al., 1990; Pitrat, 2002; Park et al., 2004). These male sterility genes are on different chromosomes, and the male sterility traits controlled by these genes vary. A few male-sterile watermelon mutants have been reported, including a glabrous male-sterile (*gms*) mutant, male-sterile G17AB, a male-sterile dwarf (*ms-dw*), male-sterile *DT-2*, *ms-2*, and male/female-sterile *MFFH*, all of which exhibit GMS (Watts, 1962, 1967; Ray and Sherman, 1988; Xia et al., 1988; Dyutin and Sokolov, 1990; Zhang and Wang, 1990; Huang et al., 1998; Liu et al., 2004; Zhang et al., 2012). Male-sterile watermelon germplasm are very precious resources useful for watermelon breeding and for clarifying the molecular mechanism underlying male sterility (Rhee et al., 2015). However, the gene controlling male sterility has not been precisely identified and mapped.

Genic male sterility has been observed and widely used in various crops. For example, a Chinese hybrid rice line has been instrumental for increasing rice production in China and worldwide (Khush, 2001; Yuan, 2004). A spontaneous mutant exhibiting photoperiod-sensitive male sterility (PSMS) was detected in China in 1973. Specifically, PSMS was detected in the japonica rice (*Oryza sativa* ssp. *japonica*) variety Non-gken 58 (referred to as 58N) in Hubei Province, China (Shi, 1985). During hybrid rice breeding, PSMS rice may be fertile under short-day conditions, thereby enabling self-reproduction. It is male-sterile under long-day conditions and produces hybrid seeds by intercropping with normally fertile lines (Ding et al., 2012). Advances in genomic research have resulted in the mapping of many nuclear genes in rice (Qi et al., 2014; Sheng et al., 2015). A previous study revealed more than 70 male-sterile cytoplasmic systems in wheat and confirmed that heterosis may lead to yield increases of 3.5–15% (Singh et al., 2015). There are at least five GMS genes and three environmentally sensitive GMS genes (Ni et al., 2017). Hundreds of maize GMS mutants have been generated and characterized, and 17 maize GMS genes have been identified and cloned (Timofejeva et al., 2013; Walbot and Egger, 2016; Zhou et al., 2017). All of these genes are recessive, with the exception of *ms44* (Fox et al., 2017).

Next-generation GMS hybrid biotechnology-based research techniques are useful for screening GMS and maintainer seeds, especially the techniques related to the seed production technology (SPT) process previously used to address the problem associated with recessive genic male-sterile line maintenance and reproduction in maize (Albertsen et al., 2006). The male sterility of watermelon cannot be restored because of a lack of male sterility maintainer lines. Establishing SPT maintainer lines *via* the production of transgenic plants requires the following: the full coding sequence of a male fertility gene for fertility restoration, a pollen-inactivating gene for disrupting transgenic pollen development, and a seed color marker gene for seed sorting (Wu et al., 2016). The SPT process has been developed in rice (Chang et al., 2016; Wang et al., 2018). To date, there is no report describing the utility of SPT in watermelon. The G17AB male-sterile watermelon line was initially selected in 1988 and was subsequently used by watermelon breeding programs (Xia et al., 1988). It has been an excellent resource for constructing a biotechnology-based male-sterile system, but the major gene controlling the male sterility of G17AB remains unknown, which has hindered the development of SPT. The primary objective of this study was to identify the major gene regulating GMS. Bulked segregant analysis (BSA) and whole-genome resequencing of two DNA pools (i.e., male-sterile pool and normal pool) derived from the F_2 population followed by genetics-, bioinformatics-, cytobiology-, and molecular biology-based analyses preliminarily identified *Cla006625* as a gene encoding a melon pollen-specific leucine-rich repeat (LRR) protein. Moreover, *Cla006625* was determined to be the major gene controlling watermelon male sterility. This study is the first to clone a male sterility gene in watermelon. The identification and characterization of the GMS gene provides the foundation for future research aimed at applying SPT for the genetic improvement of watermelon.

MATERIALS AND METHODS

Plant Materials and Phenotyping for Male Sterility

The G17AB male-sterile watermelon line ($2n = 2\times = 22$) was identified in 1997 at the experimental farm of the Henan University Genetics and Breeding Base in Kaifeng, China. Its morphological characteristics were documented annually starting in 1998 to evaluate its genetic stability. In this study, the following validation experiments were conducted. Firstly, G17AB male-sterile watermelon plants were tagged and hand-pollinated with pollen from G17AB male-fertile watermelon plants to generate the F_1 generation in the spring of 2015. In the fall of 2015, the F_1 plants were selfed to produce the F_2 generation. Secondly, G17AB male-sterile watermelon plants were analyzed by conducting test cross experiments. The plants were hand-pollinated with pollen from six inbred lines ("Zhongliu," "Cai1," "Cai7," "Kexi," "Juwang," and "Changhei") to generate the F'_1 generation in the spring of 2016. In the autumn of 2016, the F'_1 plants were self-pollinated to generate the F'_2 generation. The F'_2 seeds were sown in the spring of 2017. The male flower fertility of the F_1, F_2, F'_1, and F'_2 plants was determined. In the autumn of 2017, 60 plants in the F_2 segregating population (mixed pool comprising 30 plants exhibiting male sterility and 30 plants exhibiting male fertility) and six parent plants (male-sterile G17AB and "Zhongliu" inbred line) were used as research materials. We strictly controlled the watermelon growth conditions, with all plants cultivated under long-day conditions and examined in the

greenhouse at the Henan University Genetic Breeding Base. The temperature was maintained at 25–30°C during the day and at 15–18°C at night. All watermelon seeds were stored in a seed storage cabinet at 4°C.

Pollen Microspore Development

Buds of the G17AB watermelon plants were sampled every 2 days during the pre-flowering stage, when the flower buds were 2, 3–4, 5–10, and 10–20 mm long (Shan et al., 2016; Sheng et al., 2017). For the light microscopy examination, the anthers were fixed in a fixative solution (4% paraformaldehyde) for 24 h. They were then dehydrated, embedded in paraffin, and sliced as previously described (O'Brien et al., 1964). The slices were stained with toluidine blue and sealed in neutral gum after heating at 38°C. The samples were then observed using the ECLIPSE E100 microscope (Nikon, Tokyo, × 100 magnification).

For the transmission electron microscopy analysis, the collected anthers were immediately immersed in fixative solution (2.5% glutaraldehyde). The samples were post-fixed for 5 h in a 1% osmium tetroxide buffer solution, after which they were washed four times and dehydrated in a graded series (30, 50, 70, 80, 90, and 100%) of ethyl alcohol for 1 h. The samples were incubated at 37°C overnight and embedded in paraffin at 60°C for 48 h. Ultrathin sections (60–80 nm) were sliced with the DiATOME Ultra 45° knife (DIATOME Ltd., Biel, Switzerland) and stained with a 2% uranium acetate-saturated alcohol solution. The samples were examined using the HT7700 transmission electron microscope (Hitachi, Japan).

Sample Collection and BSA Library Preparation

Total genomic DNA was extracted from the leaves of the parents and F_2 plants after the flowering stage. Genomic DNA was purified from 60 plants in the F_2 segregating population and five parent plants for a whole-genome resequencing performed by the Beijing Biomarker Technologies Corporation (Beijing, China). To generate bulked samples, equal amounts of DNA from each plant in the male-sterile (S-pool) and normal (N-pool) groups were mixed for a final concentration of 40 ng/μl. The DNA samples were sonicated to produce 350-bp fragments. After trimming the barcodes, high-quality reads were mapped to the *C. lanatus* 97,103 genome sequence (version 1[1]). The single nucleotide polymorphisms (SNPs) were filtered, including the loci with multiple genotypes, all supporting reads for SNPs with fewer than four reads, the loci with the same genotype between mixed pools, and the loci of recessive mixed pool genes not from recessive parents. An association analysis was performed to analyze the difference between the SNP indices of the two pools. The ΔSNP/indel index reflected the significant differences in the genotype frequencies between the two pools (Fekih et al., 2013; Hill et al., 2013). Candidate regions were extracted from the linkage group that exceeded the threshold (99th percentile). The Euclidean distance (ED) algorithm uses sequencing data to identify markers of significant differences between mixed pools, after which the regions associated with specific traits are evaluated (Hill et al., 2013). Theoretically, except for the differences in the loci related to the target traits, the loci tend to be consistent between the two pools. The results of the variation analysis and the BSA correlation analysis for the samples were plotted using Circos software[2].

Analysis of Candidate Gene Expression Levels

The *Cla009408*, *Cla006737*, *Cla006738*, *Cla001244*, *Cla006625*, *Cla009378*, *Cla009382*, *Cla007521*, and *Cla009410* expression patterns were examined by quantitative real-time (qRT)-PCR. The G17AB and "Zhongliu" plants were grown for about 60 days after sowing. Three replicates of the anther samples were collected, each comprising 10 anthers from individual plants. Total RNA was extracted and gene expression was analyzed as previously described (Dong et al., 2018). Briefly, total RNA was isolated from each sample using the TRIzol reagent (Invitrogen, Carlsbad, CA, United States). qRT-PCR was completed using TB Green® Premix Ex Taq™ II (Tli RNaseH Plus) and the Roche LightCycler 480 II instrument according to the manufacturer's instructions. The PCR program was as follows: 95°C for 30 s; 40 cycles of 95°C for 5 s and 60°C for 30 s. The *ClYLS8* gene was used as an internal reference control. Primers were designed based on the *C. lanatus* 97,103 genome sequence using the Primer5 program. Details regarding the qRT-PCR primers used to analyze candidate gene expression are listed in **Table 1**.

Single Nucleotide Polymorphism Analysis of Major Genes Controlling Male Sterility

To detect the SNPs in the major genes controlling male sterility, genomic DNA was extracted from the leaves of 30 male-fertile watermelon plants and 30 male-sterile watermelon plants according to the CTAB method (Murray and Thompson, 1980). The extracted genomic DNA was analyzed by agarose gel electrophoresis to assess the extent of any DNA degradation. The DNA concentration and purity were determined using the Nanophotometer spectrophotometer (IMPLEN, CA, United States). A forward primer (5′-ATGGCTTCTTTTCATAGAAAGCAAGCT-3′) and a reverse primer (5′-TTAATAGCCAGGAAACTGTGGTGG-3′) were designed to analyze the SNPs. The PCR products were sequenced.

Bioinformatics Analysis

The homology of nucleotide sequences was analyzed online[3]. The Vector NTI Advance10 software was used to align the target gene sequence with the sequences of *Arabidopsis thaliana* homologs. A phylogenetic tree comprising the target gene and its homologous sequences was constructed using the MEGA 4.0 software (Kumar et al., 2001). A bootstrap analysis (1,000 replicates) was completed to assess the reliability of the tree (Felsenstein, 1992).

[1] www.icugi.org/pub/cucurbit/genome/watermelon/97103/v1/

[2] http://circos.ca/

[3] http://www.ncbi.nlm.nih.gov

TABLE 1 | Sequence details for the qRT-PCR primers used to analyze watermelon candidate gene expression.

Primer name	Forward primer sequence	Reverse primer sequence
Cla009408	TATGTATCGCCGAATAATCCCGC	CATTGAATTGTTCTGACCCCTCA
Cla006737	GACTGTCCATATTGCATCCCTCTACC	AGCACCACTAATTTCTACGGCTTCCT
Cla006738	TCACTTCTCCACATGTCCTCCTCA	TTTGCTTGGCTCTAAAACCTTCCT
Cla006625	TCACTCATCGTCAACTTTTGGCTC	ATTGGCTGTCATGTTTTGAGGGTC
Cla009378	GGTGATTGTTGCTCTTCATTCTTG	GGGAGGCGTCGATTTTCTTAGT
Cla009382	CCACAAGCCTCAAAACAAGCGA	GGAATCTGGGAAAGAGAACCCC
Cla007521	GCCTCATCACTTCCCCTCACCTT	AATCCTTTAGCCTCAAAACCCTG
Cla009410	TCTTCCTCCCCCTTCCATCTTC	ACCCTTTTCACTTCGCCCACTC
ClYLS8	AGAACGGCTTGTGGTCATTC	GAGGCCAACACTTCATCCAT

Watermelon Transformation

The binary RNA interference (RNAi) vector DHpart27RNAi FADP1P4 was constructed as previously described (Li et al., 2019). Briefly, a 300-bp fragment of the candidate gene was inserted between the *Hin*dIII and *Xba*I sites. The fragment was amplified by PCR using a forward primer (5′-CCCAAGCTTAACAATCGCTTCGTCGGCC-3′) and a reverse primer (5′-CTAGTCTAGAGGTTTCCTATCTCGGGTGGG-3′). The reverse sequence was inserted between the *Xho*I and *Kpn*I sites in the vector. The reverse complementary sequence was amplified by PCR using a forward primer (5′-CGGGGTACCAACAATCGCTTCGTCGGCC-3′) and a reverse primer (5′-CCGCTCGAGGGTTTCCTATCTCGGGTGGGAAA-3′). The resulting DHpart27RNAi FADP1P4-Y recombinant plasmid was inserted into the *Agrobacterium tumefaciens* strain GV3101 cells. The seeds of six inbred diploid "Kexi" lines were used as explant material to induce the development of adventitious shoots. Previously described methods were modified for the genetic transformation of watermelon (Yu et al., 2011; Liu et al., 2016; Ren et al., 2018). Briefly, watermelon seeds were dehusked and sterilized, after which they were sown on basic Murashige and Skoog solid medium and incubated for 2 days in darkness and then 2–3 days with a 16-h light/8-h dark photoperiod. The cotyledon explants were infected with the transformed *A. tumefaciens* strain GV3101 cells carrying the recombinant plasmid. The infected cotyledon explants were co-cultivated in darkness for 4 days. The timing of this step was considerably affected by the variety. The cotyledon explants were then transferred to selective induction medium and incubated for 4 weeks. They were then transferred to selective elongation medium and incubated for 2 weeks. The plantlets with well-developed roots were collected from the rooting medium and placed in plastic cups containing vermiculite.

RESULTS

Morphological and Genetic Characteristics of Male-Sterile Watermelon

After years of screening and cultivating, the genetic characteristics underlying the male sterility of G17AB were confirmed to be stable. To evaluate the genetic stability, G17AB male-sterile watermelon plants were hand-pollinated using pollen from six inbred lines ("Cai1," "Cai7," "Kexi," "Juwang," "Tianli," and "Changhei") to produce F'_1 and F'_2 generations. The characterization of the resulting plants revealed that all F_1 hybrids were male-fertile (**Figure 1A**), and the ratio of male-fertile plants to male-sterile plants in the F_2 population was 3:1, which is consistent with Mendel's segregation (the maximum χ^2 value was 0.45, $P > 0.05$). The male-sterile flowers were pale yellow and had small petals and anthers, the surface of which lacked pollen grains. The male-fertile flowers were golden and had large petals and anthers, the surface of which was covered with pollen grains (**Figure 1B**). The average sugar content, weight, length, and width of the male-fertile watermelon fruits were 10.8°Bx, 5.8 kg, 20.1 cm, and 19.6 cm, respectively. The average sugar content, weight, length, and width of the male-sterile watermelon fruits were 10.5°Bx, 5.65 kg, 19.5 cm, and 18.8 cm, respectively (**Figure 1C**). There was no difference between the fruits produced by the male-fertile and male-sterile G17AB plants. The fruits were all round with red flesh and were moderately sized. The GMS mutant G17AB is an excellent resource for constructing a biotechnology-based male-sterile system.

Microspore Development

To analyze pollen development, anthers embedded in paraffin were examined using a light microscope (**Figure 2**). Normal pollen sacs were detected in the fertile flowers and the male-sterile flowers (**Figure 2A**, parts a and e). During the early male flower development stage, the pollen sacs of male-sterile flowers developed normally, similar to the pollen sacs of fertile flowers. The microsporocyte was larger in fertile anthers than in male-sterile anthers (**Figure 2A**, parts b and g). The archesporium was divided into a parietal cell and a sporogenous cell *via* periclinal division. The microsporocyte developed into a tetrad in the fertile anthers (**Figure 2A**, part c). In contrast, the male-sterile anthers lacked a tetrad and the microsporocyte was vacuolated (**Figure 2A**, part h). In the fertile anthers, the tetrad eventually developed into pollen (**Figure 2A**, parts d and e). In the male-sterile plants, the tapetum cells disintegrated, the anthers shrank completely, and no mature pollen grains developed (**Figure 2A**, parts i and j).

The transmission electron microscopy analysis revealed many organelles, including plastids, mitochondria, and an endoplasmic reticulum, in the cytoplasm of the microsporocyte in the fertile anthers. The nucleus was large and the nucleolus was clear (**Figure 2B**, part a). The mononuclear pollen grains formed

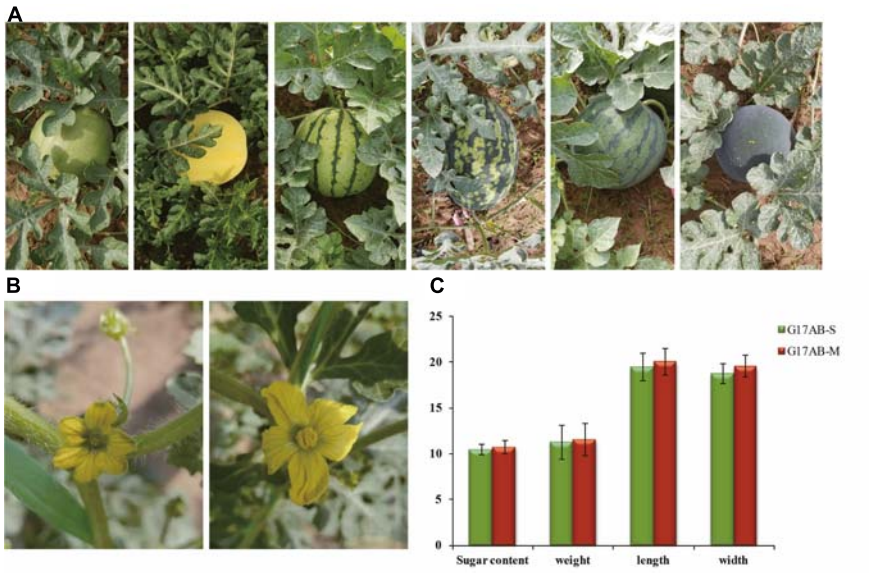

FIGURE 1 | Comparison of the male flowers and fruits between male-sterile and male-fertile watermelon plants. **(A)** Different inbred lines (from *left* to *right*: "Cai1," "Cai7," "Kexi," "Juwang," "Tianli," and "Changhei"). **(B)** Comparison of the flowers from male-sterile (*left*) and male-fertile (*right*) G17AB watermelon plants. **(C)** The sugar content, weight, length, and width of individual fruits from the male-fertile and male-sterile G17AB watermelon plants.

by meiosis were filled with organelles (**Figure 2B**, parts b and c). The mature pollen grain wall comprised two layers (i.e., inner and outer walls). The outer wall exhibited protuberant ornamentation, and the pollen contained many plastids and starch grains (**Figure 2B**, part d). The transmission electron microscopy images clearly presented the boundary between the cytoplasm and the nuclear membrane. Compared with the microsporocyte in fertile anthers, the cytoplasm of the microsporocyte in sterile anthers was thinner and included fewer organelles (**Figure 2B**, part e). As the microsporocyte grew, the number of vacuoles in the cytoplasm increased rapidly, reflecting a tendency of vacuolation (**Figure 2B**, parts f and g). Finally, the vacuoles disappeared and the microsporocyte contracted into clusters and gradually disintegrated and disappeared (**Figure 2B**, part h).

Whole-Genome Resequencing Analysis

A whole-genome resequencing analysis was completed to identify and analyze candidate genes mediating male sterility. The Illumina high-throughput sequencing resulted in 62.99 Gbp clean bases, with a Q30 of 80% after filtering. The data have been submitted to the NCBI database (submission number: SUB8801923). The average comparison efficiency between the sample and the reference genomes was 98.55%, the average coverage depth was 34.25×, and the genome coverage was 99.60% (at least one base coverage). The SNPs between the watermelon sample and the reference genomes were obtained and are presented herein in a Venn diagram (**Figure 3A**). A total of 176,751 SNPs were detected between the parents, 2,852 of which were non-synonymous mutations. Additionally, 45,865 SNPs were detected between the mixed pools, 665 of which were non-synonymous mutations. On the basis of the mapping of the clean reads to the reference genome, the insertion and deletion of small fragments in the sample and reference genomes were detected (**Figure 3B**). A comparison of the parents revealed 72,356 small indels, whereas a comparison of the mixed pools detected 26,034 small indels.

A Circos plot of the chromosomal distribution of candidate regions among samples was produced (**Figure 4A**). On the basis of the theoretical separation ratio, the correlation threshold was 0.667 (Hill et al., 2013). To more precisely locate candidate regions, the threshold was decreased to 0.56. The candidate regions were extracted from the linkage group exceeding the threshold (99th percentile). Using the SNP index association algorithm, eight candidate regions (0.32 Mb) related to specific traits were detected on chromosome 6 (**Figure 4B**). The median + 3SD of the fitted values of all loci was used as the correlation threshold (0.37) of the analysis (Hill et al., 2013). The ED association algorithm revealed one candidate region (10.73 Mb) related to specific traits on chromosome 6. This region comprised 710 genes, including 25 genes with non-synonymous SNP sites (**Figure 4C**).

Identification of the LRR Protein-Encoding Gene

The expression levels of the following seven candidate watermelon genes in the "Zhongliu" and G17AB male-sterile plants were analyzed by qRT-PCR: *Cla009408*, *Cla006737*, *Cla006738*, *Cla006625*, *Cla009382*, *Cla007521*, and *Cla009410* (**Figure 5**). The *Cla006737* and *Cla009382* expression levels were higher in the flowers than in the flower buds of the G17AB male-sterile plants. The opposite expression pattern was detected in "Zhongliu" plants. The *Cla009410* expression level was lower

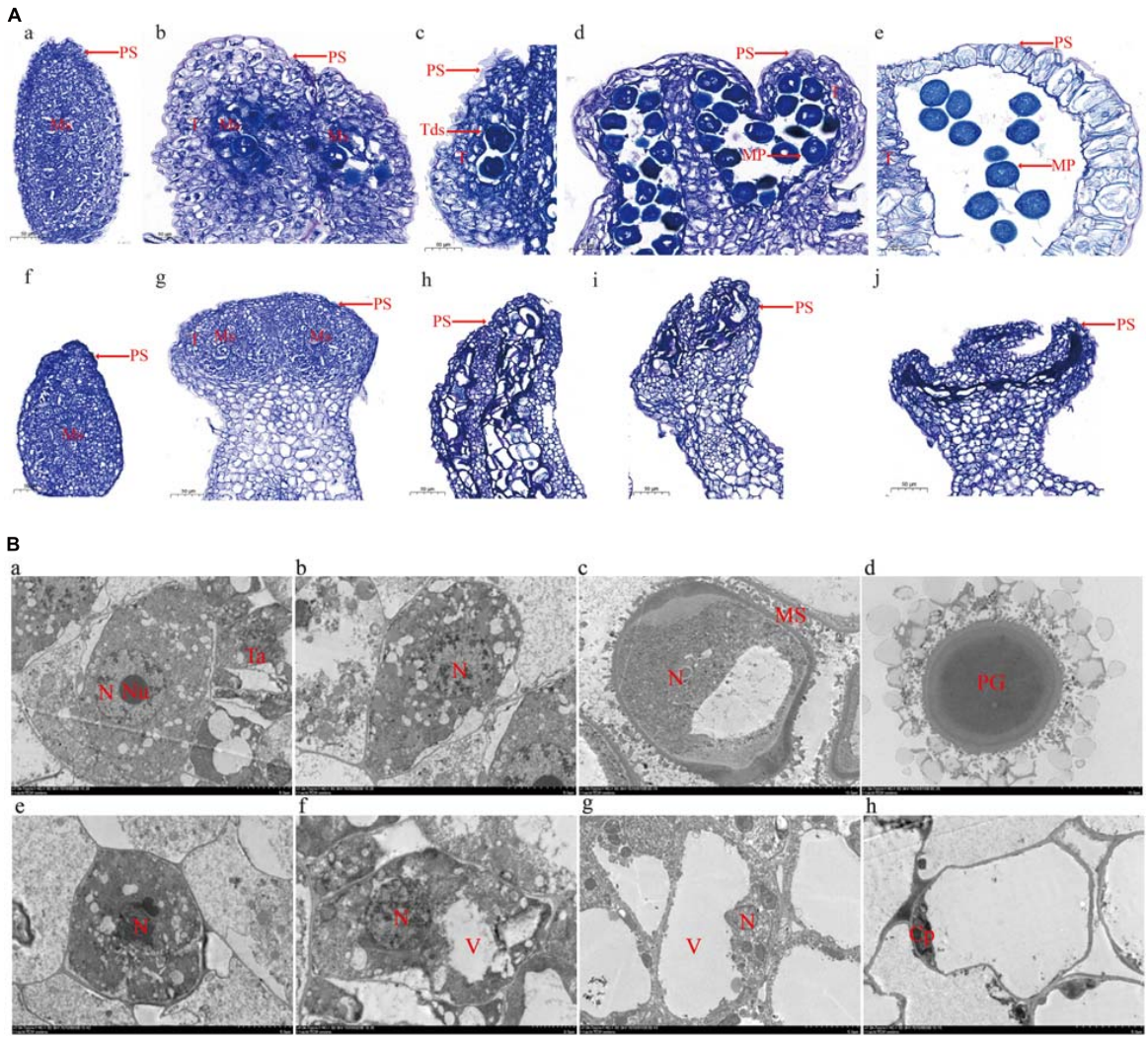

FIGURE 2 | Microscopy analysis of microspore development. **(A)** Optical microscopy images. Undifferentiated anther **(a)**, microsporocyte stage **(b)**, tetrad stage **(c)**, microspore stage **(d)**, and mature pollen stage **(e)** in male-fertile anthers. Undifferentiated anther **(f)**, microsporocyte stage **(g)**, microsporocyte abnormal division stage **(h)**, microsporocyte disaggregated stage **(i)**, and withered powder chamber **(j)** in male-sterile anthers. *PS*, pollen sac; *T*, tapetum; *Tds*, tetrads; *Ms*, microsporocyte; *MP*, mature pollen. *Bar* = 50 μm. **(B)** Transmission electron microscopy images. Sporogenous cells **(a)**, microsporocyte **(b)**, immature pollen **(c)**, and mature pollen **(d)** in male-fertile anthers. Sporogenous cells **(e)**, microsporocyte **(f)**, abnormal microsporocyte **(g)**, and hollow and wrinkled pollen **(h)** in male-sterile anthers. *N*, nucleus; *Nu*, nucleolus; *Ta*, tapetum; *MS*, microspore; *PG*, pollen grain; *V*, vacuole; *Cp*, cytoplasm. *Bar* = 50 μm (each scale = 5 μm).

in the flowers than in the flower buds of the G17AB male-sterile plants, whereas the opposite expression pattern was detected in "Zhongliu" plants. There were some inconsistencies between the candidate gene expression patterns and male sterility, which were initially excluded. The *Cla007521* gene, which is supposedly a suppressor gene, was more highly expressed in flowers than in flower buds. The *Cla006625*, *Cla006738*, and *Cla009408* expression levels were significantly higher in the flowers than in the flower buds of "Zhongliu" plants ($P < 0.05$). The expressions of the *Cla006625* and *Cla006738* genes were almost undetectable in the G17AB male-sterile line. These results indicated that the expression levels of these genes influence male sterility, implying that the genes may be responsible for male sterility in watermelon.

Alignments with sequences in the NCBI database indicated that *Cla007521* encodes a homocysteine *S*-methyltransferase, *Cla006738* encodes the MYB-related transcription factor LHY, *Cla009408* encodes a serine/threonine protein kinase, and *Cla006625* encodes a pollen-specific LRR extensin-like protein. The BLAST analysis suggested that *Cla006625* is the candidate gene most related to pollen. Consequently, it was preliminarily designated as a major gene controlling male sterility. The full-length *Cla006625* complementary DNA (cDNA) sequence consists of 2,076 bp. The SWISS-MODEL[4] results indicated that the tertiary structure of the protein encoded by *Cla006625* is similar to that of pollen-specific LRR extensin-like protein 1.

[4]https://swissmodel.expasy.org/interactive

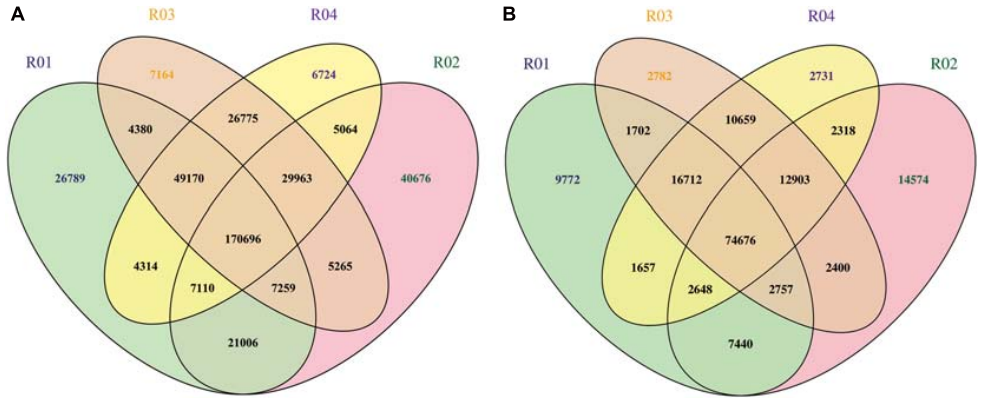

FIGURE 3 | (A) Venn diagram of the SNPs among samples. **(B)** Venn diagram of the small indels among samples. *R01* represents the male parent sample; *R02* represents the female parent sample; *R03* represents the F_2 generation male-fertile sample; *R04* represents the F_2 generation male-sterile sample.

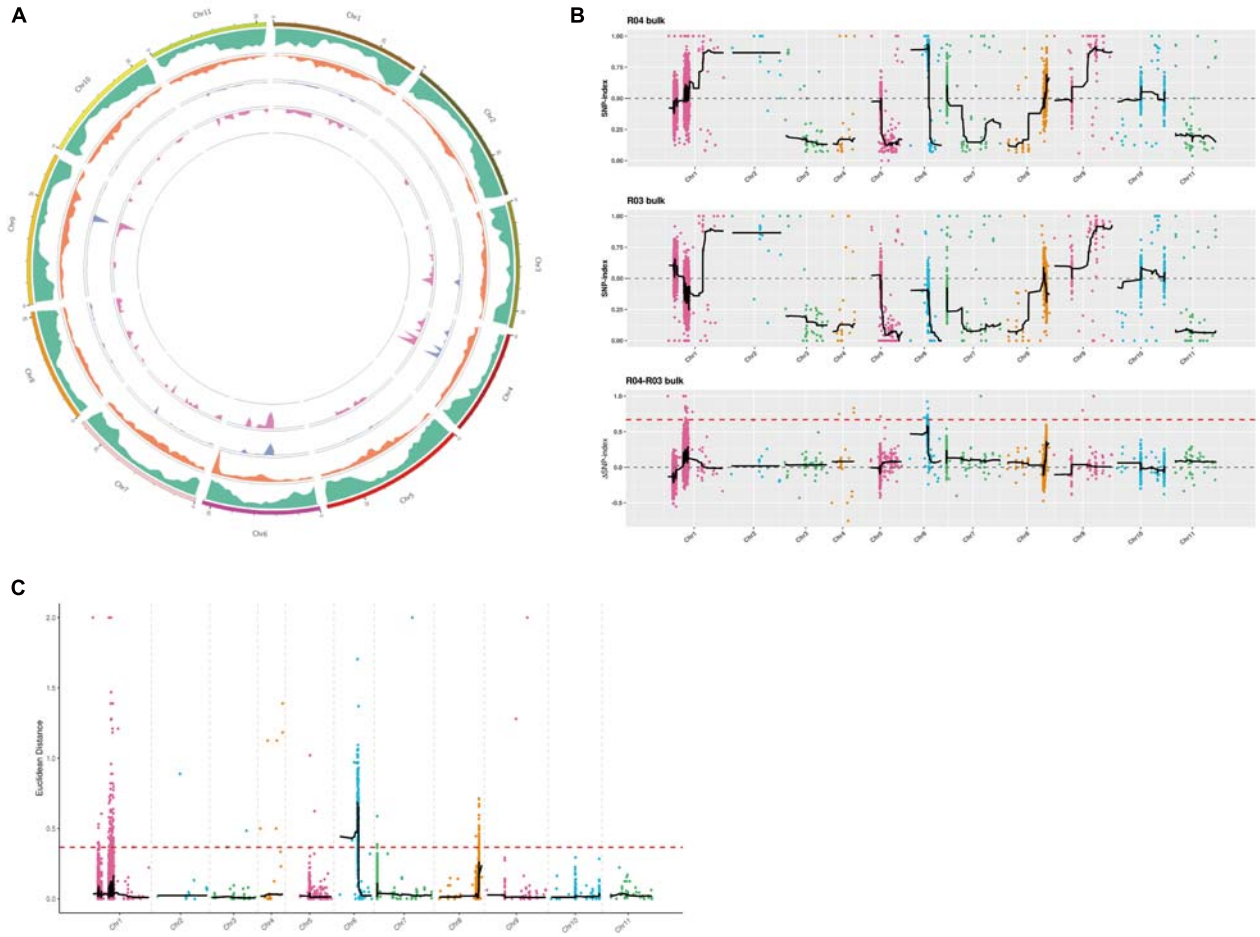

FIGURE 4 | (A) Chromosomal distribution of the candidate regions determined using Circos software. From the *outside* to the *inside*: *first circle*: chromosomal coordinates; *second circle*: gene distribution; *third circle*: single nucleotide polymorphism (SNP) density distribution; *fourth circle*: Euclidean distance (ED) value distribution; *fifth circle*: ΔSNP index value distribution. **(B)** Layout of the ΔSNP index value distribution. The *x*-axis presents the watermelon chromosome numbers. The *colored dots* represent the calculated SNP index (or ΔSNP index) values. The *black lines* represent the fitted SNP index (or ΔSNP index) values. The *top figure* presents the SNP index value distribution in the male-sterile sample mixed pool. The *middle figure* presents the SNP index value distribution in the male-fertile sample mixed pool. The *bottom figure* presents the ΔSNP index value distribution, with the *red line* indicating the 99th percentile threshold. **(C)** ED value distribution. The threshold is indicated by a *red dashed line*. The *x*-axis presents the watermelon chromosome numbers.

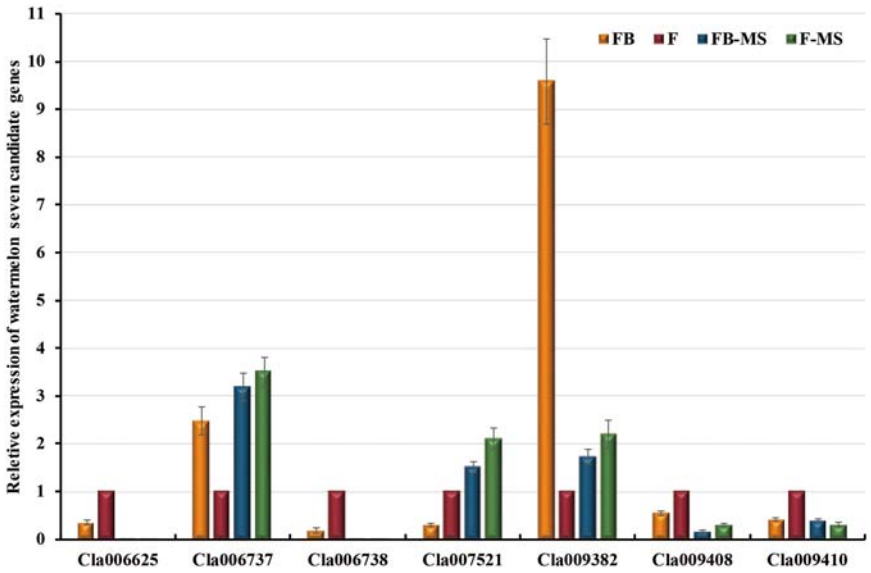

FIGURE 5 | Relative expression levels of seven candidate watermelon genes. The presented data are the average values of six independent measurements. *The error bars* represent the standard deviation of the mean. *FB*, flower bud; *F*, flower; *FB-MS*, flower bud of male-sterile plants; *F-MS*, flower of male-sterile plants.

The sequence identities between *Cla006625* and *A. thaliana AtPEX1*, *AtPEX2*, *AtPEX3*, and *AtPEX4* were revealed to be 49.58, 56.31, 58.51, and 57.12%, respectively (**Figure 6A**). Thus, we speculated that *Cla006625* is a *PEX* homolog encoding pollen-specific LRR extensin-like protein 1 in watermelon. Accordingly, the gene was named *ClaPEX1* according to established gene-naming rules. The constructed phylogenetic tree clarified the molecular evolutionary relationship between *ClaPEX1* and its homologs (**Figure 6B**). The alignment of multiple amino acid sequences suggested that *ClaPEX1* is highly similar to pollen-specific *LRX* (*PEX*) genes in *Cucumis melo* (80.03% similarity; accession number: XP_008458675.1) and *Cucumis sativus* (76.37% similarity; accession number: XP_011656352.1). Additionally, *ClaPEX1* includes a pollen-specific LRR sequence, and the maximum homology was detected within this region, confirming that this gene encodes a pollen-specific LRR extensin-like protein.

To identify the mutation site in *Cla006625*, the SNPs in the gene were detected by sequencing the DNA extracted from the samples in the F_2 population. Sixteen SNPs were identified in the *Cla006625* promoter and coding region in male-sterile F_2 plants, of which nine were non-synonymous SNPs (**Table 2**). Multiple non-synonymous mutations to the gene likely influenced the watermelon traits.

Silencing of *ClaPEX1* in Watermelon *via* RNAi

To functionally characterize *ClaPEX1*, its cDNA sequence was amplified by PCR and integrated into the RNAi vector. The resulting recombinant plasmid was used to generate transgenic plants through *A. tumefaciens*-mediated transformation. To prove the universal utility of *ClaPEX1* RNAi, the seeds of six inbred diploid "Kexi" lines, which differ from the G17AB and "Zhongliu" lines, were used for adventitious shoot induction. Sixty transgenic plants were obtained and screened to verify that they were positive clones. After another 3 weeks, the regenerated shoots were transferred to the rooting medium (**Figure 7A**). Finally, the rooted shoots were grown in plastic cups containing vermiculite, ultimately resulting in 35 individual kanamycin-resistant plants after acclimation. After another 1 month, the transgenic plants were transferred to a greenhouse for further growth (**Figure 7B**). An examination 1 month later indicated that the flowers of the transgenic plants were blooming, and both the female and male flowers were smaller than those of "Kexi" plants (**Figure 7C**). Furthermore, very few fruits were produced by the transgenic plants following self-pollination. The fruits of T_4 *ClaPEX1* RNAi watermelon plants exhibited a markedly inhibited seed set and were much smaller than the fruits of "Kexi" plants (**Figures 7D,E**).

DISCUSSION

Male sterility is a widespread phenomenon in higher plants. For crops with significant heterosis, male-sterile lines are important for generating hybrids. Therefore, there has been considerable interest in male sterility among breeders. Male-sterile germplasm resources for varieties with desirable characteristics are especially important. Genic male sterility has been exploited for the efficient production of F_1 hybrid seeds because it can decrease production costs and enhance seed quality. Thus, GMS will likely continue to be applied for the production of agriculturally valuable seeds, with far-reaching implications for large-scale hybrid seed production. Moreover, GMS plants are useful experimental materials for investigating pollen and flower development,

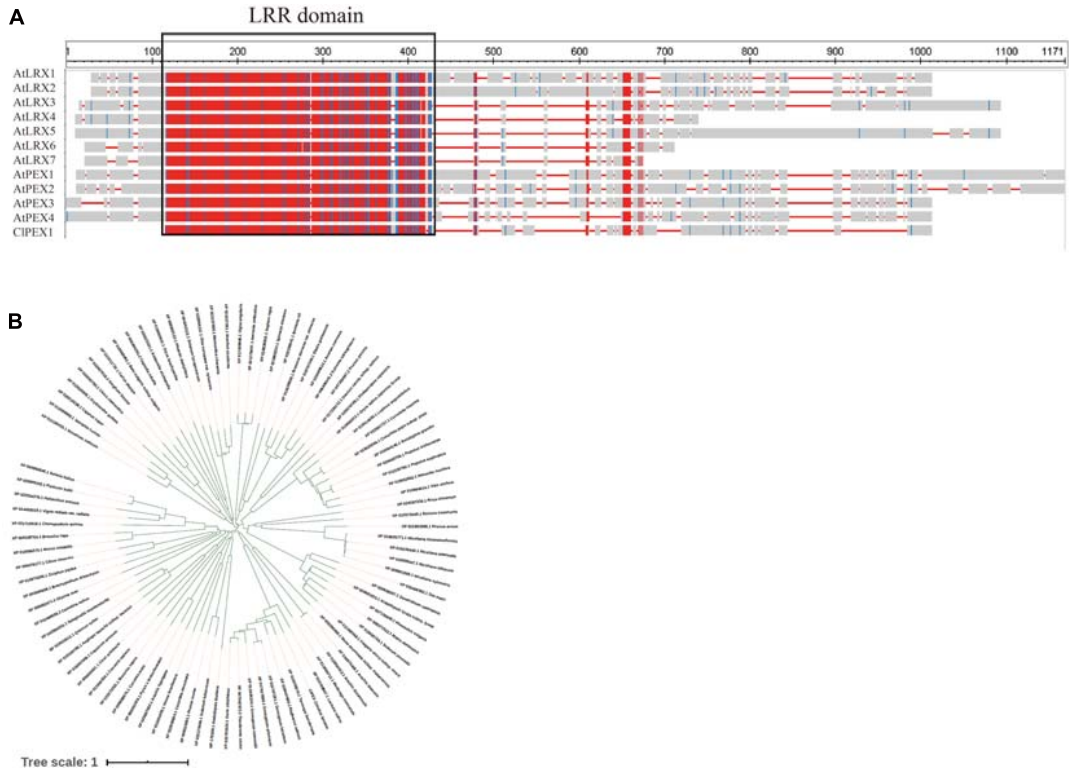

FIGURE 6 | Characterization of ClaPEX1 and its predicted product. **(A)** BLAST analysis of the pollen-specific leucine-rich repeat extensin-like protein 3 sequences in various organisms. The GenBank accession numbers of *Arabidopsis thaliana* genes are as follows: AtLRX1 (AY026364), AtLRX2 (AAF70841), AtLRX3 (CAB40769), AtLRX4 (BAB01951), AtLRX5 (CAB37452), AtLRX6 (BAB01255), AtLRX7 (NP_197937), AtPEX1 (BAB01698), AtPEX2 (AAD43152), AtPEX3 (AAD41978), and AtPEX4 (CAA19879). **(B)** Phylogenetic tree based on pollen-specific leucine-rich repeat extensin-like protein 3 sequences in different organisms. The GenBank accession numbers are provided. The sequences are in **Supplementary Material**.

especially for watermelon, which currently has relatively few GMS materials. The male sterility of the watermelon mutant G17AB is controlled by a recessive nuclear gene. This line is an excellent resource for constructing a biotechnology-based male-sterile system. However, the genes responsible for male sterility have not been cloned and the genetic mechanism underlying male sterility remains unknown. In this study, we characterized the spontaneous GMS mutant G17AB and identified a candidate gene mediating sterility.

TABLE 2 | Chromosomal positions and the codons of 16 SNPs.

Chr	Pos	Effect	Codon_change
Chr6	2,366,479	Non-synonymous coding	aTc/aGc
Chr6	2,366,489	Synonymous coding	ctA/ctG
Chr6	2,366,498	Synonymous coding	tcT/tcA
Chr6	2,366,504	Synonymous coding	gaT/gaC
Chr6	2,366,529	Non-synonymous coding	Ggt/Agt
Chr6	2,366,539	Non-synonymous coding	gGa/gAa
Chr6	2,366,558	Synonymous coding	gaG/gaA
Chr6	2,366,614	Non-synonymous coding	aTc/aCc
Chr6	2,366,656	Non-synonymous coding	gAg/gGg
Chr6	2,366,669	Synonymous coding	gcC/gcT
Chr6	2,366,678	Synonymous coding	ttG/ttA
Chr6	2,366,686	Non-synonymous coding	aTc/aCc
Chr6	2,366,697	Non-synonymous coding	Ttc/Atc
Chr6	2,366,710	Non-synonymous coding	aAc/aCc
Chr6	2,366,725	Non-synonymous coding	aAt/aGt
Chr6	2,366,786	Synonymous coding	tcT/tcC

The genetic analysis conducted in this study revealed that a single recessive nuclear gene controls the male sterility of G17AB watermelon. Firstly, the F_1 generation plants obtained *via* hybridizations with normal male-fertile watermelon plants were all male-fertile, whereas the ratio of male-fertile plants to male-sterile plants in the F_2 population was 3:1, which was in accordance with Mendel's segregation and the results of an earlier study (Xia et al., 1988). In the flowering stage, the male-sterile petals and anthers were small and pollen was undetectable on the anther surface. In contrast, the flowers of male-fertile watermelon plants had large anthers and a substantial abundance of pollen grains on the anther surface (**Figure 1B**). However, there were no differences between the fruits of the male-fertile and male-sterile G17AB plants. More specifically, all fruits were round, moderately sized, and had red flesh. In earlier investigations on cucumber, the four main types of male sterility were associated with undesirable traits (e.g., missing corollas, malformed ovaries, and unopened female flowers) (Grimbly, 1980; Zhang et al., 1994). Secondly, cytological examinations confirmed the presence of normal pollen sacs in fertile flowers, in contrast to the irregular pollen sacs in male-sterile flowers (**Figure 2A**). In a previous study, a rice

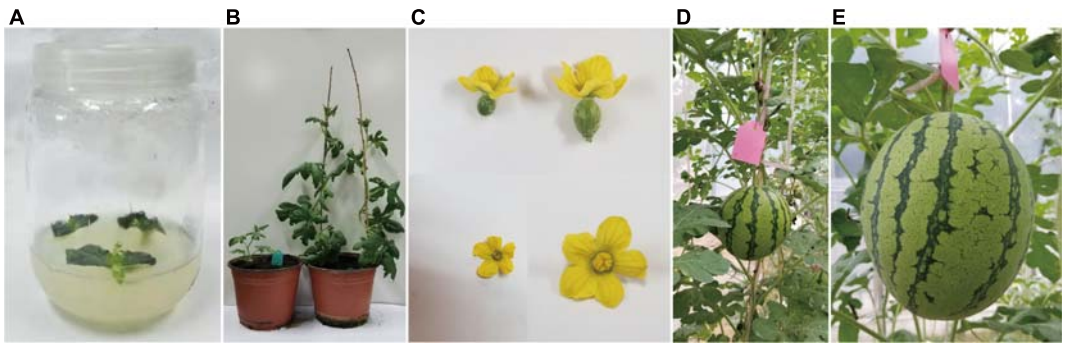

FIGURE 7 | Characteristics of the transgenic watermelon plants at different growth stages. **(A)** Bud regeneration from cotyledons after 3 weeks. **(B)** Enlarged adventitious shoots, which were transferred to plastic cups containing vermiculite. The plastic cup on the *left* contains transformed plants, whereas the plastic cup on the *right* consists of control plants. **(C)** Elongated plantlets. Female and male flowers of transgenic plants are presented on the *left*, whereas female and male flowers of control plants are presented on the *right*. **(D)** Representative fruit from a T_4 ClaPEX1 RNAi watermelon plant. **(E)** Representative fruit from a control "Kexi" plant.

male-sterile mutant (*OsMS-L*) was obtained following the ^{60}Co γ-irradiation of an M_4 population (Liu et al., 2005). Subsequent analysis of the tissue sections revealed the retarded tapetum development in the microspore stage of the male-sterile mutant. The tapetal cells expanded and the microspores degenerated. The tapetum degeneration retardation (*tdr*) rice (*O. sativa*) male-sterile mutant reportedly has a degenerated tapetum and middle layer as well as collapsed microspores (Li et al., 2006). In the current study, many cytoplasmic organelles were detected in fertile anthers during a transmission electron microscopy analysis (**Figure 2B**, part a). Additionally, as the microsporocyte grew, the number of vacuoles in the cytoplasm increased rapidly (**Figure 2B**, parts f and g). Finally, the vacuoles disappeared and the microsporocyte contracted into clusters and gradually disintegrated (**Figure 2B**, part h). These findings are consistent with the results of previous research. The anther abortion in the G17AB watermelon plants occurs during the meiosis of the pollen mother cell. An earlier investigation proved that the anther abortion of dicotyledonous plants commonly occurs from the sporogenesis period to the tetrad period (Liu et al., 2002).

Whole-genome resequencing and gene expression analyses identified *Cla006738*, *Cla009408*, *Cla007521*, and *Cla006625* as candidate genes, but the predicted functions of *Cla006738*, *Cla009408*, and *Cla007521* homologs were not associated with male sterility. Thus, of these genes, *Cla006625* is most likely the major gene contributing to male sterility. Because of the homology between the *Cla006625* sequence and the sequence encoding pollen-specific LRR extensin-like protein 1, *Cla006625* was renamed *ClaPEX1*. The LRR extensins (LRXs) are chimeric proteins that contain LRR and extensin domains (Baumberger et al., 2003). The full-length *ClaPEX1* cDNA is 2,076 bp long. On the basis of an alignment of multiple amino acid sequences, ClaPEX1 is most homologous to *C. melo* and *C. sativus* pollen-specific LRXs (PEXs). The sequence identities between *ClaPEX1* and the *A. thaliana* genes *AtPEX1*, *AtPEX2*, *AtPEX3*, and *AtPEX4* are 49.58, 56.31, 58.51, and 57.12%, respectively (**Figure 6A**).

The LRX-encoding genes can be divided into two groups based on their expression patterns. The genes in the first group are expressed in vegetative tissues, whereas the genes belonging to the second group are specifically expressed in pollen grains. For example, *TOML-4* in tomato (*Solanum lycopersicum*) and *LRX1–7* in *A. thaliana* are expressed in vegetative tissues (Zhou et al., 1992). In contrast, the gene encoding pollen extensin-like1 (*Pex1*) in maize and *LRX8–11* in *A. thaliana* are expressed exclusively in pollen grains (Rubinstein et al., 1995b; Baumberger et al., 2001). Thus, *ClaPEX1* likely belongs to the second group of LRX-encoding genes. Notably, *ClaPEX1* was substantially more highly expressed in the pollen of male-fertile G17AB plants than in the pollen of male-sterile G17AB plants. The *LRX8–11* genes in *A. thaliana* are reportedly expressed in mature pollen grains and possibly in germinating pollen grains, similar to the *ZmPEX1*, *ZmPEX2*, and *LePEX* genes (Rubinstein et al., 1995a,b; Stratford et al., 2001). The recently determined gene expression profiles of *A. thaliana LRX8–11* indicated that these genes are highly expressed in pollen tubes (Sede et al., 2018). In the current study, the T_4 *ClaPEX1* RNAi watermelon fruits exhibited a markedly inhibited seed set and were much smaller than the fruits of the male-fertile watermelon plants (**Figures 7D,E**). In *A. thaliana*, the expression patterns and functions are consistent among *LRX8–11* in mature pollen grains and pollen tubes. Phenotypic analyses of mutants in which one of these genes is mutated confirmed that pollen germination and pollen tube growth are severely affected by the mutations, which significantly decrease the seed setting rate and the mutant allele transmission efficiency (Wang et al., 2018). Another study indicated that the main characteristics of an *O. sativa* LRR receptor-like protein kinase (RLK) single mutant are an increased number of microsporocytes and a lack of middle layers and tapetal cells (Yang et al., 2016). Very few pollen tubes make it through the papillar apoplast into the ovary, ultimately leading to male sterility and an inhibited seed set (Fabrice et al., 2018). Hence, *ClaPEX1* was identified as the most likely major gene causing male sterility in G17AB watermelon plants.

The identification and characterization of GMS genes has deepened our understanding of the molecular basis of anther and pollen development. This has enabled the development and efficient use of many biotechnology-based male-sterile systems for crop hybrid breeding. Next-generation GMS hybrid biotechnology will be useful for sorting GMS and maintainer

crop seeds, and SPT will determine whether it can be successfully applied (Wu et al., 2016). In future studies, an SPT maintainer line will be developed *via* the transformation of plants with the *ClaPEX1* gene. The potential utility of the three other candidate genes identified in this study (*Cla007521*, *Cla006738*, and *Cla009408*) will be assessed in future investigations. The successful cultivation of a watermelon SPT maintainer line will improve the production of hybrid watermelon seeds by exploiting a homozygous male-sterile line. We generated preliminary evidence that *ClaPEX1* may be useful for generating an SPT maintainer line and for hybrid seed production.

DATA AVAILABILITY STATEMENT

The original contributions presented in the study are publicly available. This data can be found here: NCBI, BioProject accession PRJNA687916 (https://www.ncbi.nlm.nih.gov/bioproject/PRJNA687916).

AUTHOR CONTRIBUTIONS

WD and DFW jointly designed all experiments and conducted almost all of the molecular analyses. WD wrote the manuscript. WD and CY grew the plant materials and recorded the morphological characteristics. WD and DWW completed the whole-genome resequencing analysis. All authors contributed to the article and approved the submitted version.

FUNDING

This work was supported by funding from the National Natural Science Foundation of China (31801882), the National Postdoctoral Program for Innovative Talents (BX201700205), and Henan Province Key Science and Technology Projects (212102110044 and 192102310024).

ACKNOWLEDGMENTS

We would like to thank Liwen Bianji, Edanz Editing China (www.liwenbianji.cn/ac) for editing the English text of a draft of this manuscript.

SUPPLEMENTARY MATERIAL

The Supplementary Material for this article can be found online at: https://www.frontiersin.org/articles/10.3389/fpls.2021.639431/full#supplementary-material

REFERENCES

Albertsen, M. C., Fox, T. W., Hershey, H. P., Huffman, G. A., Trimnell, M., and Wu, Y. (2006). *Nucleotide Sequences Mediating Plant Male Fertility and Method of Using Same*.

Baumberger, N., Doesseger, B., Guyot, R., Diet, A., Parsons, R. L., Clark, M. A., et al. (2003). Whole genome comparison of leucine-rich repeat extensins in Arabidopsis and rice. A conserved family of cell wall proteins form a vegetative and a reproductive clade. *Plant Physiol.* 131, 1313–1326. doi: 10.1104/pp.102.014928

Baumberger, N., Ringli, C., and Keller, B. (2001). The chimeric leucine-rich repeat/extensin cell wall protein LRX1 is required for root hair morphogenesis in Arabidopsis thaliana. *Genes. Dev.* 15, 1128–1139. doi: 10.1101/gad.200201

Bohn, G. W., and Principe, J. A. (1964). A second male-sterility gene in the muskmelon. *J. Hered.* 55, 211–215. doi: 10.1093/oxfordjournals.jhered.a107335

Bohn, G. W., and Whitaker, T. W. (1949). A gene for male sterility in the muskmelon (*Cucumis melo* L.) *Proc. Am. Soc. Hort. Sci.* 53, 309–314.

Chang, Z., Chen, Z., Wang, N., Xie, G., Lu, J., Yan, W., et al. (2016). Construction of a male sterility system for hybrid rice breeding and seed production using a nuclear male sterility gene. *Proc. Natl. Acad. Sci. U.S.A.* 113, 14145–14150. doi: 10.1073/pnas.1613792113

Ding, J., Lu, Q., Ouyang, Y., Mao, H., Zhang, P., Yao, J., et al. (2012). A long noncoding RNA regulates photoperiod-sensitive male sterility, an essential component of hybrid rice. *Proc. Natl. Acad. Sci. U.S.A.* 109, 2654–2659. doi: 10.1073/pnas.1121374109

Dong, W., Wu, D., Li, G., Wu, D., and Wang, Z. (2018). Next-generation sequencing from bulked segregant analysis identifies a dwarfism gene in watermelon. *Sci. Rep*. 8:2908. doi: 10.1038/s41598-018-21293-1

Dyutin, K. E., and Sokolov, S. D. (1990). Spontaneous mutant of watermelon with male sterility. *Cytol. Genet*. 24, 56–57.

Fekih, R., Takagi, H., Tamiru, M., Abe, A., Natsume, S., Yaegashi, H., et al. (2013). MutMap+: genetic mapping and mutant identification without crossing in rice. *PLoS One* 8:e68529. doi: 10.1371/journal.pone.0068529

Fabrice, T. N., Vogler, H., Draeger, C., Munglani, G., Gupta, S., Herger, A. G., et al. (2018). LRX proteins play a crucial role in pollen grain and pollen tube cell wall development. *Plant Physiol.* 176, 1981–1992. doi: 10.1104/pp.17.01374

Felsenstein, J. (1992). Estimating effective population size from samples of sequences: a bootstrap Monte Carlo integration method. *Genet. Res.* 60, 209–220. doi: 10.1017/S0016672300 030962

Fox, T., DeBruin, J., Haug Collet, K., Trimnell, M., Clapp, J., Leonard, A., et al. (2017). A single point mutation in Ms44 results in dominant male sterility and improves nitrogen use efficiency in maize. *Plant Biotechnol. J.* 15, 942–952. doi: 10.1111/pbi.12689

Grimbly, P. E. (1980). *An Apetalous Male Sterile Mutant in Cucumber*. Cucurbit Genetics Cooperative Report 3:9 (article 5) 1980. Littlehampton: Glasshouse Crops Research Institute.

Gusmini, G., and Wehner, T. (2005). Foundations of yield improvement in watermelon. *Crop Sci*. 45, 141–146. doi: 10.2135/cropsci2005.0810

Han, Y., Zhao, F., Gao, S., Wang, X., Wei, A., Chen, Z., et al. (2018). Fine mapping of a male sterility gene ms-3 in a novel cucumber (*Cucumis sativus* L.) mutant. *Theor. Appl. Genet*. 131, 449–460. doi: 10.1007/s00122-017-3013-2

Hill, J. T., Demarest, B. L., Bisgrove, B. W., Gorsi, B., Su, Y., and Yost, H. J. (2013). MMAPPR: mutation mapping analysis pipeline for pooled RNA-seq. *Genome Res*. 23, 687–697. doi: 10.1101/gr.146936.112

Huang, H., Zhang, X., Wei, Z., Li, Q., and Li, X. (1998). Inheritance of male-sterility and dwarfism in watermelon [*Citrullus lanatus* (*Thunb.*) *Matsum.* and *Nakai*]. *Sci. Hortic*. 74, 175–181. doi: 10.1016/S0304-4238(97)00102-7

Khush, G. S. (2001). Green revolution: the way forward. *Nat. Rev. Genet.* 2, 815–822. doi: 10.1038/35093585

Kumar, S., Tamura, K., Jakobsen, I. B., and Nei, M. (2001). MEGA2: molecular evolutionary genetics analysis software. *Bioinformatics* 17, 1244–1245. doi: 10.1093/bioinformatics/17.12.1244

Lecouviour, M., Pitrat, M., and Risser, G. (1990). A fifth gene for male sterility in *Cucumis melo*. *Rep. Cucurbit Genet. Coop.* 13, 34–35.

Li, N., Zhang, D. S., Liu, H. S., Yin, C. S., Li, X., Liang, W., et al. (2006). The rice tapetum degeneration retardation gene is required for tapetum degradation and anther development. *Plant Cell* 18, 2999–3014. doi: 10.1105/tpc.106.044107

Li, S., Li, M., Li, Z., Zhu, Y., Ding, H., Fan, X., et al. (2019) Effects of the silencing of CmMET1 by RNA interference in chrysanthemum (Chrysanthemum morifolium). *Hortic Res.* 6:109. doi: 10.1038/s41438-019-0193-8

Liu, H., Chu, H., Li, H., Wang, H., Wei, J., Li, N., et al. (2005). Genetic analysis and mapping of rice (*Oryza sativa* L.) male-sterile (OsMS-L) mutant. *Chin. Sci. Bull.* 2, 122–125. doi: 10.1360/982004-423

Liu, H., Hou, X., and Zhang, Y. (2004). Marker linked to a male fertile gene in watermelon G17AB line. *J. Fruit Sci*. 21, 491–493.

Liu, H., Zhang, Y., and Ma, D. (2002). Study on the development of the male sterile anther in watermelon G 17 AB line. *Acta Agric. Boreali Sin*. 17, 88–92.

Liu, L., Gu, Q., Ijaz, R., Zhang, J., and Ye, Z. (2016). Generation of transgenic watermelon resistance to Cucumber mosaicvirus facilitated by an effective *Agrobacterium*-mediatedtransformation method. *Sci. Hortic*. 205, 32–38. doi: 10.1016/j.scienta.2016.04.013

McCreight, J. D., and Elmstrom, G. W. (1984). A third male sterile gene in muskmelon. *Hortic. Sci.* 19, 268–270.

Murray, M. G., and Thompson, W. F. (1980). Rapid isolation of high molecular weight plant DNA. *Nucleic Acids Res*. 8:4321. doi: 10.1093/nar/8.19.4321

Ni, F., Qi, J., Hao, Q., Lyu, B., Luo, M., Yan, W., et al. (2017). Wheat Ms2 encodes for an orphan protein that confers male sterility in grass species. *Nat. Commun*. 8:15121. doi: 10.1038/ncomms15121

O'Brien, T. P., Feder, N., and Mccully, M. E. (1964). Polychromatic staining of plant cell walls by toluidine blue O. *Protoplasma* 59, 368–373. doi: 10.1007/BF01248568

Park, S. O., Crosby, K. M., Huang, R. F., and Mirkov, T. E. (2004). Identification and confirmation of RAPD and SCAR markers linked to the *ms-3* gene controlling male sterility in melon (*Cucumis melo* L.). *J. Am. Soc. Hortic. Sci.* 129, 819–825. doi: 10.1007/s10658-004-0814-3

Pitrat, M. (2002). Gene list for melon. *Rep. Cucurbit Genet. Coop.* 25, 76–93.

Qi, Y., Liu, Q., Zhang, L., Mao, B., Yan, D., Jin, Q., et al. (2014). Fine mapping and candidate gene analysis of the novel thermo-sensitive genic male sterility tms9-1 gene in rice. *Theor. Appl. Genet*. 127, 1173–1182. doi: 10.1007/s00122-014-2289-8

Ray, D. T., and Sherman, J. D. (1988). Desynaptic chromosome behavior of the GMS mutant in watermelon. *J. Hered*. 79, 397–399. doi: 10.1093/oxfordjournals.jhered.a110537

Ren, Y., Guo, S., Zhang, J., He, H., Sun, H., Tian, S., et al. (2018). A tonoplast sugar transporter underlies a sugar accumulation QTL in watermelon. *Plant Physiol*. 176, 836–850. doi: 10.1104/pp.17.01290

Rhee, S., Seo, M., Jang, Y. J., Cho, S., and Lee, G. (2015). Transcriptome profiling of differentially expressed genes in floral buds and flowers of male sterile and fertile lines in watermelon. *BMC Genomics* 16:914. doi: 10.1186/s12864-015-2186-9

Rubinstein, A. L., Broadwater, A. H., Lowrey, K. B., and Bedinger, P. A. (1995a). PEX1, a pollen-specific gene with an extensin-like domain. *Proc. Natl. Acad. Sci. U.S.A*. 92, 3086–3090. doi: 10.1073/pnas.92.8.3086

Rubinstein, A. L., Marquez, J., Suarez Cervera, M., and Bedinger, P. A. (1995b). Extensin-like glycoproteins in the maize pollen tube wall. *Plant Cell* 7, 2211–2225. doi: 10.1105/tpc.7.12.2211

Saminathan, T., Nimmakayala, P., Manohar, S., Malkaram, S., Almeida, A., Cantrell, R., et al. (2015). Differential gene expression and alternative splicing between diploid and tetraploid watermelon. *J. Exp. Bot*. 66, 1369–1385. doi: 10.1093/jxb/eru486

Sede, A. R., Borassi, C., Wengier, D. L., Mecchia, M. A., Estevez, J. M., and Muschietti, J. P. (2018). Arabidopsis pollen extensins LRX are required for cell wall integrity during pollen tube growth. *FEBS Lett*. 592, 233–243. doi: 10.1002/1873-3468.12947

Shan, W., Ji, G., Zhang, J., Gong, G., Zhao, H., Xu, Y., et al. (2016). Cytomorphological observation on three kinds of sexual type sex differentiation in watermelon. *China Vegetables* 1, 49–54.

Sheng, Y., Wang, Y., Jiao, S., Jin, Y., Ji, P., and Luan, F. (2017). Mapping and preliminary analysis of ABORTED MICROSPORES (AMS) as the candidate gene underlying the male sterility (MS-5) mutant in melon (Cucumis melo L.). *Front. Plant Sci.* 8:902. doi: 10.3389/fpls.2017.00902

Sheng, Z., Tang, L., Shao, G., Xie, L., Jiao, G., Tang, S., et al. (2015). The rice thermo sensitive genic male sterility gene tms9: pollen abortion and gene isolation. *Euphytica* 203, 145-152. doi: 10.1007/s10681-014-1285-z

Shi, M. (1985). The discovery and preliminary studies of the photoperiod-sensitive recessive male sterile rice (*Oryza sativa* L. subsp. japonica). *Sci. Agric. Sin*. 2, 44–48.

Singh, S. P., Srivastava, R., and Kumar, J. (2015). Male sterility systems in wheat and opportunities for hybrid wheat development. *Acta Physiol. Plant*. 37:1713. doi: 10.1007/s11738-014-1713-7

Stratford, S., Barnes, W., Hohorst, D. L., Sagert, J. G., Cotter, R., Golubiewski, A., et al. (2001). A leucine-rich repeat region is conserved in pollen extensin-like (Pex) proteins in monocots and dicots. *Plant Mol. Biol*. 46, 43–56. doi: 10.1023/A:1010659425399

Timofejeva, L., Skibbe, D. S., Lee, S., Golubovskaya, I., Wang, R., Harper, L., et al. (2013). Cytological characterization and allelism testing of anther developmental mutants identified in a screen of maize male sterile lines. *G3* (*Bethesda*) 3, 231–249. doi: 10.1534/g3.112.004465

Walbot, V., and Egger, R. L. (2016). Pre-meiotic anther development: cell fate specification and differentiation. *Annu. Rev. Plant Biol*. 67, 365–395. doi: 10.1146/annurev-arplant-043015-111804

Wan, X., Wu, S., Li, Z., Dong, Z., An, X., Ma, B., et al. (2019). Maize genic male-sterility genes and their applications in hybrid breeding: progress and perspectives. *Mol. Plant* 12, 321–342. doi: 10.1016/j.molp.2019.01.014

Wang, X. X., Wang, K., Yin, G., Liu, X., Liu, M., Cao, N., et al. (2018). Pollen-expressed leucine-rich repeat extensins are essential for pollen germination and growth. *Plant Physiol*. 176, 1993–2006. doi: 10.1104/pp.17.01241

Watts, V. M. (1962). A marked male-sterile mutantin watermelon. *Proc. Am. Soc. Hort. Sci*. 81, 498–505.

Watts, V. M. (1967). Development of disease resistance and seed production in watermelon stocks carrying the MSG gene. *Proc. Am. Soc. Hort. Sci*. 91, 579–583.

Wu, Y., Fox, T. W., Trimnell, M. R., Wang, L., Xu, R. J., Cigan, A. M., et al. (2016). Development of a novel recessive genetic male sterility system for hybrid seed production in maize and other cross-pollinating crops. *Plant Biotechnol. J*. 14, 1046–1054. doi: 10.1111/pbi.12477

Xia, X., Liu, Y., and Wu, X. (1988). Selection of watermelon (*Citrullus vulgaris*) AB male-sterile line G17AB. *Acta Shenyang Agric. Univ*. 19, 9–13.

Yang, L., Qian, X., Chen, M., Fei, Q., Meyers, B. C., Liang, W., et al. (2016). Regulatory role of a receptor-like kinase in specifying anther cell identity. *Plant Physiol*. 171, 2085–2100. doi: 10.1104/pp.16.00016

Yu, T. A., Chiang, C. H., Wu, H. W., Li, C., Yang, C., Chen, J., et al. (2011). Generation of transgenic watermelon resistant to Zucchini yellow mosaicvirus and Papaya ringspot virus type W. *Plant Cell Rep*. 30, 359–371. doi: 10.1007/s00299-010-0951-4

Yuan, L. (2004). Hybrid rice technology for food security in the world. *Crop Res*. 18, 185–186.

Zhang, Q., Gabert, A. C., and Baggett, J. R. (1994). Characterizing a cucumber pollen sterile mutant: inheritance, allelism, and response to chemical and environmental factors. *J. Am. Soc. Hortic. Sci*. 119, 804–807. doi: 10.21273/jashs.119.4.804

Zhang, X. P., and Wang, M. (1990). A genetic male-sterile (ms) watermelon from China. *Cucurbit Genet. Coop. Rep*. 13:45.

Zhang, Y., Cheng, Z., Ma, J., Xian, F., and Zhang, X. (2012). Characteristics of a novel male–female sterile watermelon (*Citrullus lanatus*) mutant. *Sci. Hortic*. 140, 107–114. doi: 10.1016/j.scienta.2012.03.020

Zhou, J., Rumeau, D., and Showalter, A. M. (1992). Isolation and characterization of two wound-regulated tomato extensin genes. *Plant Mol. Biol.* 20, 5–17. doi: 10.1007/BF00029144

Zhou, L. Z., Juranic, M., and Dresselhaus, T. (2017). Germline development and fertilization mechanisms in maize. *Mol. Plant* 10, 389–401. doi: 10.1016/j.molp.2017.01.012

Conflict of Interest: The authors declare that the research was conducted in the absence of any commercial or financial relationships that could be construed as a potential conflict of interest.

Publisher's Note: All claims expressed in this article are solely those of the authors and do not necessarily represent those of their affiliated organizations, or those of the publisher, the editors and the reviewers. Any product that may be evaluated in this article, or claim that may be made by its manufacturer, is not guaranteed or endorsed by the publisher.

frontiers in Plant Science

MINI REVIEW
published: 03 September 2021
doi: 10.3389/fpls.2021.703864

The Toughest Material in the Plant Kingdom: An Update on Sporopollenin

Etienne Grienenberger[1†] *and Teagen D. Quilichini*[2*†]

[1] *Institut de biologie moléculaire des plantes, CNRS, Université de Strasbourg, Strasbourg, France,* [2] *Aquatic and Crop Resource Development Research Centre, National Research Council Canada, Saskatoon, SK, Canada*

The extreme chemical and physical recalcitrance of sporopollenin deems this biopolymer among the most resilient organic materials on Earth. As the primary material fortifying spore and pollen cell walls, sporopollenin is touted as a critical innovation in the progression of plant life to a terrestrial setting. Although crucial for its protective role in plant reproduction, the inert nature of sporopollenin has challenged efforts to determine its composition for decades. Revised structural, chemical, and genetic experimentation efforts have produced dramatic advances in elucidating the molecular structure of this biopolymer and the mechanisms of its synthesis. Bypassing many of the challenges with material fragmentation and solubilization, insights from functional characterizations of sporopollenin biogenesis *in planta*, and *in vitro,* through a gene-targeted approach suggest a backbone of polyhydroxylated polyketide-based subunits and remarkable conservation of biochemical pathways for sporopollenin biosynthesis across the plant kingdom. Recent optimization of solid-state NMR and targeted degradation methods for sporopollenin analysis confirms polyhydroxylated α-pyrone subunits, as well as hydroxylated aliphatic units, and unique cross-linkage heterogeneity. We examine the cross-disciplinary efforts to solve the sporopollenin composition puzzle and illustrate a working model of sporopollenin's molecular structure and biosynthesis. Emerging controversies and remaining knowledge gaps are discussed, including the degree of aromaticity, cross-linkage profiles, and extent of chemical conservation of sporopollenin among land plants. The recent developments in sporopollenin research present diverse opportunities for harnessing the extraordinary properties of this abundant and stable biomaterial for sustainable microcapsule applications and synthetic material designs.

Keywords: sporopollenin, biopolymer, spore, pollen, exine cell wall, polyketide, α-pyrone, molecular structure

OPEN ACCESS

Edited by:
David Honys, Institute of Experimental Botany, Academy of Sciences of the Czech Republic, Czechia

Reviewed by:
Ravishankar Palanivelu, University of Arizona, United States
Gwyneth Ingram, Université de Lyon, France

***Correspondence:**
Teagen D. Quilichini
Teagen.Quilichini@nrc-cnrc.gc.ca

***ORCID**:
Etienne Grienenberger
orcid.org/0000-0002-0555-3208
Teagen D. Quilichini
orcid.org/0000-0003-3311-3776

Specialty section:
This article was submitted to Plant Development and EvoDevo, a section of the journal Frontiers in Plant Science

Received: *30 April 2021*
Accepted: *26 July 2021*
Published: *03 September 2021*

Citation:
Grienenberger E and Quilichini TD (2021) The Toughest Material in the Plant Kingdom: An Update on Sporopollenin. Front. Plant Sci. 12:703864. doi: 10.3389/fpls.2021.703864

INTRODUCTION

A seminal innovation in plant evolution was the fortification of mobile reproductive cells with sporopollenin. Amidst novel stresses, reinforcement of spore cell walls with a desiccation-resistant, durable exterior of sporopollenin likely provided an adaptive advantage to plant terrestrial reproduction. Lauded as the "diamond of the plant world," sporopollenin is an

organic material distinguished by its extraordinary stability and recalcitrance when challenged by mechanical, thermal, hydrostatic, non-oxidative chemical, and biological pressures (Kesseler and Harley, 2004; Barrier, 2008; Montgomery et al., 2016). The inert nature of sporopollenin is perhaps best highlighted by its chemical preservation in fossil spores an estimated 450 million years old, providing the earliest record of plant life on land (Brooks and Shaw, 1971; Brown and Lemmon, 2011). The ubiquitous appearance of sporopollenin in the outer shell of land plant spores and pollen grains, and strong evolutionary conservation of genes encoding key enzymes in the biosynthesis of sporopollenin among current land plants, support a critical function for this biopolymer in the conquest and proliferative success of plants on dry land (Wallace et al., 2011; Gómez et al., 2015; Quilichini et al., 2015; Shi et al., 2015).

The definition of sporopollenin as the organic residue remaining after acetolysis conveys the nebulous understanding of this biomacromolecule that has prevailed (Zetzsche and Vicari, 1931; Brown, 1960; Hemsley et al., 2009). This is in stark contrast to other major and more widely known biopolymers that fortify plant cell walls, including cutin, suberin, and lignin, for which chemical composition and linkage data are extensive (Mackenzie et al., 2015). Much of the uncertainty surrounding sporopollenin is due to the material's extreme inertness, preventing solubilization under harsh treatments and yielding partial, modified or degraded fragments of the native polymer for biochemical characterization (Hemsley et al., 2009; Li et al., 2019a). From early models of a carotenoid-based polymer (Brooks and Shaw, 1968), the tools available for elucidating sporopollenin's composition have grown rapidly, supporting substantial revision of molecular structure models. Circumventing challenges of sporopollenin solubilization and breakdown, genetic tools predominantly in model flowering plants have uncovered a core set of biosynthetic enzymes required for sporopollenin biosynthesis. Mounting evidence from non-model species supports strong conservation of a sporopollenin metabolic pathway across the plant kingdom. Mutant analyses, *in vitro* enzyme assays, labeling studies, and chemical breakdown analyses have facilitated informed inferences on sporopollenin's composition, supporting a polyhydroxylated aliphatic backbone of polyketides, an aromatic fraction, and extensive coupling of subunits through ester and ether cross-linkages (Quilichini et al., 2015). Until recently however, genetic studies could not fully explain models from biochemical analyses and vice versa.

A recent surge in the analytical characterization of sporopollenin has produced significant breakthroughs in the elucidation of molecular structure, complimenting and challenging prevailing theories. Aided by the development of treatment approaches for interrogating the biopolymer, and the large quantities of spores/pollen available from non-flowering species, mass spectrometry, solid-state NMR, and infrared spectroscopy techniques have uncovered novel structural and compositional data on sporopollenin. Among these discoveries, subunits of varying phobicity coupled by linkages with different solvent stabilities offer plausible explanations for the unique recalcitrance of sporopollenin. While a clearer picture for sporopollenin is emerging, new discrepancies between studies from disparate plant groups and methodologies raise questions about the extent of chemical conservation versus heterogeneity of sporopollenin among land plants. Here, we highlight the latest breakthroughs and emerging controversies in sporopollenin research, and the value of solving the elusive structure of sporopollenin for biotechnological advances.

CONSERVED METABOLIC PATHWAYS FOR SPOROPOLLENIN BIOSYNTHESIS

In flowering plants, sporopollenin is synthesized in tapetal cells that line the inner surface of the anther. Following its synthesis, sporopollenin constituents must exit the tapetum, traverse a fluid-filled locule, and assemble into the structured outer pollen wall or exine surrounding immature pollen grains (or microspores). Although questions surrounding the mechanisms of sporopollenin delivery from the sporophytic tapetum to the developing male gametophyte remain largely unanswered and beyond the scope of this article, evidence from several species supports a role for transport proteins, including ATP-binding cassette transporters and lipid transfer proteins, in sporopollenin export and/or shuttling from the tapetum (Liang et al., 2010; Quilichini et al., 2010, 2014; Choi et al., 2011; Huang et al., 2013; Niu et al., 2013; Qin et al., 2013; Zhu et al., 2013; Zhao et al., 2015; Chang et al., 2016, 2018; Zaidi et al., 2020). Similarly, little is known about the polymerization of sporopollenin, but recent studies implicate reactive oxygen species (ROS) and the environment of the locule in the biopolymer's assembly (see section entitled "Cross-linkages and Assembly of Sporopollenin" below).

In contrast to sporopollenin traffic and assembly, more is known about sporopollenin biosynthesis, with a suite of tapetum-expressed genes including *MALE STERILITY2* (*MS2;* Aarts et al., 1997; Chen et al., 2011), *CYTOCHROME P450 (CYP) 703A2* (Morant et al., 2007), *CYP704B1* (Dobritsa et al., 2009), *ACYL-COA SYNTHTASE5* (*ACOS5*; Souza et al., 2009), *POLYKETIDE SYNTHASE A/LESS ADHESIVE POLLEN6* (*PKSA/LAP6), PKSB/LAP5* (Dobritsa et al., 2010; Kim et al., 2010), and *TETRAKETIDE α-PYRONE REDUCTASE1/DIHYDROFLAVONOL 4-REDUCTASE-LIKE1* (*TKPR1/DRL1;* Tang et al., 2009; Grienenberger et al., 2010) encoding enzymes required for sporopollenin biosynthesis in *Arabidopsis thaliana* (Arabidopsis; **Table 1**). Loss-of-function mutations in these genes affect male fertility and disrupt exine deposition, supporting functions for the encoded enzymes in synthesizing crucial sporopollenin constituents. Enzyme assays characterizing recombinant MS2, CYP703A2, CYP704B1, ACOS5, PKSA/LAP6, PKSB/LAP5, and TKPR1/DRL1 support a major role for lipid metabolism in sporopollenin production. *In vitro*, medium- to long-chain fatty acids with varying degrees of hydroxylation are accepted by Arabidopsis ACOS5, forming activated fatty acyl-CoA esters that can be condensed with malonyl-CoAs to form tri- and tetraketide α-pyrones by PKSA/LAP6 and PKSB/LAP5 enzymes (reviewed by Quilichini et al., 2015). Subsequent ketone reduction by TKPR1/DRL1 produces polyhydroxylated aliphatic α-pyrones

TABLE 1 | Summary of genes and putative orthologs encoding core enzymes required for sporopollenin biosynthesis.

Arabidopsis gene full name (Gene name)	Putative ortholog	Species	Plant classification	Reference
CYTOCHROME P450 703A2 (CYP703A2)	*CYP703A3*	*Oryza sativa*	Angiosperm, monocot	Yang et al., 2014, 2018
CYTOCHROME P450 704B1 (CYP704B1)	*MS1 and MS2* *CYP704B2* *MS26/CYP704B*	*Brassica napus* *Oryza sativa* *Triticum aestivum*	Angiosperm, eudicot Angiosperm, monocot Angiosperm, monocot	Yi et al., 2010 Li et al., 2010 Singh et al., 2017
ACYL-COA SYNTHETASE (ACOS5)	*ACOS5* *ACOS5* *ACOS12* *ACOS6*	*Brassica napus* *Nicotiana tobacum* *Oryza sativa* *Physcomitrella patens*	Angiosperm, eudicot Angiosperm, eudicot Angiosperm, monocot Bryophyte	Qin et al., 2016 Wang et al., 2013 Li et al., 2016; Yang et al., 2017 Li et al., 2019b
POLYKETIDE SYNTHASE A (PKSA) / LESS ADHESIVE POLLEN 6 (LAP6)	*PKSA* *PKS1* *GASCL1* and *GASCL2* *PKS1* *LAP6/PKS1* *ASCL*	*Brassica napus* *Nicotiana tobacum* *Gerbera hybrida* *Hypericum perforatum* *Oryza sativa* *Physcomitrella patens*	Angiosperm, eudicot Angiosperm, eudicot Angiosperm, eudicot Angiosperm, eudicot Angiosperm, monocot Bryophyte	Qin et al., 2016 Wang et al., 2013 Kontturi et al., 2017 Jepson et al., 2014 Wang et al., 2013; Zou et al., 2017; Shi et al., 2018 Colpitts et al., 2011; Daku et al., 2016
POLYKETIDE SYNTHASE B (PKSB) / LESS ADHESIVE POLLEN 5 (LAP5)	*PKSB* *PKS2*	*Brassica napus* *Oryza sativa*	Angiosperm, eudicot Angiosperm, monocot	Qin et al., 2016 Zhu et al., 2017; Zou et al., 2018
TETRAKETIDE α-PYRONE REDUCTASE 1 (TKPR1) / DIHYDROFLAVONOL 4-REDUCTASE-LIKE 1 (DRL1)	*TKPR1*	*Oryza sativa*	Angiosperm, monocot	Wang et al., 2013; Xu et al. 2019
MALE STERILE 2 (MS2)	*DPW* *MS6021* *MS2*	*Oryza sativa* *Zea mays* *Physcomitrella patens*	Angiosperm, monocot Angiosperm, monocot Bryophyte	Shi et al., 2011; Wang et al., 2014 Tian et al., 2017 Wallace et al., 2015

that are proposed to form core monomers of sporopollenin (**Figure 1**, blue shading). In addition, the production of fatty alcohols by reduction of long-chain fatty acyl-ACP by MS2 (Doan et al., 2009; Chen et al., 2011) supports a hypothesized secondary pathway yielding aliphatic sporopollenin precursors that could link with the aliphatic α-pyrone units (**Figure 1**, green shading). Two CYTOCHROME P450 enzymes, CYP703A2 and CYP704B1, essential for exine synthesis, catalyze in-chain and ω-hydroxylation of medium- to long-chain fatty acids (Morant et al., 2007; Dobritsa et al., 2009). These P450 enzymes could act prior to ACOS5 to produce polyhydroxylated polyketides or in the production of hydroxylated aliphatic precursors with MS2 (**Figure 1**). These highly oxygenated potential sporopollenin precursors are conducive to covalent linkage within the polymer.

In addition to a critical role for lipid metabolism, there is support for the inclusion of hydroxylated aromatics in sporopollenin (Guilford et al., 1988; Ahlers et al., 1999; Domínguez et al., 1999; Ahlers et al., 2003; Li et al., 2019a; Lutzke et al., 2020; Xue et al., 2020), although no metabolic genes have been shown to be directly involved in the addition of aromatics to the biopolymer. One of the earliest studies to identify a putative genetic link between phenylpropanoid metabolism and sporopollenin production was in Arabidopsis, in which modulated expression of *FERULIC ACID 5-HYDROXYLASE* (*F5H*) and *CAFFEIC ACID O-METHYLTRANSFERASE* (*COMT*) to form unusual lignin with elevated 5-hydroxyguaiacyl units produced male sterility and abnormal exine (Weng et al., 2010). In rice, the Defective Pollen Wall 2 (DPW2) BAHD acyltransferase catalyzing the transfer of hydroxycinnamoyl moieties to ω-hydroxy fatty acids has been shown to be essential for pollen wall formation (Xu et al., 2017), although it is unclear whether the DPW2 product is directly incorporated into sporopollenin. Further, the expression of Arabidopsis phenylpropanoid pathway genes in the tapetum, alongside *ACOS5*, *PKSA/LAP6*, *PKSB/LAP5*, *TKPR*, *MS2*, *CYP703A2*, and *CYP704B1* supports their involvement in sporopollenin production (Xue et al., 2020).

Over the last decade, the expansion of studies characterizing sporopollenin synthesis-related genes and their encoded enzymes in a variety of species has revealed crucial and largely conserved functionalities in spore/pollen wall formation among land plants. In rice, orthologous genes for each Arabidopsis sporopollenin biosynthesis-related gene have been characterized, including *DPW* (Shi et al., 2011), *CYP703A3* (Yang et al., 2014, 2018), *CYP704B2* (Li et al., 2010), *ACOS12* (Li et al., 2016; Yang et al., 2017), *PKS1/LAP6* (Wang et al., 2013; Zou et al., 2017; Shi et al., 2018), *PKS2* (Zhu et al., 2017; Zou et al., 2018), and *TKPR1* (Xu et al., 2019), and

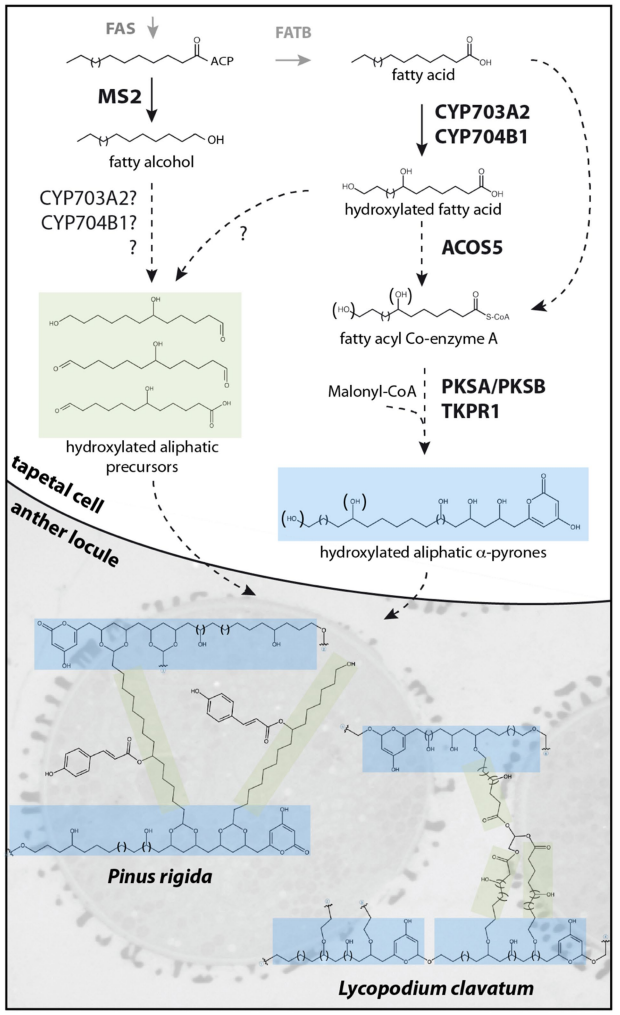

FIGURE 1 | Proposed sporopollenin metabolic pathway and simplified molecular structures of *Pinus rigida* and *Lycopodium clavatum* sporopollenin. Fatty acyl-ACP esters, synthesized de novo by the FAS complex, are reduced by MS2 to produce fatty alcohols or hydrolyzed by FATB to produce free fatty acids. After hydroxylation by CYP703A2 and CYP704B1, free fatty acids may be reduced by unknown reductases to fatty alcohols or aldehydes, forming putative hydroxylated aliphatic sporopollenin precursors. Alternatively, hydroxylation by CYP703A2 and CYP704B1 of the fatty alcohol produced by MS2 may occur. In the case of *Pinus rigida*, these aliphatic precursors might be acylated with phenolics by an unknown transferase. Hydroxylated or non-hydroxylated fatty acids are esterified to CoA by ACOS5 prior to several cycles of condensation by PKSs and reduction by TKPRs to form polyhydroxylated α-pyrone precursors. The precursors could be exported to the anther locule and polymerized on the surface of developing microspores by an unknown mechanism. In *Pinus rigida*, a simplified sporopollenin is proposed to predominantly contain hydroxylated aliphatic α-pyrone units, crosslinked at one end through an ester group and linked through a dioxane moiety to other units by a hydroxylated aliphatic chain bearing a coumaroyl moiety. In *Lycopodium clavatum*, the sporopollenin structure is proposed to contain a rigid macrocyclic backbone of several hydroxylated aliphatic α-pyrone units coupled through ether bonds to hydroxylated aliphatic networks linked together by glycerol.

exhibit largely redundant gene product activities (**Table 1**). These findings, together with the characterization of orthologs required for sporopollenin biosynthesis in monocots *Zea mays* (Tian et al., 2017) and *Triticum aestivum* (Singh et al., 2017), and eudicots *Brassica napus* (Yi et al., 2010; Qin et al., 2016), *Nicotiana tobacum* (Wang et al., 2013), *Gerbera hybrida* (Kontturi et al., 2017), and *Hypericum perforatum* (Jepson et al., 2014) support strong conservation of a core sporopollenin metabolic pathway in angiosperms (**Table 1**). Despite a deficiency in the study of sporopollenin-related orthologs in non-flowering species, characterization of *MS2* (Wallace et al., 2015), *ACOS6* (Li et al., 2019b), and *ASCL* (Colpitts et al., 2011; Daku et al., 2016) in the early emerging moss *Physcomitrella patens* supports substantial overlap in gene product activities, lending further support to the conservation of sporopollenin biosynthetic machinery among land plants (**Table 1**). Further, ACOS, PKS, and TKPR appear to function cooperatively as a metabolon, forming an ER-localized multienzyme complex in the tapetum of Arabidopsis, *Brassica napus*, and *Nicotiana tobacum* (Lallemand et al., 2013; Wang et al., 2013; Qin et al., 2016), or dually present in the tapetum and locule of rice anthers (Wang et al., 2018; Xu et al., 2019). Altogether, the hypothesis that the synthesis of core sporopollenin constituents involves a highly conserved pathway has gained broad support, reinforcing earlier phylogenetic and genomic findings (Souza et al., 2008; Colpitts et al., 2011; Wang et al., 2013; Gómez et al., 2015; Shi et al., 2015; Zhang et al., 2016) and discoveries made in Arabidopsis. Although understanding of sporopollenin's chemical composition remains incomplete, molecular genetics have provided a valued mechanism for making informed inferences on sporopollenin's composition.

PUTATIVE HETEROGENEITY OF SPOROPOLLENIN IN THE PLANT KINGDOM

Evidence from genetic and biochemical studies indicates polyhydroxylated aliphatic derivatives form major constituents of sporopollenin, which appear to be produced by conserved and ancient biochemical pathways. Yet, the extent of chemical conservation of the biopolymer among land plants remains unclear. With the growth of experimental evidence for sporopollenin-related putative orthologs and their encoded enzymes from diverse plant species (**Table 1**), data from several studies are challenging the notion of a single definition for sporopollenin. In the case of *ACOS* orthologs, Arabidopsis, rice, tobacco, and canola ACOS enzymes accept similar medium- to long-chain fatty acid substrates, indicating general conservation of enzymatic activities among flowering plants (Souza et al., 2009; Wang et al., 2013; Li et al., 2016; Qin et al., 2016; Yang et al., 2017). Interestingly however, amidst strong conservation of orthologous genes from disparate plant groups, examples of variation in substrate preferences and functional complementation capabilities for select sporopollenin-related enzymes have emerged. Notably, the abnormal exine in Arabidopsis and other dicot sporopollenin biosynthetic mutants

commonly manifests as dual abnormalities in rice and other monocots, disrupting exine and anther cuticle formation. The incomplete complementation of the Arabidopsis *acos5* mutant exine phenotype by OsACOS12, driven by the Arabidopsis *ACOS5* promoter, suggests some functional divergence between dicot and monocot ACOS enzymes (Li et al., 2016). In bryophytes, investigations of sporopollenin synthesis-related genes, including *ACOS6* (Li et al., 2019b), *ASCL*, a *PKSA*/*LAP6* ortholog (Colpitts et al., 2011; Daku et al., 2016), and *MS2* in *Physcomitrella patens* (Pp; Wallace et al., 2015), support general conservation of function, with knock-out mutations in each producing defective spore walls. However, complementation analyses using PpACOS6 or PpMS2 driven by their respective Arabidopsis promoters failed to recover *acos5* and *ms2* phenotypes (Wallace et al., 2015; Li et al., 2019b). In support of mixed complementation data, unique substrate preferences for ACOS5 and its orthologs in Physcomitrella and rice suggest sporopollenin fatty acid chain lengths may vary among species (Li et al., 2019b). The breadth of substrates accepted by PpACOS6 also appears reduced relative to AtACOS5 and OsACOS12, suggesting a degree of functional divergence in sporopollenin biosynthetic machinery that may translate into biochemical heterogeneity in the biopolymer across the plant kingdom.

THE MOLECULAR STRUCTURE OF SPOROPOLLENIN

Despite its incredible properties and perhaps because of its resilience, the molecular structure of sporopollenin has not yet been fully elucidated. Recent works, however, report important progress in defining the molecular structure of sporopollenin. Li et al. developed and optimized chemical degradation protocols in association with state-of-the-art NMR techniques to study sporopollenin from the gymnosperm *Pinus rigida* (Li et al., 2019a). With the large amounts of pollen that can be obtained from pine and an optimized thioacidolysis method, sporopollenin was partially solubilized. Analysis of the degradation products by HPLC-UV-MS and NMR detected p-coumaroylated 7-OH-C16 aliphatic chains and the flavonoid naringenin as a minor element. Acetylation of the remaining insoluble fraction allowed partial solubilization, with further NMR analysis identifying mostly polyhydroxylated aliphatic chains, polyvinylacetate (PVA)-like units, flanked at one end by an α-pyrone moiety and crosslinked at the other end through an ester group. These units were found crosslinked with coumaroylated 7-OH-C16 fatty acids through a newly described dioxane moiety (**Figure 1**). Glycerol-like units, and to a lesser extent naringenin, were linked to PVA-like units through ester bonds. It is suggested that the α-pyrone PVA-like units could be obtained through extension of a hydroxylated fatty acyl precursor with several cycles of malonyl-CoA condensation by type III polyketide synthases (such as PKSA/PKSB) followed by a reduction of the ketone, possibly by TKPR1/DRL1. These units would then be crosslinked with p-coumaroylated 7-OH-C16 aliphatics, flanked on one or both ends by aldehydes, to form the dioxane moiety. In this model, sporopollenin crosslinking involves acetal linkages (forming the dioxane moieties) and ester linkages, having distinct chemical stability. The authors suggest that this chemical linkage heterogeneity explains the superior stability of sporopollenin relative to other biopolymers that are predominantly crosslinked *via* only one linkage type.

In another recent study, Mikhael et al. report novel insights on the molecular structure of sporopollenin from *Lycopodium clavatum* non-sexual spores (Mikhael et al., 2020). Using a combination of TOF-SIMS and CID-MS/MS, MALDI-TOF-MS and CID-TOF/TOF-MS/MS and solid-state NMR, they describe two main units that form the sporopollenin exine in this pteridophyte. The backbone is reported to contain a unique macrocyclic oligomeric monomer of polyhydroxylated aliphatic α-pyrone units, linked through ether bonds, to form a ring-like structure (**Figure 1**, blue shading). The second unit is composed of polyhydroxylated aliphatic chains with glycerol as a core component, which forms a dendrimer-like structure (**Figure 1**, green shading) and is reported to be covalently attached by ether bonds to the macrocyclic backbone to form sporopollenin. In contrast to Li et al., an absence of aromaticity was reported for *L. clavatum* sporopollenin. Using infrared spectroscopy, Lutzke et al. report analysis of isolated *Pinus ponderosa* sporopollenin (Lutzke et al., 2020). In agreement with known or hypothesized constituents of sporopollenin, they show that the biopolymer consists of distinct aliphatic and aromatic domains, but in contrast with models proposed by Li et al. and Mikhael et al., α-pyrones were not detected in FTIR spectra. They also report that exine morphology is largely retained after removal of all aromatics, suggesting phenolic compounds are not critical structural components. Similarly, Xue et al. report NMR analysis of sporopollenin from a variety of seed plants, pteridophytes and bryophytes (Xue et al., 2020). Their results indicate the presence of aromatics in all tested sporopollenins, including *Lycopodium clavatum*, contrasting with data presented by Mikhael et al. (2020).

CROSS-LINKAGES AND ASSEMBLY OF SPOROPOLLENIN

To date, no enzyme is known to be involved in the polymerization and deposition of sporopollenin on the microspore surface. It has however been suggested that oxidative polymerization involving ROS takes place, similar to what is known for lignin (Matveyeva et al., 2012; Jacobowitz et al., 2019), and that sporopollenin deposition into an elaborately patterned and sculptured cell wall is guided by a cellulosic (primexine) scaffold and the physico-chemical properties of modulated phases surrounding developing microspores (Scott, 1994; Paxson-Sowders et al., 1997; Gabarayeva et al., 2019; Radja et al., 2019). The application of ROS scavenger to developing moss spores compromised spore wall formation and structural integrity in a dose-dependent manner, suggesting the involvement of ROS and peroxidases in sporopollenin polymerization and/or

deposition (Rabbi et al., 2020). In Arabidopsis, tapetum-expressed peroxidases PER9 and PER40 are reported to be mostly involved in tapetal cell wall formation. Primary or secondary effects on pollen wall formation are however also described in the null mutants (Jacobowitz et al., 2019), supporting the oxidative polymerization of sporopollenin.

DISCUSSION

Through the advancement of tools for solubilizing and fractionating sporopollenin, alongside expansion of studies characterizing sporopollenin biosynthesis in diverse plant species, immense strides toward structurally elucidating sporopollenin and the mechanisms of its biosynthesis have been made. Genetic and biochemical efforts to characterize sporopollenin are converging on similar findings, with extensive overlap in the core subunits and biosynthetic enzyme activities identified, collectively supporting a backbone of covalently coupled polyhydroxylated α-pyrones and hydroxylated aliphatic chains. Although much uncertainty surrounding this complex, resilient organic material remains, advancements in elucidating the molecular structure and biosynthetic mechanisms that form sporopollenin are enabling comparative analyses among land plants and raising new questions about the extent of sporopollenin's chemical conservation (Xue et al., 2020). Further, mechanisms of assembly, higher-order structure, and the plasticity of the polymer remain largely unexplored topics of basic and applied interest.

Recent biochemical studies reporting polymer analysis describe the presence of hydroxylated, aliphatic α-pyrones in sporopollenin (Li et al., 2019a; Mikhael et al., 2020), upholding composition predictions based on *in vitro* activities of enzymes required for sporopollenin formation. Although biochemical and genetic approaches are forming a more consistent picture of sporopollenin, significant gaps remain between models of sporopollenin proposed by biochemists and what is known of its biosynthetic pathway. In Lycopodium and pine sporopollenin models, aliphatic precursors have in-chain and terminal hydroxyl groups. It is not clear whether the known cytochrome P450 oxygenases (CYP703A2 and CYP704B1) produce these hydroxylations or if other, yet-to-be-discovered oxygenases are involved. In *Pinus rigida*, it is hypothesized that aliphatic precursors bear aldehyde groups at one or both ends to form acetal bonds with the aliphatic α-pyrone. This production would require the action of unknown alcohol dehydrogenases or reductases from alcohol or carboxylic acid precursors, respectively. Similarly, the presence of coumaroyl and naringenin moieties in pine sporopollenin suggests the involvement of not-yet-discovered acyltransferases. Thus, genetic studies have the potential to bridge the remaining gaps in our knowledge of sporopollenin biosynthesis with insights from molecular structure analyses.

The molecular structure of sporopollenin has been a mystery for decades with numerous studies only providing glimpses of functional groups or fragments of the polymer constituents, such as lipids or phenol rings. It is now suggested that some earlier discoveries identified technical artifacts arising from the harsh conditions used for sporopollenin analysis (Gonzalez-Cruz et al., 2018; Mikhael et al., 2020). Using different models, recent studies present significant progress in understanding sporopollenin's molecular composition. Li et al. describe a principal structure of hydroxylated aliphatic α-pyrone units linked by coumaroylated 7-OH-C16 aliphatic in pine. Lutzke et al. report aliphatic and aromatic domains but no polyketide-derived elements in pine sporopollenin. Mikhael et al. describe a macrocyclic backbone structure composed of hydroxylated aliphatic α-pyrone units linked by dendrimer-like, hydroxylated fatty acid units in *L. clavatum* with no aromatics, while Xue et al. report the presence of aromatics for the same plant. Thus, despite recent advances, inconsistencies remain in the available sporopollenin molecular structure data, depending on the techniques used or organism studied.

General consensus describes sporopollenin with a main polyhydroxylated aliphatic component and polyketide-derived aliphatic α-pyrone elements. This emerging picture reconciles for the first time the work of biochemists with that of geneticists that described the involvement of fatty acid oxygenase cytochrome P450s, polyketide synthases, and polyketide reductases in the biosynthesis of sporopollenin. Genetic studies have uncovered remarkable conservation of the core sporopollenin biosynthetic pathway in the plant kingdom. However, differences found recently question the extent of sporopollenin chemical conservation between evolutionary clusters. It is possible that the backbone of sporopollenin between plant clusters is conserved but differs in the way the units are assembled or "decorated" with phenolic-derived elements. Continued efforts to chemically and structurally characterize sporopollenin from flowering and early emerging plant species will help to resolve current discrepancies and provide evolutionary context for resolving sporopollenin's compositional homogeneity within the plant kingdom.

The recent acceleration of long-term efforts to uncover the mysteries of sporopollenin, particularly with solid-state methods, has provided novel understanding of the molecular features of the biopolymer that confer extreme stability. Harnessing the resilience of sporopollenin offers diverse opportunities for synthetic material design in medical science, space exploration, and environmental remediation. Further, the use of sporopollenin-based microparticles as a vector for oral vaccines and a range of macromolecules offers potential for sustainable applications of this abundant and stable biomaterial.

AUTHOR CONTRIBUTIONS

All authors listed have made a substantial, direct and intellectual contribution to the work, and approved it for publication.

FUNDING

Funding provided by the Aquatic and Crop Resource Development Research Centre, National Research Council of Canada, ACRD #58289.

ACKNOWLEDGMENTS

This work was supported by the Aquatic and Crop Resource Development Research Division of the National Research Council of Canada. The micrograph presented was prepared in the laboratory of A. L. Samuels and the BioImaging Facility at the University of British Columbia.

REFERENCES

Aarts, M. G. M., Hodge, R., Kalantidis, K., Florack, D., Wilson, Z. A., Mulligan, B. J., et al. (1997). The *Arabidopsis MALE STERILITY 2* protein shares similarity with reductases in elongation/condensation complexes. *Plant J.* 12, 615–623. doi: 10.1046/j.1365-313X.1997.d01-8.x

Ahlers, F., Lambert, J., and Wiermann, R. (2003). Acetylation and silylation of piperidine solubilized sporopollenin from pollen of *Typha angustifolia* L. *Z. Naturforsch., C. J. Biosci.* 58, 807–811. doi: 10.1515/znc-2003-11-1210

Ahlers, F., Thom, I., Lambert, J., Kuckuk, R., and Wiermann, R. (1999). 1H NMR analysis of sporopollenin from *Typha angustifolia*. *Phytochemistry* 50, 1095–1098. doi: 10.1016/S0031-9422(98)00225-8

Barrier, S. (2008). *Physical and Chemical Properties of Sporopollenin Exine Particles*. Doctoral dissertation. University of Hull.

Brooks, J., and Shaw, G. (1968). Chemical structure of the exine of pollen walls and a new function for carotenoids in nature. *Nature* 219, 532–533. doi: 10.1038/219532a0

Brooks, J., and Shaw, G. (1971). Evidence for life in the oldest known sedimentary rocks—the onverwacht series chert, Swaziland system of Southern Africa. *Grana* 11, 1–8. doi: 10.1080/00173137109427403

Brown, C. A. (1960). Palynological techniques. *Micropaleontology* 6, 329–331.

Brown, R. C., and Lemmon, B. E. (2011). Spores before sporophytes: hypothesizing the origin of sporogenesis at the algal–plant transition. *New Phytol.* 190, 875–881. doi: 10.1111/j.1469-8137.2011.03709.x

Chang, Z., Chen, Z., Yan, W., Xie, G., Lu, J., Wang, N., et al. (2016). An ABC transporter, OsABCG26, is required for anther cuticle and pollen exine formation and pollen-pistil interactions in rice. *Plant Sci.* 253, 21–30. doi: 10.1016/j.plantsci.2016.09.006

Chang, Z., Jin, M., Yan, W., Chen, H., Qiu, S., Fu, S., et al. (2018). The ATP-binding cassette (ABC) transporter OsABCG3 is essential for pollen development in rice. *Rice* 11:58. doi: 10.1186/s12284-018-0248-8

Chen, W., Yu, X. H., Zhang, K., Shi, J., De Oliveira, S., Schreiber, L., et al. (2011). *MALE STERILE2* encodes a plastid-localized fatty acyl carrier protein reductase required for pollen exine development in Arabidopsis. *Plant Physiol.* 157, 842–853. doi: 10.1104/pp.111.181693

Choi, H., Jin, J.-Y., Choi, S., Hwang, J.-U., Kim, Y.-Y., Suh, M. C., et al. (2011). An ABCG/WBC-type ABC transporter is essential for transport of sporopollenin precursors for exine formation in developing pollen. *Plant J.* 65, 181–193. doi: 10.1111/j.1365-313X.2010.04412.x

Colpitts, C. C., Kim, S. S., Posehn, S. E., Jepson, C., Kim, S. Y., Wiedemann, G., et al. (2011). PpASCL, a moss ortholog of anther-specific chalcone synthase-like enzymes, is a hydroxyalkylpyrone synthase involved in an evolutionarily conserved sporopollenin biosynthesis pathway. *New Phytol.* 192, 855–868. doi: 10.1111/j.1469-8137.2011.03858.x

Daku, R. M., Rabbi, F., Buttigieg, J., Coulson, I. M., Horne, D., Martens, G., et al. (2016). PpASCL, the *Physcomitrella patens* anther-specific chalcone synthase-like enzyme implicated in sporopollenin biosynthesis, is needed for integrity of the moss spore wall and spore viability. *PLoS One* 11:e0146817. doi: 10.1371/journal.pone.0146817

Doan, T. T. P., Carlsson, A. S., Hamberg, M., Bülow, L., Stymne, S., and Olsson, P. (2009). Functional expression of five Arabidopsis fatty acyl-CoA reductase genes in *Escherichia coli*. *J. Plant Physiol.* 166, 787–796. doi: 10.1016/j.jplph.2008.10.003

Dobritsa, A. A., Lei, Z., Nishikawa, S.-I., Urbanczyk-Wochniak, E., Huhman, D. V., Preuss, D., et al. (2010). LAP5 and LAP6 encode anther-specific proteins with similarity to chalcone synthase essential for pollen exine development in Arabidopsis. *Plant Physiol.* 153, 937–955. doi: 10.1104/pp.110.157446

Dobritsa, A. A., Shrestha, J., Morant, M., Pinot, F., Matsuno, M., Swanson, R., et al. (2009). CYP704B1 is a long-chain fatty acid omega-hydroxylase essential for sporopollenin synthesis in pollen of Arabidopsis. *Plant Physiol.* 151, 574–589. doi: 10.1104/pp.109.144469

Domínguez, E., Mercado, J. A., Quesada, M. A., and Heredia, A. (1999). Pollen sporopollenin: degradation and structural elucidation. *Sex. Plant Reprod.* 12, 171–178. doi: 10.1007/s004970050189

Gabarayeva, N. I., Grigorjeva, V. V., and Shavarda, A. L. (2019). Mimicking pollen and spore walls: self-assembly in action. *Ann. Bot.* 123, 1205–1218. doi: 10.1093/aob/mcz027

Gómez, J. F., Talle, B., and Wilson, Z. A. (2015). Anther and pollen development: a conserved developmental pathway. *J. Integr. Plant Biol.* 57, 876–891. doi: 10.1111/jipb.12425

Gonzalez-Cruz, P., Uddin, M. J., Atwe, S. U., Abidi, N., and Gill, H. S. (2018). Chemical treatment method for obtaining clean and intact pollen shells of different species. *ACS Biomater Sci. Eng.* 4, 2319–2329. doi: 10.1021/acsbiomaterials.8b00304

Grienenberger, E., Kim, S. S., Lallemand, B., Geoffroy, P., Heintz, D., Souza, C. d. A., et al. (2010). Analysis of *TETRAKETIDE* α*-PYRONE REDUCTASE* function in *Arabidopsis thaliana* reveals a previously unknown, but conserved, biochemical pathway in sporopollenin monomer biosynthesis. *Plant Cell* 22, 4067–4083. doi: 10.1105/tpc.110.080036

Guilford, W. J., Schneider, D. M., Labovitz, J., and Opella, S. J. (1988). High resolution solid state C NMR spectroscopy of sporopollenins from different plant taxa. *Plant Physiol.* 86, 134–136. doi: 10.1104/pp.86.1.134

Hemsley, A. R., Barrie, P. J., Chaloner, W. G., and Scott, A. C. (2009). The composition of sporopollenin and its use in living and fossil plant systematics. *Grana* 32, 2–11. doi: 10.1080/00173139309427446

Huang, M.-D., Chen, T.-L. L., and Huang, A. H. C. (2013). Abundant type III lipid transfer proteins in Arabidopsis tapetum are secreted to the locule and become a constituent of the pollen exine. *Plant Physiol.* 163, 1218–1229. doi: 10.1104/pp.113.225706

Jacobowitz, J. R., Doyle, W. C., and Weng, J.-K. (2019). PRX9 and PRX40 are extensin peroxidases essential for maintaining tapetum and microspore cell wall integrity during Arabidopsis anther development. *Plant Cell* 31, 848–861. doi: 10.1105/tpc.18.00907

Jepson, C., Karppinen, K., Daku, R. M., Sterenberg, B. T., and Suh, D.-Y. (2014). *Hypericum perforatum* hydroxyalkylpyrone synthase involved in sporopollenin biosynthesis – phylogeny, site-directed mutagenesis, and expression in nonanther tissues. *FEBS J.* 281, 3855–3868. doi: 10.1111/febs.12920

Kesseler, R., and Harley, M. (2004). *Pollen, the Hidden Sexuality of Flowers* Papadakis. London: Papa-dakis Publisher.

Kim, S. S., Grienenberger, E., Lallemand, B., Colpitts, C. C., Kim, S. Y., Souza, C. d. A., et al. (2010). *LAP6/POLYKETIDE SYNTHASE A* and *LAP5/POLYKETIDE SYNTHASE B* encode hydroxyalkyl α-pyrone synthases required for pollen development and sporopollenin biosynthesis in *Arabidopsis thaliana*. *Plant Cell* 22, 4045–4066. doi: 10.1105/tpc.110.080028

Kontturi, J., Osama, R., Deng, X., Bashandy, H., Albert, V. A., and Teeri, T. H. (2017). Functional characterization and expression of GASCL1 and GASCL2, two anther-specific chalcone synthase like enzymes from *Gerbera hybrida*. *Phytochemistry* 134, 38–45. doi: 10.1016/j.phytochem.2016.11.002

Lallemand, B., Erhardt, M., Heitz, T., and Legrand, M. (2013). Sporopollenin biosynthetic enzymes interact and constitute a metabolon localized to the endoplasmic reticulum of tapetum cells. *Plant Physiol.* 162, 616–625. doi: 10.1104/pp.112.213124

Li, Y., Li, D., Guo, Z., Shi, Q., Xiong, S., Zhang, C., et al. (2016). OsACOS12, an orthologue of Arabidopsis acyl-CoA synthetase5, plays an important role in pollen exine formation and anther development in rice. *BMC Plant Biol.* 16:256. doi: 10.1186/s12870-016-0943-9

Li, F.-S., Phyo, P., Jacobowitz, J., Hong, M., and Weng, J.-K. (2019a). The molecular structure of plant sporopollenin. *Nat Plants* 5, 41–46. doi: 10.1038/s41477-018-0330-7

Li, H., Pinot, F., Sauveplane, V., Werck-Reichhart, D., Diehl, P., Schreiber, L., et al. (2010). Cytochrome P450 family member CYP704B2 catalyzes the

{omega}-hydroxylation of fatty acids and is required for anther cutin biosynthesis and pollen exine formation in rice. *Plant Cell* 22, 173–190. doi: 10.1105/tpc.109.070326

Li, Y.-L., Zhang, Y.-F., Li, D.-D., Shi, Q. S., Lou, Y., Yang, Z.-N., et al. (2019b). Acyl-CoA synthetases from Physcomitrella, rice and Arabidopsis: different substrate preferences but common regulation by MS188 in sporopollenin synthesis. *Planta* 250, 535–548. doi: 10.1007/s00425-019-03189-0

Liang, W., Yin, C., Zong, J., Gu, F., and Zhang, D. (2010). *OsC6*, encoding a lipid transfer protein, is required for postmeiotic anther development In rice. *Plant Physiol.* 154, 149–162. doi: 10.1104/pp.110.158865

Lutzke, A., Morey, K. J., Medford, J. I., and Kipper, M. J. (2020). Detailed characterization of *Pinus ponderosa* sporopollenin by infrared spectroscopy. *Phytochemistry* 170:112195. doi: 10.1016/j.phytochem.2019.112195

Mackenzie, G., Boa, A. N., Diego-Taboada, A., Atkin, S. L., and Sathyapalan, T. (2015). Sporopollenin, the least known yet toughest natural biopolymer. *Front. Mater.* 2:66. doi: 10.3389/fmats.2015.00066

Matveyeva, N. P., Polevova, S. V., Smirnova, A. V., and Yermakov, I. P. (2012). Sporopollenin accumulation in *Nicotiana tabacum* L. microspore wall during its development. *Cell. Tiss. Biol.* 6, 293–301. doi: 10.1134/S1990519X12030078

Mikhael, A., Jurcic, K., Schneider, C., Karr, D., Fisher, G. L., Fridgen, T. D., et al. (2020). Demystifying and unravelling the molecular structure of the biopolymer sporopollenin. *Rapid Commun. Mass Spectrom.* 34:e8740. doi: 10.1002/rcm.8740

Montgomery, W., Potiszil, C., Watson, J. S., and Sephton, M. A. (2016). Sporopollenin, a natural copolymer, is robust under high hydrostatic pressure. *Macromol. Chem. Phys.* 217, 2494–2500. doi: 10.1002/macp.201600142

Morant, M., Jørgensen, K., Schaller, H., Pinot, F., Møller, B. L., Werck-Reichhart, D., et al. (2007). CYP703 is an ancient cytochrome P450 in land plants catalyzing in-chain hydroxylation of lauric acid to provide building blocks for sporopollenin synthesis in pollen. *Plant Cell* 19, 1473–1487. doi: 10.1105/tpc.106.045948

Niu, B.-X., He, F.-R., He, M., Ren, D., Chen, L.-T., and Liu, Y.-G. (2013). The ATP-binding cassette transporter OsABCG15 is required for anther development and pollen fertility in rice. *J. Integr. Plant Biol.* 55, 710–720. doi: 10.1111/jipb.12053

Paxson-Sowders, D. M., Owen, H. A., and Makaroff, C. A. (1997). A comparative ultrastructural analysis of exine pattern development in wild-type Arabidopsis and a mutant defective in pattern formation. *Protoplasma* 198, 53–65. doi: 10.1007/BF01282131

Qin, M., Tian, T., Xia, S., Wang, Z., Song, L., Yi, B., et al. (2016). Heterodimer formation of BnPKSA or BnPKSB with BnACOS5 constitutes a multienzyme complex in tapetal cells and is involved in male reproductive development in *Brassica napus*. *Plant Cell Physiol.* 57, 1643–1656. doi: 10.1093/pcp/pcw092

Qin, P., Tu, B., Wang, Y., Deng, L., Quilichini, T. D., Li, T., et al. (2013). *ABCG15* encodes an ABC transporter protein, and is essential for post-meiotic anther and pollen exine development in rice. *Plant Cell Physiol.* 54, 138–154. doi: 10.1093/pcp/pcs162

Quilichini, T. D., Friedmann, M. C., Samuels, A. L., and Douglas, C. J. (2010). ATP-binding cassette transporter G26 is required for male fertility and pollen exine formation in Arabidopsis. *Plant Physiol.* 154, 678–690. doi: 10.1104/pp.110.161968

Quilichini, T. D., Grienenberger, E., and Douglas, C. J. (2015). The biosynthesis, composition and assembly of the outer pollen wall: a tough case to crack. *Phytochemistry* 113, 170–182. doi: 10.1016/j.phytochem.2014.05.002

Quilichini, T. D., Samuels, A. L., and Douglas, C. J. (2014). ABCG26-mediated polyketide trafficking and hydroxycinnamoyl spermidines contribute to pollen wall exine formation in Arabidopsis. *Plant Cell* 26, 4483–4498. doi: 10.1105/tpc.114.130484

Rabbi, F., Renzaglia, K. S., Ashton, N. W., and Suh, D.-Y. (2020). Reactive oxygen species are required for spore-wall formation in *Physcomitrella patens*. *Botany* 98, 575–587. doi: 10.1139/cjb-2020-0012

Radja, A., Horsley, E. M., Lavrentovich, M. O., and Sweeney, A. M. (2019). Pollen cell wall patterns form from modulated phases. *Cell* 176, 856–868. doi: 10.1016/j.cell.2019.01.014

Scott, R. J. (1994). "Pollen exine: the sporopollenin enigma and the physics of pattern," in *Molecular and Cellular Aspects of Plant Reproduction*. eds. R. J. Scott and A. D. Stead (Cambridge, UK: Cambridge University Press), 49–81.

Shi, J., Cui, M., Yang, L., Kim, Y.-J., and Zhang, D. (2015). Genetic and biochemical mechanisms of pollen wall development. *Trends Plant Sci.* 20, 741–753. doi: 10.1016/j.tplants.2015.07.010

Shi, J., Tan, H., Yu, X.-H., Liu, Y., Liang, W., Ranathunge, K., et al. (2011). Defective pollen wall is required for anther and microspore development in rice and encodes a fatty acyl carrier protein reductase. *Plant Cell* 23, 2225–2246. doi: 10.1105/tpc.111.087528

Shi, Q. S., Wang, K.-Q., Li, Y.-L., Zhou, L., Xiong, S. X., Han, Y., et al. (2018). OsPKS1 is required for sexine layer formation, which shows functional conservation between rice and Arabidopsis. *Plant Sci.* 277, 145–154. doi: 10.1016/j.plantsci.2018.08.009

Singh, M., Kumar, M., Thilges, K., Cho, M.-J., and Cigan, A. M. (2017). MS26/CYP704B is required for anther and pollen wall development in bread wheat (Triticum aestivum L.) and combining mutations in all three homeologs causes male sterility. *PLoS One* 12:e0177632. doi: 10.1371/journal.pone.0177632

Souza, C. d. A., Barbazuk, B., Ralph, S. G., Bohlmann, J., Hamberger, B., and Douglas, C. J. (2008). Genome-wide analysis of a land plant-specific acyl:coenzyme A synthetase (ACS) gene family in Arabidopsis, poplar, rice and Physcomitrella. *New Phytol.* 179, 987–1003. doi: 10.1111/j.1469-8137.2008.02534.x

Souza, C. d. A., Kim, S. S., Koch, S., Kienow, L., Schneider, K., McKim, S. M., et al. (2009). A novel fatty Acyl-CoA Synthetase is required for pollen development and sporopollenin biosynthesis in Arabidopsis. *Plant Cell* 21, 507–525. doi: 10.1105/tpc.108.062513

Tang, L. K., Chu, H., Yip, W. K., Yeung, E. C., and Lo, C. (2009). An anther-specific dihydroflavonol 4-reductase-like gene (*DRL1*) is essential for male fertility in Arabidopsis. *New Phytol.* 181, 576–587. doi: 10.1111/j.1469-8137.2008.02692.x

Tian, Y., Xiao, S., Liu, J., Somaratne, Y., Zhang, H., Wang, M., et al. (2017). *MALE STERILE6021* (*MS6021*) is required for the development of anther cuticle and pollen exine in maize. *Sci. Rep.* 7:16736. doi: 10.1038/s41598-017-16930-0

Wallace, S., Chater, C. C., Kamisugi, Y., Cuming, A. C., Wellman, C. H., Beerling, D. J., et al. (2015). Conservation of Male Sterility 2 function during spore and pollen wall development supports an evolutionarily early recruitment of a core component in the sporopollenin biosynthetic pathway. *New Phytol.* 205, 390–401. doi: 10.1111/nph.13012

Wallace, S., Fleming, A., Wellman, C. H., and Beerling, D. J. (2011). Evolutionary development of the plant and spore wall. *AoB Plants* 2011:plr027. doi: 10.1093/aobpla/plr027

Wang, K., Guo, Z.-L., Zhou, W.-T., Zhang, C., Zhang, Z.-Y., Lou, Y., et al. (2018). The regulation of sporopollenin biosynthesis genes for rapid pollen wall formation. *Plant Physiol.* 178, 283–294. doi: 10.1104/pp.18.00219

Wang, Y., Lin, Y.-C., So, J., Du, Y., and Lo, C. (2013). Conserved metabolic steps for sporopollenin precursor formation in tobacco and rice. *Physiol Plantarum* 149, 13–24. doi: 10.1111/ppl.12018

Wang, W., Ma, Y., Suo, Y., Yan, L., Zhang, D., and Miao, C. (2014). Crystallization and preliminary crystallographic analysis of defective pollen wall (DPW) protein from Oryza sativa. *Acta Cryst.* 70, 758–760. doi: 10.1107/S2053230X14008486

Weng, J.-K., Mo, H., and Chapple, C. (2010). Over-expression of *F5H* in COMT-deficient Arabidopsis leads to enrichment of an unusual lignin and disruption of pollen wall formation. *Plant J.* 64, 898–911. doi: 10.1111/j.1365-313X.2010.04391.x

Xu, D., Qu, S., Tucker, M. R., Zhang, D., Liang, W., and Shi, J. (2019). Ostkpr1 functions in anther cuticle development and pollen wall formation in rice. *BMC Plant Biol.* 19, 1–13. doi: 10.1186/s12870-019-1711-4

Xu, D., Shi, J., Rautengarten, C., Yang, L., Qian, X., Uzair, M., et al. (2017). *Defective Pollen Wall 2* (*DPW2*) encodes an acyl transferase required for rice pollen development. *Plant Physiol.* 173, 240–255. doi: 10.1104/pp.16.00095

Xue, J.-S., Zhang, B., Zhan, H., Lv, Y.-L., Jia, X.-L., Wang, T., et al. (2020). Phenylpropanoid derivatives are essential components of sporopollenin in vascular plants. *Mol. Plant* 13, 1644–1653. doi: 10.1016/j.molp.2020.08.005

Yang, X., Liang, W., Chen, M., Zhang, D., Zhao, X., and Shi, J. (2017). Rice fatty acyl-CoA synthetase OsACOS12 is required for tapetum programmed cell death and male fertility. *Planta* 246, 105–122. doi: 10.1007/s00425-017-2691-y

Yang, X., Wu, D., Shi, J., He, Y., Pinot, F., Grausem, B., et al. (2014). Rice CYP703A3, a cytochrome P450 hydroxylase, is essential for development

of anther cuticle and pollen exine. *J. Integr. Plant Biol.* 56, 979–994. doi: 10.1111/jipb.12212

Yang, Z., Zhang, Y., Sun, L., Zhang, P., Liu, L., Yu, P., et al. (2018). Identification of cyp703a3-3 and analysis of regulatory role of CYP703A3 in rice anther cuticle and pollen exine development. *Gene* 649, 63–73. doi: 10.1016/j.gene.2018.01.058

Yi, B., Zeng, F., Lei, S., Chen, Y., Yao, X., Zhu, Y., et al. (2010). Two duplicate *CYP704B1*-homologous genes *BnMs1* and *BnMs2* are required for pollen exine formation and tapetal development in *Brassica napus*. *Plant J.* 63, 925–938. doi: 10.1111/j.1365-313X.2010.04289.x

Zaidi, M. A., O'Leary, S. J. B., Gagnon, C., Chabot, D., Wu, S., Hubbard, K., et al. (2020). A triticale tapetal non-specific lipid transfer protein (nsLTP) is translocated to the pollen cell wall. *Plant Cell Rep.* 39, 1185–1197. doi: 10.1007/s00299-020-02556-6

Zetzsche, F., and Vicari, H. (1931). Untersuchungen über die Membran der Sporen und Pollen. *Helv. Chim. Acta* 14, 58–78. doi: 10.1002/hlca.19310140104

Zhang, D., Shi, J., and Yang, X. (2016). "Role of Lipid Metabolism in Plant Pollen Exine Development," in *Lipids in Plant and Algae Development. Vol 86*. eds. Y. Nakamura and Y. Li-Beisson (Cham: Springer), 315–337.

Zhao, G., Shi, J., Liang, W., Xue, F., Luo, Q., Zhu, L., et al. (2015). Two ATP Binding cassette G transporters, rice ATP binding cassette G26 and ATP binding cassette G15 collaboratively regulate rice male reproduction. *Plant Physiol.* 169, 2064–2079. doi:10.1104/pp.15.00262.

Zhu, L., Shi, J., Zhao, G., Zhang, D., and Liang, W. (2013). Post-meiotic deficient anther1 (PDA1) encodes an ABC transporter required for the development of anther cuticle and pollen exine in rice. *J. Plant Biol.* 56, 59–68. doi: 10.1007/s12374-013-0902-z

Zhu, X., Yu, J., Shi, J., Tohge, T., Fernie, A. R., Meir, S., et al. (2017). The polyketide synthase OsPKS2 is essential for pollen exine and Ubisch body patterning in rice. *J. Integr. Plant Biol.* 59, 612–628. doi: 10.1111/jipb.12574

Zou, T., Liu, M., Xiao, Q., Wang, T., Chen, D., Luo, T., et al. (2018). OsPKS2 is required for rice male fertility by participating in pollen wall formation. *Plant Cell Rep.* 37, 759–773. doi: 10.1007/s00299-018-2265-x

Zou, T., Xiao, Q., Li, W., Luo, T., Yuan, G., He, Z., et al. (2017). OsLAP6/OsPKS1, an orthologue of Arabidopsis PKSA/LAP6, is critical for proper pollen exine formation. *Rice* 10:53. doi: 10.1186/s12284-017-0191-0

Conflict of Interest: The authors declare that the research was conducted in the absence of any commercial or financial relationships that could be construed as a potential conflict of interest.

Publisher's Note: All claims expressed in this article are solely those of the authors and do not necessarily represent those of their affiliated organizations, or those of the publisher, the editors and the reviewers. Any product that may be evaluated in this article, or claim that may be made by its manufacturer, is not guaranteed or endorsed by the publisher.

frontiers in Plant Science

ORIGINAL RESEARCH
published: 15 October 2021
doi: 10.3389/fpls.2021.735451

Hormonome Dynamics During Microgametogenesis in Different *Nicotiana* Species

Lenka Záveská Drábková[1]†, Eva Pokorná[2†], Petre I. Dobrev[2], Jana Kůrková[1], Lenka Steinbachová[1], David Honys[1] and Václav Motyka[2]**

[1] *Laboratory of Pollen Biology, Institute of Experimental Botany of the Czech Academy of Sciences, Prague, Czechia,*
[2] *Laboratory of Hormonal Regulations in Plants, Institute of Experimental Botany of the Czech Academy of Sciences, Prague, Czechia*

OPEN ACCESS

Edited by:
Kentaro K. Shimizu, University of Zurich, Switzerland

Reviewed by:
Afif Hedhli, Agrifood Research and Technology Centre of Aragon (CITA), Spain
Hiroyuki Kakui, Niigata University, Japan

***Correspondence:**
Lenka Záveská Drábková
l.zaveska.drabkova@ueb.cas.cz; lenka.zaveska.drabkova@gmail.com
Václav Motyka
motyka@ueb.cas.cz

† These authors have contributed equally to this work

Specialty section:
This article was submitted to Plant Development and EvoDevo, a section of the journal Frontiers in Plant Science

Received: *02 July 2021*
Accepted: *28 September 2021*
Published: *15 October 2021*

Citation:
Záveská Drábková L, Pokorná E, Dobrev PI, Kůrková J, Steinbachová L, Honys D and Motyka V (2021) Hormonome Dynamics During Microgametogenesis in Different Nicotiana Species. Front. Plant Sci. 12:735451. doi: 10.3389/fpls.2021.735451

Plant microgametogenesis involves stages leading to the progressive development of unicellular microspores into mature pollen. Despite the active and continuing interest in the study of male reproductive development, little is still known about the hormonomics at each ontogenetic stage. In this work, we characterized the profiles and dynamics of phytohormones during the process of microgametogenesis in four *Nicotiana* species (*Nicotiana tabacum*, *Nicotiana alata*, *Nicotiana langsdorffii*, and *Nicotiana mutabilis*). Taking advantage of advanced HPLC-ESI-MS/MS, twenty to thirty endogenous hormone derivatives were identified throughout pollen ontogenesis, including cytokinins, auxins, ABA and its derivatives, jasmonates, and phenolic compounds. The spectra of endogenous phytohormones changed dynamically during tobacco pollen ontogeny, indicating their important role in pollen growth and development. The different dynamics in the accumulation of endogenous phytohormones during pollen ontogenesis between *N. tabacum* (section *Nicotiana*) and the other three species (section *Alatae*) reflects their different phylogenetic positions and origin within the genus *Nicotiana*. We demonstrated the involvement of certain phytohormone forms, such as *cis*-zeatin- and methylthiol-type CKs, some derivatives of abscisic acid, phenylacetic and benzoic acids, in pollen development for the first time here. Our results suggest that unequal levels of endogenous hormones and the presence of specific derivatives may be characteristic for pollen development in different phylogenetic plant groups. These results represent the currently most comprehensive study of plant hormones during the process of pollen development.

Keywords: hormonome, male gametophyte, *Nicotiana* spp., ontogeny, pollen development, phytohormones

INTRODUCTION

The development of male gametophyte in vascular plants is a complex process that requires coordinated action and participation of numerous cells and both sporophyte and gametophyte tissues. The life cycle of the male gametophyte can be divided into a developmental phase leading to the formation of mature pollen grains and a functional (progamic) phase beginning

with the impingement of pollen on the stigma surface and ending with double fertilization (Hafidh and Honys, 2021).

The pollen grain of angiosperms is formed within the anthers of the flower via two successive developmental programs: microsporogenesis and microgametogenesis. During microsporogenesis, one (lineage model, Scott et al., 2004) to a few (cluster model, Kelliher and Walbot, 2011) meristematic L2-derived sporophytic cells differentiate into archesporial cells, which will undergo a series of periclinal and anticlinal divisions giving rise to the sub-epidermal anther wall layers (endothecium, middle layer, and tapetum) and the pollen mother cells. The diploid pollen mother cells will then undergo meiosis and form tetrads of haploid microspores encased by a callose layer. The digestion of callose and the release of microspores mark the beginning of microgametogenesis. Microgametogenesis comprises events that lead to the progressive development of the unicellular microspores into mature pollen. The released microspores increase their size, vacuolize, and their nuclei migrate to the periphery (McCormick, 1993; Borg and Twell, 2010). Thereafter, the microspores undergo highly asymmetric pollen mitosis I (PMI), leading to a large vegetative cell and a small generative cell. The generative cell migrates into the cytoplasm of the vegetative cell (Berger and Twell, 2011). After PMI, the generative cell moves inward, enabling gamete transport within the pollen tube (Honys et al., 2006). In *Nicotiana*, the generative cell undergoes one more cell division, pollen mitosis II (PMII), which occurs before pollen maturation in bi-cellular pollen. Two sperm cells are formed from a generative cell by PMII. The fusion of one sperm cell with the egg cell results in the formation of embryo, and the other sperm cell's fusion with the central cell initiates the endosperm, a nutritive tissue for the embryo. The endosperm and double fertilization are unique and are often used as defining features of angiosperms.

An essential role in male gametophyte development is played by phytohormones -naturally occurring low-abundance organic substances affecting numerous physiological processes in plants such as germination, seed development, vegetative growth, flowering, senescence, dormancy, mobilization of nutrients as well as the biotic and abiotic stress responses (Novák et al., 2017; Kieber and Schaller, 2018; Wybouw and de Rybel, 2019). Based on their physiological functions and chemical structures, phytohormones are classified into several groups – auxins, cytokinins (CKs), gibberellins (GAs), abscisic acid (ABA), ethylene, polyamines, brassinosteroids (BRs), jasmonates, salicylic acid (SA) plus other hormones with a phenolic nature, signaling peptides and strigolactones (Novák et al., 2017; Šimura et al., 2018). Hormonal studies of the plant microgametogenesis have been mostly limited to the effects of exogenously applied phytohormones on various aspects of pollen development (Kovaleva et al., 2015; Zuñiga-Mayo et al., 2018), their immunolocalization (Chen and Zhao, 2008), and molecular regulations (Huang et al., 2003; Chhun et al., 2007; Cecchetti et al., 2008, 2015, 2017; Kinoshita-Tsujimura and Kakimoto, 2011; Ding et al., 2012; Yao et al., 2018).

However, systematic research on the profiles of various phytohormone classes and their dynamics throughout particular pollen ontogenetic stages has not been performed yet, and the existing data are scarce and scattered. Chibi et al. (1995) reported variations in the ABA level during pollen grains maturation in *Nicotiana tabacum*, whereas changes in the endogenous auxin concentrations were sketched by Dupľáková et al. (2016) for five pollen developmental stages in *Arabidopsis thaliana*. Indirect evidence for a high IAA accumulation in the *Arabidopsis* pollen grains was provided by Salinas-Grenet et al. (2018) in transgenic plants expressing DR5::GUS promoter. A strong auxin signaling activity was detected throughout the pollen development, mainly in the uninucleate microspore, bicellular and tricellular cells. The endogenous profile of several phytohormones in the anther, leaf blade and pistil of rice was presented by Hirano et al. (2008). A marked predominance of free IAA, IAA-aspartate (IAA-Asp) and GA4, in contrast to very low levels of CK derivatives, was shown in anthers, containing mainly mature tricellular pollen grains.

Hirano et al. (2008) have given an extensive picture of the involvement of endogenous phytohormones in the microspore/pollen development. It is, however, not possible to generalize Hirano's results on rice monocotyledonous plant model for dicotyledonous plants. That's why we focused here on determining variations in the plant hormonome during microgametogenesis in tobacco as a dicotyledonous plant representative. Taking advantage of advanced high-performance liquid chromatography tandem mass spectrometry, we provide a detailed analysis of endogenous phytohormones during pollen ontogeny in four tobacco species differing in their phylogenetic position within the genus *Nicotiana*, the model plant *N. tabacum* (section *Nicotiana*) and three other species (*Nicotiana alata, Nicotiana langsdorffii,* and *Nicotiana mutabilis*; all section *Alatae*). The obtained results represent the currently most comprehensive overview of the plant hormonome during the process of pollen development in plants.

MATERIALS AND METHODS

Plant Material and Growth Conditions

All developmental pollen stages of *Nicotiana tabacum* L. were separately collected during July 2019 and 2020 on the basis of the length of the flower buds including calyx and corolla (Tupý et al., 1983). For *Nicotiana tabacum*, six main stages were obtained: stage 1 (unicellular microspores; 1-UNC) – 13–16 mm; stage 2 (early bicellular pollen; 2-early BC) – 17–21 mm, stage 3 (3-BC) – 26–31 mm, stage 4 (4-BC) – 36–45 mm, stage 5 (late bicellular pollen; 5-BC) – 48–51 mm, and stage 6 (mature pollen grain; MPG) – 52–57 mm. We also collected flower buds with different male gametophyte developmental stages from *N. alata* Link & Otto, *N. langsdorffii* Weinm., and *N. mutabilis* Stehmann & Semir during a whole season and checked them microscopically to select clearly definable stages. Selected developmental stages of *N. alata*, *N. langsdorffii,* and *N. mutabilis* were compared with *N. tabacum*. Only five developmental stages were detected and retained (**Figure 1**). Flower bud lengths and morphology were measured and determined under a Zeiss stereomicroscope (Carl Zeiss, Jena, Germany).

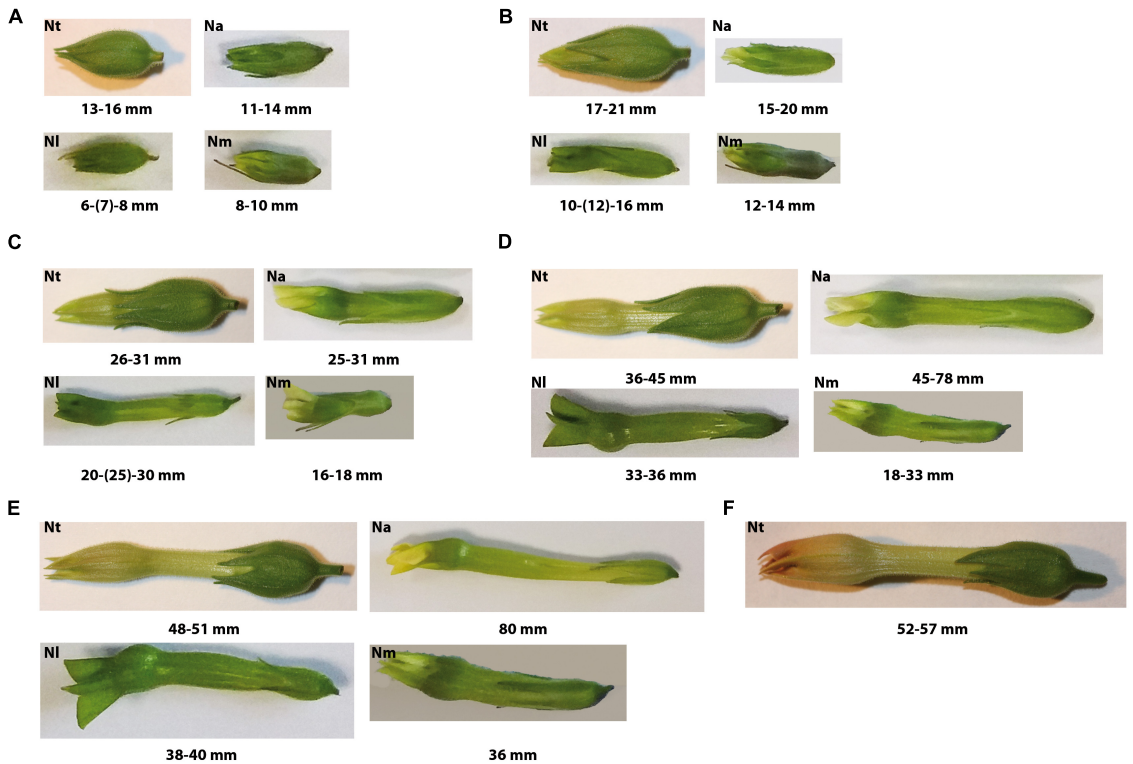

FIGURE 1 | Shape and size of floral buds containing main pollen developmental stages of genus *Nicotiana*: **(A)** Stage 1 – unicellular microspores; **(B)** Stage 2 – early bicellular young vacuolized pollen grains with beginning starch deposition in *N. alata* (Na)*, N. langsdorffii* (Nl) and *N. mutabilis* (Nm) and early bicellular young vacuolized pollen in *N. tabacum* (Nt); **(C)** Stage 3 – middle bicellular pollen in Na, Nl, and Nm and early bicellular pollen with beginning starch deposition in Nt; **(D)** Stage 4 – late bicellular pollen with spindle-shaped generative nucleus in Na, Nl, Nm, and middle bicellular pollen filled with starch in Nt; **(E)** Stage 5 – mature pollen grain in Na, Nl, Nm, and late bicellular pollen with spindle-shaped generative nucleus in Nt; **(F)** Stage 6 – mature pollen grain in Nt.

Freshly isolated anthers from 20 flower buds of particular developmental stage (Tupý et al., 1983) were collected and immediately processed by gentle crushing in a chilled mortar within a 5% sucrose solution. The mixture was vortexed immediately for 20 s to release the pollen grains and filtered through a nylon mesh (approximately 100 μm of pore size) to remove anther debris. The suspended pollen grains were then sedimented by centrifugation (2,000 *g*, 5 min, 4°C), and after decanting excess supernatant were stored at −80°C as described by Matoušek et al. (2020).

Mature pollen grains (MPG) from isolated anthers of flowers 1 day before anthesis (Tupý et al., 1983; Matoušek et al., 2020) were collected daily and were desiccated on filter paper in Petri dish to dehisce overnight at room temperature. Then, MPG were sieved through a nylon mesh to discard anther debris and stored at −80°C.

Pollen Microscopy

Small aliquots of *Nicotiana* spp. pollen of different stages (0.5–1 μL) were resuspended in DAPI staining solution (4′-6-Diamidino-2-phenylindole, Merck KGaA, Darmstadt, Germany) for cell nuclei visualization [16 μL of DAPI stock solution in 10 mL buffer, modified according to Dupľáková et al. (2016)] and Lugol's staining solution for starch grains visualization (3.5% solution: 5 g KI, 2.5 g I, 200 ml 80% ethanol). Bright field and fluorescence (UV light) microscopy were used for checking the particular stage of tobacco pollen and starch content on an inverted fluorescent microscopes Nikon Eclipse TE2000E and Zeiss Axiovert 200M. NIS-Elements (Nikon Imaging Software) and ZEN blue 3.2 (Carl Zeiss, Jena, Germany) software were used to capture images. For each pollen stage, representative images illustrating the shape of nucleus and the starch content are shown (**Figure 2**).

Phytohormone Extraction and Quantification

Endogenous phytohormones were extracted according to Dobrev and Kamínek (2002). Homogenized samples [approximately 100 mg fresh weight (FW)] were incubated in 0.5 mL Bielski extraction buffer (methanol/formic acid/water 15/1/4, v/v/v) with addition of internal standards (10 pmols each) for 1 h at −20°C. After centrifugation (20,000 *g*, 25 min, 4°C), the pellets were re-extracted with an additional 0.5 mL of Bielski buffer for 30 min at 6°C. Samples were concentrated in a vacuum concentrator (Alpha RVC, Christ, Germany), diluted with 0.5 mL of 1 M formic acid and applied to a mixed-mode reversed phase-cation exchange SPE column (Oasis-MCX, Waters, Milford, MA, United States). Two fractions were obtained: (1) fraction A

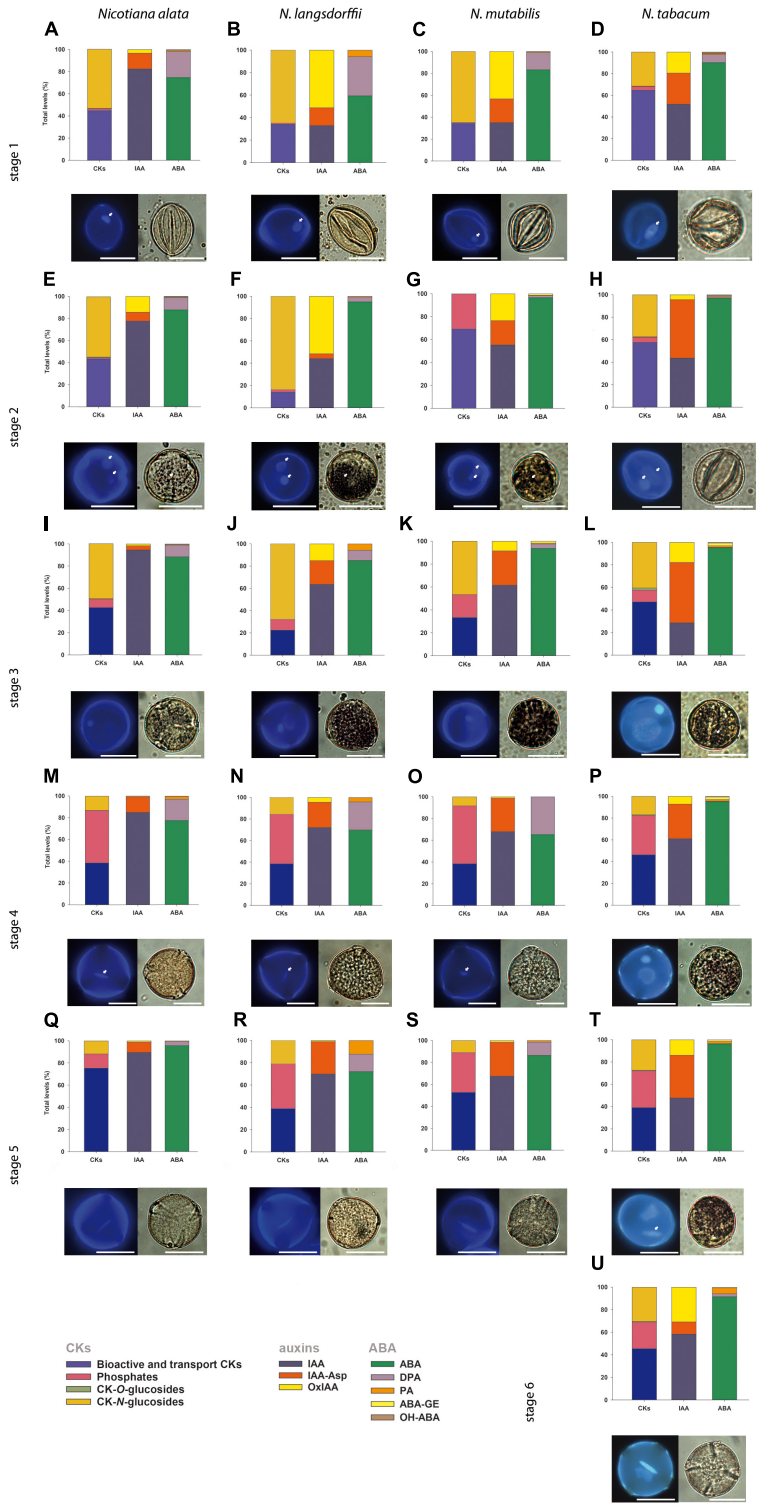

FIGURE 2 | General schematic overview demonstrating the shape of nuclei, starch content and the profiles of phytohormones cytokinins, (CKs), auxins (indole-3-acetic acid, IAA) and abscisic acid (ABA) (together with their derivatives; for specification see lower-left corner of the panel) during pollen development of *Nicotiana alata* **(A,E,I,M,Q)**, *N. langsdorffii* **(B,F,J,N,R)**, *N. mutabilis* **(C,G,K,O,S)**, and *N. tabacum* **(D,H,L,P,T,U)**. The scale is 20 μm. **(A–D)** Stage 1, **(E–H)** stage 2, **(I–L)** stage 3, **(M–P)** stage 4, **(Q–T)** stage 5, **(U)** stage 6. Characterization of individual pollen developmental stages is given in **Figure 1**, proportions of CKs, auxins, and ABA are expressed as a percentage of the total pool. Small white arrows show beginning of starch deposition at stage 2 **(E,F,G)** and at stage 3 **(L)**; one nucleolus in microspores **(A–D)** and generative and vegetative nuclei starting at stage 2 **(E–H)**; and spindle-shaped generative nucleus at stage 4 **(M–O)** and at stage 5 **(T)**.

(eluted with 0.5 mL methanol) containing hormones of acidic and neutral character (IAA, ABA, jasmonates and phenolic compounds); and (2) fraction B (eluted with 0.5 mL 0.35 M NH_4OH in 60% methanol) containing hormones of basic character (CKs). The SPE eluates were evaporated to dryness in a vacuum concentrator. The fraction A was then dissolved in 30 μL 15% of acetonitrile and the fraction B in 30 μL 5% of methanol. An aliquot (10 μL) of each extract was injected on an Ultimate 3000 high-performance liquid chromatograph (Dionex, Bannockburn, IL, United States) coupled to a hybrid triple quadrupole/linear ion trap mass spectrometer (3200 Q TRAP, Applied Biosystems, Foster City, CA, United States) using a multilevel calibration graph with [^{2}H]-labeled internal standards as described previously Dobrev and Vaňková (2012) and Djilianov et al. (2013). Methylthiolated *cis*- and *trans*-zeatin-type CKs (ribosides of *c*Z and *t*Z) were not distinguishable by HPLC-MS due to identical mass spectra and are therefore considered one substance marked in the graph legend as 2MeSZR. Phytohormone levels were recalculated to dry weight because the water content substantially differed during pollen maturation (from 13.25% in mature pollen grains up to 86.2% during pollen development).

RESULTS

Developmental Changes and Starch Accumulation During Pollen Ontogeny of Different *Nicotiana* Species

In *Nicotiana tabacum* (section *Nicotiana*), six stages of pollen development have previously been identified and distinguished on the basis of bud length, flower size and morphology, organelle development, and starch content (Tupý et al., 1983). In contrast, we determined only five developmental stages in *N. alata, N. langsdorffii,* and *N. mutabilis* (section *Alatae*). The variation in flower bud morphology and sizes of all sampled stages (**Figure 1**) were ascertained to the corresponding pollen developmental stage (**Figure 2**). Stage 1 of *Nicotiana tabacum* is characterized by unicellular, mostly polarized microspores before pollen mitosis I (PMI). Early bicellular young vacuolized pollen (stages 2) and early bicellular pollen with beginning starch deposition (stage 3) to middle bicellular pollen (stage 4) contain two nuclei, one generative and one vegetative. The generative nucleus of late bicellular pollen in premature stage 5 begins to elongate in a spindle shape. Stage 6 is represented by a mature pollen grain before anthesis (**Figure 2**). Five main developmental stages were found in the other three species, which probably reflects a faster developmental process during the first mitosis of the microspore (**Figure 2**). Stage 1 is the same as in *N. tabacum*, a unicellular microspore, but the two-celled pollen stage contains two stages of bicellular pollen described as early bicellular pollen with beginning starch deposition and middle bicellular pollen (stages 2 and 3, respectively), followed by elongation and spindle-like formation of the generative nucleus at stage 4 – late bicellular pollen, and stage 5 is the mature pollen just before anthesis.

Due to the evolutionary tendency in higher plants to store material reserves and nutrients during pollen maturation, we visualized starch content in individual *Nicotiana* pollen stages. Together with increasing flower size, the progression of pollen development from microspores to the late bicellular pollen stage and starch accumulation (**Figure 2**) between stages 2 and 5 were found to be species-dependent. In *N. tabacum*, starch accumulation does not occur at stage 2, while it becomes evident at stage 3 and peaks at stage 4. A high starch content is still detectable at stage 5 but not at stage 6. In *N. alata, N. langsdorffii,* and *N. mutabilis*, starch accumulation occurs more rapidly (starch grains are already visible at stage 2) and reaches maxima at stage 3 (**Figure 2**).

Hormonal Profiling During the Pollen Development in Different *Nicotiana* Species

Hormone analysis was performed after dual-mode solid-phase extraction and using an advanced high-performance liquid chromatography tandem mass spectrometry. This procedure allowed the simultaneous and highly reliable identification and quantification of nearly thirty phytohormones, including CKs, auxins, ABA, JA (all together with their various metabolic forms), and the phenolic compounds SA, benzoic acid (BzA), and phenylacetic acid (PAA). The concentrations of these different phytohormones varied considerably within six ontogenetic stages of *Nicotiana tabacum* and five ontogenetic stages of *N. alata, N. langsdorffii,* and *N. mutabilis*, as shown in **Figures 3–7** and **Supplementary Tables 1–4**.

A general schematic overview of the profiles of growth hormones (CKs and auxins) and the most abundant stress hormone ABA (together with its derivatives) during pollen development in different *Nicotiana* species is shown in **Figure 2**. Based on the criteria of biological function/conjugation status, the classical CKs (i.e., excluding methylthiolated derivatives) are classified here into four groups, including (1) bioactive and transport forms (free bases and ribosides, respectively), (2) immediate biosynthetic precursors (phosphates), (3) storage forms (*O*-glucosides), and (4) deactivation forms (*N*-glucosides). Although it is rather difficult to generalize variations in the proportion of particular CK forms in the total CK pool during pollen ontogeny, some clues are worth considering. These include relatively high levels of bioactive and transport CK forms (on average over 40% of total CKs) and the absence or lack of CK *O*-glucosides (less than 0.1% of the total CKs) throughout pollen development in all four species, the abundance of CK phosphates at later developmental stages (on average 48% of total CKs) and their low levels at early stages (6% of total CKs) in all species (except at stage 2 in *N. mutabilis*) and a decreasing trend in the concentrations of CK *N*-glucosides during pollen ontogeny in *N. alata* and *N. langsdorffii* (**Figure 2** and **Supplementary Tables 1–4**) are among the most important.

During pollen development only a relatively narrow spectrum of endogenous indole auxins was detected, including bioactive free indole-3-acetic acid (IAA), its major primary catabolite 2-oxindole-3-acetic acid (OxIAA) and its amino acid conjugate

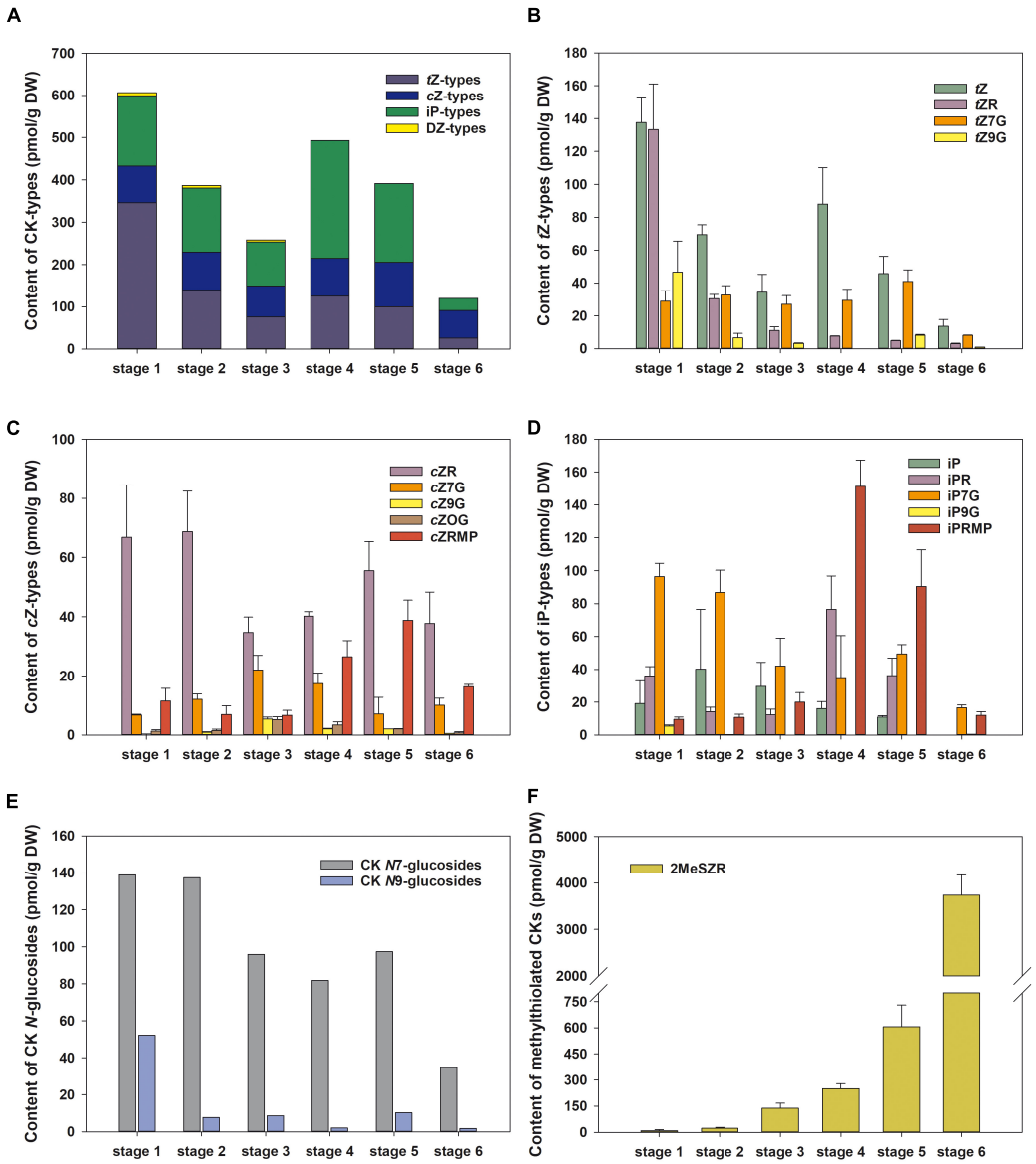

FIGURE 3 | Changes in the content of endogenous cytokinins (CKs) during six developmental stages of *Nicotiana tabacum* pollen. **(A)** Total CKs; **(B)** *trans*-zeatin (*tZ*) types; **(C)** *cis*-zeatin (cZ) types; **(D)** N^6-(Δ^2-isopentenyl)adenine (iP) types; **(E)** CK *N7*- and *N9*-glucosides; **(F)** Methylthiol-types (represented by 2MeSZR).

IAA-aspartate (IAA-Asp; **Figure 2** and **Supplementary Tables 1–4**). Among indole auxins, IAA dominated throughout pollen ontogeny in *N. alata* (averaging over 85% of the total) and at later developmental stages in all other three species. Concentrations of IAA-Asp exceeded those of OxIAA during pollen development of *N. tabacum* (except at stage 6) and at later developmental stages (stages 3–5) of *N. alata*, *N. langsdorffii,* and *N. mutabilis.*

The total pool of ABA metabolites comprised from three (*N. langsdorffii*) to five (*N. alata*, *N. tabacum*) substances, including bioactive ABA itself (**Figure 2** and **Supplementary Tables 1–4**). In all four species, ABA was the predominant form throughout pollen development, accounting for between 86% (*N. alata*) and 96% (*N. tabacum*) of the total pool. Derivatives of ABA accounted for the remaining proportion (from 4 to 14%). Among them, the deactivation product dihydrophaseic acid (DPA) predominated throughout pollen ontogeny in *N. alata*, *N. langsdorffii,* and *N. mutabilis*. In *N. tabacum*, DPA represented the major ABA metabolite at stage 1, while the other catabolite phaseic acid (PA) and the storage form ABA glucosyl ester (ABA-GE) prevailed in later stages (**Figure 2** and **Supplementary Tables 1–4**).

To summarize, our data suggest that CKs, auxins, and ABA derivatives persist predominantly in bioactive forms throughout pollen ontogeny in all four tobacco species. The levels of

bioactive forms, similar to the levels of other metabolites, change dynamically during each developmental stage. This suggests that phytohormones are integrally involved in and rigorously influence the growth and developmental processes of tobacco pollen.

Variations in Phytohormones Contents During Pollen Ontogeny of Different *Nicotiana* Species

Cytokinins

A total of eight to fifteen forms of four classical isoprenoid CKs –N^6-(Δ^2-isopentenyl)adenine (iP), *trans*-zeatin (*t*Z), *cis*-zeatin (*c*Z), and dihydrozeatin (DZ) – were detected during the course of pollen development in individual tobacco species (**Figures 3**, **4** and **Supplementary Tables 1–4**). Concentrations of each CK derivative varied in tobacco pollen from picomoles to hundreds of picomoles per g DW. Interestingly, no CK *O*-glucosides (storage forms of CKs) or only their trace amounts near the detection limit (less than 0.1% of total CKs) were found. In addition to classical CKs, CK methylthioderivatives of zeatin-type (ribosides of *c*Z and *t*Z; designated as 2MeSZR) and iP-type (riboside of iP; 2MeSiPR) occurred in pollen at high concentrations that substantially exceeded the levels of other CKs, especially at later developmental stages (**Figures 3**, **4** and **Supplementary Tables 1–4**).

In *N. tabacum*, the total pool of classical CKs in developing pollen grains was composed of *t*Z (four forms), *c*Z, iP (five forms each), and DZ (one form) derivatives (**Figure 3** and **Supplementary Table 1**). Total concentrations of CKs varied during pollen ontogeny from 119.86 (mature pollen grains; stage 6) to 606.21 pmol/g DW (microspores; stage 1). In addition to the CK maximum in microspores, another peak of CKs was detectable in bicellular pollen grains (stage 4) (**Figure 3A**). The first and most important peak observed at stage 1 in microspores was mainly caused by the maxima of *t*Z-type CKs. Among them, *t*Z and its riboside (*t*ZR) dominated, both appearing at concentrations above 130 pmol/g DW (**Figure 3B**). The iP-types represented the most abundant CKs at later developmental stages, with the exception of stage 6, where the *c*Z-types predominated (**Figures 3C,D**). The second (smaller) maximum of total CKs in *N. tabacum* pollen, detected at stage 4 (493.38 pmol/g DW) can be explained by an increase in N^6-(Δ^2-isopentenyl)adenosine-5′-monophosphate (iPRMP) level (151.31 pmol/g DW), followed by *t*Z and N^6-(Δ^2-isopentenyl)adenosine (iPR). The *c*Z-type CKs were present at moderate levels during the ontogeny of *N. tabacum* pollen (from 65.23 to 105.5 pmol/g DW). In contrast, the sole representative of the DZ-types, DZ-*N*7-glucoside (DZ7G), occurred only in very low amounts in the first three developmental stages (below 7 pmol/g DW) and was not detected in later ones. The content of *N*7-glucosides significantly exceeded that of *N*9-glucosides throughout pollen development (3- to 40-fold) (**Figure 3E**). Interestingly, a progressively increasing accumulation of 2MeSZR was detected during ontogeny of *N. tabacum* pollen (**Figure 3F**).

Total concentrations of CKs in the other three tobacco species varied considerably during pollen development, ranging from 77.84 (*N. mutabilis*, stage 2) to 2933.43 pmol/g DW (*N. alata*, stage 4) (**Figure 4** and **Supplementary Tables 2–4**). In general, *c*Z- and iP-type CKs predominated, followed by *t*Z-types. Similar to *N. tabacum*, the DZ-types represented the least abundant or absent CK forms (**Figures 4A–C**). The total CK pool in the pollen of all three tobacco species reached the characteristic maxima at stage 4, mainly caused by the peaks of the bioactive and phosphate *c*Z and iP forms (**Figures 4D–L**). The spectra of classical CKs in pollen differed among tobacco species and included eight (*N. langsdorffii*), ten (*N. mutabilis*), and fifteen (*N. alata*) derivatives. In analogy to *N. tabacum*, *N*7-glucoside concentrations in *N. alata* significantly exceeded *N*9-glucosides (7- to 35-fold) during pollen development, whereas CK *N*9-glucosides were completely absent in *N. langsdorffii* and *N. mutabilis* pollen (**Figures 4M–O** and **Supplementary Tables 2–4**). Accumulation of methylthiolated CKs (2MeSZR in *N. alata* and both 2MeSZR and 2MeSiPR in *N. langsdorffii* and *N. mutabilis*) had a similar pattern to classical CKs, with maxima at stage 4 (**Figures 4P–R**).

Overall, CK screening during pollen development revealed some trends for classical and methylthiolated CKs that differ between *N. tabacum* and the other three (*N. alata*, *N. langsdorffii*, and *N. mutabilis*) species. Among them, two concentration maxima of the total pool of classical CKs (stages 1 and 4) in *N. tabacum* pollen compared to one peak (stage 4) in the other three species and/or the progressive increase in the content of CK methylthioderivatives during the ontogeny of *N. tabacum* pollen compared to. their maximum accumulation at stage 4 in the other three species are worth mentioning and deserve further attention.

Auxins

Only three endogenous auxins (IAA, OxIAA, and IAA-Asp) were found during pollen ontogeny in all four tobacco species (**Figures 5**, **6** and **Supplementary Tables 1–4**). In *N. tabacum* pollen, total auxin concentrations ranged from 250.52 (mature pollen grains; stage 6) to 1338 pmol/g DW (early bicellular pollen; stage 2). The auxin peak at stage 2 was mainly due to the IAA and IAA-Asp concentration maxima (584.47 and 693.94 pmol/g DW, respectively; **Figure 5A**). In the other tobacco species, the dynamics of total auxin accumulation were similar to those of CKs, with maxima at stage 4 (from 9459.23 in *N. mutabilis* to 24171.9 pmol/g DW in *N. alata*) caused in particular by IAA itself (**Figures 6A–C**). Interestingly, the highest IAA concentrations in pollen of all three species at stage 4 essentially overlapped the IAA maximum observed in *N. tabacum* at stage 2 (11-fold in *N. mutabilis* to 35-fold in *N. alata*). The concentrations of PAA, a phenolic non-indole compound with weak auxin activity, considerably exceeded those of indole auxins and showed analogous dynamics with the maximum at stage 4 in *N. alata*, *N. langsdorffii,* and *N. mutabilis* (**Figures 5E**, **6M–O**).

To conclude, different dynamics of auxin accumulation were observed in the pollen of selected tobacco species, peaking at the earlier stage of development (stage 2) in *N. tabacum* and at the later stage (stage 4) in the other three species.

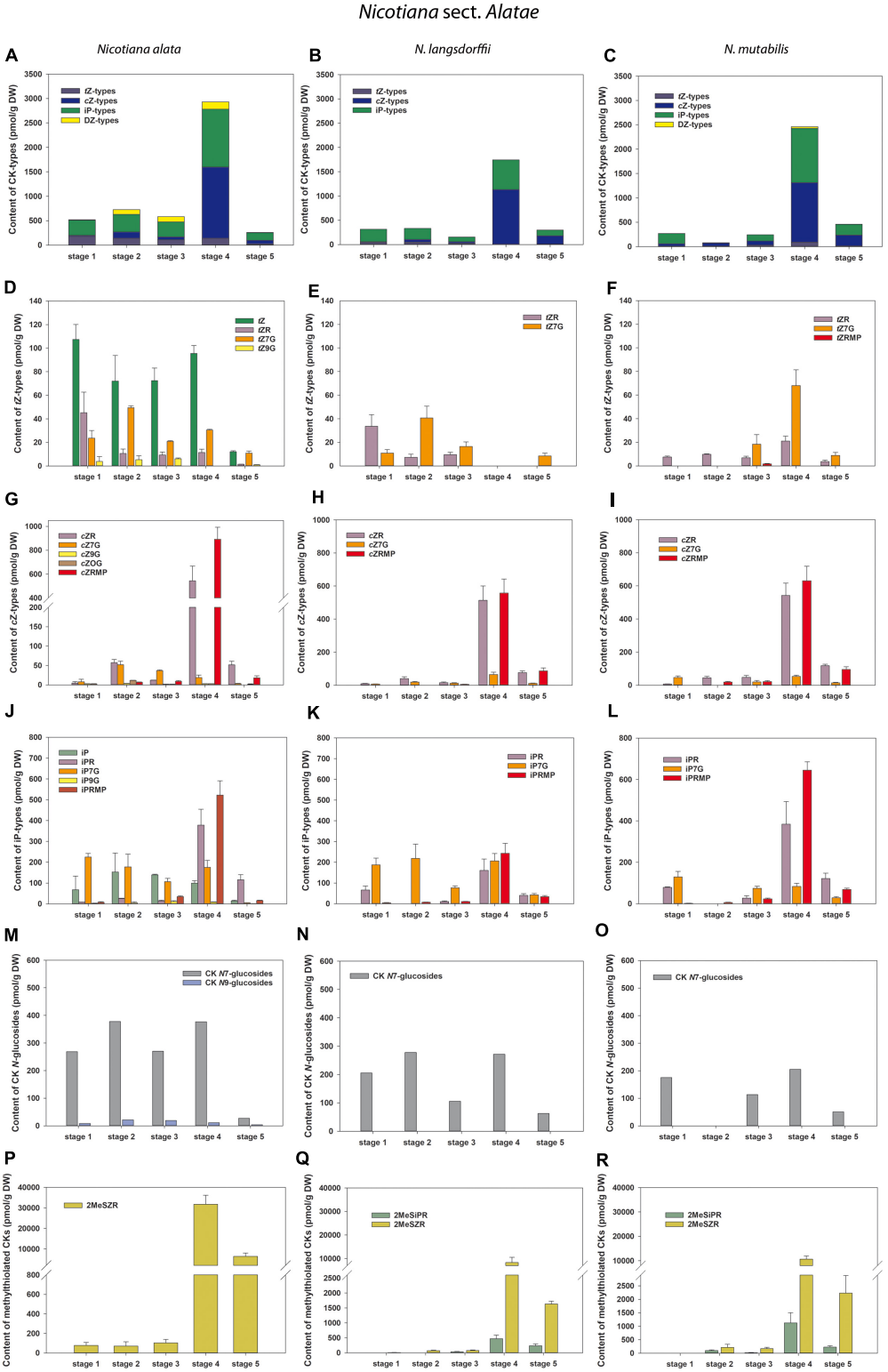

FIGURE 4 | Changes in the content of endogenous cytokinins (CKs) during five developmental stages of *Nicotiana alata* **(A,D,G,J,M,P)**, *N. langsdorffii* **(B,E,H,K,N,Q)**, and *N. mutabilis* **(C,F,I,L,O,R)**. **(A–C)** Total CKs; **(D–F)** *trans*-zeatin (*t*Z) types; **(G–I)** *cis*-zeatin (cZ) types; **(J–L)** N^6-(Δ^2-isopentenyl)adenine (iP) types; **(M–O)** CK *N*7- and *N*9-glucosides; **(P–R)** Methylthiol-types (represented by 2MeSZR and 2MeSiPR).

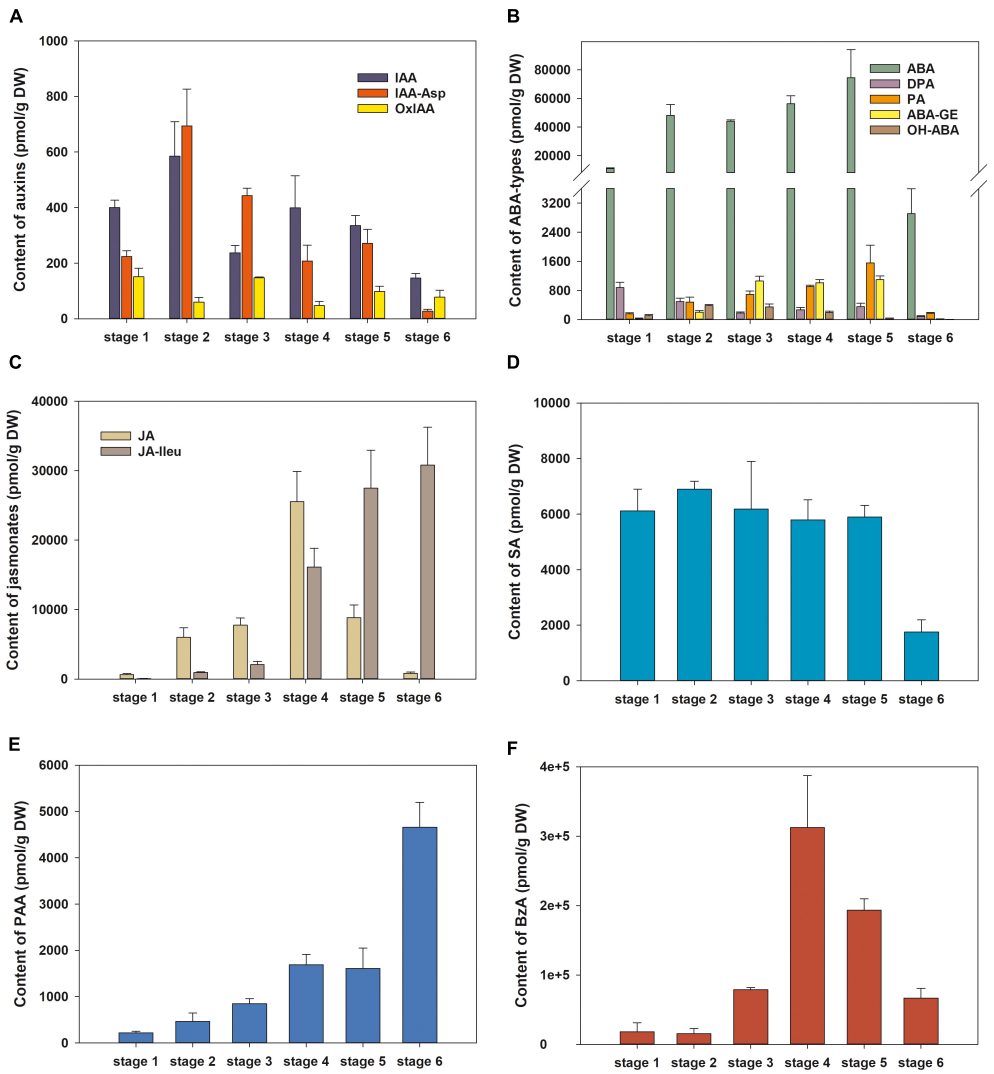

FIGURE 5 | Changes in the content of endogenous auxins, ABA and its derivatives, jasmonates and phenolic compounds during six developmental stages of *Nicotiana tabacum* pollen. **(A)** Auxins (IAA, indole-3-acetic acid; IAA-Asp, IAA-aspartate; OxIAA, 2-oxindole-3-acetic acid); **(B)** Abscisic acid (ABA) types [DPA, dihydrophaseic acid; PA, phaseic acid; (ABA-GE), ABA glucosyl ester; OH-ABA, 9-hydroxy-ABA]; **(C)** Jasmonates (JA, jasmonic acid; JA-Ileu, JA-isoleucine); **(D–F)** Phenolic compounds (**D** SA, salicylic acid; **E** PAA, phenylacetic acid; **F** BzA, benzoic acid).

Stress Hormones (Abscisic Acid, Jasmonates)

Abscisic acid was present at relatively high concentrations throughout pollen development of all four tobacco species, ranging from 663.72 (*N. langsdorffii* at stage 1) to 74563.27 pmol/g DW (*N. tabacum* at stage 5) (**Figures 5**, **6** and **Supplementary Tables 1**–**4**). In *N. tabacum* pollen, an increasing trend of ABA content until stage 5 and its subsequent dramatic decrease at stage 6 (over 25-fold) were observed (**Figure 5B**). In the other three species, the ABA contents reached the concentration maxima at stage 2 (between 21028.12 and 30476.93 pmol/g DW in *N. langsdorffii* and *N. mutabilis*, respectively), and then decreased (9- to 16-fold) until stage 5 (**Figures 6D**–**F**).

In addition, several ABA derivatives were detected during tobacco pollen ontogeny. These included the deactivation products DPA and PA (in all four species), the storage form ABA-GE (except in *N. langsdorffii*) and another physiologically inactive ABA catabolite, 9-hydroxy-ABA (9OH-ABA) (only in *N. tabacum* and *N. alata*). However, their concentrations were substantially lower than those of ABA itself (10-fold on average), and no clear trends in their dynamics across pollen development were observed that could be generalized.

Jasmonates were detected in a wide range of concentrations during pollen development in all four tobacco species (**Figures 5**, **6** and **Supplementary Tables 1**–**4**). Jasmonic acid (JA) and its active conjugate, JA-isoleucine (JA-Ileu), represented the

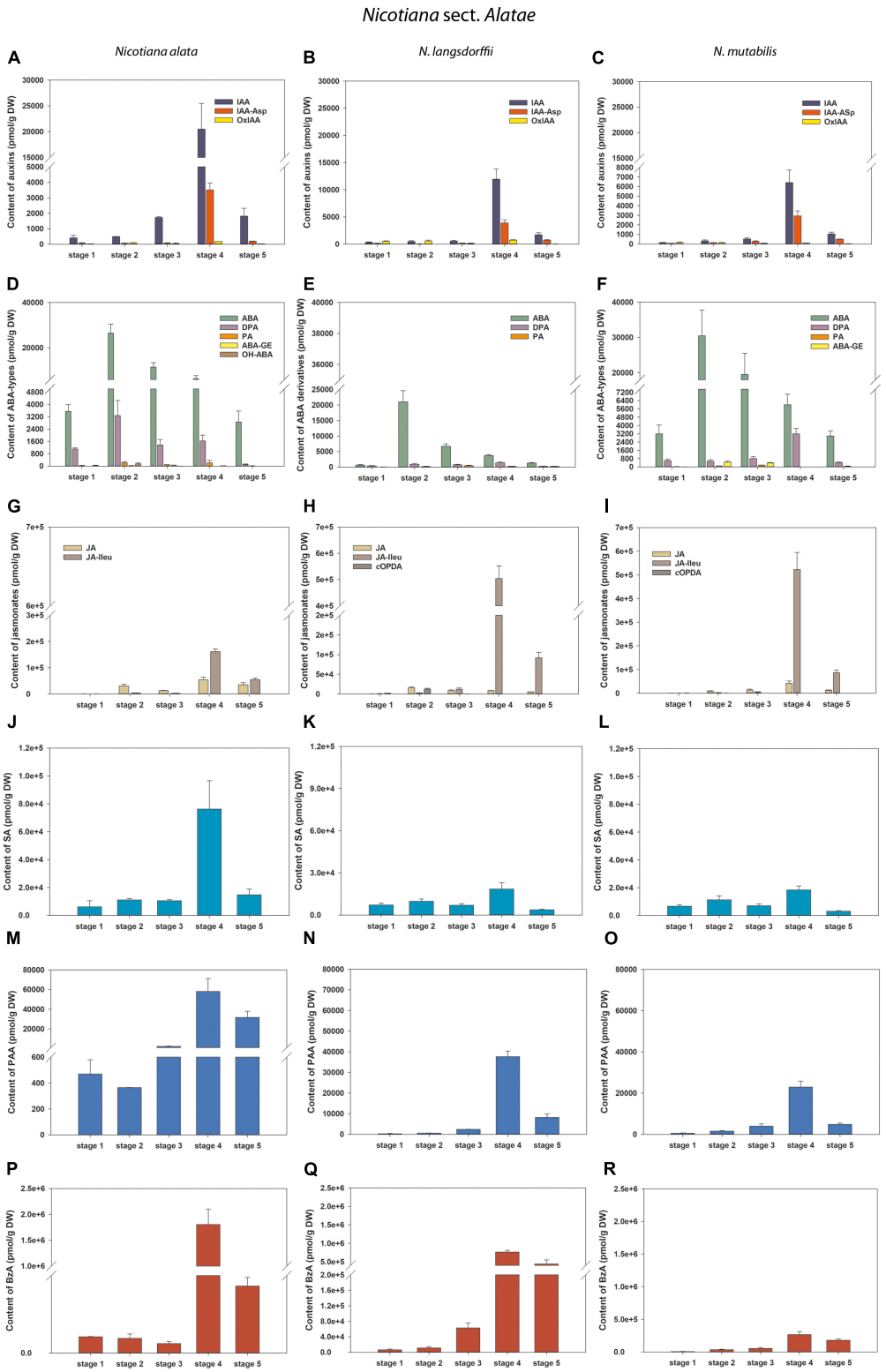

FIGURE 6 | Changes in the content of endogenous auxins, ABA and its derivatives, jasmonates and salicylic acid during five developmental stages of *Nicotiana alata* **(A,D,G,J,M,P)**, *N. langsdorffii* **(B,E,H,K,N,Q)**, and *N. mutabilis* **(C,F,I,L,O,R)** pollen. **(A–C)** Auxins (IAA, indole-3-acetic acid; IAA-Asp, IAA-aspartate; OxIAA, 2-oxindole-3-acetic acid); **(D–F)** Abscisic acid (ABA) types [DPA, dihydrophaseic acid; PA, phaseic acid; (ABA-GE), ABA glucosyl ester; OH-ABA, 9-hydroxy-ABA]; **(G–I)** Jasmonates [JA, jasmonic acid; JA-Ileu, JA-isoleucine; cOPDA, *cis*-(+)-12-oxo-phytodienoic acid]; **(J–L)** Salicylic acid (SA); **(M–O)** Phenylacetic acid (PAA); **(P–R)** Benzoic acid (BzA).

most conspicuous derivatives. In addition, small amounts of the JA precursor, *cis*-(C)-12-oxo-phytodienoic (*c*OPDA), were found at earlier developmental stages of *N. langsdorffii* and *N. mutabilis*. In *N. tabacum*, total jasmonate levels ranged from 705.44 (microspores; stage 1) to 41619.42 pmol/g DW (middle bicellular pollen; stage 4). The concentration of JA significantly exceeded that of JA-Ileu at the earlier developmental stages, with the maximum JA values recorded at stage 4 (25511.39 pmol/g DW). In contrast, a progressively increasing accumulation of JA-Ileu was observed until stage 6 (30795.9 pmol/g DW) (**Figure 5C**).

The highest amounts of jasmonates in the pollen of the other three tobacco species were detected at stage 4 (**Figures 6G–I**). The maxima (from 215176.3 in *N. alata* to 564432.26 pmol/g DW in *N. mutabilis)* were caused mainly by JA-Ileu concentrations significantly exceeding the value of JA (3- to 61-fold in *N. alata* and *N. langsdorffii*, respectively).

To sum up, the dynamics in the accumulation of stress hormones (ABA-types and jasmonates) during pollen ontogeny differed significantly between *N. tabacum* and the other three species (*N. alata*, *N. langsdorffii,* and *N. mutabilis*).

Phenolic Compounds

Three phenolic compounds, SA, BzA, and PAA, were abundant in the pollen of all four tobacco species, with extremely high levels in *N. alata* (**Figures 5**, **6** and **Supplementary Tables 1–4**). In all, BzA concentrations substantially exceeded SA and PAA throughout ontogeny.

The dynamics of each of the three phenolics differed significantly during pollen development in *N. tabacum*. While SA appeared in relatively high amounts from stage 1 to stage 5 (in the range 5796.62 and 6895.33 pmol/g DW) and then decreased at stage 6 (about 3.5-fold), the accumulation of PAA gradually increased (from 219.54 at stage 1 to 4656.99 pmol/g DW at stage 6), and BzA clearly peaked at stage 4 (312682.51 pmol/g DW) (**Figures 5D–F**). In contrast, the same trends in the dynamics of phenolic compounds with concentration maxima at stage 4 were observed in the pollen of the other three tobacco species (**Figures 6J–R**). Interestingly, PAA, which can also be categorized as a weak non-indole auxin, had similar dynamics to the indole auxins IAA and OxIAA in *N. alata*, *N. langsdorffii,* and *N. mutabilis* pollen (**Figures 6A–C,M–O**).

Overall, the dynamics of the analyzed phenolic compounds across pollen development, analogous to growth and stress hormones, were significantly different between *N. tabacum* and the other three tobacco species.

DISCUSSION

The function of phytohormones in the control of seed plant growth and development is well known (Taiz and Zeiger, 2002), but there is limited knowledge (e.g., Hirano et al., 2008; Song et al., 2013) about their involvement in pollen development. In this work, a number of phytohormone groups were detected in developing pollen grains in four *Nicotiana* species. We characterized the profiles and dynamics of specific phytohormone forms in individual pollen developmental stages to postulate how they might be involved in regulating male gametophyte development.

Following the work of Tupý et al. (1983), we recognized six developmental stages in *Nicotiana tabacum* pollen. In contrast, only five developmental stages of pollen-based morphological characteristics of flowers, organelle development and starch content were distinguished in *N. alata, N. langsdorffii,* and *N. mutabilis* (**Figure 1**). The differences in pollen ontogeny between *N. tabacum* and the other three tobacco species reflect a different phylogeny of the genus *Nicotiana*. This genus, comprising approximately 75 species, 40 diploids, and 35 allopolyploids, displays a range of diverse genomic changes (including gene conversion, tandem and dispersed sequence evolution, intergenomic translocations, dysploidy, polyploidy, etc., Clarkson et al., 2004). Whereas *N. tabacum* belongs to section *Nicotiana* with a basic chromosome number $n = 24$, the other species analyzed in our study belong to section *Alatae* with $n = 10$ (Clarkson et al., 2004). Similarly, there is a slight shift during pollen ontogeny in other *Nicotiana* species, such as *Nicotiana benthamiana* ($n = 16$) from section *Suaveolentes* (Steinbachová et al., in preparation).

Endogenous phytohormones and their dynamics were closely related to pollen ontogenesis in all four tobacco species. We found that CKs, auxins and ABA-type derivatives were present mainly in bioactive forms throughout pollen development (**Figure 2**). This confirms that pollen ontogenesis is a highly active process (Bedinger, 1992) under hormonal control.

Transcriptome analyses in pollen of *Arabidopsis* (Honys and Twell, 2004) and *N. tabacum* (Bokvaj et al., 2015) showed that all major components of the core cell cycle machinery are expressed at stage 1, the microspores, and their expression generally decreases during pollen development. However, phytohormone-related genes are expressed in a continuously increasing manner during pollen maturation (Záveská Drábková et al., in preparation), which is analogous to the concentration dynamics of numerous hormone derivatives shown here. Moreover, many transcripts have been found to persist in mature pollen (Chambers and Shuai, 2009; Grant-Downton et al., 2009). In this work, the levels of some hormones such as 2MeSZR, JA-Ileu and PAA in *N. tabacum* showed a similar trend, increasing progressively and reaching maxima at stage 6.

In general, there are two prominent maxima in the sum of phytohormones in all four *Nicotiana* species during their pollen development, a major one at stage 4 and a minor one at stage 2 (**Supplementary Figure 1**). These two maxima correspond well with the beginning and the end of the accumulation of starch and other material reserves. As for the differences in pollen ontogeny, the onset of starch accumulation is later in *N. tabacum* compared to *N. alata*, *N. langsdorffii,* and *N. mutabilis* (**Figure 2**). Moreover, the transition from polarized microspores (stage 1) after asymmetric division during pollen mitosis I (PMI) to binucleate pollen (stage 2) represents a critical moment in male gametophyte development (Hafidh et al., 2016), which is essential for determining germ cell fate (Hackenberg and Twell, 2019).

There are few and scattered reports on the role of CKs in male gametophyte development. Hirano et al. (2008) showed

that synthesis of CKs occurs preferentially during the early developmental stage of rice pollen and that bioactive CKs are deactivated by cytokinin oxidase/dehydrogenase (CKX) in the later ontogenic stages. In *N. tabacum* pollen, most classical CKs were correspondingly present at stage 1, although another smaller peak was also found at stage 4 (**Figure 3**). In contrast, only one CK maximum was found at stage 4 in the other three species (**Figure 4**). However, it is not possible to compare our results on tobacco with those of Hirano et al. (2008) on rice because only microspores and late pollen were included in their study. Relatively high contents of bioactive and transport CK forms, CK phosphates and *N*-glucosides (mainly *N*7-glucosides) and, on the other hand, the absence or lack of CK *O*-glucosides represented the most typical features of developing pollen in all four tobacco species (**Figure 2**). Accordingly, no CK *O*-glucosides were detected in *N. tabacum* chloroplasts (Benková et al., 1999), while CK *N*-glucosides represented the predominant CK forms in *N. tabacum* shoots (Gelová et al., 2018) and leaves (Uzelac et al., 2016).

In general, *t*Z- and iP-type CKs predominated throughout the pollen development of *N. tabacum* whereas *c*Z- and iP-types prevailed in the other three tobacco species. CKs of DZ-type were completely absent in the developing pollen of *N. langsdorffii* as well as in three stages of pollen ontogeny of *N. tabacum* and two of *N. mutabilis* (**Figures 3A**, **4A–C** and **Supplementary Tables 1–4**). The absence of DZ-types has also been observed in anthers of rice (Hirano et al., 2008), and the lack of these CK-types appears to be characteristic of some evolutionarily older non-vascular plants (e.g., Stirk et al., 2003; Záveská Drábková et al., 2015; Žižková et al., 2017). In *Arabidopsis* seedlings, Hošek et al. (2020) showed that DZ-type CKs are metabolically independent of other CK metabolic pathways, indicating their low abundance (e.g., Pokorná et al., 2021) compared with iP- or *t*Z-types, which might also be related to tobacco pollen.

In addition to classical CKs, hormonal analysis of tobacco pollen ontogeny revealed high levels of CK methylthioderivatives represented by 2MeSZR in all four species and 2MeSiPR in *N. langsdorffii* and *N. mutabilis* (**Figures 3F**, **4P–R** and **Supplementary Tables 1–4**). To our knowledge, the methylthiolated CKs were detected here for the first time in developing pollen grains. Their accumulation differed markedly between *N. tabacum* and the other three species. While the levels of CK methylthioderivatives increased progressively during ontogeny of *N. tabacum* with a maximum at stage 6, they peaked (analogous to classical CKs) at stage 4 in *N. alata, N. langsdorffii*, and *N. mutabilis.* This suggests increasing *t*RNA turnover at stage 4 in the latter three species, as methylthiol-type CKs are known to arise exclusively *via* the *t*RNA degradation pathway (Tarkowski et al., 2010; Gibb et al., 2020). It also agrees well with the findings of Tupý (1982) that during pollen maturation, gene expression activity decreases, mRNA dissociates from ribosomes, and the uptake capacity of pollen grains further increases, indicating active utilization of metabolites released from the degenerating tapetal cytoplasm. Kambhampati et al. (2017) reported that high levels of methylthiolated *t*Z(R) could positively affect seed filling and yield formation, which was supported by the observation that methylthiol types can interact with CK receptors to trigger growth responses in plants (Daudu et al., 2017).

Auxin plays an important role in both early and late pollen development (Cecchetti et al., 2008; Chen and Zhao, 2008). The authors suggested that auxin is preferentially synthesized in anthers of *Arabidopsis* plants. Auxin appears to be involved in the coordination of pollen development and maturation by regulating cell cycle entry, controlling dehiscence and stamen filament growth (Cecchetti et al., 2008). In addition, two auxin response transcription factors ARF6 and ARF8 have been found to act redundantly in *Arabidopsis* floral organ development, in part by inducing the production of JA or reducing the conjugation or degradation of JA, which regulates anther dehiscence and flower opening (Nagpal et al., 2005).

Determination of endogenous auxin levels during *Arabidopsis* pollen development (Dupľáková et al., 2016) revealed relatively low concentrations of auxin metabolites (no more than 30 pmol/g FW). This is in contrast to our analyzed tobacco pollen samples, where auxin concentrations were mainly in the range of hundreds to thousands of picomoles per g FW (**Figures 5A**, **6A–C** and **Supplementary Tables 1–4**). In both *Arabidopsis* and tobacco pollen, IAA, IAA-Asp, and OxIAA contributed to the total auxin pool. On the other hand, some auxin metabolites, such as OxIAA-glucose ester and the auxin precursor indole-3-acetonitrile, found in *Arabidopsis* were not detected during tobacco pollen ontogeny. These results suggest that unequal levels of endogenous auxins and the presence of specific auxin derivatives may be characteristic of pollen development in different phylogenetic plant groups.

The dynamics of auxin accumulation in pollen of selected tobacco species with maxima at the earlier stage of development (stage 2) in *N. tabacum* and at the later stage (stage 4) in the other three species seems to reflect their different phylogenetic positions and the origin as well (see below). The concentration of PAA, a non-indole phenolic compound with weak auxin activity, had the same trajectory as indole auxins (peak at stage 4) in *N. alata*, *N. langsdorffii,* and *N. mutabilis* but not in *N. tabacum* pollen. Interestingly, the identical dynamics of indole auxins and PAA accumulation have also been demonstrated in other developmental processes in plants, such as somatic embryogenesis of conifers (Vondráková et al., 2018).

Pollen desiccation is an internal stress-like process in pollen formation (Reňák et al., 2014), and pollen grains are likely exposed to water stress conditions at some point during dehydration (Pacini and Dolferus, 2019). Thus, stress hormones play an essential role in pollen development. Free ABA and proline were analyzed in intact anthers and isolated pollen grains of *N. tabacum*, and variations in their patterns during pollen maturation were evaluated (Chibi et al., 1995). In contrast to our results, no conjugated forms of ABA were detected. The maximum accumulation of free ABA throughout the anthers occurred at the mid-binucleate stage when nearly 95% of ABA was located in the pollen (Chibi et al., 1995). This ABA distribution was not observed in the microspores or mature stages of the anthers, where the sporophytic tissues yielded more ABA than the pollen (Chibi et al., 1995). In

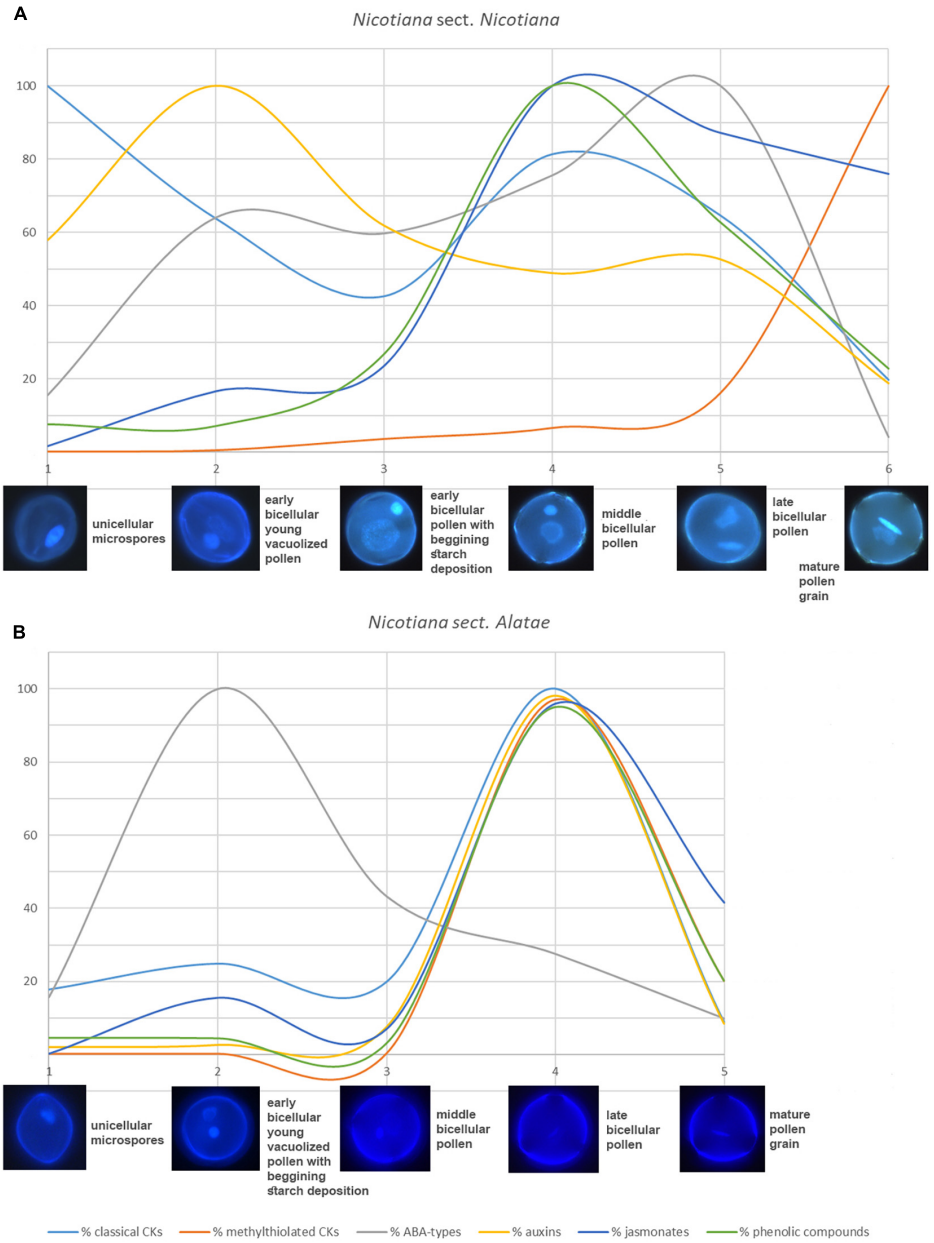

FIGURE 7 | General summary of changes and schematic representation of different trends in all analyzed phytohormone levels between **(A)** *Nicotiana* sect. *Nicotiana* (*Nicotiana tabacum*) and **(B)** *Nicotiana* sect. *Alatae* (*N. alata, N. langsdorffii*, and *N. mutabilis* that showing same trends). Different colors represent percentage of particular phytohormones [light blue – classical cytokinins, red – methylthiolated cytokinins, gray – abscisic acid (ABA) types, yellow – auxins, dark blue – jasmonates, green – phenolic compounds].

our work, ABA itself represented the predominant metabolite throughout pollen ontogeny, with concentration maxima at developmental stage 5 in *N. tabacum* and at stage 2 in the other three species, followed by deactivation products (DPA, PA) and the storage form (ABA-GE), which, however, occurred at much lower concentrations (**Figures 5B**, **6D–F** and **Supplementary Tables 1–4**).

Jasmonates are important regulators in plant development and response to biotic and abiotic stresses (Wasternack and Hause, 2013). An essential role of jasmonates in stamen and pollen maturation has been shown in *Arabidopsis* (Mandaokar et al., 2006), mediated by the induction of flower-specific MYB transcription factors (Yang et al., 2007). In our study, JA and its active conjugate JA-Ileu were the most prominent jasmonates detected during pollen development in all four tobacco species (**Figures 5C**, **6G–I** and **Supplementary Tables 1–4**). In *N. tabacum* pollen, the highest concentration of JA was detected at developmental stage 4, corresponding

with its requirement for male fertility and many aspects of flower and pollen development (Wilson and Zhang, 2009). High levels of JA localized in rice anthers, with microspores/pollen functioning cell-autonomously, were reported by Hirano et al. (2008). For JA-Ileu, our work found a progressively increasing accumulation up to stage 6 in *N. tabacum* and a peak at stage 4 in *N. alata*, *N. langsdorffii,* and *N. mutabilis*, respectively. Biologically active JA derivatives derived from isoleucine and tyramine have also been identified in the pollen of *Pinus mugo* and *Petunia hybrida* (Knöfel and Sembdner, 1995; Miersch et al., 1998). They have been shown to inhibit pollen germination and pollen tube elongation to maintain pollen dormancy (Yamane et al., 1982; Knöfel and Sembdner, 1995).

Three phenolic compounds, SA, BzA, and PAA were detected during pollen ontogeny in all four tobacco species. Among them, SA represents an important component in the regulation of plant defense, growth, and development (Yan and Dong, 2014). Although little information exists on the role of phenolics in pollen development, Rong et al. (2016) reported the regulation of pollen tip growth by SA in the *Arabidopsis* pollen tube model system. In our study, the same trends in the dynamics of SA, BzA, and PAA with concentration maxima at stage 4 were found for *N. alata*, *N. langsdorffii,* and *N. mutabilis*. In contrast, the dynamics of the three phenolics differed significantly during pollen development of *N. tabacum*.

Analogous to CKs and auxins, the concentration dynamics of stress hormones (ABA-types, jasmonates, SA) and other phenolic compounds differed significantly during pollen development between *N. tabacum* (section *Nicotiana*) and *N. alata*, *N. langsdorffii,* and *N. mutabilis* (section *Alatae*).

A general summary of changes and schematic representation of different trends in all analyzed phytohormone levels between *N. tabacum* and the other three tobacco species is shown in **Figure 7**. It clearly demonstrates the same tendencies in accumulation of analyzed phytohormones for all three *Alatae* representatives with the highest levels in the late bicellular pollen (stage 4). The only exception to this generalization is ABA-types reaching the maxima in early bicellular pollen (stage 2). In contrast, the same uniformity in phytohormone dynamics does not occur in *N. tabacum* representing the section *Nicotiana* (**Figure 7** and **Supplementary Figure 2**). The mismatched dynamics in the accumulation of endogenous phytohormones, demonstrated during pollen ontogeny between *N. tabacum* and the other three species, reflect the different phylogenetic position and origin within the genus *Nicotiana* (Clarkson et al., 2004). The section *Nicotiana* is phylogenetically younger than the section *Alatae*. Moreover, *N. tabacum* is a hybrid allotetraploid between two species differing in their phylogenetic history, *Nicotiana sylvestris* (belonging to phylogenetically younger section *Sylvestres*) and *Nicotiana tomentosiformis* (phylogenetically older section *Tomentosae*; **Supplementary Figure 2**). This fact should be taken into consideration when assessing different hormonal trends of selected tobacco representatives during pollen development, making the story even more complex.

CONCLUSION

The profiles and dynamics of phytohormones were characterized during the process of microgametogenesis in four *Nicotiana* species (*N. tabacum*, *N. alata*, *N. langsdorffii,* and *N. mutabilis*). Taking advantage of advanced HPLC-ESI-MS/MS, we identified twenty to thirty endogenous hormone derivatives, including CKs, auxins, ABA, and its derivatives, jasmonates and phenolic compounds, and tracked their concentration changes throughout pollen development.

Interestingly, all three species of the section *Alatae* have shown the same trend of all measured phytohormones with concentration maxima in the late bicellular pollen (stage 4), except for ABA-types peaking in early bicellular pollen (stage 2). On the contrary, we did not reveal the same uniformity in phytohormone dynamics in *N. tabacum* representing the section *Nicotiana* (**Figure 7**), which strongly reflected a different origin of representatives of the two *Nicotiana* sections.

To our knowledge, this work represents the most comprehensive review of plant hormones during the process of pollen development currently available, and evidence for the involvement of certain phytohormone forms, such as *cZ*- and methylthiol-type CKs, ABA derivatives, PAA and BzA, in pollen ontogeny has been provided for the first time here.

DATA AVAILABILITY STATEMENT

The original contributions presented in the study are included in the article/**Supplementary Material**, further inquiries can be directed to the corresponding authors.

AUTHOR CONTRIBUTIONS

LZD conceived and designed the experiments. LZD, EP, and PD performed the experiments. LZD and EP analyzed the data. JK, LS, and LZD performed microscopic observations and documentation. LZD, EP, VM, and DH wrote the manuscript. All authors have read the manuscript and approved it for submission.

FUNDING

The authors gratefully acknowledge the financial support from the Czech Science Foundation (Nos. 19-02699S and 19-12262S) and the Ministry of Education, Youth and Sports of the Czech Republic from European Regional Development Fund-Project "Centre for Experimental Plant Biology" (No. CZ.02.1.01/0.0/0.0/16_019/0000738).

ACKNOWLEDGMENTS

We thank Josef Lacek for mass spectrometer data processing and Marie Korecká for superb technical assistance, and Martina

Snášelová and Mikuláš Honys for help with pollen harvesting. We are grateful to two reviewers for their constructive comments and suggestions, which helped us to substantially improve the manuscript.

SUPPLEMENTARY MATERIAL

The Supplementary Material for this article can be found online at: https://www.frontiersin.org/articles/10.3389/fpls.2021.735451/full#supplementary-material

Supplementary Figure 1 | Changes in the sum of phytohormones during pollen development of *Nicotiana tabacum* **(A)**, *N. alata* **(B)**, *N. langsdorffii* **(C)**, and *N. mutabilis* **(D)**. The total pool of phytohormones includes auxins, abscisic acid (ABA) and its derivatives, cytokinins (CKs), salicylic acid (SA), and jasmonates (JA).

Supplementary Figure 2 | Summary of phylogenetic relationships of the genus *Nicotiana* diploid based on plastid and nuclear markers with hybrid origin of *Nicotiana tabacum.* Modified and adapted from Clarkson et al. (2004).

Supplementary Table 1 | Concentrations (pmol/g DW) of endogenous phytohormones during six developmental stages of *Nicotiana tabacum* pollen.

Supplementary Table 2 | Concentrations (pmol/g DW) of endogenous phytohormones during five developmental stages of *Nicotiana alata* pollen.

Supplementary Table 3 | Concentrations (pmol/g DW) of endogenous phytohormones during five developmental stages of *Nicotiana langsdorffii* pollen.

Supplementary Table 4 | Concentrations (pmol/g DW) of endogenous phytohormones during five developmental stages of *Nicotiana mutabilis* pollen.

REFERENCES

Bedinger, P. (1992). The remarkable biology of pollen. *Plant Cell* 4, 879–887. doi: 10.1105/tpc.4.8.879

Benková, E., Witters, E., Van Dongen, W., Kolář, J., Motyka, V., Brzobohatý, B., et al. (1999). Cytokinins in tobacco and wheat chloroplasts, occurrence and changes due to light/dark treatment. *Plant Physiol.* 121, 245–251. doi: 10.1104/pp.121.1.245

Berger, F., and Twell, D. (2011). Germline specification and function in plants. *Ann. Rev. Plant Biol.* 62, 461–484. doi: 10.1146/annurev-arplant-042110-103824

Bokvaj, P., Hafidh, S., and Honys, D. (2015). Transcriptome profiling of male gametophyte development in *Nicotiana tabacum*. *Genom. Data* 3, 106–111. doi: 10.1016/j.gdata.2014.12.002

Borg, M., and Twell, D. (2010). Life after meiosis: patterning the angiosperm male gametophyte. *Biochem. Soc. Trans.* 38, 577–582. doi: 10.1042/BST0380577

Cecchetti, V., Altamura, M. M., Falasca, G., Costantino, P., and Cardarelli, M. (2008). Auxin regulates *Arabidopsis* anther dehiscence, pollen maturation, and filament elongation. *Plant Cell* 20, 1760–1774. doi: 10.1105/tpc.107.057570

Cecchetti, V., Brunetti, P., Napoli, N., Fattorini, L., Altamura, M. M., Costantino, P., et al. (2015). ABCB1 and ABCB19 auxin transporters have synergistic effects on early and late *Arabidopsis* anther development. *J. Integr. Plant Biol.* 57, 1089–1098. doi: 10.1111/jipb.12332

Cecchetti, V., Celebrin, D., Napoli, N., Ghelli, R., Brunetti, P., Costantino, P., et al. (2017). An auxin maximum in the middle layer controls stamen development and pollen maturation in *Arabidopsis*. *New Phytol.* 213, 1194–1207. doi: 10.1111/nph.14207

Chambers, C., and Shuai, B. (2009). Profiling microRNA expression in *Arabidopsis* pollen using microRNA array and real-time PCR. *BMC Plant Biol.* 9:87. doi: 10.1186/1471-2229-9-87

Chen, D., and Zhao, J. (2008). Free IAA in stigmas and styles during pollen germination and pollen tube growth of *Nicotiana tabacum*. *Physiol. Plant.* 134, 202–215. doi: 10.1111/j.1399-3054.2008.01125.x

Chhun, T., Aya, K., Asano, K., Yamamoto, E., Morinaka, Y., Watanabe, M., et al. (2007). Gibberellin regulates pollen viability and pollen tube growth in rice. *Plant Cell* 19, 3876–3888. doi: 10.1105/tpc.107.054759

Chibi, F., Angosto, T., and Matilla, A. (1995). Variations of the patterns of abscisic acid and proline during maturation of *Nicotiana tabacum* pollen grains. *J. Plant Physiol.* 147, 355–358. doi: 10.1016/S0176-1617(11)82167-X

Clarkson, J. J., Knapp, S., Garcia, V. F., Olmstead, R. G., Leitch, A. R., and Chase, M. W. (2004). Phylogenetic relationships in *Nicotiana* (Solanaceae) inferred from multiple plastid DNA regions. *Mol. Phylogenet. Evol.* 33, 75–90. doi: 10.1016/j.ympev.2004.05.002

Daudu, D., Allion, E., Liesecke, F., Papon, N., Courdavault, V., de Bernonville, T. D., et al. (2017). CHASE-containing histidine kinase receptors in apple tree: from a common receptor structure to divergent cytokinin binding properties and specific functions. *Front. Plant Sci.* 8:1614. doi: 10.3389/fpls.2017.01614

Ding, Z. J., Wang, B. J., Moreno, I., Dupl'áková, N., Simon, S., Carraro, N., et al. (2012). ER-localized auxin transporter PIN8 regulates auxin homeostasis and male gametophyte development in *Arabidopsis*. *Nat. Commun.* 3:941. doi: 10.1038/ncomms1941

Djilianov, D. L., Dobrev, P. I., Moyankova, D. P., Vaňková, R., Georgieva, D. T., Gajdošová, S., et al. (2013). Dynamics of endogenous phytohormones during desiccation and recovery of the resurrection plant species *Haberlea rhodopensis*. *J. Plant Growth Regul.* 32, 564–574. doi: 10.1007/s00344-013-9323-y

Dobrev, P. I., and Kamínek, M. (2002). Fast and efficient separation of cytokinins from auxin and abscisic acid and their purification using mixed-mode solid-phase extraction. *J. Chromatogr. A* 950, 21–29. doi: 10.1016/S0021-9673(02)00024-9

Dobrev, P. I., and Vaňková, R. (2012). Quantification of abscisic acid, cytokinin, and auxin content in salt-stressed plant tissues. *Methods Mol. Biol.* 913, 251–261. doi: 10.1007/978-1-61779-986-0_17

Dupl'áková, N., Dobrev, P. I., Reňák, D., and Honys, D. (2016). Rapid separation of *Arabidopsis* male gametophyte developmental stages using a Percoll gradient. *Nat. Protoc.* 11, 1817–1832. doi: 10.1038/nprot.2016.107

Gelová, Z., ten Hoopen, P., Novák, O., Motyka, V., Pernisová, M., Dabravolski, S., et al. (2018). Antibody-mediated modulation of cytokinins in tobacco: organ-specific changes in cytokinin homeostasis. *J. Exp. Bot* 69, 441–454. doi: 10.1093/jxb/erx426

Gibb, M., Kisiala, A. B., Morrison, E. N., and Emery, R. J. N. (2020). The Origins and Roles of Methylthiolated Cytokinins: evidence From Among Life Kingdoms. *Front. Cell Dev. Biol.* 8:605672. doi: 10.3389/fcell.2020.605672

Grant-Downton, R., Hafidh, S., Twell, D., and Dickinson, H. G. (2009). Small RNA pathways are present and functional in the angiosperm male gametophyte. *Mol. Plant* 2, 500–512. doi: 10.1093/mp/ssp003

Hackenberg, D., and Twell, D. (2019). The evolution and patterning of male gametophyte development. *Plant Dev. Evol.* 131, 257–298. doi: 10.1016/bs.ctdb.2018.10.008

Hafidh, S., Fíla, J., and Honys, D. (2016). Male gametophyte development and function in angiosperms: a general concept. *Plant Reprod.* 29, 31–51. doi: 10.1007/s00497-015-0272-4

Hafidh, S., and Honys, D. (2021). Reproduction multitasking: the male gametophyte. *Ann. Rev. Plant Biol.* 72, 581–614. doi: 10.1146/annurev-arplant-080620-021907

Hirano, K., Aya, K., Hobo, T., Sakakibara, H., Kojima, M., Shim, R. A., et al. (2008). Comprehensive transcriptome analysis of phytohormone biosynthesis and signaling genes in microspore/pollen and tapetum of rice. *Plant Cell Physiol.* 49, 1429–1450. doi: 10.1093/pcp/pcn123

Honys, D., Oh, S. A., Reňák, D., Donders, M., Šolcová, B., Johnson, J. A., et al. (2006). Identification of microspore-active promoters that allow targeted manipulation of gene expression at early stages of microgametogenesis in *Arabidopsis*. *BMC Plant Biol.* 6:31. doi: 10.1186/1471-2229-6-31

Honys, D., and Twell, D. (2004). Transcriptome analysis of haploid male gametophyte development in *Arabidopsis*. *Genome Biol.* 5:R85. doi: 10.1186/gb-2004-5-11-r85

Hošek, P., Hoyerová, K., Kiran, N. S., Dobrev, P. I., Zahajská, L., Filepová, R., et al. (2020). Distinct metabolism of *N*-glucosides of isopentenyladenine and *trans*-zeatin determines cytokinin metabolic spectrum in *Arabidopsis*. *New Phytol.* 225, 2423–2438. doi: 10.1111/nph.16310

Huang, S. R., Černý, E., Qi, Y., Bhat, D., Aydt, C. M., Hanson, D. D., et al. (2003). Transgenic studies on the involvement of cytokinin and gibberellin in male development. *Plant Physiol.* 131, 1270–1282. doi: 10.1104/pp.102.018598

Kambhampati, S., Kurepin, L. V., Kisiala, A. B., Bruce, K. E., Cober, E. R., Morrison, M. J., et al. (2017). Yield associated traits correlate with cytokinin profiles in

developing pods and seeds of field-grown soybean cultivars. *Field Crops Res.* 214, 175–184. doi: 10.1016/j.fcr.2017.09.009

Kelliher, T., and Walbot, V. (2011). Emergence and patterning of the five cell types of the *Zea mays* anther locule. *Dev. Biol.* 350, 32–49. doi: 10.1016/j.ydbio.2010.11.005

Kieber, J. J., and Schaller, G. E. (2018). Cytokinin signaling in plant development. *Development* 145:dev149344. doi: 10.1242/dev.149344

Kinoshita-Tsujimura, K., and Kakimoto, T. (2011). Cytokinin receptors in sporophytes are essential for male and female functions in *Arabidopsis thaliana*. *Plant Signal. Behav.* 6, 66–71. doi: 10.4161/psb.6.1.13999

Knöfel, H. D., and Sembdner, G. (1995). Jasmonates from pine pollen. *Phytochemistry* 38, 569–571. doi: 10.1016/0031-9422(94)00748-I

Kovaleva, L. V., Voronkov, A. S., and Zakharova, E. V. (2015). Role of auxin and cytokinin in the regulation of the actin cytoskeleton in the *in vitro* germinating male gametophyte of *Petunia*. *Russ. J. Plant Physiol.* 62, 179–186. doi: 10.1134/S1021443715020107

Mandaokar, A., Thines, B., Shin, B., Lange, B. M., Choi, G., Koo, Y. J., et al. (2006). Transcriptional regulators of stamen development in *Arabidopsis* identified by transcriptional profiling. *Plant J.* 46, 984–1008. doi: 10.1111/j.1365-313X.2006.02756.x

Matoušek, J., Steinbachová, L., Záveská Drábková, L., Kocábek, T., Potěšil, D., Mishra, A. K., et al. (2020). Elimination of viroids from tobacco pollen involves a decrease in propagation rate and an increase of the degradation processes. *Int. J. Mol. Sci.* 21:3029. doi: 10.3390/ijms21083029

McCormick, S. (1993). Male gametophyte development. *Plant Cell* 5, 1265–1275.

Miersch, O., Knöfel, H. D., Schmidt, J., Kramell, R., and Parthier, B. (1998). A jasmonic acid conjugate, N- (-)-jasmonoyl -tyramine, from *Petunia* pollen. *Phytochemistry* 47, 327–329. doi: 10.1016/S0031-9422(97)00617-1

Nagpal, P., Ellis, C. M., Weber, H., Ploense, S. E., Barkawi, L. S., Guilfoyle, T. J., et al. (2005). Auxin response factors ARF6 and ARF8 promote jasmonic acid production and flower maturation. *Development* 132, 4107–4118. doi: 10.1242/dev.01955

Novák, O., Napier, R., and Ljung, K. (2017). Zooming in on plant hormone analysis: tissue- and cell-specific approaches. *Annu. Rev. Plant Biol.* 68, 323–348. doi: 10.1146/annurev-arplant-042916-040812

Pacini, E., and Dolferus, R. (2019). Pollen developmental arrest: maintaining pollen fertility in a world with a changing climate. *Front. Plant Sci.* 10:679. doi: 10.3389/fpls.2019.00679

Pokorná, E., Hluska, T., Galuszka, P., Hallmark, H. T., Dobrev, P. I., Záveská Drábková, L., et al. (2021). Cytokinin *N*-glucosides: occurrence, metabolism and biological activities in plants. *Biomolecules* 11:24. doi: 10.3390/biom11010024

Reňák, D., Gibalová, A., Šolcová, K., and Honys, D. (2014). A new link between stress response and nucleolar function during pollen development in *Arabidopsis* mediated by AtREN1 protein. *Plant Cell Environ.* 37, 670–683.

Rong, D., Luo, N., Mollet, J. C., Liu, X., and Yang, Z. (2016). Salicylic acid regulates pollen tip growth through an npr3/npr4-independent pathway. *Mol. Plant* 9, 1478–1491. doi: 10.1016/j.molp.2016.07.010

Salinas-Grenet, H., Herrera-Vasquez, A., Parra, S., Cortez, A., Gutierrez, L., Pollmann, S., et al. (2018). Modulation of auxin levels in pollen grains affects stamen development and anther dehiscence in *Arabidopsis*. *Int. J. Mol. Sci.* 19:2480. doi: 10.3390/ijms19092480

Scott, R. J., Spielman, M., and Dickinson, H. G. (2004). Stamen structure and function. *Plant Cell* 16, S46–S60. doi: 10.1105/tpc.017012

Šimura, J., Antoniadi, I., Široká, J., Tarkowská, D., Strnad, M., Ljung, K., et al. (2018). Plant hormonomics: multiple phytohormone profiling by targeted metabolomics. *Plant Physiol.* 177, 476–489. doi: 10.1104/pp.18.00293

Song, S. S., Qi, T. C., Huang, H., and Xie, D. X. (2013). Regulation of stamen development by coordinated actions of jasmonate, auxin, and gibberellin in *Arabidopsis*. *Mol. Plant* 6, 1065–1073. doi: 10.1093/mp/sst054

Stirk, W. A., Novák, O., Strnad, M., and van Staden, J. (2003). Cytokinins in macroalgae. *Plant Growth Regul.* 41, 13–24. doi: 10.1023/A:1027376507197

Taiz, L., and Zeiger, E. (2002). *Plant Physiology. 3rd Edition*. Sunderland: Sinauer Associates, Inc. Publishers.

Tarkowski, P., Václavíková, K., Novák, O., Pertry, I., Hanuš, J., Whenham, R., et al. (2010). Analysis of 2-methylthio-derivatives of isoprenoid cytokinins by liquid chromatography-tandem mass spectrometry. *Anal. Chim. Acta* 680, 86–91. doi: 10.1016/j.aca.2010.09.020

Tupý, J. (1982). Alterations in polyadenylated RNA during pollen maturation and germination. *Biol. Plant.* 24, 331–340. doi: 10.1007/BF02909098

Tupý, J., Süss, J., Hrabětová, E., and Říhová, L. (1983). Developmental changes in gene expression during pollen differentiation and maturation in *Nicotiana tabacum* L. *Biol. Plant.* 25, 231–237. doi: 10.1007/BF02902110

Uzelac, B., Janošević, D., Simonović, A., Motyka, V., Dobrev, P. I., and Budimir, S. (2016). Characterization of natural leaf senescence in tobacco (*Nicotiana tabacum*) plants grown *in vitro*. *Protoplasma* 253, 259–275. doi: 10.1007/s00709-015-0802-9

Vondráková, Z., Dobrev, P. I., Pešek, B., Fischerová, L., Vágner, M., and Motyka, V. (2018). Profiles of endogenous phytohormones over the course of Norway spruce somatic embryogenesis. *Front. Plant Sci.* 9:1283. doi: 10.3389/fpls.2018.01283

Wasternack, C., and Hause, B. (2013). Jasmonates: biosynthesis, perception, signal transduction and action in plant stress response, growth and development. An update to the 2007 review in Annals Botany. *Ann. Bot.* 111, 1021–1058.

Wilson, Z. A., and Zhang, D. B. (2009). From *Arabidopsis* to rice: pathways in pollen development. *J. Exp. Bot.* 60, 1479–1492. doi: 10.1093/jxb/erp095

Wybouw, B., and de Rybel, B. (2019). Cytokinin - A developing story. *Trends Plant Sci.* 24, 177–185. doi: 10.1016/j.tplants.2018.10.012

Yamane, H., Abe, H., and Takahashi, N. (1982). Jasmonic acid and methyl jasmonate in pollens and anthers of three camellia species. *Plant Cell Physiol.* 23, 1125–1127.

Yan, S., and Dong, X. (2014). Perception of the plant immune signal salicylic acid. *Curr. Opin. Plant Biol.* 20, 64–68. doi: 10.1016/j.pbi.2014.04.006

Yang, C., Xu, Z., Song, J., Conner, K., Vizcay Barrena, G., and Wilson, Z. A. (2007). *Arabidopsis* MYB26/MALE STERILE35 regulates secondary thickening in the endothecium and is essential for anther dehiscence. *Plant Cell* 19, 534–548. doi: 10.1105/tpc.106.046391

Yao, X., Tian, L., Yang, J., Zhao, Y. N., Zhu, Y. X., Dai, X., et al. (2018). Auxin production in diploid microsporocytes is necessary and sufficient for early stages of pollen development. *PLoS Genet.* 14:e1007397. doi: 10.1371/journal.pgen.1007397

Záveská Drábková, L., Dobrev, P. I., and Motyka, V. (2015). Phytohormone Profiling across the Bryophytes. *PLoS One* 10:e0125411. doi: 10.1371/journal.pone.0125411

Žižková, E., Kubeš, M., Dobrev, P. I., Přibyl, P., Šimura, J., Zahajská, L., et al. (2017). Control of cytokinin and auxin homeostasis in cyanobacteria and algae. *Ann. Bot.* 119, 151–166. doi: 10.1093/aob/mcw194

Zuñiga-Mayo, V. M., Baños-Bayardo, C. R., Díaz-Ramírez, D., Marsch-Martinez, N., and de Folter, S. (2018). Conserved and novel responses to cytokinin treatments during flower and fruit development in *Brassica napus* and *Arabidopsis thaliana*. *Sci. Rep.* 8:6836. doi: 10.1038/s41598-018-25017-3

Conflict of Interest: The authors declare that the research was conducted in the absence of any commercial or financial relationships that could be construed as a potential conflict of interest.

Publisher's Note: All claims expressed in this article are solely those of the authors and do not necessarily represent those of their affiliated organizations, or those of the publisher, the editors and the reviewers. Any product that may be evaluated in this article, or claim that may be made by its manufacturer, is not guaranteed or endorsed by the publisher.

frontiers in Plant Science

ORIGINAL RESEARCH
published: 29 October 2021
doi: 10.3389/fpls.2021.765277

PsEND1 Is a Key Player in Pea Pollen Development Through the Modulation of Redox Homeostasis

*Rim Hamza, Edelín Roque, Concepción Gómez-Mena, Francisco Madueño, José Pío Beltrán and Luis A. Cañas**

Department of Plant Development and Hormone Action, Instituto de Biología Molecular y Celular de Plantas (CSIC-Universitat Politècnica de València), Ciudad Politécnica de la Innovación, Valencia, Spain

OPEN ACCESS

Edited by:
Michael Gerard Muszynski, University of Hawai'i at Mānoa, United States

Reviewed by:
José A. Feijó, University of Lisbon, Portugal
Eduardo Zabaleta, CONICET Mar del Plata, Argentina

***Correspondence:**
Luis A. Cañas
lcanas@ibmcp.upv.es

Specialty section:
This article was submitted to Plant Development and EvoDevo, a section of the journal Frontiers in Plant Science

Received: *26 August 2021*
Accepted: *11 October 2021*
Published: *29 October 2021*

Citation:
Hamza R, Roque E, Gómez-Mena C, Madueño F, Beltrán JP and Cañas LA (2021) PsEND1 Is a Key Player in Pea Pollen Development Through the Modulation of Redox Homeostasis. Front. Plant Sci. 12:765277. doi: 10.3389/fpls.2021.765277

Redox homeostasis has been linked to proper anther and pollen development. Accordingly, plant cells have developed several Reactive Oxygen Species (ROS)-scavenging mechanisms to maintain the redox balance. Hemopexins constitute one of these mechanisms preventing heme-associated oxidative stress in animals, fungi, and plants. *Pisum sativum ENDOTHECIUM 1 (PsEND1*) is a pea anther-specific gene that encodes a protein containing four hemopexin domains. We report the functional characterization of *PsEND1* and the identification in its promoter region of *cis*-regulatory elements that are essential for the specific expression in anthers. *PsEND1* promoter deletion analysis revealed that a putative CArG-like regulatory motif is necessary to confer promoter activity in developing anthers. Our data suggest that *PsEND1* might be a hemopexin regulated by a MADS-box protein. *PsEND1* gene silencing in pea, and its overexpression in heterologous systems, result in similar defects in the anthers consisting of precocious tapetum degradation and the impairment of pollen development. Such alterations were associated to the production of superoxide anion and altered activity of ROS-scavenging enzymes. Our findings demonstrate that *PsEND1* is essential for pollen development by modulating ROS levels during the differentiation of the anther tissues surrounding the microsporocytes.

Keywords: *Pisum sativum*, *PsEND1* promoter, anther-specific gene, *cis*-regulatory motifs, CArG boxes, hemopexin-like, redox homeostasis

INTRODUCTION

Anthers development is a critical step in plant reproduction as it is required for male gametophytes generation and fertility. Anthers are composed of three outer layers (epidermis, middle layer, and endothecium) and an inner cell layer (tapetum) surrounding the microsporocytes. Pollen production requires coordinated development of sporophytic and gametophytic tissues

(Parish and Li, 2010; Chang et al., 2011; Hafidh et al., 2016; Fu et al., 2020). Haploid microspores are generated from pollen mother cells (PMC) through meiosis; then, two successive mitoses lead to the formation of binucleate and trinucleate mature pollen grains. During this process, the tapetum undergoes programmed cell death (PCD), providing the enzymes required for the release of the microspores from the tetrads, nutrients for pollen development and maturation and components for the pollen wall (Wilson and Zhang, 2009; Zhu et al., 2011; Zheng et al., 2020). Thus, the production of viable pollen grains requires a fine timing of tapetum degradation involving several key intracellular factors. Reactive oxygen species (ROS) have been shown to play an essential role in tapetum function and PCD in Arabidopsis and rice (Hu et al., 2011; Luo et al., 2013; Yi et al., 2016). For instance, high ROS levels in rice resulted in male sterility due to a delayed tapetum degradation (Hu et al., 2011; Luo et al., 2013), while low levels lead to early tapetum degradation (Xie et al., 2014). In both cases, the imbalance of ROS levels caused severe impairment of pollen development. Redox homeostasis is also critical for the regulation of different plant biological processes, including cell proliferation and differentiation (Zafra et al., 2010; Schippers et al., 2016; Huang et al., 2019; Lodde et al., 2021).

ROS are present in cells both in ionic and molecular states. Hydroxyl radical.OH and superoxide anion $O_2^{\cdot -}$ represent the ionic state, while the molecular state consists mainly of singlet oxygen $^1O_2$ and hydrogen peroxide H_2O_2. $O_2^{\cdot -}$ is the precursor of different ROS and can be dismutated to H_2O_2 by the superoxide dismutase (SOD). Hydrogen peroxide is considered the most important ROS due to its high stability in the cell with a half-life of 10^{-3} s (Mittler, 2017; Mhamdi and van Breusegem, 2018). It can be transported through the cell membrane via aquaporins causing long-distance damage and participating in cell signaling (Miller et al., 2010; Lodde et al., 2021). $^{\cdot}OH$ is the most reactive ROS, and it can react with all biological molecules. However, it has a very short half-life, and thus, can only act locally at the cells where it is produced.

Cells have developed a diverse arsenal of mechanisms to deal with oxidative stress. ROS-scavenging mechanisms may be classified into two types: enzymatic and non-enzymatic. The enzymatic mechanisms rely on three main enzymes: superoxide dismutases (SOD), peroxidases and catalases (Arora et al., 2002; Huang et al., 2019; Lodde et al., 2021). The non-enzymatic mechanisms use low mass antioxidant molecules such as glutathione, ascorbic acid and flavonoids.

Pisum sativum ENDOTHECIUM 1 (PsEND1) is a pea (*Pisum sativum* L.) anther-specific gene displaying very early expression in the anther primordium and during anther development (Gómez et al., 2004). *PsEND1* promoter drives heterologous gene expression exclusively to the anthers, being equally active in dicots and monocots (Gómez et al., 2004; Roque et al., 2007, 2019; Briones et al., 2020). A −2.7 Kb region of *PsEND1* promoter has been used to drive the expression of the cytotoxic ribonuclease *barnase* gene (Hartley, 1988). *PsEND1* promoter was used to generate male-sterile plants by cell ablation of specific anther tissues, preventing the production of mature pollen grains in different ornamental (*Kalanchoe, Pelargonium*) and crops species (tomato, oilseed rape, tobacco, rice, wheat, poplar) (Roque et al., 2019; Briones et al., 2020). This ability makes *PsEND1* promoter a valuable tool for biotechnological applications, such as the production of hybrids, the elimination of allergenic pollen or gene containment.

PsEND1 encodes a protein (25.7 KDa; Genbank accession number: AAM12036.1) containing four copies of a hemopexin-type conserved repeat (Beltrán et al., 2007). Hemopexins are heme-scavenging proteins preventing heme-associated oxidative stress in animals, fungi and plants. Heme is an electron transfer molecule of vital importance in several biological processes involving proteins associated with redox activity, such as peroxidases and hemopexins. However, free heme can be highly toxic for cells generating ROS (Vercellotti et al., 1994; Jeney et al., 2002; Kumar and Bandyopadhyay, 2005; Tolosano et al., 2010; Gáll et al., 2018). PsEND1 shows 72.17% sequence homology with the atypical pea storage protein PsPA2 (Higgins et al., 1987; Vigeoles et al., 2008; Robinson and Domoney, 2021) while it does not seem to have any homolog in *A. thaliana*. The role of hemopexins during anthers development has only been reported for the rice *OsHFP* gene (Chattopadhyay et al., 2015). It has been suggested that the heme-binding properties of OsHFP could regulate PCD in the anther tissues of rice through the regulation of ROS levels (Chattopadhyay et al., 2015).

In this work, we have functionally characterized the *PsEND1* gene of pea. Our findings suggest that *PsEND1* might be a target of MADS-domain transcription factors, playing an essential role during pollen development. The importance of this gene lies in its function as a ROS-scavenger during the differentiation of the anther tissues surrounding the microsporocytes.

MATERIALS AND METHODS

Plant Material and Growth Conditions

Arabidopsis thaliana cv. Columbia plants were grown in the greenhouse under long-day conditions (16 h light/8 h dark) at 21°C. *Pisum sativum* cv. Bonneville, *Nicotiana benthamiana,* and *Nicotiana tabacum* cv. Xhanti plants were grown in the greenhouse under long-day conditions (16 h light/8 h dark) at 22°C (day) and 18°C (night).

Promoter Sequence Analyses

PsEND1 promoter region (Genbank accession number: AY324651) was analyzed in search for regulatory elements using the online software PLACE (Higo et al., 1999). We used the promoter region −986/−6, which is sufficient to direct the spatio-temporal expression of *PsEND1*.

Promoter Cloning and Site-Directed Mutagenesis

The *PsEND1* promoter fragments were cloned in the plasmid pKGWFS7.0 and transcriptionally fused to the *uidA* reporter gene. Site-directed mutagenesis of the CArG-like motif was performed using the QuikChange II Site-directed

mutagenesis kit (Agilent) according to the manufacturer instructions and using the primers END1mutF and END1mutR (**Supplementary Table 1**).

GUS Staining

Floral tissues were infiltrated using three vacuum pulses of 5 min in GUS assay buffer [0.1 M NaH_2PO_4, 10 mM $Na_2EDTA.H_2O$, 0.5 M $K_3Fe(CN)_6$, 0.1% Triton X-100 and 0.3% 5-bromo-4-chloro-3-indolyl β-D-glucuronide (X-Gluc)] and incubated in this solution at 37°C for 16 h. Afterward, de-staining was carried out using successive washes with ethanol at 50, 70, and 90%. Subsequently, stained flowers were observed under a stereoscope (Leica MZ16F). GUS-positive zones were identified as those colored in blue.

Subcellular Localization

The coding sequence of *PsEND1* was cloned in the plasmid pEarlyGate104 downstream the CaMV35S promoter and transcriptionally fused to the Yellow Fluorescent Protein (YFP). The construct was transformed into *Agrobacterium tumefaciens* strain C58C1. The transformed bacteria were used to transform leaves of *Nicotiana benthamiana* transiently. After 3 days, the leaves were infiltrated with an aniline blue solution (0.005% Aniline Blue in potassium phosphate buffer 70 mM, pH 9.0). Ten min later, fluorescence was detected in the leaves under a confocal microscope (AxioObserver 780, Zeiss).

Prediction of PsEND1 3D Structure and Heme Binding Motifs

Prediction of PsEND1 3D structure was performed using the online tool swissmodel.expasy.org using the crystal structure of hemopexin fold protein CP4 from cowpea (SMTL ID: 3oyo.1; Gaur et al., 2011) as a template. The predicted 3D structure was visualized using the software Chimera (Pettersen et al., 2004) and the heme binding motifs using the online server HeMoQuest[1] (George et al., 2020). This online interface detects transient heme binding nonapeptide motifs.

Virus-Induced Gene Silencing

We used the plasmids pCAPE1 and pCAPE2 as vectors for gene silencing (Constantin et al., 2004). A fragment of the *PsEND1* coding sequence was amplified by PCR using the primers VIGSEND1F and VIGSEND1R (**Supplementary Table 1**) and cloned in the vector pCAPE2. The construct was transferred to the *Agrobacterium tumefaciens* strain C58C1. *Pisum sativum* cv. Bonneville 2-week-old plants were infiltrated as described by Constantin et al. (2004).

Gene Expression Analyses by qRT-PCR

RNA was extracted using the E.Z.N.A.® Plant RNA Kit (Omega Bio-tek) according to the manufacturer instructions. Two micrograms of total RNA were treated with DNase I (Thermo Scientific) following the manufacturer protocol. The first strand of cDNA was synthesized using 1 μg of treated RNA with the Primescript™ RT-PCR kit (TAKARA, Tokyo, Japan). qRT-PCR was performed in a 7,500 Fast Real-time PCR System (Applied Biosystems, Foster City, CA, United States) using 20 ng of template cDNA mixed with EvaGreen® Master Mix (Cultek, Madrid, Spain). For *PsEND1* expression analysis in the VIGS-*PsEND1* plants, we used the primers qEND1VIGSF and qEND1VIGSR (**Supplementary Table 1**). The constitutive gene *PsEF1* was used to normalize according to the $2^{\Delta\Delta Ct}$ method (Livak and Schmittgen, 2001).

Pollen Viability Assay

Pollen was recovered from pre-dehiscent anthers under a stereomicroscope and incubated with Alexander stain at 50°C for 2 min (Alexander, 1969). The slides were later observed under an optical microscope (Leica DM5000).

Overexpression of *PsEND1* in *Arabidopsis thaliana* and *Nicotiana tabacum*

The coding sequence of *PsEND1* was cloned downstream of the strong promoter CaMV35S in the plasmids pK2GW7. The construct was then transformed into the Agrobacterium strains C58C1 and LBA4404 to transform *A. thaliana* and *N. tabacum*, respectively. *A. thaliana* plants were transformed using the flower dip method (Zhang et al., 2006). Seeds of the transformed plants were recovered and germinated on a kanamycin selective medium. Tobacco plants were transformed as previously described (Hamza et al., 2018). Genomic DNA was extracted from the obtained plants using the E.Z.N.A.® Plant DNA Kit (Omega Bio-tek). The integration of the transgenic DNA was checked by PCR using the primers PsEND1ATG and PsEND1STOP (**Supplementary Table 1**).

Superoxide Anion Detection

In order to detect superoxide anion ($O_2^{\cdot -}$) accumulation, Arabidopsis seedlings were immersed in a 0.2% w/v NBT solution in sodium phosphate buffer (pH 7.5). NBT reacts with superoxide anion forming a dark blue insoluble formazan compound. The seedlings were incubated overnight at room temperature, then the solution was discarded, and the seedlings were washed several times with 70% ethanol until complete removal of the chlorophyll.

TdT-Mediated dUTP Nick-End Labeling Assay

TdT-mediated dUTP Nick-End Labeling (TUNEL) assay was performed with the DeadEND™Fluoremetric TUNEL System kit (Promega) according to the manufacturer instructions. Samples were analyzed with a fluorescent microscope (Leica DM5000). Cells were stained with propidium iodide (1 μ/ml).

Histological Sectioning

Flowers of *Pisum sativum* and *Arabidopsis thaliana* were fixed in formaldehyde/acetic acid/ethanol (10%:5%:50%). The flowers that were intended for the TUNEL assay were embedded in

[1]http://131.220.139.55/SeqDHBM/

paraffin, while the rest of the samples were embedded in synthetic resin (Leica). The samples were later sectioned and stained either with 1% Toluidine Blue or with 1 μg/ml 2-(4-aminophenyl)-1H-indole-6-carboxamidine (DAPI). Toluidine blue stained sections were imaged by light microscopy, while DAPI stained slides were observed by fluorescence microscopy (Leica DM5000).

Superoxide Dismutase and Peroxidase Activity

To measure SOD and PRX activity, pea flowers of each developmental stage were collected from different plants and mixed to form pools, as the level of gene silencing varies between plants. VIGS and control flowers were collected simultaneously. Frozen flowers of pea or leaves of *A. thaliana* and *N. tabacum* were ground in liquid nitrogen to a fine powder and homogenized in 500 μl of ice-cold extraction buffer (0.1 M Tris pH 7.0, 0.1% ascorbic acid, 0.1% L-cysteine, 0.5 M sucrose and 10 mg/ml PVP). The mixture was then centrifuged for 15 min at 4°C, and the supernatant was recovered. The total protein content of the crude extract was determined by the Bradford method (Bradford, 1976). The activity of SOD was determined using 5 μl of crude extract mixed with 200 μl of SOD buffer (PBS 50 mM pH 7.6, 0.1 mM EDTA, 50 mM sodium carbonate, 12 mM L-methionine, 10 μM riboflavin, 50 μM NBT in PBS 50 mM pH 7.6). The mixture was incubated for 10 min at room temperature under white light, and absorbance was measured at 560 nm. One unit of SOD activity is defined as the amount of enzyme required to inhibit 50% of the NBT photoreduction. PRX activity was measured adding 5 μl of crude extract to 200 μl PRX buffer (0.85 mM hydrogen peroxide in HEPES pH 7.0, 0.125 M 4-aminoantipyrene, 8.1 mg/ml phenol). The change in absorbance at 510 nm was measured for 2 min. Horseradish peroxidase at different known concentrations was used as a reference to generate a standard curve.

Statistical Analyses

Statistical analyses were performed with the GraphPad Prism 9 software. ANOVA test was used to analyze the SOD and PRX activity assays in *A. thaliana* and *N. tabacum*, while *t*-test was used to compare enzymatic activity in pea flowers between the VIGS-*PsEND1* flowers and the control.

RESULTS

Characterization and Functional Analysis of the *PsEND1* Promoter

In a first approach, we have corroborated that the −986/−6 region of the *PsEND1* promoter is able to drive a strong anther-specific expression of the *uidA* (GUS) reporter gene in Arabidopsis. *In silico* analysis of this promoter region, using the online software PLACE, detected several putative regulatory motifs (**Supplementary Table 2**). Among these, we focused on the transcription factor binding DNA motifs associated to specific gene expression in anthers: GTGANTG10 (−799/−795; −794/−790; −693/−599; −597/−593; −81/−77) (Rogers et al., 2001) and Pollen1lellat2 (−607/−602; −551/−546) (Bate and Twell, 1998; Filichkin et al., 2004). In addition, we paid special interest to the DNA sequences recognized by transcription factors containing MADS-box domains, termed CArG motifs (Shore and Sharrocks, 1995; Riechmann and Meyerowitz, 1997; Folter and Angenent, 2006). We found three CARGCW8GAT motifs (Tang and Perry, 2003; CWWWWWWWWG at positions −375/−366; −247/−238; −57/−48 (**Figure 1**). We also included in our analysis a regulatory element previously described (Gómez et al., 2004) as a putative CArG-like motif (CCATTTTGG; −112/−104).

To identify the minimal promoter region sufficient to drive *PsEND1* anther-specific expression, we performed several promoter-reporter (*uidA*, GUS) constructs. The successive deletions contained the fragments −986/−6 (C1), −685/−6 (C2), −426/−6 (C3), −366/−6 (C4), and −309/−6 (C5) (**Figure 1A**). *Arabidopsis thaliana* plants were transformed with each of these constructs. The inflorescent apices from several primary (T0) transgenic plants were analyzed using flowers at different stages of development. The flowers of the Arabidopsis plants that contained the constructs C1 to C4 (**Figure 1B**) showed GUS staining in the anthers since the early stages of development. GUS staining was qualitatively high when all of these sequential deletions of the *PsEND1* promoter were used. However, no GUS signal was detected in the flowers of the transgenic plants transformed with the C5 construct (**Figure 1C**).

We tested whether the regulatory motif at position −112/−104 (CCATTTTGG), described by Gómez et al. (2004) as a putative CArG-like motif, might be critical for *PsEND1* gene expression. For this purpose, we generated a construct in which an internal fragment containing this motif was removed. The flowers of Arabidopsis plants harboring this construct did not show any GUS activity. This indicates that the CArG-like box motif (Gómez et al., 2004) present in the deleted fragment could be essential for *PsEND1* expression, at least within the context of the −366/−6 promoter. To confirm the importance of this regulatory element for the spatio-temporal expression pattern of the *PsEND1* gene, we performed a site-directed mutagenesis strategy. The CCATTTTGG sequence was converted into GGATTTTGG, thus lacking the conserved motif CArG. The Arabidopsis flowers harboring the mutated *PsEND1*promoter did not show any GUS staining in their anthers (**Figure 1D**). These findings confirm the importance of the putative CArG-like element for the regulation of *PsEND1*expression.

Subcellular Localization of PsEND1

In previous studies (Gómez et al., 2004), PsEND1 protein was immunolocalized in the anther tissues, but its subcellular localization was not determined. To investigate the subcellular localization of PsEND1protein, the *PsEND1* coding sequence was transcriptionally fused to the Yellow Fluorescent Protein (YFP). PsEND1 YFP-tagged protein was transiently expressed in *Nicotiana benthamiana* leaves. PsEND1 was detected by confocal microscopy in the cytoplasm and in plasmodesmata. Localization in plasmodesmata was confirmed by co-localization with aniline blue, a plasmodesmata marker (**Figure 2**).

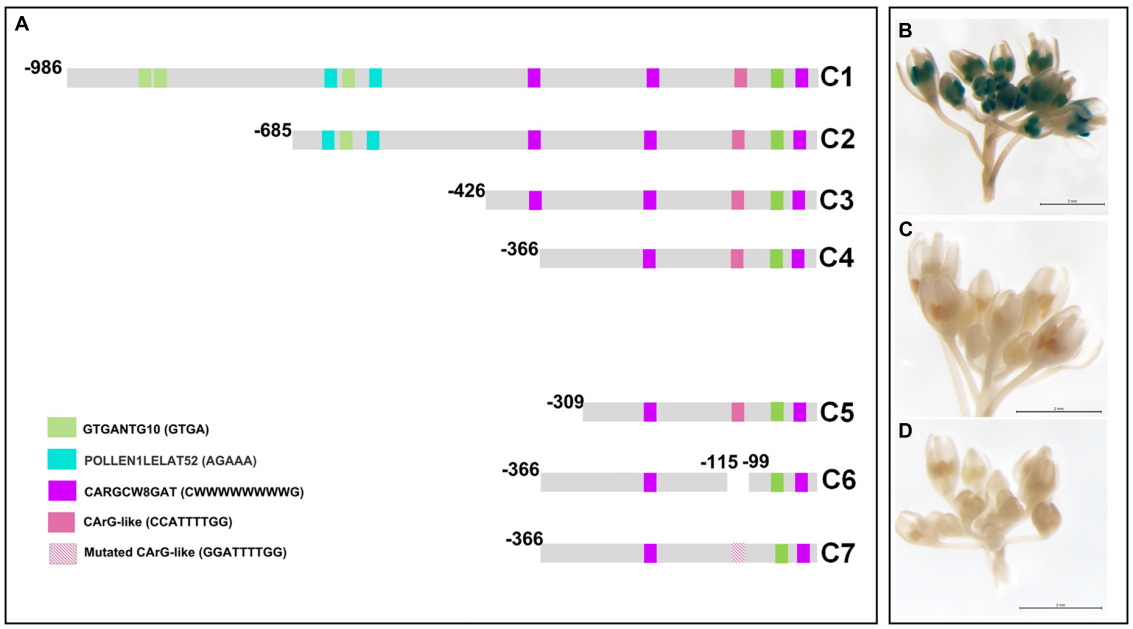

FIGURE 1 | Deletion analysis of the *PsEND1* promoter. **(A)** Promoter regions used in the different constructs (C1–C7). The regulatory motifs related to the specific expression in anthers, GTGANTG10 and Pollen1lellat2, are highlighted in green and blue, respectively. CARG-like motifs are highlighted in pink and purple. **(B)** GUS staining of *Arabidopsis thaliana* flowers carrying the construct C4. **(C)** Gus staining of *A. thaliana* flowers carrying the construct C5. **(D)** Gus staining of *A. thaliana* flowers carrying the construct C7.

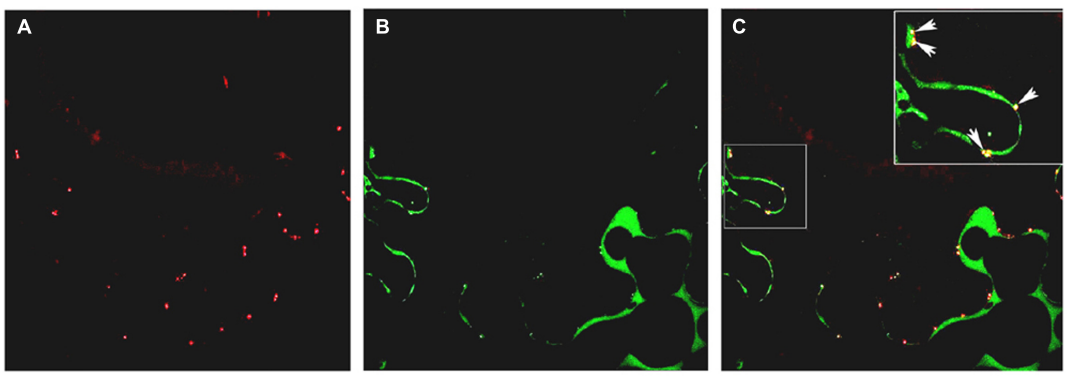

FIGURE 2 | Subcellular localization of PsEND1 in *Nicotiana benthamiana* leaves as observed by confocal microscopy. **(A)** Plasmodesmata stained by aniline blue (red). **(B)** Localization of PsEND1 fused to YFP (green). **(C)** Co-localization of plasmodesmata and PsEND1. The yellow dots indicate the co-localization of both fluorescent signals.

Prediction of PsEND1 3D Structure and Heme Binding Motifs

As previously described, PsEND1 presents four hemopexin domains (**Supplementary Figure 2A**; Beltrán et al., 2007). *In silico* 3D modeling based on the template of the cowpea, hemopexin fold protein showed that the hemopexin domains form a beta-propeller typical of hemopexins, surrounding a hollow shaft (**Supplementary Figure 2B**). This structure was described in different hemopexins (Paoli et al., 1999; Gaur et al., 2010; Chattopadhyay et al., 2012) and is thought to be responsible for binding heme groups (Paoli et al., 1999). Transient heme binding motifs were predicted using the online software HeMoQuest. Eight heme binding motifs were detected (**Supplementary Figure 2C**). These putative heme binding motifs were located on the PsEND1 3D model (**Supplementary Figure 2D**).

Virus Induced Gene Silencing of *PsEND1* in Pea

To investigate the function of *PsEND1*, we generated pea plants with reduced levels of the gene, using Virus Induced Gene

Silencing (VIGS) technology. As a negative control, we used the pCAPE1 vector. We analyzed nine independent VIGS-*PsEND1* lines and observed that the expression of *PsEND1* was highly reduced, ranging from 47 to 99% (**Figure 3A**). The majority of the flowers of the partially silenced plants presented a varying number of white anthers that appeared to contain few pollen grains (**Figure 3B**). Some anthers from silenced plants were also smaller in size. We recovered the pollen from control and VIGS-*PsEND1* plants and assessed its viability using Alexander's stain (Alexander, 1969). Alexander's stain colors aborted pollen grains blue-green and non-aborted pollen grains magenta-red. While the control plants showed over 98% viable pollen, the partially silenced plants contained between 16 and 91% aborted pollen (**Figures 3C,D**).

To further study the effect of *PsEND1*downregulation on pea anthers, we embedded flowers at different developmental stages and sizes in resin and performed histological cross-sections (**Figures 3E–J**). We observed that at the stage of 3 mm, the control anthers showed a thin layer of tapetal cells and round-shaped PMC where the cytoplasm is close to the membrane (**Figure 3E**). However, in the VIGS-*PsEND1* anthers, both the tapetal cells and PMC are swollen, and their cytoplasms shrunk (**Figure 3H**). At 5 mm stage, while in the control anthers, the pollen is normally formed and the tapetum is still present (**Figure 3F**), in the VIGS-*PsEND1* anthers, the tapetum has been degraded, and pollen grains seem to have collapsed and had been replaced by an amorphous mass (**Figure 3I**). Moreover, the endothecium has started to show secondary thickening and lignification, characteristics which were not observed in the control anthers. Later, at 7 mm size, the VIGS-*PsEND1* anthers presented no tapetal cells; the pollen was either collapsed or altered (**Figure 3G**), while the control still showing an intact tapetum and normal pollen cells (**Figure 3J**).

To analyze the effect of *PsEND1* gene silencing on tapetum development, we performed a TUNEL assay to visualize the cleavage of nuclear DNA (**Figures 3K–P**). In the VIGS-*PsEND1* anthers, we were able to detect chromatin fragmentation, the hallmark of PCD, in the tapetum of 5 mm flowers (**Figure 3N**). The fluorescent signal was maintained through stages of 6 mm (**Figure 3O**) and 7 mm (**Figure 3P**) in some locules. However, in the control anthers, no chromatin degradation could be detected at stages of 5 mm (**Figure 3K**) and 6 mm (**Figure 3L**). The first signal of PCD was detected in the 7 mm stage (**Figure 3M**). Therefore, while in the control anthers this process appears to be brief and initiated at late microspore state (7 mm flower), in the VIGS-*PsEND1* flowers, it seems to occur earlier and at a slow pace.

Different studies have shown that anther development and tapetum degeneration are highly sensitive to ROS balance (Hu et al., 2011; Xie et al., 2014; Yi et al., 2016; Jacobowitz et al., 2019; Zheng et al., 2019). ROS concentration in anther tissues is dynamic and finely regulated by several ROS-scavenging mechanisms in which participate enzymes such as peroxidases (PRX) and SOD. With the aim to investigate how *PsEND1* levels impact the enzymes involved in ROS regulation, we measured SOD and PRX activities in the VIGS-*PsEND1* pea flowers at four flower developmental stages (1–4 mm length flowers) (**Figure 4**). We found that in the control flowers, PRX and SOD activity follows antagonist patterns, varying during the development of the flower. When PRX activity increased (**Figure 4B**), SOD activity decreased (**Figure 4A**). In the VIGS-*PsEND1* flowers, at early stages, we observed a decreased SOD activity compared to the control, while PRX activity was increased. A dramatic reduction of SOD activity was observed at the flower sizes of 1 and 3 mm. While in the WT, SOD activity varied along developmental stages, in the VIGS-*PsEND1* flowers, the activity remains almost stable and low at the different flower developmental stages.

Overexpression of *PsEND1* in *Arabidopsis thaliana* and *Nicotiana tabacum*

To further study *PsEND1* function, we expressed the gene under the control of the strong constitutive promoter CaMV35S in *Arabidopsis thaliana* and *Nicotiana tabacum,* two plant species containing no *PsEND1* homologs in their genomes.

A. thaliana transformed seeds were grown on selective media. After germination, some seedlings developed to a similar size to the control ones, while others remained small and presented a dark color (**Figures 5A,B**). To investigate if these changes might be due to ROS accumulation, we stained the seedlings with NBT. The overexpressing plants showed an accumulation of superoxide radical $O_2^{\cdot -}$ as shown by the intense staining of the rosette leaves (**Figures 5C–E**). It is noteworthy to mention that the most affected plants in size and development presented the highest $O_2^{\cdot -}$ levels (**Figures 5D,E**). Several transgenic plants were later acclimatized in the greenhouse, although the smaller plants did not grow and died. The rest of the plants managed to grow but were smaller in size than the control ones.

The flowers of the 35S:*PsEND1* plants showed two types of developmental anther defects that coexist in the same plants: early anther dehiscence or complete anther collapse. In pre-anthesis flowers, at an early stage where the stamens were still shorter than the style, some anthers were already dehiscent (**Figure 5G**). The second type corresponds to flowers that showed collapsed stamens, with short filaments and arrow-shaped anthers with an intense yellow color (**Figure 5H**). These flowers were embedded in resin and stained with toluidine blue to visualize the effect on the internal structure of the anthers (**Figures 5I–K**). The histological analysis confirmed the macroscopic observations. In the anthers that seemed to have precocious dehiscence, the septum and the stomium have already been disrupted, thus liberating the pollen (**Figure 5J**). Moreover, the endothecium showed secondary thickening, and the tapetum was absent. Mutant flowers were compared to the wild type ones (**Figure 5I**) at the same stage. The developmental stage of the flowers was determined by the development of the carpel. The floral sections were subsequently stained with DAPI. We observed that the pollen grains of the dehiscent transformed anthers were mature and trinucleate (**Figure 5M**), while the pollen grains of the control flowers were still binucleate (**Figure 5N**). The anthers of transgenic flowers had an accelerated development leading to early dehiscence and pollen maturation. Arrow-shaped anthers of transgenic flowers were also sectioned

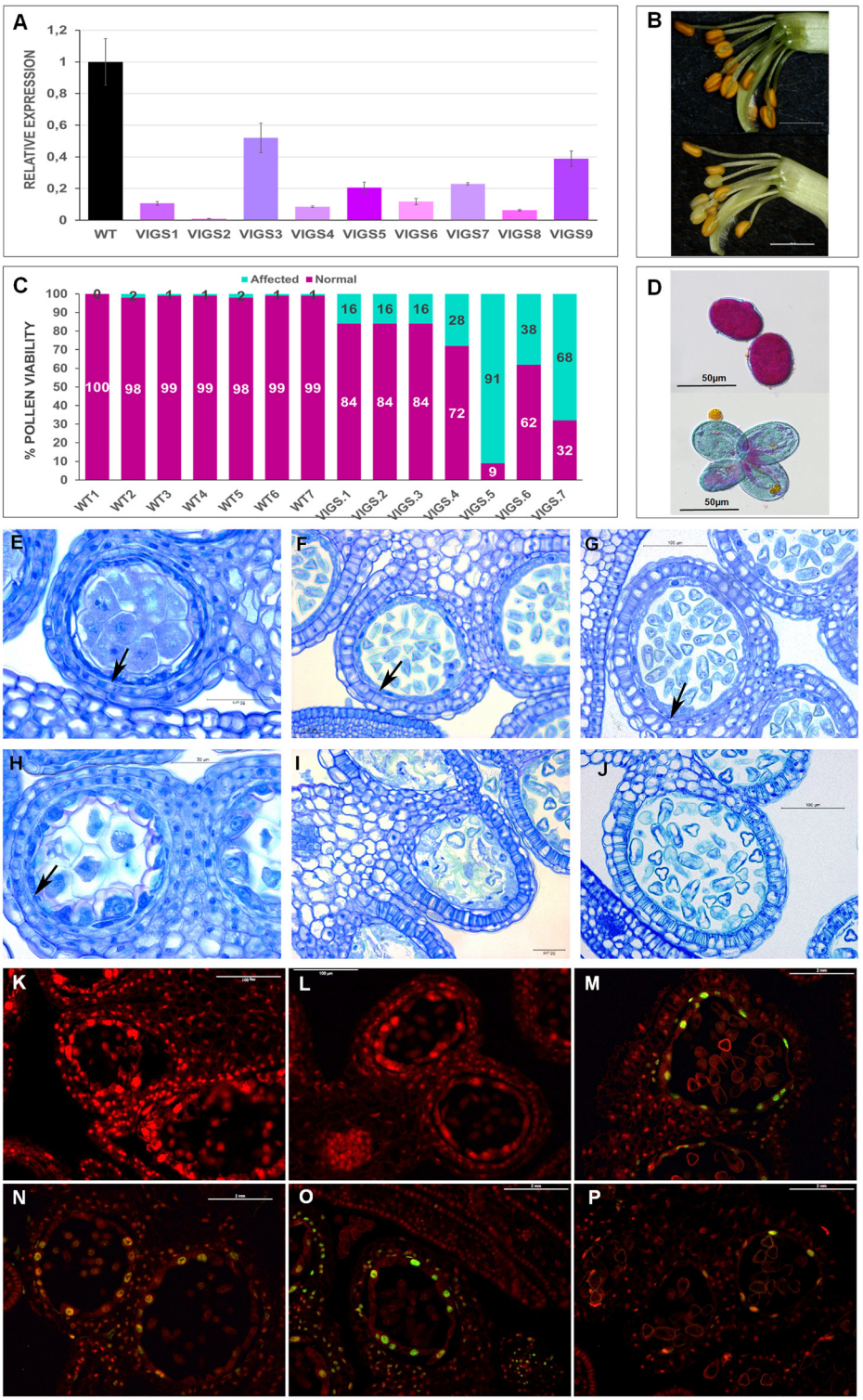

FIGURE 3 | Phenotypic characterization of VIGS-*PsEND1* pea flowers. **(A)** Expression of *PsEND1* in flower buds of different VIGS plants. **(B)** Detail of the stamens of wild type (upper) and VIGS-*PsEND1* (bottom) plants. The anthers of the VIGS-*PsEND1* plants showed a white color and small size. **(C)** Percentage of viable pollen in the wild type and VIGS-*PsEND1* plants. **(D)** Alexander's staining of pollen; wild type (upper) and VIGS plant (bottom). Viable pollen protoplasm is stained pink, while dead pollen is stained blue. Histological sections of wild type **(E–G)** and VIGS-*PsEND1* **(H–J)** pea flowers. **(E,H)** 3 mm flowers, **(F,I)** 5 mm flowers, **(G,J)** 7 mm flowers. Arrows in **(E–H)** indicate the presence of tapetal cells. Scale bars in **(E–J)** correspond to 100 µm. **(K–P)** Detection of DNA fragmentation by TUNEL assays of pea anthers of the wild type **(K–M)** and VIGS-*PsEND1* anthers **(N–P)**. Cell wall or membranes showed red fluorescence and the positive apoptotic nuclei stained with TUNEL were deep green.

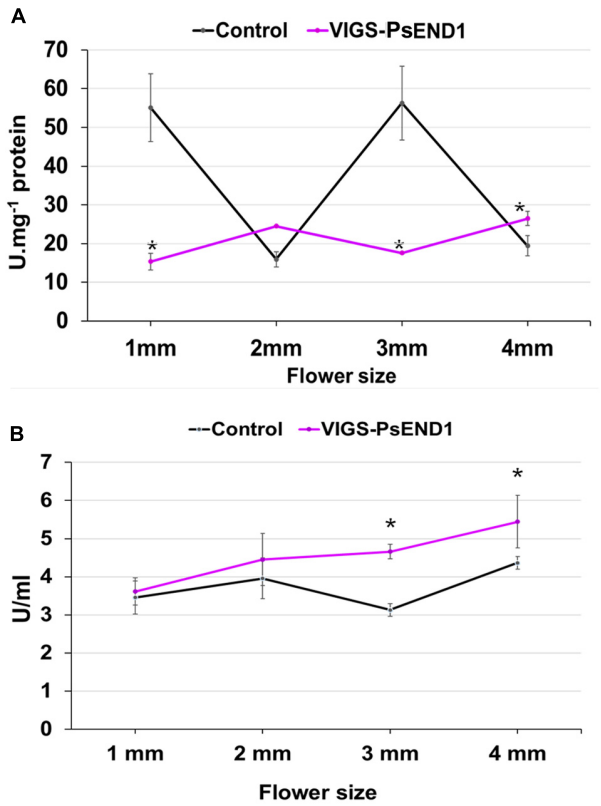

FIGURE 4 | Superoxide dismutase and peroxidase activity in transgenic pea plants. **(A)** SOD activity in control and VIGS-*PsEND1* flowers at different developmental stages. SOD activity is significantly reduced in the VIGS-*PsEND1* flowers. **(B)** Peroxidase activity in control and VIGS-PsEND1 flowers at different developmental stages. At stages 3 and 4 mm, peroxidase activity increases in the VIGS-*PsEND1* plants compared to the control. $^{*}p \leq 0.05$, $^{**}p \leq 0.01$, $^{***}p \leq 0.001$.

and observed. Their locules were surrounded by a single cell layer corresponding to the epidermis, while the endothecium and the tapetum were absent. Inside the locules, the anthers presented an intense yellow colored amorphous mass instead of the pollen cells (**Figures 5K,N**), probably due to an accumulation of flavonoids. At early stages, the anthers were similar to the wild type, being the first alterations observed at the stage of meiocytes, previous to the formation of tetrads. Indeed, tetrads could not be observed in the more affected anthers; the last stage observed being the meiocyte one. After this stage, the PMC and the tapetum degenerated (**Supplementary Figure 1**).

We also overexpressed *PsEND1* in *Nicotiana tabacum*. Only a few plantlets were regenerated because most of the calli failed to differentiate. Most of them remained small and did not succeed to root (**Figure 6A**). Three plants were acclimatized in the greenhouse. Similarly to what was observed with *A. thaliana* plants, these transgenic tobacco plants were smaller than the control ones (**Figure 6B**), and some of the transgenic flowers presented smaller anthers or anthers formed by only two locules (**Figure 6C**). We recovered the pollen of these anthers and stained it with Alexander's stain. We found that this pollen was non-viable (**Figure 6D**).

We then analyzed SOD and peroxidase activity in the rosette of *A. thaliana* and the leaves of N. *tabacum* overexpressing *PsEND1*. Similarly, in the overexpressing transgenic Arabidopsis and tobacco plants, SOD activity (**Figures 7A,B**) decreased, and PRX activity (**Figures 7C,D**) increased. This effect was stronger in the tobacco plant Nt.1, which was the most altered in size.

DISCUSSION

The Hemopexin-Like Protein PsEND1 Is a Putative Target of MADS-Box Transcription Factors

The *PsEND1* promoter deletion analysis showed in this work indicates that a region of approximately 0.3 kb (−366 to −6) upstream of the transcriptional start site contains the PsEND1 minimal promoter. Deleted sequences between C4 and C5 constructs (from −336 to −309) comprises different TF-binding sites as well as different common regulatory elements to eukaryotes and plants, such as the DOF (DOFCOREZM) (Yanagisawa and Schmidt, 1999; Yanagisawa, 2000) and MYC (MYCCONSENSUSAT) (Chinnusamy et al., 2003, 2004; Oh et al., 2005). These TFs binding elements seem to be essential for *PsEND1* regulation in the context of the −366 to −6 domain. This defined minimal promoter region (−366 to −6) contains a transcription binding DNA motif associated with the specific gene expression in anthers (GTGANTG10) (Rogers et al., 2001), two CARGCW8GAT motifs (Tang and Perry, 2003; Folter and Angenent, 2006) and a putative CArG-like motif (Gómez et al., 2004; **Figure 1A**). The absence of GUS staining in the anthers of the Arabidopsis plants containing the construct C5 (−309 to −6) may be explained by a possible cooperative protein-protein interaction between MADS-domain proteins with other transcription factors. One of the CARGCW8GAT (−247 to −238) motifs falls in the vicinity of the removed TF binding sites from −366 to −309. It has been suggested that the presence of other transcription factor binding sites in the proximity of CArG-box motifs could be essential for MADS-domain proteins interactions and, consequently, target gene regulation (Aerts et al., 2018).

We demonstrated that the CArG-like regulatory motif present at the position −112 to −104 (CCATTTTGG; Gómez et al., 2004) is essential to confer promoter activity in developing anthers. MADS-box proteins possess similar DNA-binding specificities, although some differences between each protein exist in this regard (Folter and Angenent, 2006). This DNA-binding site is termed CArG motif with the overall consensus $CC(A/T)_6GG$ (Shore and Sharrocks, 1995; Riechmann and Meyerowitz, 1997; Folter and Angenent, 2006), recently renamed perfect CArG-box (Aerts et al., 2018). Several variants of this sequence have been recognized as regulatory motifs for binding to some MADS-domain proteins (Folter and Angenent, 2006; Aerts et al., 2018). These motifs still conserve the DNA-binding properties

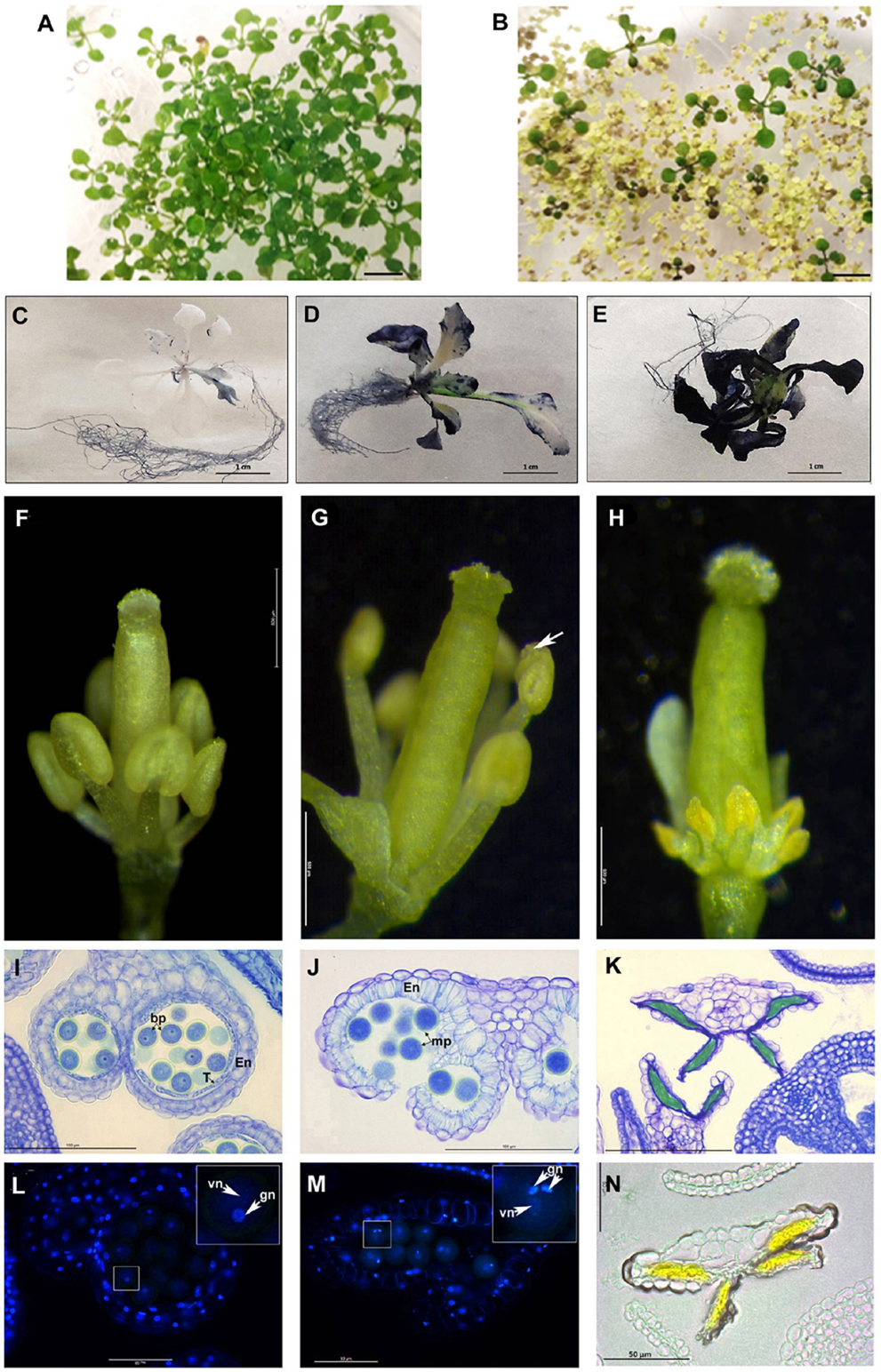

FIGURE 5 | *PsEND1* ectopic expression in Arabidopsis plants. **(A–F)** Vegetative phenotype of 2-weeks-old Arabidopsis seedlings from the wild-type **(A)** and 35S:*PsEND1* plants **(B)**. **(C–E)** Detection of reactive oxygen species (ROS) production in *Arabidopsis thaliana* seedlings overexpressing *PsEND*1 by Nitroblue tetrazolium (NBT) staining. **(F–H)** Floral phenotypes of *A. thaliana* plants overexpressing *PsEND1* (the petals and sepals have been removed). **(F)** Wild type flower. **(G)** 35S:*PsEND1* flower showing early dehiscence (white arrow). **(H)** 35S:*PsEND1* flower showing collapsed, arrow-shaped anthers**. (I–K)** Histological sections of

(Continued)

FIGURE 5 | (Continued)
anthers stained with toluidine blue. **(I)** Wild type flower anther showing a layer of intact tapetal cells and no endothecium secondary thickening. **(J)** Cross-section of a 35S:PsEND1 anther showing a disrupted septum and stomium secondary thickening of the endothecium and degenerated tapetum. **(K)** Cross-section of an arrow-shaped 35S:*PsEND1* anther where the pollen cells were replaced by an amorphous mass and the tapetal cell layer is absent. **(L–M)** Cross-section of wild type **(L)** and 35S:*PsEND1* anthers **(M)** of the same flower size, stained with DAPI and observed under a fluorescence microscope. **(L)** Cross-section of a wild type anther, presenting binucleate pollen (inset) and an intact tapetum. **(M)** Cross-section of a 35S:PsEND1 anther, with trinucleate pollen (inset) and no tapetal cell layer. **(N)** The collapsed locules of the 35S:PsEND1 anthers presenting an intense yellow colored amorphous mass. En, endotecium; T, tapetum; Bp, bicellular pollen; vn, vegetative nucleus; gn, generative nucleus. Bars in **(A,B)** represent 1 cm.

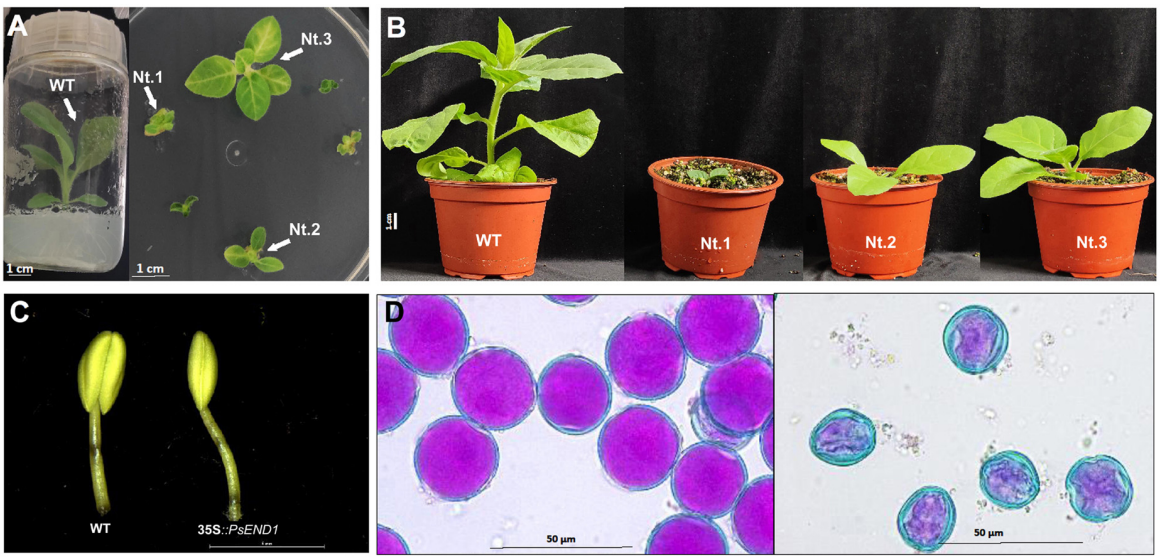

FIGURE 6 | Phenotypes of transgenic tobacco plants overexpressing *PsEND1*. **(A)** Tobacco plants 8 weeks after transformation. The control plant (left) has elongated and rooted and are ready to be acclimatized. The transgenic plants (right) are still much smaller and have not elongated nor rooted, yet. **(B)** Wild type (WT) and transgenic (Nt1, Nt2, and Nt3) tobacco plants 1 week after acclimatization in the greenhouse. The transgenic plants are smaller than the control. **(C)** Anthers of the transgenic plants (right) are smaller and lack two locules. **(D)** Alexander's staining of pollen grains from the control (left) and transgenic tobacco plants (right). Viable pollen is round-shaped and stained in pink.

of the MADS domain proteins as long as the mismatches do not eliminate either the C or G sequences flanking the A/T core. The A/T core can include C or G and may be formed by six to eight nucleotides (Gómez-Mena et al., 2005; Folter and Angenent, 2006). Besides, it has been reported that the most chosen DNA binding motif of MADS-box proteins was a CArG-box with an NAA extension comparing with a perfect CArG-box (Folter and Angenent, 2006; Aerts et al., 2018). The sequences CCATTTTGG found in the 5' *PsEND1* sequence is an almost perfect CArG motif. It features the typical dyad symmetry ending as CC and GG but differs from the rest since it has five nucleotides in the A/T core instead of six. However, this CArG-like regulatory motif (Gómez et al., 2004) contains an extension NAA: $CC(CA/T)_5GGGAA$ at position 13. CArG-box has 10 positions, being the first C, the position 1 and the last G, the defined position 10 (Aerts et al., 2018). It has been demonstrated that there is a preference for adenines at positions 12 and 13, thus extending the consensus motif of a perfect CArG-box to $CC(A/T)_6GGNAA$ (Aerts et al., 2018). Therefore, the sequence $CC(CA/T)_5GGGAA$ found in the 5′ region of the pea *PsEND1* gene might be a new CArG-box regulatory motif variant.

In summary, the flexibility of the CArG-box sequences recognized by MADS target genes, the early specific expression of *PsEND1* in the anther primordia and the results showed in this work suggest that *PsEND1* could be a target of the MADS-domain proteins that specify the stamen identity in *Pisum sativum*. Further experiments will be needed to confirm that the Pisum MADS-box proteins that confer stamen identity can interact with this putative CArG-box regulatory motif. Interestingly, the rice hemopexin fold protein gene (*OsHFP*) promoter also presents a CArG-like regulatory element essential for its specific expression in anthers (Chattopadhyay et al., 2012). In line with this, the C-function MADS-box gene *MADS3* has been related to the promoter of a ROS-scavenging gene in rice (Hu et al., 2011). Accordingly, our data suggest that *PsEND1* could be a hemopexin regulated by a MADS-box protein, modulating redox homeostasis during early anther development in pea.

PsEND1 Is Essential for Proper Pollen Development in *Pisum sativum*

In this work, we have shown that *PsEND1* is of major importance for the development of pollen and the surrounding

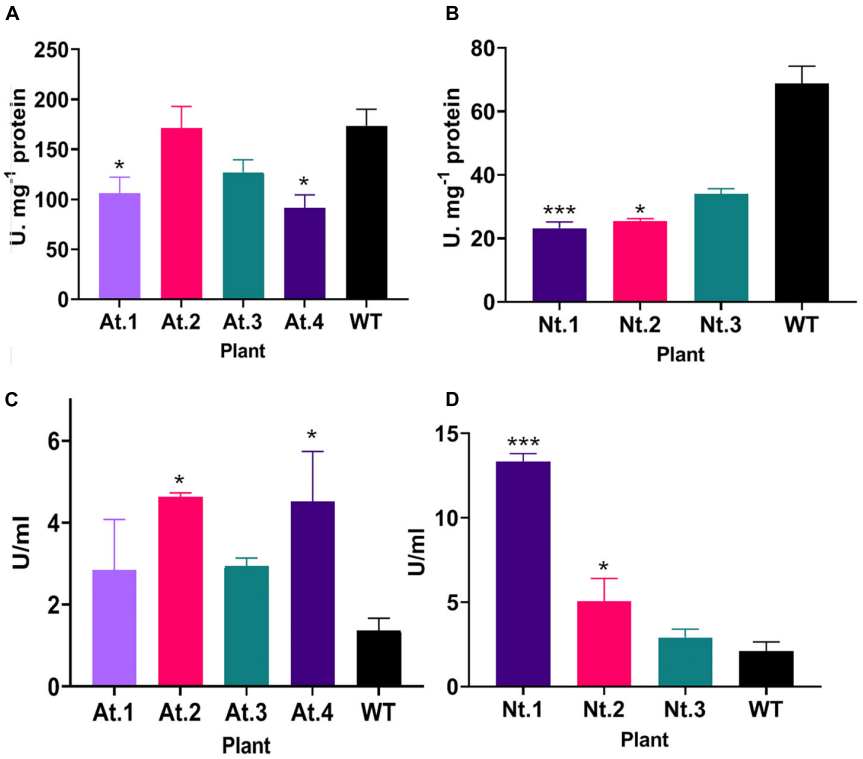

FIGURE 7 | Superoxide dismutase and peroxidase activity in transgenic *Arabidopsis thaliana* and *Nicotiana tabacum* plants. **(A)** SOD activity in transgenic *A. thaliana* plants. Plants At.1 and At.4 show a significant decrease in SOD activity compared to the wild type. **(B)** SOD activity in transgenic *N. tabacum* plants. The transgenic plants Nt.1 and Nt.2 show a significant decrease in SOD activity compared to the wild type. **(C)** Peroxidase activity in transgenic *A. thaliana* plants. Plants At.2 and At.4 show a significant increase in peroxidase activity compared to the wild type. **(D)** Peroxidase activity in transgenic *N. tabacum* plants. The transgenic plants Nt.1 and Nt.2 show a significant increase in peroxidase activity compared to the wild type. $^{*}p \leq 0.05$, $^{**}p \leq 0.01$, $^{***}p \leq 0.001$.

tissues. *PsEND1* expression begins at an early stage of anther development, in the stamen primordium. Later, it is expressed in the primary parietal cells, precursor cells of the endothecium, middle layer, and tapetum tissues (Gómez et al., 2004). At this stage, these cells are contiguous with the primary sporogenous cell lineage, and *PsEND1* is participating in the modulation of ROS in the cells that will differentiate into different sporophytic tissues, including the tapetum. Therefore, its downregulation affects the development and degeneration of the tapetal cells and causes the abortion of pollen. The tapetum is a transitory apoptotic tissue that provides nutrients to microspores. Hence, a functional tapetum is essential for the proper development of microspores. In fact, different male-sterile mutants present tapetum ablation or affected tapetum (Mariani et al., 1990; Goldberg et al., 1993; Sanders et al., 1999; Kawanabe et al., 2006; Parish and Li, 2010; García et al., 2017). Tapetum PCD occurs at late microsporogenesis stages. The precise timing of this process is of vital importance for pollen development (Ko et al., 2017; Sun et al., 2018; Bai et al., 2019; Gao et al., 2019; Shukla et al., 2019; Xu et al., 2019; Zheng et al., 2019; Lei and Liu, 2020; Mondol et al., 2020). In this context, different studies have demonstrated that the arrest of tapetum development at early stages results in meiotic cell cycle arrest and meiocytes maturation failure (Murmu et al., 2010; Cui et al., 2018). Accordingly, our findings show that *PsEND1* plays an essential role in the synchronization of tapetum degeneration and, thus, in the development of viable pollen grains in *Pisum sativum*.

PsEND1 Participates in Pollen Development Through the Modulation of Redox Homeostasis

Through *in silico* 3D modeling, we have shown that PsEND1 presents the typical beta-propeller structure responsible for heme binding in the hemopexins (Paoli et al., 1999). The presence of eight possible heme binding motifs in the PsEND1 protein has been predicted using the online HeMoQuest software, which shows a high level of accuracy (92%) in identifying heme binding motifs (George et al., 2020). Taken together, these results suggest that PsEND1 possesses the biochemical capacity of binding heme and, consequently, could participate in redox modulation.

The overexpression of *PsEND1* in Arabidopsis seedlings produces an accumulation of superoxide anion $O_2^{\cdot -}$ supporting its implication in ROS modulation. Previous studies have linked heme with ROS scavenging enzymes. For instance, in *Saccahromyces cerevisiae* it had been shown that heme regulates the expression of SOD (Pinkham et al., 1997). Moreover, it has

been demonstrated that the expression of the rice Hemopexin *OsHFP* in *E. coli* affects the expression of a SOD isozyme (Chattopadhyay et al., 2015). Accordingly, the downregulation of *PsEND1* in pea and its ectopic overexpression in *A. thaliana* and tobacco affected the enzymatic activities of SOD and peroxidase. Additionally, Arabidopsis plants overexpressing *PsEND1* accumulated flavonoids in their anthers, which are also ROS-scavenging molecules. This confirms that *PsEND1* interferes with different ROS-scavenging mechanisms involved in the maintenance of balanced redox levels. ROS have been shown to play an essential role in tapetum development and PCD in model dicots and rice (Hu et al., 2011; Xie et al., 2014; Yi et al., 2016; Jacobowitz et al., 2019; Zheng et al., 2019). Several studies have shown that the loss of redox balance, either by an increase or a decrease in ROS, impairs tapetum degradation and pollen development (Hu et al., 2011; Luo et al., 2013; Xie et al., 2014). For instance, in tomato (Yan et al., 2020) and rice (Yi et al., 2016) it has been found that a decrease in ROS levels caused a delay in tapetum degradation. Nonetheless, in wheat, an excess of ROS levels has been associated with delayed tapetum degeneration (Liu et al., 2018). These studies are in agreement with the anther defects observed here by downregulation or overexpression of *PsEND1* in different species.

In Arabidopsis, it has been shown that the apoplastic class III peroxidases (PRX9 and PRX40*)* are required for the correct development of the anthers. *prx9-1* and *prx40-2* mutants showed defects similar to those observed in the VIGS-*PsEND1* anthers, with swollen tapetal cells at early meiosis stages and aborted pollen (Jacobowitz et al., 2019). It is also noteworthy that this class of peroxidases have also been found in pollen cells and, therefore, could play an essential role in their development (Sankaranarayanan et al., 2020). In tobacco and tomato plants, the manipulation of the expression of Rbohs proteins, which are involved in ROS regulation, resulted in the impairment of tapetal degradation and pollen development. Similarly over-accumulation of ROS in rice anthers generated premature initiation of tapetum PCD and pollen abortion (Zheng et al., 2019). These results are in accordance with the phenotype observed in the VIGS-*PsEND1* anthers where we detected by TUNEL assay the early degradation of the tapetum cells, leading to pollen abortion.

It is noteworthy that in the pea VIGS-*PsEND1* and *A. thaliana* 35S:*PsEND1* flowers, the first defects in pollen are observed approximately at the same stage: when the PMC are undergoing the first meiosis. Indeed, ROS have been suggested, for a long time, to play a role in cell cycle progression as an intrinsic signal (Ho and Dowdy, 2002; Jorgensen and Tyers, 2004). For instance, Reichheld et al. (1999) have shown that oxidative stress affect cell divisions and SOD expression in *Nicotiana tabacum* both in plant cell culture and plants. Moreover, it has been shown that in Arabidopsis embryogenic roots, the G1 phase is accelerated in the oxidized state and slowed in the reduced state (de Simone et al., 2017). Our findings are in accordance with these results. Under the oxidative stress caused by the overexpression of *PsEND1* in Arabidopsis and after the early meiosis stage, the PMC and surrounding tissues (tapetum and endothecium) either degenerated and collapsed or presented an accelerated development leading to early pollen maturation, tapetum degradation and endothecium lignification. In plants, studies have shown that there is a tightly regulated gradient of ROS during the development of the pollen and throughout the meiosis (Zafra et al., 2010; Xu et al., 2019). In pea, the regulation of ROS and the activity of antioxidant enzymes in flowers have not been described previously. In our work, we determined the activity of two of the major ROS detoxifying enzymes: SOD and PRX, during the early anther developmental stages. Interestingly, the activity of both enzymes is altered at the same stage in the VIGS-*PsEND1* flowers, where the depletory effects on tapetum and PMC are observed (stage 3 mm). These findings confirm that the fine quantitative and spatio-temporal regulation of redox homeostasis at early anther developmental stages and, especially at the start of meiosis, is critical for the correct development of anther tissues and proper pollen development.

Subcellular localization of hemopexins has not been described in plants before. Our work is the first to report the localization of a plant hemopexin in plasmodesmata. These channels allow the communication between neighboring cells as well as distantly located cells through the symplastic pathway (Ding et al., 2003; Cilia and Jackson, 2004; Heinlein and Epel, 2004). They are responsible for transporting non-cell-autonomous signaling molecules such as transcription factors, small RNAs or ROS (Haywood et al., 2002; Heinlein, 2002; Wu et al., 2002; Sager and Lee, 2018). Also, due to their proximity to the cell wall, it has been suggested by previous studies that plasmodesmata act as a bridge between the symplastic and apoplastic compartments (Stahl and Simon, 2013). In plants, peroxidases are heme-containing enzymes that have been found in the apoplast, where they participate in redox homeostasis. PsEND1 localization suggests that this protein might interact directly or indirectly with peroxidases to modulate ROS levels and transport through plasmodesmata.

During early pollen development stages, plasmodesmata exist at the junction of different tissues: middle layer-tapetum, between tapetum cells, tapetum- PMC and between pre-meiotic PMC (Steer, 1977; Radice et al., 2008; Sager and Lee, 2014). This connection permits the feeding of the developing PMC by the tapetum. This would explain the effect of *PsEND1* expression alteration on tapetum and pollen cells even though the gene is not expressed in these cells. H_2O_2, which is produced in the apoplast by dismutation of $O_2^{\cdot -}$, is the most stable ROS, with a half-life of 10^{-3} s (Mittler, 2017; Mhamdi and van Breusegem, 2018). Then, it can be transported through the plasma membrane and participate in cell signaling or cause long-distance damage (Bienert et al., 2006; Lodde et al., 2021). *PsEND1* is expressed since very early developmental stages of the anthers in the cell layers neighboring those that will produce the tapetum and pollen. Thus, *PsEND1* might be participating in the communication among cell layers modulating ROS accumulation during the early stages of anther development.

Taken together, our results indicate that *PsEND1* is a central player in the maintenance of balanced redox levels during anther development. Further studies with fine monitoring of heme levels, ROS and oxidants production would provide further

insight into the biochemical mechanisms by which *PsEND1* modulates redox homeostasis in the anthers.

DATA AVAILABILITY STATEMENT

The original contributions presented in the study are included in the article/**Supplementary Material**, further inquiries can be directed to the corresponding author/s.

AUTHOR CONTRIBUTIONS

RH, ER, and CG-M performed the experiments. RH, ER, CG-M, FM, JB, and LC conceived the experiments and analyzed the data. LC and CG-M wrote the grants that funded this work. RH, ER, and LC wrote the manuscript. All authors read and approved the final version of this manuscript.

FUNDING

This work was funded by the grants PID2019-106060RB-I00 and RTI2018-094280-100 from the Spanish Ministry of Science and Innovation (MICINN).

ACKNOWLEDGMENTS

We acknowledge the support of the publication fee by the CSIC Open Access Publication Support Initiative through its Unit of Information Resources for Research (URICI).

SUPPLEMENTARY MATERIAL

The Supplementary Material for this article can be found online at: https://www.frontiersin.org/articles/10.3389/fpls.2021.765277/full#supplementary-material

Supplementary Figure 1 | Comparative cross-sections of WT and 35S:*PsEND1* *Arabidopsis thaliana* flowers stained with toluidine blue. **(A)** Wild type; **(B,C)** 35S:*PsEND1*. At the first stages of development, we do not observe differences between anthers in **(A,B)**, while at the stage of meiocytes **(C)** most of the anthers have collapsed. After this stage, the pollen mother cells and the tapetum degenerate.

Supplementary Figure 2 | PsEND1 sequence and predicted 3D structure showing the heme binding sites. **(A)** PsEND1 sequence, the hemopexin motifs are highlighted in blue boxes. **(B)** Predicted PsEND1 3D structure. Cyan: Hemopexin domain at position 4–55; Pink: Hemopexin domain at position 62–112; Orange: Hemopexin domain at position 118–165; Green: Hemopexin domain at position 171–222. **(C)** Heme binding motifs predicted by the software HeMoQuest. **(D)** PsEND1 3D model showing the localization of eight heme binding motifs predicted by the software HeMoQuest. The predicted heme binding sites are represented by spheres of different colors.

REFERENCES

Aerts, N., de Bruijn, S., van Mourik, H., Angenent, G. C., and van Dijk, A. D. (2018). Comparative analysis of binding patterns of MADS-domain proteins in *Arabidopsis thaliana*. *BMC Plant Biol.* 18:131. doi: 10.1186/s12870-018-1348-8

Alexander, M. P. (1969). Differential staining of aborted and non aborted pollen. *Stain Technol.* 44, 117–122. doi: 10.3109/10520296909063335

Arora, A., Sairam, R. K., and Srivastava, G. C. (2002). Oxidative stress and antioxidative system in plants. *Curr. Sci.* 82, 1227–1238.

Bai, W., Wang, P., Hong, J., Kong, W., Xiao, Y., Yu, X., et al. (2019). *Earlier Degraded Tapetum1* (*EDT1*) encodes an ATP-citrate lyase required for tapetum programmed cell death. *Plant Physiol.* 181, 1223–1238. doi: 10.1104/pp.19.00202

Bate, N., and Twell, D. (1998). Functional architecture of a late pollen promoter: pollen-specific transcription is developmentally regulated by multiple stage-specific and co-dependent activator elements. *Plant Mol. Biol.* 37, 859–869.

Beltrán, J. P., Roque, E., Medina, M., Madueño, F., Gómez, M. D., and Cañas, L. A. (2007). Androesterilidad inducida mediante ingeniería genética en plantas: fundamentos y aplicaciones biotecnológicas. *Anal. Real Acad. Nacional Farmacia* 73, 1237–1264.

Bienert, G. P., Schjoerring, J. K., and Jahn, T. P. (2006). Membrane transport of hydrogen peroxide. *Biochem. Biophys. Acta* 1758, 994–1003.

Bradford, M. M. (1976). A rapid and sensitive method for the quantitation of microgram quantities of protein utilizing the principle of protein-dye binding. *Analyt. Biochem.* 72, 248–254.

Briones, M. V., Hoenicka, H., Cañas, L. A., Beltrán, J. P., Hanelt, D., Sharry, S., et al. (2020). Efficient evaluation of a gene containment system for poplar through early flowering induction. *Plant Cell Rep.* 39, 577–587.

Chang, F., Wang, Y., Wang, S., and Ma, H. (2011). Molecular control of microsporogenesis in Arabidopsis. *Curr. Opin. Plant Biol.* 14, 66–73. doi: 10.1016/j.pbi.2010.11.001

Chattopadhyay, T., Bhattacharyya, S., Das, A. K., and Maiti, M. K. (2012). A structurally novel hemopexin fold protein of rice plays role in chlorophyll degradation. *Biochem. Biophys. Res. Commun.* 420, 862–868. doi: 10.1016/j.bbrc.2012.03.089

Chattopadhyay, T., Das, P. K., Roy, S., and Maiti, M. K. (2015). Proposed physiological mode of action of rice hemopexin fold protein OsHFP: linking heme-binding with plant cell death. *Acta Physiol. Plantarum* 37:95.

Chinnusamy, V., Ohta, M., Kanrar, S., Lee, B. H., Hong, X., Agarwal, M., et al. (2003). ICE1: a regulator of cold-induced transcriptome and freezing tolerance in *Arabidopsis*. *Genes Dev.* 17, 1043–1054. doi: 10.1101/gad.1077503

Chinnusamy, V., Schumaker, K., and Zhu, J. K. (2004). Molecular genetic perspectives on cross-talk and specificity in abiotic stress signalling in plants. *J. Exper. Bot.* 55, 225–236. doi: 10.1093/jxb/erh005

Cilia, M. L., and Jackson, D. (2004). Plasmodesmata form and function. *Curr. Opin. Cell Biol.* 16, 500–506. doi: 10.1016/j.ceb.2004.08.002

Constantin, G. D., Krath, B. N., MacFarlane, S. A., Nicolaisen, M., Johansen, I. E., and Lund, O. S. (2004). Virus-induced gene silencing as a tool for functional genomics in a legume species. *Plant J.* 40, 622–631. doi: 10.1111/j.1365-313x.2004.02233.x

Cui, Y., Hu, C., Zhu, Y., Cheng, K., Li, X., Wei, Z., et al. (2018). CIK receptor kinases determine cell fate specification during early anther development in *Arabidopsis*. *Plant Cell* 30, 2383–2401. doi: 10.1105/tpc.17.00586

Folter, S., and Angenent, G. C. (2006). Trans meets cis in MADS science. *Trends Plant Sci.* 11, 224–231. doi: 10.1016/j.tplants.2006.03.008

de Simone, A., Hubbard, R., De La Torre, N. V., Velappan, Y., Wilson, M., Considine, M. J., et al. (2017). Redox changes during the cell cycle in the embryonic root meristem of Arabidopsis thaliana. *Antioxid. Redox Signal.* 27, 1505–1519. doi: 10.1089/ars.2016.6959

Ding, B., Itaya, A., and Qi, Y. (2003). Symplasmic protein and RNA traffic: regulatory points and regulatory factors. *Curr. Opin. Plant Biol.* 6, 596–602.

Filichkin, S. A., Leonard, J. M., Monteros, A., Liu, P. P., and Nonogaki, H. (2004). A novel endo-β-mannanase gene in tomato LeMAN5 is associated with anther and pollen development. *Plant Physiol.* 134, 1080–1087.

Fu, Y., Li, M., Zhang, S., Yang, Q., Zhu, E., You, C., et al. (2020). Analyses of functional conservation and divergence reveal requirement of bHLH010/089/091 for pollen development at elevated temperature in *Arabidopsis*. *J. Genet. Genom.* 47, 477–492. doi: 10.1016/j.jgg.2020.09.001

Gáll, T., Pethő, D., Nagy, A., Hendrik, Z., Méhes, G., Potor, L., et al. (2018). Heme induces endoplasmic reticulum stress (HIER stress) in human aortic smooth muscle cells. *Front. Plant Sci.* 9:1595. doi: 10.3389/fphys.2018.01595

Gao, J., Li, Q., Wang, N., Tao, B., Wen, J., Yi, B., et al. (2019). Tapetal expression of BnaC. MAGL8. a causes male sterility in Arabidopsis. *Front. Plant Sci.* 10:763. doi: 10.3389/fpls.2019.00763

García, C. C., Nepi, M., and Pacini, E. (2017). It is a matter of timing: asynchrony during pollen development and its consequences on pollen performance in angiosperms-a review. *Protoplasma* 254, 57–73. doi: 10.1007/s00709-016-0950-6

Gaur, V., Chanana, V., Jain, A., and Salunke, D. M. (2011). The structure of a haemopexin-fold protein from cow pea (*Vigna unguiculata*) suggests functional diversity of haemopexins in plants. *Acta Crystallogr. Sect. F Struct. Biol. Cryst. Commun.* 67, 193–200. doi: 10.1107/s1744309110051250

Gaur, V., Qureshi, I. A., Singh, A., Chanana, V., and Salunke, D. M. (2010). Crystal structure and functional insights of hemopexin fold protein from grass pea. *Plant Physiol.* 152, 1842–1850. doi: 10.1104/pp.109.150680

George, A. A. P., Lacerda, M., Syllwasschy, B. F., Hopp, M.-T., Wißbrock, A., and Imhof, D. (2020). HeMoQuest: a webserver for qualitative prediction of transient heme binding to protein motifs. *BMC Bioinform.* 21:124. doi: 10.1186/s12859-020-3420-2

Goldberg, R. B., Beals, T. P., and Sanders, P. M. (1993). Anther development: basic principles and practical applications. *Plant Cell* 5:1217. doi: 10.2307/3869775

Gómez, M. D., Beltrán, J. P., and Cañas, L. A. (2004). The pea END1 promoter drives anther-specific gene expression in different plant species. *Planta* 219, 967–981. doi: 10.1007/s00425-004-1300-z

Gómez-Mena, C., de Folter, S., Costa, M. M. R., Angenent, G. C., and Sablowski, R. (2005). Transcriptional program controlled by the floral homeotic gene *AGAMOUS* during early organogenesis. *Development* 132, 429–438. doi: 10.1242/dev.01600

Hafidh, S., Fíla, J., and Honys, D. (2016). Male gametophyte development and function in angiosperms: a general concept. *Plant Reproduc.* 29, 31–51. doi: 10.1007/s00497-015-0272-4

Hamza, R., Pérez-Hedo, M., Urbaneja, A., Rambla, J. L., Granell, A., Gaddour, K., et al. (2018). Expression of two barley proteinase inhibitors in tomato promotes endogenous defensive response and enhances resistance to *Tuta absoluta*. *BMC Plant Biol.* 18:24. doi: 10.1186/s12870-018-1240-6

Hartley, R. W. (1988). *Barnase* and *barstar*: expression of its cloned inhibitor permits expression of a cloned ribonuclease. *J. Mol. Biol.* 202, 913–915.

Haywood, V., Kragler, F., and Lucas, W. J. (2002). Plasmodesmata: pathways for protein and ribonucleoprotein signaling. *Plant Cell* 14, S303–S325.

Heinlein, M. (2002). Plasmodesmata: dynamic regulation and role in macromolecular cell-to-cell signaling. *Curr. Opin. Plant Biol.* 5, 543–552. doi: 10.1016/s1369-5266(02)00295-9

Heinlein, M., and Epel, B. L. (2004). Macromolecular transport and signaling through plasmodesmata. *Int. Rev. Cytol.* 235, 93–164.

Higgins, T. J. V., Beach, L. R., Spencer, D., Chandler, P. M., Randall, P. J., Blagrove, R. J., et al. (1987). cDNA and protein sequence of a major pea seed albumin (PA2: Mr 26.000). *Plant Mol. Biol.* 8, 37–45. doi: 10.1007/bf00016432

Higo, K., Ugawa, Y., Iwamoto, M., and Korenaga, T. (1999). Plant cis-acting regulatory DNA elements (PLACE) database: 1999. *Nucleic Acids Res.* 27, 297–300. doi: 10.1093/nar/27.1.297

Ho, A., and Dowdy, S. F. (2002). Regulation of G1 cell-cycle progression by oncogenes and tumor suppressor genes. *Curr. Opin. Genet. Dev.* 12, 47–52. doi: 10.1016/s0959-437x(01)00263-5

Hu, L., Liang, W., Yin, C., Cui, X., Zong, J., Wang, X., et al. (2011). Rice MADS3 regulates ROS homeostasis during late anther development. *Plant Cell* 23, 515–533.

Huang, H., Ullah, F., Zhou, D.-X., Yi, M., and Zhao, Y. (2019). Mechanisms of ROS regulation of plant development and stress responses. *Front. Plant Sci.* 10:800. doi: 10.3389/fpls.2019.00800

Jacobowitz, J. R., Doyle, W. C., and Weng, J. K. (2019). PRX9 and PRX40 are extensin peroxidases essential for maintaining tapetum and microspore cell wall integrity during Arabidopsis anther development. *Plant Cell* 31, 848–861. doi: 10.1105/tpc.18.00907

Jeney, V., Balla, J., Yachie, A., Varga, Z., Vercellotti, G. M., Eaton, J. W., et al. (2002). Pro-oxidant and cytotoxic effects of circulating heme. *Blood* 100, 879–887. doi: 10.1182/blood.v100.3.879

Jorgensen, P., and Tyers, M. (2004). How cells coordinate growth and division. *Curr. Biol.* 14, R1014–R1027.

Kawanabe, T., Ariizumi, T., Kawai-Yamada, M., Uchimiya, H., and Toriyama, K. (2006). Abolition of the tapetum suicide program ruins microsporogenesis. *Plant Cell Physiol.* 47, 784–787. doi: 10.1093/pcp/pcj039

Ko, S. S., Li, M. J., Lin, Y. J., Hsing, H. X., Yang, T. T., Chen, T. K., et al. (2017). Tightly controlled expression of bHLH142 is essential for timely tapetal programmed cell death and pollen development in rice. *Front. Plant Sci.* 8:1258. doi: 10.3389/fpls.2017.01258

Kumar, S., and Bandyopadhyay, U. (2005). Free heme toxicity and its detoxification systems in human. *Toxicol. Lett.* 157, 175–188.

Lei, X., and Liu, B. (2020). Tapetum-dependent male meiosis progression in plants: increasing evidence emerges. *Front. Plant Sci.* 10:1667. doi: 10.3389/fpls.2019.01667

Liu, Z., Shi, X., Li, S., Hu, G., Zhang, L., and Song, X. (2018). Tapetal-delayed programmed cell death (PCD) and oxidative stress-induced male sterility of Aegilops uniaristata cytoplasm in wheat. *Int. J. Mol. Sci.* 19:1708. doi: 10.3390/ijms19061708

Livak, K. J., and Schmittgen, T. D. (2001). Analysis of relative gene expression data using real-time quantitative PCR and the 2- ΔΔCT method. *Methods* 25, 402–408. doi: 10.1006/meth.2001.1262

Lodde, V., Morandini, P., Costa, A., Murgia, I., and Ezquer, I. (2021). cROStalk for life: uncovering ROS signaling in plants and animal systems, from gametogenesis to early embryonic development. *Genes* 12:525. doi: 10.3390/genes12040525

Luo, D., Xu, H., Liu, Z., Guo, J., Li, H., Chen, L., et al. (2013). A detrimental mitochondrial-nuclear interaction causes cytoplasmic male sterility in rice. *Nat. Genet.* 45, 573–577. doi: 10.1038/ng.2570

Mariani, C., De Beuckeleer, M., Truettner, J., Leemans, J., and Goldberg, R. B. (1990). Induction of male sterility in plants by a chimaeric ribonuclease gene. *Nature* 347, 737–741. doi: 10.1038/347737a0

Mhamdi, A., and van Breusegem, F. (2018). Reactive oxygen species in plant development. *Development* 145:dev164376.

Miller, G. A. D., Suzuki, N., Ciftci-Yilmaz, S. U. L. T. A. N., and Mittler, R. O. N. (2010). Reactive oxygen species homeostasis and signalling during drought and salinity stresses. *Plant Cell Environ.* 33, 453–467.

Mittler, R. (2017). ROS are good. *Trends Plant Sci.* 22, 11–19. doi: 10.1016/j.tplants.2016.08.002

Mondol, P. C., Xu, D., Duan, L., Shi, J., Wang, C., Chen, X., et al. (2020). Defective Pollen Wall 3 (DPW3), a novel alpha integrin-like protein, is required for pollen wall formation in rice. *New Phytol.* 225, 807–822. doi: 10.1111/nph.16161

Murmu, J., Bush, M. J., DeLong, C., Li, S., Xu, M., Khan, M., et al. (2010). Arabidopsis basic leucine-zipper transcription factors TGA9 and TGA10 interact with floral glutaredoxins ROXY1 and ROXY2 and are redundantly required for anther development. *Plant Physiol.* 154, 1492–1504. doi: 10.1104/pp.110.159111

Oh, S. J., Song, S. I, Kim, Y. S., Jang, H. J., Kim, S. Y., Kim, M., et al. (2005). Arabidopsis CBF3/DREB1A and ABF3 in transgenic rice increased tolerance to abiotic stress without stunting growth. *Plant Physiol.* 138, 341–351. doi: 10.1104/pp.104.059147

Paoli, M., Anderson, B. F., Baker, H. M., Morgan, W. T., Smith, A., and Baker, E. N. (1999). Crystal structure of hemopexin reveals a novel high-affinity heme site formed between two β-propeller domains. *Nat. Struc. Biol.* 6, 926–931.

Parish, R. W., and Li, S. F. (2010). Death of a tapetum: a programme of developmental altruism. *Plant Sci.* 178, 73–89. doi: 10.1016/j.plantsci.2009.11.001

Pettersen, E. F., Goddard, T. D., Huang, C. C., Couch, G. S., Greenblatt, D. M., Meng, E. C., et al. (2004). UCSF Chimera-a visualization system for exploratory research and analysis. *J. Comput. Chem.* 25, 1605–1612. doi: 10.1002/jcc.20084

Pinkham, J. L., Wang, Z., and Alsina, J. (1997). Heme regulates SOD2 transcription by activation and repression in *Saccharomyces cerevisiae*. *Curr. Genet.* 31, 281–291. doi: 10.1007/s002940050207

Radice, S., Ontivero, M., Giordani, E., and Bellini, E. (2008). Anatomical differences on development of fertile and sterile pollen grains of *Prunus salicina* Lindl. *Plant Syst. Evol.* 273, 63–69. doi: 10.1007/s00606-008-0011-5

Reichheld, J. P., Vernoux, T., Lardon, F., Van Montagu, M., and Inzé, D. (1999). Specific checkpoints regulate plant cell cycle progression in response to oxidative stress. *Plant J.* 17, 647–656.

Riechmann, J. L., and Meyerowitz, E. M. (1997). MADS-domain proteins in plant development. *Biol. Chem.* 378, 1079–1102.

Robinson, G. H. J., and Domoney, C. (2021). Perspectives on the genetic improvement of health- and nutrition-related traits in pea. *Plant Physiol. Biochem.* 158, 353–362. doi: 10.1016/j.plaphy.2020.11.020

Rogers, H. J., Bate, N., Combe, J., Sullivan, J., Sweetman, J., Swan, C., et al. (2001). Functional analysis of cis-regulatory elements within the promoter of the tobacco late pollen gene *g10*. *Plant Mol. Biol.* 45, 577–585.

Roque, E., Gómez, M. D., Ellul, P., Wallbraun, M., Madueño, F., Beltrán, J. P., et al. (2007). The PsEND1 promoter: a novel tool to produce genetically engineered male-sterile plants by early anther ablation. *Plant Cell Rep.* 26, 313–325. doi: 10.1007/s00299-006-0237-z

Roque, E., Hamza, R., Gómez-Mena, C., Beltrán, J. P. and Cañas, L. A. (2019). Engineered male sterility by early anther ablation using the anther-specific promoter PsEND1. *Front. Plant Sci.* 10:819. doi: 10.3389/fpls.2019.00819

Sager, R., and Lee, J. Y. (2014). Plasmodesmata in integrated cell signalling: insights from development and environmental signals and stresses. *J. Exper. Bot.* 65, 6337–6358. doi: 10.1093/jxb/eru365

Sager, R. E., and Lee, J. Y. (2018). Plasmodesmata at a glance. *J. Cell Sci.* 131:jcs209346.

Sanders, P. M., Bui, A. Q., Weterings, K., McIntire, K. N., Hsu, Y. C., Lee, P. Y., et al. (1999). Anther developmental defects in *Arabidopsis thaliana* male-sterile mutants. *Sex. Plant Reproduc.* 11, 297–322. doi: 10.1007/s004970050158

Sankaranarayanan, S., Ju, Y., and Kessler, S. A. (2020). Reactive oxygen species as mediators of gametophyte development and double fertilization in flowering plants. *Front. Plant Sci.* 11:1199. doi: 10.3389/fpls.2020.01199

Schippers, J. H., Foyer, C. H., and van Dongen, J. T. (2016). Redox regulation in shoot growth, SAM maintenance and flowering. *Curr. Opin. Plant Biol.* 29, 121–128. doi: 10.1016/j.pbi.2015.11.009

Shore, P., and Sharrocks, A. D. (1995). The MADS-box family of transcription factors. *Eur. J. Biochem.* 229, 1–13.

Shukla, P., Gautam, R., Singh, N. K., Ahmed, I., and Kirti, P. B. (2019). A proteomic study of cysteine protease induced cell death in anthers of male sterile tobacco transgenic plants. *Physiol. Mol. Biol. Plants* 25, 1073–1082. doi: 10.1007/s12298-019-00642-y

Stahl, Y., and Simon, R. (2013). Gated communities: apoplastic and symplastic signals converge at plasmodesmata to control cell fates. *J. Exper. Bot.* 64, 5237–5241. doi: 10.1093/jxb/ert245

Steer, M. W. (1977). Differentiation of the tapetum in Avena. I. The cell surface. *J. Cell Sci.* 25, 125–138. doi: 10.1242/jcs.25.1.125

Sun, L., Xiang, X., Yang, Z., Yu, P., Wen, X., Wang, H., et al. (2018). *OsGPAT3* plays a critical role in anther wall programmed cell death and pollen development in rice. *Int. J. Mol. Sci.* 19:4017. doi: 10.3390/ijms19124017

Tang, W., and Perry, S. E. (2003). Binding site selection for the plant MADS-domain protein AGL15: an *in vitro* and *in vivo* study. *J. Biol. Chem.* 278, 28154–28159. doi: 10.1074/jbc.m212976200

Tolosano, E., Fagoonee, S., Morello, N., Vinchi, F., and Fiorito, V. (2010). Heme-scavenging and the other facets of hemopexin. *Antioxid. Redox Signal.* 12, 305–320. doi: 10.1089/ars.2009.2787

Vercellotti, G. M., Balla, G., Balla, J., Nath, K., Eaton, J. W., and Jacob, H. S. (1994). Heme and the vasculature: an oxidative hazard that induces antioxidant defenses in the endothelium. *Artif. Cells Blood Substit. Immobil. Biotechnol.* 22, 207–213. doi: 10.3109/10731199409117415

Vigeoles, H., Chinoy, C., Zuther, E., Blessington, B., Geigenberger, P., and Domoney, C. (2008). Combined metabolomic and genetic approaches reveal a link between the polyamine pathway and albumin 2 in developing pea seeds. *Plant Physiol.* 146, 74–82.

Wilson, Z. A., and Zhang, D. B. (2009). From Arabidopsis to rice: pathways in pollen development. *J. Exper. Bot.* 60, 1479–1492. doi: 10.1093/jxb/erp095

Wu, X., Weigel, D., and Wigge, P. A. (2002). Signaling in plants by intercellular RNA and protein movement. *Genes Dev.* 16, 151–158. doi: 10.1101/gad.952002

Xie, H. T., Wan, Z. Y., Li, S., and Zhang, Y. (2014). Spatiotemporal production of reactive oxygen species by NADPH oxidase is critical for tapetal programmed cell death and pollen development in *Arabidopsis*. *Plant Cell* 26, 2007–2023. doi: 10.1105/tpc.114.125427

Xu, D., Qu, S., Tucker, M. R., Zhang, D., Liang, W., and Shi, J. (2019). *Ostkpr1* functions in anther cuticle development and pollen wall formation in rice. *BMC Plant Biol.* 19:104. doi: 10.1186/s12870-019-1711-4

Yan, M. Y., Xie, D. L., Cao, J. J., Xia, X. J., Shi, K., Zhou, Y. H., et al. (2020). Brassinosteroid-mediated reactive oxygen species are essential for tapetum degradation and pollen fertility in tomato. *Plant J.* 102, 931–947. doi: 10.1111/tpj.14672

Yanagisawa, S. (2000). *Dof1* and *Dof2* transcription factors are associated with expression of multiple genes involved in carbon metabolism in maize. *Plant J.* 21, 281–288. doi: 10.1046/j.1365-313x.2000.00685.x

Yanagisawa, S., and Schmidt, R. J. (1999). Diversity and similarity among recognition sequences of Dof transcription factors. *Plant J.* 17, 209–214.

Yi, J., Moon, S., Lee, Y. S., Zhu, L., Liang, W., Zhang, D., et al. (2016). Defective tapetum cell death 1 (DTC1) regulates ROS levels by binding to metallothionein during tapetum degeneration. *Plant Physiol.* 170, 1611–1623. doi: 10.1104/pp.15.01561

Zafra, A., Rodríguez-García, M. I., and de Dios Alché, J. (2010). Cellular localization of ROS and NO in olive reproductive tissues during flower development. *BMC Plant Biol.* 10:36. doi: 10.1186/1471-2229-10-36

Zhang, X., Henriques, R., Lin, S. S., Niu, Q. W., and Chua, N. H. (2006). Agrobacterium-mediated transformation of *Arabidopsis thaliana* using the floral dip method. *Nat. Protocols* 1, 641–646.

Zheng, S., Li, J., Ma, L., Wang, H., Zhou, H., Ni, E., et al. (2019). *OsAGO2* controls ROS production and the initiation of tapetal PCD by epigenetically regulating *OsHXK1* expression in rice anthers. *Proc. Natl. Acad. Sci.* 116, 7549–7558.

Zheng, X., He, L., Liu, Y., Mao, Y., Wang, C., Zhao, B., et al. (2020). A study of male fertility control in *Medicago truncatula* uncovers an evolutionarily conserved recruitment of two tapetal bHLH subfamilies in plant sexual reproduction. *New Phytol.* 228, 1115–1133.

Zhu, J., Lou, Y., Xu, X., and Yang, Z. N. (2011). A genetic pathway for tapetum development and function in Arabidopsis. *J. Integr. Plant Biol.* 53, 892–900.

Conflict of Interest: The authors declare that the research was conducted in the absence of any commercial or financial relationships that could be construed as a potential conflict of interest.

Publisher's Note: All claims expressed in this article are solely those of the authors and do not necessarily represent those of their affiliated organizations, or those of the publisher, the editors and the reviewers. Any product that may be evaluated in this article, or claim that may be made by its manufacturer, is not guaranteed or endorsed by the publisher.

frontiers in Plant Science

REVIEW
published: 07 January 2022
doi: 10.3389/fpls.2021.751230

Androgenesis-Based Doubled Haploidy: Past, Present, and Future Perspectives

Brett Hale[1,2], Alison M. R. Ferrie[3], Sreekala Chellamma[4], J. Pon Samuel[4] and Gregory C. Phillips[2,5,6]*

[1]Molecular Biosciences Graduate Program, Arkansas State University, Jonesboro, AR, United States, [2]Arkansas Biosciences Institute, Arkansas State University, Jonesboro, AR, United States, [3]National Research Council Canada, Saskatoon, SK, Canada, [4]Corteva Agriscience, Johnston, IA, United States, [5]College of Agriculture, Arkansas State University, Jonesboro, AR, United States, [6]Agricultural Experiment Station, University of Arkansas System Division of Agriculture, Jonesboro, AR, United States

Androgenesis, which entails cell fate redirection within the microgametophyte, is employed widely for genetic gain in plant breeding programs. Moreover, androgenesis-responsive species provide tractable systems for studying cell cycle regulation, meiotic recombination, and apozygotic embryogenesis within plant cells. Past research on androgenesis has focused on protocol development with emphasis on temperature pretreatments of donor plants or floral buds, and tissue culture optimization because androgenesis has different nutritional requirements than somatic embryogenesis. Protocol development for new species and genotypes within responsive species continues to the present day, but slowly. There is more focus presently on understanding how protocols work in order to extend them to additional genotypes and species. Transcriptomic and epigenetic analyses of induced microspores have revealed some of the cellular and molecular responses required for or associated with androgenesis. For example, microRNAs appear to regulate early microspore responses to external stimuli; trichostatin-A, a histone deacetylase inhibitor, acts as an epigenetic additive; ά-phytosulfokine, a five amino acid sulfated peptide, promotes androgenesis in some species. Additionally, present work on gene transfer and genome editing in microspores suggest that future endeavors will likely incorporate greater precision with the genetic composition of microspores used in doubled haploid breeding, thus likely to realize a greater impact on crop improvement. In this review, we evaluate basic breeding applications of androgenesis, explore the utility of genomics and gene editing technologies for protocol development, and provide considerations to overcome genotype specificity and morphogenic recalcitrance in non-model plant systems.

Keywords: androgenesis, doubled haploidy, microspore culture, plant breeding, pollen

OPEN ACCESS

Edited by:
Concepción Gómez-Mena, Polytechnic University of Valencia, Spain

Reviewed by:
Petr Smýkal, Palacký University, Olomouc, Czechia
Shivali Sharma, International Crops Research Institute for the Semi-Arid Tropics (ICRISAT), India

****Correspondence:***
Brett Hale
brett.hale@smail.astate.edu

Specialty section:
This article was submitted to Plant Development and EvoDevo, a section of the journal Frontiers in Plant Science

Received: *31 July 2021*
Accepted: *22 November 2021*
Published: *07 January 2022*

Citation:
Hale B, Ferrie AMR, Chellamma S, Samuel JP and Phillips GC (2022) Androgenesis-Based Doubled Haploidy: Past, Present, and Future Perspectives. Front. Plant Sci. 12:751230. doi: 10.3389/fpls.2021.751230

INTRODUCTION

In the vast majority of higher plants, a reproductive lineage is established by post-embryonic cell division that culminates with gametogenesis. Resultant gametes provide a basis for sporophyte-gametophyte life cycle alternation and allow the continuation of species through fertilization-mediated embryogenesis. In addition, plants have the capacity to undergo apozygotic embryogenesis

(Soriano et al., 2013). This phenomenon is observed commonly during *in vivo*, asexual reproduction (e.g., recurrent and nonrecurrent apomixis; uniparental chromosome elimination) and is exploited *in vitro* (e.g., gametophyte culture; somatic embryogenesis) for the genetic improvement of commercially-relevant species (Ferrie and Caswell, 2011). The most efficient method for artificially-induced, gametophyte-based apozygotic embryogenesis is androgenesis – a developmental program characterized by the generation of male-derived haploid progeny.

The primary benefit of androgenesis is the recovery of genetically-fixed, doubled haploid (DH) tissues, derived by leveraging the haploid state of the microspore and subsequent genome doubling. Given their homozygous nature, DH plants are ideal for rapid cultivar development in self-pollinated crops (**Figure 1**), for the generation of inbred parental lines during F_1 hybrid production, and for the discovery and introgression of novel traits (Ferrie and Möllers, 2011; Germanà, 2011). In the same context, DH technology has the potential to reduce undesirable events that may arise during the breeding pipeline, such as self-incompatibility during hybrid development and hemizygosity during transgenesis and genome editing (Dwivedi et al., 2015; Niazian and Shariatpanahi, 2020). Androgenesis-based doubled haploidy also serves as a model for fundamental research. The microspore is derived post-meiosis; thus, microspore-derived androgenic plants are useful for the construction of linkage maps, estimation of recombination frequencies, and for the manipulation of cell cycle machinery (**Figure 1**; Touraev et al., 1997; Ferrie and Möllers, 2011). Androgenesis also provides a tractable approach for the study of cell fate determination that may be extended to somatic and zygotic embryogenesis platforms (Hale et al., 2021).

Techniques for *in vivo* androgenic induction have been discussed recently (Ren et al., 2017); thus, this review focuses primarily on *in vitro* haploidization, its application in commercial plant breeding systems, and potential methods to expand protocols to recalcitrant species. In doing so, we emphasize the value of single-cell based approaches for improved selection efficiency and cultivar development, highlight advances in gene product delivery systems to drive cell fate redirection, and consider 'omic' and tissue culture-related strategies for improved androgenic response.

PLANT BREEDING APPLICATIONS: FROM LAB TO FIELD

In a conventional, science-based plant breeding process, genetic variability is created by cross-pollinating different parents with desirable trait combinations, followed by continuous selection and selfing. In traditional plant breeding strategies, such variability was evaluated, and selections based purely on the observed phenotype of the individual entries (Breseghello and Coelho, 2013). Later, with the development of molecular breeding techniques, selection of plants was fast-tracked using molecular markers linked to the desirable traits. Genetic variation was also generated using techniques such as mutagenesis, so that desirable traits were incorporated and later, selection was done to identify and select those recombinants (McNally et al., 2009). Since reducing timelines was a major goal in improving the plant breeding process, speed breeding was later introduced as a technique to reduce the total time to develop improved plant varieties (Ahmar et al., 2020). In this context, DHs allow homozygous inbred lines to be developed much faster and more efficiently than traditional breeding methods (Jarrod, 2020). Combining DHs and marker-assisted selection (MAS) has resulted in a significant advancement of the breeding systems in many major crops (Tuvesson et al., 2007). Genomic selection (GS), as a recently emerged technology to predict the performance of plants without phenotyping, has proven to be effective in plant breeding (Li et al., 2020; Krishnappa et al., 2021).

DH methods have been, and are being, used to accelerate the breeding programs in a variety of crop plants, including maize (*Zea mays*), barley (*Hordeum vulgare*), *Brassica* sp., wheat (*Triticum aestivum*), and several vegetable crops (Ho and Jones, 1980; Ferrie and Möllers, 2011; Krishnappa et al., 2021). Maize is a crop where such an increase in improvement efficiency has resulted in a significant increase in genetic gain (Li et al., 2020). Geiger et al. (2013) reported that genetic variances and *per se* performance were substantially increased in haploids and DH in maize. This might have significantly contributed to progress in maize hybrid and population breeding. Wheat is another species where the use of DH technology has significantly reduced the breeding timelines and increased genetic gain (Barkley and Chumley, 2012). *Brassica* sp. was identified as one of the best responding species for androgenesis. Most of the currently grown *B. napus* varieties originated from DH technology and many of the *B. oleracea* vegetable breeding programs also use doubled haploidy (Ferrie and Möllers, 2011). In vegetable crops such as cauliflower (*Brassica oleracea* var. *botrytis*), a high degree of cross-pollination and strong S-allele results in enormous heterozygosity. This makes conventional selfing for the development of homozygous inbreds practically impossible (Nieuwhof, 1963). Therefore, the development of complete homozygous lines through the androgenesis process remains very attractive. In crops like cassava (*Manihot esculenta*), genetic improvement is slow due to long breeding cycles, large genetic load, and the heterozygous nature of parents and progeny (Ceballos et al., 2015). In such circumstances, the development of a DH system would greatly benefit breeding efforts.

The use of DHs in the breeding process was originally determined based on the plant mode of reproduction. In crops that are self-pollinated, DHs can be used directly as the final varieties/cultivars. Homozygosity created by the DHs allows the selection of both qualitative and quantitative characters (Murovec and Bohanec, 2012). Self-pollination allows further propagation of these cultivars as true-breeding lines. DHs can also be used as parental lines or test-cross lines in the hybrid breeding of cross-pollinated species (Rudolf-Pilih et al., 2019). Additionally, they can be used in a recurrent selection scheme in which superior doubled haploids of one cycle can be used as parents for the next hybridization cycle (Murovec and Bohanec, 2012). More recently, DHs have been recommended as breeding material in reverse breeding-based combining ability tests (Rudolf-Pilih et al., 2019) to enhance the hybrid breeding process.

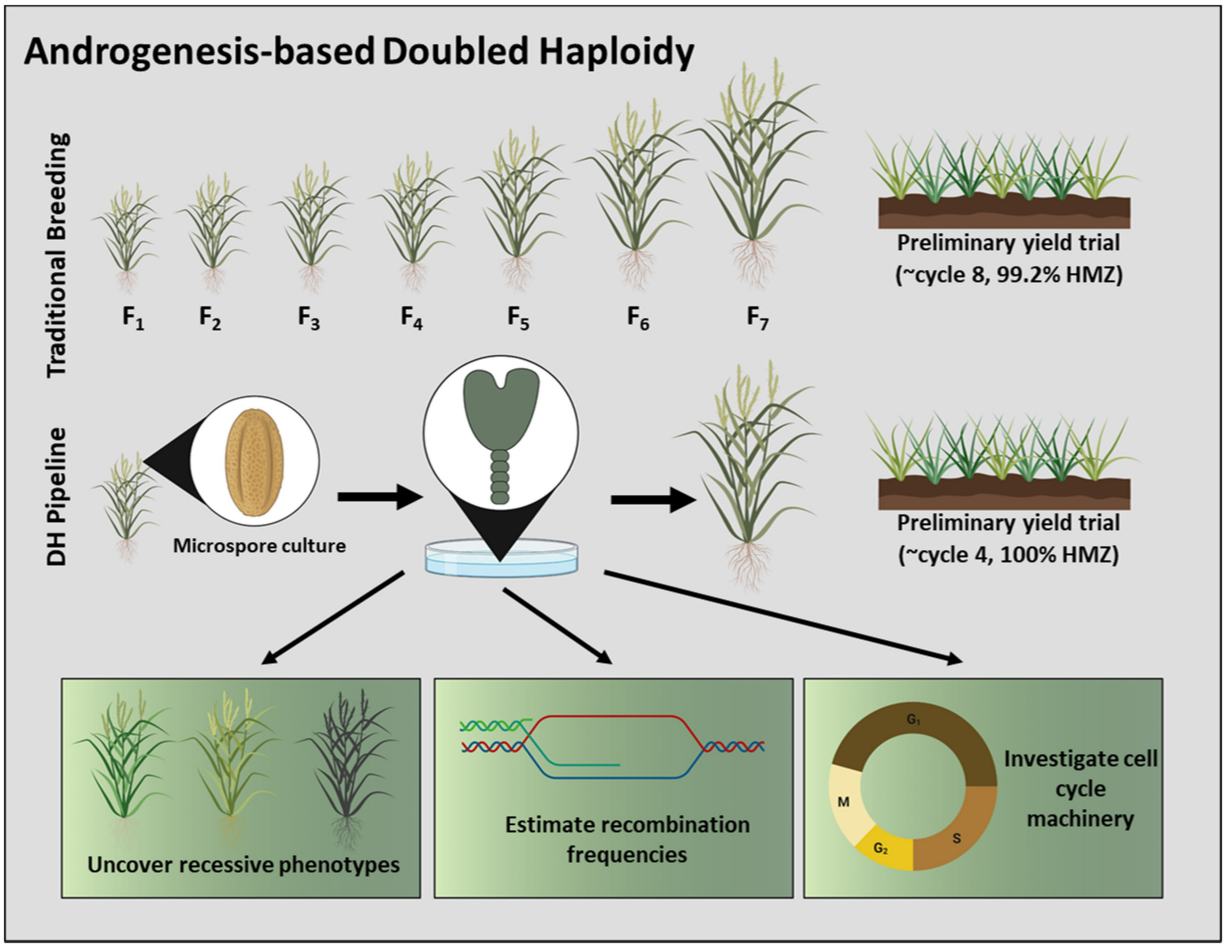

FIGURE 1 | Schematic overview of androgenesis-based doubled haploidy and its uses in plant breeding. A DH pipeline has the capacity to advance cultivar development in a timeframe unmatched by traditional methods. The nature of microspore-derived DH's permits their exploitation to uncover recessive phenotypes, to estimate recombination frequencies, and to investigate cell cycle machinery, among other benefits. Note that wheat (*Triticum aestivum*) is depictive of all species, and the number of cycles is plant-specific. Moreover, this illustration considers *in vitro* embryogenesis to be a cycle in the breeding process.

Hybrid breeding systems have replaced conventional variety development in many major crops of economic value, irrespective of their mode of reproduction. This is due primarily to rapid advancement in the development of hybridization systems (Nienhuis and Sills, 1992; Murovec and Bohanec, 2012; Mette et al., 2015; Hooghvorst et al., 2020). There are inherent advantages of using DHs in a hybrid breeding program, e.g., the creation of genetically distant, distinct, pure, inbred lines and their combination for the highest possible combining ability (Murovec and Bohanec, 2012; Dezfouli et al., 2019). Thus, the advancement of DH platforms has become a focal point in hybrid breeding systems for many crops of interest (Begheyn et al., 2016). DHs have more relevance in perennial crops or outcrossing plants with severe inbreeding depression (Seeja and Sreekumar, 2020).

There are two different approaches for creating DH lines. These include androgenic and gynogenic methods (Forster et al., 2007). From a breeding perspective, both systems have their own advantages and disadvantages. When obtained in a genotype-independent manner with high efficiency, the androgenic system provides some distinct advantages. For example, androgenesis provides an agile platform for the incorporation/complementation of emerging genomic technologies (explained in different sections within this article). While androgenesis and gynogenesis methods are employed commercially for genetic gain, this review emphasizes the use of androgenesis-based doubled haploidy in a plant breeding program.

Major Applications of DH in Plant Breeding

In short, doubled haploids have enormous potential to improve agronomic characters in crop plants (Krishnappa et al., 2021). Breeding/selection approaches that allow a rapid increase in selection intensity, genetic diversity in the breeding population and/or heritability of traits, and a reduction in the length of the breeding cycle are needed to obtain higher genetic gain in breeding programs (Cooper et al., 2014). Described below are some ways that DHs drive such genetic gain. It is noteworthy that, in addition to the outlined methodologies, haploids and

doubled haploids contribute to several other components in a seed product development pipeline.

Create Variability/A Greater Number of Recombinants That Can Be Selected

DHs provide a unique opportunity to create a large number of fixed recombinants simultaneously, allowing selection within the same time window and environment. Compared to gynogenic methods, where the total number of recombinants from a single event is limited, the androgenesis system (microspores) provides the flexibility to generate a large number of recombinants. Tadesse et al. (2012) reported that, theoretically, if a hybrid has n pairs of independently segregating genes, the chance to select a particular homozygous genotype from the F2 population in a conventional breeding program is $(1/2)2n$, whereas in haploid breeding, it is $(1/2)n$ (Chu, 1982). In other words, the selection efficiency in haploid breeding is $2n$ times greater than that of conventional methods.

Bradshaw et al. (1995, 1998) reported that a larger population allowed the detection of quantitative trait loci (QTLs) of smaller effect. In general, to improve quantitatively-inherited traits such as yield, it is highly important to increase the population size by nominating a limited number of elite x elite crosses for DH production (Tadesse et al., 2012). It is also important to note that linkage between genes plays a role in determining the genetic recombination for selectable traits (Choo, 1981). Therefore, as more traits are considered, a higher number of starting recombinants results in a more desirable combination of traits.

Reduce Time, Space and Efficiency for Breeding

Urgent development of new cultivars is required to meet the demands of an increasing population and challenges of a changing climate, yet cultivar development is a lengthy and time-consuming process (Dwivedi et al., 2015). Comparing conventional and DH wheat variety development, Barkley and Chumley (2012) predicted that a 150% increase in yield potential may be achieved with the use of DH. In addition, they also estimated a 4-year reduction in variety development using the DH method for the same overall outcome at the end of the breeding cycle. Similarly, for sorghum (*Sorghum bicolor* L.), a DH breeding system allows parental lines to be developed in 2 years, where it takes up to 7 years to complete similar developments conventionally (Hussain and Franks, 2019).

Availability of novel technologies has further enabled reduction in the breeding time, or an improved genetic gain using DHs in a breeding program. For example, through the development of DH wheat lines containing rust resistance genes, Wessels and Botes (2014) showed that integration of MAS and DH technology into conventional breeding processes could increase the speed of cultivar development. Genome sequences of many food crops are available today and can be readily leveraged in any breeding program, in addition to the information on markers and genomic regions associated with agronomically beneficial traits (Dwivedi et al., 2007, 2015; Varshney et al., 2009, 2013; Thudi et al., 2012). Development of abundant genomic resources (Dwivedi et al., 2007), high throughput, cost-effective phenotyping (Cobb et al., 2013; Fiorani and Schurr, 2013; Araus and Cairns, 2014), and genotyping tools (Varshney et al., 2009; Thudi et al., 2012, 2020) contributes to the enhancement of breeding selections from DHs. This allows the best opportunity to use scientific knowledge generated through DH technology for several years in crops [e.g., barley, *Brassica* sp., maize, rice (*Oryza sativa*), and wheat]s, and integrate them with phenomics and genomics to accelerate breeding pipelines. Li et al. (2020) simulated DH-based genomic selection procedures and reported that it is possible to obtain substantial long-term genetic gain along with the feasibility of increasing multiple traits simultaneously (Brauner et al., 2019).

If n loci are segregating, the probability of getting the desirable genotype is $(1/2)^n$ by the haploid method and $(1/4)^n$ by the diploid method, due to the occurrence of additional segregating progenies compared to the distinct allelic families (Badu et al., 2017). Therefore, as the number of traits that are considered in a breeding process increases, the efficiency of the doubled haploid method increases. Mayor and Bernardo (2009) studied GS and MAS in DH versus F2 populations and found that GS was superior to MAS and DH populations were superior to F2-derived populations using GS (Ren et al., 2017).

Large numbers of finished inbred lines are attained at once in a DH-based breeding pipeline compared to multiple years and stages in a conventional method. This eliminates the need for handling larger numbers of breeding materials from different generations of inbreeding. In other words, significant field resources are saved by allowing smaller population sizes to produce a homozygous (fixed) trait, and/or evaluation of better performing lines (Park et al., 1976; Ho and Jones, 1980; Dwivedi et al., 2015; Li et al., 2020). In addition to the advantage of evaluating all the possible recombinants together, logistics like shipping the seed, managing inventories, planting nurseries, selfing, and maintaining lines are simplified (Röber et al., 2005; Prasanna et al., 2012; Chaikam et al., 2019). Simplified logistics in overall operations lead to significant cost savings in the long term (Jumbo, 2010).

DHs Provide Excellent Recombinant Inbred Lines for Molecular Mapping Applications and Trait Stacking

DHs can be repeatedly tested to recover reliable data in multiple generations, owing to their uniform genetic identity, and provide high value in quantitative and qualitative trait mapping (Yang et al., 2020). Complete homozygosity of DH lines offers a higher phenotype to genotype correlation, thereby facilitating better estimation of QTL effects in marker-trait association studies (Hyne et al., 1995). In addition, DH lines are expected to improve the selection response compared to F2 populations when dealing with complex traits of low heritability controlled by many QTLs (Mayor and Bernardo, 2009) based on simulation studies in marker-assisted recurrent selection and genome-wide selection. The ability to generate DHs enabled the establishment of chromosome maps in a range of species, such as barley, rice, rapeseed, and wheat

(Forster and Thomas, 2005). In addition, it also provided most mapped genetic markers, >90% in some species (Forster et al., 2007). Due to low population structure and quick decay of linkage disequilibrium DH lines derived from landraces were proposed to be ideal for association mapping (Strigens et al., 2013; Melchinger et al., 2018). DHs are also of high utility in establishing marker–trait associations in bulked segregant analysis (BSA; Michelmore et al., 1991). Several disease and pest resistance breeding traits, as well as quality traits, were established using marker-assisted selection in BSA using DHs (Forster et al., 2007; Melchinger et al., 2018). Therefore, integration of DHs with MAS provides an excellent opportunity to maximize selection gains and accelerate development of crop cultivars (Belicuas et al., 2007). In genomic selections, the genome-wide marker data along with phenotyping are used to estimate genomic estimated breeding values (GEBVs) for predicting performance. In comparison to MAS, genomic selection incorporates all marker information, thereby avoiding biased marker effect estimates and capturing more of the variation due to small-effect QTL (Dwivedi et al., 2015). This information is then used to predict performance of a data set where only genomic information is available (Heffner et al., 2009). Predictions for GEBV can be done without phenotypic characterization, which enables breeders to make early selection decisions and may shorten breeding cycles (Daetwyler et al., 2015). Purely homozygous nature of DHs provides an excellent opportunity to increase accuracy in genomic predictions.

Expressed sequence tags (ESTs) can be used as a tool to identify genes controlling a certain trait and map them to a chromosomal location associated with said trait (Wang et al., 2001). In addition, co-locating markers/traits and their associations can be verified (Badu et al., 2017). DHs play a vital role in integrating the genetic and physical maps. This enables precision in targeting candidate genes (Künzel et al., 2000; Forster et al., 2007). Another way to link genes and phenotypes is to induce mutations and analyze their phenotypes (Szarejko and Forster, 2007) for forward and reverse genetics approaches, where use of a DH line will help in increasing precision (Forster et al., 2007; Badu et al., 2017). Doubled haploids are also useful in rapid isolation and purification of selected mutants in subsequent generations.

Assessing Effect of Environment on the Expression of Traits

DHs provide the best material for assessing gene expression across different environments when compared to early selfing generations (Foiada et al., 2015; Yan et al., 2017). Strigens et al. (2013) showed that DH lines from landraces and open-pollinated varieties (OPVs) could be evaluated in replicated trials with high precision, which is not possible when using landraces and OPVs due to their high heterogeneity. Moreover, a high genetic load of deleterious alleles and high heterogeneity prevented the use of landraces and OPVs in hybrid maize breeding (Wilde et al., 2010; Melchinger et al., 2018). Due to the occurrence of a single chromosome during haploid generation, deleterious alleles are readily expressed and eliminated through natural or artificial selection.

Ease With Variety Registration/Protection

The plant variety protection act (USDA) provides intellectual property protection for new varieties of plants, giving owners 20-plus years of exclusive rights. An application for Plant Variety Protection requires submission of seed/plant material, which will be assessed for novelty, distinctness, uniformity, and stability. It is unlikely to develop conventional inbred lines with 100% homozygosity or homogeneity. Consequently, residual heterozygosity in these conventional inbred lines can sometimes delay plant variety registration (Chaikam et al., 2019). The aforementioned criteria of a variety can be easily established due to the complete homozygosity of DH lines, making variety registration/protection relatively easy (Röber et al., 2005), which in turn results in reduced time to commercialization (Bordes et al., 2006; Chaikam et al., 2019).

Use in Genetic Transformation

Use of haploid tissue in genetic transformation has been previously discussed (Swanson and Erickson, 1989; Chauhan and Khurana, 2011; Brew-Appiah et al., 2013; Shen et al., 2015). Integration of the transgene at a haploid state would allow creation of homozygous transgenic events with 100% pure genetic background. This facilitates stable fixation of the integrated gene (Chauhan and Khurana, 2011). Transformation can be done using any type of haploid plant tissue (Murovec and Bohanec, 2012), but microspores provide an ideal single cell and have proven to be feasible in many species (Eudes and Chugh, 2008; Chugh et al., 2009). For species where germplasm response to androgenesis and transformation are low, trait introgression will be significantly benefited by haploid transformation. For single gene introgression, the expected probability of individuals with a desired homozygous genotype is 1/4. If n represents the number of independently segregating genes, the frequency of expected genotypes decreases exponentially following the formula $1/4^n$ (Lübberstedt and Frei, 2012; Shen et al., 2015). Haploid target genotypes are generated with a frequency of $1/2^n$, and thus significantly reduces population size required to achieve successful genetic combinations (Ren et al., 2017).

Androgenesis From Single Cells Can Be Used as a Source of Artificial Variability Creation

Induced mutations have been used mainly to improve particular characters in well-adapted local varieties or to generate variation, which is difficult to be found in germplasm collections (Ferrie and Möllers, 2011; Germanà, 2011; Geiger et al., 2013). About 70% of developed mutant cultivars were released as direct mutants, i.e., without any further breeding; the remaining 30% were developed through cross-breeding programs (Maluszynski et al., 2000). DH systems have many attractive benefits for inducing, selecting, and fixing mutations (Szarejko and Forster, 2007). Haploid cells provide an ideal target for mutation induction and selection, for the screening of both recessive and dominant mutants in the first generation after mutagenic treatment, for the avoidance of chimerism, and for the shortening of breeding times. Induced mutations are predominantly recessive and are normally selected in the second or third (M2 and M3) generation after mutagenic

treatment. Mutation of haploid cells enables the immediate expression of recessive mutations and recovery of homozygous diploids by chromosome doubling (Howland and Hart, 1977). Application of DH systems enhances the effectiveness of the selection of desired recombinants, shortening the time required for mutation detection and evaluation (Forster and Thomas, 2005; DePauw et al., 2011). If the mutagenic treatment is carried out on quiescent seed and the M1 plants are used as gamete donors for DH production, which saves many generations normally needed to produce pure breeding lines. Another option is *in vitro* mutagenic treatment of haploid cells. If microspores are used in this option, it works best if the mutagenic agent is applied at the uninucleate stage, before the first nuclear division, in order to avoid heterozygosity and/or chimerism caused by spontaneous diploidization through nuclear fusion. *In vitro* mutagenic treatment can also be accompanied by *in vitro* selection of desired traits.

Ploidy-Based Breeding Strategies

Polyploid organisms may often exhibit increased vigor and, in some cases, outperform their diploid relatives in several aspects. In many species, improved plant cultivars were developed for the increment in plant organs ("gigas" effect), buffering of deleterious mutations, increased heterozygosity, heterosis (hybrid vigor), high yield, improved product quality, tolerance to both biotic and abiotic stresses, and as a tool for gene transfer in interspecific crosses (Sattler et al., 2016). DHs can be used as a tool in enabling ploidy breeding strategy in crops where a DH system is possible (Bhatia et al., 2017). In a cauliflower breeding program, it was reported that tetraploid lines had more than a 50% economic yield increased as compared to the diploids and exhibited normal fertility. A triploid hybrid was produced by using these tetraploid lines as the pollen parent with a diploid cytoplasmic male sterility (CMS) line as the female (Bhatia et al., 2017). In cauliflower, heterosis is very low because of a narrow gene pool (Nieuwhof, 1963). Therefore, ploidy breeding may serve as a better strategy to the conventional breeding program. Chromosomal stability of the tetraploid lines (Szadkowski et al., 2011) needs to be worked out before their long-term use.

In fruit crops, DHs offers specific opportunities to manipulate seed size with ploidy (Germanà, 2011). Another potential avenue is to create seedless triploids (Germanà, 2009). In papaya (*Carica papaya* L.), gametic embryogenesis, particularly obtained *via* anther culture, seemed to contribute directly to the production of female pure lines (Rimberia et al., 2006).

Landraces and Diversity Inclusion

DH technologies open new opportunities for characterizing and utilizing the genetic diversity present in GenBank accessions. This is well-illustrated in maize, where heterogeneous populations of landraces helped in unlocking genetic diversity (Wilde et al., 2010). Their genetic heterogeneity and heavy genetic load are two distinct reasons for the limited use of landraces in breeding programs. These limitations may be overcome by *in vivo* DH techniques (Strigens et al., 2013). Wilde et al. (2010) reported that large genotypic variances among DH lines derived from landraces allowed the identification of DH lines with grain yields comparable to those of elite flint (EF) lines, enabling selected DH lines to be introgressed into elite germplasm without impairing yield potential. Large genetic distances of DH lines derived from landraces help to broaden the genetic base of the EF germplasm. Due to the low population structure and rapid decrease of linkage disequilibrium within populations of DH lines landraces, these would be an ideal tool for association mapping. However, Zeitler et al. (2020) reported that landrace DH lines may result in a decreased genetic diversity.

APPLICATIONS FOR GAMETOPHYTE REPROGRAMMING

As described in previous sections, androgenesis is a biological process that culminates in an entity linked entirely to an individual male gametophyte. Conventionally, this inferred spontaneous, *in vivo* haploidy in which a fertilized embryo sac contained an inactivated female nucleus, resulting in an embryo with an exclusively paternal genetic program (Kermicle, 1974). More accurately today, the definition of androgenesis is expanded to *in vitro* male-derived haploidy that can be induced in the laboratory through multiple approaches, including (i) anther culture; (ii) isolated microspore culture; (iii) shed microspore culture; and (iv) meiocyte-derived callogenesis (Seguí-Simarro, 2010). These androgenic pathways differ oftentimes in the induction stage but lead to the same final haploid or doubled haploid product. Microspore embryogenesis is widely studied and applied (discussed elsewhere in this chapter). The developmental ontogeny of microspore embryogenesis typically follows a division pattern similar to zygotic embryogenesis (Zaki and Dickinson, 1991; Maraschin et al., 2005b; Supena et al., 2008); however, in some species, the sequence of differentiation involves several randomly oriented initial cell divisions that resemble sporophytic growth (Radoeva and Weijers, 2014). Subsequently, a well-defined protoderm can be recognized, and is the marker for embryo formation. At this stage of development, compact masses with a protoderm are defined as embryo-like structures (ELS) that give rise to an embryo with all primary tissues found in zygote-derived embryos (Soriano et al., 2013). It is unclear whether the competence to undergo microspore embryogenesis generates a reproductive edge or whether parallel processes occur naturally. Alternatively, given the derivation of embryogenesis from spore-like evolutionary precursors (Taylor et al., 2009), microspore embryogenesis may be a remnant of an essential developmental potential. Although the molecular mechanisms for induction have yet to be elucidated, it was recently shown that chromatin regulation using Trichostatin-like compounds contributed to developmental control (Li et al., 2014). However, the universal application of epigenetic additives (and other exogenous biomolecules) across crop species and genotypes to trigger androgenesis-based embryogeny remains to be realized, and attempts of expanding methods across genotypes and taxa are in progress (see succeeding text). This section focuses on the use of molecular manipulation *in vitro*, resulting in the induction

of androgenic events and targeted mutagenesis using DNA-free transduction approaches.

Embryogenesis-relevant genes can be used ingeniously to trigger microspore de-and redifferentiation and are expected to provide much-needed DH methods. DNA-free delivery of gene products could enable the adoption and expansion of DH platforms across species and genotypes (Sinha et al., 2021). Moreover, regulating androgenesis-associated gene expression by internalizing exogenously supplied molecules [e.g., RKD Transcription activator-like effector (TALE) proteins in wheat] has potential to enhance androgenic response and ultimately accelerate plant breeding programs (Barkley and Chumley, 2012). Sinha et al. (2021) analyzed RKD promoters from wheat and triticale (× *Triticosecale*) and custom-synthesized a TaRKD-TALE protein for delivery using a cell penetrating peptide (CPP) Nano-carrier. The purified protein was covalently conjugated with R9 CPP, (Cys (Npys)-(D-Arg)9), and successfully transduced into wheat microspores. The embryogenesis-related marker genes early-culture abundant (ECA1), RWP-RK domain-containing proteins (RKD1), and Tapetum determinant 1 (TPD1) were upregulated significantly in the TALE-transduced microspores compared to the control. In addition, microspores cultured after the transduction of the R9-TaRKD-TALE protein yielded a considerably higher number of ELS and green plants in wheat cultivar, AC Fielder. The researchers also reported that microspore quality was not affected by the internalization of R9-TaRKD-TALE; on the contrary, transduced microspores showed a higher recovery post 120 h of culture. This work demonstrated the successful deployment of the TALE protein to improve the androgenesis process, and has potential for expansion to other crops/genotypes in the future.

Recently, Bélanger et al. (2020) investigated the role of miRNA for developmental plasticity and cell fate reprogramming within the barley microspore. Their findings indicated that the switch toward embryo differentiation involved miRNA-directed regulation of members of the ARF, SPL, GRF, and HD-ZIPIII transcription factor families. Approximately 41.5% of these targets were shared between day-2 and day-5 microspores, while 26.8% were unique to day-5 microspores. The former set may disrupt transcripts driving the destined pollen development, while the latter group may direct the microspore toward embryogenic pathways. There has been diligent research investigation into the epigenetic regulation of androgenesis, including the exploration of DNA methylation (El-Tantawy et al., 2014), histone methylation (Berenguer et al., 2017), acetylation (Li et al., 2014), and the upregulation of embryogenesis genes by TaRKD-TALE (Sinha et al., 2021). While these mechanisms are capable of disrupting gametophytic gene expression, they are not capable of degrading transcripts altogether. This further suggests a role for small regulatory RNAs (sRNAs) in microspore dedifferentiation. In wheat, increased expression of 24-nucleotide (nt) sRNAs was correlated with the progression of an embryogenic program, while sRNAs ≥23-nt demonstrated an opposing expression pattern (Seifert et al., 2016). Furthermore, sRNAs play essential functions in key developmental processes, including embryo, leaf, and meristem patterning and flower development (D'Ario et al., 2017). Thus, it is possible that *in vitro* modulation of sRNA expression may help drive the gametophyte to sporophyte transition.

Microspore embryogenesis is employed for practical breeding purposes and genetic mapping in many species; yet, is restricted oftentimes to a few responsive genotypes. A deeper understanding of the molecular mechanisms controlling gametophyte totipotency and subsequent histodifferentiation are needed to overcome species and genotypes dependencies. A combination of genomic (e.g., next-generation sequencing and network/meta-analyses) and biotechnological approaches could help establish more universal androgenesis induction protocols in the foreseeable future. Additional applications for gametophyte reprogramming are described by Dwivedi et al. (2015).

EXPANSION OF PROTOCOLS ACROSS GENOTYPES AND TAXA

Development of genotype-independent DH methods and protocols are essential for breeding purposes. However, this is not always possible during androgenesis, as genotypic differences do occur and in some cases differences between plants within the same genotype also exist. Several DH methods have shown that genotype has no or a limited role in DH response, for example, haploid inducer lines (Jacquier et al., 2020) or CENH3 (centromere variant of histone 3). These methods are currently not available for all species and are not discussed in this review.

In many species, embryogenic lines have been identified and these are used as model genotypes to conduct genetic, genomic, biochemical, or physiological experiments. Microspore embryogenesis is generally regarded as routine in *B. napus* but differences in embryogenic response do exist among genotypes. The highly embryogenic line Topas DH4079 (Pechan and Keller, 1988; Ferrie, 2003), which has been used as the model in countless experiments, is derived from the cultivar Topas, which is a poor responding cultivar in terms of microspore embryogenesis. Embryogenic lines are also available in other *Brassica* species (Ferrie et al., 1995; Hiramatsu et al., 1995; Barro and Martín, 1999; Lionneton et al., 2001).

Embryogenic Biomarkers

Over the years, many DH protocols have been developed by systematically evaluating the different factors that influence microspore embryogenesis (donor plant conditions, genotype, developmental stage of the microspore, pretreatments, media components, and culture conditions). More recent studies are utilizing 'omics' methods and targeting the genes and the biochemical processes that trigger the switch from microspore development to embryo development.

Over the years, simple markers like morphological or physiological characteristics have been identified to denote induction or early embryogenesis. An observed indicator is the "star-like" morphology (Indrianto et al., 2001; Maraschin et al., 2005a) which occurs when the nucleus moves to the center of the cell and the vacuole splits into fragments.

It has also been shown that the identification of certain genes can indicate an embryogenic response. In *Brassica*, genes such as BABY BOOM (Boutilier et al., 2002), LEC2 (Malik et al., 2007), SERK1, and SERK2 (Ahmadi et al., 2016) have

been shown to be involved in the steps of microspore embryogenesis and subsequent plant regeneration. The expression of LEC2 was useful in distinguishing embryogenic and non-embryogenic cultures after 3 days (Malik et al., 2007). SERK1 was up-regulated during the first few days of culture (day 1–5) and then decreased from globular to torpedo embryo stages. However, SERK2 expression levels increased throughout the early stages of embryogenesis and through to regeneration (Ahmadi et al., 2016). BABY BOOM and AINTEGUMENTA-like 5 (AIL5) were also identified in wheat when comparing freshly isolated microspores, microspores exposed to a pretreatment, and after 8 days of culture (Seifert et al., 2016).

Omics methods (e.g., transcriptomics, proteomics) can open up new avenues to understand the mechanism of microspore embryogenesis. In these experiments, there is a requirement for comparing a cultivar or culture treatment that is responsive with a cultivar or condition that is not. This is not always possible in the recalcitrant species, hence most of the work has been done in *Brassica*, barley, or wheat. There are only a few studies that have looked at protein changes during the different steps of the *Brassica* DH process. Early studies identified heat shock proteins (HSPs) associated with cell proliferation (Pechan, 1991). HSP synthesis has been reported during stress-induced microspore embryogenesis across many platforms (Cordewener et al., 1995; Telmer et al., 1995; Zarsky et al., 1995; Bárány et al., 2001; Seguí-Simarro et al., 2003); however, it remains unclear if HSP activity coincides primarily with the onset of embryogenesis or cytoprotection (Zhao et al., 2003; Testillano, 2019; Hale et al., 2020). In another study, cabbage (*B. oleracea* L. var. *capitata* L.) microspores were subjected to the high temperature pretreatment of 32°C as well as the 25°C untreated control (Su et al., 2020). The authors were able to identify 97 differentially expressed proteins found in the highly responsive embryogenic line at 32°C but not in the recalcitrant line. These proteins could then be classified based on their function, that being carbohydrate metabolism, protein synthesis and degradation in the endoplasmic reticulum, signal transduction, and cutin, suberin, and wax biosynthesis (Su et al., 2020).

The pollen transcriptome has been described for several species (soybean, rice, maize) and has been the subject of several reviews (Rutley and Twell, 2015; Liu and Wang, 2021). However, there are limited publications on transcriptomics in microspore embryogenesis. In wheat, the different stages of microspore embryogenesis have been analyzed using transcriptome and small RNA sequencing (Seifert et al., 2016). The authors were able to identify up-regulated genes that were involved in DNA methylation, histone methylation, and histone deacetylation. In barley, 96 differentially expressed EST's were identified when freshly isolated microspores were compared to pretreated microspores (4°C). These encoded genes were involved in protein degradation, starch and sugar hydrolysis, stress response, and cell signaling (Maraschin et al., 2006). In a more recent study in barley (Bélanger et al., 2018), microspores at day 0, 2, 5 were compared. It was determined that there were approximately 14 K genes, with 3,382 differentially expressed genes between the microspore populations. This corresponded to the up-regulation of genes associated with glutathione s-transferase and heat shock proteins and the down-regulation of ribosomal subunit protein genes. From day 2 to 5, there was an induction of genes involved in early embryogenesis, hormone biosynthesis, hormone signaling, and secondary metabolism. Gene expression profiling in temperature-stressed soybean microspores reinforced these findings, suggesting that cellular reprogramming of the microspore entailed a traditional stress response, suppression of gametogenesis-relevant transcripts, and an increase in genes involved in cell division and proliferation (Hale et al., 2020).

As demonstrated, "omic" methods are beneficial in trying to tease out the components or genes involved in microspore embryogenesis; however, the most critical aspect is how to take these results and use them to enhance or develop an efficient protocol in recalcitrant species that will generate sufficient embryos for breeding or basic research purposes.

Tissue Culture-Based Protocol Expansion

Traditional and less-traditional tissue culture additives used to promote androgenesis have been reviewed previously (Niazian and Shariatpanahi, 2020). Thus, we focus on a few tissue culture additives that have proven effective in recalcitrant systems, which may be useful for protocol expansion to additional genotypes and species. Arabinogalactan proteins (AGPs), polyamines, and epigenetic modifiers will be reviewed briefly here. A recent book compiled of 62 chapters including detailed DH protocols for 44 species has been published and is a useful resource for DH methodology (Seguí-Simarro, 2021).

Arabinogalactan Proteins and Extracellular Matrices

Extracellular matrices secreted by cell cultures may contain clues for protocol expansion. Borderies et al. (2004) observed the formation of an extracellular matrix in the culture of maize microspores, consisting of secreted AGPs, cell wall invertase, thaumatin, β-1,3-glucanase, and chitinase. Rye anther cultures exhibited high activities of β-1,3-glucanases and chitinases in androgenic embryos, and AGPs were found to accumulate in the vesicles and inner walls of the anthers (Zieliński et al., 2021). *Brassica* microspores and pollen actively produce and secrete AGPs (El-Tantawy et al., 2013). Testillano (2019) reported that AGPs, cell wall remodeling, and pectin demethylesterification were essential features for androgenesis. Niazian and Shariatpanahi (2020) identified programmed cell death in a subpopulation of cultured microspores as leading to the secretion of the matrix, and the AGPs in the matrix coordinated with cell wall remodeling. In addition, the extracellular matrix contained polyamines and antioxidants to ameliorate stress.

Rodríguez-Sanz et al. (2014) found that cultures of androgenic embryos and zygotic embryos of *Quercus* shared several similarities, including cell wall remodeling by pectin esterification, DNA hypomethylation, and an increase in auxin. AGPs and pectin demethylesterification were deemed essential for somatic embryogenesis in *Quercus* (Pérez-Pérez et al., 2019). Leljak-Levanić et al. (2015) noted similarities between somatic embryos and zygotic embryos of several species, including the formation of an extracellular matrix containing polysaccharides and AGPs,

and pathogenesis-related (PR) β-1,3-glucanases and chitinases. A fibrous- and vesicle-rich matrix was essential for somatic embryogenesis. AGPs were found to be secreted in somatic embryogenic but not in non-embryogenic cultures of hybrid *Abies* (Šamaj et al., 2008), and AGPs from one cereal genus stimulated zygotic embryo development of another cereal genus (Paire et al., 2003). AGPs released in cultures act as signaling molecules (Hernández-Sánchez et al., 2009). These findings taken together indicate that plant embryos – whether zygotic, somatic, or androgenic in origin – secrete AGPs that coordinate with cell wall modifying enzymes to direct cells into an embryogenic pathway and/or maintain embryogenesis.

Letarte et al. (2006) reported improvement of wheat isolated microspore culture response with the use of a commercial source (10 mg/L Larcoll) of arabinogalactans (AGs) and gum Arabic (10 mg/L) as a source of AGPs added to the culture medium. Similarly, addition of 10 mg/L gum Arabic promoted microspore embryogenesis in white cabbage (*Brassica oleracea* var. *capitata*, Yuan et al., 2012) and eggplant (*Solanum melongena*, Corral-Martinez and Segui-Simarro, 2014). Kale (*Brassica oleracea* var. *sabellica*) microspore embryogenesis was enhanced with the addition of 10 mg/L AGs (Niu et al., 2015), and 10 mg/L gum Arabic promoted androgenesis in barley anther cultures (Makowska et al., 2017). Ovary co-culture combined with the addition of AGPs further enhanced wheat microspore embryogenesis (Coskun and Savaskan, 2017). Pepper (*Capsicum*) microspore response improved with addition of 120 mg/L gum Arabic (Pourmohammad et al., 2021). Evidently, the amount, source, and quality of AGs and AGPs required by different species may differ, but addition of AGs/AGPs shows promise for extending androgenesis protocols to additional genotypes and species.

To our knowledge, application of chitinases or glucanases have not been reported in androgenesis protocols.

Polyamines

Cha-um et al. (2009) included 0.5 mm spermidine in the culture of rice anthers with an improvement in androgenic response. Redha and Suleman (2011) pretreated wheat anthers with 1 mm putrescine or spermine for 1 h prior to culture with an improved androgenic response. In contrast, *Brassica* isolated microspore cultures utilized 0.5–1.0 mg/L putrescine (micromolar range) with beneficial results, but higher concentrations were inhibitory (Ahmadi et al., 2014; Bhatia et al., 2021). Similarly, pepper isolated microspores were exposed to 0.5–1.0 mg/L putrescine during the temperature stress and sugar starvation stages of the protocol with improved androgenic response, and higher concentrations were inhibitory (Heidari-Zefreh et al., 2019). The much lower effective concentrations of polyamines in isolated microspore culture are likely due to their direct availability to androgenic cells, whereas anther cultures have multiple layers of cells to penetrate in order to access the androgenic cell (e.g., the microspore).

Epigenetic Additives

The understanding of the embryogenesis process and the identification of epigenetic reprogramming has led to incorporating additives (enzyme inhibitors) that are involved in epigenetic reprogramming. Histone deacetylase inhibitors (i.e., Trichostatin-A, scriptaid, sodium butyrate) have been shown to enhance embryogenesis in several species. Trichostatin-A has been shown to induce embryogenesis in *B. napus*, *B. rapa*, and wheat (Li et al., 2014; Zhang et al., 2016; Jiang et al., 2017; Wang et al., 2019; Castillo et al., 2020). Concentrations ranged from 0.008 to 0.4 μm depending on the species as well as the method of incorporation (short incubation period or kept continuously in culture). Not only was embryogenesis increased, but there was an increase in green plant production in wheat (Jiang et al., 2017; Wang et al., 2019). Scriptaid, another histone deacetylase inhibitor, has also resulted in an increase in embryogenesis and green plant production in wheat, however the plant morphology was classified as abnormal (Wang et al., 2019). In both spring wheat and winter wheat, the addition of sodium butyrate did not show any added benefit in inducing microspore embryogenesis, as embryo numbers decreased (although embryos appeared to be of better quality with a higher regeneration rate; Kathiria et al., 2016; Wang et al., 2019).

The histone methyltransferase inhibitor, BIX-01294, has also been evaluated in microspore culture of *B. napus* and barley (Berenguer et al., 2017). Embryo production was highest with the BIX-01294 treatment of 1.0 or 2.5 μm for 4–6 days, however detrimental effects were observed with long term treatment (30 days). The addition of 5-azacytidine (5-AzaC), inhibitor of DNA methyltransferase, to barley and *B. napus* microspores showed that a 4 day treatment of 2.5 μm AzaC increased embryo induction, but longer treatments were detrimental to embryo production (Solís et al., 2015). Other studies in triticale indicated that the addition of 5-AzaC or 2′-deoxy-5-azacytidine was not able to overcome the recalcitrant nature of the low responding line but was able to enhance embryo production and plant regeneration in the highly embryogenic line (Nowicka et al., 2019).

Advances in Embryo Conversion

Some species (e.g., *Brassica*) undergo microspore embryogenesis through to conversion into plantlets readily, while others (e.g., *Capsicum*) exhibit induction of microspore embryogenesis but significant bottlenecks at the conversion stage (Ferrie and Caswell, 2011). Recent advances in the conversion of pepper microspore embryos may provide a strategy for extending conversion success to other species.

One of the best protocols for conversion of pepper plants from anther cultures was described by Dolcet-Sanjuan et al. (1997). A two-layer culture system was used with a semisolid medium underlayer and a liquid medium overlay based on NN (Nitsch and Nitsch, 1969) using 2% maltose as sugar source, except the underlayer medium included 0.5% activated charcoal (AC) as well as gelling agent. Cultures were incubated in dark at 7°C for 1 week then moved to 28°C for 8 week Cultures were transferred to fresh semisolid medium with 2% maltose but lacking AC for 3–4 week in light conditions, then finally to fresh medium with 2% sucrose for plantlet recovery.

This anther-based bilayer protocol was adapted to the shed-microspore culture of pepper by Supena et al. (2006a,b) and Supena and Custers (2011). The shed-microspore cultures were

incubated in the dark at 9°C for 1 week, then 28°C for 3 week, then 21°C for 4 week prior to exposure to light. The underlayer semisolid medium was based on NN with 2% maltose and 1.0% AC. The overlayer liquid medium lacked AC. After 4 week incubation (when temperature was reduced), the liquid overlayer medium was supplemented with 2.5 µm zeatin and 5.0 µm indole acetic acid. These modifications resulted in enhanced pepper microspore embryo yield and quality.

Progress in Androgenesis of Recalcitrant Grain Legumes

The legume species are considered recalcitrant in tissue culture. Pratap et al. (2018) stated that slow morphogenesis, albinism, genotypic specificity, and vitreous tissues can hinder plant regeneration from cells and tissues. Croser et al. (2006) reviewed DH progress within the Fabaceae and stated that DH technology is not being used in breeding programs for any leguminous species because of the recalcitrant nature of the family. There have been a few reports of anther culture and isolated microspore culture with legumes but there are no efficient, routine methods. Bayliss et al. (2004) cultured isolated microspores of several species of lupin (*Lupinus* spp.) and reported the production of pro-embryos, but there was no further development. There have been some positive initial results on isolated microspore culture of field pea (*Pisum sativum* L.; Ochatt et al., 2009; Bobkov, 2018). Microcalli (Bobkov, 2018) and embryogenic/organogenic calli (Ochatt et al., 2009) resulted in a few (8) embryos; however, these were of poor quality and did not survive transfer to soil (Ochatt et al., 2009).

Legumes are recalcitrant to androgenesis, especially the commercially important grain legumes. Recent progress in chickpea and soybean bode well for resolving this challenge. Panchangam et al. (2014) induced chickpea anthers with cold stress and cultured them on a high osmoticum medium containing high auxin. After 4 day of culture, microspores were observed with 3–5 nuclei from all four genotypes tested, and these were subjected to expressed sequence tag (EST) analysis. Two members of the Agamous-like (AGL) transcription factor family, AGL-16 and AGL-6, were among the chickpea ESTs, which coincide with androgenesis activity in *Arabidopsis*. Abdollahi and Rashidi (2018) cultured chickpea anthers on medium containing 10 mg/L 2,4-D and 15–25 mg/L $AgNO_3$ and successfully recovered haploid plants. Grewal et al. (2009) combined several stress treatments, including cold shock (4°C for 4 day), electric pulse (125–200 V), centrifugation (168 *g* for 10 min), and high osmotic stress (563 mmol) to generate embryogenic structures. From these experiments (Grewal et al., 2009; Abdollahi and Rashidi, 2018), 52 plants survived and were transferred to soil. Many of the chickpea androgenesis experiments have focused on anther culture methods; however isolated microspore culture is often the preferred method, as it can be more efficient than anther culture. Isolated microspore culture of chickpea have resulted in early stage embryo development (Croser et al., 2011), but there was no further development. If this protocol can be enhanced, doubled haploid breeding will be feasible for chickpea.

Similarly, a two-step donor plant cold temperature stress defined using soybean anther cultures (Garda et al., 2020) elicited characteristic responses from isolated microspores at the cellular (Hale et al., 2021) and molecular (Hale et al., 2020) levels, similar to model systems. Nitrogen starvation, but not sugar starvation (imposed using maltose instead of sucrose), enhanced androgenic response in anther cultures (Garda et al., 2020). Phytohormones were required for isolated microspores to undergo sustained cell divisions, but anther cultures did not require phytohormone supplementation (Garda et al., 2020). Soybean isolated microspore cultures exhibited matrix formation, and the matrix contained AGPs (Hale et al., 2020, 2021). While conversion into plants has yet to be achieved, the soybean induction protocol presents a significant advancement for this crop.

CONCLUSION

In 1964 the first report was published on the regeneration of plants from anther culture (Guha and Maheshwari, 1964). Now, planst breeders are routinely using these methods to develop new cultivars. For example, the majority of the canola breeding organizations in Canada are utilizing the DH methods and most of the varieties are DH. As outlined, these DH methods have been instrumental in speeding up the breeding program in many crops. We have also been able to acquire some understanding of the molecular and biochemical processes that are involved in the induction of the microspore to change the developmental process to one of embryo development. These haploid cells can be manipulated through mutagenesis, transformation, or gene editing to generate variation and generate lines with the desired trait of interest.

Despite these successes, there are still many commercially important crops that are considered recalcitrant when it comes to DH methodology. There may be a few publications indicating microspore induction, early stages of embryo development, or even plant development, but a routine protocol that would yield sufficient embryos and subsequent plants for breeding purposes is not available.

AUTHOR CONTRIBUTIONS

All authors contributed equally to this work. BH and GP wrote the abstract. BH wrote the introduction, incorporated edits, modified writing style, and constructed reference section. SC wrote Section "Plant Breeding Applications: From Lab to Field." JS wrote Section "Applications for Gametophyte Reprogramming." GP and AF wrote Section "Expansion of Protocols Across Genotypes and Taxa." AF wrote Section "Conclusion." BH, AF, and SC edited the manuscript.

FUNDING

This study was funded through support from USDA-NIFA Non-Land Grant Colleges of Agriculture Capacity Building award number 2018-70001-28762 and Corteva Agriscience Open Innovation.

REFERENCES

Abdollahi, M. R., and Rashidi, S. (2018). Production and conversion of haploid embryos in chickpea (*Cicer arietinum* L.) anther cultures using high 2, 4-D and silver nitrate containing media. *Plant Cell Tissue Organ Cult.* 133, 39–49. doi: 10.1007/s11240-017-1359-4

Ahmadi, B., Masoomi-Aladizgeh, F., Shariatpanahi, M. E., Azadi, P., and Keshavarz-Alizadeh, M. (2016). Molecular characterization and expression analysis of SERK1 and SERK2 in *Brassica napus* L.: implication for microspore embryogenesis and plant regeneration. *Plant Cell Rep.* 35, 185–193. doi: 10.1007/s00299-015-1878-6

Ahmadi, B., Shariatpahani, M. E., Ojaghkandi, M. A., and Heidari, A. A. (2014). Improved microspore embryogenesis induction and plantlet regeneration using putrescine, cefotaxime and vancomycin in *Brassica napus* L. *Plant Cell Tissue Organ Cult.* 118, 497–505. doi: 10.1007/s11240-014-0501-9

Ahmar, S., Gill, R. A., Jung, K. H., Faheem, A., Qasim, M. U., Mubeen, M., et al. (2020). Conventional and molecular techniques from simple breeding to speed breeding in crop plants: recent advances and future outlook. *Int. J. Mol. Sci.* 21:2590. doi: 10.3390/ijms21072590

Araus, J. L., and Cairns, J. E. (2014). Field high-throughput phenotyping: the new crop breeding frontier. *Trends Plant Sci.* 19, 52–61. doi: 10.1016/j.tplants.2013.09.008

Badu, M., Tripathy, B., Sahu, G. S., and Jena, A. K. (2017). Role of doubled haploids in vegetable crop improvement. *J. Pharmacogn. Phytochem*. 2017, 384–389.

Bárány, I., Testillano, P. S., Mitykó, J., and Risueno, M. C. (2001). The switch of the microspore program in capsicum involves HSP70 expression and leads to the production of haploid plants. *Int. J. Dev. Biol.* 45, 39–40.

Barkley, A. P., and Chumley, F. G. (2012). A doubled haploid laboratory for Kansas wheat breeding: an economic analysis of biotechnology adoption. *Int Food Agri Man Rev.* 15, 99–120. doi: 10.22004/ag.econ.127109

Barro, F., and Martín, A. (1999). Response of different genotypes of *Brassica carinata* to microspore culture. *Plant Breed.* 118, 79–81. doi: 10.1046/j.1439-0523.1999.118001079.x

Bayliss, K. L., Wroth, J. M., and Cowling, W. A. (2004). Pro-embryos of *Lupinus* spp. produced from isolated microspore culture. *Aust. J. Agric. Res.* 55, 589–593. doi: 10.1071/AR03226

Begheyn, R., Lübberstedt, T., and Studer, B. (2016). Haploid and doubled haploid techniques in perennial ryegrass (*Lolium perenne* L.) to advance research and breeding. *Agronomy* 6:60. doi: 10.3390/agronomy6040060

Bélanger, S., Baldrich, P., Lemay, M. A., Marchand, S., Esteves, P., Meyers, B. C., et al. (2020). The commitment of barley microspores into embryogenesis correlates with miRNA-directed regulation of members of the SPL, GRF and HD-ZIPIII transcription factor families. *Plant Direct.* 4:e00289. doi: 10.1002/pld3.289

Bélanger, S., Marchand, S., Jacques, P.-E., Meyers, B., and Belzile, F. (2018). Differential expression profiling of microspores during the early stages of isolated microspore culture using the responsive barley cultivar Gobernadora. *G3-Gen. Genom. Genet.* 8, 1603–1614. doi: 10.1534/g3.118.200208

Belicuas, P. R., Guimarães, C. T., Paiva, L. V., Duarte, J. M., Maluf, W. R., and Paiva, E. (2007). Androgenetic haploids and SSR markers as tools for the development of tropical maize hybrids. *Euphytica* 156, 95–102. doi: 10.1007/s10681-007-9356-z

Berenguer, E., Bárány, I., Solís, M. T., Pérez-Pérez, Y., Risueño, M. C., and Testillano, P. S. (2017). Inhibition of histone H3K9 methylation by BIX-01294 promotes stress-induced microspore totipotency and enhances embryogenesis initiation. *Front. Plant Sci.* 8:1161. doi: 10.3389/fpls.2017.01161

Bhatia, R., Dey, S. S., Sood, S., Sharma, K., Parkash, C., and Kumar, R. (2017). Efficient microspore embryogenesis in cauliflower (*Brassica oleracea* var. botrytis L.) for development of plants with different ploidy level and their use in breeding programme. *Sci Hort.* 216, 83–92. doi: 10.1016/j.scienta.2016.12.020

Bhatia, R., Sharma, K., Parkash, C., Pramanik, A., Singh, D., Singh, S., et al. (2021). Microspore derived population developed from an inter-specific hybrid (*Brassica oleracea*× *B. carinata*) through a modified protocol provides insight into B genome derived black rot resistance and inter-genomic interaction. *Plant Cell Tissue Organ Cult.* 145, 417–434. doi: 10.1007/s11240-021-02018-1

Bobkov, S. (2018). Initiation of microcalli in culture of pea (*Pisum sativum* L.) isolated microspores. *Asia Pac. J. Mol. Biol.* 26, 20–26.

Borderies, G., Le Béchec, M., Rossignol, M., Lafitte, C., Le Deunff, E., Beckert, M., et al. (2004). Characterization of proteins secreted during maize microspore culture: arabinogalactan proteins (AGPs) stimulate embryo development. *Euro. J. Cell Bio.* 83, 205–212. doi: 10.1078/0171-9335-00378

Bordes, J., Charmet, G., de Vaulx, R. D., Pollacsek, M., Beckert, M., and Gallais, A. (2006). Doubled haploid versus S1 family recurrent selection for testcross performance in a maize population. *Theor. Appl. Genet.* 112, 1063–1072. doi: 10.1007/s00122-006-0208-3

Boutilier, K., Offringa, R., Sharma, V. K., Kieft, H., Ouellet, T., Zhang, L., et al. (2002). Ectopic expression of BABY BOOM triggers a conversion from vegetative to embryonic growth. *Plant Cell* 14, 1737–1749. doi: 10.1105/tpc.001941

Bradshaw, H. D., Otto, K. G., Frewen, B. E., McKay, J. K., and Schemske, D. W. (1998). Quantitative trait loci affecting differences in floral morphology between two species of monkeyflower (Mimulus). *Genetics* 149, 367–382. doi: 10.1093/genetics/149.1.367

Bradshaw, H. D., Wilbert, S. M., Otto, K. G., and Schemske, D. W. (1995). Genetic mapping of floral traits associated with reproductive isolation in monkeyflowers (Mimulus). *Nature* 376, 762–765. doi: 10.1038/376762a0

Brauner, P. C., Schipprack, W., Utz, H. F., Bauer, E., Mayer, M., Schön, C., et al. (2019). Testcross performance of doubled haploid lines from European flint maize landraces is promising for broadening the genetic base of elite germplasm. *Theor. Appl. Genet.* 132, 1897–1908. doi: 10.1007/s00122-019-03325-0

Breseghello, F., and Coelho, A. S. (2013). Traditional and modern plant breeding methods with examples in rice (*Oryza sativa* L.). *J. Agric. Food Chem.* 61, 8277–8286. doi: 10.1021/jf305531j

Brew-Appiah, R. A., Ankrah, N., Liu, W., Konzak, C. F., von Wettstein, D., and Rustgi, S. (2013). Generation of doubled haploid transgenic wheat lines by microspore transformation. *PLoS One* 8:e80155. doi: 10.1371/journal.pone.0080155

Castillo, A. M., Valero-Rubira, I., Burrell, M. Á., Allué, S., Costar, M. A., and Vallés, M. P. (2020). Trichostatin A affects developmental reprogramming of bread wheat microspores towards an embryogenic route. *Plan. Theory* 9:1442. doi: 10.3390/plants9111442

Ceballos, H., Kawuki, R. S., Gracen, V. E., Yencho, G. C., and Hershey, C. H. (2015). Conventional breeding, marker-assisted selection, genomic selection and inbreeding in clonally propagated crops: a case study for cassava. *Theor. Appl. Genet.* 128, 1647–1667. doi: 10.1007/s00122-015-2555-4

Chaikam, V., Molenaar, W., Melchinger, A. E., and Boddupalli, P. M. (2019). Doubled haploid technology for line development in maize: technical advances and prospects. *Theor. Appl. Genet.* 132, 3227–3243. doi: 10.1007/s00122-019-03433-x

Chauhan, H., and Khurana, P. (2011). Use of doubled haploid technology for development of stable drought tolerant bread wheat (*Triticum aestivum* L.) transgenics. *Plant Biotech. J.* 9, 408–417. doi: 10.1111/j.1467-7652.2010.00561.x

Cha-um, S., Srianan, B., Pichakum, A., and Kirdmanee, C. (2009). An efficient procedure for embryogenic callus induction and double haploid plant regeneration through anther culture of Thai aromatic rice (*Oryza sativa* L. subsp. *indica*). *In Vitro Cell Dev. Biol. Plant* 45, 171–179. doi: 10.1007/s11627-009-9203-0

Choo, T. M. (1981). Doubled haploids for studying the inheritance of quantitative characters. *Genetics* 99, 525–540. doi: 10.1093/genetics/99.3-4.525

Chu, C. (1982). "Haploids in plant improvement," in *Plant Improvement and Somatic Cell Genetics* eds. I. K. Vasil, W. R. Scowcroft and K. J. Frey (United States: Academic Press Inc.), 129–157.

Chugh, A., Amundsen, E., and Eudes, F. (2009). Translocation of cell-penetrating peptides and delivery of their cargoes in triticale microspores. *Plant Cell Rep.* 28, 801–810. doi: 10.1007/s00299-009-0692-4

Cobb, J. N., DeClerck, G., Greenberg, A., Clark, R., and McCouch, S. (2013). Next-generation phenotyping: requirements and strategies for enhancing our understanding of genotype–phenotype relationships and its relevance to crop improvement. *Theor. Appl. Genet.* 126, 867–887. doi: 10.1007/s00122-013-2066-0

Cooper, M., Messina, C. D., Podlich, D., Totir, L. R., Baumgarten, A., Hausmann, N. J., et al. (2014). Predicting the future of plant breeding: complementing empirical evaluation with genetic prediction. *Crop and Pasture Sci.* 65, 311–336. doi: 10.1071/CP14007

Cordewener, J. H., Hause, G., Görgen, E., Busink, R., Hause, B., Dons, H. J., et al. (1995). Changes in synthesis and localization of members of the 70-kDa class of heat-shock proteins accompany the induction of embryogenesis in *Brassica napus* L. microspores. *Planta* 196, 747–755. doi: 10.1007/BF01106770

Corral-Martinez, P., and Segui-Simarro, J. M. (2014). Refining the method for eggplant microspore culture: effect of abscisic acid, epibrassinolide, polyethylene glycol, naphthaleneacetic acid, 6-benzylaminopurine and arabinogalactan proteins. *Euphytica* 195, 369–382. doi: 10.1007/s10681-013-1001-4

Coskun, Y., and Savaskan, C. (2017). Plant regeneration through isolated microspore culture in recalcitrant durum wheat genotypes. *Indian J. Biotechnol.* 16, 119–125.

Croser, J. S., Lülsdorf, M. M., Davies, P. A., Clarke, H. J., Bayliss, K. L., Mallikarjuna, N., et al. (2006). Toward doubled haploid production in the Fabaceae: progress, constraints, and opportunities. *Crit. Rev. Plant Sci.* 25, 139–157. doi: 10.1080/07352680600563850

Croser, J. S., Lulsdorf, M. M., Grewal, R. K., Usher, K. M., and Siddique, K. H. M. (2011). Isolated microspore culture of chickpea (*Cicer arietinum* L.): induction of androgenesis and cytological analysis of early haploid divisions. *In Vitro Cell. Dev. Biol. Plant* 47, 357–368. doi: 10.1007/s11627-011-9346-7

Daetwyler, H. D., Hayden, M. J., Spangenberg, G. C., and Hayes, B. J. (2015). Selection on optimal haploid value increases genetic gain and preserves more genetic diversity relative to genomic selection. *Genetics* 200, 1341–1348. doi: 10.1534/genetics.115.178038

D'Ario, M., Griffiths-Jones, S., and Kim, M. (2017). Small RNAs: big impact on plant development. *Trends Plant Sci.* 22, 1056–1068. doi: 10.1016/j.tplants.2017.09.009

DePauw, R. M., Knox, R. E., Humphreys, D. G., Thomas, J. B., Fox, S. L., Brown, P. D., et al. (2011). New breeding tools impact Canadian commercial farmer fields. *Czech J. Genet. Plant Breed.* 47, S28–S34. doi: 10.17221/3250-CJGPB

Dezfouli, P. M., Sedghi, M., Shariatpanahi, M. E., Niazian, M., and Alizadeh, B. (2019). Assessment of general and specific combining abilities in doubled haploid lines of rapeseed (*Brassica napus* L.). Ind crops. *Prod.* 141:111754. doi: 10.1016/j.indcrop.2019.111754

Dolcet-Sanjuan, R., Claveria, E., and Huerta, A. (1997). Androgenesis in *Capsicum annuum* L.-effects of carbohydrate and carbon dioxide enrichment. *J. Amer. Soc. Hort. Sci.* 122, 468–475. doi: 10.21273/JASHS.122.4.468

Dwivedi, S. L., Britt, A. B., Tripathi, L., Sharma, S., Upadhyaya, H. D., and Ortiz, R. (2015). Haploids: constraints and opportunities in plant breeding. *Biotech Adv.* 33, 812–829. doi: 10.1016/j.biotechadv.2015.07.001

Dwivedi, S. L., Crouch, J. H., Mackill, D. J., Xu, Y., Blair, M. W., Ragot, M., et al. (2007). The molecularization of public sector crop breeding: progress, problems, and prospects. *Adv. Agron.* 95, 163–318. doi: 10.1016/S0065-2113(07)95003-8

El-Tantawy, A. A., Solís, M. T., De Costa, M. L., Coimbra, S., Risueño, M. C., and Testillano, P. S. (2013). Arabinogalactan protein profiles and distribution patterns during microspore embryogenesis and pollen development in *Brassica napus*. *Plant Reprod.* 26, 231–243. doi: 10.1007/s00497-013-0217-8

El-Tantawy, A. A., Solís, M. T., Risueño, M. C., and Testillano, P. S. (2014). Changes in DNA methylation levels and nuclear distribution patterns after microspore reprogramming to embryogenesis in barley. *Cytogenet. Genome Res.* 143, 200–208. doi: 10.1159/000365232

Eudes, F., and Chugh, A. (2008). Nanocarrier based plant transfection and transduction. WO 2008/148223 A1, Patent Application 25. Available at: http://www.lens.org/lens/patent/WO_2008_148223_A1 (Accessed March 25, 2015).

Ferrie, A. M. R. (2003). "Microspore culture of brassica species," in *Doubled Haploid Production in Crop Plants. A Manual*. eds. M. Maluszynski, K. J. Kasha, B. P. Forster and I. Szarejko (Dordrecht, Netherlands: Kluwer Academic Publishers), 195–204.

Ferrie, A. M. R., and Caswell, K. L. (2011). Isolated microspore culture techniques and recent progress for haploid and doubled haploid plant production. *Plant Cell Tissue Organ Cult.* 104, 301–309. doi: 10.1007/s11240-010-9800-y

Ferrie, A. M. R., Epp, D. J., and Keller, W. A. (1995). Evaluation of *Brassica rapa* L. genotypes for microspore culture response and identification of a highly embryogenic line. *Plant Cell Rep.* 14, 580–584. doi: 10.1007/BF00231942

Ferrie, A. M. R., and Möllers, C. (2011). Haploids and doubled haploids in brassica spp. for genetic and genomic research. *Plant Cell Tissue Organ Cult.* 104, 375–386. doi: 10.1007/s11240-010-9831-4

Fiorani, F., and Schurr, U. (2013). Future scenarios for plant phenotyping. *Annu. Rev. Plant Biol.* 64, 267–291. doi: 10.1146/annurev-arplant-050312-120137

Foiada, F., Westermeier, P., Kessel, B., Ouzunova, M., Wimmer, V., Mayerhofer, W., et al. (2015). Improving resistance to the European corn borer: a comprehensive study in elite maize using QTL mapping and genome-wide prediction. *Theor. Appl. Genet.* 128, 875–891. doi: 10.1007/s00122-015-2477-1

Forster, B. P., Heberle-Bors, E., Kasha, K. J., and Touraev, A. (2007). The resurgence of haploids in higher plants. *Trends Plant Sci.* 12, 368–375. doi: 10.1016/j.tplants.2007.06.007

Forster, B. P., and Thomas, W. T. B. (2005). Doubled haploids in genetics and plant breeding. *Plant Breed Rev.* 25, 57–88. doi: 10.1002/9780470650301

Garda, M., Hale, B., Rao, N., Lowe, M., Bright, M., Goodling, S., et al. (2020). Soybean androgenesis I: identification of pyramidal stressors in anther cultures that sustain cell divisions and putative embryo formation from isolated microspore cultures. *In vitro Cell. Dev. Biol. Plant* 56, 415–429. doi: 10.1007/s11627-020-10074-z

Geiger, H. H., Gordillo, A. G., and Koch, S. (2013). Genetic correlations among haploids, doubled haploids, and testcrosses in maize. *Crop Breed Genet.* 56, 2313–2320. doi: 10.2135/cropsci2013.03.0163

Germanà, M. A. (2009). "Haploids and doubled haploids in fruit trees," in *Advances in Haploid Production in Higher Plants*. eds. A. Touraev, B. P. Forster and S. M. Jain (Dordrecht: Springer).

Germanà, M. A. (2011). Anther culture for haploid and doubled haploid production. *Plant Cell Tissue Organ Cult.* 104, 283–300. doi: 10.1007/s11240-010-9852-z

Grewal, R. K., Lulsdorf, M., Croser, J., Ochatt, S., Vandenberg, A., and Warkentin, T. (2009). Doubled-haploid production in chickpea (*Cicer arietinum* L.): role of stress treatments. *Plant Cell Rep.* 28, 1289–1299. doi: 10.1007/s00299-009-0731-1

Guha, S., and Maheshwari, S. (1964). *In vitro* production of embryos from anthers of Datura. *Nature* 204:497. doi: 10.1038/204497a0

Hale, B., Phipps, C., Rao, N., Kelley, C., and Phillips, G. C. (2021). Soybean androgenesis II: non-gametophytic morphologies in isolated microspore culture. *In Vitro Cell Dev. Biol. Plant* 57, 356–364. doi: 10.1007/s11627-020-10144-2

Hale, B., Phipps, C., Rao, N., Wijeratne, A., and Phillips, G. C. (2020). Differential expression profiling reveals stress-induced cell fate divergence in soybean microspores. *Plan. Theory* 9:1510. doi: 10.3390/plants9111510

Heffner, E. L., Sorrells, M. E., and Jannink, J. L. (2009). Genomic selection for crop improvement. *Crop Sci.* 49, 1–12. doi: 10.2135/cropsci2008.08.0512

Heidari-Zefreh, A. A., Shariatpanahi, M. E., Mousavi, A., and Kalatejari, S. (2019). Enhancement of microspore embryogenesis induction and plantlet regeneration of sweet pepper (*Capsicum annuum* L.) using putrescine and ascorbic acid. *Protoplasma* 256, 13–24. doi: 10.1007/s00709-018-1268-3

Hernández-Sánchez, A. M., Capitaz-Tafur, J., Rodríguez-Monroy, M., and Sepúlveda-Jiménez, G. (2009). Arabinogalactan proteins in plant cell cultures. *Interciencia* 34, 170–176.

Hiramatsu, M., Odahara, K., and Matsue, Y. (1995). A survey of microspore embryogenesis in leaf mustard (*Brassica juncea*). *Acta Hort.* 392, 139–145. doi: 10.17660/ActaHortic.1995.392.16

Ho, K. M., and Jones, G. E. (1980). Mingo barley. *Can. J. Plant Sci.* 60, 279–280. doi: 10.4141/cjps80-041

Hooghvorst, I., Torrico, O., Hooghvorst, S., and Nogués, S. (2020). In situ parthenogenetic doubled haploid production in melon "Piel de Sapo" for breeding purposes. *Front. Plant Sci.* 11:378. doi: 10.3389/fpls.2020.00378

Howland, G. P., and Hart, R. W. (1977). "Radiation biology of cultured plant cells," in *Applied and Fundamental Aspects of Plant Cell, Tissue, and Organ Culture*. eds. J. Reinert and B. YPS (Berlin: Springer-Verlag), 732–756.

Hussain, T., and Franks, C. (2019). "Discovery of sorghum haploid induction system," in *Sorghum, Methods in Molecular Biology. Vol. 1931*. eds. Z. Y. Zhao and J. Dahlberg (New York, NY: Humana Press), 49–59.

Hyne, V., Kearsey, M. J., Pike, D. J., and Andsnape, J. W. (1995). QTL analysis: unreliability and bias in estimation procedures. *Mol. Breed.* 1, 273–282. doi: 10.1007/BF02277427

Indrianto, A., Barinova, I., Touraev, A., and Heberle-Bors, E. (2001). Tracking individual wheat microspores *in vitro*: identification of embryogenic microspores and body axis formation in the embryo. *Planta* 212, 163–174. doi: 10.1007/s004250000375

Jacquier, N. M. S., Gilles, L. M., Pyott, D. E., Martinant, J. P., Rogowsky, P. M., and Widiez, T. (2020). Puzzling out plant reproduction by haploid induction

for innovations in plant breeding. *Nature Plants* 6, 610–619. doi: 10.1038/s41477-020-0664-9

Jarrod, F. (2020). Doubled haploid breeding methods in maize and soybean. *Creative Components* 583.

Jiang, F., Ryabova, D., Diedhiou, J., Hucl, P., Randhawa, H., Marillia, E. F., et al. (2017). Trichostatin A increases embryo and green plant regeneration in wheat. *Plant Cell Rep.* 36, 1701–1706. doi: 10.1007/s00299-017-2183-3

Jumbo, M. B. (2010). *Comparison of Conventional, Modified Single Seed Descent, and Doubled Haploid Breeding Methods for Maize Inbred Line Development Using GEM Breeding Crosses*. Delaware: University of Delaware.

Kathiria, P., Diedhiou, J., and Marillia, E. F. (2016). "Improvement in wheat carbon flux for increased yield and harvest index," in Canadian Wheat Alliance Meetings, Saskatoon; July, 2016.

Kermicle, J. L. (1974). "Origin of androgenetic haploids and diploids induced by the indeterminate gametophyte (ig) mutation in maize." in *Haploids in Higher Plants: Advances and Potential*. ed. K. J. Kasha (Guelph, Canada: University of Guelph), 137.

Krishnappa, G., Savadi, S., Tyagi, B. S., Singh, S. K., Masthigowda, M. H., Kumar, S., et al. (2021). Integrated genomic selection for rapid improvement of crops. *Genomics* 113, 1070–1086. doi: 10.1016/j.ygeno.2021.02.007

Künzel, G., Korzun, L., and Meister, A. (2000). Cytologically integrated physical restriction fragment length polymorphism maps for the barley genome based on translocation breakpoints. *Genetics* 154, 397–412. doi: 10.1093/genetics/154.1.397

Leljak-Levanić, D., Mihaljevic, S., and Bauer, N. (2015). Somatic and zygotic embryos share common developmental features at the onset of plant embryogenesis. *Acta Physiol. Plant.* 37, 1–14. doi: 10.1007/s11738-015-1875-y

Letarte, J., Simion, E., Miner, M., and Kasha, K. J. (2006). Arabinogalactans and arabinogalactan-proteins induce embryogenesis in wheat (*Triticum aestivum* L.) microspore culture. *Plant Cell Rep.* 24, 691–698. doi: 10.1007/s00299-005-0013-5

Li, J., Cheng, D., Guo, S., Yang, Z., Chen, M., Chen, C., et al. (2020). Genomic selection to optimize doubled haploid-based hybrid breeding in maize. *bioRxiv* [Preprint]. doi: 10.1101/2020.09.08.287672

Li, H., Soriano, M., Cordewener, J., Muiño, J. M., Riksen, T., Fukuoka, H., et al. (2014). The histone deacetylase inhibitor trichostatin a promotes totipotency in the male gametophyte. *Plant Cell* 26, 195–209. doi: 10.1105/tpc.113.116491

Lionneton, E., Beuret, W., Delaitre, C., Ochatt, S., and Rancillac, M. (2001). Improved microspore culture and doubled-haploid plant regeneration in the brown condiment mustard (*Brassica juncea*). *Plant Cell Rep.* 20, 126–130. doi: 10.1007/s002990000292

Liu, L., and Wang, T. (2021). Male gametophyte development in flowering plants: a story of quarantine and sacrifice. *J. Plant Physiol.* 258:153365. doi: 10.1016/j.jplph.2021.153365

Lübberstedt, T., and Frei, U. K. (2012). Application of doubled haploids for target gene fixation in backcross programmes of maize. *Plant Breed.* 131, 449–452. doi: 10.1111/j.1439-0523.2011.01948.x

Makowska, K., Kałużniak, M., Oleszczuk, S., Zimny, J., Czaplicki, A., and Konieczny, R. (2017). Arabinogalactan proteins improve plant regeneration in barley (*Hordeum vulgare* L.) anther culture. *Plant Cell Tissue Organ Cult.* 131, 247–257. doi: 10.1007/s11240-017-1280-x

Malik, M. R., Wang, F., Dirpaul, J. M., Zhou, N., Polowick, P. L., Ferrie, A. M., et al. (2007). Transcript profiling and identification of molecular markers for early microspore embryogenesis in *Brassica napus*. *Plant Physiol.* 144, 134–154. doi: 10.1104/pp.106.092932

Maluszynski, M., Nichterlein, K., van Zanten, L., and Ahloowalia, B. S. (2000). Officially released mutant varieties – the FAO/IAEA database. *Mut. Breed Rev.* 12, 1–84.

Maraschin, S. D. F., Caspers, M., Potokina, E., Wülfert, F., Graner, A., Spaink, H. P., et al. (2006). cDNA array analysis of stress-induced gene expression in barley androgenesis. *Physiol. Plant.* 127, 535–550. doi: 10.1111/j.1399-3054.2006.00673.x

Maraschin, S. D. F., De Priester, W., Spaink, H. P., and Wang, M. (2005b). Androgenic switch: an example of plant embryogenesis from the male gametophyte perspective. *J. Exp. Bot.* 56, 1711–1726. doi: 10.1093/jxb/eri190

Maraschin, S. D. F., Vennik, M., Lamers, G. E., Spaink, H. P., and Wang, M. (2005a). Time-lapse tracking of barley androgenesis reveals position-determined cell death within pro-embryos. *Planta* 220, 531–540. doi: 10.1007/s00425-004-1371-x

Mayor, P. J., and Bernardo, R. (2009). Genomewide selection and marker-assisted recurrent selection in doubled haploid versus F2 populations. *Crop Sci.* 49, 1719–1725. doi: 10.2135/cropsci2008.10.0587

McNally, K. L., Childs, K. L., Bohnert, R., Davidson, R. M., Zhao, K., Ulat, V. J., et al. (2009). Genomewide SNP variation reveals relationships among landraces and modern varieties of rice. *Proc. Natl. Acad. Sci. U. S. A.* 106, 12273–12278. doi: 10.1073/pnas.0900992106

Melchinger, A. E., Böhm, J., Utz, H. F., Müller, J., Munder, S., and Mauch, F. J. (2018). High-throughput precision phenotyping of the oil content of single seeds of various oilseed crops. *Crop Sci.* 58, 670–678. doi: 10.2135/cropsci2017.07.0429

Mette, M. F., Gils, M., Longin, C. F. H., and Reif, J. C. (2015). "Hybrid breeding in wheat," in *Advances in Wheat Genetics: From Genome to Field*. eds. Y. Ogihara, S. Takumi and H. Handa (Tokyo: Springer).

Michelmore, R. W., Paran, I., and Kesseli, R. V. (1991). Identification of markers linked to disease-resistance genes by bulked segregant analysis: a rapid method to detect markers in specific genomic regions by using segregating populations. *Proc. Natl. Acad. Sci. U. S. A.* 88, 9828–9832. doi: 10.1073/pnas.88.21.9828

Murovec, J., and Bohanec, B. (2012). "Haploids and doubled haploids," in *Plant Breeding*. ed. I. Abdurakhmonov (China: InTech), 87–106.

Niazian, M., and Shariatpanahi, M. E. (2020). *In vitro*-based doubled haploid production: recent improvements. *Euphytica* 216, 1–21. doi: 10.1007/s10681-020-02609-7

Nienhuis, J., and Sills, G. (1992). "The potential of hybrid varieties in self-pollinating vegetables," in *Reproductive Biology and Plant Breeding*. eds. Y. Dattée, C. Dumas and A. Gallais (Berlin, Heidelberg: Springer).

Nieuwhof, M. (1963). Pollination and contamination of *Brassica oleracea* L. *Euphytica* 12, 17–26. doi: 10.1007/BF00033588

Nitsch, J. P., and Nitsch, C. (1969). Haploid plants from pollen grains. *Science* 163, 85–87. doi: 10.1126/science.163.3862.85

Niu, R. Q., Zhang, Y., Tong, Y., Liu, Z. Y., Wang, Y. H., and Feng, H. (2015). Effects of p-chlorophenoxyisobutyric acid, arabinogalactan, and activated charcoal on microspore embryogenesis in kale. *Gen Mol Res.* 14, 3897–3909. doi: 10.4238/2015.April.27.4

Nowicka, A., Juzoń, K., Krzewska, M., Dziurka, M., Dubas, E., Kopeć, P., et al. (2019). Chemically-induced DNA de-methylation alters the effectiveness of microspore embryogenesis in triticale. *Plant Sci.* 287:110189. doi: 10.1016/j.plantsci.2019.110189

Ochatt, S., Pech, C., Grewal, R., Conreux, C., Lulsdorf, M., and Jacas, L. (2009). Abiotic stress enhances androgenesis from isolated microspores of some legume species (Fabaceae). *J. Plant Physiol.* 166, 1314–1328. doi: 10.1016/j.jplph.2009.01.011

Paire, A., Devaux, P., Lafitte, C., Dumas, C., and Matthys-Rochon, E. (2003). Proteins produced by barley microspores and their derived androgenic structures promote *in vitro* zygotic maize embryo formation. *Plant Cell Tissue Organ Cult.* 73, 167–176. doi: 10.1023/A:1022805623167

Panchangam, S. S., Mallikarjuna, N., Gaur, P. M., and Suravajhala, P. (2014). Androgenesis in chickpea: anther culture and expressed sequence tags derived annotation. *Indian J. Exp. Biol.* 52, 181–188.

Park, S. J., Walsh, E. J., Reinbergs, E., Song, L. S. P., and Kasha, K. J. (1976). Field performance of doubled haploid barley lines in comparison with lines developed by the pedigree and single seed descent methods. *Can. J. Plant Sci.* 56, 467–474. doi: 10.4141/cjps76-077

Pechan, P. M. (1991). Heat shock proteins and cell proliferation. *FEBS Lett.* 280, 1–4. doi: 10.1016/0014-5793(91)80190-E

Pechan, P. M., and Keller, W. A. (1988). Identification of potentially embryogenic microspores in *Brassica napus*. *Physiol. Plant.* 74, 377–384. doi: 10.1111/j.1399-3054.1988.tb00646.x

Pérez-Pérez, Y., Carneros, E., Berenguer, E., Solís, M. T., Bárány, I., Pintos, B., et al. (2019). Pectin de-methylesterification and AGP increase promote cell wall remodeling and are required during somatic embryogenesis of *Quercus suber*. *Front. Plant Sci.* 9:1915. doi: 10.3389/fpls.2018.01915

Pourmohammad, A., Moieni, A., Dehghani, H., and Monfared, S. R. (2021). Field-grown donor plants and arabinogalactan proteins improve microspore embryogenesis in sweet pepper (*Capsicum annuum* L.). *In Vitro Cell Dev. Biol. Plant* 57, 510–518. doi: 10.1007/s11627-020-10152-2

Prasanna, B. M., Chaikam, V., and Mahuku, G. (2012). *Doubled Haploid Technology in Maize Breeding: Theory and Practice*. Mexico: CIMMYT.

Pratap, A., Prajapati, U., Singh, C. M., Gupta, S., Rathore, M., Malviya, N., et al. (2018). Potential, constraints and applications of *in vitro* methods in improving grain legumes. *Plant Breed.* 137, 235–249. doi: 10.1111/pbr.12590

Radoeva, T., and Weijers, D. (2014). A roadmap to embryo identity in plants. *Trends Plant Sci.* 19, 709–716. doi: 10.1016/j.tplants.2014.06.009

Redha, A., and Suleman, P. (2011). Effects of exogenous application of polyamines on wheat anther cultures. *Plant Cell Tissue Organ Cult.* 105, 345–353. doi: 10.1007/s11240-010-9873-7

Ren, J., Wu, P., Trampe, B., Tian, X., Lübberstedt, T., and Chen, S. (2017). Novel technologies in doubled haploid line development. *Plant Biotechnol. J.* 15, 1361–1370. doi: 10.1111/pbi.12805

Rimberia, F. K., Adaniya, S., Etoh, T., and Ishimine, Y. (2006). Sex and ploidy of anther culture derived papaya (*Carica papaya* L.). *Euphytica* 149, 53–59. doi: 10.1007/s10681-005-9051-x

Röber, F. K., Gordillo, G. A., and Geiger, H. H. (2005). In vivo haploid induction in maize – performance of new inducers and significance of doubled haploid lines in hybrid breeding. *Maydica* 50, 275–283.

Rodríguez-Sanz, H., Manzanera, J. A., Solís, M. T., Gómez-Garay, A., Pintos, B., Risueño, M. C., et al. (2014). Early markers are present in both embryogenesis pathways from microspores and immature zygotic embryos in cork oak, *Quercus suber* L. *BMC Plant Bio.* 14, 1–18. doi: 10.1186/s12870-014-0224-4

Rudolf-Pilih, K., Petkovšek, M., Jakše, J., Štajner, N., Murovec, J., and Bohanec, B. (2019). Proposal of a new hybrid breeding method based on genotyping, inter-pollination, phenotyping and paternity testing of selected elite F1 hybrids. *Front. Plant Sci.* 10:1111. doi: 10.3389/fpls.2019.01111

Rutley, N., and Twell, D. (2015). A decade of pollen transcriptomics. *Plant Reprod.* 28, 73–89. doi: 10.1007/s00497-015-0261-7

Šamaj, J., Salaj, T., Matúšová, R., Salaj, J., Takáč, T., and Volkmann, D. (2008). Arabinogalactan-protein epitope Gal4 is differentially regulated and localized in cell lines of hybrid fir (*Abies alba*× *Abies cephalonica*) with different embryogenic and regeneration potential. *Plant Cell Rep.* 27, 221–229. doi: 10.1007/s00299-007-0429-1

Sattler, M. C., Carvalho, C. R., and Clarindo, W. R. (2016). The polyploidy and its key role in plant breeding. *Planta* 243, 281–296. doi: 10.1007/s00425-015-2450-x

Seeja, G., and Sreekumar, S. (2020). Doubled haploids in genetic improvement: a review. *Int. J. Recent Sci. Res.* 11, 36941–36949. doi: 10.24327/ijrsr.2020.1101.5029

Seguí-Simarro, J. M. (2010). Androgenesis revisited. *Bot. Rev.* 76, 377–404. doi: 10.1007/s12229-010-9056-6

Seguí-Simarro, J. M. (2021). "Doubled haploid technology," in *Methods in Molecular Bsiology*. *Vol.* 2287. New York: Springer Science+ Business Media.

Seguí-Simarro, J. M., Testillano, P. S., and Risueño, M. C. (2003). Hsp70 and Hsp90 change their expression and subcellular localization after microspore embryogenesis induction in *Brassica napus* L. *J. Struct Biol.* 142, 379–391. doi: 10.1016/S1047-8477(03)00067-4

Seifert, F., Bössow, S., Kumlehn, J., Gnad, H., and Scholten, S. (2016). Analysis of wheat microspore embryogenesis induction by transcriptome and small RNA sequencing using the highly responsive cultivar "Svilena". *BMC Plant Biol.* 16:97. doi: 10.1186/s12870-016-0782-8

Shen, Y., Pan, G., and Lübberstedt, T. (2015). Haploid strategies for functional validation of plant genes. *Trends Biotech.* 33, 611–620. doi: 10.1016/j.tibtech.2015.07.005

Sinha, R. K., Jiang, F., and Eudes, F. (2021). TALE protein mediated overexpression of embryogenesis related marker genes in wheat microspores. *South African J. Bot.* 138, 50–56. doi: 10.1016/j.sajb.2020.12.004

Solís, M. T., El-Tantawy, A. A., Cano, V., Risueño, M. C., and Testillano, P. S. (2015). 5-azacytidine promotes microspore embryogenesis initiation by decreasing global DNA methylation, but prevents subsequent embryo development in rapeseed and barley. *Front. Plant Sci.* 6:472. doi: 10.3389/fpls.2015.00472

Soriano, M., Li, H., and Boutilier, K. (2013). Microspore embryogenesis: establishment of embryo identity and pattern in culture. *Plant Rep.* 26, 181–196. doi: 10.1007/s00497-013-0226-7

Strigens, A., Schipprack, W., Reif, J. C., and Melchinger, A. E. (2013). Unlocking the genetic diversity of maize landraces with doubled haploids opens new avenues for breeding. *PLoS One* 8:e57234. doi: 10.1371/journal.pone.0057234

Su, H., Chen, G., Yang, L., Zhang, Y., Wang, Y., Fang, Z., et al. (2020). Proteomic variations after short-term heat shock treatment reveal differentially expressed proteins involved in early microspore embryogenesis in cabbage (*Brassica oleracea*). *PeerJ* 8:e8897. doi: 10.7717/peerj.8897

Supena, E. D. J., and Custers, J. B. M. (2011). Refinement of shed-microspore protocol to increase normal embryos production in hot pepper (*Capsicum annuum* L.). *Scientia Hort.* 130, 769–774. doi: 10.1016/j.scienta.2011.08.037

Supena, E. D. J., Muswita, W., Suharsono, S., and Custers, J. B. M. (2006a). Evaluation of crucial factors for implementing shed-microspore culture of Indonesian hot pepper (*Capsicum annuum* L.) cultivars. *Scientia Hort.* 107, 226–232. doi: 10.1016/j.scienta.2005.08.006

Supena, E. D. J., Suharsono, S., Jacobsen, E., and Custers, J. B. M. (2006b). Successful development of a shed-microspore culture protocol for doubled haploid production in Indonesian hot pepper (*Capsicum annuum* L.). *Plant Cell Rep.* 25, 1–10. doi: 10.1007/s00299-005-0028-y

Supena, E. D. J., Winarto, B., Riksen, T., Dubas, E., Van Lammeren, A., Offringa, R., et al. (2008). Regeneration of zygotic-like microspore-derived embryos suggests an important role for the suspensor in early embryo patterning. *J. Exp. Bot.* 59, 803–814. doi: 10.1093/jxb/erm358

Swanson, E. B., and Erickson, L. R. (1989). Haploid transformation in *Brassica napus* using an octopine-producing strain of agrobacterium tumefaciens. *Theoret. Appl. Genet* 78, 831–835. doi: 10.1007/BF00266666

Szadkowski, E., Eber, F., Huteau, V., Lode, M., Coriton, O., Jenczewski, E., et al. (2011). Polyploid formation pathways have an impact on genetic rearrangements in resynthesized *Brassica napus*. *New Phytol.* 191, 884–894. doi: 10.1111/j.1469-8137.2011.03729.x

Szarejko, I., and Forster, B. P. (2007). Doubled haploidy and induced mutation. *Euphytica* 158, 359–370. doi: 10.1007/s10681-006-9241-1

Tadesse, W., Inagaki, M., Tawkaz, S., Baum, M., and van Ginkel, M. (2012). Recent advances and application of doubled haploids in wheat breeding Africa. *J. Biotechnol.* 11, 15484–15492. doi: 10.5897/AJB12.2124

Taylor, E. L., Taylor, T. N., and Krings, M. (2009). *Paleobotany: The Biology and Evolution of Fossil Plants*. United States: Academic Press.

Telmer, C. A., Newcomb, W., and Simmonds, D. H. (1995). Cellular changes during heat shock induction and embryo development of cultured microspores of *Brassica napus* cv. *Topas*. *Protoplasma* 185, 106–112. doi: 10.1007/BF01272758

Testillano, P. S. (2019). Microspore embryogenesis: targeting the determinant factors of stress-induced cell reprogramming for crop improvement. *J. Exp. Bot.* 70, 2965–2978. doi: 10.1093/jxb/ery464

Thudi, M., Li, Y., Jackson, S. A., May, G. D., and Varshney, R. K. (2012). Current state-of-art of sequencing technologies for plant genomics research. *Brief. Funct. Genomics* 11, 3–11. doi: 10.1093/bfgp/elr045

Thudi, M., Palakurthi, R., Schnable, J. C., Chitikineni, A., Dreisigacker, S., Mace, E., et al. (2020). Genomic resources in plant breeding for sustainable agriculture. *J. Plant Phys.* 257:153351. doi: 10.1016/j.jplph.2020.153351

Touraev, A., Vicente, O., and Heberle-Bors, E. (1997). Initiation of microspore embryogenesis by stress. *Trends Plant Sci.* 2, 297–302. doi: 10.1016/S1360-1385(97)89951-7

Tuvesson, S., Dayteg, C., Hagberg, P., Manninen, O., Tanhuanpää, P., Tenhola-Roininen, T., et al. (2007). Molecular markers and doubled haploids in European plant breeding programmes. *Euphytica* 158, 305–312. doi: 10.1007/s10681-006-9239-8

Varshney, R., Nayak, S., May, G., and Jackson, S. (2009). Next-generation sequencing technologies and their implications for crop genetics and breeding. *Trends Biotech.* 27, 522–530. doi: 10.1016/j.tibtech.2009.05.006

Varshney, R. K., Roorkiwal, M., and Nguyen, H. T. (2013). Legume genomics: from genomic resources to molecular breeding. *Plant Genome* 6, 1–7. doi: 10.3835/plantgenome2013.12.0002in

Wang, H. M., Enns, J. L., Nelson, K. L., Brost, J. M., Orr, T. D., and Ferrie, A. M. R. (2019). Improving the efficiency of wheat microspore culture methodology – evaluation of pretreatments, gradients, and epigenetic chemicals. *Plant Cell Tissue Organ Cult.* 139, 589–599. doi: 10.1007/s11240-019-01704-5

Wang, Z., Taramino, G., Yang, D., Liu, G., Tingey, S. V., Miao, G. H., et al. (2001). Rice ESTs with disease-resistance gene-or defense-response gene-like sequences mapped to regions containing major resistance genes or QTLs. *Mol. Gen. Genom.* 265, 302–310. doi: 10.1007/s004380000415

Wessels, E., and Botes, W. C. (2014). Accelerating resistance breeding in wheat by integrating marker-assisted selection and doubled haploid technology. *South African J. Plant. Soil.* 31, 35–43. doi: 10.1080/02571862.2014.903434

Wilde, K., Burger, H., Prigge, V., Presterl, T., Schmidt, W., Ouzunova, M., et al. (2010). Testcross performance of doubled-haploid lines developed from European flint maize landraces. *Plant Breed.* 129, 181–185. doi: 10.1111/j.1439-0523.2009.01677.x

Yan, G., Liu, H., Wang, H., Lu, Z., Wang, Y., Mullan, D., et al. (2017). Accelerated generation of selfed pure line plants for gene identification and crop breeding. *Front. Plant Sci.* 8:1786. doi: 10.3389/fpls.2017.01786

Yang, J., Liu, Z., Chen, Q., Qu, Y., Tang, J., Lübberstedt, T., et al. (2020). Mapping of QtL for grain yield components based on a DH population in maize. *Sci. Rep.* 10, 1–11. doi: 10.1038/s41598-020-63960-2

Yuan, S. X., Su, Y. B., Liu, Y. M., Fang, Z. Y., Yang, L. M., Zhuang, M., et al. (2012). Effects of pH, MES, arabinogalactan-proteins on microspore cultures in white cabbage. *Plant Cell Tissue Organ Cult.* 110, 69–76. doi: 10.1007/s11240-012-0131-z

Zaki, M., and Dickinson, H. (1991). Microspore-derived embryos in *brassica*: the significance of division symmetry in pollen mitosis I to embryogenic development. *Sex. Plant Reprod.* 4, 48–55. doi: 10.1007/BF00194572

Zarsky, V., Garrido, D., Eller, N., Tupy, J., Vicente, O., Schöffl, F., et al. (1995). The expression of a small heat shock gene is activated during induction of tobacco pollen embryogenesis by starvation. *Plant. Cells Env.* 18, 139–147. doi: 10.1111/j.1365-3040.1995.tb00347.x

Zeitler, L., Ross-Ibarra, J., and Stetter, M. G. (2020). Selective loss of diversity in doubled-haploid lines from European maize landraces. *G3: Gen. Genom. Genet.* 10, 2497–2506. doi: 10.1534/g3.120.401196

Zhang, L., Zhang, Y., Gao, Y., Jiang, X., Zhang, M., Wu, H., et al. (2016). Effects of histone deacetylase inhibitors on microspore embryogenesis and plant regeneration in Pakchoi (*Brassica rapa* ssp. *chinensis* L.). *Sci Hort.* 209, 61–66. doi: 10.1016/j.scienta.2016.05.001

Zhao, J., Newcomb, W., and Simmonds, D. (2003). Heat-shock proteins 70 kDa and 19 kDa are not required for induction of embryogenesis of *Brassica napus* L. cv. *Topas microspores. Plant Cell Phys.* 44, 1417–1421. doi: 10.1093/pcp/pcg162

Zieliński, K., Dubas, E., Gerši, Z., Krzewska, M., Janas, A., Nowicka, A., et al. (2021). β-1, 3-Glucanases and chitinases participate in the stress-related defence mechanisms that are possibly connected with modulation of arabinogalactan proteins (AGP) required for the androgenesis initiation in rye (*Secale cereale* L.). *Plant Sci.* 302:110700. doi: 10.1016/j.plantsci.2020.110700

Conflict of Interest: The authors declare that this review was written in the absence of any commercial or financial relationships that could be construed as a potential conflict of interest.

Publisher's Note: All claims expressed in this article are solely those of the authors and do not necessarily represent those of their affiliated organizations, or those of the publisher, the editors and the reviewers. Any product that may be evaluated in this article, or claim that may be made by its manufacturer, is not guaranteed or endorsed by the publisher.

frontiers in Plant Science

ORIGINAL RESEARCH
published: 11 January 2022
doi: 10.3389/fpls.2021.768584

Pollen Number and Ribosome Gene Expression Altered in a Genome-Editing Mutant of *REDUCED POLLEN NUMBER1* Gene

*Hiroyuki Kakui[1,2,3], Takashi Tsuchimatsu[1,4,5,6,7], Misako Yamazaki[1], Masaomi Hatakeyama[1,8] and Kentaro K. Shimizu[1,2,4]**

[1] Department of Evolutionary Biology and Environmental Studies, University of Zurich, Zurich, Switzerland, [2] Kihara Institute for Biological Research, Yokohama City University, Yokohama, Japan, [3] Graduate School of Science and Technology, Niigata University, Niigata, Japan, [4] Department of Plant and Microbial Biology & Zurich-Basel Plant Science Center, University of Zurich, Zurich, Switzerland, [5] Gregor Mendel Institute, Austrian Academy of Sciences, Vienna BioCenter, Vienna, Austria, [6] Department of Biology, Chiba University, Chiba, Japan, [7] Department of Biological Sciences, University of Tokyo, Tokyo, Japan, [8] Functional Genomics Center Zurich, Zurich, Switzerland

The number of pollen grains varies within and between species. However, little is known about the molecular basis of this quantitative trait, in contrast with the many studies available on cell differentiation in the stamen. Recently, the first gene responsible for pollen number variation, *REDUCED POLLEN NUMBER1* (*RDP1*), was isolated by genome-wide association studies of *Arabidopsis thaliana* and exhibited the signature of natural selection. This gene encodes a homolog of yeast Mrt4 (mRNA turnover4), which is an assembly factor of the large ribosomal subunit. However, no further data were available to link ribosome function to pollen development. Here, we characterized the *RDP1* gene using the standard *A. thaliana* accession Col-0. The frameshift mutant, *rdp1-3* generated by CRISPR/Cas9 revealed the pleiotropic effect of *RDP1* in flowering, thus demonstrating that this gene is required for a broad range of processes other than pollen development. We found that the natural Col-0 allele conferred a reduced pollen number against the Bor-4 allele, as assessed using the quantitative complementation test, which is more sensitive than transgenic experiments. Together with a historical recombination event in Col-0, which was identified by sequence alignment, these results suggest that the coding sequence of *RDP1* is the candidate region responsible for the natural phenotypic variation. To elucidate the biological processes in which *RDP1* is involved, we conducted a transcriptome analysis. We found that genes responsible for ribosomal large subunit assembly/biogenesis were enriched among the differentially regulated genes, which supported the hypothesis that ribosome biogenesis is disturbed in the *rdp1-3* mutant. Among the pollen-development genes, three key genes encoding basic helix-loop-helix (bHLH) transcription factors (*ABORTED MICROSPORES* (*AMS*), *bHLH010*, and *bHLH089*), as well as direct downstream genes of *AMS*, were downregulated in the *rdp1-3* mutant. In summary, our results suggest a specialized function of ribosomes in pollen development through *RDP1*, which harbors natural variants under selection.

Keywords: pollen number, *REDUCED POLLEN NUMBER1*, complementation test, CRISPR/Cas9, transcriptome, ribosomal protein

OPEN ACCESS

Edited by:
David Honys, Institute of Experimental Botany of the Czech Academy of Sciences, Czechia

Reviewed by:
Gorou Horiguchi, Rikkyo University, Japan
Etienne Delannoy, UMR 9213 Institut des Sciences des Plantes de Paris Saclay (IPS2), France

***Correspondence:**
Kentaro K. Shimizu
kentaro.shimizu@uzh.ch

Specialty section:
This article was submitted to Plant Development and EvoDevo, a section of the journal Frontiers in Plant Science

Received: *31 August 2021*
Accepted: *08 December 2021*
Published: *11 January 2022*

Citation:
Kakui H, Tsuchimatsu T, Yamazaki M, Hatakeyama M and Shimizu KK (2022) Pollen Number and Ribosome Gene Expression Altered in a Genome-Editing Mutant of REDUCED POLLEN NUMBER1 Gene. Front. Plant Sci. 12:768584. doi: 10.3389/fpls.2021.768584

INTRODUCTION

Pollen grain number in seed plants is a key reproductive trait that has been studied extensively for decades, from agricultural and evolutionary viewpoints. Domesticated crop species generally produce fewer pollen grains than wild relative species, whereas a high pollen number is preferred in some cultivation strategies, such as hybrid crops and artificial pollination (Oka and Morishima, 1967; Franco-Mora et al., 2005; Langer et al., 2014; Shimizu and Tsuchimatsu, 2015; Boeven et al., 2016). Despite its agricultural and evolutionary importance, the genetic basis of pollen grain number has remained elusive, mainly because of its quantitative nature. Recently, the *REDUCED POLLEN NUMBER1* (*RDP1*) gene, which is responsible for the natural variation in pollen number, was identified through a genome-wide association study of *Arabidopsis thaliana* (Tsuchimatsu et al., 2020). The CRISPR/Cas9-generated *RDP1* frameshift mutants in the Col-0 background produced about half of the number of pollen grains compared with wild-type and was considered non-functional or null. The Uod-1 accession had a long-haplotype variant at the *RDP1* region, which conferred a lower number of pollen grains and exhibited a signature of selective sweep. The Bor-4 accession had an alternative variant that conferred a greater number of pollen grains. Both variants did not contain a gene disruptive mutation. Causal evidence of the allelic effects of *RDP1* was obtained using Uod-1 and Bor-4 via the quantitative complementation test (also known as reciprocal hemizygosity test) (Tsuchimatsu et al., 2020), which compares allelic effects under the same copy number and positions of genes (Stern, 1998, 2014; Turner, 2014). Although functional tests using transgenesis are often used to examine exact causal mutations, a subtle allelic effect may not be detected in this manner because of the uncertainty of the insertion position in the genome in plants. Further quantitative complementation testing using an accession that experienced historical recombination events (such as Col-0) is another experiment that can narrow down the specific region responsible for the allelic effect of *RDP1*.

In contrast with pollen-number regulation, the molecular basis of cell differentiation in stamen development has been well studied (Alvarez-Buylla et al., 2010; Walbot and Egger, 2016; Ferguson et al., 2017; Li et al., 2017; Xue et al., 2021). Pollen and tapetal cell lineages differentiate from archesporial cells, with the latter being essential for the development of the former (Sanders et al., 1999; Feng and Dickinson, 2010; Walbot and Egger, 2016). The development of tapetum and pollen lineages is governed by a genetic pathway called "DYT1-TDF1-AMS-MS188-MS1" (Li et al., 2017), which is composed of transcriptional factors (Zhu et al., 2011; Lou et al., 2018). Two of them, DYSFUNCTIONAL TAPETUM1 (DYT1) and ABORTED MICORSPORES (AMS), are basic helix-loop-helix (bHLH) transcription factors that interact with three other bHLH factors, bHLH10, bHLH89, and bHLH91. Their protein interactions and transcriptional feedback regulations were reported (Feng et al., 2012; Zhu et al., 2015; Cui et al., 2016). Among these bHLH factors, AMS is known as a master regulator of pollen wall formation (Sorensen et al., 2003; Xu et al., 2010; Zhu et al., 2011; Xu et al., 2014). Transcriptome data showed that many genes are differentially expressed between wild-type and *ams* mutant. Li et al. (2017) detected 825 downregulated genes from tapetum cells in the *ams* mutant. Xu et al. (2014) reported 23 genes that were directly regulated by AMS based on microarray and qChIP-PCR experiments. Based on these detailed characterizations of transcriptional regulation and protein interaction in the pollen/anther pathway (Zhu et al., 2011; Ma et al., 2012; Cui et al., 2016; Ferguson et al., 2017; Wang et al., 2018; Chen et al., 2019), we investigated these pollen development genes in the mutants of *RDP1*.

RDP1 encodes a protein with homology to the mRNA turnover 4 (Mrt4) protein. Mrt4 acts as a pre-60S ribosomal component in yeast (Schmidt et al., 2013; Salih et al., 2020; Tsuchimatsu et al., 2020). The *Mrt4* gene is not essential in yeast, but null mutants of *mrt4* show slow-growth phenotypes, suggesting its role in cell proliferation (Rodriguez-Mateos et al., 2009a,b). However, it is unclear whether RDP1 is working as a component of ribosome and affect the translation in *A. thaliana*. Ribosomal genes were traditionally considered housekeeping genes of the protein synthesis machinery, and to function uniformly in all cells. Nevertheless, increasing evidence has shown ribosome specialization in plant and other model species (Martinez-Seidel et al., 2020; Norris et al., 2021). Many mutants of ribosome-related genes exhibit organ specific phenotypes, such as the reduction of leaf cell number, larger leaf cell size (Fujikura et al., 2009; Horiguchi et al., 2011), reduced root length (Creff et al., 2010), and reduction of stamen number (Stirnberg et al., 2012). Transcriptome studies of ribosome biogenesis factor mutants of *Arabidopsis* reported the upregulation of ribosomal genes as well as altered regulation of other genes, which supported the importance of transcriptome data of ribosome biogenesis factors mutant (Beine-Golovchuk et al., 2018; Cheong et al., 2021).

Here, we focused on the standard Col-0 background for further characterization of the *RDP1* gene. First, the phenotypes at different developmental stages were examined in the frameshift *rdp1-3* mutant in the Col-0 background. Second, the *RDP1* genomic sequences of Col-0, Uod-1, and Bor-4 were aligned to characterize the Col-0 sequence, and the quantitative complementation test was used to narrow down the candidate regions responsible for the natural phenotypic variation. Subsequently, we performed transcriptome analyses to detect differentially expressed genes (DEGs) between the wild-type and *rdp1-3* plants focusing on ribosome-related and pollen development genes. Finally, we assessed whether ribosome genes were upregulated, as previously observed in *Arabidopsis* ribosome mutants. Our data support the specific function of the ribosome in the developing pollen cell lineage.

Abbreviations: AMS, *ABORTED MICROSPORES*; bHLH, basic helix-loop-helix; DEG, differentially expressed gene; DYT1, *DYSFUNCTIONAL TAPETUM1*; FAA, formaldehyde acetic acid; FDR, false discovery rate; GO, gene ontology; Mrt4, mRNA turnover4; RDP1, *REDUCED POLLEN NUMBER1*.

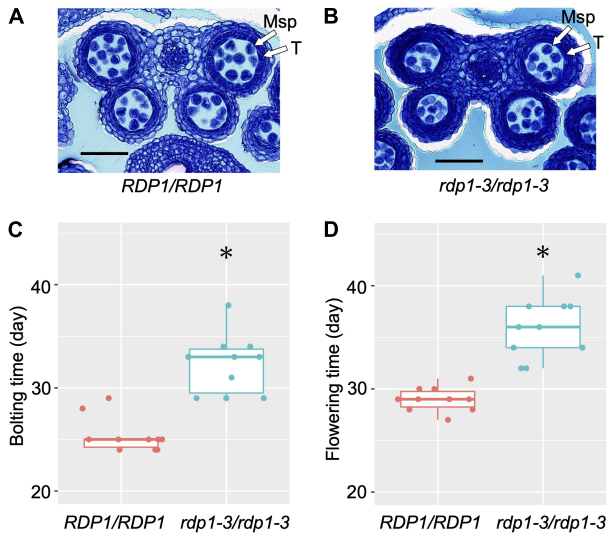

FIGURE 1 | Anther sections, bolting time, and flowering time of wild-type (*RDP1/RDP1*) and null mutant (*rdp1-3/rdp1-3*) plants. Transverse sections of *RDP1/RDP1* **(A)** and *rdp1-3/rdp1-3* **(B)** anthers (anther stage 8). Msp, microspores; T, tapetum. Scale bars, 50 μm. Bolting **(C)** and flowering **(D)** time of *RDP1/RDP1* and *rdp1-3/rdp1-3* plants (n = 10 and 10 for **C,D**, respectively; Asterisks indicate significant differences, determined by Wilcoxon rank-sum test, P = 4.33e–05 for **C**, P = 1.08e–05 for **D**). Boxplots **(C,D)** show center line: median; box limits: upper and lower quartiles; dots: individual data points.

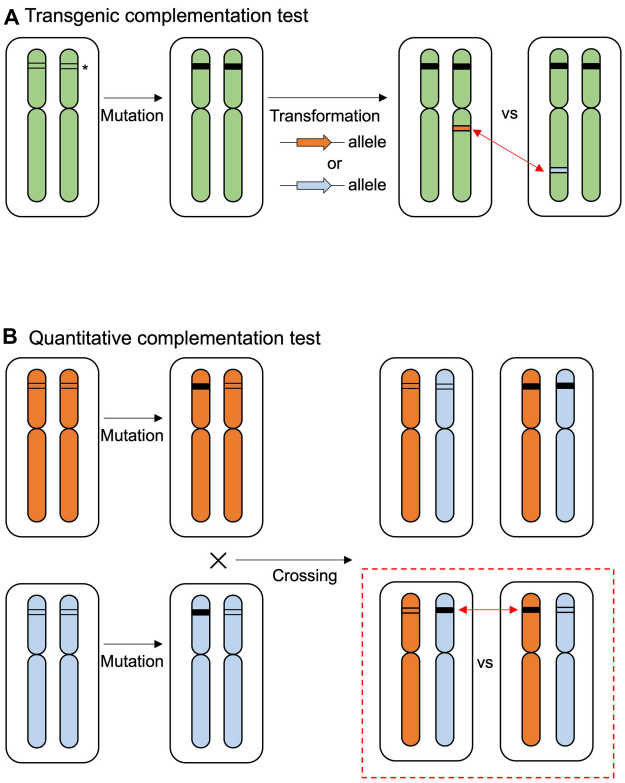

FIGURE 2 | Overview of the complementation tests. **(A)** The traditional transgenic complementation test compares the effects of inserted alleles (indicated by orange or blue arrows) in the null mutant background. The allelic effect of the target gene is compared from different insertion positions (red two-sided arrows). The asterisk indicates the target gene. The black box at the target gene indicates the mutated sequence. **(B)** Quantitative complementation test using null mutation of different alleles. Allelic effects are evaluated in the F_1 progenies of heterozygous mutants (red dashed square). The allelic effect of the target gene is compared from the original position in the genome (red two-sided arrows).

MATERIALS AND METHODS

Plant Materials and Growth Conditions

Four accessions of *A. thaliana*, Col-0 (N22625), Bor-4 (N22591), Mz-0 (N22636), and Uod-1 (N22612), as well as *A. lyrata* ssp. *lyrata* (CS22696), were used in this study. *Arabidopsis* seeds were sown on soil mixed with the insecticide ActaraG (Syngenta Agro, Switzerland) and stratified for 3–4 days at 4°C in the dark. The plants were grown under 16 h of light at 22°C and 8 h of dark at 20°C, with weekly treatments with insecticide (Kendo Gold, Syngenta Agro). The frameshift mutants of *RDP1* created by CRISPR/Cas9, i.e., *rdp1-3* (Col-0) and *rdp1-6* (Bor-4), were generated previously (Tsuchimatsu et al., 2020). The frameshift of *rdp1-3* and *rdp1-6* were identical. These frameshift mutants were genotyped by PRIMA using primers (Forward primer, 5′–TAGGCACAATGGAAAGTTAG–3′; Reverse primer, 5′–TTAACATAAAAGAACCATTGTAAG–3′) and 40-mer probe (5′–GGAGACTTTGTAGATACCAGAGTTCATCTTCTGCAGAACG–3′) as described previously (Kakui et al., 2021). T-DNA fragments containing CRISPR/Cas9 and GFP marker were removed from each strain of *rdp1-3* and *rdp1-6* by selecting non-fluorescence seeds (Tsutsui and Higashiyama, 2017). Bolting time was determined when the main inflorescence stem reached 3 cm. Flowering time was recorded when the first flower opened. Time-lapse movie of plant growth from Col-0 and *rdp1-3* was obtained using a TLC200 Pro camera (Brinno, Taiwan).

Histological Analysis of Anthers

For histological analysis, inflorescences were fixed with FAA (formaldehyde:acetic acid:70% ethanol = 1:1:18), dehydrated, and embedded in Technovit 7100 according to the manufacturer's instructions (Heraeus Kulzer GmbH, Wehrheim, Germany). Five-micrometer sections were cut with a microtome (RM2145, Leica, Germany) and stained with toluidine blue before observation under a Leica microscope (DM5000, Leica) equipped with a color camera (DMC2900, Leica).

Traditional Transgenic Complementation

The *RDP1* sequence of Col-0, including the 1,960 bp upstream region from the coding sequence to 661 bp downstream from the stop codon, was amplified using the following primers: 3795_At1g25260F (5′–TTTCTCCCCACATTTCTC–3′) and 3988_At1g25260R (5′–TATGTTATCAAAATTCATAAAATG–3′). The *RDP1* sequences from different accessions were amplified from Mz-0, Col-0, Bor-4, and *A. lyrata* by PCR (PrimeSTAR GXL, Takara Bio, Japan). These PCR products were cloned

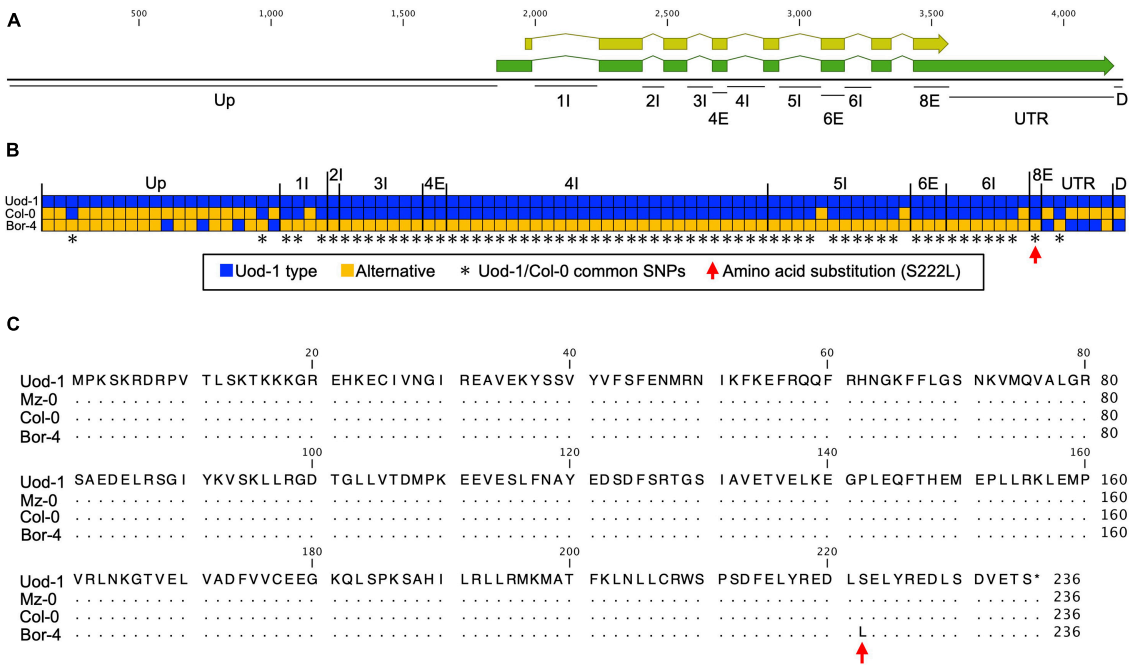

FIGURE 3 | Comparison of *RDP1* sequences among Uod-1, Col-0, and Bor-4. **(A)** Schematic structure of the *RDP1* gene. The green and yellow boxes indicate mRNA and coding regions, respectively. Up, upstream; I, intron; E, exon; UTR, 3′UTR; D, downstream. Each annotation was defined by NCBI information (NM_102335.4). The number with I or E stands for the ordinal number of each intron or exon. Only the names of polymorphic regions are indicated. **(B)** Haplotype map of the *RDP1* gene. All SNPs and gaps (indels) of the *RDP1* region are shown. Each box corresponds to a polymorphism. Continuous gaps (indels) are displayed as a single box. The blue box indicates the Uod-1 type, and the orange box indicates an alternative polymorphism. The asterisks indicate common SNPs between Uod-1 and Col-0. The red arrow indicates an amino acid substitution in *RDP1* (S222L). The nucleic acid sequences of the *RDP1* region corresponding to **(A)** region from Uod-1, Col-0, and Bor-4 are shown in **Supplementary Figure 1**. **(C)** Amino acid sequences of *RDP1* from Uod-1, Mz-0, Col-0, and Bor-4. Dots represent identical sequence with Uod-1. Single amino acid substitution alone was identified among these accessions (S222L, red arrow). Sequence annotations and multiple sequence alignment were generated using the CLC Main Workbench (version 21.0.5)(**A,C**, and **Supplementary Figure 1**).

into pFAST-R01 (Shimada et al., 2010). Each construct was independently transformed into *rdp1-3* (Col-0 background) plants using the floral-dip method (Clough and Bent, 1998) with *Agrobacterium tumefaciens* (GV3101).

Quantitative Complementation

Arabidopsis thaliana plants with heterozygous *RDP1* alleles from two accessions, i.e., the Col-0 accession (*RDP1*/*rdp1-3*, termed $RDP1^{Col}/rdp1^{Col}$ hereafter) and the Bor-4 accession (*RDP1*/*rdp1-6*, termed $RDP1^{Bor}/rdp1^{Bor}$ hereafter), were prepared (Tsuchimatsu et al., 2020). F_1 plants were generated by crossing $RDP1^{Col}/rdp1^{Col}$ and $RDP1^{Bor}/rdp1^{Bor}$. Subsequently, F1 progenies are genotyped and analyzed.

Pollen-Number Counting Using a Cell Counter

We sampled flower buds and counted pollen numbers using a cell counter as described previously (Kakui et al., 2020; Tsuchimatsu et al., 2020). In summary, flowers of stage 12 [unopened anther with mature pollen grains (Smyth et al., 1990)] were collected and incubated overnight at 60°C. Flowers were collected from the side stem because flowers of the main stem have significantly larger pollen numbers (Tsuchimatsu et al., 2020). 1st and 2nd flowers of flower buds were excluded from sampling because they tend to show abnormal flower shapes (Kakui et al., 2020). We collected flowers from the start of flowering until approximately 2 weeks later. Subsequently, 30 μL of 5% Tween-20 was added, and the mixture was sonicated using a sonicator (Bioruptor Plus, Diagenode, Belgium), to release the pollen grains. The pollen suspension was mixed with a pollen counting solution (CASYton, OMNI Life Science, Germany), and particles were counted on a cell counter (CASY cell counter, OMNI Life Science). Pollen-number data were statistically analyzed and plots were constructed in R (R Core Team, 2013).

Transcriptome Analysis

Total RNA was isolated from four replicates of flower buds of the wild-type and *rdp1-3* plants using the RNeasy plant mini kit (Qiagen, Germany). The samples encompassed a wide range of developmental stages (flower stages 1–12) (Sanders et al., 1999), excluding opened flowers. Next, 75-bp single-end read sequencing was performed on a NextSeq 500 sequencer (Illumina, San Diego, CA, United States). The sample information and the number of reads are listed in **Supplementary Table 1**. The transcriptome data obtained were analyzed using the SUSHI framework (Hatakeyama et al., 2016). We defined DEGs based on a false discovery rate (FDR) < 0.1. All DEGs data

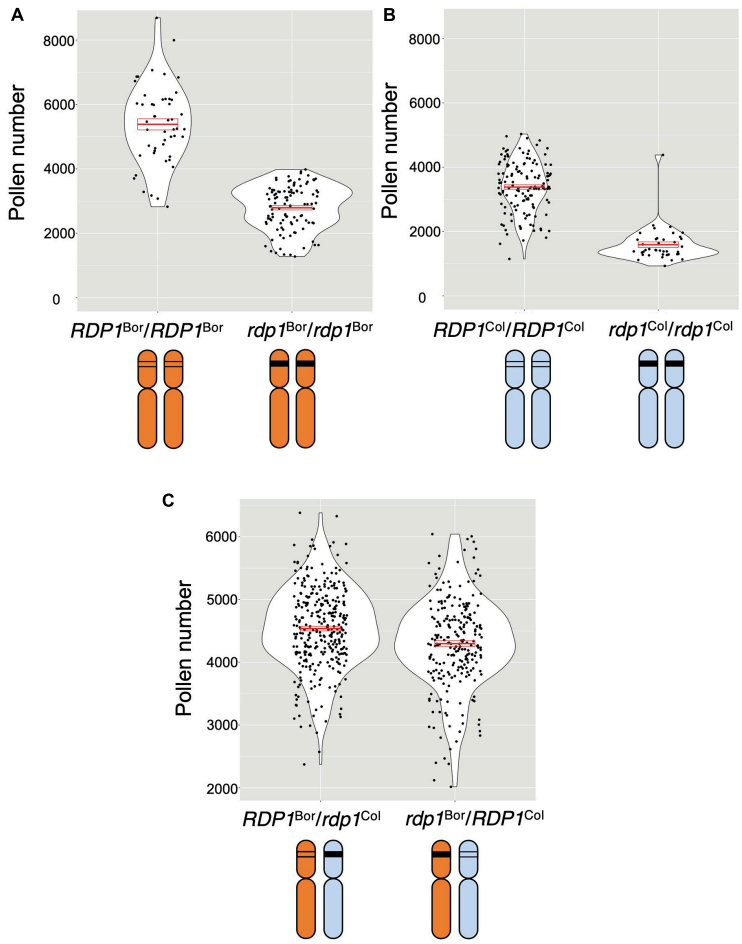

FIGURE 4 | Quantitative complementation test of the *RDP1* gene. Pollen number per flower was analyzed. Violin plots with means and standard errors of means indicated by red bold bars and boxes, respectively. **(A,B)** Pollen-number difference between the wild-type and a homozygote of a frameshift allele generated by the CRISPR/Cas9 technique in the Bor-4 background **(A**; n = 50 [$RDP1^{Bor}/RDP1^{Bor}$]; n = 106 [$rdp1^{Bor}/rdp1^{Bor}$]) and in the Col-0 background (**B**; n = 135 [$RDP1^{Col}/RDP1^{Col}$]; n = 40 [$rdp1^{Col}/rdp1^{Col}$]). **(C)** Difference in the effect of two natural alleles, $RDP1^{Bor}$ and $RDP1^{Col}$, on pollen number. The pollen number in the plants with $RDP1^{Bor}$ was significantly higher than that in the plants with $RDP1^{Col}$ (nested analysis of variance; $P = 1.10 \times 10^{-5}$; n = 315 [$RDP1^{Bor}/rdp1^{Col}$, median = 4,528 pollen grains/flower]; n = 247 [$rdp1^{Bor}/RDP1^{Col}$, median = 4,302 pollen grains/flower]). The two alleles were compared in the heterozygous state with a frameshift CRISPR/Cas9 allele in an identical genomic background. F_1 plants were obtained from the cross of two heterozygotes, $RDP1^{Col}/rdp1^{Col}$ and $RDP1^{Bor}/rdp1^{Bor}$. Results from four genotypes including $RDP1^{Bor}/RDP1^{Col}$ and $rdp1^{Bor}/rdp1^{Col}$ were shown in **Supplementary Figure 3**.

are listed in **Supplementary Table 2**. The gene ontology (GO) enrichment analysis was performed using the ShinyGO v0.66 software (Ge et al., 2020).

RESULTS

Natural Variation of *RDP1* Sequences and the Validation of Allelic Functional Differences Using the Quantitative Complementation Test

The CRISPR/Cas9-generated frameshift *rdp1-3* mutant in the Col-0 background produced about half the number of pollen grains compared with the wild-type counterpart (Tsuchimatsu et al., 2020). We further observed the section of the developing anther and confirmed that the number of microspores was already decreased in the mutant at the anther stage 8 (Sanders et al., 1999; **Figures 1A,B**). Tsuchimatsu et al. (2020) reported that the frameshift *rdp1-3* mutants exhibited other pleiotropic phenotypes, such as reduced ovule number and delayed growth, in contrast with the effect of natural variants. Here, we found that the bolting and flowering times were significantly delayed (Wilcoxon rank-sum test; P = 4.33e–05 for bolting time, P = 1.08e–05 for flowering time, **Figures 1C,D** and **Supplementary Video 1**). These results support the notion that *RDP1* functions as an Mrt4 homolog in *A. thaliana*, in accordance with the slower growth observed in the Mrt4 null mutant in yeast (Rodriguez-Mateos et al., 2009a).

To narrow down the causal sequence/region underlying the allelic effect of *RDP1*, we performed functional experiments

using natural accessions. We first performed a traditional transgenic test to detect the allelic effect of *RDP1* (**Figure 2A**), but found that the resolution was not sufficient to detect it, as follows. The prepared *RDP1* sequences ranged from the upstream region (1,960 bp in Col-0) to the downstream region (661 bp in Col-0, **Supplementary Figure 1**) of three *A. thaliana* accessions (Col-0, Mz-0, and Bor-4), as well as *A. lyrata* ssp. *lyrata*. Mz-0 was among the accessions with the lowest pollen number, and the predominantly outcrossing species *A. lyrata* produced a much greater number of pollen grains than the *A. thaliana* accessions (Tsuchimatsu et al., 2020). Each sequence was introduced into the CRISPR/Cas9-generated *rdp1* null (non-functional) mutant (*rdp1-3/rdp1-3*, Col-0 background), and more than 10 independent transformants were obtained for each of the four constructs. However, the variation in pollen number was high, even among the transformants of the same construct, and the range of the number of pollen grains largely overlapped between the four constructs (**Supplementary Figures 2A,B**). When these data were compared with those obtained for wild-type Col-0, three of them showed no significant difference, whereas, unexpectedly, the construct with Col-0 showed a slight increase in pollen number, although a previous complementation test on another *rdp1* mutant background (*rdp1-1*) showed no significant difference compared with Col-0 (Tsuchimatsu et al., 2020). We speculate that the positional effect of the insertion site was too large to detect a subtle allelic difference. In *Arabidopsis* transgenic experiments, it is difficult to control the insertion sites of transgenes. Depending on the insertion position, the expression level, timing, and/or tissue type of the transgenes may be affected and other genes can be disrupted. Although a drastic increase in the number of independent transgenic lines may eventually result in significant differences, the construction of these lines and the measurement of phenotypes would be highly tedious.

We then used the quantitative complementation test to detect the allelic effect of *RDP1*. Previously, we showed the allelic differences of *RDP1* between Uod-1 (a variant conferring reduced pollen number) and Bor-4 (a variant conferring increased pollen number) via the quantitative complementation test (**Figure 2B**; Tsuchimatsu et al., 2020). Here, we tested quantitative complementation using the Bor-4 and Col-0 accessions. We aligned the *RDP1* genomic region of Col-0 to that of Uod-1 and Bor-4 (**Figure 3A** and **Supplementary Figure 1**). The analysis of the alignment of genomic sequences showed that Col-0 experienced a historical recombination event near the start of the transcribed region, i.e., between its upstream and transcribed (exon/intron) regions (**Figure 3B**; Tsuchimatsu et al., 2020). The upstream sequence of Col-0 was close to that of Bor-4. However, the exonic and intronic sequences of Col-0 were very close to those of Uod-1, and there was only a single amino acid substitution differentiating Bor-4 from the three other accessions (S222L, **Figures 3B,C**). This amino acid position was deduced to be functionally important because the corresponding serine residues at the C-terminal region of human Mrt4 regulate cellular localization under the stress condition (Michalec-Wawiorka et al., 2015). In addition, the 3′UTR and downstream regions of Col-0 had several unique substitutions

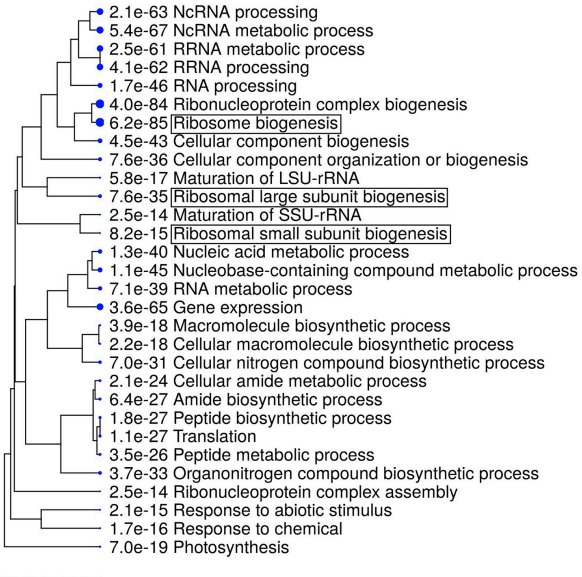

FIGURE 5 | Gene ontology (GO) enrichment analysis of upregulated differentially expressed genes (DEGs) in *rdp1* compared with the wild-type (1284 genes). The top 30 hits on the GO list are shown in this figure, and the top 500 hits in the GO data are listed in **Supplementary Table 3**. Hierarchical clustering tree summarizing the correlation among the significant pathways listed in the Enrichment tab. Larger dots indicate smaller *P*-values. GO terms containing "ribosome" are highlighted by boxes.

compared with Uod-1 and Bor-4. Phenotypically, Col-0 and Uod-1 had smaller numbers of pollen grains (Col-0, 3,355 pollen grains/flower; Uod-1, 3,277 pollen grains/flower) in contrast with Bor-4 (4,528 pollen grains/flower) (Tsuchimatsu et al., 2020). The unique sequence character of Col-0 prompted us to study whether the coding region has a variant conferring reduced pollen number.

To compare the *RDP1* allele, plants were prepared as follows (**Figure 2B**): (1) *RDP1* heterozygous plants (*RDP1/rdp1*) were prepared from the Bor-4 and Col-0 accessions; (2) two heterozygous plants were crossed; and (3) $RDP1^{Bor}/rdp1^{Col}$ and $rdp1^{Bor}/RDP1^{Col}$ plants were selected. These plants had a single different functional *RDP1* allele in the original chromosomal position, but all other genome sequences were identical: a single disrupted *RDP1* allele with the same frameshift position and the same genome constitution (one chromosome from Bor-4 and the other from Col-0) outside of *RDP1*. We found that the plants with the functional Bor-4 allele of *RDP1* ($RDP1^{Bor}/rdp1^{Col}$) had a significantly higher pollen number than those with a functional Col-0 allele ($rdp1^{Bor}/RDP1^{Col}$) ($P = 1.10 \times 10^{-5}$; **Figure 4**). We estimated allelic effect of *RDP1* based on median in the quantitative complementation test. $RDP1^{Bor}$ is 1,599 pollen grain increasing [$RDP1^{Bor}/rdp1^{Col}$ (4,528 pollen grain) vs. $rdp1^{Bor}/rdp1^{Col}$ (2,929 pollen grain)] and $RDP1^{Col}$ is 1,373 pollen grain increasing [$rdp1^{Bor}/RDP1^{Col}$ (4,302 pollen grain) vs. $rdp1^{Bor}/rdp1^{Col}$ (2,929 pollen grain)] (**Supplementary Figure 3**). This result elucidated the allelic difference between Bor-4 and Col-0.

TABLE 1 | DEGs from ribosomal small and large subunit-related genes (FDR < 0.1).

Locus	RP family	RP name	WT_FPKM	*rdp1-3*_FPKM	Fold change (*rdp1-3*/WT)	Up/Down	FDR
Small subunit							
AT2G17360	S4	RPS4A	301.750	417.175	1.383	Up	0.03901
AT2G37270	S5	RPS5A	174.325	242.650	1.392	Up	0.04229
AT4G31700	S6	RPS6A	500.050	716.100	1.432	Up	0.03465
AT5G39850	S9	RPS9C	21.920	29.573	1.349	Up	0.08566
AT5G09500	S15	RPS15C	270.500	139.763	0.517	Down	0.0001105
AT5G63070	S15	RPS15F	2.147	0.656	0.306	Down	0.003703
AT3G04920	S24	RPS24A	362.125	472.675	1.305	Up	0.08819
AT1G23410	S27a	RPS27aA	20.613	33.018	1.602	Up	0.002746
Large subunit							
AT2G40010	P0	RPP0A	33.220	45.148	1.359	Up	0.0401
AT3G09200	P0	RPP0B	730.525	1018.125	1.394	Up	0.05074
AT1G01100	P1	RPP1A	172.625	249.500	1.445	Up	0.01443
AT5G47700	P1	RPP1C	225.475	291.725	1.294	Up	0.08017
AT4G25890	P3	RPP3A	49.863	70.398	1.412	Up	0.07064
AT1G61580	L3	RPL3B	6.506	4.296	0.660	Down	0.0688
AT3G09630	L4	RPL4A	219.625	353.675	1.610	Up	0.0004233
AT5G02870	L4	RPL4D	289.350	475.600	1.644	Up	0.001281
AT5G39740	L5	RPL5B	165.500	214.700	1.297	Up	0.08304
AT1G80750	L7	RPL7A	47.308	63.925	1.351	Up	0.04856
AT2G44120	L7	RPL7C	221.250	318.225	1.438	Up	0.02429
AT2G47610	L7a	RPL7aA	440.875	581.925	1.320	Up	0.08774
AT2G18020	L8	RPL8A	771.800	1106.525	1.434	Up	0.03117
AT4G36130	L8	RPL8C	64.268	89.533	1.393	Up	0.02703
AT4G10450	L9	RPL9D	39.513	65.113	1.648	Up	0.0004775
AT5G22440	L10a	RPL10aC	117.043	154.350	1.319	Up	0.09077
AT3G58700	L11	RPL11B	38.113	49.583	1.301	Up	0.09166
AT5G45775	L11	RPL11D	305.325	395.375	1.295	Up	0.09226
AT2G37190	L12	RPL12A	131.750	172.075	1.306	Up	0.07142
AT3G53430	L12	RPL12B	425.450	552.250	1.298	Up	0.0906
AT5G60670	L12	RPL12C	160.125	216.100	1.350	Up	0.08106
AT3G07110	L13a	RPL13aA|	368.900	574.000	1.556	Up	0.004389
AT2G20450	L14	RPL14A	54.750	78.120	1.427	Up	0.01233
AT4G17390	L15	RPL15B	462.025	610.425	1.321	Up	0.08518
AT3G16780	L19	RPL19B	46.078	68.470	1.486	Up	0.0467
AT2G33370	L23	RPL23B	120.215	164.650	1.370	Up	0.0819
AT2G39460	L23a	RPL23aA	1465.250	1984.000	1.354	Up	0.09487
AT2G44860	L24	RPL24C	108.735	145.025	1.334	Up	0.06166
AT3G49910	L26	RPL26A	496.375	711.675	1.434	Up	0.04323
AT4G29410	L28	RPL28C	120.538	178.900	1.484	Up	0.007889
AT4G18100	L32	RPL32A	332.650	442.025	1.329	Up	0.06263
AT3G28900	L34	RPL34C	149.325	193.750	1.298	Up	0.06931
AT2G39390	L35	RPL35B	22.165	32.263	1.456	Up	0.06232

The pink and blue highlights indicate gene upregulation and downregulation, respectively. The list of cytosolic ribosomal genes was taken from previous reports (Barakat et al., 2001; Hummel et al., 2015).

Enhanced Transcription of Ribosome-Related Genes and the Reduction of That of Specific Anther/Pollen Development Genes in *rdp1-3*

Next, we examined which biological processes are disturbed by the disruption of the *RDP1* gene in flower bud tissues, and whether the expression of ribosome-related genes is altered as previously described for other *Arabidopsis* ribosome mutants. We performed a transcriptome analysis using wild-type of Col-0 and *rdp1-3* plants. A large number of DEGs between the wild-type and *rdp1-3* plants was detected using the criterion of FDR < 0.1 (3,020 genes, **Supplementary Table 2**). Among them, 1,284 genes were upregulated and 1,736 genes were downregulated in *rdp1-3* plants. A GO term analysis showed the enrichment

of many ribosome-related genes in the upregulated gene set (**Figure 5** and **Table 1** and **Supplementary Table 3**). These results strongly support the notion that *RDP1* of *A. thaliana* functions in the biogenesis of the ribosome as a yeast Mrt4 homolog (Lo et al., 2010; Michalec-Wawiorka et al., 2015; Greber, 2016; Saez-Vasquez and Delseny, 2019).

The GO term analysis also revealed the enrichment of genes relevant for pollen development, as well as pollen-related categories in the downregulated gene set (e.g., "Pollen development," "Pollen wall assembly," and "Pollen tube growth"; **Figure 6** and **Supplementary Table 4**). Among the genes relevant for pollen development, three bHLH transcription factor genes, *bHLH010*, *bHLH089*, and *AMS*, were downregulated (**Table 2**), all of which interact with the DYT1 during anther development (Feng et al., 2012; Ferguson et al., 2017). Although their fold change itself was modest (29.7–34.4% reduction; **Table 2**), we also observed a systematic downregulation of genes that were directly regulated by AMS (19 out of 23, $P = 2.901e{-}15$, Fisher's exact test; **Table 2**; Xu et al., 2014). These data suggest that the bHLH pathway and its downstream genes were downregulated in the *rdp1-3* mutant. By contrast, we did not find any enrichment of GO terms related to ovule development, although ovule number was also reduced in the *rdp1-3* (Tsuchimatsu et al., 2020). This expression analysis in the flower bud suggests a distinctive role for *RDP1* in anther development through transcription factor regulation.

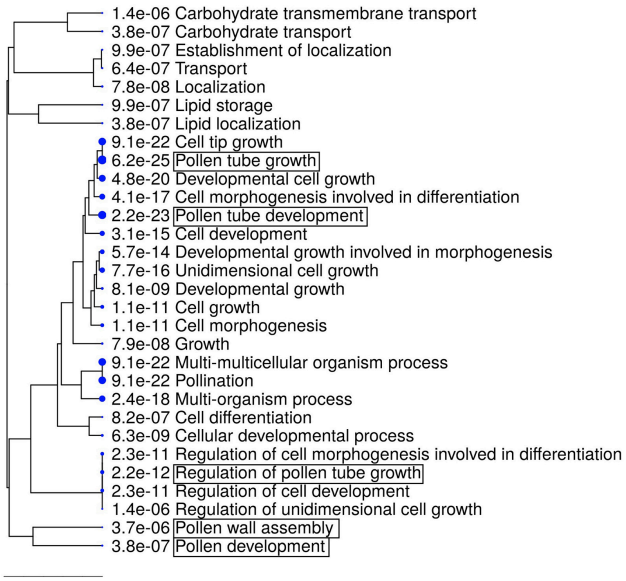

FIGURE 6 | GO enrichment analysis of downregulated DEGs (1736 genes). The top 30 hits on the GO list are shown in this figure, and all GO data are listed in **Supplementary Table 4**. Hierarchical clustering tree summarizing the correlation among the significant pathways listed in the Enrichment tab. Larger dots indicate smaller *P*-values. GO terms containing "pollen" are highlighted by boxes.

DISCUSSION

Quantitative Complementation Tests of Multiple Combinations to Narrow Down the Genomic Regions Responsible for Pollen-Number Regulation

Although the quantitative complementation test has been validated in several animal and bacterial species, such as yeast, *Drosophila*, mosquito, fish, and mouse (Steinmetz et al., 2002; Stern, 2014; Turner, 2014; Podobnik et al., 2020), the preparation of mutants in a specific site of a gene represents a bottleneck regarding the application of quantitative complementation tests in plants (Stern, 2014). Recent progress in genome-editing technologies has allowed the efficient generation of frameshift non-functional mutants at the targeted gene in several different accessions. Thus, a quantitative complementation test will have a broader application of obtaining causal evidence of subtle allelic effects in plant species.

In this study, we performed a quantitative complementation test of *RDP1* between Col-0 and Bor-4. A key of the method is to generate equivalent non-functional alleles in two different backgrounds by CRISPR/Cas9. We generated frameshift mutants at the same position, i.e., *rdp1-3* and *rdp1-6* in Col-0 and Bor-4, respectively. We consider them as null mutants because frameshift mutants are in general disruptive, and the yeast studies suggested the importance of C-terminal domains (Michalec et al., 2010), but we note that the quantitative complementation test can work even if they are not completely null. Combined with the previously reported results of the quantitative complementation test between Uod-1 and Bor-4 (Tsuchimatsu et al., 2020), our data support the notion that both Col-0 and Uod-1 have alleles that confer reduced pollen number against Bor-4. Although it is formally possible that more than two functional variants exist, the selective sweep signature of the long-haplotype variants suggests that a single mutation conferring reduced pollen number spread to many accessions, including Col-0 and Uod-1. This implies that the causal mutation of the reduced pollen number is shared between Col-0 and Uod-1, in contrast with Bor-4. The alignment of the genomic sequences of the three accessions revealed that such substitutions were mostly found in exon/intron regions, and not in upstream or downstream regions, reflecting the historical recombination inferred in Col-0. Although it is possible that mutations outside of the aligned region may have contributed to this phenomenon, substitutions in the exon/intron regions, including S222L, are promising candidate causal mutations of the reduced pollen number (**Figures 3B,C**), which warrants further experimental verification. In short, quantitative complementation tests using multiple accessions serve as a tool to narrow down the candidate regions of causal mutations of quantitative traits when transgenic experiments are not sufficiently powerful.

RDP1 and the Biogenesis of the Ribosomal Large Subunit

Remarkably, we detected two ontologies related to the ribosomal large subunit ("Ribosomal large subunit

TABLE 2 | Downregulated pollen/anther development-related genes.

ID	Gene symbol	Gene name/description	FPKM		Fold change	Up/Down	FDR
			WT	*rdp1-3*	(*rdp1-3*/WT)		
Fifty-one downregulated genes in GO "Pollen development" (51 of 344 genes)							
AT4G27420	ABCG9	ATP-BINDING CASSETTE G9	10.36	6.73675	0.650	Down	0.03768
AT3G13220	ABCG26	ATP-BINDING CASSETTE G26	32.95	24.17	0.734	Down	0.07096
AT3G21180	ACA9	AUTOINHIBITED CA(2 +)-ATPASE 9	13.565	5.79125	0.427	Down	0.001642
AT2G03060	AGL30	AGAMOUS-LIKE 30	20.29	11.8888	0.586	Down	0.003651
AT1G77980	AGL66	AGAMOUS-LIKE 66	9.15675	3.65205	0.399	Down	0.01597
AT1G69540	AGL94	AGAMOUS-LIKE 94	4.50075	2.462	0.547	Down	0.01472
AT1G22130	AGL104	AGAMOUS-LIKE 104	21.21	10.585	0.499	Down	0.006843
AT5G14380	AGP6	ARABINOGALACTAN PROTEIN 6	695.075	212.25	0.305	Down	0.0004339
AT2G16910	AMS	ABORTED MICROSPORES	20.7625	13.3375	0.642	Down	0.009175
AT5G54470	BBX29	B-BOX DOMAIN PROTEIN 29	1.01833	0.44235	0.434	Down	0.05074
AT2G31220	bHLH010	BASIC HELIX LOOP HELIX PROTEIN 10	11.089	7.27475	0.656	Down	0.03039
AT1G06170	bHLH089	BASIC HELIX LOOP HELIX PROTEIN 89	27.22	19.1275	0.703	Down	0.08885
AT3G57370	BRP4	transcription factor IIB-related protein	7.012	3.73475	0.533	Down	0.004574
AT5G59030	COPT1	COPPER TRANSPORTER 1	126.868	77.21	0.609	Down	0.03737
AT1G01280	CYP703A2	CYTOCHROME P450, FAMILY 703, SUBFAMILY A, POLYPEPTIDE 2	26.2025	18.22	0.695	Down	0.06944
AT3G04620	DAN1	D NUCLDUO1-ACTIVATEEIC ACID BINDING PROTEIN 1	50.7075	29.4975	0.582	Down	0.002855
AT3G60460	DUO1	DUO POLLEN 1	2.4205	1.26045	0.521	Down	0.07064
AT4G10950	GELP77	GDSL-TYPE ESTERASE/LIPASE 77	2.621	1.49225	0.569	Down	0.07858
AT5G54800	GPT1	GLUCOSE 6-PHOSPHATE/PHOSPHATE TRANSLOCATOR 1	55.88	36.22	0.648	Down	0.02275
AT4G22600	INP1	INAPERTURATE POLLEN1	1.95575	0.9254	0.473	Down	0.06207
AT1G19180	JAZ1	JASMONATE-ZIM-DOMAIN PROTEIN 1	36.1125	22.34	0.619	Down	0.01786
AT5G11110	KNS2	KAONASHI 2	6.718	4.33975	0.646	Down	0.02011
AT2G35210	MEE28	MATERNAL EFFECT EMBRYO ARREST 28	5.495	2.2425	0.408	Down	0.01798
AT4G14080	MEE48	MATERNAL EFFECT EMBRYO ARREST 48	445.275	249.95	0.561	Down	0.00152
AT1G19890	MGH3	MALE-GAMETE-SPECIFIC HISTONE H3	5.827	3.23475	0.555	Down	0.06423
AT3G11980	MS2	MALE STERILITY 2	85.015	59.585	0.701	Down	0.05185
AT5G46795	MSP2	MICROSPORE-SPECIFIC PROMOTER 2	28.515	16.8475	0.591	Down	0.004003
AT2G26960	MYB81	MYB DOMAIN PROTEIN 81	9.4635	6.213	0.657	Down	0.06235
AT2G32460	MYB101	MYB DOMAIN PROTEIN 101	22.33	14.6225	0.655	Down	0.06215
AT5G41090	NAC095	NAC DOMAIN CONTAINING PROTEIN 95	8.23725	4.3635	0.530	Down	0.02754
AT2G29940	PDR3	PLEIOTROPIC DRUG RESISTANCE 3	8.95675	5.879	0.656	Down	0.02452
AT5G05850	PIRL1	PLANT INTRACELLULAR RAS GROUP-RELATED LRR 1	19.8625	11.5435	0.581	Down	0.02079
AT4G34850	PKSB	POLYKETIDE SYNTHASE B	95.7175	67.7175	0.707	Down	0.09108
AT4G29470	PLA2-DELTA	PHOSPHOLIPASE A2 DELTA	5.387	1.73778	0.323	Down	0.005243
AT4G29460	PLA2-GAMMA	PHOSPHOLIPASE A2 GAMMA	0.65675	0.07614	0.116	Down	0.004069
AT5G39400	PTEN1	PHOSPHATASE AND TENSIN HOMOLOG DELETED ON CHROMOSOME TEN 1	3.12565	0.68463	0.219	Down	0.09549
AT4G20050	QRT3	QUARTET 3	68.4625	43.4175	0.634	Down	0.004464
AT4G17530	RAB1C	RAB GTPASE HOMOLOG 1C	70.8125	46.1975	0.652	Down	0.01514
AT5G40260	RPG1	RUPTURED POLLEN GRAIN1	12.3375	7.75825	0.629	Down	0.04411
AT5G50800	RPG2	RUPTURED POLLEN GRAIN 2	19.1675	6.2265	0.325	Down	0.0006463
AT1G09180	SAR1	SECRETION-ASSOCIATED RAS 1	4.53925	2.48025	0.546	Down	0.06193
AT1G06515	ssSPTa	SMALL SUBUNIT OF SPT A	68.015	44.575	0.655	Down	0.03059
AT1G07340	STP2	SUGAR TRANSPORTER 2	39.175	27.415	0.700	Down	0.02665
AT3G47440	TIP5;1	TONOPLAST INTRINSIC PROTEIN 5;1	3.16325	1.8435	0.583	Down	0.09475
AT4G35420	TKPR1	TETRAKETIDE ALPHA-PYRONE REDUCTASE 1	265	163.175	0.616	Down	0.009035
AT1G68540	TKPR2	TETRAKETIDE ALPHA-PYRONE REDUCTASE 2	18.45	12.1625	0.659	Down	0.05092
AT4G12920	UND	UNDEAD	11.3435	6.2965	0.555	Down	0.04017
AT4G26440	WRKY34	WRKY DNA-BINDING PROTEIN 34	7.033	4.24575	0.604	Down	0.009744
AT2G35070		transmembrane protein;(source:Araport11)	8.2975	4.489	0.541	Down	0.01696

(Continued)

TABLE 2 | (Continued)

ID	Gene symbol	Gene name/description	FPKM		Fold change	Up/Down	FDR
			WT	*rdp1-3*	(*rdp1-3*/WT)		
AT3G10470		C2H2-type zinc finger family protein;(source:Araport11)	1.9	0.54983	0.289	Down	0.06933
AT3G28780		transmembrane protein, putative (DUF1216);(source:Araport11)	127.82	40.83	0.319	Down	0.00002049
Twenty-three genes directly regulated by AMS (Xu et al., 2014)							
AT4G14080	MEE48	MATERNAL EFFECT EMBRYO ARREST 48	445.28	249.95	0.561	Down	0.00152
AT4G20050	QRT3	QUARTET 3	68.46	43.42	0.634	Down	0.004464
AT3G52160	KCS15	3-KETOACYL-COA SYNTHASE 15	47.29	35.54	0.752	n.s.	0.1359
AT5G49070	KCS21	03-KETOACYL-COA SYNTHASE 21	8.12	8.72	1.074	n.s.	0.8009
AT1G71160	KCS7	03-KETOACYL-COA SYNTHASE 7	14.41	12.24	0.850	n.s.	0.4758
AT3G51590	LTP12	LIPID TRANSFER PROTEIN 12	2847.00	1431.10	0.503	Down	0.00206
AT1G66850		LTP family protein	1532.75	815.58	0.532	Down	0.00003572
AT5G62080		LTP family protein	519.88	285.28	0.549	Down	0.001196
AT3G13220	ABCG26	ATP-Binding Cassette G subfamily 26	32.95	24.17	0.734	Down	0.07096
AT4G34850	PKSB/LAP5	POLYKETIDE SYNTHASE B/LESS ADHESIVE POLLEN 5	95.72	67.72	0.707	Down	0.09108
AT4G35420	TKPR1	TETRAKETIDE ALPHA-PYRONE REDUCTASE 1	265.00	163.18	0.616	Down	0.009035
AT4G00040	CHS	Chalcone and stilbene synthase family protein	82.51	55.72	0.675	Down	0.01389
AT1G75920	EXL5	EXTRACELLULAR LIPASE 5	54.14	27.89	0.515	Down	0.000005513
AT1G75910	EXL4	EXTRACELLULAR LIPASE 4	408.30	210.20	0.515	Down	0.000004671
AT1G75930	EXL6	EXTRACELLULAR LIPASE 6	244.13	120.38	0.493	Down	7.601e–07
AT1G06990		GDSL-like Lipase/Acylhydrolase superfamily protein	32.87	19.16	0.583	Down	0.003785
AT1G69500	CYP704B1	CYTOCHROME P450, FAMILY 704, SUBFAMILY B, POLYPEPTIDE 1	14.82	11.20	0.756	n.s.	0.219
AT1G01280	CYP703A2	CYTOCHROME P450, FAMILY 703, SUBFAMILY A, POLYPEPTIDE 2	26.20	18.22	0.695	Down	0.06944
AT1G74540	CYP98A8	CYTOCHROME P450, FAMILY 98, SUBFAMILY A, POLYPEPTIDE 8	40.58	27.55	0.679	Down	0.02009
AT1G74550	CYP98A9	CYTOCHROME P450, FAMILY 98, SUBFAMILY A, POLYPEPTIDE 9	55.92	37.84	0.677	Down	0.01419
AT1G13140	CYP86C3	CYTOCHROME P450, FAMILY 86, SUBFAMILY C, POLYPEPTIDE 3	59.11	43.66	0.739	Down	0.0959
AT5G07520	GRP18	GLYCINE-RICH PROTEIN 18	63.58	31.91	0.502	Down	1.898e–07
AT5G07550	GRP19	GLYCINE-RICH PROTEIN 19	5613.75	2498.00	0.445	Down	0.0002736

The genes highlighted in blue are downregulated.

assembly" and "Ribosomal large subunit biosynthesis") in the transcriptome analysis of *rdp1-3*. We found that 23.0% of the genes involved in the ribosomal large subunit were significantly differentially expressed (33 out of 143 genes), with most of them being upregulated (32 out of 33 genes) (**Table 1**). Conversely, only 8.2% of the genes involved in the ribosomal small subunit were significantly different (8 out of 98 genes). Furthermore, S222L was the only non-synonymous mutation in the mapped region revealed by the two complementation tests; thus, it was a candidate causal mutation for the pollen-number phenotype (as discussed above). Moreover, this amino acid position was shown to be important for the cellular localization and ribosomal function of human *RDP1* (Michalec-Wawiorka et al., 2015). Taken together, our results strongly support the contention that *RDP1* of *A. thaliana* functions in the biogenesis of the ribosomal large subunit as a yeast Mrt4 homolog (Lo et al., 2010; Michalec-Wawiorka et al., 2015; Greber, 2016; Saez-Vasquez and Delseny, 2019).

Regulation of the Expression of Pollen Development Genes in the Mutant of *RDP1*

The mechanisms underlying where and how *RDP1* affects the expression of bHLH transcriptional factor genes, such as *AMS*, *bHLH010*, and *bHLH089*, remain unknown. Previous studies have reported that the spatial expression pattern of these transcriptional factor genes and that of *RDP1* overlap partly in the same cell types (Zhu et al., 2011; Zhu et al., 2015; Tsuchimatsu et al., 2020). Real-time PCR, promoter-GUS assay, and *in situ* hybridization studies have suggested that *RDP1* is expressed broadly and strongly in proliferating cells, including sporogenous cells (Tsuchimatsu et al., 2020). A transcriptome study of dissected tissues also demonstrated that *RDP1* is expressed in both tapetal cells and the pollen lineage (microspore, bicellular, and tricellular stages) (Honys and Twell, 2004; Li et al., 2017). The expressions of *bHLH010* and *bHLH089* were detected in both microspores and tapetum

cells via *in situ* hybridization (Zhu et al., 2015). Moreover, *in situ* hybridization suggested that *AMS* is expressed in both tapetum cells and microspores (Zhu et al., 2011), although the defect of *ams* mutants is primarily found in surrounding tapetum cells that provide pollen wall to the germ lines (Xu et al., 2010). These expression data suggest that these bHLH genes are co-expressed with *RDP1* in tapetum and microspore cells. It is reported that the feedback regulation of bHLH transcription factor genes (*DYT1*, *bHLH010*, *bHLH089*, and *bHLH091*) occurs during anther development (Cui et al., 2016). Because this feedback regulation requires the synthesis of the protein encoded by each gene, *RDP1* may contribute to the expression of these genes through translation by ribosomes. This hypothesis was supported by the observation that two of these genes (*bHLH010* and *bHLH089*) were downregulated in the *rdp1-3* mutant. We also considered the possibility that the transcriptional reduction of these bHLH genes in tapetal cells has an indirect effect on tapetum development via the microspore reduction afforded by *RDP1* mutation. However, this is unlikely because the expression patterns of other genes that are essential for tapetum development, such as *DYT1*, *TPD1*, and *MS188*, were not affected in *rdp1-3*. We could not exclude the possibility that the aberrant translational machinery of *rdp1-3* may affect the mRNA abundance, or of downstream transcription independent from the feedback (Tiruneh et al., 2013; Beine-Golovchuk et al., 2018; Cheong et al., 2021) or multi-functionalization of *RDP1* independent from the ribosome. Further detailed analyses are required to evaluate this scenario. In addition, previous transcriptome data obtained for the *bhlh* triple mutant (*bhlh010/bhlh089/bhlh091*) (Zhu et al., 2015) did not show an obvious transcriptional difference for ribosomal genes, including *RDP1*, suggesting that *RDP1* or ribosome function is not located downstream of the bHLH gene regulatory network.

The Reduction in Pollen Number and Slower Growth Observed in the *rdp1-3* Mutant Are Possibly Caused by Ribosomal Specialization

The ribosome is a protein biosynthesis machinery that is present in all living cells. Although the ribosome has been considered a solid component common to all cells, organ-specific phenotypes are revealed from mutant analysis of ribosome and ribosome-biogenesis genes in yeast, humans, and plants. This ribosome specialization is now suggested as not being a rare phenomenon (Martinez-Seidel et al., 2020; Norris et al., 2021). Reproductive defects of ribosomal mutants were observed, such as reduced stamen number, smaller pollen size, slower pollen tube elongation, and reduced functional ovules (Stirnberg et al., 2012; Luo et al., 2020). *RDP1* is considered a homolog of yeast Mrt4, which is a key component for the 60S ribosomal assembly. We found that the expression level of *RDP1* varied among different cell types and was higher in proliferating cells (Tsuchimatsu et al., 2020). Natural variants under selection supported the critical role of *RDP1* in adaptive evolution (Tsuchimatsu et al., 2020). Furthermore, a non-functional *RDP1* mutant exhibited reduced pollen number and slower growth speed. These data support the idea that the high expression level of *RDP1* is required to respond to the high demand of ribosome production in proliferation cells. Interestingly, Tsuchimatsu et al. (2020) reported that quantitative complementation test with Uod-1 and Bor-1 showed allelic differences for pollen number but not growth speed (rosette size and bolting/flowering date). This result may suggest the ribosome specialization for pollen number. At first glance, this may be similar to cytoplasmic sterility, where the reduction of mitochondrial function results in pollen-specific phenotype, where high energy consumption may be necessary (Warmke and Lee, 1978; Chase, 2007). However, our transcriptome data does not support this idea because there was no GO term "mitochondria" in down-regulated genes. Further analysis of *RDP1* will provide clues regarding how ribosome specialization affects the pollen number regulation.

CONCLUSION

A previous study showed that natural variation of the *RDP1* gene was responsible for pollen number in *A. thaliana*. Here, we showed that the standard accession Col-0 had a natural variant that reduced pollen number. Moreover, the frameshift mutant *rdp1*-3 in the Col-0 background confirmed pleiotropic effects, including that on flowering time. A transcriptome analysis of the *rdp1-3* mutant suggested the function of *RDP1* in ribosome assembly and pollen development. These data support the specialized function of the ribosome in pollen development.

DATA AVAILABILITY STATEMENT

The datasets presented in this study can be found in online repositories. The names of the repository/repositories and accession number(s) can be found in the **Supplementary Table 1**.

AUTHOR CONTRIBUTIONS

HK, TT, MY, and KKS planned and designed the study and wrote the manuscript. HK and MY performed the experiments. HK and TT analyzed the data and drew the figures. MH managed the sequencing data. All authors contributed to the article and approved the submitted version.

FUNDING

This work was supported by a Swiss National Science Foundation grant 31003A_182318 to KKS, by MEXT KAKENHI (Grant Numbers 16H06469 to KKS, and 17H05833 and 19H04851 to TT), JSPS KAKENHI (Grant Number 19K05976 to HK), the University Research Priority Program (URPP) Evolution in Action of the University of Zurich, and a JST CREST JPMJCR16O3 to KKS.

ACKNOWLEDGMENTS

We thank Aluri Sirisha (Functional Genomics Center Zurich) for technical support in the transcriptome analysis, and Naoto-Benjamin Hamaya (University of Zurich) and Daisuke Maruyama (Yokohama City University) for valuable suggestions.

SUPPLEMENTARY MATERIAL

The Supplementary Material for this article can be found online at: https://www.frontiersin.org/articles/10.3389/fpls.2021.768584/full#supplementary-material

Supplementary Figure 1 | Nucleic acid comparison of the *RDP1* region from Uod-1, Col-0, and Bor-4. The green and yellow boxes indicate mRNA and coding regions, respectively. Each annotation was defined by NCBI information (NM_102335.4).

Supplementary Figure 2 | Traditional transgenic complementation test of pollen number per flower in the *rdp1-3* background. No significant difference was detected in each case in line-wise **(A)** and in allele-wise **(B)** analyses (*n* = 269 *(RDP1/RDP1)*, 908 *(rdp1-3/rdp1-3 +* $RDP1^{Col-0}$), 932 *(rdp1-3/rdp1-3 +* $RDP1^{Mz-0}$), 713 *(rdp1-3/rdp1-3 +* $RDP1^{Bor-4}$), and 788 *(rdp1-3/rdp1-3 +* $RDP1^{Alyrata}$)). Boxplots show center line: median; box limits: upper and lower quartiles; dots: outliers.

Supplementary Figure 3 | Pollen number from four genotypes of quantitative complementation test between Bor-4 and Col-0 accession. Sample numbers are shown above the plots. Boxplots show center line: median; box limits: upper and lower quartiles; whiskers: not greater than 1.5 times the interquartile range; point: outlier. Violin shape corresponds to the density of data.

Supplementary Table 1 | Sample information and read numbers of transcriptome analysis in this study.

Supplementary Table 2 | List of differentially expressed genes (3020 genes) between wild-type and *rdp1-3* plants.

Supplementary Table 3 | TOP500 GO enrichment list (Biological process) for upregulated DEGs in *rdp1-3* plants.

Supplementary Table 4 | Complete GO enrichment list (Biological process) for downregulated DEGs in *rdp1-3* plants.

Supplementary Video 1 | Time-lapse movie of *RDP1/RDP1* (left) and *rdp1-3/rdp1-3* (right) plants. Photos were taken every hour from 10h00 to 19h00 for 39 days under the long-day condition.

REFERENCES

Alvarez-Buylla, E. R., Benitez, M., Corvera-Poire, A., Chaos Cador, A., de Folter, S., Gamboa de Buen, A., et al. (2010). Flower development. *Arabidopsis Book* 8:e0127. doi: 10.1199/tab.0127

Barakat, A., Szick-Miranda, K., Chang, I. F., Guyot, R., Blanc, G., Cooke, R., et al. (2001). The organization of cytoplasmic ribosomal protein genes in the *Arabidopsis* genome. *Plant Physiol.* 127, 398–415. doi: 10.1104/pp.010265

Beine-Golovchuk, O., Firmino, A. A. P., Dabrowska, A., Schmidt, S., Erban, A., Walther, D., et al. (2018). Plant temperature acclimation and growth rely on cytosolic ribosome biogenesis factor homologs. *Plant Physiol.* 176, 2251–2276. doi: 10.1104/pp.17.01448

Boeven, P. H., Longin, C. F., Leiser, W. L., Kollers, S., Ebmeyer, E., and Wurschum, T. (2016). Genetic architecture of male floral traits required for hybrid wheat breeding. *Theor. Appl. Genet.* 129, 2343–2357. doi: 10.1007/s00122-016-2771-6

Chase, C. D. (2007). Cytoplasmic male sterility: a window to the world of plant mitochondrial-nuclear interactions. *Trends Genet.* 23, 81–90. doi: 10.1016/j.tig.2006.12.004

Chen, W., Lv, M., Wang, Y., Wang, P. A., Cui, Y., Li, M., et al. (2019). BES1 is activated by EMS1-TPD1-SERK1/2-mediated signaling to control tapetum development in *Arabidopsis thaliana*. *Nat. Commun.* 10:4164. doi: 10.1038/s41467-019-12118-4

Cheong, B. E., Beine-Golovchuk, O., Gorka, M., Ho, W. W. H., Martinez-Seidel, F., Firmino, A. A. P., et al. (2021). *Arabidopsis* REI-LIKE proteins activate ribosome biogenesis during cold acclimation. *Sci. Rep.* 11:2410. doi: 10.1038/s41598-021-81610-z

Clough, S. J., and Bent, A. F. (1998). Floral dip: a simplified method for *Agrobacterium*-mediated transformation of *Arabidopsis thaliana*. *Plant J.* 16, 735–743. doi: 10.1046/j.1365-313x.1998.00343.x

Creff, A., Sormani, R., and Desnos, T. (2010). The two *Arabidopsis RPS6* genes, encoding for cytoplasmic ribosomal proteins S6, are functionally equivalent. *Plant Mol. Biol.* 73, 533–546. doi: 10.1007/s11103-010-9639-y

Cui, J., You, C. J., Zhu, E. G., Huang, Q., Ma, H., and Chang, F. (2016). Feedback regulation of DYT1 by interactions with downstream bHLH factors promotes DYT1 nuclear localization and anther development. *Plant Cell* 28, 1078–1093. doi: 10.1105/tpc.15.00986

Feng, B. M., Lu, D. H., Ma, X., Peng, Y. B., Sun, Y. J., Ning, G., et al. (2012). Regulation of the *Arabidopsis* anther transcriptome by DYT1 for pollen development. *Plant J.* 72, 612–624. doi: 10.1111/j.1365-313X.2012.05104.x

Feng, X., and Dickinson, H. G. (2010). Tapetal cell fate, lineage and proliferation in the *Arabidopsis* anther. *Development* 137, 2409–2416. doi: 10.1242/dev.049320

Ferguson, A. C., Pearce, S., Band, L. R., Yang, C. Y., Ferjentsikova, I., King, J., et al. (2017). Biphasic regulation of the transcription factor ABORTED MICROSPORES (AMS) is essential for tapetum and pollen development in *Arabidopsis*. *New Phytol.* 213, 778–790. doi: 10.1111/nph.14200

Franco-Mora, O., Tanabe, K., Tamura, F., and Itai, A. (2005). Effects of putrescine application on fruit set in 'Housui' Japanese pear (*Pyrus pyrifolia* Nakai). *Sci. Hortic.* 104, 265–273. doi: 10.1016/j.scienta.2004.10.005

Fujikura, U., Horiguchi, G., Ponce, M. R., Micol, J. L., and Tsukaya, H. (2009). Coordination of cell proliferation and cell expansion mediated by ribosome-related processes in the leaves of *Arabidopsis thaliana*. *Plant J.* 59, 499–508. doi: 10.1111/j.1365-313X.2009.03886.x

Ge, S. X., Jung, D., and Yao, R. (2020). ShinyGO: a graphical gene-set enrichment tool for animals and plants. *Bioinformatics* 36, 2628–2629. doi: 10.1093/bioinformatics/btz931

Greber, B. J. (2016). Mechanistic insight into eukaryotic 60S ribosomal subunit biogenesis by cryo-electron microscopy. *RNA* 22, 1643–1662. doi: 10.1261/rna.057927.116

Hatakeyama, M., Opitz, L., Russo, G., Qi, W. H., Schlapbach, R., and Rehrauer, H. (2016). SUSHI: an exquisite recipe for fully documented, reproducible and reusable NGS data analysis. *BMC Bioinformatics* 17:228. doi: 10.1186/s12859-016-1104-8

Honys, D., and Twell, D. (2004). Transcriptome analysis of haploid male gametophyte development in *Arabidopsis*. *Genome Biol.* 5:R85. doi: 10.1186/gb-2004-5-11-r85

Horiguchi, G., Molla-Morales, A., Perez-Perez, J. M., Kojima, K., Robles, P., Ponce, M. R., et al. (2011). Differential contributions of ribosomal protein genes to *Arabidopsis thaliana* leaf development. *Plant J.* 65, 724–736. doi: 10.1111/j.1365-313X.2010.04457.x

Hummel, M., Dobrenel, T., Cordewener, J., Davanture, M., Meyer, C., Smeekens, S., et al. (2015). Proteomic LC-MS analysis of *Arabidopsis* cytosolic ribosomes: identification of ribosomal protein paralogs and re-annotation of the ribosomal protein genes. *J. Proteom.* 128, 436–449. doi: 10.1016/j.jprot.2015.07.004

Kakui, H., Yamazaki, M., Hamaya, N.-B., and Shimizu, K. K. (2020). "Pollen grain counting using a cell counter," in *Pollen and Pollen Tube Methods*, ed A. Geitmann (New York: Springer), 1–11. doi: 10.1007/978-1-0716-0672-8

Kakui, H., Yamazaki, M., and Shimizu, K. K. (2021). PRIMA: a rapid and cost-effective genotyping method to detect single-nucleotide differences using probe-induced heteroduplexes. *Sci. Rep.* 11:20741. doi: 10.1038/s41598-021-99641-x

Langer, S. M., Longin, C. F. H., and Wurschum, T. (2014). Phenotypic evaluation of floral and flowering traits with relevance for hybrid breeding in wheat (*Triticum aestivum* L.). *Plant Breed.* 133, 433–441. doi: 10.1111/pbr.12192

Li, D. D., Xue, J. S., Zhu, J., and Yang, Z. N. (2017). Gene regulatory network for tapetum development in *Arabidopsis*

thaliana. *Front. Plant Sci.* 8:1559. doi: 10.3389/fpls.2017.01559

Lo, K. Y., Li, Z., Bussiere, C., Bresson, S., Marcotte, E. M., and Johnson, A. W. (2010). Defining the pathway of cytoplasmic maturation of the 60S ribosomal subunit. *Mol. Cell* 39, 196–208. doi: 10.1016/j.molcel.2010.06.018

Lou, Y., Zhou, H. S., Han, Y., Zeng, Q. Y., Zhu, J., and Yang, Z. N. (2018). Positive regulation of *AMS* by TDF1 and the formation of a TDF1–AMS complex are required for anther development in *Arabidopsis thaliana*. *New Phytol.* 217, 378–391. doi: 10.1111/nph.14790

Luo, A., Zhan, H. D., Zhang, X. C., Du, H. W., Zhang, Y. B., and Peng, X. B. (2020). Cytoplasmic ribosomal protein L14B is essential for fertilization in *Arabidopsis*. *Plant Sci.* 292:110394. doi: 10.1016/j.plantsci.2019.110394

Ma, X., Feng, B. M., and Ma, H. (2012). AMS-dependent and independent regulation of anther transcriptome and comparison with those affected by other *Arabidopsis* anther genes. *BMC Plant Biol.* 12:23. doi: 10.1186/1471-2229-12-23

Martinez-Seidel, F., Beine-Golovchuk, O., Hsieh, Y. C., and Kopka, J. (2020). Systematic review of plant ribosome heterogeneity and specialization. *Front. Plant Sci.* 11:948. doi: 10.3389/fpls.2020.00948

Michalec, B., Krokowski, D., Grela, P., Wawiorka, L., Sawa-Makarska, J., Grankowski, N., et al. (2010). Subcellular localization of ribosomal P0-like protein MRT4 is determined by its N-terminal domain. *Int. J. Biochem. Cell Biol.* 42, 736–748. doi: 10.1016/j.biocel.2010.01.011

Michalec-Wawiorka, B., Wawiorka, L., Derylo, K., Krokowski, D., Boguszewska, A., Molestak, E., et al. (2015). Molecular behavior of human Mrt4 protein, MRTO4, in stress conditions is regulated by its C-terminal region. *Int. J. Biochem. Cell Biol.* 69, 233–240. doi: 10.1016/j.biocel.2015.10.018

Norris, K., Hopes, T., and Aspden, J. L. (2021). Ribosome heterogeneity and specialization in development. *Wiley Interdiscip. Rev. RNA* 12:e1644. doi: 10.1002/wrna.1644

Oka, H. I., and Morishima, H. (1967). Variations in the breeding systems of a wild rice, *Oryza perennis*. *Evolution* 21, 249–258. doi: 10.1111/j.1558-5646.1967.tb00153.x

Podobnik, M., Frohnhofer, H. G., Dooley, C. M., Eskova, A., Nusslein-Volhard, C., and Irion, U. (2020). Evolution of the potassium channel gene *Kcnj13* underlies colour pattern diversification in *Danio* fish. *Nat. Commun.* 11:6230. doi: 10.1038/s41467-020-20021-6

R Core Team (2013). *R: A Language and Environment for Statistical Computing*. Vienna: R Foundation for Statistical Computing.

Rodriguez-Mateos, M., Abia, D., Garcia-Gomez, J. J., Morreale, A., de la Cruz, J., Santos, C., et al. (2009a). The amino terminal domain from Mrt4 protein can functionally replace the RNA binding domain of the ribosomal P0 protein. *Nucl. Acids Res.* 37, 3514–3521. doi: 10.1093/nar/gkp209

Rodriguez-Mateos, M., Garcia-Gomez, J. J., Francisco-Velilla, R., Remacha, M., de la Cruz, J., and Ballesta, J. P. (2009b). Role and dynamics of the ribosomal protein P0 and its related *trans*-acting factor Mrt4 during ribosome assembly in *Saccharomyces cerevisiae*. *Nucl. Acids Res.* 37, 7519–7532. doi: 10.1093/nar/gkp806

Saez-Vasquez, J., and Delseny, M. (2019). Ribosome biogenesis in plants: from functional 45S ribosomal DNA organization to ribosome assembly factors. *Plant Cell* 31, 1945–1967. doi: 10.1105/tpc.18.00874

Salih, K. J., Duncan, O., Li, L., Trosch, J., and Millar, A. H. (2020). The composition and turnover of the *Arabidopsis thaliana* 80S cytosolic ribosome. *Biochem. J.* 477, 3019–3032. doi: 10.1042/BCJ20200385

Sanders, P. M., Bui, A. Q., Weterings, K., McIntire, K. N., Hsu, Y. C., Lee, P. Y., et al. (1999). Anther developmental defects in *Arabidopsis thaliana* male-sterile mutants. *Sex. Plant Reprod.* 11, 297–322. doi: 10.1007/s004970050158

Schmidt, S., Dethloff, F., Beine-Golovchuk, O., and Kopka, J. (2013). The REIL1 and REIL2 proteins of *Arabidopsis thaliana* are required for leaf growth in the cold. *Plant Physiol.* 163, 1623–1639. doi: 10.1104/pp.113.223925

Shimada, T. L., Shimada, T., and Hara-Nishimura, I. (2010). A rapid and non-destructive screenable marker, FAST, for identifying transformed seeds of *Arabidopsis thaliana*. *Plant J.* 61, 519–528. doi: 10.1111/j.1365-313X.2009.04060.x

Shimizu, K. K., and Tsuchimatsu, T. (2015). Evolution of selfing: recurrent patterns in molecular adaptation. *Annu. Rev. Ecol. Evol. Syst.* 46, 593–622. doi: 10.1146/annurev-ecolsys-112414-054249

Smyth, D. R., Bowman, J. L., and Meyerowitz, E. M. (1990). Early flower development in *Arabidopsis*. *Plant Cell* 2, 755–767. doi: 10.1105/tpc.2.8.755

Sorensen, A. M., Krober, S., Unte, U. S., Huijser, P., Dekker, K., and Saedler, H. (2003). The *Arabidopsis ABORTED MICROSPORES (AMS)* gene encodes a MYC class transcription factor. *Plant J.* 33, 413–423. doi: 10.1046/j.1365-313x.2003.01644.x

Steinmetz, L. M., Sinha, H., Richards, D. R., Spiegelman, J. I., Oefner, P. J., McCusker, J. H., et al. (2002). Dissecting the architecture of a quantitative trait locus in yeast. *Nature* 416, 326–330. doi: 10.1038/416326a

Stern, D. L. (1998). A role of *Ultrabithorax* in morphological differences between *Drosophila* species. *Nature* 396, 463–466. doi: 10.1038/24863

Stern, D. L. (2014). Identification of loci that cause phenotypic variation in diverse species with the reciprocal hemizygosity test. *Trends Genet.* 30, 547–554. doi: 10.1016/j.tig.2014.09.006

Stirnberg, P., Liu, J. P., Ward, S., Kendall, S. L., and Leyser, O. (2012). Mutation of the cytosolic ribosomal protein-encoding *RPS10B* gene affects shoot meristematic function in *Arabidopsis*. *BMC Plant Biol.* 12:160. doi: 10.1186/1471-2229-12-160

Tiruneh, B. S., Kim, B. H., Gallie, D. R., Roy, B., and von Arnim, A. G. (2013). The global translation profile in a ribosomal protein mutant resembles that of an eIF3 mutant. *BMC Biol.* 11:123. doi: 10.1186/1741-7007-11-123

Tsuchimatsu, T., Kakui, H., Yamazaki, M., Marona, C., Tsutsui, H., Hedhly, A., et al. (2020). Adaptive reduction of male gamete number in the selfing plant *Arabidopsis thaliana*. *Nat. Commun.* 11:2885. doi: 10.1038/s41467-020-16679-7

Tsutsui, H., and Higashiyama, T. (2017). pKAMA-ITACHI vectors for highly efficient CRISPR/Cas9-mediated gene knockout in *Arabidopsis thaliana*. *Plant Cell Physiol.* 58, 46–56. doi: 10.1093/pcp/pcw191

Turner, T. L. (2014). Fine-mapping natural alleles: quantitative complementation to the rescue. *Mol. Ecol.* 23, 2377–2382. doi: 10.1111/mec.12719

Walbot, V., and Egger, R. L. (2016). Pre-meiotic anther development: cell fate specification and differentiation. *Annu. Rev. Plant Biol.* 67, 365–395. doi: 10.1146/annurev-arplant-043015-111804

Wang, K., Guo, Z. L., Zhou, W. T., Zhang, C., Zhang, Z. Y., Lou, Y., et al. (2018). The regulation of sporopollenin biosynthesis genes for rapid pollen wall formation. *Plant Physiol.* 178, 283–294. doi: 10.1104/pp.18.00219

Warmke, H. E., and Lee, S.-L. J. (1978). Pollen abortion in T cytoplasmic male-sterile corn (*Zea mays*): a suggested mechanism. *Science* 200, 561–563. doi: 10.1126/science.200.4341.561

Xu, J., Ding, Z., Vizcay-Barrena, G., Shi, J., Liang, W., Yuan, Z., et al. (2014). ABORTED MICROSPORES acts as a master regulator of pollen wall formation in *Arabidopsis*. *Plant Cell* 26, 1544–1556. doi: 10.1105/tpc.114.122986

Xu, J., Yang, C., Yuan, Z., Zhang, D., Gondwe, M. Y., Ding, Z., et al. (2010). The *ABORTED MICROSPORES* regulatory network is required for postmeiotic male reproductive development in *Arabidopsis thaliana*. *Plant Cell* 22, 91–107. doi: 10.1105/tpc.109.071803

Xue, J. S., Yao, C., Xu, Q. L., Sui, C. X., Jia, X. L., Hu, W. J., et al. (2021). Development of the middle layer in the anther of *Arabidopsis*. *Front. Plant Sci.* 12:634114. doi: 10.3389/fpls.2021.634114

Zhu, E. G., You, C. J., Wang, S. S., Cui, J., Niu, B. X., Wang, Y. X., et al. (2015). The DYT1-interacting proteins bHLH010, bHLH089 and bHLH091 are redundantly required for *Arabidopsis* anther development and transcriptome. *Plant J.* 83, 976–990. doi: 10.1111/tpj.12942

Zhu, J., Lou, Y., Xu, X., and Yang, Z. N. (2011). A genetic pathway for tapetum development and function in *Arabidopsis*. *J. Integr. Plant Biol.* 53, 892–900. doi: 10.1111/j.1744-7909.2011.01078.x

Conflict of Interest: The authors declare that the research was conducted in the absence of any commercial or financial relationships that could be construed as a potential conflict of interest.

Publisher's Note: All claims expressed in this article are solely those of the authors and do not necessarily represent those of their affiliated organizations, or those of the publisher, the editors and the reviewers. Any product that may be evaluated in this article, or claim that may be made by its manufacturer, is not guaranteed or endorsed by the publisher.

frontiers in Plant Science

REVIEW
published: 13 January 2022
doi: 10.3389/fpls.2021.789789

Molecular Control of Sporophyte-Gametophyte Ontogeny and Transition in Plants

*Saurabh Pandey[1], Amir Bahram Moradi[1], Oleksandr Dovzhenko[1,2], Alisher Touraev[3], Klaus Palme[1,2,4] and Ralf Welsch[1]**

[1] Faculty of Biology, Institute of Biology II, Albert-Ludwigs-University of Freiburg, Freiburg, Germany, [2] ScreenSYS GmbH, Freiburg, Germany, [3] National Center for Knowledge and Innovation in Agriculture, Ministry of Agriculture of the Republic of Uzbekistan, Tashkent, Uzbekistan, [4] BIOSS Center for Biological Signaling Studies, Albert-Ludwigs-University of Freiburg, Freiburg, Germany

OPEN ACCESS

Edited by:
Pilar S. Testillano, Margarita Salas Center for Biological Research, Spanish National Research Council (CSIC), Spain

Reviewed by:
Maria Pilar Valles, Aula Dei Experimental Station, Spanish National Research Council (CSIC), Spain
Ikram Blilou, Wageningen University and Research, Netherlands

***Correspondence:**
Ralf Welsch
ralf.welsch@biologie.uni-freiburg.de

Specialty section:
This article was submitted to Plant Development and EvoDevo, a section of the journal Frontiers in Plant Science

Received: 05 October 2021
Accepted: 23 December 2021
Published: 13 January 2022

Citation:
Pandey S, Moradi AB, Dovzhenko O, Touraev A, Palme K and Welsch R (2022) Molecular Control of Sporophyte-Gametophyte Ontogeny and Transition in Plants. Front. Plant Sci. 12:789789. doi: 10.3389/fpls.2021.789789

Alternation of generations between a sporophytic and gametophytic developmental stage is a feature common to all land plants. This review will discuss the evolutionary origins of these two developmental programs from unicellular eukaryotic progenitors establishing the ability to switch between haploid and diploid states. We will compare the various genetic factors that regulate this switch and highlight the mechanisms which are involved in maintaining the separation of sporophytic and gametophytic developmental programs. While haploid and diploid stages were morphologically similar at early evolutionary stages, largely different gametophyte and sporophyte developments prevail in land plants and finally allowed the development of pollen as the male gametes with specialized structures providing desiccation tolerance and allowing long-distance dispersal. Moreover, plant gametes can be reprogrammed to execute the sporophytic development prior to the formation of the diploid stage achieved with the fusion of gametes and thus initially maintain the haploid stage. Upon diploidization, doubled haploids can be generated which accelerate modern plant breeding as homozygous plants are obtained within one generation. Thus, knowledge of the major signaling pathways governing this dual ontogeny in land plants is not only required for basic research but also for biotechnological applications to develop novel breeding methods accelerating trait development.

Keywords: ontogeny, sporophyte, gametophyte, alternation of generations, phase transition

ALTERNATION OF GENERATION – DEFINITION AND COMMON THEMES

The life cycle of land plants alternates between two generations: a diploid sporophyte and a haploid gametophyte, with each generation developing a multicellular body. The concept of alternation of generations was first proposed by the German botanist Hofmeister (1851). Hofmeister (1851) termed these fundamental phase transitions with the German word *Generationswechsel* which

is still used to specifically describe the process (Horst and Reski, 2016). With the advance of molecular techniques and knowledge, these morphological observations have accumulated the molecular support that allows us to precisely define and understand the *Generationswechsel*. At the molecular level, a single plant genome encodes two fundamentally different programs, governing the development of two different body plans (ontogenies; Horst and Reski, 2016). The gametophytic generation represents the haploid phase of the plant's life cycle during which gametes are produced by mitotic division of haploid spores, whereas the sporophytic generation represents the spore-producing diploid generation (Friedman, 2013). In land plants, both haploid and diploid cells can divide by mitosis leading to the formation of different multicellular haploid and diploid plant bodies (Bowman et al., 2016). The haploid plant body representing the gametophyte produces gametes by mitosis which after fertilization form the diploid zygote. Following mitotic divisions, the zygote produces the sporophytic plant body. Depending on the relative period of the developmental process that each phase occupies, either the gametophyte or the sporophyte is considered the dominant stage in the respective plant species (Bowman et al., 2016). In mosses, the haploid gametophyte generation is dominant, whereas in vascular plants (ferns, gymnosperms, and angiosperms), the diploid sporophyte is the prevalent generation. Fertilization, the fusion of two haploid gametes to a diploid sporophyte and the generation of haploid gametophytes from a diploid sporophyte through meiosis, are two processes that act as switching points for haploid-to-diploid and diploid-to-haploid transitions, respectively (Horst and Reski, 2016).

Remarkably, a single genome governs the two generations or ontogenies as well as encodes the regulatory mechanisms to switch from one to the other (Friedman, 2013). Improper phase transition can have severe consequences for any of the plant species including loss of the capability of sexual reproduction (see below). Thus, this transition must be under tight molecular control including key regulatory genes which initiate phase transitions and govern distinct developmental processes occurring in the gametophyte and the sporophyte. Obviously, regarding the fundamentally different programs as well as the resetting of cellular identities with the switch from one program to another, epigenetic control mechanisms are similarly involved. Some of the genes known to be involved in ontogeny determination and phase transitions are discussed in the following section while epigenetic control mechanisms from haploid-to-diploid switch are covered by other excellent review articles (Borg et al., 2021; Ono and Kinoshita, 2021; Vigneau and Borg, 2021). Moreover, the focus of this review is on mechanisms of diploid-to-haploid and haploid-to-diploid switches in angiosperms as a requirement for the development of novel biotechnological breeding approaches.

The complexity of multicellular flowering plants has its origins in relatively simple early land plants (**Figure 1**). *Phaeophyta* (brown algae) evolved 150–200 million years ago and colonize mostly marine environments, and *Sargassum*, *Ascophyllum*, *Fucus*, and *Ectocarpus* are some of the best-known members of this phylum. Their evolution parallels that of the green algae and red algae as all three groups possess complex multicellular species with an alternation of generations. With the origin of a phase transition, the gametophytic and the sporophytic generations were morphologically indistinguishable (isomorphic) while during evolution distinct developmental programs were accompanied with partially large morphological differences between the two generations. Accordingly, members of *Phaeophyta* show various types of alternation of generation, i.e., isomorphic (*Ectocarpus*) or heteromorphic (*Laminaria*; Bringloe et al., 2020).

Species of *Chlorophyta* (green algae) are common inhabitants of marine, freshwater and terrestrial environments with a simple body plan and *Chlamydomonas* is one of the most studied members of this phylum. All land plants (*Embryophyta*) are believed to have evolved from *Chlorophyta* and feature a progressive increase in complexity with the evolution of bryophytes, pteridophytes, gymnosperms to angiosperms (flowering plants). The progenitors of early land plants (*Chlorophyta* and *Charophyta*) developed multicellularity, but do not have dual ontogenies (Finet et al., 2010). Dual ontogeny came into existence in land plants only after the appearance of *Bryophyta* and it remained in all the land plants thereafter (Jill Harrison, 2017).

The coordination of reprogramming events at the molecular/genetic level defines the integrity of ontogenic decisions (Hafidh and Honys, 2021). Here, developmental decisions mediated by members of the three-amino-acid-loop-extension (TALE) class of homeoproteins characterized by a highly conserved DNA-binding homeodomain (HD), are prominent (Bowman et al., 2016). The most important HD proteins belong to the families of KNOTTED1-like (KNOX) and BEL1-like (BLH or BELL) which function as heterodimers (Arnaud and Pautot, 2014).

In bryophytes, the gametophytic phase dominates the plants' lifecycle, whereas the sporophytic phase is very short. In contrast, the sporophyte phase became dominant in vascular plants (gymnosperms and angiosperms), however, the evolutionary pressure which caused this development is still an open and intriguing question for evolutionary biologists. Possible investigations could focus on finding the genetic factors that control following aspects:

- Molecular mechanism of the phase transition.
- The maintenance of specific body plans.
- The timing of transitions between one body plan to another.

The pervasive influence of ontogeny control exerts a strong evolutionary pressure that would be expected to result in the evolution of rigid checkpoints and the clear separation of the two developmental programs. Initial elucidation of the genetic control of gametophyte-sporophyte ontogeny determination and phase transition in different plant species has already provided strong evidence for a common genetic program controlling all haploid-to-diploid transitions. Homeodomain proteins play a central role in this checkpoint (Bowman et al., 2016). Here, we review our understanding of some of these molecular controls in different taxa.

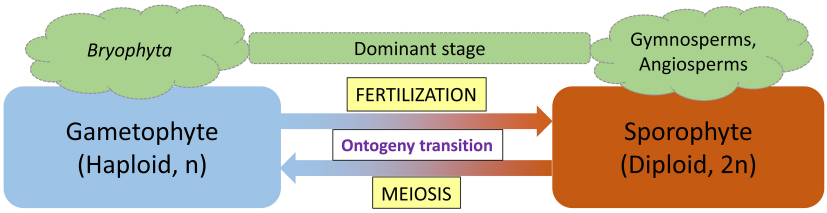

FIGURE 1 | Alternation of generation life cycle pattern of land plants. Lower plants (*Bryophyta*) spend the majority of their life in the gametophyte stage, whereas the sporophyte stage is the dominant stage in vascular plants (gymnosperms and angiosperms). Fertilization and meiosis function as ontogeny switch points.

ALTERNATION OF GENERATIONS IN ALGAE

Brown Algae (*Phaeophyta*)

The majority of brown algae (*Phaeophyta*) exhibit an alternation of generations in which either the gametophyte or sporophyte can be the dominant stage. *Ectocarpus* is a filamentous brown alga that is used as a model organism to study the life cycle and developmental events (Coelho et al., 2012). Life cycle mutants *ouroboros* (*oro*) and *immediate upright* (*imm*) were identified in *Ectocarpus* and provide molecular information about life cycle progression in brown algae. *Oro* acts as a single, recessive Mendelian locus that is unlinked to the locus of *imm* mutant and is crucial for sporophyte development. ORO is considered to be a master regulator of the gametophyte-to-sporophyte life cycle transition (Coelho et al., 2011), whereas IMM is required to induce the partial conversion of sporophytic to gametophytic generations (Peters et al., 2008). Transcriptome analysis shows that ORO induces the sporophyte developmental program and represses the gametophyte genetic program (Coelho et al., 2011). More recently, SAMSARA (SAM) has been identified as an interacting partner of ORO (Arun et al., 2019). SAM and ORO form a heterodimer that regulates the expression of genes controlling gametophyte to sporophyte generation, mainly associated with functional categories like "Cell wall and extracellular" and "Cellular regulation and signaling" (Arun et al., 2019). This suggests that TALE-HD transcription factors are of ancient origin and function as gene regulators during sporophytic developmental events.

Green Algae (*Chlorophyta*)

Chlamydomonas reinhardtii, a unicellular green alga generates two types of gametes, plus-gametes and minus-gametes. The fusion of the gametes, the haploid-to-diploid transition, is regulated by many factors, including GAMETE-SPECIFIC MINUS1 (GSM1)/GAMETE-SPECIFIC PLUS1 (GSP1) which form a heterodimeric transcription factor (**Table 1**).

The plus-gametes express *Gsp1* which encodes a BELL-related TALE-HD protein whereas the minus-gametes express *Gsm1* encoding a KNOX–related TALE-HD protein (Lee et al., 2008). Interestingly, these proteins are structural and functional homologs to KNOX/BELL homeobox heterodimers which are engaged in the sporophytic, diploid phase in vascular plants (Lee et al., 2008). During nitrogen starvation in *Chlamydomonas*, the vegetative cells differentiate into plus- and minus-gametes which display SAG1 (sexual agglutination) and SAD1 (sexual adhesion) agglutinins on their flagella membranes, respectively. The agglutinins on their flagella surface cause adhesion between complementary gametes leading to initial recognition events, triggering an intracellular cAMP burst that activates gametolysin, an enzyme that degrades the cell wall to allow membrane fusion between two gametes. This takes place between plus and minus mating loci structures expressing membrane fusion-enabling factors such as FUS1 and HAP2 on the plasma membrane, respectively (Liu et al., 2010). The *fus1* gene encodes a glycoprotein that enables fusion and binding to minus-gametes, while HAP2 plays an essential role in the completion of the membrane fusion process. The species-specific adhesion initiates the fusogenic reorganization of HAP2 from a labile form into a stable homotrimeric form. Hydrophobic residues of the HAP2 homotrimer subsequently interact with lipid bilayers and are involved in converting them into a single lipid bilayer as the fusion product. The adhesion thus exhibits two functions: it allows sex cells to recognize each other, and initiates the biochemical conformational changes required to activate the fusion machinery (Zhang et al., 2021). Following cytoplasmic fusion, FUS1 and HAP2 are degraded (Liu et al., 2010), and the two HD proteins GSP1 and GSM1 physically interact to form a heterodimer and translocate from the cytosol to the nucleus, initiating the zygote developmental program (Liu et al., 2010).

The ectopic expression of GSP1 in minus-gametes results in the transcription of certain genes that would otherwise be exclusively transcribed in zygotes. Lee et al. (2008) extended these findings and reported the molecular regulation of haploid-to-diploid transition through the KNOX-TALE genes in *Chlamydomonas reinhardtii*. Moreover, the ectopic expression of these proteins in vegetative cells is sufficient to activate the zygote development. A broader comparative analysis led to

TABLE 1 | Gamete-type specific proteins in *Chlamydomonas*.

Gamete type	Expressed protein	Protein family
+	Gamete-specific plus1 (Gsp1)	BELL-related TALE homeodomain protein
−	Gamete-specific minus1 (Gsm1)	KNOX-related TALE homeodomain protein
Zygote+ −	GSM1 + GSP1	

KNOX-TALE genes in land plants being proposed as candidates for the regulation of alternation of generations (Lee et al., 2008).

ALTERNATION OF GENERATION IN *BRYOPHYTA* AND *LYCOPHYTA*

Land plants comprise bryophytes, lycophytes, ferns, gymnosperms, and angiosperms. There is a good amount of evidence to highlight the conservation and evolution of ontogeny control and determination in these land plants as described below.

Bryophyta

Bryophytes spend the majority of their life cycle as persistent haploid gametophytes and exhibit only a short-lived diploid sporophyte generation (Cove, 2005; Szövényi et al., 2021). Bryophytes include three lineages, namely hornworts, liverworts, and mosses.

Hornworts

Hornworts are a small clade consisting of about 220 species with the majority being present in tropical regions. *Anthoceros agrestis* is the model plant species for this clade whose genome was recently sequenced (Li et al., 2020; Frangedakis et al., 2021). Hornworts share some common features that connect them with both the green algae and other land plant lineages. Similar to green algae, they have a single chloroplast per cell with a characteristic pyrenoid which is functionally associated with carbon-concentrating mechanisms. Similar to vascular plants, the sporophyte of hornworts is long-lived and develops moderately independent from the gametophyte which represents the dominant stage (Li et al., 2020). While a KNOX1 ortholog is absent in the *Anthoceros* genome, several *KNOX2* genes are present. In *A. agrestis* a single BELL and a single KNOX2 gene are specifically expressed in the sporophyte phase (Li et al., 2020). As BELL is expressed during early stages of sporophyte development while KNOX2 shows the opposite pattern with expression during later stages, sporophyte identity might not be determined by KNOX2/BELL interaction. However, detailed functional reports are presently lacking which would be instrumental to understand the involvement of KNOX and BELL genes in zygote activation and ontogeny control in hornworts.

Liverworts

In contrast to hornworts, liverworts or *Marchantiophyta* are a larger clade with an estimated number of 9,000 species (Christenhusz and Byng, 2016). Like all *Bryophyta* they are gametophyte-dominant. *Marchantia polymorpha* is the model system of liverworts with its genome sequenced in 2017 (Bowman et al., 2017). Analysis of its genome for HD-containing genes involved in haploid-to-diploid transition revealed four *KNOX* genes and five *BELL* genes. Among the *KNOX* genes, three belong to the KNOX1 subclass, however, only one gene, *MpKNOX1*, encodes a HD protein while the remaining two (MpKNOX1A and MpKNOX1B) lack a HD. *MpKNOX1* is expressed specifically in developing and mature egg cells and is absent in the male gametophyte. In contrast, the forth *Marchantia polymorpha KNOX* gene, *MpKNOX2* is not detected in unfertilized reproductive organs and expressed primarily during sporophyte development (Dierschke et al., 2021; Hisanaga et al., 2021). Thus, *MpKNOX1* is the only *KNOX* gene in *Marchantia polymorpha* involved in phase transition regulation.

Among the five *BELL* genes, *MpBELL1* is expressed primarily during sporophyte development similar to *MpKNOX2*, while *MpBELL5* is expressed in archegonia and functionally not characterized. In contrast, the remaining three *BELL* genes, *MpBELL2*, *MpBELL3* and *MpBELL4* are expressed in the antheridia in cells which will develop into sperm cells (Dierschke et al., 2021; Hisanaga et al., 2021). Upon fertilization, egg-derived MpKNOX1 and sperm-derived MpBELL3/4 heterodimerize and activate the transcription of zygote-specific genes, which is essentially required for diploid sporophyte development. Confusingly, however, *MpBELL2*,*3*,*4* expression is not exclusive for sperm cell, alternative short transcripts of *MpBELL3* and *MpBELL4* are also detected in egg cells. However, truncated MpBELL3 and MpBELL4 proteins are incapable to interact efficiently with MpKNOX1 in split YFP BiFC assays in a heterologous system, which is considered as one reason that sperm-derived full-length MpBELL3 and MpBELL4 are required for KNOX/BELL heterodimer formation. One hypothetic function of maternal MpBELL3/4 presence is a backup function to ensure diploid development following fertilization (Dierschke et al., 2021).

Interestingly, ectopic expression of either *MpBELL3* or co-expression of *MpKNOX1* and *MpBELL3* in the vegetative gametophyte for 72 h is sufficient to activate both *MpKNOX2* and *MpBELL1*, whose expression is normally limited to sporophyte development. Thus, MpBELL3 alone controls *MpKNOX2* expression, which is reminiscent of the post-zygotic activation of MpKNOX2 after fertilization (Dierschke et al., 2021).

In summary the zygote-activating function of KNOX/BELL is conserved between *C. reinhardtii* and *M. polymorpha* (Dierschke et al., 2021; Hisanaga et al., 2021). This striking conservation of KNOX/BELL functions in the promotion of karyogamy across phylogenetically distant *M. polymorpha* and *C. reinhardtii* suggests that functions of KNOX/BELL heterodimers shifted from zygote activation to sporophyte development as land plants evolved (Hisanaga et al., 2021).

Mosses

The two ontogenies can be changed easily by modulating the culture conditions making them an ideal system to understand the molecular controls of sporophyte-gametophyte determination and transition (Horst and Reski, 2016). *Physcomitrium patens* is a widely-used model system that has been used to understand the ontogenic switch due to its small genome, non-redundant gene structure, short life span, and the simple mechanical induction of two types of asexual reproduction processes: apogamy (haploid) and apospory (diploid; Cove, 2005).

Apospory can be induced by mechanically injuring sporophytic vegetative tissue (Pringsheim, 1876; Horst and Reski, 2016), whereas apogamy occurs spontaneously in old

cultures of several moss species (Bauer, 1959). Interestingly, this feature is lost in isolated apogamous sporophytes. Bauer (1959) suggested that a mobile self-replicating "sporogonial factor" is produced in moss sporophytes that can induce the development of further sporophytes from gametophytic cells (Horst and Reski, 2016). Based on this hypothesis, Ripetsky (1985) postulated that the hypothetical sporogonial factor is under epigenetic control and is switched on for sporophyte development and also observed that a gametophyte moss culture can be established via aposporous regeneration of sporophytic cells. These diploid gametophytes would continuously give rise to apogamous sporophytes, even in the absence of previously established sporophytes.

In the past decade, these observations have received molecular support. In the moss *Physcomitrium patens*, it has been shown that the two transcription factors of the KNOTTED1-LIKE HOMEOBOX (KNOX2) class MKN1 and MKN6 are necessary for maintaining the sporophyte developmental program. Accordingly, *mkn1* and *mkn6* double knockout show gametophyte morphological features in diploid sporophytes (Sakakibara et al., 2013).

In another recent report in *Physcomitrium patens*, it has been shown that the ectopic overexpression of the homeobox gene *BELL1* (*PpBELL1*) in specific gametophytic cells induces embryo formation and subsequent development of reproductive diploid sporophytes without undergoing fertilization (Horst et al., 2016). This demonstrates that PpBELL1 represents the central molecular trigger for gametophyte-to-sporophyte transitions in *P. patens* (Horst et al., 2016). Similar sporophytic features in the haploid gametophytic stage are observed in *P. patens* mutants of the Polycomb repressive complex 2 (PRC2), which is involved in the control of epigenetic memory (Okano et al., 2009). Moreover, as PRC2 represses BELL1 function in *P. patens* and PRC2 homologs are present also in *Chlamydomonas*, it is appealing to envision a PRC2-mediated control of phase transition before the emergence of land plants (Schubert, 2019).

Lycophyta

Lycophyta are one of the oldest lineages of extant vascular plants. Similar to other vascular plants lycophytes reproduce by spores and the sporophyte generation is dominant in these plants. *Lycophytes* consist of three families namely: *Lycopodiaceae* (club mosses), *Isoeteaceae* (quillworts) and *Selginellaceae*. *Lycopodiaceae* members produce one single type of spores (homosporous), whereas *Isoeteaceae* and *Selginellaceae* species are heterosporous and produce megaspores and microspores. The distinct differentiation of male and female sporophytes with largely different sizes and properties in seed plants is considered to be originated in these species, although heterospory is thought to have evolved independently in several plant groups. Living lycophytes represent a sister group to the seed plant clade and diverged from a common ancestor around 420 million years ago. Thus, they are frequently exploited for comparative studies regarding conservative traits and convergent evolution of traits which have evolved independently, such as leaves and roots.

Selaginella is the model genus for detailed studies of these plants. *Selaginella* is of particular interest as it retained an autonomous but water-dependent gametophyte generation that is typical of all non-seed plants. In contrast to angiosperms, their gametophytes are not buried within maternal tissues of the sporophyte, so it offers a useful experimental system for investigating how the alternation of generations is regulated. Free-living gametophytes also make it a suitable system to study gametogenesis, gamete recognition, fertilization, and early embryonic developments. Identification of genes involved in the ontogeny control and transition in these plants would help to investigate the evolution of genes and their speciation (Banks, 2009).

Compared to the primary expansion of the number of *KNOX* genes during the evolution from algae to moss, a second expansion occurred during the transition from lycophytes to angiosperms (Gao et al., 2015). While lycophytes contain four *KNOX* genes, angiosperms contain a much higher number which is also interpreted in the context of the development of complex leaves with many specialized tissues leading to a neofunctionalization of several *KNOX* gene duplications during angiosperm evolution.

ALTERNATION OF GENERATION IN ANGIOSPERMS

In Angiosperms, the development of the male gametes from microsporocytes or pollen mother cells occurs within anthers, finally forming fertile male gametes - pollen. Angiosperm anthers usually consist of four layers that nourish and protect developing male gametes: epidermis, endothecium, middle layer, and tapetum. The innermost layer, the tapetum, contains sporophytic helper cells that control the development of microspores into pollen but die soon after the first pollen mitosis. The dynamic crosstalk between the reproductive cells and somatic helper cells happens at multiple levels throughout the gamete development. Any defect in this crosstalk leads to non-viable pollen grains which highlight the complexity of the relationship and significance of this developmental process (Feng et al., 2013).

Diploid-to-Haploid Switch

The main functions of meiosis are the reduction of chromosome numbers and recombination which provides genetic variability. However, it also represents a critical stage for the ontogeny switch, representing the sporophyte-to-gametophyte transition (Hafidh and Honys, 2021). Our efforts to understand meiotic gene functions during the transition from the sporophyte cell lineage (the pollen mother cell) to the gametophyte cell lineage (microspore) are still in their infancy. In contrast, the molecular control of tapetum development has been extensively studied. Tapetal cells never change their ontogeny but instead undergo programmed cell death after performing their specific functions (Ma, 2005; Parish and Li, 2010). Unlike the tapetum cells, the scenario is very different for the pollen mother cells, which after the completion of meiosis have to alter their physiology to accommodate the new ontogeny of gametophyte development (Hafidh and Honys, 2021). Extensive chromatin changes are expected during this transition, with genes involved

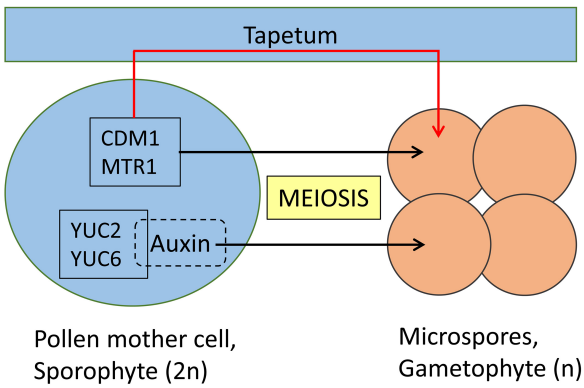

FIGURE 2 | Meiotic genes controlling the gametophyte development in Angiosperms. Pollen mother cell (PMC) and tapetum are sporophyte stages. A diploid PMC (2n) undergoes meiosis to produce four haploid (n) microspores, which are gametophytes. Among the genes expressed in PMC, the function of certain genes is in the development of microspores, thus the PMC development remains unaffected in corresponding knockout mutant lines. CDM1 (in *Arabidopsis thaliana*) and MTR1 (in *Oryza sativa*) are essential for male gamete development which occurs indirectly through the tapetum. Auxin produced by YUC2 and YUC6 plays a direct essential role for the development of microspores. Sporophyte and gametophyte developmental stages are represented in blue and orange, respectively. Direct role of meiotic factors is represented with black arrows, whereas indirect role is represented with a red arrow.

in this phase transition forming the keys to our understanding of the molecular events that govern the two ontogenies (Hafidh and Honys, 2021).

Rice MICROSPORE AND TAPETUM REGULATOR1 (MTR1) is a fascilin glycoprotein that is essential for the development of male gametes (**Figure 2**). *MTR1* is absent in the tapetum but is expressed from early meiotic (stage 7), tetrad (stage 8) stages until microspore development (stage 9; Tan et al., 2012). Interestingly, even though MTR1 is present at the sporophyte stage of wild-type male reproductive cells, *mtr1* plants show no defects at the meiotic and tetrad stages, but fail to undergo mitosis 1 and 2 and are, thus, male sterile. The programmed cell death of tapetum cells, which is their final developmental stage in normal pollen development, is delayed in *mtr1* mutants resulting in defective sporopollenin deposition which in turn detaches microspores from their tapetal inner surface. This indicates a crosstalk between MTR1 and tapetal cells, which is suggested to involve a secretion of MTR1 during early microspore development regulating tapetum development via interaction with surface proteins. In conclusion, MTR1 serves as a critical signaling protein that coordinates the development of microspore and tapetal cells (Tan et al., 2012; Feng et al., 2013).

Further cases of male sterility were recently observed in crosses made with pigeon pea (*Cajanus cajan*) with its wild relative *Cajanus sericeus* (Pazhamala et al., 2020). One of the lines generated was the thermosensitive male sterile line *Evs Sel 107* in which pollen mother cells undergo normal meiosis and form normal tetrads, however, microspores fail to separate and eventually die. The male-sterile condition of this mutant could be reversed to fertility by reducing the day temperature below the critical threshold temperature of 24°C. The morphological studies were compared with transcriptomic, proteomic and metabolomic experiments revealing that the male sterility was caused by a perturbation of auxin homeostasis (Pazhamala et al., 2020). Confirmatory, external application of a natural auxin, indole-3-acetic acid (IAA), rescued the sterile phenotype emphasizing the critical role of auxin in gametophyte development.

Further support for the involvement of auxins in pollen development has also been reported in *Arabidopsis*. Here, the expression of two auxin biosynthetic genes, *YUC2* and *YUC6*, in the sporophytic pollen mother cell was essential for the early stages of pollen development (Yao et al., 2018). *yuc2yuc6* is a male sterile double mutant, and the expression of the bacterial auxin biosynthetic gene *iaaM* under the control of the *YUC6* promoter could restore the fertility of *yuc2yuc6*, indicating that the fertility defects of *yuc2yuc6* were caused by partial auxin deficiency during anther development (Cheng et al., 2006). One open question was whether the sporophytic effect comes from the pollen mother cell directly or through the tapetum. To address this question, ectopic production of auxin in the tapetum failed to rescue the sterile phenotype of *yuc2yuc6*. Whereas, production of auxin in either pollen mother cells or microspores rescued the defects of pollen development in *yuc2yuc6* double mutants. This establishes the direct involvement of genetic factors to control the diploid-to-haploid ontogeny switch (Yao et al., 2018).

The important role of auxins in microspore development is further corroborated by several investigations focusing on the characterization of stress-induced microspore embryogenesis (Rodríguez-Sanz et al., 2015; Testillano, 2019). As this process is extremely taxa-specific, understanding the function of auxins during this process will have commercial benefits in accelerating crop breeding and improvement. Taxa-independent establishment of microspore embryogenesis and increased efficiency will improve the production of isogenic doubled haploid lines suitable for breeding purposes (Pérez-Pérez et al., 2019).

In Arabidopsis, *CALLOSE DEFECTIVE MICROSPORE1* (*CDM1*) is another meiotic gene that is essential for the development of microspores (Lu et al., 2014). CDM1 plays an important role in the regulation of callose metabolism which is highly expressed in meiocytes and tapetum and the *cdm1* knockout mutant is male sterile and here also the onset of phenotype starts after the tetrad stage.

All these diverse studies as presented in **Figure 2** establish the direct involvement of sporophytic genetic factors in controlling the development and transition of the sporophyte-to-gametophyte stage. In Arabidopsis, *BELL1* expression is high during female gametophyte development; in *bel1*, the female gametophyte fails to develop (Ray et al., 1994; Reiser et al., 1995). It is interesting to note that *BELL1* expression remains low during pollen developmental stages. It will be worth testing the ectopic overexpression of *BELL1* during the pollen developmental stages (**Table 2**; data obtained from Arabidopsis eFP Browser, Winter et al., 2007).

Haploid-to-Diploid Switch

Genetic control for the haploid-to-diploid switch is not yet thoroughly established. One of the genes that perform this

TABLE 2 | Tissue-specific expression levels of BELL1 (At5g41410) in Arabidopsis.

Tissue	*AtBELL1* expression level (Absolute)
Cauline leaf	222.3
Cotyledon	109.3
Flower stage 9	33
Flower stage 10/11	70
Mature pollen	24.7

TABLE 3 | Number of *BELL* and KNOTTED1-like (*KNOX*) family proteins across the plant species.

	Clamydomonas	*Physcomitrium*	*Arabidopsis*	Poplar	Rice
BELL	1	4	13	15	12
KNOX	1	5	8	19	14

function is *SHORT SUSPENSOR* (*SSP*). *SSP* is an interleukin-1 receptor-associated kinase (IRAK)/Pelle-like kinase gene that is expressed in pollen but remains untranslated until fertilization and thereafter accumulates in the zygote and the endosperm. SSP acts upstream to YODA (YDA) which requires MAPKKK activity for its activation and proper differentiation of the zygote (Lukowitz et al., 2004). SSP protein produced from paternal transcripts upon fertilization triggers zygotic YDA activity (Bayer et al., 2009). This is a classical study to establish how genes expressed in one ontogeny are required to regulate the essential function of another ontogeny.

It is, thus, evident that ORO, SAM, GSM1, GSP1, KNOX2, and BELL1 are molecular regulators that control gametophyte-to-sporophyte phase transitions in *Phaeophyta*, *Chlorophyta*, and *Bryophyta*. However, in angiosperms such studies are still lacking, possibly because, with the increasing occurrence of gene duplications the molecular controls are much more complex. For instance, the number of *BELL* and *KNOX* genes is much higher in dicots and monocots compared with those in the non-vascular plants (Horst et al., 2016; **Table 3**). Accordingly, the identification of individual functions is hampered by difficulties in generating a loss of function mutants. Moreover, based on different interacting partners at different developmental stages, the same protein performs multiple functions at different developmental stages. This makes it a challenge to decipher specific *BELL* and *KNOX* genes involved in the transition of ontogeny.

TRANSLATIONAL APPLICATIONS OF ONTOGENY REGULATION

Microspore embryogenesis is an *in vitro* system in which the haploid microspore is reprogrammed by the application of external stress treatments to enter into the embryogenesis pathway which usually characterizes the diploid sporophytic development and occurs after fertilization (Shariatpanahi et al., 2006). The resulting embryo can be diploidized by the application of chromosome doubling agents, producing doubled haploid (DH) plants. DH plants are important biotechnological tools in plant breeding mainly because they permit the breeding process to be considerably shortened. This is due to the fact that homozygous stable lines are produced within only one generation while this process usually requires at least six generations of backcrossings when traditional breeding is applied (Testillano, 2019). Despite numerous stress applications and chemicals which are known to induce microspore embryogenesis, a better understanding of genes involved in ontogeny transition and regulation would help to engineer the expression of these genes to increase the frequency of microspore embryogenesis. Also, it might help to break the recalcitrance in certain plant species where microspore embryogenesis is not yet successful.

Usually, the embryogenesis event happens from tetrad, microspore, and bicellular pollen stages of the pollen developmental pathway. Stress-induced alterations of the chromatin architecture occurring during these stages to allow access and transcription of key genes is required to skip the pollen development pathway and follow the embryogenesis pathway. A better understanding of ontogeny regulatory genes and their association to the chromatin architecture at different pollen developmental stages might help to engineer and initiate embryogenic pathways at meiotic stages to obtain diploid embryos from the pollen mother cell.

The genetic segregation accompanying meiosis during the diploid-to-haploid switch is causal for the recurrent need to generate seeds for hybrid crops from their homozygous, genetically different parents. Thus, the advantageous heterozygosity of hybrids could be maintained if clonal progenies were generated through seed propagation, e.g., through induced embryogenesis in gametophytes which were generated by mitosis and not by meiosis in corresponding mutants. Recent findings on the capability to induce embryogenesis associated with the transcription factor BABY BOOM1 (BBM1) suggest a possible solution. BBM1 belongs to the superfamily of APETALA 2/ETHYLENE RESPONSE FACTOR (AP2/ERF) transcription factors and was shown to induce somatic embryogenesis when expressed ectopically in several taxa (Boutilier, 2002; Lowe et al., 2016; Méndez-Hernández et al., 2019; Wójcik et al., 2020). In rice gametes, *BBM1* is exclusively expressed in sperm cells but not in egg cells. Moreover, it has recently been found that *BBM1* expression in rice zygotes is specific for the *BBM1* allele introduced with the male gamete, but is expressed biallelic several hours following fertilization (Khanday et al., 2019). Moreover, a triple knockout of *BBM1* along with its two homologs in rice, *BBM2* and *BBM3*, causes embryo arrest and abortion, but can be fully rescued by male-transmitted *BBM1*. These findings suggest that embryogenesis following fertilization requires *BBM1* transmitted from the male genome. Interestingly, this can be applied to induce embryogenesis in egg cells prior to fertilization by male gametes as shown by transgenic rice lines expressing *BBM1* under control of an egg-cell-specific promoter which are parthenogenetic. If *BBM1* is expressed egg-cell-specifically in a genetic background in which meiosis was substituted with mitosis and thus recombination was eliminated (*MiMe* lines; Mieulet et al., 2016), sexual propagation without genetic segregation can be engineered in a sexually reproducing plant. These clonal progenies retain genome-wide parental heterozygosity which is beneficial, e.g., for maintaining hybrids with favorable gene combinations.

Dual ontogeny is an integral part of land plants. A better understanding of ontogeny determinants and controls is not only important for a better understanding of the evolution of plant diversity but will also have commercial benefits. Identifying key genes and altering their expression to switch microspores to reprogram themselves to a diploid ontogeny will be highly beneficial for faster breeding of crop plants, e.g., via the induced production of dihaploids.

AUTHOR CONTRIBUTIONS

SP, AT, KP, and RW wrote the manuscript. AM and OD discussed the manuscript. All authors have read the manuscript and approved it for submission.

FUNDING

KP, RW, and SP received funding from the BMBF (KMU-innovativ-20, project Haploswitch, 031B0503A). KP, RW, SP, and AM received funding from the BMBF (Plant Breeding Research for Bioeconomy, project InnoBeet, 031B0556). The article processing charge was funded by the University of Freiburg in the funding programme Open Access Publishing.

ACKNOWLEDGMENTS

We are indebted to William Teale (Institute for Biology II, University of Freiburg) for his critical and constructive comments.

REFERENCES

Arnaud, N., and Pautot, V. (2014). Ring the BELL and tie the KNOX: roles for TALEs in gynoecium development. *Front. Plant Sci.* 5:93. doi: 10.3389/fpls.2014.00093

Arun, A., Coelho, S. M., Peters, A. F., Bourdareau, S., Pérès, L., Scornet, D., et al. (2019). Convergent recruitment of TALE homeodomain life cycle regulators to direct sporophyte development in land plants and brown algae. *Elife* 8:e43101. doi: 10.7554/eLife.43101

Banks, J. A. (2009). Selaginella and 400 million years of separation. *Annu. Rev. Plant Biol.* 60, 223–238. doi: 10.1146/annurev.arplant.59.032607.092851

Bauer, L. (1959). Auslösung apogamer Sporogonbildung am Regenerations-Protonema von Laubmoosen durch einen vom Muttersporogon abgegebenen Faktor. *Naturwissenschaften* 46, 154–155.

Bayer, M., Nawy, T., Giglione, C., Galli, M., Meinnel, T., and Lukowitz, W. (2009). Paternal Control of Embryonic Patterning in *Arabidopsis thaliana*. *Science* 323, 1485–1488. doi: 10.1126/science.1167784

Borg, M., Papareddy, R. K., Dombey, R., Axelsson, E., Nodine, M. D., Twell, D., et al. (2021). Epigenetic reprogramming rewires transcription during the alternation of generations in *arabidopsis*. *Elife* 10:e61894. doi: 10.7554/eLife.61894

Boutilier, K. (2002). Ectopic Expression of BABY BOOM.Pdf. *Plant Cell* 14, 1737–1749. doi: 10.1105/tpc.001941.tissue

Bowman, J. L., Kohchi, T., Yamato, K. T., Jenkins, J., Shu, S., Ishizaki, K., et al. (2017). Insights into Land Plant Evolution Garnered from the Marchantia polymorpha Genome. *Cell* 171, 287–304.e15. doi: 10.1016/J.CELL.2017.09.030

Bowman, J. L., Sakakibara, K., Furumizu, C., and Dierschke, T. (2016). Evolution in the Cycles of Life. *Annu. Rev. Genet.* 50, 133–154. doi: 10.1146/annurev-genet-120215-035227

Bringloe, T. T., Starko, S., Wade, R. M., Vieira, C., Kawai, H., De Clerck, O., et al. (2020). Phylogeny and Evolution of the Brown Algae. *CRC. Crit. Rev. Plant Sci.* 39, 281–321. doi: 10.1080/07352689.2020.1787679

Cheng, Y., Dai, X., and Zhao, Y. (2006). Auxin biosynthesis by the YUCCA flavin monooxygenases controls the formation of floral organs and vascular tissues in *Arabidopsis*. *Genes Dev.* 20, 1790–1799. doi: 10.1101/gad.1415106.molecular

Christenhusz, M. J. M., and Byng, J. W. (2016). The number of known plants species in the world and its annual increase. *Phytotaxa* 261, 201–217. doi: 10.11646/phytotaxa.261.3.1

Coelho, S. M., Godfroy, O., Arun, A., Le Corguille, G., Peters, A. F., and Cock, J. M. (2011). OUROBOROS is a master regulator of the gametophyte to sporophyte life cycle transition in the brown alga Ectocarpus. *Proc. Natl. Acad. Sci. U. S. A.* 108, 11518–11523. doi: 10.1073/pnas.1102274108

Coelho, S. M., Scornet, D., Rousvoal, S., Peters, N. T., Dartevelle, L., Peters, A. F., et al. (2012). Ectocarpus: a model organism for the brown algae. *Cold Spring Harb. Protoc.* 7, 193–198. doi: 10.1101/pdb.emo065821

Cove, D. (2005). The moss Physcomitrella patens. *Annu. Rev. Genet.* 39, 339–358. doi: 10.1146/annurev.genet.39.073003.110214

Dierschke, T., Flores-Sandoval, E., Rast-Somssich, M. I., Althoff, F., Zachgo, S., and Bowman, J. L. (2021). Gamete expression of tale class hd genes activates the diploid sporophyte program in marchantia polymorpha. *Elife* 10:e57088. doi: 10.7554/eLife.57088

Feng, X., Zilberman, D., and Dickinson, H. (2013). A Conversation across Generations: soma-Germ Cell Crosstalk in Plants. *Dev. Cell* 24, 215–225. doi: 10.1016/j.devcel.2013.01.014

Finet, C., Timme, R. E., Delwiche, C. F., and Marlétaz, F. (2010). Multigene phylogeny of the green lineage reveals the origin and diversification of land plants. *Curr. Biol.* 20, 2217–2222. doi: 10.1016/j.cub.2010.11.035

Frangedakis, E., Shimamura, M., Villarreal, J. C., Li, F. W., Tomaselli, M., Waller, M., et al. (2021). The hornworts: morphology, evolution and development. *New Phytol.* 229, 735–754. doi: 10.1111/nph.16874

Friedman, W. E. (2013). One Genome, Two Ontogenies. *Science* 339, 1045–1046. doi: 10.1126/science.1234992

Gao, J., Yang, X., Zhao, W., Lang, T., and Samuelsson, T. (2015). Evolution, diversification, and expression of KNOX proteins in plants. *Front. Plant Sci.* 6:882. doi: 10.3389/fpls.2015.00882

Hafidh, S., and Honys, D. (2021). Reproduction Multitasking: the Male Gametophyte. *Annu. Rev. Plant Biol.* 72, 581–614. doi: 10.1146/annurev-arplant-080620-021907

Hisanaga, T., Fujimoto, S., Cui, Y., Sato, K., Sano, R., Yamaoka, S., et al. (2021). Deep evolutionary origin of gamete-directed zygote activation by knox/ bell transcription factors in green plants. *Elife* 10:e57090. doi: 10.7554/eLife.57090

Hofmeister, W. F. B. (1851). *Vergleichende Untersuchungen der Keimung, Entfaltung und Fruchtbildung höherer Kryptogame*. Leipzig: Friedrich Hofmeister Verlag.

Horst, N. A., Katz, A., Pereman, I., Decker, E. L., Ohad, N., and Reski, R. (2016). A single homeobox gene triggers phase transition, embryogenesis and asexual reproduction. *Nat. Plants* 2:15209. doi: 10.1038/nplants.2015.209

Horst, N. A., and Reski, R. (2016). Alternation of generations - unravelling the underlying molecular mechanism of a 165-year-old botanical observation. *Plant Biol.* 18, 549–551. doi: 10.1111/plb.12468

Jill Harrison, C. (2017). Development and genetics in the evolution of land plant body plans. *Philos. Trans. R. Soc. B Biol. Sci.* 372:20150490. doi: 10.1098/rstb.2015.0490

Khanday, I., Skinner, D., Yang, B., Mercier, R., and Sundaresan, V. (2019). A male-expressed rice embryogenic trigger redirected for asexual propagation through seeds. *Nature* 565, 91–95. doi: 10.1038/s41586-018-0785-8

Lee, J. H., Lin, H., Joo, S., and Goodenough, U. (2008). Early Sexual Origins of Homeoprotein Heterodimerization and Evolution of the Plant KNOX/BELL Family. *Cell* 133, 829–840. doi: 10.1016/j.cell.2008.04.028

Li, F. W., Nishiyama, T., Waller, M., Frangedakis, E., Keller, J., Li, Z., et al. (2020). Anthoceros genomes illuminate the origin of land plants and the unique biology of hornworts. *Nat. Plants* 6, 259–272. doi: 10.1038/s41477-020-0618-2

Liu, Y., Misamore, M. J., and Snell, W. J. (2010). Membrane fusion triggers rapid degradation of two gamete-specific, fusion-essential proteins in a membrane

block to polygamy in Chlamydomonas. *Development* 137, 1473–1481. doi: 10.1242/dev.044743

Lowe, K., Wu, E., Wang, N., Hoerster, G., Hastings, C., Cho, M.-J., et al. (2016). Morphogenic Regulators Baby boom and Wuschel Improve Monocot Transformation. *Plant Cell* 28, 1998–2015. doi: 10.1105/tpc.16.00124

Lu, P., Chai, M., Yang, J., Ning, G., Wang, G., and Ma, H. (2014). The *Arabidopsis* CALLOSE DEFECTIVE MICROSPORE1 gene is required for male fertility through regulating callose metabolism during microsporogenesis. *Plant Physiol.* 164, 1893–1904. doi: 10.1104/pp.113.233387

Lukowitz, W., Roeder, A., Parmenter, D., and Somerville, C. (2004). A MAPKK Kinase Gene Regulates Extra-Embryonic Cell Fate in *Arabidopsis*. *Cell* 116, 109–119. doi: 10.1016/S0092-8674(03)01067-5

Ma, H. (2005). Molecular Genetic Analyses of Microsporogenesis and Microgametogenesis in Flowering Plants. *Annu. Rev. Plant Biol.* 56, 393–434. doi: 10.1146/annurev.arplant.55.031903.141717

Méndez-Hernández, H. A., Ledezma-Rodríguez, M., Avilez-Montalvo, R. N., Juárez-Gómez, Y. L., Skeete, A., Avilez-Montalvo, J., et al. (2019). Signaling overview of plant somatic embryogenesis. *Front. Plant Sci.* 10:77. doi: 10.3389/fpls.2019.00077

Mieulet, D., Jolivet, S., Rivard, M., Cromer, L., Vernet, A., Mayonove, P., et al. (2016). Turning rice meiosis into mitosis. *Cell Res.* 26, 1242–1254. doi: 10.1038/cr.2016.117

Okano, Y., Aono, N., Hiwatashi, Y., Murata, T., Nishiyama, T., Ishikawa, T., et al. (2009). A polycomb repressive complex 2 gene regulates apogamy and gives evolutionary insights into early land plant evolution. *Proc. Natl. Acad. Sci. U. S. A.* 106, 16321–16326. doi: 10.1073/pnas.0906997106

Ono, A., and Kinoshita, T. (2021). Epigenetics and plant reproduction: multiple steps for responsibly handling succession. *Curr. Opin. Plant Biol.* 61:102032. doi: 10.1016/j.pbi.2021.102032

Parish, R. W., and Li, S. F. (2010). Death of a tapetum: a programme of developmental altruism. *Plant Sci.* 178, 73–89. doi: 10.1016/j.plantsci.2009.11.001

Pazhamala, L. T., Chaturvedi, P., Bajaj, P., Srikanth, S., Ghatak, A., Chitikineni, A., et al. (2020). Multiomics approach unravels fertility transition in a pigeonpea line for a two-line hybrid system. *Plant Genome* 13, 1–20. doi: 10.1002/tpg2.20028

Pérez-Pérez, Y., El-Tantawy, A. A., Solís, M. T., Risueño, M. C., and Testillano, P. S. (2019). Stress-Induced Microspore Embryogenesis Requires Endogenous Auxin Synthesis and Polar Transport in Barley. *Front. Plant Sci.* 10:1200. doi: 10.3389/fpls.2019.01200

Peters, A. F., Scornet, D., Ratin, M., Charrier, B., Monnier, A., Merrien, Y., et al. (2008). Life-cycle-generation-specific developmental processes are modified in the immediate upright mutant of the brown alga Ectocarpus siliculosus. *Development* 135, 1503–1512. doi: 10.1242/dev.016303

Pringsheim, N. (1876). *Über die vegetative Sprossung der Moosfrüchte. Monatsberichte der königlich-preussischen Akad. der Wissenschaften zu Berlin*. Berlin: Berlin-Brandenburgische Akademie der Wissenschaften, 425–429.

Ray, A., Robinson-Beers, K., Ray, S., Baker, S. C., Lang, J. D., Preuss, D., et al. (1994). *Arabidopsis* floral homeotic gene BELL (BEL1) controls ovule development through negative regulation of AGAMOUS gene (AG). *Proc. Natl. Acad. Sci. U. S. A.* 91, 5761–5765. doi: 10.1073/pnas.91.13.5761

Reiser, L., Modrusan, Z., Margossian, L., Samach, A., Ohad, N., Haughn, G. W., et al. (1995). The Bell1 Gene Encodes a Homeodomain Protein Involved in Pattern-Formation in the *Arabidopsis* Ovule Primordium. *Cell* 83, 735–742.

Ripetsky, R. T. (1985). Experimental apomixis in mosses and the problem of stability of the determined and differentiated states. *Ontogeny* 16, 229–241.

Rodríguez-Sanz, H., Solís, M.-T., López, M.-F., Gómez-Cadenas, A., Risueño, M. C., and Testillano, P. S. (2015). Auxin Biosynthesis, Accumulation, Action and Transport are Involved in Stress-Induced Microspore Embryogenesis Initiation and Progression in *Brassica napus*. *Plant Cell Physiol.* 56, 1401–1417. doi: 10.1093/pcp/pcv058

Sakakibara, K., Ando, S., Yip, H. K., Tamada, Y., Hiwatashi, Y., Murata, T., et al. (2013). KNOX2 genes regulate the haploid-to-diploid morphological transition in land plants. *Science* 339, 1067–1070. doi: 10.1126/science.1230082

Schubert, D. (2019). Evolution of Polycomb-group function in the green lineage. *F1000Res.* 8:268. doi: 10.12688/f1000research.16986.1

Shariatpanahi, M. E., Bal, U., Heberle-Bors, E., and Touraev, A. (2006). Stresses applied for the re-programming of plant microspores towards in vitro embryogenesis. *Physiol. Plant.* 127, 519–534. doi: 10.1111/j.1399-3054.2006.00675.x

Szövényi, P., Gunadi, A., and Li, F. W. (2021). Charting the genomic landscape of seed-free plants. *Nat. Plants* 7, 554–565. doi: 10.1038/s41477-021-00888-z

Tan, H., Liang, W., Hu, J., and Zhang, D. (2012). MTR1 Encodes a Secretory Fasciclin Glycoprotein Required for Male Reproductive Development in Rice. *Dev. Cell* 22, 1127–1137. doi: 10.1016/j.devcel.2012.04.011

Testillano, P. S. (2019). Microspore embryogenesis: targeting the determinant factors of stress-induced cell reprogramming for crop improvement. *J. Exp. Bot.* 70, 2965–2978. doi: 10.1093/jxb/ery464

Vigneau, J., and Borg, M. (2021). The epigenetic origin of life history transitions in plants and algae. *Plant Reprod.* 34, 267–285. doi: 10.1007/s00497-021-00422-3

Winter, D., Vinegar, B., Nahal, H., Ammar, R., Wilson, G. V., and Provart, N. J. (2007). An "electronic fluorescent pictograph" Browser for exploring and analyzing large-scale biological data sets. *PLoS One* 2:e718. doi: 10.1371/journal.pone.0000718

Wójcik, A. M., Wójcikowska, B., and Gaj, M. D. (2020). Current perspectives on the auxin-mediated genetic network that controls the induction of somatic embryogenesis in plants. *Int. J. Mol. Sci.* 21:1333. doi: 10.3390/ijms21041333

Yao, X., Tian, L., Yang, J., Zhao, Y.-N., Zhu, Y.-X., Dai, X., et al. (2018). Auxin production in diploid microsporocytes is necessary and sufficient for early stages of pollen development. *PLoS Genet.* 14:e1007397. doi: 10.1371/journal.pgen.1007397

Zhang, J., Pinello, J. F., Fernández, I., Baquero, E., Fedry, J., Rey, F. A., et al. (2021). Species-specific gamete recognition initiates fusion-driving trimer formation by conserved fusogen HAP2. *Nat. Commun.* 12:4380. doi: 10.1038/s41467-021-24613-8

Conflict of Interest: The authors declare that the research was conducted in the absence of any commercial or financial relationships that could be construed as a potential conflict of interest.

Publisher's Note: All claims expressed in this article are solely those of the authors and do not necessarily represent those of their affiliated organizations, or those of the publisher, the editors and the reviewers. Any product that may be evaluated in this article, or claim that may be made by its manufacturer, is not guaranteed or endorsed by the publisher.

frontiers in Plant Science

ORIGINAL RESEARCH
published: 08 February 2022
doi: 10.3389/fpls.2022.806865

Transcript Profiling Analysis and ncRNAs' Identification of Male-Sterile Systems of *Brassica campestris* Reveal New Insights Into the Mechanism Underlying Anther and Pollen Development

*Dong Zhou[1], Caizhi Chen[1,2], Zongmin Jin[1], Jingwen Chen[1], Sue Lin[3], Tao Lyu[1], Dandan Liu[1,2], Xinpeng Xiong[4], Jiashu Cao[1,2] and Li Huang[1,2]**

[1] Laboratory of Cell & Molecular Biology, Institute of Vegetable Science, Zhejiang University, Hangzhou, China, [2] Hainan Institute of Zhejiang University, Sanya, China, [3] Institute of Life Sciences, Wenzhou University, Wenzhou, China, [4] College of Bioengineering, Jingchu University of Technology, Jingmen, China

OPEN ACCESS

Edited by:
Concepción Gómez-Mena, Polytechnic University of Valencia, Spain

Reviewed by:
Hui Feng, Shenyang Agricultural University, China
Ying Miao, Fujian Agriculture and Forestry University, China

***Correspondence:**
Li Huang
lihuang@zju.edu.cn

Specialty section:
This article was submitted to Plant Development and EvoDevo, a section of the journal Frontiers in Plant Science

Received: 01 November 2021
Accepted: 10 January 2022
Published: 08 February 2022

Citation:
Zhou D, Chen C, Jin Z, Chen J, Lin S, Lyu T, Liu D, Xiong X, Cao J and Huang L (2022) Transcript Profiling Analysis and ncRNAs' Identification of Male-Sterile Systems of Brassica campestris Reveal New Insights Into the Mechanism Underlying Anther and Pollen Development. Front. Plant Sci. 13:806865. doi: 10.3389/fpls.2022.806865

Male-sterile mutants are useful materials to study the anther and pollen development. Here, whole transcriptome sequencing was performed for inflorescences in three sterile lines of Chinese cabbage (*Brassica campestris* L. ssp. *chinensis* Makino, syn. *B. rapa* ssp. *chinensis*), the genic male-sterile line (A line), the *Polima* cytoplasmic male-sterile (CMS) line (P line), and the *Ogura* CMS line (O line) along with their maintainer line (B line). In total, 7,136 differentially expressed genes (DEGs), 361 differentially expressed long non-coding RNAs (lncRNAs) (DELs), 56 differentially expressed microRNAs (miRNAs) (DEMs) were selected out. Specific regulatory networks related to anther cell differentiation, meiosis cytokinesis, pollen wall formation, and tapetum development were constructed based on the abortion characteristics of male-sterile lines. Candidate genes and lncRNAs related to cell differentiation were identified in sporocyteless P line, sixteen of which were common to the DEGs in *Arabidopsis spl/nzz* mutant. Genes and lncRNAs concerning cell plate formation were selected in A line that is defected in meiosis cytokinesis. Also, the orthologs of pollen wall formation and tapetum development genes in *Arabidopsis* showed distinct expression patterns in the three different sterile lines. Among 361 DELs, 35 were predicted to interact with miRNAs, including 28 targets, 47 endogenous target mimics, and five precursors for miRNAs. Two lncRNAs were further proved to be functional precursors for bra-miR156 and bra-miR5718, respectively. Overexpression of *bra-miR5718HG* in *B. campestris* slowed down the growth of pollen tubes, caused shorter pollen tubes, and ultimately affected the seed set. Our study provides new insights into molecular regulation especially the ncRNA interaction during pollen development in *Brassica* crops.

Keywords: *Brassica campestris*, pollen development, long non-coding RNA, miRNA, endogenous target mimic, miRNA precursor

INTRODUCTION

Anther development starts from an archesporial cell that produces sporogenous cells that further differentiate into the endothecium, middle layer, tapetum, and pollen mother cells (PMCs) (Murmu et al., 2010). In *Arabidopsis*, *Sporocyteless*/*Nozzle* (*SPL/NZZ*) is the key regulator of anther cell differentiation, whose mutation blocks the formation of sporocytes (Yang et al., 1999). The basic leucine-zipper transcription factors *TGACG motif-binding protein 9* (*TGA9*) and *TGA10* work downstream of *SPL/NZZ* and interact with floral CC-type glutaredoxins ROXY1 and ROXY2 (Murmu et al., 2010). Ath-miR156 is downregulated in *spl/nzz* and its overexpression in *spl8* mutant leads to similar phenotypes of *spl/nzz* mutant (Xing et al., 2010). Although several key regulators have been found, molecular networks controlling anther cell specification remain largely unknown.

Pollen development can be divided into two major phases: the developmental phase and the functional phase (Hafidh and Honys, 2021). The latter refers to the interaction between pollen and stigma in which pollen grains rehydrate and germinate with pollen tubes to accomplish double fertilization (Johnson et al., 2019). The developmental stage of pollen is initiated by the meiosis of diploid PMCs. Tetrads formed by four haploid microspores are generated after simultaneous-type cytokinesis in dicotyledon, which means cell plates form between four haploid nuclei simultaneously (De Storme and Geelen, 2013). The position of the meiotic cell plate is determined by radial microtubule arrays, a phragmoplast-like structure consisting of actin filaments and microtubules. In *Arabidopsis*, there is a classical mitogen-activated protein kinase (MAPK) cascade signaling pathway, *Kinesin-like protein NPK1-activating kinase 1/2* (*AtNACK1/2*)-*Arabidopsis NPK1-related protein kinase* (*ANP1/2/3*)-*MAPK kinase* (*MAPKK6*)-*MAPK4*, regulating mitotic cell plate expansion *via* affecting the phosphorylation of microtubule crosslinker protein MAP65s (De Storme and Geelen, 2013). Notably, *AtNACK2*, *MAPKK6*, and *MAPK4* also function in male-specific meiotic cytokinesis while no evidence showed that ANP1 and ANP3 work in male meiosis as yet (Yang et al., 2003; Zeng et al., 2011). Thus, the MAPK cascade is still incomplete for male meiosis. During somatic cytokinesis, the Exocyst complex regulates fusion of clathrin-coated vesicles in the midzone and compromised initial cell plate assembly was observed in the Exocyst complex subunit EXO70A1 mutants (Fendrych et al., 2010). In contrast to mitotic cytokinesis, little is known about the regulatory network underlying plant male meiotic cytokinesis.

The second meiotic division is usually accompanied by the formation of a callose wall (Shen et al., 2019). *Callose synthase 5* (*Cals5*) is the key gene responsible for the synthesis of callose surrounding tetrads (Dong et al., 2005). *Arabidopsis Ruptured pollen grain 1* (*RPG1*), a sugar transporter encoding gene, shares a redundant function with *RPG2* in regulating the expression of *Cals5* (Sun et al., 2013). The callose wall is degraded by callose secreted by the tapetum to release free microspores. Tapetum is the last structure surrounding the developing PMCs and microspores, supplying essential substances and enzymes required for microsporogenesis and pollen maturation. A well-defined genetic pathway, *Dysfunctional tapetum 1* (*DYT1*)-*Defective in tapetal development and function 1* (*TDF1*)-*Aborted microspores* (*AMS*)-*MYB domain protein 80* (*MYB80*)-*MS1* has been identified for tapetal development (Parish and Li, 2010). *Vanguard 1* (*VGD1*) and *Glyoxal oxidase 1* (*GLOX1*) are direct targets of *MYB80* and may be involved in the formation of the pollen coat (Phan et al., 2011). Three cysteine proteases [Carbohydrate epimerase 1 (CEP1), RD19A, and RD19C] play irreplaceable roles in tapetal PCD and their maturation is regulated by β vacuolar processing enzyme (βVPE) (Cheng et al., 2020). After the degradation of the callose wall, the synthesis of the pollen wall starts. The pollen wall includes an inner intine mainly composed of pectin, cellulose, and hemicellulose, and an outer exine mainly composed of sporopollenin (Jiang et al., 2013). Pectin and cellulose are synthesized from sucrose by enzymes, such as cell wall invertases (cwINVs) and fructokinases (FRKs), in microspores (Shi et al., 2015). Sporopollenin is synthesized in the tapetum and secreted to the surface of the microspore to form exine. Although the exact structure of sporopollenin remains unknown, several genes like *Arabidopsis male sterility 2* (*MS2*), *acyl-CoA synthetase 5* (*ACOS5*), and *cytochrome p450 family 703 subfamilies A polypeptide 2* (*CYP703A2*) have been revealed to involve in its synthesis (Shi et al., 2015).

In recent years, a vital role of non-coding RNAs (ncRNAs) including microRNAs (miRNAs) and long ncRNAs (lncRNAs) have been revealed in reproductive processes. For example, overexpression of bra-miR158 reduced the pollen viability and pollen germination ratio in *B. campestris* (Ma et al., 2017). Reduced expression of *Long-day-specific male-fertility-associated RNA* (*LDMAR*) triggered premature PCD of tapetum and then resulted in male sterility in rice under long-day conditions (Ding et al., 2012). In addition, interactions between ncRNAs have also been discovered: lncRNAs can act as miRNA decoys that are also known as endogenous target mimics (eTMs). Excessive expression of *osa-eTM160* impaired the repression of osa-miR160 on its targets, resulting in less seed set in rice (Wang et al., 2017). Our previous study also predicted 15 lncRNAs as the potential eTMs for 13 miRNAs during pollen development and fertilization in *B. campestris* and demonstrated that identified two functional eTMs for miR160 in pollen development (Huang et al., 2018). LncRNAs can also act as miRNA targets and precursors. In sweet orange (*Citrus sinensis*), three lncRNAs, *csi-eTM166*, *XLOC_009399* (a precursor of csi-miR166c), and *XLOC_016898* (a target of csi-miR166c) together with csi-miR166c could form an eTM166-miR166c-targeted lncRNA regulatory network, which possibly affected citrus fruit development (Ke et al., 2019). To uncover the interactions between different types of transcripts is undoubtedly important to interpret gene expression networks during anther and/or pollen development.

With anther and/or pollen abortion as the most common variable defect, male-sterile lines are suitable materials to study the molecular and cellular mechanisms underlying anther and pollen development. According to the mode of inheritance, male sterility can be divided into genic male-sterile (GMS) and cytoplasmic male-sterile (CMS). The former is controlled by nuclear genes and the latter is caused by mitochondrial genes

together with nuclear genes. *Polima* (*Pol*) and *Ogura* (*Ogu*) CMS are widely used in the breeding of *Brassica* crops. In *Pol* CMS lines, sporogenous cells fail to differentiate into the endothecium, middle layer, and tapetum, and ultimately no pollen sac is formed (An et al., 2014). In *Ogu* type CMS lines, the obvious malformation is discovered during the late tetrad and uninucleate stage where tapetal cells are radially expanded and vacuolated, and the deposition of sporopollenin is delayed (Kang et al., 2014; Xing et al., 2018). As a typical GMS line, Chinese cabbage (*B. campestris* ssp. *chinensis* cv. Aijiaohuang) '*Bcajh97-01A*' has been demonstrated to undergo aberrant cytokinesis during male meiosis with defective exine formation, and premature tapetal PCD (Huang et al., 2009; Shen et al., 2019). To systematically explore the molecular mechanisms underlying anther/pollen development in *Brassica* crops, we created the GMS line '*Bcajh97-01A*,' a *Pol* CMS line '*Bcpol97-05A*,' and an *Ogu* CMS line '*Bcogu97-06A*' of Chinese cabbage (hereafter called A line, P line, and O line, respectively) that shared the same maintainer line '*Bcajh97-01B*' (B line) by successive selection and backcrossing (Huang et al., 2008; Liang et al., 2019). In this study, whole transcriptome sequencing was performed to disclose the regulatory networks between mRNAs and ncRNAs, and interactions of different types of ncRNAs during anther and/or pollen development in *B. campestris*. Differentially expressed genes (DEGs) and ncRNAs associated with pollen development were identified in different sterile lines. We also constructed the interplay between lncRNAs and miRNAs, which will broaden our knowledge on the molecular mechanisms underlying male sterility and proceed with its utilization in breeding.

MATERIALS AND METHODS

Plant Materials

The *Ogu* CMS line (*B. napus*) was transferred into '*Aijiaohuang*' (*B. campestris*) through successive backcrossing four times. And then, the fertile plant (B line) in the '*Aijiaohuang*' two-type line '*Bcajh97-01A/B*' were backcrossed to *Ogu* CMS in *B. campestris* for four generations. The fertility and morphology characteristics like height and width of backcross progeny were observed over successive years. Finally, we established an O line that shared the common maintainer line (B line) with the A line.

The three sterile lines (A line, P line, and O line) and their common maintainer line (B line) in Chinese cabbage were cultivated in the experimental farm of Zhejiang University, Hangzhou, China at the same time. Inflorescences were harvested from plants at the full flowering stage with the removal of open flowers. Each sample of inflorescences was collected from more than 10 individual plants, frozen in liquid nitrogen immediately, and stored at −75°C for further use. Three replicates were performed.

Whole Transcriptome Sequencing

Total RNA was extracted using TRIzol reagent (Invitrogen, Carlsbad, CA, United States) following the manufacturer's instructions. Libraries for mRNA-Seq and lncRNA-Seq were generated using NEBNext® Ultra™ Directional RNA Library Prep Kit for Illumina® (NEB, Ipswich, MA, United States) as the instruction manual described. Libraries for miRNA-Seq were generated using NEBNext® Ultra™ small RNA Sample Library Prep Kit for Illumina® (NEB) following the manufacturer's recommendations and index codes were added to attribute sequences to each sample. RNA-Seq was performed by the Biomarker Technologies Co., Ltd., Beijing, China[1] on an Illumina Hi-Seq platform.

Identification of ncRNAs and Differential Expression Analysis

The transcriptome was assembled using the StringTie package based on the reads mapped to the reference genome downloaded from the Brassica database, Institute of Vegetables and Flowers, Beijing, China (version 1.5, BRAD)[2] and annotated using the gffcompare program. Coding-Non-Coding Index (CNCI), coding potential assessment tool (CPAT), coding potential calculator (CPC), and Pfam were used to predict lncRNAs. The secondary structure of lncRNAs was generated by the Mfold web server.[3] Known miRNAs were identified by aligning the mapped reads with the mature miRNAs' sequences in miRBase, University of Manchester, Manchester, United Kingdom (version 21).[4] Reads were identified as known miRNAs when the alignment was identical. Novel miRNAs were predicted by a modified miRDeep2, Max Delbrück Center for Molecular Medicine, Berlin, Germany with plant-specific parameters (version 2.0.5). DESeq R package, Dana-Farber Cancer Institute, MA, United States (version 1.10.1) was used for screening DEGs, differentially expressed lncRNAs (DELs), DECs, and differentially expressed miRNAs (DEMs). The criteria were a |fold change (FC)| $\geq$ 2 and a false discovery rate (FDR) $\leq$ 0.05.

Construction of lncRNA-mRNA, lncRNA-miRNA, and Transcription Factors Networks

Adjacent genes within 100 kb of lncRNAs were considered to be their *cis*-targets and *trans*-targets, which were predicted by LncTar software (Casero et al., 2015). Pearson bivariate correlation was adopted to estimate the expression relationships between ncRNAs and their targets. The correlation is significant at a confidence level (bilateral) $\leq$ 0.05 ($P < 0.05$) and extremely significant when P-value $\leq$ 0.01. Targets of DEMs were predicated by TargetFinder, Beijing Institute of Radiation Medicine, Beijing, China (version 1.6). LncRNAs as potential miRNA targets were selected by the psRNATarget website[5] with the default parameter. LncRNAs as miRNA precursors were predicted by comparing lncRNAs with miRNA precursor sequences. LncRNAs as miRNA eTMs were predicted by a local Perl script (Ye et al., 2014). The transcription factor network was constructed by iGRN, a newly developed tool for transcriptional networks, and visualized using Cytoscape, Institute for Systems Biology, Washington, WA, United States (version 3.8) (Meng et al., 2021).

[1]http://www.biomarker.com.cn
[2]http://brassicadb.cn/#/
[3]http://www.unafold.org/RNA_form.php
[4]http://www.mirbase.org/
[5]http://plantgrn.noble.org/psRNATarget/

Nicotiana benthamiana Transient Expression Assay

Fragments of *bra-miR156HG* and *bra-miR5718HG* were amplified and inserted into the pBI121 vector under two CaMV 35S promoters, respectively. Primers used for vector construction are listed in **Supplementary Table 1**. Plasmids were transformed into *Agrobacterium tumefaciens* strain GV3101 and then infiltrated into tobacco leaves when OD_{600} reached 1.0–1.2. The leaves were collected, frozen in liquid nitrogen immediately, and stored at −75°C for RNA extraction after 48 h of infiltration.

Semi-Quantitative and Real-Time Quantitative RT-PCR

For transient expression assay, semi-quantitative reverse transcription (RT)-PCR of lncRNAs was performed with 2 × TSINGKE master mix (Tsingke Biotechnology Co., Ltd., Beijing, China) and *nbe-18S rRNA* was used as a reference. Expression of miRNAs was detected by real-time quantitative PCR (RT-qPCR) on a CFX96 Real-Time System (Bio-Rad, Hercules, CA, United States) using TB Green Premix Ex Taq II (TaKaRa, Dalian, China) and *nbe-5.8S rRNA* was used for normalization. For validation of RNA-Seq, RT-qPCR was performed using the same samples for RNA-Seq. The expressions of DEGs and DELs were normalized against *BraUBC10* and those of DEMs were normalized against *bra-5.8S rRNA*. The relative expression levels were calculated using the $2^{-\Delta\Delta CT}$ method. The cDNAs used for the RT-qPCR analysis of miRNA were synthesized by a Mir-X^{TM} miRNA First-Strand Synthesis Kit (TaKaRa). All primers are shown in **Supplementary Table 1**.

Data Availability

Transcriptome data supporting the findings of this study have been deposited in National Center for Biotechnology Information Sequence Read Archive (SRA) under the accession number PRJNA753197. All other relevant data are available from the corresponding author on request.

RESULTS

Transcripts Were Identified Genome-Wide in *Brassica campestris*

As the general morphology of inflorescences and flowers of the three sterile lines did not differ from those of the common fertile maintainer line except for the anthers, inflorescences without opened flowers of A line, P line, O line, and B line were taken for transcriptome sequencing to analyze the transcriptome during pollen and anther development (**Figure 1A**). For lncRNAs and mRNAs, a total of 141.89 GB of clean data were obtained for 12 samples, with an average of 10.20 GB of clean data per sample. For microRNA, a total of 253.31 M clean data were obtained, and clean reads of each sample no less than 14.40 M. A total of 41,133 mRNAs, 13,879 putative lncRNAs, and 342 miRNAs were identified (**Supplementary Figures 1A–C**). The identified lncRNAs were classified into lincRNAs, antisense lncRNAs, sense lncRNAs, and intronic lncRNAs, which were evenly distributed on different chromosomes (**Supplementary Figures 1D,E**). The expression difference of transcripts between each male-sterile line and the maintainer line was then compared respectively. Totally, 7,136 DEGs, 361 DELs, 56 DEMs were selected out (**Figures 1B–D**). A total of 2,277 DEGs, 77 DELs, and 11 DEMs were common to all sterile lines. Further, 608, 1,139, and 715 DEGs were specific to A line, P line, and O line, respectively (**Figures 1B–D**). As for DELs, 22, 52, and 78 DELs were specifically expressed in A line, P line, and O line, respectively. No line-specific DEMs were found in the A line, 20 DEMs were specifically expressed in the P line, and only six DEMs were specifically expressed in the O line. Compared with the B line, 3,376, 4,779, and 4,480 DEGs were identified in A line, P line, and O line, respectively, 79% of which on average were downregulated (**Figures 1B,E**). Among the three sterile lines, the largest number of DELs was discovered in O line (242), followed by P line (179), and the least was in A line (142) (**Figures 1C,F**). The number of miRNAs expressed in four lines was comparatively lower than other transcripts. There were 18, 47, and 32 differentially expressed microRNAs (DEMs) identified in A line, P line, and O line, respectively (**Figures 1D,G**). All the expression data of DEGs, DELs, and DEMs were concluded in **Supplementary Data 1**. Interestingly, like mRNAs, the proportion of downregulated non-coding transcripts in sterile lines including lncRNAs and miRNAs was significantly higher than that of upregulated transcripts (**Figures 1E–G**). Further, we carried out the RT-qPCR experiments of seven DEGs, six DELs, and three DEMs to validate the results of RNA-Seq. The results showed that the expression pattern of these candidate genes was consistent with the results of RNA-Seq, which suggest the transcriptome data were reliable (**Supplementary Figure 2**).

Using the P Line We Found Candidate Transcripts Involved in Anther Cell Differentiation

To excavate genes related to anther cell differentiation, firstly, the expression of genes that were experimentally confirmed to function in anther differentiation (reviewed by Walbot and Egger, 2016) was analyzed in the B line and the sterile lines. Our results showed that five out of them were DEGs in sterile lines compared with the fertile line (**Figure 2A**). Homolog genes of *Arabidopsis SPL/NZZ*, *Bra026359* (*NZZ-1*), and its putative downstream genes, *Bra018634* (*TGA9-1*), *Bra031622* (*TGA9-2*), *Bra009233* (*TGA10-1*), *Bra005914* (*TGA10-2*), and *Bra009231* (*STRUBBELIG-receptor family 2*, *SRF2*) were downregulated in P line, and so did miR156. While the expression of another homolog to *Arabidopsis SPL/NZZ*, *Bra019056* (*NZZ-2*) and four downstream genes except for *Bra009231* (*SRF2*) was also decreased in the O line and only miR156 was downregulated in the A line. Additionally, through target prediction and expression correlation analysis, five lncRNAs were found to target *SPL/NZZ* and its downstream genes (**Supplementary Data 2**). Two lncRNAs target *Bra009233* and one targets *Bra026359*, *Bra019056*, *Bra009233*, and *Bra005914*. *MSTRG.2229.1* was predicted to positively regulate *Bra026359* (*NZZ-1*) while *Bra019056* (*NZZ-2*) was negatively related with

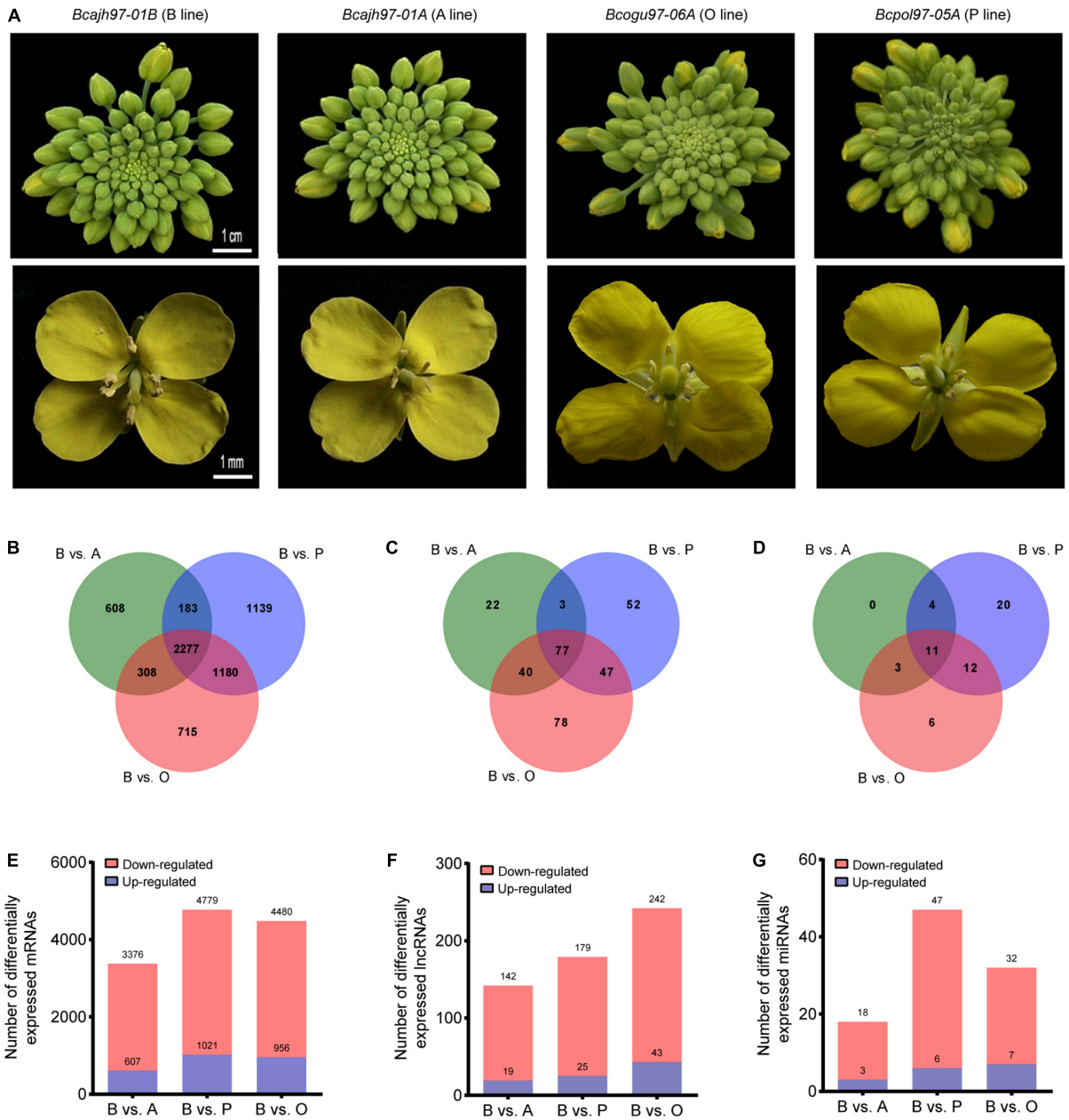

FIGURE 1 | Genome-wide identification and characteristics of transcripts in *Brassica campestris*. **(A)** Photographs for inflorescences and flowers from the sterile and the fertile line. **(B,E)** Statistics of differentially expressed mRNAs in three sterile lines and the fertile line. **(C,F)** Statistics of differentially expressed long non-coding RNAs in three sterile lines and fertile line. **(D,G)** Statistics of differentially expressed microRNAs in three sterile lines and fertile line. B line, the maintainer line '*Bcajh97-01B*'; A line, the genic male-sterile line '*Bcajh97-01A*'; P line, *Polima* cytoplasmic male-sterile line '*Bcpol97-05A*'; O line, *Ogura* cytoplasmic male-sterile line '*Bcogu97-06A*'.

lncRNA *MSTRG.17700.1*. *MSTRG54890.1* was predicted to target *Bra009233* (*TGA10-1*).

Considering that molecular networks regulating anther cell differentiation are not well studied, it is reasonable that only several function-known DEGs related to it were identified in the three sterile lines. To further elucidate molecular networks in anther cell differentiation, all line-specific DEGs were filtered by gene ontology (GO) term "cell differentiation." The number of DEGs annotated in P line (72) was approximately twice that of A line (31) and O line (38) (**Figure 2B**). For further analysis, only DEGs specifically expressed in the P line were included because a previous study described that sporogenous cells in *Pol* CMS anthers failed to differentiate, which was largely different from the phenotype of A line and O line (An et al., 2014). As *B. campestris* and *Arabidopsis* have a common ancestor, functional analysis of homologous genes in

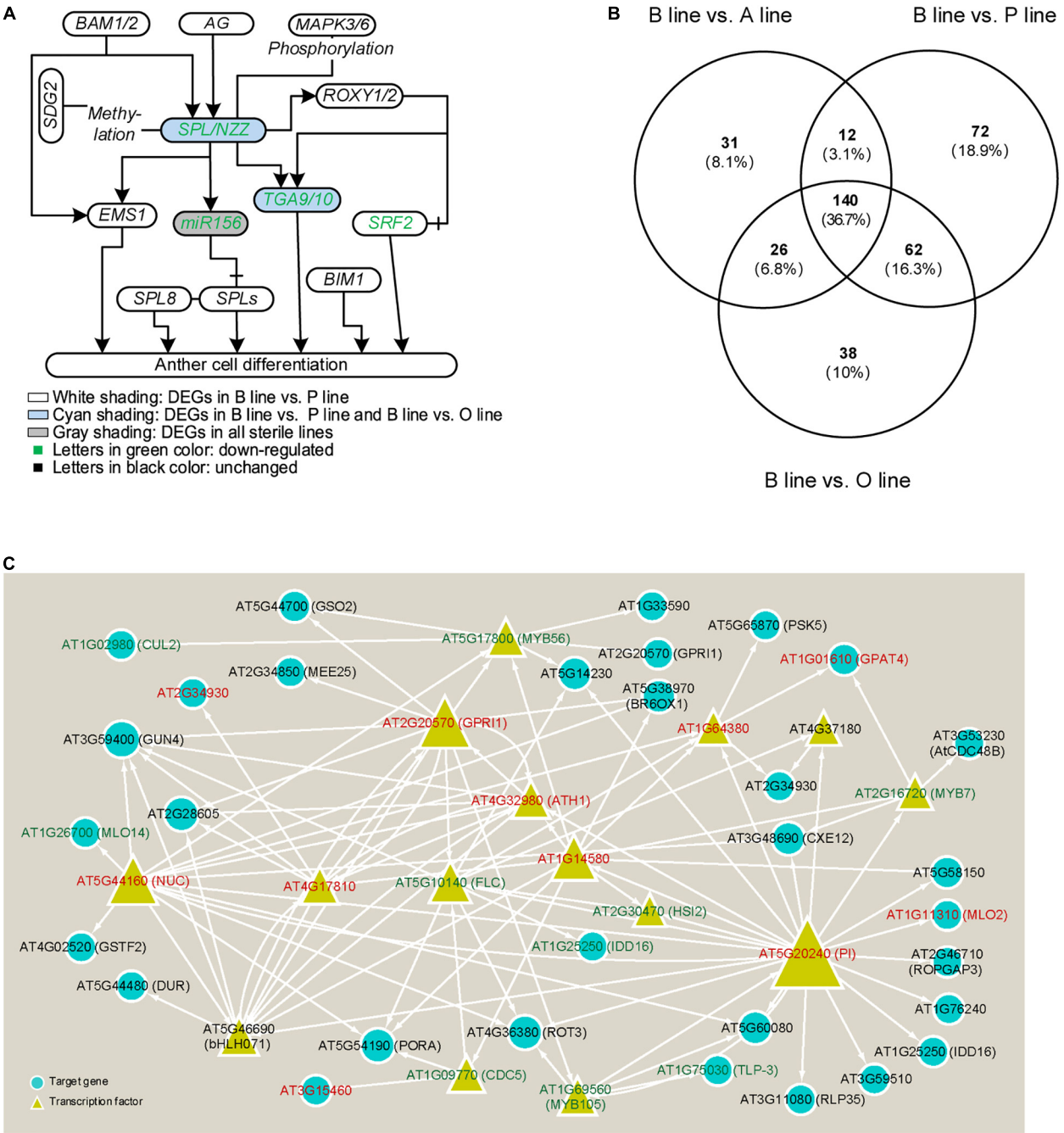

FIGURE 2 | Analysis of genes in anther cell differentiation in three sterile lines of *Brassica campestris*. **(A)** Genic network of anther cell differentiation. **(B)** Venn diagram of differentially expressed genes (DEGs) number involved in cell differentiation in fertile line and sterile lines. **(C)** Regulatory network of transcription factors annotated to participate in cell differentiation predicted by integrated gene regulatory network (iGRN). Genes in red mean upregulated DEGs, while genes in green represent downregulated DEGs. B line, the fertile line '*Bcajh97-01B*'; A line, the sterile line '*Bcajh97-01A*'; P line, *Polima* (*Pol*) cytoplasmic male-sterile (CMS) line '*Bcpol97-05A*'; O line, *Ogura* (*Ogu*) CMS line '*Bcogu97-06A*'; BAM1/2, β-amylase 1/2; SDG2, SET domain protein 2; EMS1, excess microsporocytes 1; AG, agamous; SPL/NZZ, sporocyteless/nozzle; SPL8, SQUAMOSA promoter binding protein-like 8; MAPK3/6, mitogen-activated protein kinase 3/6; ROXY1/2, CC-type glutaredoxin 1/2; TGA9/10, TGACG (TGA) motif-binding protein 9/10; BIM1, brassinosteroid insensitive 1 (BRI1)-EMS-suppressor 1 (BES1)-interacting MYC-like protein 2; SRF2, STRUBBELIG-receptor family 2; CUL2, cullin 2; GUN4, genomes uncoupled 4; MLO2/14, mildew resistance locus O; NUC, nutcracker; GSTF2, Glutathione s-transferase phi 2; DUR, defective uge in root; bHLH071, basic helix-loop-helix protein 71; GSO2, gassho 2; MEE25, maternal effect embryo arrest 25; MYB7/56/105, MYB domain protein 7/56/105; GPRI1, GBF's pro-rich region-interacting factor 1; FLC, flowering locus C; CDC5/48B, cell division cycle 5/48B; BR6OX1, brassinosteroid-6-oxidase 1; HSI2, high-level expression of sugar-inducible gene 2; IDD16, indeterminate(id)-domain 16; TLP-3, thaumatin-like protein 3; RLP35, receptor like protein 35; PSK5, phytosulfokine 5 precursor; GPAT4, glycerol-3-phosphate sn-2-acyltransferase 4; CXE12, carboxylesterase 12; PI, pistillata; ROPGAP3, ROP guanosine triphosphatase (GTPASE)-activating protein 3.

TABLE 1 | Common DEGs between *Polima* cytoplasmic male-sterile of *Brassica campestris* and the *Arabidopsis spl/nzz* mutant.

ID in BRAD	Expression in B line	Expression in P line	Regulated	Homologous genes in *Arabidopsis*		Gene annotation
				ID in TAIR	Gene name	
Bra021188	2.043	0.345	**Down**	AT3G16650	*Pleiotropic regulatory locus 2* (*PRL2*)	RNA processing and modification
Bra029913	56.944	6.537	**Down**	AT3G48690	*Carboxylesterase 12* (*CXE12*)	Serine hydrolases hydrolyzing 2,4-D-methyl
Bra002042	8.613	3.164	**Down**	AT2G16720	*MYB domain protein 7* (*MYB7*)	Cell differentiation, regulation of flavanol biosynthetic process
Bra009231	2.731	0.958	**Down**	AT5G06820	*Strubbelig-receptor family 2* (*SRF2*)	Protein phosphorylation
Bra006422	1.419	0.580	**Down**	AT5G17800	*MYB56*	Negative regulation of cell division
Bra008175	134.316	6.473	**Down**	AT1G75030	*Thaumatin-like protein 3* (*TLP-3*)	Defense response
Bra002513	1.757	0.045	**Down**	AT5G60080	-	Protein phosphorylation
Bra009055	2.000	0.198	**Down**	AT5G10140	*Flowering locus C* (*FLC*)	Floral transition repression and temperature compensation of the circadian clock
Bra003995	1.451	0.393	**Down**	AT1G69560	*MYB105*	Boundary specification, meristem initiation and maintenance, and organ patterning
Bra006978	1.560	0.197	**Down**	AT3G53230	*Cell division cycle 48B* (*CDC48B*)	Mitotic spindle disassembly
Bra039531	0.449	1.612	Up	AT5G44700	*Gassho2* (*GSO2*)	Regulation of cell division and cell fate specification
Bra003889	1.895	4.182	Up	AT1G72180	*C-terminally encoded peptide (CEP)* receptor 2 (*CEPR2*)	Receptor for CEP1 peptide
Bra028006	8.508	19.272	Up	AT1G33590	-	Response to Karrikin, signal transduction
Bra017533	0.699	2.011	**Up**	AT5G46690	*Basic helix-loop-helix protein 71* (*bHLH071*)	Interacting with FAMA to regulate stomatal differentiation
Bra026499	0.661	1.526	**Up**	AT5G23400	-	Signal transduction
Bra011403	2.550	5.431	**Up**	AT4G32980	*Arabidopsis thaliana homeobox 1* (*ATH1*)	Regulation of gibberellin biosynthetic genes

The expression of genes was presented as fragments per kilobase of exon model per million mapped fragments. B line and P line refer to the fertile line 'Bcajh97-01B' and the Polima cytoplasmic male-sterile line 'Bcpol97-05A' of B. ampestris, respectively. Bold characters in the column "regulated" represent genes that showed the same expression change and non-bold ones represent genes that showed the opposite change in the Arabidopsis spl/nzz mutant and P line of B. ampestris. DEG, differentially expressed gene; TAIR, the Arabidopsis information resource; BRAD, Brassica database.

Arabidopsis can provide a reference to the function of genes in *B. campestris*. Integrated gene regulatory network (iGRN), a newly developed tool for transcription factors regulatory network prediction in *Arabidopsis* was used to investigate the relationship between homologs of the 72 P line-specific DEGs. Finally, 15 DEGs were screened out to form a regulatory network (**Figure 2C**). Twenty genes were found to interact with *Pistillata* (*PI*, *AT5G20240*) that controls the differentiation of petals and stamen, and 13 genes were found to interact with *Nutcracker* (*NUC*, *AT5G44160*) which affects flowering time *via* sugar metabolism (Bowman et al., 1989; Jeong et al., 2015). As the phenotype of the P line was similar to the *Arabidopsis spl/nzz* mutant, all P line-specific DEGs and the microarray data from anthers of *spl/nzz* were compared to discover more genes involved in anther cell differentiation (Wijeratne et al., 2007). Consequently, 16 common DEGs between *spl/nzz* and P line were identified and 13 of them showed the same expressional changes, among which six transcription factors (*FLC*, *bHLH071*, *ATH1*, *MYB56*, *MYB105*, and *MYB7*) were also identified with iGRN (**Table 1**). Five lncRNAs and three miRNAs were predicted to interact with seven DEGs (**Supplementary Data 2**). Notably, *Bra002042* (*MYB7*) were predicted to be the target of one lncRNA, *MSTRG.33978.1*, and two miRNAs, bra-miR159a and bra-miR319-3p (**Supplementary Data 2**).

Utilizing A Line We Selected Potential Transcripts Related to Cell Plate Formation During Meiotic Cytokinesis

Previous cytological observations showed that failure of tetrads formation in the A line was caused by the aberrant cytokinesis (Huang et al., 2009; Shen et al., 2019). To explore the network that participated in male meiotic cytokinesis, DEGs concerning it were selected *via* GO analysis, Swiss-Prot, and NR annotation. Finally, 13 DEGs, 11 of which were A line-specific and two were expressed in both A line and P line were identified (**Table 2**). Generally, dicotyledonous male meiocytes undergo simultaneous-type cytokinesis where cell plates determined by

TABLE 2 | Specifically expressed genes involved in cytoplasmic cell plate formation in '*Bcajh97-01A*' of *Brassica campestris*.

ID in BRAD	Expression in B line	Expression in A line	Regulated	Homologous genes in *Arabidopsis*		Swiss-Prot annotation	NR annotation
				ID in TAIR	Gene name		
Bra014865	50.911	25.592	Down	AT3G53750	Actin 3 (ACT3)	ACT3	ACT3
Bra033236	12.236	3.862	Down	AT1G01750	Actin-depolymerizing factor 10 (ADF10)	ADF10	A hypothetical ADF (CARUB_v10011760mg)
Bra020294	1.205	3.251	Up	AT5G59730	Exocyst subunit exo70 family protein H7 (EXO70H7)	–	EXO70H7
Bra031138	84.051	40.448	Down	AT2G20760	Clathrin light chain 1 (CLC1)	CLC1	A Hypothetical CLC protein (ARALDRAFT_900444)
Bra033472	2.534	6.372	Up	AT3G51890	CLC3	CLC3	CLC protein
Bra002635	0.141	0.672	Up	–	–	MAPKKK [Nicotiana protein kinase 1 (NPK1)]	Hypothetical MAPKKK A-like protein
Bra013771	0.638	0.255	Down	AT4G24170	–	Kinesin-like protein NPK1-activating kinase 1 (NACK1)	ATP binding microtubule motor family protein
Bra037232	2.729	1.305	Down	AT2G18170	Mitogen-activated protein kinase 7 (MAPK7)	MAPK7	P-loop containing nucleoside triphosphate hydrolases superfamily protein
Bra016220	2.731	1.439	Down	AT1G70430	–	MAPKK1	Kinase family protein
Bra021794	0.544	3.531	Up	AT2G32510	MAPKK kinase 17 (MAPKKK17)	MAPKKK3	MAPKKK17
Bra030001	0.187	0.927	Up	AT3G50310	MAPKKK20	MAPKKK20	MAPKKsK20
Bra034123	12.917	6.961	Down	AT3G10525	Siamese related 1 (SMR1)	Cyclin-dependent protein kinase inhibitor SMR1	Hypothetical protein (ARALDRAFT_478386)
Bra001367	12.750	6.011	Down	AT3G10525	SMR1	Cyclin-dependent protein kinase inhibitor SMR1	Unknown

The expression of genes was presented as fragments per kilobase of exon model per million mapped fragments. B line, the fertile line 'Bcajh97-01B'; A line, the genic male-sterile line 'Bcajh97-01A'; TAIR, the Arabidopsis information resource; BRAD, Brassica database.

radial microtubule arrays form between all four haploid nuclei at the same time (**Figure 3A**). As one of the main components of radial microtubule arrays, actin plays an important role in cytokinesis (De Storme and Geelen, 2013). *Bra014865* (*ACT3*) and *Bra033236* (*ADF10*) annotated to encode an actin protein and an actin-depolymerizing factor 10, respectively, were downregulated in A line (**Table 2**). Clathrin light protein was reported to be the coating materials of vesicles secreted from the Golgi/Trans-Golgi network in somatic cytokinesis (Buschmann and Muller, 2019). In A line, two genes, *Bra031138* (*Clathrin light chain 1*, *CLC1*) and *Bra033472* (*CLC3*) were annotated to encode clathrin light protein (**Table 2**). During cytokinesis, a fusion of vesicles carrying substances required for cell plate synthesis is a crucial process, which is regulated by the Exocyst complex (De Storme and Geelen, 2013). Mutation of Exocyst complex subunit EXO70A1 is compromised the initial cell plate assembly (Fendrych et al., 2010). In A line, *Bra020294* was annotated as the Exocyst subunit exo70 and downregulated in A line (**Table 2**). Moreover, genes responsible for callose synthesis were downregulated in the A line as well (see below **Figure 4**). Three lncRNAs interacted with *Bra033472* (*CLC3*) and *Bra033236* (*ADF10*), two of which were targeted *Bra033472* (*CLC3*) (**Supplementary Data 3**).

In mitotic cytokinesis, the phosphorylation of MAP65 protein affects the expansion of phragmoplast, which is regulated by a classical MAPK cascade signaling pathway (De Storme and Geelen, 2013). To explore the MAPK pathway involved in male meiosis of *B. campestris*, DEGs specifically expressed in A line were screened out and a putative cascade signaling pathway was proposed according to the annotation of DEGs (**Figure 3B**). In this cascade signaling pathway, three MAPKKKs (NPK1, MAPKKK17, and MAPKKK20) worked downstream of *Bra013771*, which was annotated as the kinesin-like protein NACK1; then, three MAPKKKs targeted MAPKK1 that was encoded by *Bra016220*, and subsequently, MAPK7 was activated to phosphate the protein MAP65. Expression analysis showed that the expression of *Bra037232* encoding the protein MAPK7 was decreased (**Supplementary Data 1**). Eleven lncRNAs were presumed to target three MAPKKKs (**Supplementary Data 3**). Seven of them targeted *Bra021794* (*MAPKKK17*) while two targeted *Bra002635* (*NPK1*) and two targeted *Bra030001* (*MAPKKK20*), respectively (**Supplementary Data 3**).

Transcripts Related to Pollen Wall Formation Showed Distinct Expression Patterns in Different Sterile Lines

Previous morphological observation showed that a rough and irregular surface rather than a reticulate exine structure existed on pollen grains in A line (Shen et al., 2019). Although the differentiation of sporogenous cells was arrested, a few anther sacs with withered pollen still reside in *Pol* CMS (An et al., 2014).

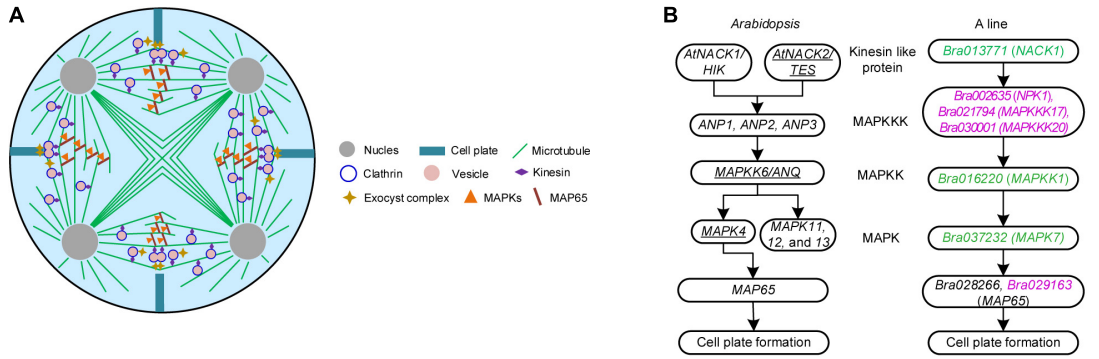

FIGURE 3 | Pathways concerning meiosis cytokinesis in *Brassica campestris*. **(A)** Schematic diagram of simultaneous-type plant male cytokinesis. **(B)** Mitogen-activated protein kinase signaling cascade mediating *de novo* cell plate formation in *Arabidopsis* and the genic male-sterile line '*Bcajh97-01A*' (A line) of *B. campestris*. The left was adapted from De Storme and Geelen (2013) and the right was a putative pathway hypothesized in this study. Underlined genes have been proved to function in male meiotic cytokinesis. Differentially expressed genes down and upregulated were colored in green and rose red, respectively. B line, the fertile line '*Bcajh97-01B*'; A line, the genic male-sterile line '*Bcajh97-01A*'; MAPKK, MAPK kinase; MAPKKK, MAPKK kinase; NACK1/2, Nicotiana protein kinase 1 (NPK1)-activating kinesin 1; HIK, hinkel; TES, tetraspore; ANP1/2/3, Arabidopsis NPK1-related protein kinase 1/2/3; ANQ, Arabidopsis Nicotiana kinase next to NPK1 (NQK1).

In the *Ogu* CMS line, the exine of pollen was thinner than that in the fertile line (Lin et al., 2019). To explore the network regulating the pollen wall formation, the expression levels of genes involved in the metabolism of pollen wall components in the three sterile lines were analyzed. In this study, sporopollenin and callose synthesis and degradation pathways were concluded based on (Shi et al., 2015), and cellulose and pectin synthesis pathways were drawn according to the Kyoto Encyclopedia of Genes and Genomes (KEGG) analysis.

A total of 32 DEGs were selected out and 13 for sporopollenin synthesis and transportation, 9 for the synthesis and degradation of callose, and 11 of them were responsible for the biosynthesis of pectin and cellulose (**Figure 4**). Compared with the B line, genes involved in sporopollenin synthesis and transportation like homolog genes of *Arabidopsis MS2*, *ACOS5*, and *CYP703A2* were downregulated in the P line, while most of them showed no differential expression in the A line and O line. The expression level of *Bra037213*, orthologs of *Arabidopsis Cals5*, was decreased in all sterile lines. *Bra025595*, which is isogenous with *Arabidopsis RPG1*, was also reduced in all three sterile lines. However, *Bra022761*, orthologs of *Arabidopsis RPG2* that shares a redundant function with *RPG1*, was downregulated in A line and P line but not in O line. The expression of *Bra029746*, a syngenic gene of *Defective in exine formation 1* (*DEX1*) encoding a membrane calcium-binding protein that is required for the primexine matrix formation, was decreased only in the O line. *Bra000704* and *Bra003378* are orthologs of *Arabidopsis FRK5* and *FRK7* encoding fructokinases that phosphorylate fructose in cellulose and pectin synthesis, respectively, were downregulated in all sterile lines. Furthermore, ncRNAs interacting with DEGs in the synthesis and/or degradation metabolism pathways of sporopollenin, cellulose, pectin, and callose were predicted. Finally, 29 lncRNAs and one miRNA significantly correlated with corresponding DEGs were obtained (**Supplementary Data 4**). Fifteen DEGs were targeted by only one lncRNAs, three targeted by two lncRNAs, and two targeted by three lncRNAs. In contrast to the similar expression pattern between *MSTRG.16387.1* and *Bra013041* (*AMS*), *MSTRG.16374.1* showed the reverse expression trend with *Bra013041* (*AMS*).

Tapetum Degradation-Related Genes Were Downregulated in Three Sterile Lines

It has been reported that tapetum cells in A line exhibited premature PCD after meiosis (Shen et al., 2019), however, in *Ogu* CMS, tapetum cells became vacuolized and elongated radially at the uninucleate stage with delayed degradation (Kang et al., 2014; Xing et al., 2018). To unearth the underlying regulatory network of tapetum development, the expression of genes related to it in the three sterile lines was analyzed. Thirty protein-coding genes were included based on (Parish and Li, 2010). Among these genes, 12 of them were DEGs (**Figure 5**). Further analysis of gene expression changes showed that 11 of them were downregulated in the P line, half in the O line, and only four in the A line. Compared with the B line, all homogenous genes to the *DYT1-TDF1-AMS-MYB80-MS1* pathway except *Bra013519* (*DYT1*) were downregulated in the P line. Expression of genes correlated with tapetum formation and differentiation was not discrepant in the O line and A line, but the expression of genes interrelated with tapetum degradation declined in the two sterile lines. All copies of three homogenous genes of *Arabidopsis VGD1*, *GLOX1*, and *RD19C* relevant to tapetum degradation were downregulated, but *Bra000615*, a homolog to *CEP1*, was upregulated in the O line (**Figure 5**).

ncRNAs that interact with protein-coding genes in the network were selected out *via* target prediction and expression correlation analysis. Finally, 21 lncRNAs and one miRNA targeted 14 DEGs were obtained (**Supplementary Data 5**). The expression of *Bra025337* (*TDF1*) was negatively related to a newly defined miRNA, unconservative_A03_9803 (P = 0.039). Three lncRNAs, *MSTRG.33891.1*, *MSTRG.33874.2*, and

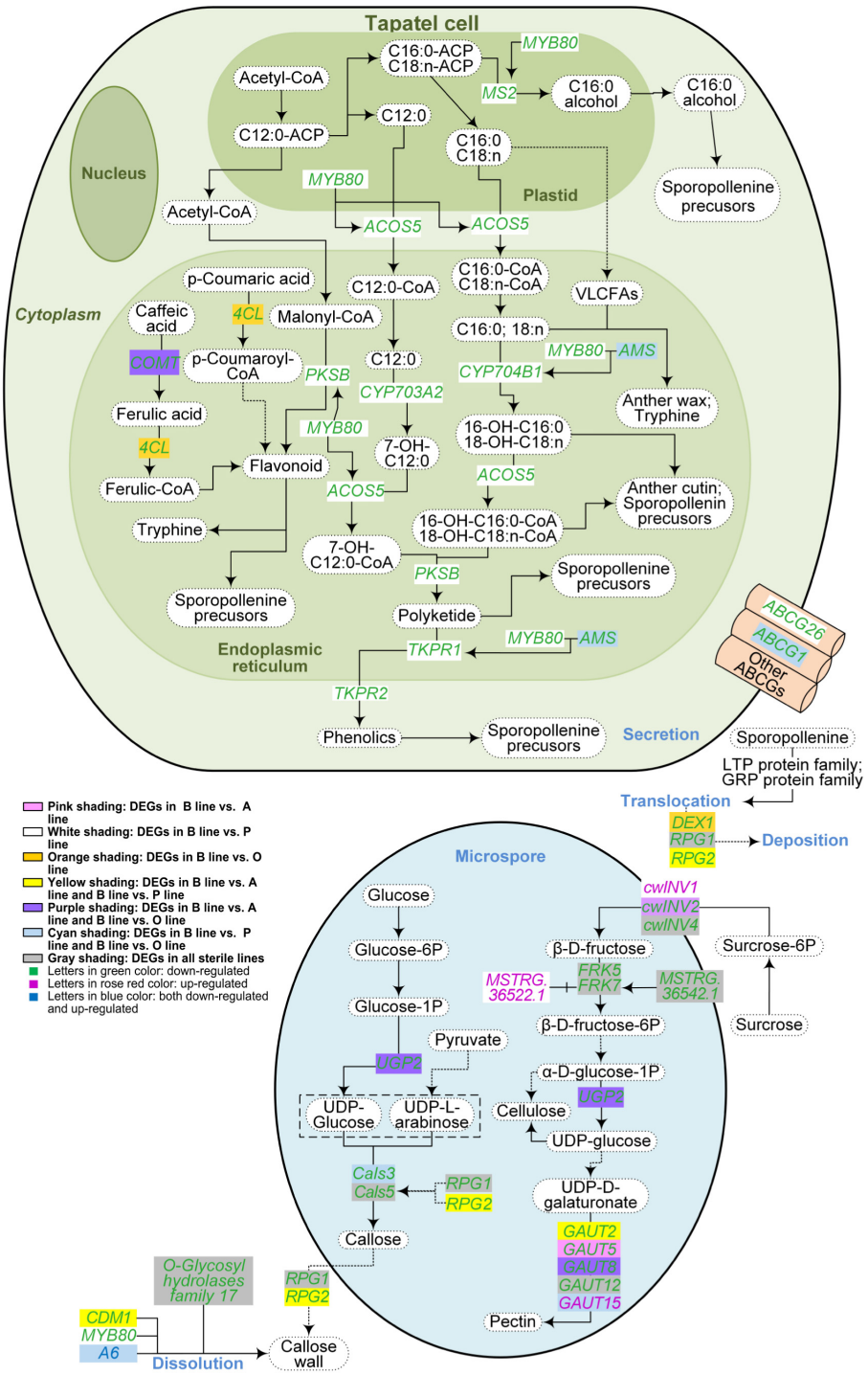

FIGURE 4 | Metabolism pathways of pollen wall components in the three sterile lines of *Brassica campestris*. Differentially expressed genes associated with the metabolism of sporopollenin, cellulose, pectin, and callose were indicated in the figure. The solid arrows represent a direct relationship, and the dotted arrows indicate an indirect relationship. B line, the fertile line '*Bcajh97-01B*'; A line, the genic male-sterile line '*Bcajh97-01A*'; P line, the *Polima* cytoplasmic male-sterile line '*Bcpol97-05A*'; O line, the *Ogura* cytoplasmic male-sterile line '*Bcogu97-06A*'; MYB80, MYB domain protein 80; MS2, male sterility 2; ACOS5, acyl-CoA synthetase 5; COMT, caffeate O-methyltransferase; 4CL, 4-coumarate:CoA ligase; PKSB, polyketide synthase B; CYP703A2, cytochrome p450 family 703 subfamilies A polypeptide 2; CYP704B1, cytochrome p450 family 704 subfamily B polypeptide 1; AMS, aborted microspores; VLCFAs, very-long-chain fatty acids; TKPR1/2, tetraketide α-pyrone reductase 1/2; ABCG, Adenosine triphosphate (ATP)-binding cassette, subfamily G; UGP, uridine diphosphate (UDP)-glucose pyrophosphorylase; Cals, callose synthase; DEX1, defective in exine formation 1; RPG1/2, ruptured pollen grain 1/2; CDM1, callose defective microspore 1; cwINV, cell wall invertase; FRK, fructokinase; GAUT, galacturonosyl transferase.

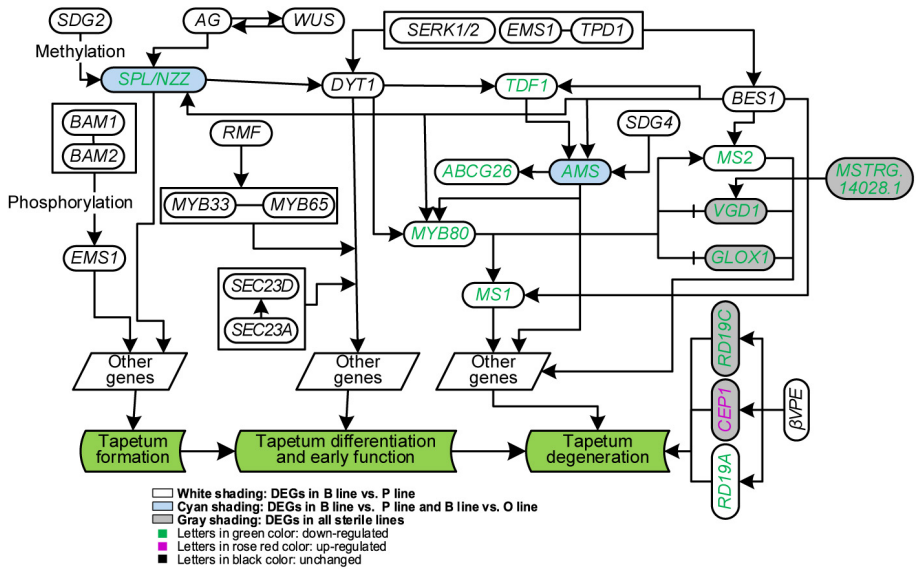

FIGURE 5 | Analysis of genes in tapetum development of *Brassica campestris*. Genes in the same box were worked together to regulate downstream genes. B line, the fertile line '*Bcajh97-01B*'; P line, the *Polima* cytoplasmic male-sterile line '*Bcpol97-05A*'; O line, the *Ogura* cytoplasmic male-sterile line '*Bcogu97-06A*.' SDG2/4, SET domain protein 2/4; BAM1/2, β-amylase 1/2; AG, agamous; WUS, wuschel; SPL/NZZ, sporocyteless/nozzle; RMF, reduced male fertility; MYB33/65, MYB domain protein 33/65; DYT1, dysfunctional tapetum 1; SERK1/2, somatic embryogenesis receptor-like kinase 1/2; EMS1, excess microsporocytes 1; TPD1, tapetum determinant 1; TDF1, defective in tapetal development and function 1; ABCG26, Adenosine triphosphate (ATP)-binding cassette subfamily G 26; AMS, Aborted microspores; MYB80, MYB domain protein 80; MS1/2, male sterility 1/2; VGD1, Vanguard 1; GLOX1, Glyoxal oxidase 1; CEP1, cysteine endopeptidase 1; βVPE, β vacuolar processing enzyme.

MSTRG.33884.1 were found to target the meristem control gene *Bra039894* (*WUS*).

Extensive Interactions Between DELs and miRNAs Were Found During Anther and Pollen Development

LncRNAs and miRNAs have been shown to play critical roles in regulating gene expression *via* complex interaction networks (Han et al., 2021). To further investigate their functions in anther/pollen development, the interaction between DELs and miRNAs in the three sterile lines was explored. As a result, 35 DELs were predicted to interact with miRNAs, with most of which were identified in P line (23), followed by O line (21), and the least in A line (11) (**Table 3**). Twenty-eight DELs were putative targets of 43 miRNAs. Notably, six common DELs targeted by miRNAs were downregulated in the three sterile lines. Although 47 lncRNAs were predicted to work as eTMs for miRNA, only *MSTRG.30876.5* was DEL in the P line and O line, and no DEL functioned as eTM was found in the A line (**Table 3** and **Supplementary Data 6**). Another six DELs were identified as host genes of nine miRNAs according to the similarity of sequences. Two lncRNAs, *MSTRG.50087.1* and *MSTRG.44699.1* (renamed as *bra-miR156HG* and *bra-miR5718HG*) were predicted to work as host genes for bra-miR156 and bra-miR5718, respectively (**Supplementary Figure 3** and **Supplementary Data 6**).

miR156 is a conserved miRNA in plants, which is widely known to participate in diverse processes of plant growth and development, especially vegetative phase change in *Arabidopsis* (He et al., 2018). miR5718 has been reported to respond to heat stress in *B. campestris* (Yu et al., 2012). In the inflorescences of *B. campestris*, the expression pattern of these two lncRNAs was positively correlated with that of *bra-miR156* ($P = 0.005$) and *bra-miR5718* ($P = 0.003$) (**Figure 6A**), respectively. To confirm whether *bra-miR156HG* and *bra-miR5718HG* could generate corresponding miRNAs or not, the fragments of the two lncRNAs were inserted into the pBI121 vector (**Figure 6B**), respectively, and a transient transformation assay in tobacco was performed. Semi-quantitative RT-PCR showed that both lncRNAs were successfully expressed in tobacco leaves (**Figure 6C**). The expression levels of bra-miR156 and bra-miR5718 were significantly increased in leaves injected with relevant specific fragments of host genes (**Figure 6D**). These results proved that *bra-miR156HG* and *bra-miR5718HG* can generate mature miRNAs *in vivo*.

Overexpression of *bra-miR5718HG* in *Brassica campestris* Upregulated *bra-miR5718* and Affected Pollen Tube Growth and Seed Set

To answer whether the host gene of miRNA would function in pollen development or not, we created the *bra-miR5718HG*-overexpressed transgenic plants in *B. campestris*. Two transgenic lines, namely OE-83 and OE-91, with successful overexpression were obtained. The expression of bra-miR5718 was correspondingly increased while its target gene *braPAP10*

TABLE 3 | Summary of differentially expressed lncRNAs acting as miRNAs' targets, precursors, and eTMs in *Brassica campestris*.

miRNA	Different roles of DELs								
	eTM			Target			Host gene		
	A line	P line	O line	A line	P line	O line	A line	P line	O line
Bra-miR156c	–	–	–	–	–	–	–	*MSTRG.50087.1*	–
Bra-miR156f	–	–	–	–	–	–	–	*MSTRG.50087.1*	–
Bra-miR158-5p	–	–	–	–	*MSTRG.20734.1*	*MSTRG.20734.1; MSTRG.20734.2*	–	–	–
Bra-miR162-5p	–	***MSTRG.30876.5***	*MSTRG.30876.5*	–	–	–	–	–	–
Bra-miR403-5p	–	–	–	***MSTRG.13936.3***	–	–	–	–	–
Bra-miR408-3p	–	–	–	*MSTRG.39657.1*	*MSTRG.39657.1*	–	–	–	–
Bra-miR5712	–	–	–	*MSTRG.6099.1*	*MSTRG.6099.1*	*MSTRG.6099.1*	–	–	–
Bra-miR5719	–	–	–	–	***MSTRG.55412.1***	***MSTRG.55412.1***	–	–	–
Bra-miR9408-3p	–	–	–	***MSTRG.12676.1***	–	–	–	–	–
Bra-miR9558-3p	–	–	–	–	–	***MSTRG.7520.4***	–	–	–
Bra-miR9562-5p	–	–	–	–	–	***MSTRG.7012.1***	–	–	–
Unconservative_A01_124	–	–	–		–	–	–	*MSTRG.50087.1*	–
Unconservative_A01_2822	–	–	–	***MSTRG.12676.1***	–	–	–	–	–
Unconservative_A01_337	–	–	–	*MSTRG.6099.1*	*MSTRG.6099.1*	*MSTRG.6099.1*	–	–	–
Unconservative_A01_3874	–	–	–	–	–	–	–	*MSTRG.10680.1; MSTRG.26529.1*	*MSTRG.10680.1*
Unconservative_A02_5263	–	–	–	–	*MSTRG.26116.1*	–	–	*MSTRG.21862.1*	–
Unconservative_A02_5624	–	–	–	–	–	***MSTRG.31712.2***	–	–	–
Unconservative_A02_9408	–	–	–	*MSTRG.47571.3*	***MSTRG.22869.1***	–	–	–	–
Unconservative_A02_9409	–	–	–	*MSTRG.47571.3*	***MSTRG.22869.1***	–	–	–	–
Unconservative_A03_10008	–	–	–	–	*MSTRG.20239.1*	–	–	–	–
Unconservative_A03_10228	–	–	–	*MSTRG.38026.1*	*MSTRG.38026.1*	*MSTRG.38026.1*	–	–	–
Unconservative_A03_10294	–	–	–	–	–	*MSTRG.17213.1*	–	–	–
Unconservative_A03_12816	–	–	–	*MSTRG.6099.1*	*MSTRG.6099.1*	*MSTRG.6099.1*	–	–	–
Unconservative_A03_13897	–	–	–	–	–	–	–	*MSTRG.50087.1*	–
Unconservative_A04_16774	–	–	–	–	***MSTRG.22869.1***	–	–	–	–
Unconservative_A04_16775	–	–	–	–	***MSTRG.22869.1***	–	–	–	–
Unconservative_A04_16989	–	–	–	–	–	–	–	–	–
Unconservative_A05_19537	–	–	–	***MSTRG.13936.3***	–	–	–	–	–
Unconservative_A05_21515	–	–	–	*MSTRG.16423.1*	*MSTRG.16423.1*	*MSTRG.16423.1*	–	–	–
Unconservative_A06_22943	–	–	–	–	***MSTRG.22869.1***	–	–	–	–
Unconservative_A06_23503	–	–	–	–	*MSTRG.26116.1*	–	–	–	–
Unconservative_A06_25032	–	–	–	–	***MSTRG.34516.1***	***MSTRG.34516.1***; *MSTRG.25360.2*	–	–	–
Unconservative_A06_25702	–	–	–	–	***MSTRG.22869.1***	–	–	–	–
Unconservative_A07_27582	–	–	–	–	*MSTRG.41319.2*	*MSTRG.41319.2*	–	–	–
Unconservative_A07_28347	–	–	–	–	*MSTRG.56775.1*	–	***MSTRG.25551.2***	*MSTRG.25551.3; MSTRG.25550.1*	*MSTRG.25550.1; MSTRG.25551.1; MSTRG.25551.3*
Unconservative_A07_29448	–	–	–	–	***MSTRG.22869.1***	–	–	–	–
Unconservative_A07_29750	–	–	–	–	***MSTRG.8026.1***	–	–	–	–
Unconservative_A07_29886	–	–	–	–	***MSTRG.8026.1***	–	–	–	–
Unconservative_A08_30911	–	–	–	***MSTRG.27755.1***	–	–	–	–	–
Unconservative_A08_33222	–	–	–	–	–	*MSTRG.25360.2*	–	–	–
Unconservative_A09_33893	–	–	–	–	***MSTRG.22869.1***	–	–	–	–
Unconservative_A09_36589	–	–	–	–	***MSTRG.22869.1***	–	–	–	–
Unconservative_A09_36656	–	–	–	–	–	–	–	*MSTRG.50087.1*	–
Unconservative_A09_40282	–	–	–	–	***MSTRG.22869.1***	–	–	–	–
Unconservative_A09_40283	–	–	–	–	***MSTRG.22869.1***	–	–	–	–
Unconservative_A10_40369	–	–	–	*MSTRG.51803.1*	*MSTRG.51803.1*	*MSTRG.51803.1*	–	–	–
Unconservative_A10_41812	–	–	–	–	***MSTRG.22869.1***	–	–	–	–
Unconservative_A10_41813	–	–	–	–	***MSTRG.22869.1***	–	–	–	–
Unconservative_A10_42634	–	–	–	–	***MSTRG.22869.1***	–	–	–	–
Unconservative_A10_42699	–	–	–	–	*MSTRG.56864.1*	*MSTRG.56864.1*	–	–	–
Unconservative_scaffold036722_49811	–	–	–	–	*MSTRG.21147.1*	–	–	–	–

Long non-coding RNAs (lncRNAs) in bold font were upregulated and lncRNAs non-bolded were downregulated in sterile lines. eTMs, endogenous target mimics; A line, the genic male-sterile line 'Bcajh97-01A'; P line, the Polima cytoplasmic male-sterile line 'Bcpol97-05A'; O line, the Ogura cytoplasmic male-sterile line 'Bcogu97-06A'.

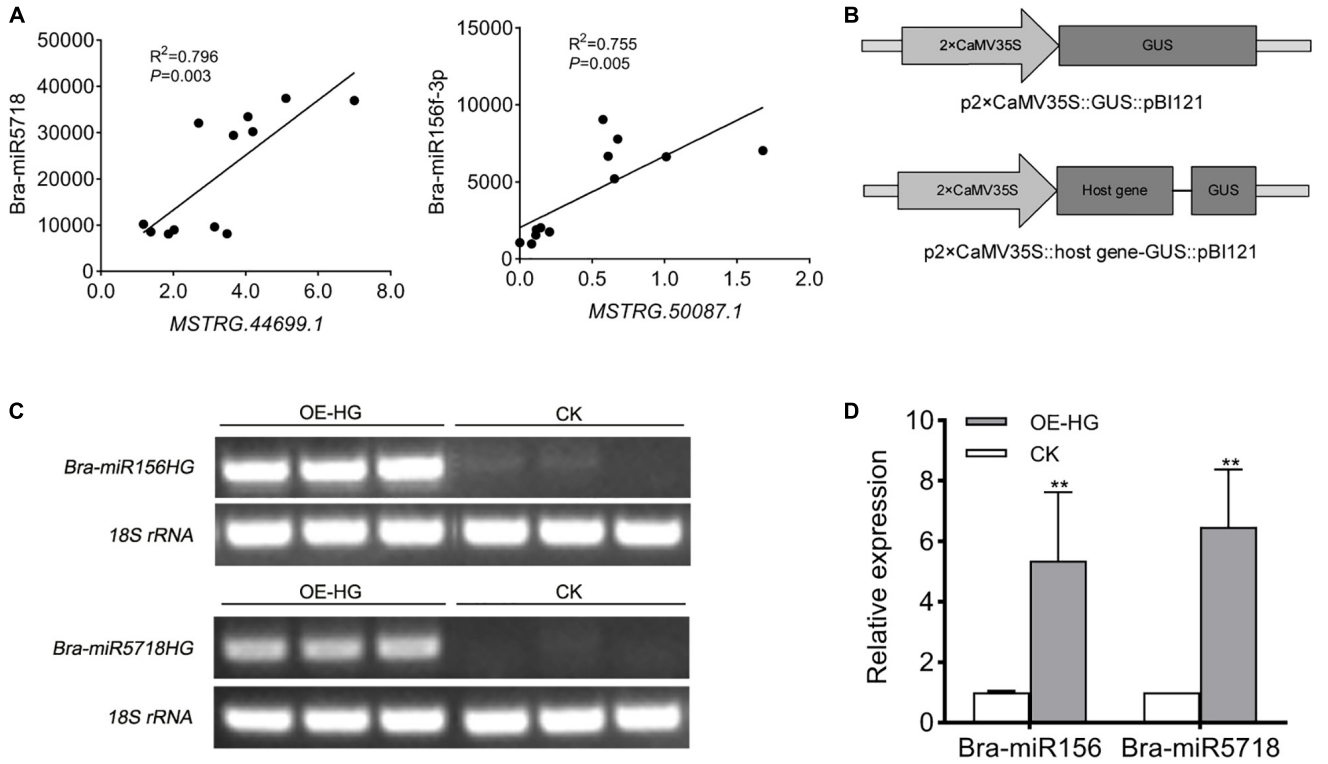

FIGURE 6 | LncRNAs, *bra-miR156HG* and *bra-miR5718HG*, worked as host genes for miR156 and miR5718 in *Brassica campestris*. **(A)** Expression correlation between *bra-miR5718HG* and *bra-miR156HG* and the corresponding miRNAs. **(B)** Structure of expression vectors used for transient agroinfiltration assay. **(C)** Semi reverse transcriptase PCR verifying the overexpression of lncRNAs in tobacco leaves. The lane of OE-HG represents samples containing corresponding lncRNA overexpression vectors. **(D)** Real-time quantitative PCR revealing the up-regulation of miR156 and miR5718. Data were presented as mean ± SD and the *t*-test was used for significance analysis. $^{**}P < 0.01$. Triplicate experiments were conducted. LncRNAs, long non-coding RNAs; miRNAs, microRNAs.

was downregulated in these lines (**Figure 7A**). Compared with wild type (WT), no obvious abnormality was observed during the vegetative phase, but the flowering time of transgenic plants was slightly delayed for 3 days (**Figure 7B**). Alexander staining of pollen grains showed that pollen viability was not affected in the two transgenic lines (**Figure 7C**). However, *in vitro* germination assay showed that the length of pollen tubes in transgenic plants was significantly shorter than that in WT plants, thus, a time-series *in vitro* germination assay was performed to observe the growth rate of pollen tubes in the transgenic plants. At 20 min after germination, the average pollen tube length of WT was 17.34 μm, yet it was 14.27 μm of OE-83 and OE-91 (**Figures 7D,E**). With the increase of germination time, the difference in pollen tube length was more obvious. The average pollen tube length of WT reached 74.95 μm at 60 min after germination, while it was only 64.27 μm of OE-83 and OE-91, which was significantly shortened ($P < 0.01$) (**Figures 7D,E**). Further, to see if the shorter pollen tubes affect seed set, take the line OE-83 as an example, we crossed OE-83 (♀) with WT (♂) through fertilizing the stigma of emasculated OE-83 (♀) flower buds with WT (♂) pollen grains. The resultant pollinated OE-83 (♀) flowers were 100% fertile and produced normal silique in which vigor seeds developed. By contrast, the reciprocal WT (♀) × OE-83 (♂) cross caused shorter silique and fewer seeds inside. Such infertility was also observed in OE-83 self-crossed plant but not in WT self-crossed plant. This result suggested that over-expression of *bra-miR5718HG* influenced the seed set in *B. campestris* (**Figures 7F,G**).

DISCUSSION

Whole Transcriptome Analysis Helps Us to Deeply Understand the Gene Regulation During Anther and Pollen Development in *Brassica* Crops

Sporocyte formation and meiosis are the early stages of pollen development. *SPL/NZZ* is required for the initiation of sporogenesis in *Arabidopsis* (Wijeratne et al., 2007). In the present study, *Bra026359* (*SPL/NZZ*) were degraded in P line. Analysis of P line-specific DEGs identified candidate genes for anther cell differentiation (**Figure 2A** and **Table 1**). Most of P line-specific DEGs were transcription factors and their homologous genes in *Arabidopsis* formed a network, in which PI seemed to target most genes. PI could form a higher-order heterotetrametric complex with Agamous-like 13 (AGL13)-AG-Apetala 3 (AP3)

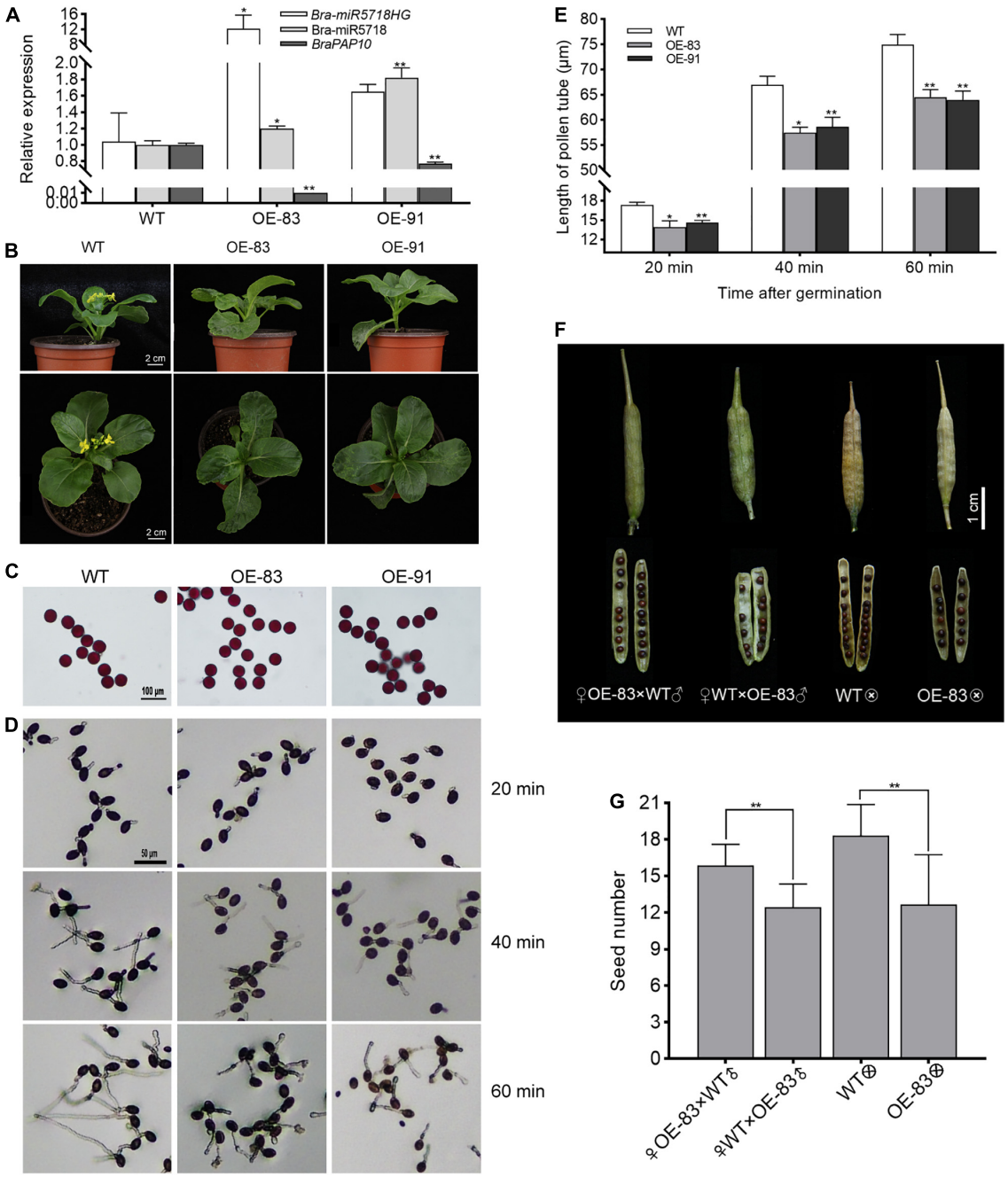

FIGURE 7 | *Bra-miR5718HG* slow down pollen tube growth *via* working as host genes for miR5718 in *B. campestris*. **(A)** Relative expression of *bra-miR5718HG*, bra-miR5718, and *braPAP10* in transgenic and wild-type (WT) plants. **(B)** Photograph of *bra-miR5718HG* overexpression transgenic lines and WT. **(C)** Alexander staining of pollen grains from *bra-miR5718HG* overexpressing plants in *B. camperstris*. **(D)** Representative photograph of pollen germination *in vitro* of overexpression lines and WT. **(E)** Pollen tubes length of overexpression lines and WT at different times after germination. **(F)** Representative photograph of siliques from reciprocal cross and self-cross of transgenic and WT plants. **(G)** statistics of seed number of siliques from reciprocal cross and self-cross of transgenic and WT plants. Data were presented as mean ± SD and the *t*-test was used for significance analysis. $^{**}P < 0.01$. Triplicate experiments were conducted.

to regulate the expression of *SPL/NZZ* (Hsu et al., 2014). Thirteen DEGs displayed the same expression changes between P line and *spl/nzz* mutant and half of them belong to the MYB or Receptor-like protein kinases (RLKs) families. MYB7, MYB56, and MYB105 were MYB family members who worked in different parts of the plant reproductive process. *AtMYB7* and its homologs *AtMYB4* affected pollen exine formation, *AtMYB56* negatively regulated the flowering time, and the double mutants of *AtMYB105* and *AtMYB117* presented disordered floral organ boundary specification, and meristem initiation and maintenance

(Lee et al., 2009; Chen et al., 2015; Wang et al., 2020). Serval RLKs have been studied in anther development including *Arabidopsis Excess microsporocytes 1 (EMS1)* and *Barely any meristem 1/2* (*BAM1/2*) (Cai and Zhang, 2018). Here, three members of RLKs, *STRUBBELIG-RECEPTOR FAMILY* (*SRF2*), *Gassho2* (*GSO2*), and *C-terminally encoded peptide (CEP) receptor 2* (*CEPR2*) have also been identified (**Table 1**). It was more diverse for the function of the three members. *AtSRF2* negatively affected plant fertility while *GSO2* and *CEPR2* regulate the morphological architecture of plant roots through sucrose response (Eyuboglu et al., 2007; Racolta et al., 2014; Dimitrov and Tax, 2018). Although its roles in anther cell differentiation remain to be explored, *GSO2* positively regulates root cell proliferation and differentiation (Racolta et al., 2014). Interactions between these transcription factors and *SPL*/*NZZ* will create new windows of pollen development.

Whole transcriptome analysis showed that expression changes of well-known networks in anther/pollen development varied in different male sterile lines with different abortion phenotypes (**Figures 4**, **5**). Pollen wall and tapetum are essential structures for functional pollen grains and the synthesis or regulatory pathways for them have been well studied (Parish and Li, 2010; Shi et al., 2015). In the A line and O line, most of the genes related to pectin, cellulose, and callose synthesis were downgraded. *Bra006395* (*UGP2*) was downregulated only in the two male sterile lines, A line and O line. UDP-glucose pyrophosphorylase (UGPase) catalyzes glucose-1-phosphate to UDP-glucose, which makes it a key enzyme in carbohydrate metabolism. Suppressing of *OsUGP1* and *OsUGP2* resulted in reduced callose production and delayed tapetum and middle layer degeneration, and further produced degenerated microspores (Chen et al., 2007). Strikingly, all orthologs of sporopollenin synthesis genes were downregulated in the P line. Considering that few pollen sacs were formed in the anthers of the P line as the standstill of cell differentiates, down-regulation of these genes may be caused by a decreased amount of pollen grains (An et al., 2014). The proper degradation of tapetum is essential for pollen wall formation and microspores maturation. In this study, the majority of tapetum development-related genes showed declined expression in the P line, while only genes that functioned in tapetum degradation were downregulated in the A line and O line.

Interplays Between mRNAs and ncRNAs Are Universal During Anther and Pollen Development

Although transcriptome analysis for different male-sterile lines has been performed in Cruciferae crops, such as cabbage (Kang et al., 2008), broccoli (Shu et al., 2018), and turnip (Lin et al., 2019), the participation of ncRNAs, especially newly defined lncRNAs, and the cross-talk between mRNAs and ncRNAs still need to be explored. The whole transcriptome sequencing in this study revealed that among the transcripts identified in the three male sterile lines of *B. campestris*, mRNAs were the most abundant transcripts. However, a considerable number of lncRNAs and miRNAs were also identified. Interestingly, the proportion of downregulated mRNAs and ncRNAs was significantly higher than that of the upregulated ones (**Figure 1**). It was inferred that most of the expressed genes and ncRNAs play a positive role in pollen development and lower expression of them contributed to the infertility of *B. campestris*.

LncRNA-mRNA interaction was found in pollen wall construction, tapetum development, anther cell differentiation, and pollen meiosis (**Figures 2–5** and **Supplementary Data 2–5**). Except for coding genes, lncRNA and miRNA have been proved to play a part in male sterility *via* forming complex interaction networks (Han et al., 2021). Interplays between lncRNAs and miRNAs are various. In this study, 35 DELs were predicted to be miRNA targets, eTMs, and precursors (**Table 3**). Among them, *bra-miR156HG* and *bra-miR5718HG* were experimentally validated to be miRNA precursors. In *Arabidopsis*, miR156 is the main factor for the phase change and is responsible for leaf morphology, trichome distribution, and lateral organogenesis (Zheng et al., 2019). Bra-miR5718 is a novel potential heat-responsive miRNA, which may also contribute to pollen development considering its relatively high expression level in *Ogu* CMS Chinese cabbages (Yu et al., 2012; Wei et al., 2015). Given the extremely significant positive correlation between the expression of two host genes and corresponding miRNAs, and the results of transient transformation assay, it can be assumed that *bra-miR156HG* and *bra-miR5718HG* generated the corresponding miRNAs *in vivo* (**Figure 6**).

Bra-miR5718HG Negatively Regulated Pollen Tube Growth in *Brassica campestris*

In the top30 GO enrichment items, "nucleus" and "plasma membrane" were included in most of the DEGs. Furtherer, we found that 461 DEGs were enriched to the term "pollen tube growth" (**Supplementary Figure 4**). Our transgenic assay revealed that overexpression of *bra-miR5718HG* led to the upregulation of bra-miR5718 and reduced expression of *braPAP10* (**Figure 7A**). Delayed pollen tube growth *in vitro* of the transgenic plants overexpressing *bra-miR5718HG* was observed, which resulted in shorter pollen tubes and finally caused less seed set in *B. campestris* (**Figures 7D–G**). *AtPAP10* (*AT2G16430*), the *Arabidopsis* homolog of *braPAP10*, is a member of the purple acid phosphorylase (PAP) family (Xie and Shang, 2018). PAPs are usually involved in the acquisition and distribution of phosphorus in plants, yet more functions of them have been revealed besides Pi deficiency adaption (Bhadouria and Giri, 2021). Overexpression of *AtPAP2* improved sucrose phosphate synthase (SPS) activity and the levels of sugars and tricarboxylic acid (TCA) metabolites, resulting in earlier bolting and higher seed yield (Sun et al., 2012). Interestingly, many PAPs showed relatively higher expression in reproductive tissues, and 21 PAP genes in *Arabidopsis* were detected expression in dry pollen and germinated pollen tubes in microarray analysis (Kuang et al., 2009; Qin et al., 2009; Xie and Shang, 2018). *AtPAP10*, *AtPAP18*, and *AtPAP27* were upregulated two or threefolds in the transcriptome of pollen tubes compared to the mature pollen, which meant that they might have a positive role in pollen tube growth (Yu et al., 2012). *AtPAP15* (*At3g07130*),

a PAP with phytase activity, showed an obvious GUS signal in mature pollen grains and germinated pollen tubes (Kuang et al., 2009). Consistent with its expression, mutants of *AtPAP15* presented lower pollen germination (30–35%) compared with WT (78%), which can be explained by its phytase activity since the major storage form of phosphorus in pollen grains is phytate (Kuang et al., 2009). Biochemical properties analysis of *AtPAP10* revealed that it has hydrolysis activity on ATP, ADP, dATP, pyrophosphate, polyphosphate, and phytate (Wang et al., 2011). In this study, shorter pollen tubes were observed in *bra-miR5718HG* overexpressing plants and the expression of *braPAP10* was downregulated. These results indicated that *braPAP10* may play a positive role in pollen tube growth of *B. campestris* and its expression was regulated by *bra-miR5718HG*.

Above all, it is apparent that interactions between mRNAs and ncRNAs, as well as different ncRNAs, are universal and widespread during pollen and anther development, and the discovery of these interactions can help to better understand the molecular mechanism underlying this process. Moreover, our study provides many candidate genes and ncRNAs, and further confirmation for the function and the interaction of them will unveil the complex network for pollen development.

DATA AVAILABILITY STATEMENT

The datasets presented in this study can be found in online repositories. The names of the repository/repositories and accession number(s) can be found below: https://www.ncbi.nlm.nih.gov/, PRJNA753197.

AUTHOR CONTRIBUTIONS

LH designed the research. DZ, ZJ, JWC, and DL analyzed the transcriptome data. DZ, CC, and TL generated the transgenic plants and performed the experiments. JSC constructed the male sterile lines. DZ, XX, SL, and LH wrote the manuscript. All authors have read and approved the manuscript.

FUNDING

This work was funded by the National Natural Science Foundation of China (Nos. 31872109, 32072587, and 31972418), the Grand Science and Technology Special Project of Zhejiang Province (No. 2021C02065), the Natural Science Foundation of Zhejiang Province (No. LY21C150004), and the Science and Technology Project of Jiaxing City (No. 201900012).

SUPPLEMENTARY MATERIAL

The Supplementary Material for this article can be found online at: https://www.frontiersin.org/articles/10.3389/fpls.2022.806865/full#supplementary-material

REFERENCES

An, H., Yang, Z., Yi, B., Wen, J., Shen, J., Tu, J., et al. (2014). Comparative transcript profiling of the fertile and sterile flower buds of pol CMS in *B. napus*. *BMC Genomics* 15:258. doi: 10.1186/1471-2164-15-258

Bhadouria, J., and Giri, J. (2021). Purple acid phosphatases: roles in phosphate utilization and new emerging functions. *Plant Cell Rep*. doi: 10.1007/s00299-021-02773-7

Bowman, J. L., Smyth, D. R., and Meyerowitz, E. M. (1989). Genes directing flower development in *Arabidopsis*. *Plant Cell* 1, 37–52. doi: 10.1105/tpc.1.1.37

Buschmann, H., and Muller, S. (2019). Update on plant cytokinesis: rule and divide. *Curr. Opin. Plant Biol.* 52, 97–105. doi: 10.1016/j.pbi.2019.07.003

Cai, W., and Zhang, D. (2018). The role of receptor-like kinases in regulating plant male reproduction. *Plant Reprod.* 31, 77–87. doi: 10.1007/s00497-018-0332-7

Casero, D., Sandoval, S., Seet, C. S., Scholes, J., Zhu, Y., Ha, V. L., et al. (2015). LncRNA profiling of human lymphoid progenitors reveals transcriptional divergence of B and T lineages. *Nat. Immunol.* 16, 1282–1291. doi: 10.1038/ni.3299

Chen, L. Y., Bernhardt, A., Lee, J., and Hellmann, H. (2015). Identification of *Arabidopsis* MYB56 as a novel substrate for CRL3(BPM) E3 ligases. *Mol. Plant* 8, 242–250. doi: 10.1016/j.molp.2014.10.004

Chen, R. Z., Zhao, X., Shao, Z., Wei, Z., Wang, Y. Y., Zhu, L. L., et al. (2007). Rice UDP-glucose pyrophosphorylase1 is essential for pollen callose deposition and its cosuppression results in a new type of thermosensitive genic male sterility. *Plant Cell* 19, 847–861. doi: 10.1105/tpc.106.044123

Cheng, Z., Guo, X., Zhang, J., Liu, Y., Wang, B., Li, H., et al. (2020). betaVPE is involved in tapetal degradation and pollen development by activating proprotease maturation in *Arabidopsis thaliana*. *J. Exp. Bot.* 71, 1943–1955. doi: 10.1093/jxb/erz560

De Storme, N., and Geelen, D. (2013). Cytokinesis in plant male meiosis. *Plant Signal. Behav.* 8:e23394. doi: 10.4161/psb.23394

Dimitrov, I., and Tax, F. E. (2018). Lateral root growth in *Arabidopsis* is controlled by short and long distance signaling through the LRR RLKs XIP1/CEPR1 and CEPR2. *Plant Signal. Behav.* 13:e1489667. doi: 10.1080/15592324.2018.1489667

Ding, J., Lu, Q., Ouyang, Y., Mao, H., Zhang, P., Yao, J., et al. (2012). A long noncoding RNA regulates photoperiod-sensitive male sterility, an essential component of hybrid rice. *Proc. Natl. Acad. Sci. U.S.A.* 109, 2654–2659. doi: 10.1073/pnas.1121374109

Dong, X. Y., Hong, Z. L., Sivaramakrishnan, M., Mahfouz, M., and Verma, D. P. S. (2005). Callose synthase (CalS5) is required for exine formation during microgametogenesis and for pollen viability in *Arabidopsis*. *Plant J.* 42, 315–328. doi: 10.1111/j.1365-313X.2005.02379.x

Eyuboglu, B., Pfister, K., Haberer, G., Chevalier, D., Fuchs, A., Mayer, K. F. X., et al. (2007). Molecular characterisation of the STRUBBELIG-RECEPTOR FAMILY of genes encoding putative leucine-rich repeat receptor-like kinases in *Arabidopsis thaliana*. *BMC Plant Biol.* 7:16. doi: 10.1186/1471-2229-7-16

Fendrych, M., Synek, L., Pecenkova, T., Toupalova, H., Cole, R., Drdova, E., et al. (2010). The *Arabidopsis* exocyst complex is involved in cytokinesis and cell plate maturation. *Plant Cell* 22, 3053–3065. doi: 10.1105/tpc.110.074351

Hafidh, S., and Honys, D. (2021). Reproduction multitasking: the male gametophyte. *Annu. Rev. Plant Biol.* 72, 581–614. doi: 10.1146/annurev-arplant-080620-021907

Han, Y., Zhao, Y., Wang, H., Zhang, Y., Ding, Q., and Ma, L. (2021). Identification of ceRNA and candidate genes related to fertility conversion of TCMS line YS3038 in wheat. *Plant Physiol. Biochem.* 158, 190–207. doi: 10.1016/j.plaphy.2020.10.037

He, J., Xu, M., Willmann, M. R., McCormick, K., Hu, T., Yang, L., et al. (2018). Threshold-dependent repression of SPL gene expression by miR156/miR157 controls vegetative phase change in *Arabidopsis thaliana*. *PLoS Genet.* 14:e1007337. doi: 10.1371/journal.pgen.1007337

Hsu, W. H., Yeh, T. J., Huang, K. Y., Li, J. Y., Chen, H. Y., and Yang, C. H. (2014). AGAMOUS-LIKE13, a putative ancestor for the E functional genes,

specifies male and female gametophyte morphogenesis. *Plant J.* 77, 1–15. doi: 10.1111/tpj.12363

Huang, L., Cao, J., Ye, W., Liu, T., Jiang, L., and Ye, Y. (2008). Transcriptional differences between the male-sterile mutant bcms and wild-type *Brassica campestris* ssp. *chinensis* reveal genes related to pollen development. *Plant Biol.* 10, 342–355. doi: 10.1111/j.1438-8677.2008.00039.x

Huang, L., Dong, H., Zhou, D., Li, M., Liu, Y., Zhang, F., et al. (2018). Systematic identification of long non-coding RNAs during pollen development and fertilization in *Brassica rapa*. *Plant J.* 96, 203–222. doi: 10.1111/tpj.14016

Huang, L., Ye, W. Z., Liu, T. T., and Cao, J. S. (2009). Characterization of the male-sterile line Bcajh97-01A/B and identification of candidate genes for genic male sterility in Chinese cabbage-pak-choi. *J. Am. Soc. Hortic. Sci.* 134, 632–640. doi: 10.21273/Jashs.134.6.632

Jeong, E. Y., Seo, P. J., Woo, J. C., and Park, C. M. (2015). AKIN10 delays flowering by inactivating IDD8 transcription factor through protein phosphorylation in *Arabidopsis*. *BMC Plant Biol.* 15:110. doi: 10.1186/s12870-015-0503-8

Jiang, J., Zhang, Z., and Cao, J. (2013). Pollen wall development: the associated enzymes and metabolic pathways. *Plant Biol.* 15, 249–263. doi: 10.1111/j.1438-8677.2012.00706.x

Johnson, M. A., Harper, J. F., and Palanivelu, R. (2019). A fruitful journey: pollen tube navigation from germination to fertilization. *Annu. Rev. Plant Biol.* 70, 809–837. doi: 10.1146/annurev-arplant-050718-100133

Kang, J., Zhang, G., Bonnema, G., Fang, Z., and Wang, X. (2008). Global analysis of gene expression in flower buds of Ms-cd1 *Brassica oleracea* conferring male sterility by using an *Arabidopsis* microarray. *Plant Mol. Biol.* 66, 177–192. doi: 10.1007/s11103-007-9261-9

Kang, J. E., Guo, Y. Y., Chen, Y. J., Li, H. L., Zhang, L., and Liu, H. X. (2014). Upregulation of the AT-hook DNA binding gene BoMF2 in OguCMS anthers of *Brassica oleracea* suggests that it encodes a transcriptional regulatory factor for anther development. *Mol. Biol. Rep.* 41, 2005–2014. doi: 10.1007/s11033-014-3048-2

Ke, L. L., Zhou, Z. W., Xu, X. W., Wang, X., Liu, Y. L., Xu, Y. T., et al. (2019). Evolutionary dynamics of lincRNA transcription in nine citrus species. *Plant J.* 98, 912–927. doi: 10.1111/tpj.14279

Kuang, R. B., Chan, K. H., Yeung, E., and Lim, B. L. (2009). Molecular and biochemical characterization of AtPAP15, a purple acid phosphatase with phytase activity, in *Arabidopsis*. *Plant Physiol.* 151, 199–209. doi: 10.1104/pp.109.143180

Lee, D. K., Geisler, M., and Springer, P. S. (2009). LATERAL ORGAN FUSION1 and LATERAL ORGAN FUSION2 function in lateral organ separation and axillary meristem formation in *Arabidopsis*. *Development* 136, 2423–2432. doi: 10.1242/dev.031971

Liang, Y., Zhang, Y., Xu, L., Zhou, D., Jin, Z., Zhou, H., et al. (2019). CircRNA expression pattern and ceRNA and miRNA-mRNA networks involved in anther development in the CMS line of *Brassica campestris*. *Int. J. Mol. Sci.* 20:4808. doi: 10.3390/ijms20194808

Lin, S., Miao, Y., Su, S., Xu, J., Jin, L., Sun, D., et al. (2019). Comprehensive analysis of Ogura cytoplasmic male sterility-related genes in turnip (*Brassica rapa* ssp. *rapifera*) using RNA sequencing analysis and bioinformatics. *PLoS One* 14:e0218029. doi: 10.1371/journal.pone.0218029

Ma, Z., Jiang, J., Hu, Z., Lyu, T., Yang, Y., Jiang, J., et al. (2017). Over-expression of miR158 causes pollen abortion in *Brassica campestris* ssp. *chinensis*. *Plant Mol. Biol.* 93, 313–326. doi: 10.1007/s11103-016-0563-7

Meng, X., Li, A., Yu, B., and Li, S. (2021). Interplay between miRNAs and lncRNAs: mode of action and biological roles in plant development and stress adaptation. *Comput. Struct. Biotechnol. J.* 19, 2567–2574. doi: 10.1016/j.csbj.2021.04.062

Murmu, J., Bush, M. J., DeLong, C., Li, S., Xu, M., Khan, M., et al. (2010). Arabidopsis basic leucine-zipper transcription factors TGA9 and TGA10 interact with floral glutaredoxins ROXY1 and ROXY2 and are redundantly required for anther development. *Plant Physiol.* 154, 1492–1504. doi: 10.1104/pp.110.159111

Parish, R. W., and Li, S. F. (2010). Death of a tapetum: a programme of developmental altruism. *Plant Sci.* 178, 73–89. doi: 10.1016/j.plantsci.2009.11.001

Phan, H. A., Iacuone, S., Li, S. F., and Parish, R. W. (2011). The MYB80 transcription factor is required for pollen development and the regulation of tapetal programmed cell death in *Arabidopsis thaliana*. *Plant Cell* 23, 2209–2224. doi: 10.1105/tpc.110.082651

Qin, Y., Leydon, A. R., Manziello, A., Pandey, R., Mount, D., Denic, S., et al. (2009). Penetration of the stigma and style elicits a novel transcriptome in pollen tubes, pointing to genes critical for growth in a pistil. *PLoS Genet.* 5:e1000621. doi: 10.1371/journal.pgen.1000621

Racolta, A., Bryan, A. C., and Tax, F. E. (2014). The receptor-like kinases GSO1 and GSO2 together regulate root growth in *Arabidopsis* through control of cell division and cell fate specification. *Dev. Dyn.* 243, 257–278. doi: 10.1002/dvdy.24066

Shen, X., Xu, L., Liu, Y., Dong, H., Zhou, D., Zhang, Y., et al. (2019). Comparative transcriptome analysis and ChIP-sequencing reveals stage-specific gene expression and regulation profiles associated with pollen wall formation in *Brassica rapa*. *BMC Genomics* 20:264. doi: 10.1186/s12864-019-5637-x

Shi, J., Cui, M., Yang, L., Kim, Y. J., and Zhang, D. (2015). Genetic and biochemical mechanisms of pollen wall development. *Trends Plant Sci.* 20, 741–753. doi: 10.1016/j.tplants.2015.07.010

Shu, J., Zhang, L., Liu, Y., Li, Z., Fang, Z., Yang, L., et al. (2018). Normal and abortive buds transcriptomic profiling of *Broccoli ogu* cytoplasmic male sterile line and its maintainer. *Int. J. Mol. Sci.* 19:2501. doi: 10.3390/ijms19092501

Sun, F., Suen, P. K., Zhang, Y. J., Liang, C., Carrie, C., Whelan, J., et al. (2012). A dual-targeted purple acid phosphatase in *Arabidopsis thaliana* moderates carbon metabolism and its overexpression leads to faster plant growth and higher seed yield. *New Phytol.* 194, 206–219. doi: 10.1111/j.1469-8137.2011.04026.x

Sun, M. X., Huang, X. Y., Yang, J., Guan, Y. F., and Yang, Z. N. (2013). *Arabidopsis* RPG1 is important for primexine deposition and functions redundantly with RPG2 for plant fertility at the late reproductive stage. *Plant Reprod.* 26, 83–91. doi: 10.1007/s00497-012-0208-1

Walbot, V., and Egger, R. L. (2016). Pre-meiotic anther development: cell fate specification and differentiation. *Annu. Rev. Plant Biol.* 67, 365–395. doi: 10.1146/annurev-arplant-043015-111804

Wang, L. S., Li, Z., Qian, W. Q., Guo, W. L., Gao, X., Huang, L. L., et al. (2011). The *Arabidopsis* purple acid phosphatase AtPAP10 is predominantly associated with the root surface and plays an important role in plant tolerance to phosphate limitation. *Plant Physiol.* 157, 1283–1299. doi: 10.1104/pp.111.183723

Wang, M., Wu, H. J., Fang, J., Chu, C. C., and Wang, X. J. (2017). A long noncoding RNA involved in rice reproductive development by negatively regulating osa-miR160. *Sci. Bull.* 62, 470–475. doi: 10.1016/j.scib.2017.03.013

Wang, X. C., Wu, J., Guan, M. L., Zhao, C. H., Geng, P., and Zhao, Q. (2020). *Arabidopsis* MYB4 plays dual roles in flavonoid biosynthesis. *Plant J.* 101, 637–652. doi: 10.1111/tpj.14570

Wei, X. C., Zhang, X. H., Yao, Q. J., Yuan, Y. X., Li, X. X., Wei, F., et al. (2015). The miRNAs and their regulatory networks responsible for pollen abortion in Ogura-CMS Chinese cabbage revealed by high-throughput sequencing of miRNAs, degradomes, and transcriptomes. *Front. Plant Sci.* 6:891. doi: 10.3389/fpls.2015.00894

Wijeratne, A. J., Zhang, W., Sun, Y., Liu, W., Albert, R., Zheng, Z., et al. (2007). Differential gene expression in *Arabidopsis* wild-type and mutant anthers: insights into anther cell differentiation and regulatory networks. *Plant J.* 52, 14–29. doi: 10.1111/j.1365-313X.2007.03217.x

Xie, L. L., and Shang, Q. M. (2018). Genome-wide analysis of purple acid phosphatase structure and expression in ten vegetable species. *BMC Genomics* 19:646. doi: 10.1186/s12864-018-5022-1

Xing, M., Sun, C., Li, H., Hu, S., Lei, L., and Kang, J. (2018). Integrated analysis of transcriptome and proteome changes related to the Ogura cytoplasmic male sterility in cabbage. *PLoS One* 13:e0193462. doi: 10.1371/journal.pone.0193462

Xing, S., Salinas, M., Hohmann, S., Berndtgen, R., and Huijser, P. (2010). miR156-targeted and nontargeted SBP-box transcription factors act in concert to secure male fertility in *Arabidopsis*. *Plant Cell* 22, 3935–3950. doi: 10.1105/tpc.110.079343

Yang, C. Y., Spielman, M., Coles, J. P., Li, Y., Ghelani, S., Bourdon, V., et al. (2003). TETRASPORE encodes a kinesin required for male meiotic cytokinesis in *Arabidopsis*. *Plant J.* 34, 229–240. doi: 10.1046/j.1365-313X.2003.01713.x

Yang, W. C., Ye, D., Xu, J., and Sundaresan, V. (1999). The SPOROCYTELESS gene of *Arabidopsis* is required for initiation of sporogenesis and encodes a novel nuclear protein. *Gene Dev.* 13, 2108–2117. doi: 10.1101/gad.13.16.2108

Ye, C. Y., Xu, H., Shen, E., Liu, Y., Wang, Y., Shen, Y., et al. (2014). Genome-wide identification of non-coding RNAs interacted with microRNAs in soybean. *Front. Plant. Sci.* 5:743. doi: 10.3389/fpls.2014.00743

Yu, X., Wang, H., Lu, Y., de Ruiter, M., Cariaso, M., Prins, M., et al. (2012). Identification of conserved and novel microRNAs that are responsive to heat stress in *Brassica rapa*. *J. Exp. Bot.* 63, 1025–1038. doi: 10.1093/jxb/err337

Zeng, Q. N., Chen, J. G., and Ellis, B. E. (2011). AtMPK4 is required for male-specific meiotic cytokinesis in *Arabidopsis*. *Plant J.* 67, 895–906. doi: 10.1111/j.1365-313X.2011.04642.x

Zheng, C., Ye, M., Sang, M., and Wu, R. (2019). A regulatory network for miR156-SPL module in *Arabidopsis thaliana*. *Int. J. Mol. Sci.* 20:6166. doi: 10.3390/ijms20246166

Conflict of Interest: The authors declare that the research was conducted in the absence of any commercial or financial relationships that could be construed as a potential conflict of interest.

Publisher's Note: All claims expressed in this article are solely those of the authors and do not necessarily represent those of their affiliated organizations, or those of the publisher, the editors and the reviewers. Any product that may be evaluated in this article, or claim that may be made by its manufacturer, is not guaranteed or endorsed by the publisher.

frontiers in Plant Science

ORIGINAL RESEARCH
published: 08 March 2022
doi: 10.3389/fpls.2022.767339

A Plastid-Bound Ankyrin Repeat Protein Controls Gametophyte and Early Embryo Development in *Arabidopsis thaliana*

Katarína Kulichová[1†‡], Janto Pieters[1], Vinod Kumar[1], David Honys[1,2†] and Said Hafidh[1†‡]*

[1] Laboratory of Pollen Biology, Institute of Experimental Botany of the Czech Academy of Sciences, Prague, Czechia,
[2] Department of Plant Experimental Biology, Faculty of Science, Charles University, Prague, Czechia

OPEN ACCESS

Edited by:
Paloma Moncaleán,
Neiker-Tecnalia, Spain

Reviewed by:
Gabriela Carolina Pagnussat,
National University of Mar del Plata, Argentina
Silvia Vieira Coimbra,
University of Porto, Portugal
Daisuke Kurihara,
Nagoya University, Japan

***Correspondence:**
Said Hafidh
hafidh@ueb.cas.cz

†ORCID:
Katarína Kulichová
orcid.org/0000-0002-1115-9899
David Honys
orcid.org/0000-0002-6848-4887
Said Hafidh
orcid.org/0000-0002-3970-713X

‡These authors have contributed equally to this work

Specialty section:
This article was submitted to Plant Development and EvoDevo, a section of the journal Frontiers in Plant Science

Received: 30 August 2021
Accepted: 10 January 2022
Published: 08 March 2022

Citation:
Kulichová K, Pieters J, Kumar V, Honys D and Hafidh S (2022) A Plastid-Bound Ankyrin Repeat Protein Controls Gametophyte and Early Embryo Development in Arabidopsis thaliana. Front. Plant Sci. 13:767339. doi: 10.3389/fpls.2022.767339

Proplastids are essential precursors for multi-fate plastid biogenesis, including chloroplast differentiation, a powerhouse for photosynthesis in plants. Arabidopsis ankyrin repeat protein (AKRP, AT5G66055) is a plastid-localized protein with a putative function in plastid differentiation and morphogenesis. Loss of function of *akrp* leads to embryo developmental arrest. Whether AKRP is critical pre-fertilization has remained unresolved. Here, using reverse genetics, we report a new allele, *akrp-3*, that exhibited a reduced frequency of mutant embryos (<13%) compared to previously reported alleles. *akrp-3* affected both male and female gametophytes resulting in reduced viability, incompetence in pollen tube attraction, altered gametic cell fate, and embryo arrest that were depleted of chlorophyll. AKRP is widely expressed, and the AKRP-GFP fusion localized to plastids of both gametophytes, in isolated chloroplast and co-localized with a plastid marker in pollen and pollen tubes. Cell-type-specific complementation of *akrp-3* hinted at the developmental timing at which AKRP might play an essential role. Our findings provide a plausible insight into the crucial role of AKRP in the differentiation of both gametophytes and coupling embryo development with chlorophyll synthesis.

Keywords: proplastid, pollen, embryo development, pollen tube reception, fertilization

INTRODUCTION

Proplastids are essential organelles for plant life cycle; they provide nutrients and monomers for energy, act as a precursor for chloroplast differentiation, and function in biosynthesis and storage of pigments, hormones, starch, fats, proteins, and terpenes. During embryo development, proplastids differentiate into chloroplasts from the globular stage, and later, during seed maturation, differentiate into storage plastids, elaioplasts (Demarsy et al., 2012; Allorent et al., 2013; reviewed in Liebers et al., 2017). Many plastid genes are, thus, critical for early plant development, and mutations often result in embryo lethality (Tzafrir et al., 2004; Meinke et al., 2008; Ajjawi et al., 2010; Myouga et al., 2010, 2013; Bryant et al., 2011). Defects in plastid function might also manifest prior to embryo development in the male or female gametophyte. Energy production in mature pollen and growing pollen tubes (PTs) is mainly supplied from mitochondrial respiration and ATP production; nevertheless, glycolysis within plastids is also a contributing source of energy (reviewed in Selinski and Scheibe, 2014). Accumulation of starch during pollen maturation is, therefore, critical, as it serves later as an energy source. Knockout mutants in enzymes catalyzing the regeneration of NAD + during glycolysis, *gapcp1* and *gapcp2*, are sterile males

(Muñoz-Bertomeu et al., 2010). The double mutant genes, *gapcp1* and *gapcp2,* exhibit defects in pollen morphology and viability in addition to having a disorganized tapetal layer. Several other mutants involved in glycolytic processes and maintaining redox homeostasis with defects in gametophyte and embryo development have been described (Prabhakar et al., 2010; Chen et al., 2011; Zhao and Assmann, 2011; reviewed in Selinski and Scheibe, 2014).

Almost all types of plastids are present during pollen development in several layers of the microsporangium and are essential in the formation of functional male gametophytes (Clément and Pacini, 2001; Hafidh and Honys, 2021). They play a supportive function to other cells as in the case of tapetum and the vegetative cell, but proplastids in sperm cells play a direct role in reproductive events through biparental cytoplasmic inheritance to the newly formed zygote. In angiosperms, only proplastids and amyloplasts are present from meiocytes to pollen maturity. Amyloplasts differentiated from proplastids in microspores are preceded by vacuolization as pollen matures (Pacini, 1994). In contrast, proplastids from tapetum undergo division during the early stages of microsporogenesis and differentiate into elaioplasts (Dickinson, 1973; Pacini and Juniper, 1979). Both tapetosomes and elaioplasts generate tapetal lipids that are secreted into the locule to form tryphine when the tapetal plasma membrane breaks down (Dickinson and Lewis, 1973). They also constitute oleosins and triacylglycerols, which later reach the coat of pollen and form a major lipid component (Ting et al., 1998).

Arabidopsis *EMB2036*, an ankyrin repeat protein (AKRP), is a single copy gene with five ankyrin repeats (Zhang et al., 1992). Ankyrin repeat-containing domains (ANK) are described as protein-protein interaction domains found in viruses, archea, bacteria, and eukaryotes. Ankyrin repeats have been found in numerous proteins with functions, such as cell signaling, cytoskeleton integrity, transcription and cell–cycle regulation, inflammatory response, development, and various transport pathways. No enzymatic function has been detected in any ankyrin repeat-containing proteins (reviewed in Mosavi et al., 2004). In Arabidopsis, there are 105 ANK-containing proteins, but only a few were described functionally (reviewed in Becerra et al., 2004). Two ankyrin repeat-containing plastid-targeted proteins, NPR1-like protein 3 and NPR1-like protein 4, are receptors for salicylic acid and are important for basal defense against pathogens (reviewed in Kuai et al., 2015). A mitochondrial protein, ANK6, is an example with function in gametophyte development and male-female gamete recognition during double fertilization (Yu et al., 2010). An *AKRP* expression was reported to be developmentally and lightly regulated. Plants transformed with sense or antisense constructs exhibited a chlorotic phenotype caused by a loss of chloroplast ultrastructure and lower amounts of chlorophylls and carotenoids (Zhang et al., 1992). Interestingly, the expression of selected photosynthesis-related genes was not affected in AKRP-deficient plants (Zhang et al., 1994). An AKRP interacted through ankyrin domains with a sequentially and functionally similar protein, EMB506 (Albert et al., 1999). Two predicted splice isoforms of *AKRP* were experimentally confirmed to be expressed (Garcion et al., 2006). Based on the observed mutant phenotype, AKRP was predicted to function in plastid differentiation. A recent study described a mechanistic role of AKRP (STT2) and EMB506 (STT1) as essential in the sorting of chloroplast twin-arginine translocation (cpTat) pathway proteins to thylakoid membranes (Ouyang et al., 2020). In this study, we have characterized a previously unknown gametophytic defect identified in a new T-DNA insertion allele of *akrp-3* that was absent in other reported *emb2036* alleles. Using gametophytic promoters, we provide a potential time window for AKRP function, pre- and post-fertilization.

RESULTS

Isolation of Novel *akrp* Allele

Two previous embryo-lethal alleles of *AKRP*, *emb2036-1* and *emb2036-2*, were reported to show 25% of pale mutant homozygous seeds containing embryos arrested at globular stage but exhibited no gametophytic defects (Garcion et al., 2006; Meinke et al., 2008). Public RNA-seq data suggest that AKRP transcripts are higher in microspores but are drastically reduced by pollen maturity, and were detected in isolated egg cell of Arabidopsis thaliana (Julca et al., 2021). As a single copy gene, the lack of gametophytic defect was puzzling. We, therefore, performed RT-qPCR measurements and verified that AKRP is broadly expressed and exhibits variation in abundance among sporophytic and gametophytic tissues with the highest expression in reproductive tissues (**Figure 1A**). Two splice variants are predicted to arise from alternative splicing of an *AKRP* single locus, with the shorter isoform lacking the last two ankyrin repeats (**Figure 1B** and **Supplementary Figure S1**). The RT-qPCR revealed that, on average, the longer isoform is >2.5-fold more abundant in both sporophytic and reproductive tissues (**Figure 1A**). We fused a 997bp putative AKRP promoter fragment with a beta-glucuronidase enzyme (GUS) and detected a promoter activity throughout development, with the strongest GUS staining specifically in the early stages of pollen development in ovules and the embryo, as well as in mature seeds (**Supplementary Figure S2**). Therefore, we screened numerous Gabi-kat T-DNA collections ([1]Kleinboelting et al., 2012) with putative insertion in the *AKRP* locus and isolated a new allele, *akrp-3* (Gk_0876D05), which exhibited both pollen and female gametophytic defects as well as a similar embryo-lethal phenotype but in a reduced frequency. We confirmed the position of insertion by Sanger sequencing, which revealed T-DNA insertion between 609 and 624 bp of exon 1 (**Figure 1B**). No homozygous individuals were recovered, confirming a gametophytic or embryo lethality. However, among segregating heterozygous individuals, some contained the canonical wild type and a mutant T-DNA band (Ht22), and others had an extra band (Ht3 and HT15) that we confirmed by sequencing as a back-to-back T-DNA inserted 6 bp away from the first insertion (**Figures 1B,C**). Both types originated from a common parent stock; therefore, we assumed that they were identified and merged as a single event at the stock center. No significant phenotypic variations

[1]https://www.gabi-kat.de

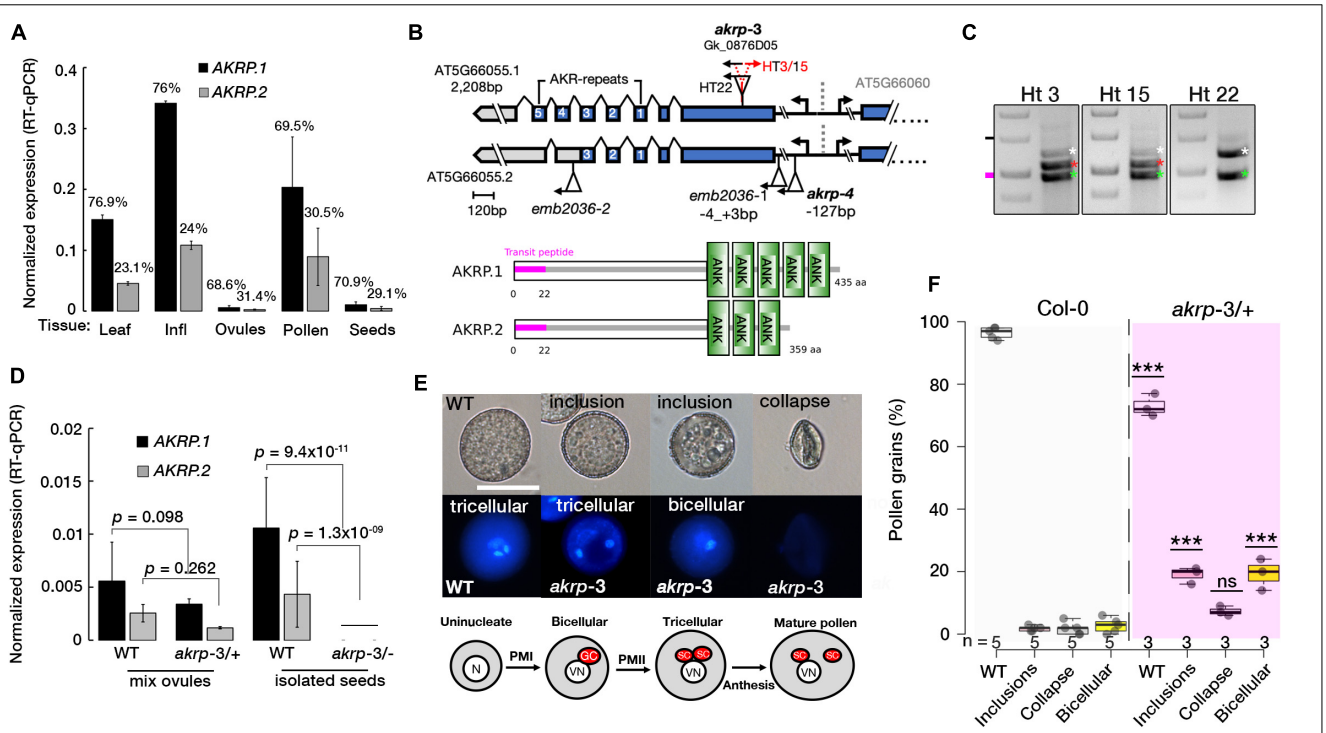

FIGURE 1 | The *akrp-3* allele exhibits abnormal pollen maturation and loss of gametic cell fate. **(A)** Quantification of AKRP splice isoform expression by RT-qPCR. Percentages represent the relative abundance of each isoform in respective tissues. **(B)** Gene and protein models of two AKRP isoforms with the position of *akrp* T-DNA insertions and ankyrin repeats (ANK). Alignment of the isoforms is presented in **Supplementary Figure S1**. **(C)** PCR genotyping of *akrp*-3 (Gk_0876D05) revealed two groups of segregating heterozygous; with three bands (HT3/15) and those with two bands (HT22), wild-type band (white asterisks), mutant (green asterisks) and a second T-DNA band (red asterisks) 6 bp apart. **(D)** Estimation of knockdown of both isoforms in *akrp*-3 mixed ovules and isolated homozygous *akrp*-3 seeds. **(E)** Abnormal pollen development observed in *akrp-3/ +* includes segregant WT pollen, reduced size pollen grains with cytoplasmic inclusion bodies with a single undivided generative nucleus (binucleate pollen) or with two sperm cells, and totally collapsed pollen grains with no DNA content. Below, a schematic of a normal pollen maturation. The N/VN are nuclei of the microspore and vegetative cell, GC/SC are the products of pollen mitosis I and II, the generative and the sperm cells, respectively. **(F)** Frequency of pollen phenotype observed in panel **(E)**. Statistical evaluation was performed using one-way ANOVA with Tukey's multiple comparisons test, with "n"-representing individual M3 plants assessed. ***$p < 0.0001$, ns, not significant. N = 12,463 pollen grains, scale bar = 20 μm.

were observed between plants with single T-DNA or those with back-to-back T-DNA insertion genotypes, however, were possible we present both types separately. We quantified the expression of both *AKRP* isoforms by RT-qPCR and verified their downregulation in *akrp-3*/+ heterozygous ovules and complete knockout in isolated *akrp-3* homozygous mutant seeds (**Figure 1D**).

Loss of Function of *akrp* Produced Abnormally Developed Pollen Without Gametic Cell Fate

In pollen, multiple aberrant phenotypes were identified *akrp*-3/+ plants. Among the aberrant pollen phenotype they include underdeveloped smaller pollen grains with cytoplasmic inclusion bodies, bi-nucleate pollen that failed to undergo the second pollen mitotic division (PMII) of the generative cell to produce two sperm cells, and the most severe was the appearance of aborted pollen grains (**Figure 1E**). No similar phenotypes were observed in segregating wild-type progenies or in screening of the original *emb*2036-1 allele (**Figure 1B**). The screening of an independent allele, *akrp-4*, with an insertion at *AKRP5*′UTR, did not exhibit any aberrant phenotypes. To rule out a T-DNA effect on a neighboring gene, AT5G66060, we screened three T-DNA alleles belonging to the AT5G66060 locus. None of the AT5G66060 alleles recapitulated the *akrp*-3 phenotype, which strongly supports that the observed phenotype is linked to *akrp*-3 loss of function.

To better understand the nature of the *akrp-3*/+ gametophytic defect, multiple assays were performed to assess viability and pollen fitness. Alexander staining revealed fully viable pollen grains alongside partially stained pollen grains containing cytoplasmic inclusion bodies, whereas *in vitro* germination showed slight reduction in *akrp*-3/+ pollen germination (**Supplementary Figures S3a–c**). The PT length appeared similar whether *in vivo*, semi-*in vivo* or *in vitro* (**Supplementary Figures S3d,e**). However, *akrp*-3 PT length perturbation could be masked by the mixture with wild-type PTs, as they are not phenotypically differentiated. The failure of *akrp*-3 generative cell to undergo PMII and appearance of inclusion bodies in the *akrp*-3 pollen implied possible pollen developmental perturbation. We therefore investigated if *akrp* gametic cell fate

is correctly specified. We crossed multiple gametophyte cell-specific markers into *akrp-3*/+ plants. These included an egg cell marker (pEC1.1-H2B-mRFP), a sperm cell marker (pHTR10-HTR10:RFP), and vegetative cell markers (pLat52-GFP and pLat52-GUS). The screening of *akrp-3*/+ plants homozygous for cell fate markers revealed that pEC1.1-H2B-mRFP egg cell expression was reduced to half of the ovules compared to that of wild-type control (35.9%, n = 1733), indicative of an effect on *akrp*-3 ovule egg cell differentiation (**Supplementary Figures S3f,g**). Similarly, the expressions of pLat52-GFP, pLat52-GUS, and pHTR10-HTR10:RFP in the vegetative cell and sperm cells were respectively reduced by 78 (n = 1,885), 47 (n = 2,211), and 60% (n = 3,889) on the *akrp-3*/+ background (**Supplementary Figures S3f,g**), indicative of *akrp*-3 pollen effect on vegetative and sperm cell differentiation. Rarely, some of the *akrp*-3 bi-cellular pollen or those containing cytoplasmic inclusions expressed both vegetative and sperm cell markers (**Supplementary Figures S3f,g**). When germinated *in vitro*, only a small population of bicellular PTs was observed, and its growth appeared retarded, with no or rare expression of cell fate markers (**Supplementary Figures S3f,g**). Collectively, these results suggest that the *akrp-3* loss of function mutant failed to correctly differentiate the male and female gametic cell fates. However, selfed *akrp*-3/+ heterozygous plants did not show significant segregation distortion, whereas reciprocal test crosses showed a decreased transmission only through the female (78% TE), but not through the male gametophyte (97% TE) (**Supplementary Figures S4a,b**).

Arabidopsis Ankyrin Repeat Protein in Ovules Is Required for Pollen Tube Attraction

In *akrp*-3/+ siliques, a high percentage of seed gaps appeared, indicating a likely fertilization defect. To establish whether untargeted ovules resulting in collapse ovules are those with *akrp-3* loss of function, we conducted a live cell imaging to visualize a correct PT reception (PT arrest, burst, and sperm cell release in the receptive synergid cell) in a*krp-3*/+ pistils. Flowers were emasculated and pollinated with a homozygous double marker for sperm cells (pHTR10-HTR10:RFP) and vegetative cell (pLat52-GFP) (**Figures 2A,B**). Twenty-four hours after pollination, ovules in pollinated pistils were exposed by dissecting the carpel walls, and confocal live-cell imaging was performed to visualize the position of GFP-labeled pollen tubes and HTR10-RFP-labeled sperm cells in wild-type and *akrp-3* ovules. On average, 43.1% (n = 250) of the ovules in *akrp*-3/+ pistil did not attract any PTs and, thus, were not fertilized (**Figures 2B,C**). In some infrequent events, mutant *akrp*-3 ovules attracted multiple PTs containing sperm cells, a phenomenon termed polytubey (Beale et al., 2012; Maruyama et al., 2013). However, none of the PTs appeared to enter the mutant *akr* ovules and burst to release sperm cells (**Figure 2C**). An independent analysis using a blue dot assay with Lat52-GUS pollen unveiled a reduced PT targeting in the *akrp*-3/+ pistil, where nearly 46% (n = 264) of the ovules were not targeted by the Lat52-GUS-expressing PT (**Supplementary Figure S4c**). These data support the live-cell imaging observations and, together, imply that *akrp*-3 ovules are incompetent in PT attraction for fertilization.

A Fraction of Targeted *akrp* Ovules Exhibits a Range of Pollen Tube Reception Defects and Fails to Develop an Embryo

The tendency of *akrp*-3 ovules we observed in live cell imaging not to attract PTs or attract multiple PTs without PT burst prompted us to investigate the frequency of PT attraction by *akrp*-3 ovules. We additionally questioned whether *akrp*-3 attracted PT experience PT reception defects and/or fertilization blockage. Since pollen tube reception and fertilization improve with longer hours after pollination (HAP) (Grossniklaus, 2017; Johnson et al., 2019; Nagahara et al., 2021), we manually crossed Col-0 × Col-0 and compared with *akrp*-3/+ × Col-0 24-to-48 HAP. Callose staining of in-pistil PTs revealed a similar *akrp*-3 untargeted event 24 HAP to that observed by live-cell imaging and the blue dot assay as the predominant phenotype (**Figure 3a**). However, a careful look unveiled that the tendency of *akrp*-3 PT attraction, polytubey attraction, as well as PT reception defects (PT overgrowth), increased at the 48 HAP time point (**Figures 3b,c**). We noticed, on average, that about 2% (n = 28) of *akrp*-3 ovules are targeted and arrested PT at micropylar entry, although without clear pollen tube burst (**Figure 3b**, scene 2). Another 1.5% (n = 19) also showed polytubey without clear PT entry, and majority of *akrp*-3-targeted ovules (3.2%, n = 23) showed a PT overgrowth, indicating a PT reception defect (**Figure 3b**, scenes 3 and 4 respectively). Nevertheless, this suggests that if given time, some of the *akrp*-3 ovules (up to 6.5%, n = 70 pistils) can eventually at least attract PTs or be targeted by a PT (**Figure 3c**). But, do these *akrp*-3-targeted ovules undergo fertilization? Whether targeted by a PT or not, mutant *akrp*-3 ovules lag behind in development, as they are clearly distinguishable by their small size at the 48 HAP time point (**Figure 3a**). Dissection of these retarded ovules revealed no presence of initiated embryos in *akrp*-3 ovules and the female gametic cells remained clearly visible and unfertilized 48 HAP (**Figure 3d**). At this time point, the wild-type targeted ovules are at the minimum 32-cell embryo stage (**Figure 3d**). We, therefore, conclude that although a fraction of *akrp*-3 ovules is successfully targeted, they likely exhibit later PT reception incompetence, as seen in PT overgrowth or the inability to induce PT burst, and, therefore, do not undergo fertilization. Forty-eight hours after pollination, on average, 55.8% (n = 44 pistils) of the ovules (corresponding to wild-type ovules) were correctly targeted in *akrp*-3/+ pistils pollinated by Col-0 pollen compared to 92.5% (n = 14 pistils) targeted ovules in Col-0 pistils also pollinated by Col-0 (**Figure 3e**). To support the observation that the majority of *akrp*-3 ovules do not proceed with fertilization and embryo development, we measured seed area 24 and 48 HAP in Col-0 and *akrp*-3/+ pistils pollinated with Col-0 pollen. Our analysis identified two distinguishable populations at 48 HAP in the *akrp*-3/+ pistils but not in the Col-0 pistils, supporting lack of fertilization and

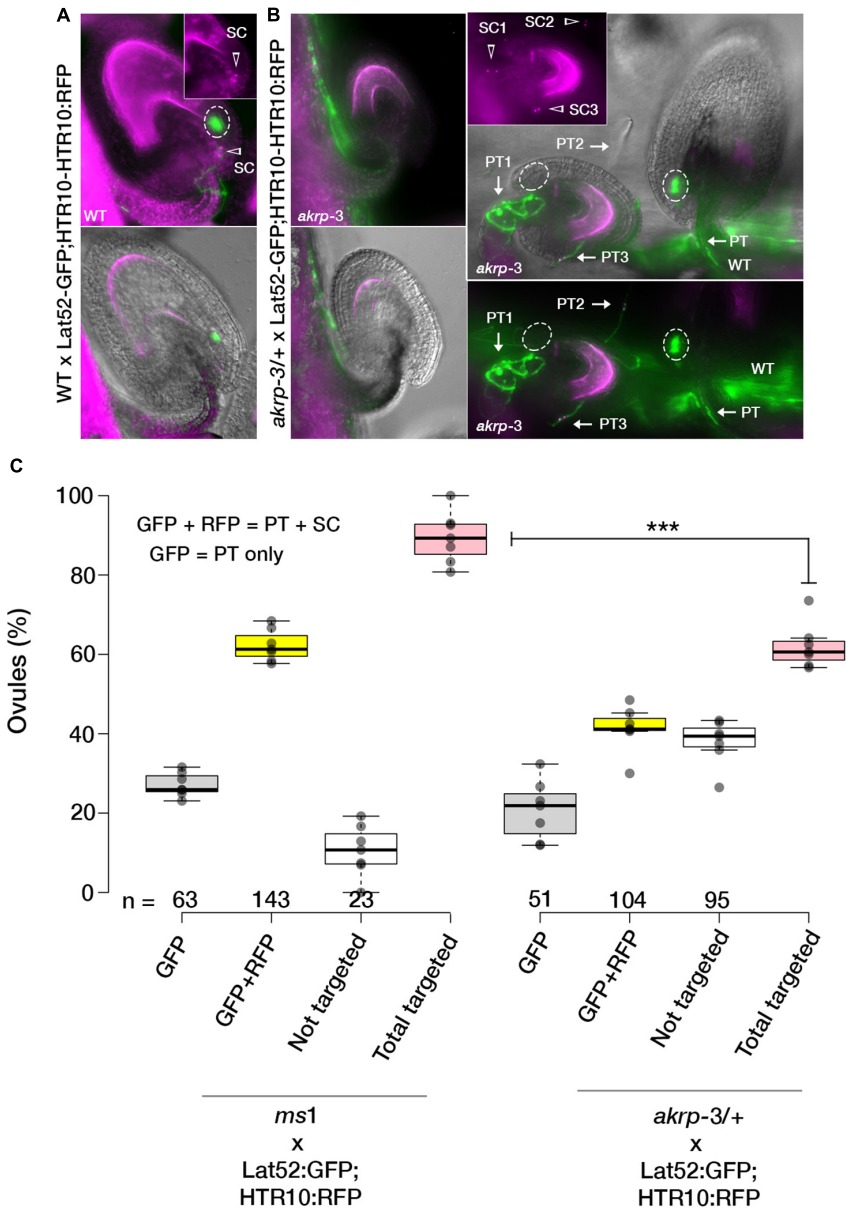

FIGURE 2 | The AKRP function in ovules is critical for pollen tube attraction. Double fertilization events in WT and *akrp*-3/+ pistils were observed after pollination with a double marker for sperm cells (pHTR10-HTR10:RFP) and vegetative cell (pLat52-GFP) 24 h after pollination. **(A)** Normal ovule targeting and reception are scored as a uniform GFP halo (ellipses) at the micropylar and presence of sperm cells (arrow head). **(B)** In *akrp*-3/+ pistil, a mixture of normal targeted and non-targeted ovules or with attraction/reception defects including up to three pollen tubes (arrows) without entry or display of GFP halo were observed. **(C)** Box plot quantification of attraction defects in respective crosses. Center lines represent the medians, and dots outside the quartile are outlier pistils, $n = 175$ and 166 ovules respectively. Statistics were conducted by two-sided non-parametric multiple comparisons with Dunnett contrast and logit approximation, $^{***}p < 0.0005$. PT, pollen tube; SC, sperm cells. Scale bar = 50 μm.

embryogenesis of Col-0 targeted mutant *akrp*-3 ovules (**Figure 3f** and **Supplementary Figure S4d**).

Arabidopsis Ankyrin Repeat Protein Post-fertilization Is Essential for Embryo Progression and Chlorophyll Synthesis

Self-pollinated *akrp*-3/+ generates, on average, 10% of homozygous *akrp* pale mutant seeds on top of the 44.2% average aborted ovule phenotype (**Figures 4A,B**). This suggests that mutant *akrp*-3 gametes from both gametophytes can get together and initiate an embryo in the aforementioned frequency. Isolation and dissection of the mutant pale seeds revealed that approximately 93% ($n = 173$) *akrp*-3 embryos are arrested at the globular stage, with the remaining 7% proceeding to late heart stage (**Figure 4C**), while the wild type segregant and Col-0 control had completed cotyledon development at similar time point (**Figure 4C**). Because of the

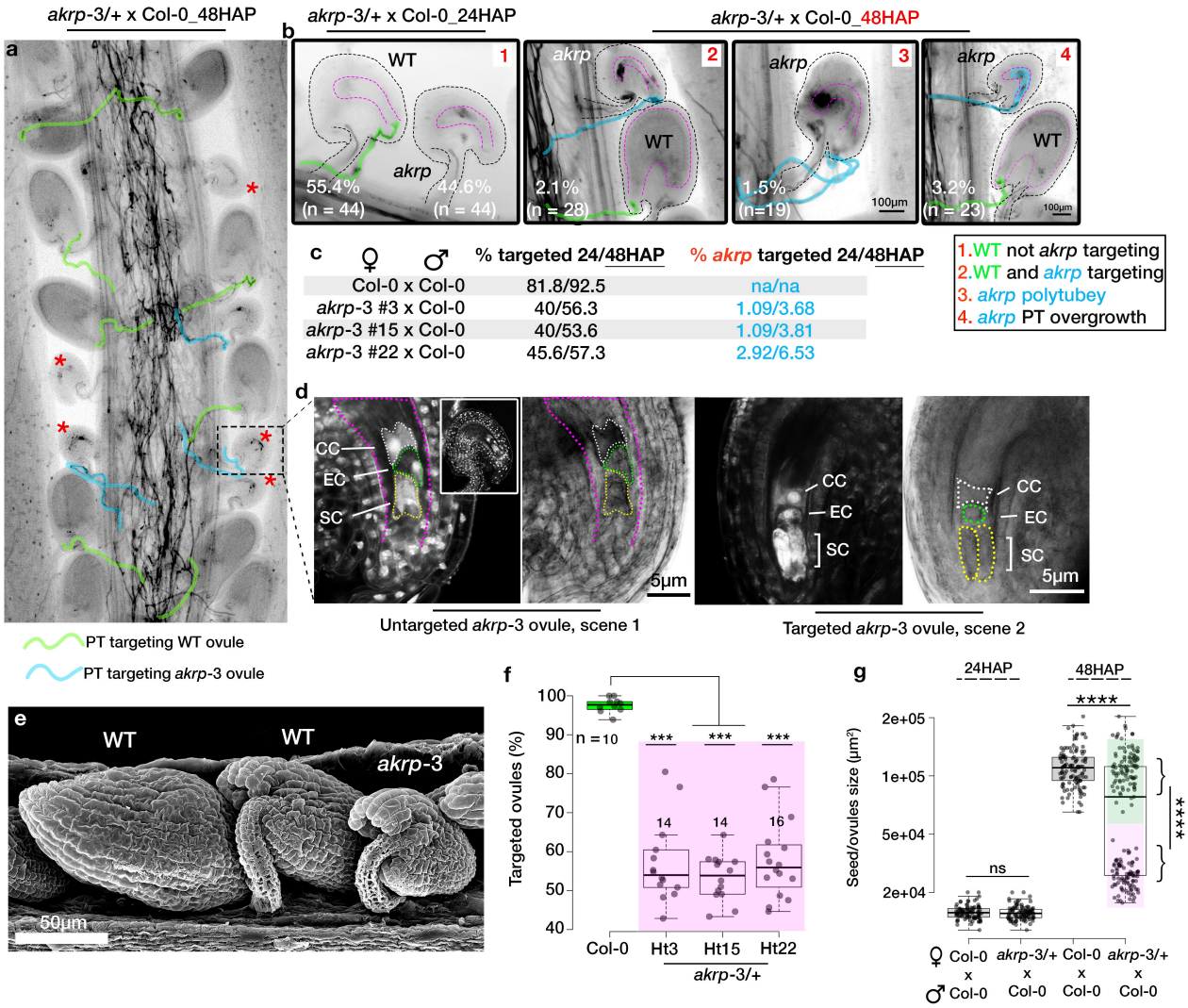

FIGURE 3 | Fraction of targeted *akrp* ovules fails to develop an embryo. *In vivo* pollen tube attraction between Col-0 × Col-0 and *akrp*-3/+ × Col-0 was assayed 24 and 48 h after pollination (HAP). **(a)** Representative pistil section from *akrp*-3/+ × Col-0 stained for callose showing wild-type (unmarked) and mutant ovules (red asterisks) and pollen tube traces (PT) targeting respective ovules. **(b)** Four phenotypic scenarios at 24 and 48 HAP were observed in *akrp*-3/+ × Col-0 pistil but not in wild-type pistil. n represents the number of pistils analyzed. **(c)** Quantification of total targeted ovules and a fraction of *akrp*-3 targeted ovules 24 and 48 HAP using both types of heterozygous *akrp*-3 with single or back-to-back insertion (**Figure 1C**). An increase in *akrp*-3 targeting can be seen 48 HAP. **(d)** Despite *akrp*-3 ovule targeting, the majority of the *akrp*-3 ovules do not produce an embryo, and the female gametophyte remains unfertilized. **(e)** Scanning electron microscopy images using secondary electron detector of *akrp*-3/+ pistil pollinated with Col-0 pollen 48 HAP demonstrated clear presence of underdeveloped *akrp*-3 seeds despite potential pollen tube targeting. **(f)** Variability in the frequency of ovule targeting as seen in individual pistils 48 HAP from respective genotypes. **(g)** Estimation of seed/ovule sizes 48 HAP clearly highlighting lack of fertilization and development of the majority of *akrp*-3 ovules. Statistics were conducted by two-sided non-parametric multiple comparisons with Dunnett contrast and logit approximation or by Student's *t*-test, ***/****$p < 0.0005/0.0001$. ns, not significant. PT, pollen tube; SC, synergid cell; EC, egg cell; CC, central cell.

genotyping variation we observed (**Figure 1C**), we investigated if this has an association with the *akrp*-3/+ silique phenotype. We dissected siliques from HT3, HT15, and HT22 (from **Figure 1C**) and observed the variable penetrance of pale seeds and unfertilized ovule phenotypes that were independent of genotypic origin (**Figures 4D,E**). Since mutant *akrp*-3 ovules are phenotypically without pigments (**Figure 4F**), we isolated mutant seeds and measured chlorophylls a and b, and total chlorophyll levels. All chlorophylls a and b levels as well as total chlorophyll were significantly depleted in the mutant *akrp*-3 seeds, suggesting lack of chlorophyll synthesis in the *akrp*-3 mutant seeds.

Arabidopsis Ankyrin Repeat Protein Localized to Proplastid in Gametophyte and in Isolated Chloroplast

A previous study colocalized 35S-spAKRP:GFP (first 50 amino acids from AKRP containing N-terminal transit peptide) with chlorophyll autofluorescence in transiently transformed

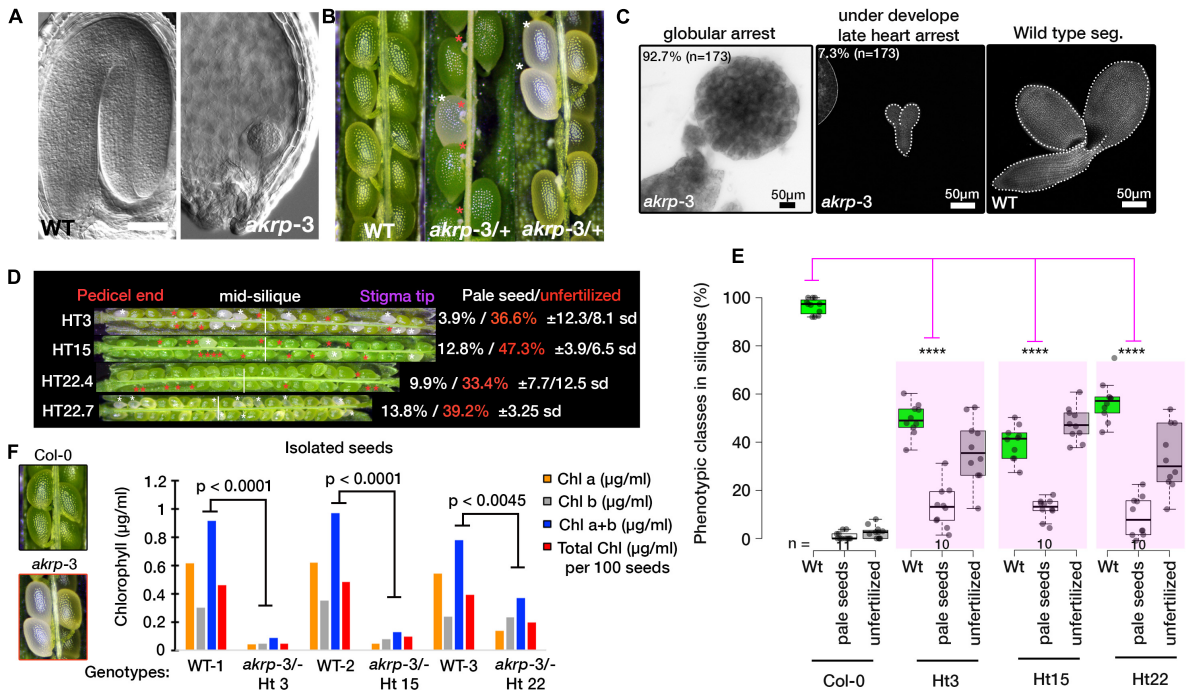

FIGURE 4 | Homozygous *akrp* arrests at globular embryo and is depleted of chlorophyll synthesis. **(A,B)** Fully developed seedlings of wild-type and globular arrested embryo of *akrp*-3 from cleared seeds of WT (green) and *akrp*-3 (pale, labeled with white asterisks, and red asterisks mark unfertilized *akrp*-3 ovules). Some siliques showed a more unfertilized phenotype over embryo arrest as quantified in panel **(D)**. **(C)** Although globular embryo arrest is a dominant *akrp*-3 embryo phenotype, some *akrp*-3 embryos halt their development in the later heart stage. **(D)** Phenotypic penetrance among *akrp*-3/+ hemizygous individuals from a common parent showing variation in the appearance of unfertilized ovules (red asterisks) and a pale embryo lethal phenotype (white asterisks). *N* = 15 siliques per genotype. **(E)** Measured frequency and variation of the *akrp*-3/+ seeds phenotype at silique maturity. **(F)** Chlorophyll measurements from isolated seeds of the respective genotypes. Data represent an average of pooled triplicates. Statistical analysis was performed by one-tail Student's *t*-test assuming unequal variance. ****$p < 0.0001$.

Nicotiana benthamiana guard cells but not the full length 35S-AKRP:GFP as proven deleterious to the chloroplast (Garcion et al., 2006). More recently, both EMB506 (STT1) and AKRP (STT2), under the control of their endogenous promoters, were reported to localize in a punctate pattern in the chloroplasts of an isolated protoplast (Ouyang et al., 2020). However, because of weakness of the *AKRP* promoter, we could not reliably detect any visible GFP signal in stable pAKRP-AKRP:GFP transformants. Nevertheless, the expression of AKRP under pLat52 (pollen vegetative cell-specific), egg cell specific EC1.1, or pDD1 (antipode-specific, AT1G36340, Steffen et al., 2007) promoters clearly localized the AKRP-GFP fusion protein into likely proplastids or differentiated elaioplasts in mature pollen, pollen tubes, the egg cell, and antipodal cells of the female gametophyte (**Figures 5A–C**). Only egg cell localization appeared less punctate and more cytoplasmically distributed (**Figure 5C**). We also isolated chloroplast from transiently transformed *Nicotiana benthamiana* leaves expressing a full-length AKRP-GFP and detected an AKRP localization in the chloroplast stroma (**Figure 5D**). To confirm AKRP-GFP plastid localization in pollen, we co-transformed pLat52-AKRP:GFP plants with a UBIQUITIN 10 promoter-driven pBINU-CHYA vector expressing 85 amino acids of the chloroplast NADPH-dependent thioredoxin reductase C (NTRC) destined to the chloroplast stroma fused to an aequorin calcium sensor and a YFP fluorophore (Mehlmer et al., 2012). Both fluorophores strongly colocalized in proplastids or differentiated elaioplasts of the pollen and pollen tubes, as supported by the GFP-YFP spectral overlap and online emission fingerprint (**Figures 5E–G**). These results confirmed AKRP-NTRC plastid co-localization (**Figure 5G**). Similar results from mature pollen were obtained by independent channel excitation (**Supplementary Figure S6**). Collectively, these data provide evidence that AKRP is likely to function in plastid differentiation and in chloroplast.

Cell-Type-Specific Complementation of *akrp-3* Revealed Timing of Arabidopsis Ankyrin Repeat Protein Function

To confirm the *akrp-3* unique gametophytic phenotype that was not observed in other alleles, we performed-complementation using a native AKRP promoter and cell type-specific promoters in an attempt to identify the developmental timing at which AKRP functions.

We fused the complete AKRP genomic fragment, including the 997-bp intergenic fragment, as a putative promoter region to N-terminal eGFP and transformed mutant *akrp*-3/+ plants. Intriguingly, the introduction of AKRP-GFP either complemented both male and female *akrp*-3 gametophytic

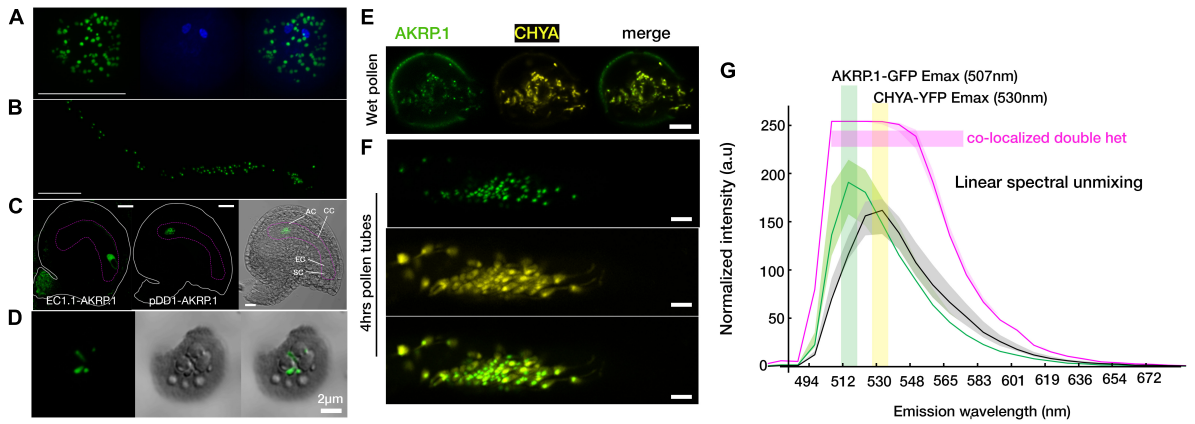

FIGURE 5 | Arabidopsis ankyrin repeat protein localized to the plastid in gametophyte and in an isolated chloroplast. **(A,B)** Punctate AKRP.1::GFP localization in pollen and *in vitro* pollen tubes expressed with the pollen-specific Lat52 promoter. **(C)** Under the egg cell promoter EC.1.1 (left panel) and an antipodal specific promoter DD1 (ubiquitin-conjugating enzyme 31, AT1G36340) (middle and right panels), AKRP.1::GFP punctate localization were observed specifically in the egg cell and antipodal cells of the wild-type embryo sac. **(D)** In isolated chloroplast, AKRP.1::GFP localized mainly in the stroma of the central chloroplast. **(E)** Co-expression of pLat52- AKRP::GFP with a plastid specific marker, pBINU-CHYA(K), in the pollen and **(F)** pollen tubes revealed strong co-localization and confirmed AKRP plastid localization in the gametophyte. **(G)** Representative linear unmixing spectra plot from double hemizygous pollen tubes for both constructs, *N* = 55 pollen tubes, ×32 ROI each. Quantification was performed with the ImageJ plug-in using fixed-size ROI. This panel is also supported by **Supplementary Figure S6**. Scale bar = 10 μm.

defects but not fully the embryo defect (lines 9, 11, and 26), or resulted in increased frequency of gametophytic defects and reduced embryo defects (lines 4, 7, and 10) (**Figure 6A**). In line 11, the complete rescue of both gametophytic *akrp* defects resulted in an increased average of pale *akrp*-3 homozygous mutant embryos, suggesting a possible uncoupling of gametophytic and embryogenic AKRP functions (**Figure 6A**). However, such individuals were underrepresented among the complemented lines.

Since AKRP encodes two splice isoforms, AKRP.1 and AKRP.2 (**Figures 1A,B** and **Supplementary Figure S1**), we tested both isoforms for their ability to complement the *akrp*-3/+ phenotype in a cell-specific manner. Using pLat52-AKRP.1/2::GFP constructs, we identified that only the longer isoform (AKRP.1) partially rescued the embryo-lethal phenotype but not the pollen phenotype, and that the gametophytes remained predominantly sterile (**Figure 6B**). This suggests that the time window for AKRP activity is much earlier during pollen maturation (as shown by the AKRP promoter activity) compared to the late onset of the Lat52 promoter activity (bicellular pollen), and that the shorter isoform is unlikely to function during the embryo development. Most of the Lat52-AKRP.1 rescued embryos were able to develop much further, forming complete cotyledons, compared to the original globular arrested *akrp-3* embryos (**Figures 6C–F**). The rescued embryos still exhibited cotyledons malformations and lacked the normal levels of chlorophyll; therefore, they remained white to pale green even during the vegetative phase in soil (**Figure 6G**). To establish how far the rescued embryos could develop, *akrp*-3/*akrp*-3 germinated seedlings were transferred into glass jars containing half MS medium and grown *in vitro* under 16-h/8-h light/dark cycle. Some of the complemented lines were able to produce flowers, although with long delays and high sterility (with only scarce seed set) compared to the control wild- type plants (**Figures 6H,I**).

To get a broader perspective of AKRP function, we complemented the *akrp-3*/+ plants with a CaMV 35S promoter-driven AKRP.1:GFP. Although the seeds remained pale, we again observed a partial 35S-AKRP.1 complementation of the pale seedlings, which later recovered the cotyledon chlorotic phenotype and produced viable flowering plants (**Supplementary Figures S5a–e**). While some of the lines retained a patchy white-green pattern on leaves, the others fully recovered and produced green organelles (**Supplementary Figures S5c,d**). A similar patchy appearance was observed when the 35S-AKRP:GFP construct was introduced into WT Col-0, suggesting that the observed phenotype was likely due to the nature of 35S overexpression-induced silencing.

To assess AKRP function in the female gametophyte, two promoters driving the expression of the longer *AKRP.1* isoform were used: an antipode-specific DD1 (AT3G36340) as a potential negative control for embryo sac cell-specific complementation and an egg cell-specific EC1.1 (AT1G76750) promoter. Intriguingly, the pEC1.1-driven AKRP complementation was not sufficient to rescue the embryo-lethal phenotype or the ovule-pollen tube attraction defect of *akrp*-3 (**Supplementary Figure S5f**). However, the pDD1-driven complementation construct was able to partially rescue the embryo developmental defects. Several lines were recovered with fully developed embryo; however, some had pale seeds that resembled the pLat52-AKRP:GFP-complemented lines (**Supplementary Figure S5g**). This suggests that the spatial-temporal DD1 promoter activity is sufficient to drive the AKRP embryo function.

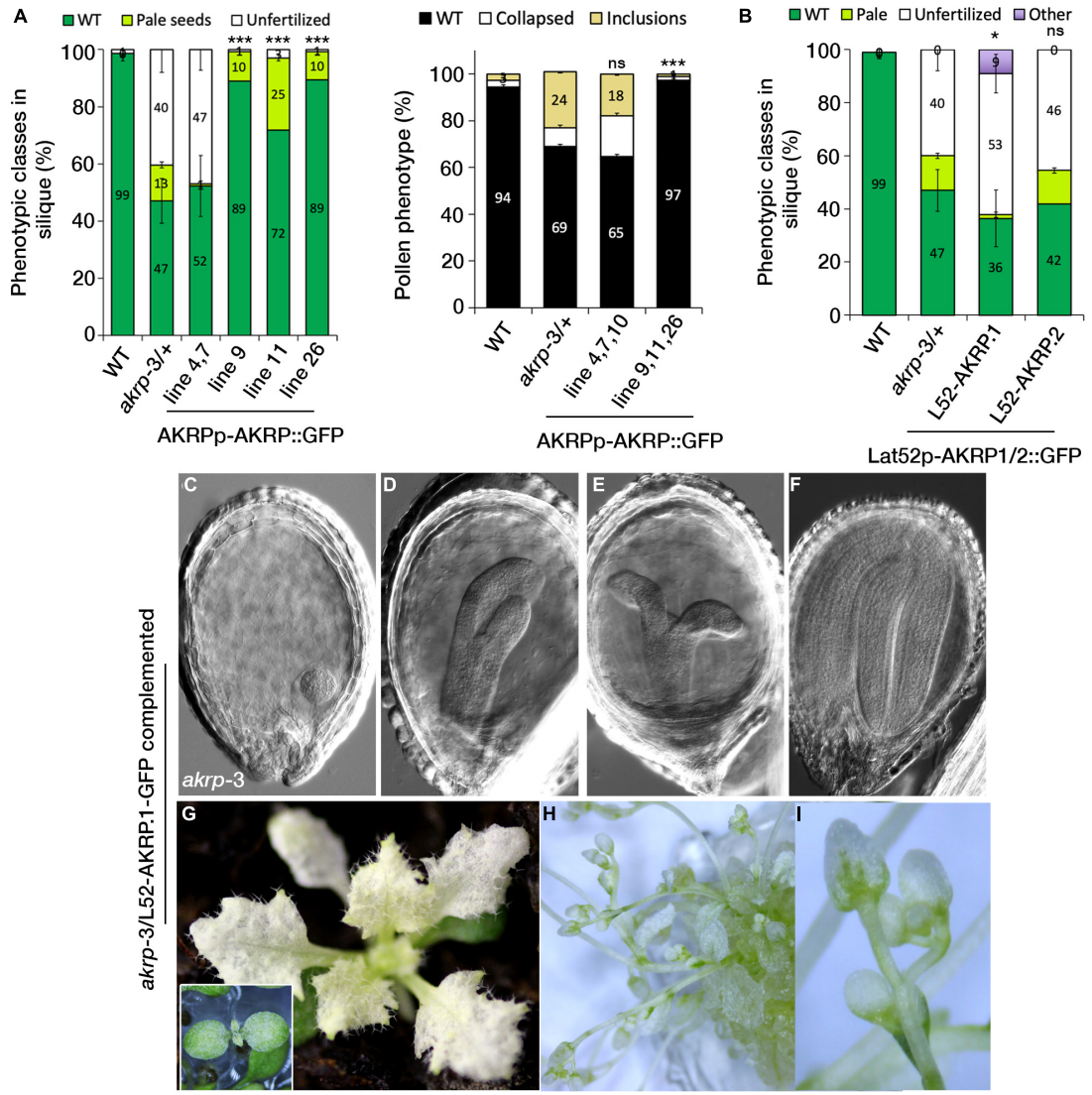

FIGURE 6 | Cell type-specific expression of *AKRP* longer isoform partially rescues embryo developmental perturbation and reveals the timing of AKRP function. **(A)** Native promoter-driven complementation resulted in two groups of complemented plants: those with reduced embryo phenotype but persistent gametophytic defects (lines 4, 7, and 10) and those with fully restored pollen defects (right panel) but with remnant pale seed embryo defects (lines 9, 11, and 26). **(B–I)** Complementation of *akrp*-3/+ with the pLat52-AKRP.1::GFP longer isoform partially complemented the *akrp-3* embryo defect ("other" category), producing rescued embryos beyond the globular arrested embryo of *akrp*-3. Some *akrp*-3 homozygote seeds were able to germinate and flower *in vitro*. Statistical tests were performed by Student's *t*-test assuming unequal variance, $*p < 0.05$, $***p < 0.001$; ns, not significant. Scale bar = 50 μm.

DISCUSSION

In this study, we have identified and functionally associated AKRP with a role in gametophyte competence to undergo fertilization. Previous studies highlighted the role of AKRP in embryonic development, but the alleles studied exhibited no gametophytic defects (Garcion et al., 2006; Meinke et al., 2008). The AKRP falls under the category of embryo-defective genes (EMB) where the fusion of two mutant gametes results in a lethal embryonic development. We show for the first time that AKRP functions earlier not only during embryonic development but also at the gametophytic level (**Figures 1–3**). In Arabidopsis, it is not yet clear how many EMB genes also have a role in the gametophyte, but 27% of the EMB genes exhibit embryo arrest in the globular stage, same stage as the *akrp*-3 mutant, whereas the others arrest earlier or later pass the globular stage, implying a differential timing of EMB gene function (Muralla et al., 2011; Meinke, 2019).

Putative Timing of Arabidopsis Ankyrin Repeat Protein Function in Gametophyte and Embryonic Development

An emerging role of plastids during pollen maturation, as assessed by transmission electron microscope, suggests an

essential role in carbohydrate storage that serves to provide energy and monomers for the construction of a PT wall. Moreover, in *Lolium perenne*, plastids store brassinosteroids during pollen maturation and later promote PT growth post pollination in stigmatic papillae and in transmitting tract tissues (Taylor et al., 1993). Therefore, the timing of genes associated with plastid biogenesis is crucial in the gametophyte and post fertilization.

The rescue of the *akrp*-3 embryo phenotype but not the pollen phenotype by the Lat52-AKRP:GFP construct is spatially intriguing. We suspect a possible inheritance of pollen-expressed AKRP: GFP post-fertilization. This possibility of sporophyte-to-gametophyte carryover inheritance (meiocytes to microspores in the male gametophyte), which masks the gametophytic phenotype, or gametophytic-to-diploid zygote carryover inheritance (ovule or pollen tube-to-zygote during double fertilization), which rescues early embryo defects, has been previously reported for several genes (Muralla et al., 2011; Nodine and Bartel, 2012; Meinke, 2019). The Lat52 promoter is known to be active only in pollen (Ursin et al., 1989; Twell et al., 1990); however, its activity was also reported in roots, as verified by protein gel blot analysis (Van Damme et al., 2006). Therefore, it is possible that the ectopic activity of the Lat52 promoter post-fertilization might be an alternative explanation over a pollen-originated AKRP transcript inheritance for the sufficient rescue of the *akrp-3* embryo phenotype. Partial complementation of the *akrp* embryo phenotype has also been previously reported by Garcion et al. (2006) using an embryo-specific promoter AB13, implying that the timing of AKRP expression is crucial for its function. Similar explanation could be hypothesized for the lack of *akrp*-3 pollen phenotype complementation by the pLat52-driven construct. The LAT52 promoter is active in vegetative cell from the bicellular stage (Brownfield et al., 2009a,b), whereas the AKRP promoter was most active in the earlier microspore stage and the tapetum (**Supplementary Figures S2c–f**), and the first defects in *akrp-3*/+ pollen morphology were already visible in the bicellular pollen stage. As such, Lat52-driven AKRP expression is far late to rescue the *akrp*-3 pollen phenotype, as supported by the lack of *akrp*-3 pollen complementation we observed (**Figure 6B**).

Interestingly, in the embryo sac, the antipodal cell-specific expression of AKRP.1 by the DD1 promoter, but not the egg cell-specific expression by EC1.1 promoter, partially complemented the *akrp*-3 globular arrest embryo phenotype (**Figures 4**, **6**). The antipodal-driven complementation of *akrp*-3 embryo arrest was unexpected because of the fact that antipodal cells degenerate post fertilization. We suspect that, perhaps, the window of expression by the DD1 promoter was sufficient to accumulate AKRP.1 transcripts to allow for AKRP.1 function post fertilization. On the other hand, the lack of *akrp*-3 complementation through egg cell-specific expression by the EC1.1 promoter can be explained by the fact that the EC1.1 promoter itself did not appear activated in *akrp*-3 ovules; therefore, the EC1.1-AKRP.1:GFP construct was not active in the *akrp*-3 egg cell (**Supplementary Figure S3g**). It will be informative in the future to express the AKRP.1, specifically in the egg cell, using a different promoter.

We also observed *akrp*-3 embryo complementation by 35S-AKRP: GFP. The construct seemed to improve pollen fitness in the rescued homozygous lines (**Supplementary Figure S4**). However, some of the rescued lines lacked pigmentation and developed deformation on leaves. The chlorotic patchiness in leaves might be the result of overexpression-induced silencing of AKRP in developing embryos. The AKRP-coding sequence contains a + 31-1,110-bp nonsense-mediated decay target sequence (Thierry-Mieg and Thierry-Mieg, 2006); therefore, its strong expression by the 35S promoter could likely induce silencing. A similar observation was reported by Zhang et al. (1992, 1994) from multiple transgenic lines with chlorotic phenotype after transformation with both sense and antisense AKRP constructs. A similar construct was also used to complement the *emb2036*-1 and generated homozygotes lines with a similar outcome (Garcion et al., 2006). In summary, our complementation analyses hinted that if the promoter used has a broader pattern of expression in either of the gametophytes (female proDD1 or male proLat52), it was sufficient to rescue the lethal embryo arrest phenotype. This is potentially substantiated through the inheritance of parental-originated macromolecules (transcripts or proteins) during double fertilization. The next step will be to structurally dissect isolated gametophytic plastids (predominantly from the vegetative cell of pollen and developing ovules) from *akrp*-3 mutant to evaluate their structures relative to those from the wild type. A similar analysis on developing embryos revealed a striking difference and assigned a role of AKRP in plastid differentiation (Garcion et al., 2006).

EMB-Defective Allele Non-canonical Penetrance

The two other mutant alleles of AKRP, *emb2036-1* and *emb2036-2*, are phenocopies, both showing 25% homozygous embryo arrest at the globular stage (Tzafrir et al., 2004; Meinke et al., 2008). Here, we have screened three alleles of *AKRP*, *emb2036-1*, *akrp-3,* and *akrp-4*. *emb2036-1,* with T-DNA inserted at the 5UTR showing no gametophytic defects, whereas *akrp-3* loss of function, with T-DNA inserted at the beginning of exon 1 exhibiting various pollen, ovule, and embryo defects (**Figures 1–3**). We suspect that these allelic variations might also be explained by T-DNA positional effect. The *AKRP* encodes two isoforms that we verified to be expressed in pollen, ovules, and seeds with the longer isoform up to three times more abundance (**Figure 1**). In pollen, only the longer isoform can complement the pollen defect, and in *akrp*-3 knockout, both isoforms are disrupted (**Figure 1**). It is unclear to us whether the *emb2036-1* and *emb2036-2* alleles that exhibit only the embryo phenotype result in the disruption of both isoforms. Because of the close proximity of AKRP with the neighboring AT5G66060 gene sharing the putative promoter region, our screening confirmed that none of the AT5G66060-associated T-DNA insertions exhibit any aberrant phenotypes. Together with the complementation of *akrp*-3 by the AKRP.1-GFP native construct, this confirms that the gametophytic phenotype we observed is linked to *akrp-3* loss of function.

Despite the substantial amount of aberrant pollen with altered cell fate and significant lack of pollen tube attraction leading

to an ovule abortion in *akrp*-3, there were no transmission defects through the male and only a reduced transmission (78%) through the female. This reduction does not correspond to the penetrance of the *akrp*-3 gametophytic phenotype (**Figures 1–3** and **Supplementary Figure S4**). A similar example of *akrp*-3 non-characteristic pattern of allele inheritance was observed in another plastidial isoform of NAD-MDH that produced NAD + required to generate ATP by glycolysis. Knockout plNAD-MDH is embryo-lethal and exhibits impaired pollen tube growth *in vitro,* which can be rescued by exogenous application of NADH-GOGAT substrates (Selinski and Scheibe, 2014). Just like *akrp*-3 pollen tubes, *plnad-mdh in vivo*-grown pollen tubes are functional and able to fully compete with the wild-type pollen tubes for fertilization (Selinski and Scheibe, 2014). This explains the normal transmission of the *plnad-mdh* mutant allele through the male despite the pollen and pollen tube phenotype. These results suggest that *in vivo*, female reproductive tissues play a key role in supporting semi-functional pollen tubes compromised by the knockout of some essential loci.

Allelic variation in *emb* mutants is also not uncommon. A T-DNA insertion in the GEX1 gene produces a truncated fragment sufficient to rescue a *gex1* gametophyte defect but not an embryo defect (Alandete-Saez et al., 2011). Similarly, a truncated fragment of ZAR1 receptor kinase results in dominant-negative effect on embryo development, a phenotype not visible in other *zar1* null alleles (Yu et al., 2016). A more similar example of *akrp*-3 allelic variation is disruption of geranylgeranyl diphosphate synthase required for isoprenoid biosynthesis that also encodes two isoforms, a short isoform and a longer isoform (Ruiz-Sola et al., 2016). A T-DNA disrupting only the longer isoform which is targeted to plastids shows a defect in seedling pigmentation, whereas disruption of the shorter isoform, exhibits embryo lethal phenotype (Ruiz-Sola et al., 2016).

Extensive screening of *emb*-defective genes by integrated multi-omics analysis has produced a consistent phenotypic profile that is transcription-linked to elaborate the behavior of *emb*-defective genes, including allelic variation, and their potential unusual inheritance (Muralla et al., 2011). Among *EMB* loci categories, those with functional male gametophyte but with pre-globular embryo arrest, 85% of the *EMB* genes in this category are maintained as heterozygous, and their transcripts are detected pre-meiosis in microsporocytes (pollen mother cell) and then in early microspores, suggesting a transcript inheritance from the microsporocytes to the microspores (Muralla et al., 2011; Meinke, 2019). By anthesis, their transcripts disappear. This is consistent with the masking of their gametophytic phenotype through a "maternal rescue," and they, instead, exhibit an onset of early embryo arrest phenotype. In other *EMB* genes with moderate-to-severe male gametophyte defect, their transcription tends to be throughout the pollen development with later onset of embryo arrest phenotype. *De novo* post-meiotic expression (over pre-meiotic transcript inheritance) is, therefore, likely essential for this category of *EMB* genes to allow sufficient levels for gene function throughout pollen ontogenesis. The profile of *akrp*-3 perfectly fits to the second category, exhibiting mild pollen phenotype yet functional to allow for normal transmission of the mutant *akrp*-3 allele. Transcripts of AKRP are detectable in microsporocytes and drastically decreased during pollen maturation, and the *akrp*-3 exhibits a pre-globular embryo arrest (**Figures 1**, **4**). The mild pollen phenotype also suggests that either *de novo* AKRP post-meiotic transcription is necessary for full AKRP function, or the *akrp*-3 allele that disrupts both isoforms of *AKRP* is a true null allele over the previously reported *emb2036*-1 and *emb2036*-2 alleles that did not exhibit the gametophytic phenotype. To summarize, RNA and/or protein storage in the gametophyte is emerging as a substantial element of sporophyte-gametophyte reinforced fitness in flowering plants to support the isolated gametophyte function for successful fertilization and sustain an early embryo development pre-zygotic gene activation. The complexity of an EMBRYO-DEFECTIVE gene (EMB) allelic variations and the non-canonical allelic inheritance patterns have recently been reviewed by the group of David W. Meinke, who initiated and characterized over 1,000 *emb* mutants more than 40 years ago. The resources presented in his review (Meinke, 2019) and the curated database, SeedGenes[2], exclusively documenting *emb* mutants, with gametophytic or embryo developmental role, are extremely valuable and are a must-explore data source.

Mechanistic Insight Into the Function of Arabidopsis Ankyrin Repeat Protein

Per cell, a chloroplast contains over 3,000 proteins; the majority of which are nuclear-encoded. These are synthesized in the cytosol with an N-terminal transit peptide and are subsequently translocated into chloroplasts (Jarvis and Loìpez-Juez, 2013; Lee et al., 2017). Chloroplasts constitute of multi-suborganellar membranes, outer envelope, inner envelope, and thylakoid membranes, and thus create three separate compartments, the intermembrane space, stroma, and the lumen (Ouyang et al., 2020). Therefore, nuclear-imported proteins need to be further resolved into subcellular organelles. The initial import into the stroma is done by the Toc/Tic import complex located in the outer/inner membrane of the chloroplast *via* N-terminal transit peptide recognition (Jarvis and Loìpez-Juez, 2013; Chen et al., 2018). To further sort nuclear-imported proteins, thylakoid membrane-destined proteins follow the chloroplast signal recognition particle pathway (RP), whereas thylakoid lumen proteins are sorted using an additional targeting signal at their N-terminal and enter either the chloroplast secretory (cpSec) or the chloroplast twin-arginine translocation (cpTat) pathway (Schuenemann et al., 1998; Yuan et al., 1994; Settles et al., 1997). Recently, AKRP (STT2) and EMB506 (STT1) were shown to be integral in the formation of liquid-liquid phase-separated droplets as a mechanistic novel mechanism of intra-chloroplast cargo sorting *via* the cpTat pathway to transport thylakoid membrane proteins (Ouyang et al., 2020). STT1-STT2 interacts to create a heterodimer and *via* N-terminal intrinsically disordered regions of the STT complex induces liquid-liquid phase

[2]https://seedgenes.org

separation (Ouyang et al., 2020). The RNAi silencing of either STT1 or STT2 led to a defective thylakoid membrane biogenesis and plastid morphogenesis, resulting in growth retardation, chlorotic leaves, and disrupted chlorophyll levels.

CONCLUSION

We report for the first time that the role of AKRP in intra-chloroplastic cargo protein sorting *via* a liquid-liquid phase translocon driven separation (Ouyang et al., 2020), plays a crucial role not only in pigmentation and embryonic development, but also in gametophytic-fertilization competence likely *via* plastidial morphogenetic function. Our data also suggest that this AKRP role is extended throughout plant development in sorting chloroplast import proteins from crowded stroma to thylakoid membranes, as partially rescued *akrp*-3 adult plants remain chlorotic with morphological distortion throughout plant development.

MATERIALS AND METHODS

Plant Material and Growth Conditions

Arabidopsis (*Arabidopsis thaliana* L. Heynh.) plants were grown at 22 and 60% humidity in Conviron PGC Flex growth chambers under 16-h light/8-h dark conditions. Seeds of Col-0 wild type (WT) and T-DNA lines of EMB2036/AKRP (At5g66055), and At5g66060 plants were obtained from The European *Arabidopsis* Stock Centre. Segregating T-DNA line Gabi-Kat GK_876D05, located in the first exon (in reverse orientation upstream of nucleotide 614) of AKRP was the main experimental material used in this study and herein referred to as *emb2036-3*. The second studied T-DNA line was SAIL_98_F02 (*emb2036-4*, located in 5′UTR). For At5g66060, located on chromosome 5 downstream of AKRP, three T-DNA insertion lines were grown (SALK_098611C, SAIL_595_H12, and SAIL_1262_D08). The T-DNA lines were genotyped using either Gabi-Kat o8474 or o8760, SALK LBb1.3, or SAIL LB2 primers in combination with gene-specific primers. Primer sequences are listed in **Supplementary Table S1**.

Phenotypic Screening

The T-DNA insertion lines were screened for defects in pollen and embryo development phenotypes. Mature pollen samples were screened in brightfield and UV on a Nikon TE-2000 microscope. Siliques in the cotyledon stage of embryo development were dissected and screened for the presence of pale white/transparent mutant seeds. The phenotypic screening was conducted on two subsequent generations.

Transmission Analysis

The *emb2036-3* heterozygous plants were back-crossed into Col-0 wild-type background to determine female transmission and crossed into male-sterile *ms1-/-* (Yang et al., 2007) to study male transmission. The progeny of these crosses was genotyped by PCR for presence of T-DNA insertion, and transmission efficiency (number of seedlings containing *emb2036-3* insertion/number of wild-type seedlings) was calculated. Siliques from the reciprocal crosses were screened for the presence of gametophytic or embryo phenotypes that could be caused by a single mutant parent.

Blue Dot Assay

Young buds of WT Col-0 and *emb2036-3/+* plants before dehiscence of stamens were emasculated and let to mature for 2-3 days until stigma papillae developed. The pistils were then pollinated with pollen containing the pLat52-GUS construct and collected 24 h after pollination. Fertilized pistils were dissected under a binocular dissection microscope (Leica, Germany), and the stripes of fertilized ovules attached to the septum were transferred to a GUS staining solution (view section Histochemical GUS staining). After 2 h of staining, fertilized ovules were observed under the Nikon TE-2000 microscope for the presence of a blue dot following pollen tube micropylar entry and burst.

Pollen Viability Stain and Aniline Blue Staining

Alexander staining was performed according to the protocol by Schoft et al. (2011). Stamens of WT and *akrp-3/+* plants were stained in a droplet of the solution. For aniline blue staining, pistils of 24-h self-pollinated WT Col-0 and *akrp-3/+* plants or cross-pollinated *ms1* plants with WT or *akrp-3/+* pollen (24-h growth *in vivo*) were stained for callose according to the protocol by Mori et al., 2006.

Pollen Tube Cultivation

In vitro pollen tube growth was performed according to the protocol by Boavida and McCormick (2007). After 8 h of *in vitro* growth, pollen germination rate and pollen tube length were measured using the NIS Elements software. For semi-*in vivo* pollen tube growth assay, sterile *ms1/-* pistils were pollinated with WT Col-0 or *akrp-3/+* pollen, and pistils were collected 1 h after pollination. The pistils were excised at the stigma shoulder with a needle and transferred to the growth medium (Palanivelu and Preuss, 2006) on a small Petri dish. The pistils were tilted to enable the pollen tubes to emerge on the surface of the solid medium and cultivated in a humidified growth chamber at 22°C for 24 h. Pollen tube length was measured using the NIS Elements software from the point where they emerged from the cut pistil.

Chloroplast Isolation and Chlorophyll Measurements

Six leaves of old *Nicotiana benthamiana* were infiltrated with0.4 O.D p35S-AKRP.1:GFP, as described in Billey et al., 2021. Two days post-infiltration (dpi), approximately 4g of transformed leaf segments were collected, rinsed with ddH2O, and ground with mortar and pestle in a 10-ml 1 × chloroplast isolation buffer (CIB):0.33M sorbitol,0.1M tris-Cl (pH 7.8), 5 mM MgCl2,

10 mM NaCl, and 2 mM EDTA supplemented with0.1% BSA. Here, all steps were performed on ice. Grounded leaves were passed through a 100-micron mesh filter into 15-ml falcon tubes and centrifuged at 1,000 × g for 3 min at 4oC. The supernatant were transferred to a sterile chilled 15-ml falcon tube and centrifuged for additional 7 min at 1,000 × *g*. The pellet was resuspended in 1 ml CIB with0.1% BSA. The mixture was gently loaded on a 40/80% percoll gradient (2.5 ml 80% and 5 ml 40%) in a 15-ml falcon tube. The gradient was centrifuged at 3,200 × *g* for 15 min at 4°C. Using a 1-ml cut tip, intact chloroplast from the gradient interface was transferred and suspended in 3 × volume CIB and centrifuged for 1 min at 1,700 × *g* table. Pelleted chloroplasts were resuspended in 50 ul CIB and aliquoted for live cell imaging or stored at −80°C for protein extraction.

For chlorophyll quantification, mature siliques from the wild-type Col-0 and *akrp*-3/+ plants were dissected, and wild-type green as well as mutant white *akrp*-3 seeds (100–200 seeds; see **Figure 6**) were collected in 1 ml dimethylformide (DMF) in triplicates: WT seeds: 200 seeds/replicate, Ht3: 200 seeds/replicate, Ht15: 133 seeds/replicate, and Ht22: 119 seeds/replicate. All the samples were incubated overnight at 4oC. Absorbance was measured at 664, 665, and 647 nm. The samples were diluted 3 × to fit the optical range and measured using a CLARIOstar microplate reader (BMG LABTECH, Ortenberg, Germany). The final amount (in ug/ml) of chlorophylls a and b, and total chlorophyll a + b was calculated according to Harris and Baulcombe (2015), as follows:

for chlorophyll a content (in μg/ml):
= (12 × A664.5) − (2.79 × A647),
for chlorophyll b content (in μg/ml):
= (20.78 × A647) − (4.88 × A664.5), and
for total chlorophyll content (in μg/ml): Chla + Chlb, later normalized to μg/ml per 100 ovules for each respective sample.

Histochemical GUS Staining

Stable transformants were screened for promoter-GUS activity in two subsequent generations. Selected plant organs were incubated in a GUS staining buffer:0.2 M Na_2HPO_4,0.2 M NaH_2PO_4, 10 mM EDTA„1% Triton X-100, 1 mM $K_3Fe(CN)_6$, and 2 mM X-Gluc, and stained for up to 48 h. Stained tissues were cleared from chlorophyll by bleaching in ethanol series (90, 70, and 50% (v/v)) prior to imaging.

Microscopy

For mutant embryo phenotypic screening, seeds were cleared in a solution of chloral hydrate. Samples were observed under the DIC optics on a Nikon TE-2000 microscope. Images were processed in the NIS Elements software (LIM). Confocal images were taken on a Nikon Eclipse Ti confocal microscope equipped with a CSU-X1 spinning disk module and an Andor iXon3 EMCCD camera, as well as with a Zeiss LSM880 confocal microscope, and captured with the ZEN 2.3v software. The images were analyzed and assembled with the ImageJ/Fiji[3][4], Adobe Photoshop CS6[5], Ink-scape[6], and NIS Elements (LIM) software. For colocalization study (based on a publication by Marcus and Raulet, 2013), a Zeiss LSM880 confocal microscope with these settings was used: 405-nm laser for excitation of GFP and 514-nm laser for excitation of YFP; emission was captured in a range of 481-508 nm for GFP and 552-561 nm for YFP.

Statistics

All the statistical analyses were performed using the Chi square test at $p < 0.01$ or as specified in respective sections.

RNA Extraction and qRT-PCR Analysis

Tissue samples were collected from the WT Col-0, *emb2036-3*/+ plants and complemented lines, and frozen in liquid nitrogen. The RNA was extracted using RNeasy Plant Mini Kit (Qiagen, Germany) and treated with RQ1 RNAse-free DNase I (Promega, Maryland, MD, United States). First-strand cDNA synthesis was conducted using a recombinant M-MLV reverse transcriptase (Promega, Maryland, MD, United States). Measurements of qRT-PCR were performed using a LightCycler 480 Instrument (Roche, Basel, Switzerland). Primers were designed to distinguish among splicing isoforms of AKRP. Translation initiation factor 1 alpha4 (AT560390G) was used as a reference gene. All the measurements were conducted in three biological and two technical replicates. A list of primers can be found in **Supplementary Table S1**.

Cloning Strategies

All the PCR reactions were performed using Phusion and Q5 Polymerase (New England Biolabs, Hitchin, United Kingdom) according to the instructions of the manufacturer. Primer sequences are listed in **Supplementary Table S1**. For the AKRP promoter, 997 bp upstream of the start codon was cloned into the pENTR/D-TOPO vector (Invitrogen, Thermo Fisher, Germany) and recombined into the destination vector pKGWFS7 (Karimi et al., 2002) bearing two reporter genes, GUS and GFP. For full-length AKRP, an AKRP putative promoter (997 bp) and a coding sequence with/without stop codon were amplified from gDNA, cloned into the pENTR/D-TOPO vector, and recombined into the destination vector pB7FWG,0 (Karimi et al., 2002) bearing the eGFP marker. For complementation under the control of different promoters (pEC1.1, pDD1, p35S, and pLat52), CDS was amplified from cDNA and recombined into the pENTR/D-TOPO vector. Complementation constructs were created using either only the longer isoform (p35S, pEC1.1, pDD1) or both isoforms (pLat52) *via* Multisite Gateway technology (Invitrogen, Thermo Fisher Scientific, Germany). The pB7m34GW, 0 backbone, and eGFP marker were used. These vectors were transformed into *Arabidopsis* WT Col-0 and/or *emb2036-3*/+ plants by floral dipping (Clough and Bent, 1998).

[3]http://imagej.net/
[4]http://fiji.sc/Fiji
[5]www.adobe.com
[6]www.inkscape.org

DATA AVAILABILITY STATEMENT

Theoriginal contributions presented in the study are included in the article/**Supplementary Material**, further inquiries can be directed to the corresponding author/s.

AUTHOR CONTRIBUTIONS

SH and KK designed the experiments. KK, SH, VK, and JP conducted the experiments and analyzed the data with supervision by SH. SH, KK, and DH wrote the manuscript. All the authors read and approved the manuscript.

FUNDING

We gratefully acknowledge Stefanie Sprunck for providing us the egg cell marker. This research was supported the Czech Science Foundation grants 21-15856S and 22-29717S and the Ministry of Education, Youth and Sports of the Czech Republic (projects LTAIN19030, and LTC20028). We acknowledge the Imaging Facility of the Institute of Experimental Botany AS CR supported by the MEYS CR (LM2018129 Czech-BioImaging) and IEB AS CR.

ACKNOWLEDGMENTS

We thank Laboratory of Electron Microscopy – IMCF Viničná, Faculty of Science, Charles University for assisting with scanning electron microscopy. We also thank Lenka Steinbachová and Jana Fecikova for help with genotyping, Christos Michaelidis for careful reading of the manuscript and Ivan Kulich for valuable comments and help throughout the study.

SUPPLEMENTARY MATERIAL

The Supplementary Material for this article can be found online at: https://www.frontiersin.org/articles/10.3389/fpls.2022.767339/full#supplementary-material

Supplementary Figure S1 | Protein alignment of two AKRP splice variants. The short isoform differs by one amino acid substitution and 75 amino acid deletion comprising two ankyrin repeats at the C-terminus. 1. Alignment was performed with Clustal Omega using HMM model and visualized in Jalview v2.9.0b2.

Supplementary Figure S2 | Profiling of AKRP promoter activity in various plant tissues. Detection of AKRP promoter activity in various tissues: cotyledons and stipules of 7-day old seedlings **(a,b)**, inflorescence **(c)**, uninucleate microspores **(d)**, bicellular pollen **(e)**, mature pollen **(f)**, immature **(g)**, and mature **(h)** ovules, and globular to cotyledon stage seeds and embryos **(i–k)**. Scale bar = 20 μm.

Supplementary Figure S3 | Gametophytic viability and pollen tube assays. **(a,b)** Alexander staining and quantification of pollen viability, (n = 664). **(c)** Comparative assessment of *in vitro* pollen germination. **(d)** Aniline blue staining of self-pollinated pistils 24 h after pollination revealed severe targeting defect (n = 953); this panel supports **Figure 2**. **(e)** Estimation of *in vitro* and semi-*in vivo* pollen tube length. **(f)** Confocal imaging of egg cell (EC1.1)-specific pEC1.1-H2B-mRFP (n = 2,511), vegetative cell-specific pLat52-GUS (n = 3,233) and a double marker for sperm cell (SC) pHTR10-HTR10:RFP (n = 4,342) and vegetative cell (VC) pLat52-GFP (n = 2,313). **(g)** Quantification of marker expression in *akrp-3*/+ and segregated WT plants. AC, antipodal cell expression of pDD1-AKRP.1::GFP.

Supplementary Figure S4 | The *akrp-3* transmission test and blue dot assay. **(a)** Segregation of self-fertilized *akrp-3*/+ on sulfadiazine antibiotic. **(b)** Transmission test of the *akrp-3* allele after reciprocal crosses. TE = transmission efficiency (Wt/Het × 100), χ^2 test: not significant at $p < 0.01$. **(c)** Blue dot assay to assess ovule attractivity following pollination with pLAT52-GUS-expressing pollen suggests a dramatic decrease in *akrp*-3 pollen tube attraction efficiency 24h after pollination (n = 824). This panel supports **Figure 2**. χ^2test, significant at $p < 0.01$. Scale bar = 50 μm. **(d)** Induction of aborted ovule phenotype through an *akrp*-3 female after reciprocal crosses.

Supplementary Figure S5 | Cell type-specific complementation of *akrp-3* mutation. **(a,b)** Complementation using a p35S promoter (35S-AKRP.1:GFP) yielded rescued homozygous plants already in the first generation. The complementation was not absolute, because some lines retained some levels of embryonic defects; **(c,d)** Chlorotic cotyledons that recovered in newly emerged true leaves and **(e)** lesions in rosette leaves. **(f)** Complementation with an egg cell-specific promoter (pEC1.1) was not sufficient to rescue *akrp*-3 fertilization or embryo-lethal phenotype (n = 11). **(g)** Complementation under an antipode-specific pDD1 promoter weakly rescued the embryo-lethal *akrp-3* phenotype (class labeled as "other," phenotypically similar to **Figure 6B** "other" category, n = 5).

Supplementary Figure S6 | AKRP.1 plastid co-localization in mature pollen. Analysis of double heterozygous Lat52-AKRP.1:GFP and pBINU-CHYA(K) marker in mature pollen by independent GFP and YFP channel excitation with Argon 488 laser in a Zeiss confocal microscope. Intensity values were plotted using the Prism software.

Supplementary Table S1 | List of primers used in this study.

REFERENCES

Ajjawi, I., Lu, Y., Savage, L. J., Bell, S. M., and Last, R. L. (2010). Large-scale reverse genetics in *Arabidopsis*: case studies from the Chloroplast 2010 Project. *Plant Physiol.* 152, 529–540. doi: 10.1104/pp.109.148494

Alandete-Saez, M., Ron, M., Leiboff, S., and McCormick, S. (2011). *Arabidopsis* thaliana GEX1 has dual functions in gametophyte development and early embryogenesis. *Plant J.* 68, 620–632. doi: 10.1111/j.1365-313X.2011.04713.x

Albert, S., Despres, B., Guilleminot, J., Bechtold, N., Pelletier, G., Delseny, M., et al. (1999). The EMB 506 gene encodes a novel ankyrin repeat containing protein that is essential for the normal development of *Arabidopsis* embryos. *Plant J.* 17, 169–179. doi: 10.1046/j.1365-313x.1999.00361.x

Allorent, G., Courtois, F., Chevalier, F., and Lerbs-Mache, S. (2013). Plastid gene expression during chloroplast differentiation and dedifferentiation into non-photosynthetic plastids during seed formation. *Plant Mol. Biol.* 82, 59–70. doi: 10.1007/s11103-013-0037-0

Beale, K. M., Leydon, A. R., and Johnson, M. A. (2012). Gamete fusion is required to block multiple pollen tubes from entering an *Arabidopsis* ovule. *Curr. Biol.* 22, 1090–1094. doi: 10.1016/j.cub.2012.04.041

Becerra, C., Jahrmann, T., Puigdomènech, P., and Vicient, C. M. (2004). Ankyrin repeat-containing proteins in *Arabidopsis*: characterization of a novel and abundant group of genes coding ankyrin-transmembrane proteins. *Gene* 340, 111–121. doi: 10.1016/j.gene.2004.06.006

Billey, E., Hafidh, S., Cruz-Gallardo, I., Litholdo, C. G., Jean, V. J., Carpentier, M. C., et al. (2021). LARP6C orchestrates posttranscriptional reprogramming of gene expression during hydration to promote pollen tube guidance. *Plant Cell* 33, 2637–2661. doi: 10.1093/plcell/koab131

Boavida, L. C., and McCormick, S. (2007). TECHNICAL ADVANCE: temperature as a determinant factor for increased and reproducible in vitro pollen germination in *Arabidopsis thaliana*. *Plant J.* 52, 570–582. doi: 10.1111/j.1365-313X.2007.03248.x

Brownfield, L., Hafidh, S., Borg, M., Sidorova, A., Mori, T., and Twell, D. (2009a). A plant germline-specific integrator of sperm specification and cell cycle progression. *PLoS Genet.* 5:e1000430. doi: 10.1371/journal.pgen.1000430

Brownfield, L., Hafidh, S., Durbarry, A., Khatab, H., Sidorova, A., Doerner, P., et al. (2009b). *Arabidopsis* DUO POLLEN3 is a key regulator of male germline development and embryogenesis. *Plant Cell* 21, 1940–1956. doi: 10.1105/tpc.109.066373

Bryant, N., Lloyd, J., Sweeney, C., Myouga, F., and Meinke, D. (2011). Identification of nuclear genes encoding chloroplast-localized proteins required for embryo development in *Arabidopsis*. *Plant Physiol.* 155, 1678–1689. doi: 10.1104/pp.110.168120

Chen, Y. L., Chen, L. J., Chu, C. C., Huang, P. K., Wen, J. R., and Li, H. M. (2018). TIC236 links the outer and inner membrane translocons of the chloroplast. *Nature* 564, 125–129. doi: 10.1038/s41586-018-0713-y

Chen, W., Yu, X. H., Zhang, K., Shi, J., De Oliveira, S., Schreiber, L., et al. (2011). Male Sterile2 encodes a plastid-localized fatty acyl carrier protein reductase required for pollen exine development in *Arabidopsis*. *Plant Physiol.* 157, 842–853. doi: 10.1104/pp.111.181693

Clément, C., and Pacini, E. (2001). Anther plastids in angiosperms. *Bot. Rev.* 67, 54–73. doi: 10.1007/BF02857849

Clough, S. J., and Bent, A. F. (1998). Floral dip: a simplified method forAgrobacterium-mediated transformation of*Arabidopsis thaliana*. *Plant J.* 16, 735–743. doi: 10.1046/j.1365-313x.1998.00343.x

Demarsy, E., Buhr, F., Lambert, E., and Lerbs-Mache, S. (2012). Characterization of the plastid-specific germination and seedling establishment transcriptional programme. *J. Exp. Bot.* 63, 925–939. doi: 10.1093/jxb/err322

Dickinson, H. G. (1973). The role of plastids in the formation of pollen grain coatings. Cytobios 8: 2 1981. The structure and chemistry ofplastid differentiation during male meiosis in Lilium heryi. *J. Cell Sci.* 52, 223–241. doi: 10.1242/jcs.52.1.223

Dickinson, H. G., and Lewis, D. (1973). The formation of tryphine coating the pollen grains of Raphanus and its properties relating to the self incompatibility system. *Proc. R. Soc. Lond B* 184, 149–156.

Garcion, C., Guilleminot, J., Kroj, T., Parcy, F., Giraudat, J., Devic, M., et al. (2006). AKRP and EMB506 are two ankyrin repeat proteins essential for plastid differentiation and plant development in *Arabidopsis*. *Plant J.* 48, 895–906. doi: 10.1111/j.1365-313X.2006.02922.x

Grossniklaus, U. (2017). Polyspermy produces tri-parental seeds in maize. *Curr. Biol.* 27, R1300–R1302. doi: 10.1016/j.cub.2017.10.059

Hafidh, S., and Honys, D. (2021). Reproduction multitasking - The male gametophyte. *Annu. Rev. Plant Biol.* 72, 581–614. doi: 10.1146/annurev-arplant-080620-021907

Harris, C. J., and Baulcombe, D. C. (2015). Chlorophyll Content Assay to Quantify the Level of Necrosis Induced by Different R Gene/Elicitor Combinations after Transient Expression. *Bio-Protoc.* 5:e1670. doi: 10.21769/BioProtoc.1670

Jarvis, P., and Loìpez-Juez, E. (2013). Biogenesis and homeostasis of chloroplasts and other plastids. *Nat. Rev. Mol. Cell Biol.* 14, 787–802. doi: 10.1038/nrm3702

Johnson, M. A., Harper, J. F., and Palanivelu, R. A. (2019). fruitful journey: pollen tube navigation from germination to fertilization. *Annu. Rev. Plant Biol.* 70, 809–837. doi: 10.1146/annurev-arplant-050718-100133

Julca, I., Ferrari, C., Flores-Tornero, M., Proost, S., Lindner, A.-C., Hackenberg, D., et al. (2021). Comparative transcriptomic analysis reveals conserved programmes underpinning organogenesis and reproduction in land plants. *Nat. Plants* 7, 1143–1159. doi: 10.1038/s41477-021-00958-2

Karimi, M., Inzé, D., and Depicker, A. (2002). GATEWAY vectors for Agrobacterium-mediated plant transformation. *Trends Plant Sci.* 7, 193–195. doi: 10.1016/S1360-1385(02)02251-3

Kleinboelting, N., Huep, G., Kloetgen, A., Viehoever, P., and Weisshaar, B. (2012). GABI-Kat SimpleSearch: new features of the *Arabidopsis thaliana* T-DNA mutant database. *Nucleic Acids Res.* 40, D1211–D1215. doi: 10.1093/nar/gkr1047

Kuai, X., MacLeod, B. J., and Després, C. (2015). Integrating data on the *Arabidopsis* NPR1/NPR3/NPR4 salicylic acid receptors; a differentiating argument. *Front. Plant Sci.* 6:235. doi: 10.3389/fpls.2015.00235

Lee, D. W., Lee, J., and Hwang, I. (2017). Sorting of nuclear-encoded chloroplast membrane proteins. *Curr. Opin. Plant Biol.* 40, 1–7. doi: 10.1016/j.pbi.2017.06.011

Liebers, M., Grübler, B., Chevalier, F., Lerbs-Mache, S., Merendino, L., Blanvillain, R., et al. (2017). Regulatory Shifts in Plastid Transcription Play a Key Role in Morphological Conversions of Plastids during Plant Development. *Front. Plant Sci.* 8:23. doi: 10.3389/fpls.2017.00023

Marcus, A., and Raulet, D. H. (2013). A simple and effective method for differentiating GFP and YFP by flow cytometry using the violet laser. *Cytometry A* 83, 973–974. doi: 10.1002/cyto.a.22347

Maruyama, D., Hamamura, Y., Takeuchi, H., Susaki, D., Nishimaki, M., Kurihara, D., et al. (2013). Independent control by each female gamete prevents the attraction of multiple pollen tubes. *Dev. Cell* 25, 317–323. doi: 10.1016/j.devcel.2013.03.013

Mehlmer, N., Parvin, N., Hurst, C. H., Knight, M. R., Teige, M., Vothknecht, U. C., et al. (2012). A toolset of aequorin expression vectors for in planta studies of subcellular calcium concentrations in *Arabidopsis thaliana*. *J. Exp. Bot.* 63, 1751–1761. doi: 10.1093/jxb/err406

Meinke, D. (2019). Genome-wide identification of EMBRYO- DEFECTIVE (EMB) genes required for growth and development in *Arabidopsis*. *New Phytol.* 226, 306–325. doi: 10.1111/nph.16071

Meinke, D., Muralla, R., Sweeney, C., and Dickerman, A. (2008). Identifying essential genes in *Arabidopsis thaliana*. *Trends Plant Sci.* 13, 483–491. doi: 10.1016/j.tplants.2008.06.003

Mori, T., Kuroiwa, H., Higashiyama, T., and Kuroiwa, T. (2006). GENERATIVE CELL SPECIFIC 1 is essential for angiosperm fertilization. *Nat. Cell Biol.* 8, 64–71. doi: 10.1038/ncb1345

Mosavi, L. K., Cammett, T. J., Desrosiers, D. C., and Peng, Z.-Y. (2004). The ankyrin repeat as molecular architecture for protein recognition. *Protein Sci.* 13, 1435–1448. doi: 10.1110/ps.03554604

Muñoz-Bertomeu, J., Cascales-Miñana, B., Irles-Segura, A., Mateu, I., Nunes-Nesi, A., Fernie, A. R., et al. (2010). The plastidial glyceraldehyde-3-phosphate dehydrogenase is critical for viable pollen development in *Arabidopsis*. *Plant Physiol.* 152, 1830–1841. doi: 10.1104/pp.109.150458

Muralla, R., Lloyd, J., and Meinke, D. (2011). Molecular Foundations of Reproductive Lethality in *Arabidopsis thaliana*. *PLoS One* 6:e28398. doi: 10.1371/journal.pone.0028398

Myouga, F., Akiyama, K., Motohashi, R., Kuromori, T., Ito, T., Iizumi, H., et al. (2010). The Chloroplast Function Database: a large-scale collection of *Arabidopsis Ds/Spm* - or T-DNA-tagged homozygous lines for nuclear-encoded chloroplast proteins, and their systematic phenotype analysis. *Plant J.* 61, 529–542. doi: 10.1111/j.1365-313X.2009.04074.x

Myouga, F., Akiyama, K., Tomonaga, Y., Kato, A., Sato, Y., Kobayashi, M., et al. (2013). The Chloroplast Function Database II: a Comprehensive Collection of Homozygous Mutants and Their Phenotypic/Genotypic Traits for Nuclear-Encoded Chloroplast Proteins. *Plant Cell Physiol.* 54:e2. doi: 10.1093/pcp/pcs171

Nagahara, S., Takeuchi, H., and Higashiyama, T. (2021). Polyspermy Block in the Central Cell During Double Fertilization of *Arabidopsis thaliana*. *Front. Plant Sci.* 11:588700. doi: 10.3389/fpls.2020.588700

Nodine, M. D., and Bartel, D. P. (2012). Maternal and paternal genomes contribute equally to the transcriptome of early plant embryos. *Nature* 482, 94–97. doi: 10.1038/nature10756

Ouyang, M., Li, X., Zhang, J., Feng, P., Pu, H., Kong, L., et al. (2020). Liquid-Liquid phase transition drives Intra-chloroplast cargo sorting. *Cell* 180, 1144–1159. doi: 10.1016/j.cell.2020.02.045

Pacini, E. (1994). "Cell biology of anther and pollen development," in *Genetic control of self-incompatibility and reproductive development in flowering plants*, eds E. G. Williams, A. E. Clarke, and R. B. Knox (Dordrecht, Netherlands: Kluwer Academic), 289–308. doi: 10.1007/978-94-017-1669-7_14

Pacini, E., and Juniper, B. E. (1979). The ultrastructure of pollen-grain development in the olive (Olea euro- pea), 2. Secretion by the tapetal cells. *New Phytol.* 83, 165–174. doi: 10.1111/j.1469-8137.1979.tb00738.x

Palanivelu, R., and Preuss, D. (2006). Distinct short-range ovule signals attract or repel *Arabidopsis thaliana* pollen tubes in vitro. *BMC Plant Biol.* 6:7. doi: 10.1186/1471-2229-6-7

Prabhakar, V., Löttgert, T., Geimer, S., Dörmann, P., Krüger, S., Vijayakumar, V., et al. (2010). Phosphoenolpyruvate provision to plastids is essential for gametophyte and sporophyte development in *Arabidopsis thaliana*. *Plant Cell* 22, 2594–2617. doi: 10.1105/tpc.109.073171

Ruiz-Sola, M. A., Barja, M. V., Manzano, D., Llorente, B., Schipper, B., Beekwilder, J., et al. (2016). A single *Arabidopsis* gene encodes two differentially targeted geranylgeranyl diphosphate synthase isoforms. *Plant Physiol.* 172, 1393–1402. doi: 10.1104/pp.16.01392

Schoft, V. K., Chumak, N., Choi, Y., Hannon, M., Garcia-Aguilar, M., Machlicova, A., et al. (2011). Function of the DEMETER DNA glycosylase in the *Arabidopsis thaliana* male gametophyte. *Proc. Natl. Acad. Sci. U. S. A.* 108, 8042–8047. doi: 10.1073/pnas.1105117108

Schuenemann, D., Gupta, S., Persello-Cartieaux, F., Klimyuk, V. I., Jones, J. D., Nussaume, L., et al. (1998). A novel signal recognition particle targets light-harvesting proteins to the thylakoid membranes. *Proc. Natl. Acad. Sci. U.S.A.* 95, 10312–10316. doi: 10.1073/pnas.95.17.10312

Settles, A. M., Yonetani, A., Baron, A., Bush, D. R., Cline, K., and Martienssen, R. (1997). Sec-independent protein translocation by the maize Hcf106 protein. *Science* 278, 1467–1470. doi: 10.1126/science.278.5342.1467

Selinski, J., and Scheibe, R. (2014). Pollen tube growth: where does the energy come from? *Plant Signal. Behav.* 9:e977200. doi: 10.4161/15592324.2014.977200

Steffen, J. G., Kang, H., Macfarlane, J., and Drew, G. N. (2007). Identification of genes expressed in the *Arabidopsis* female gametophyte. *Plant J.* 51, 281–292. doi: 10.1111/j.1365-313x.2007.03137.x

Taylor, P. E., Spuck, K., Smith, P. M., Sasse, J. M., Yokota, T., Griffiths, P. G., et al. (1993). Detection of brassinosteroids in pollen of Lolium perenne L. by immunocytochemistry. *Planta* 189, 91–100.

Thierry-Mieg, D., and Thierry-Mieg, J. (2006). AceView: a comprehensive cDNA-supported gene and transcripts annotation. *Genome Biol.* 7, S12.1–S12.14. doi: 10.1186/gb-2006-7-s1-s12

Ting, J. T. L., Wu, S. S. H., Ratnayake, C., and Huang, A. H. C. (1998). Constituents of tapetasomes and elaioplasts in Brassica campestris tapetum and their degradation and retention during microsporogenesis. *Plant J.* 16, 541–551. doi: 10.1046/j.1365-313x.1998.00325.x

Twell, D., Yamaguchi, J., and McCormick, S. (1990). Pollen-specific gene expression in transgenic plants: coordinate regulation of two different tomato gene promoters during microsporogenesis. *Development* 109, 705–713.

Tzafrir, I., Pena-Muralla, R., Dickerman, A., Berg, M., Rogers, R., Hutchens, S., et al. (2004). Identification of Genes Required for Embryo Development in *Arabidopsis*. *Plant Physiol.* 135, 1206–1220. doi: 10.1104/pp.104.045179. published

Ursin, V. M., Yamaguchi, J., and McCormick, S. (1989). Gametophytic and sporophytic expression of anther-specific genes in developing tomato anthers. *Plant Cell* 1, 727–736. doi: 10.1105/tpc.1.7.727

Van Damme, D., Coutuer, S., De Rycke, R., Bouget, F. Y., Inzé, D., Geelen, D., et al. (2006). Somatic cytokinesis and pollen maturation in *Arabidopsis* depend on TPLATE, which has domains similar to coat proteins. *Plant Cell* 18, 3502–3518. doi: 10.1105/tpc.106.040923

Yang, C., Vizcay-Barrena, G., Conner, K., and Wilson, Z. A. (2007). MALE STERILITY1 is required for tapetal development and pollen wall biosynthesis. *Plant Cell* 19, 3530–3548. doi: 10.1105/tpc.107.054981

Yu, F., Shi, J., Zhou, J., Gu, J., Chen, Q., Li, J., et al. (2010). ANK6, a mitochondrial ankyrin repeat protein, is required for male-female gamete recognition in *Arabidopsis thaliana*. *Proc. Natl. Acad. Sci. U. S. A.* 107, 22332–22337. doi: 10.1073/pnas.1015911107

Yu, T. Y., Shi, D. Q., Jia, P. F., Tang, J., Li, H. J., Liu, J., et al. (2016). The *Arabidopsis* receptor kinase ZAR1 is required for zygote asymmetric division and its daughter cell fate. *PLoS Genet.* 12:e1005933. doi: 10.1371/journal.pgen.1005933

Yuan, J., Henry, R., McCaffery, M., and Cline, K. (1994). SecA homolog in protein transport within chloroplasts: evidence for endosymbiont-derived sorting. *Science* 266, 796–798. doi: 10.1126/science.7973633

Zhang, H., Scheirer, D. C., Fowle, W. H., and Goodman, H. M. (1992). Expression of antisense or sense RNA of an ankyrin repeat-containing gene blocks chloroplast differentiation in *arabidopsis*. *Plant Cell* 4, 1575–1588. doi: 10.1105/tpc.4.12.1575

Zhang, H., Wang, J., and Goodman, H. M. (1994). Expression of the *Arabidopsis* Gene AKRP Coincides with Chloroplast Development. *Plant Physiol.* 106, 1261–1267.

Zhao, Z., and Assmann, S. M. (2011). The glycolytic enzyme, phosphoglycerate mutase, has critical roles in stomatal movement, vegetative growth, and pollen production in *Arabidopsis thaliana*. *J. Exp. Bot.* 62, 5179–5189. doi: 10.1093/jxb/err223

Conflict of Interest: The authors declare that the research was conducted in the absence of any commercial or financial relationships that could be construed as a potential conflict of interest.

Publisher's Note: All claims expressed in this article are solely those of the authors and do not necessarily represent those of their affiliated organizations, or those of the publisher, the editors and the reviewers. Any product that may be evaluated in this article, or claim that may be made by its manufacturer, is not guaranteed or endorsed by the publisher.

Advantages of publishing in Frontiers

OPEN ACCESS
Articles are free to read for greatest visibility and readership

FAST PUBLICATION
Around 90 days from submission to decision

HIGH QUALITY PEER-REVIEW
Rigorous, collaborative, and constructive peer-review

TRANSPARENT PEER-REVIEW
Editors and reviewers acknowledged by name on published articles

Frontiers
Avenue du Tribunal-Fédéral 34
1005 Lausanne | Switzerland

Visit us: www.frontiersin.org
Contact us: frontiersin.org/about/contact

REPRODUCIBILITY OF RESEARCH
Support open data and methods to enhance research reproducibility

DIGITAL PUBLISHING
Articles designed for optimal readership across devices

FOLLOW US
@frontiersin

IMPACT METRICS
Advanced article metrics track visibility across digital media

EXTENSIVE PROMOTION
Marketing and promotion of impactful research

LOOP RESEARCH NETWORK
Our network increases your article's readership